Chiral-at-Metal Iridium(III) and Rhodium(III) Lewis Acid Catalysts for the α-Functionalization of 2-Acyl Imidazoles

Dissertation

zur Erlangung des Grades eines Doktors
der Naturwissenschaften
(Dr. rer. nat.)

dem Fachbereich Chemie
der Philipps-Universität Marburg

vorgelegt von

Wei Zuo

aus
Hebei, China

Marburg/Lahn
2017

Die vorliegende Dissertation entstand in der Zeit von Dezember 2012 bis Dezember 2015 am Fachbereich Chemie der Philipps-Universität Marburg in der Arbeitsgruppe und unter Betreuung von Herrn Prof. Dr. Eric Meggers.

Vom Fachbereich Chemie der Philipps-Universität Marburg (Hochschulkennziffer 1180) als Dissertation am …….. angenommen.

Abgabedatum:
Erstgutachter: Prof. Dr. Eric Meggers
Zweitgutachter: Prof. Dr. Jörg Sundermeyer

“When nothing seems to help, I go and look at a stonecutter hammering away at his rock perhaps a hundred times without as much as a crack showing in it. Yet at the hundred and first blow it will split in two, and I know it was not that blow that did it -- but all that had gone before.”

Jacob Riis

For my parents and my wife

Acknowledgement

First of all, I would like to express my sincere gratitude to Prof. Eric Meggers for giving me the opportunity to work in his research group. Since my initial research internship in February 2012 as a master student, I have enjoyed participating in the development of the chiral-at-metal transition metal complexes for asymmetric catalysis. I am indebted to him for the academic support, the patient guidance, and being open for discussions throughout the years. His enthusiasm for chemistry research have made it a pleasure for me to work with him. Moreover, I am grateful to the freedom that he granted me to finish this thesis.

I would like to thank Prof. Jörg Sundermeyer for accepting to review this thesis as well as his wonderful lectures in organometallic chemistry, which I enjoyed a lot during my studies in Marburg.

I also want to thank Prof. Armin Geyer for participating in the defense committee.

I want to express my gratitude to all the present and former group members in the Meggers and Höbenreich group. Zhijie Lin was my supervisor during my research internship in the Meggers group and has led me into this exciting research area. I also want to thank Haohua Huo, Xiaodong Shen and Chuanyong Wang for the help and discussions in the laboratory. My special thanks go to Thomas Cruchter and Thomas Mietke for both the support in the laboratory and the companionship beyond chemistry. I also want to thank them for proofreading this thesis. I want to express my gratitude to Vladimir "Vova" Larionov for the short but enjoyable time together during his postdoctoral stay in Marburg. I am grateful to Jens Henker, Melanie Helms, Cornelia Ritter, Markus Dörr, Elisabeth Martin, Timo Völker, Nathalie Nett, Sabine Düwel, Jie Qin, Xiao Zhang, Xiaoqiang Huang, Jiajia Ma, and Yu Zheng for their kindness and the pleasant working environment.

I thank my master students Jenny Kouretova, Bo Zhang, Luomo Li for their contributions to this thesis.

My gratefulness also goes to all members of the analytical team of the chemistry department of the Philipps-University of Marburg for rapid and reliable analysis of my samples.

I want to thank Ina Pinnschmidt, Andrea Tschirch, and Lilu Zhang for ordering chemicals and their organizational efforts.

I want to thank Fang Yang from the Hampp group for the companionship both in the chemistry faculty and on the basketball court. Moreover, I want to thank Roland Hüttl and Ingrid Hain for help and support in my daily life.

Last but not least, I want to thank my parents and especially my wife Ziyin Fan. Without their constant support this thesis would not have been accomplished.

Abstract

This work describes the development of applications of chiral-at-metal iridium(III)- and rhodium(III) Lewis acid catalysts. Based on the reversible coordination to their metal center and enolization upon coordination, chiral Lewis acids are capable to facilitate various α-functionalizations of 2-acyl imidazoles. In the first part, the visible-light driven enantioselective α-alkylation with α-cyanoalkyl bromides is presented. By merging photoredox catalysis with chiral Lewis acid catalysis, the α-cyanoalkylated 2-acyl imidazoles could be obtained with excellent enantiocontrol. This is the first example that such chiral metal enolate complexes react with branched carbon-centered radicals. In the second part, the results of the development of the asymmetric α-benzoyloxylation are presented. While the chiral rhodium Lewis acid complex demonstrated excellent catalytic activity to facilitate the reaction, the enantioselectivity remains to be improved. In the third part, results of the direct coupling of electron-rich arenes with the α-position of 2-acyl imidazoles are presented. The Lewis acid catalysts were found to promote the α-bromination of 2-acyl imidazoles with 2-bromo-1,3-dicarbonyl compounds and a subsequent Friedel-Crafts alkylation with electron rich arenes yielding the coupling products. Because it appears that the latter step proceeds predominantly through a planar cationic intermediate, which results in low enantioselectivity, the investigations are focused on the racemic variants and arene scope under the optimized reaction conditions is presented.

Die vorliegende Arbeit beschreibt die Anwendungsentwicklung von Iridium(III)- und Rhodium(III)-Lewis-Säure-Katalysatoren mit metallzentrierter Chiralität. 2-Acylimidazole lassen sich durch die reversible Koordination an die Metallzentren und Enolisierung an den α-Positionen funktionalisieren. Der erste Teil behandelt die durch sichtbares Licht vermittelte, asymmetrische α-Alkylierung von 2-Acylimidazolen mit α-Cyanoalkylbromiden. Die Photoredox-Katalyse ermöglicht die Generierung der Cyanoalkylradikale, welche sich dann an die chiralen Rhodium-Enolat-Komplexe mit exzellenter Enantio-selektivität addieren. Diese Synthese ist das erste Beispiel dafür, dass solche Metall-Enolat-Komplexe mit am Kohlenstoff verzweigten Radikalen reagieren. Der zweite Teil behandelt die Entwicklung der α-Benzoyloxylierung von 2-Acylimidazolen. Der Rhodium-Lewis-Säure-Komplex zeigt ausgezeichnete katalytische Aktivität, die Enantioselektivität der Reaktion ist allerdings in der Zukunft noch zu verbessern. Der dritte Teil behandelt die direkte Kupplungsreaktion von elektronenreichen Arenen mit 2-Acylimidazolen. Die Lewis-Säure-Komplexe katalysieren zuerst die α-Brominierung mit 2-Brom-1,3-dicarbonyl-Verbindungen und die Kupplungsreaktion verläuft dann über die bromierten Zwischenprodukte über die Friedel-Crafts-Alkylierung. Da der Alkylierungsschritt vermutlich über eine planare kationische Zwischenstufe verläuft und deshalb keine Stereokontrolle erreicht wird, werden die verschiedene Arene nur in der racemischen Reaktion untersucht.

Table of Contents

Chapter 1. Introduction

1.1. Asymmetric Synthesis of Chiral-at-Metal Octahedral Complexes

The word "chirality" originates from the Greek word for hand "χειρ (kheir)" and refers to the handedness of an object.[1] Today it's defined by IUPAC as: "*The geometric property of a rigid object (or spatial arrangement of points or atoms) of being non-superimposable on its mirror image; If the object is superimposable on its mirror image the object is described as being achiral.*"[2] In case of chiral objects, each of both non-superimposable mirror images is called enantiomer. A classic example are human's hands where left and right hands are non-superimposable mirror images of each other. In chemistry, a chiral molecule can not be superposed onto its mirror image. Well-known examples for enantiomers in chemistry are molecules with a tetrahedral carbon atom bearing four different substituents (Figure 1) and the theoretical support for this idea was proposed by Le Bel and van't Hoff nearly 150 years ago.[3,4]

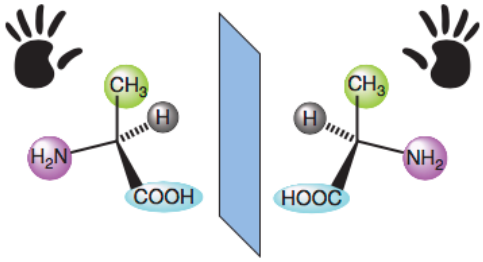

Figure 1: Human hands and a molecule with a tetrahedral carbon atom bearing four different substituents.

Since Pasteur's discovery of molecular chirality in 1848,[5] chemists have been intrigued by chiral molecules because most biomolecules are chiral and exist in only one enantiomeric form, such as the natural amino acids, which are building blocks for proteins. On the other hand, DNA is based on chiral deoxyriboses. For this reason, an organism reacts to both enantiomers of a chiral molecule in a different fashion as this chiral molecule interacts with chiral biomolecules.[6] Great efforts have been spent in developing enantioselective transformations in order to obtain enantioenriched compounds.[7,8] Among different strategies to obtain enantioenriched or enantiopure molecules, such as the resolution of a racemic mixture or by using enantiopure precursor from nature's chiral pool, asymmetric catalysis is considered to be an efficient, elegant, and economical, in which a only catalytic amount of chiral reagent is added and induces an enantioselective transformation.[9] The achievements in this area have been honored by awarding the Nobel Prize in chemistry to Knowles, Noyori, and Sharpless in 2001 for their contributions.[10-13]

In organometallic chemistry, metal complexes with chiral ligands are highly investigated because of their applicability as chiral catalysts in organic synthesis.[14] Chiral complexes with metal-located stereocenter remain much less explored, although the first example has already been reported by Alfred Werner in 1911. By applying Le Bel's and van't Hoff's stereochemical idea to hexacoordinated metal complexes, Alfred Werner predicted that some of these compounds could exist as enantiomers.[15] His prediction was soon proved by the successfully resolution of the two enantiomers of $[Co(en)_2(NH_3)X]^{2+}$ **1** (X = Cl, Br, en =

ethylene diamine) with (+)-3-bromo-camphor-9-sulphonate (**2**) as chiral anion in 1911 (Figure 2), which demonstrated for the first time that the spatial arrangement of achiral ligands around a metal center can also lead to a chiral compound.[16]

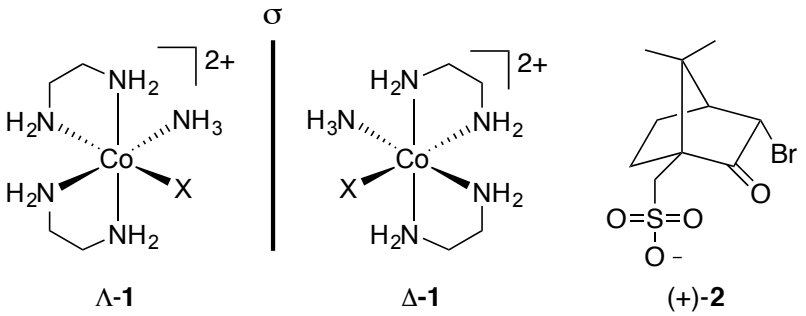

Λ-**1** Δ-**1** (+)-**2**

Figure 2: Structures of both enantiomers of the chiral cation **1**; The resolution was achieved by Alfred Werner with the chiral anion (+)-**2**.[16]

Since Werner's discovery, various strategies have been developed to obtain enantioenriched metal complexes with achiral ligands, for examples through spontaneous resolution,[17] resolution through high performance liquid chromatography (HPLC) with a chiral stationary phase,[18] and through asymmetric catalysis.[19,20] Compared to other strategies, asymmetric catalysis is highly attractive due to its efficiency and has received a lot of attention, especially in the last decade. In order to establish chirality on the metal center, it is necessary to employ enantiopure chiral auxiliaries, whose absolute configurations are predetermined, thus diastereomers with different physicochemical properties are formed which can be separated from each other through different techniques. One class of such chiral auxiliaries are chiral ions. Because many complexes exist as salts, exchange of achiral counterions against chiral counterions enables the formation of diastereomeric salts. Common ions for this purpose are tris[tetrachlorobenzene-1,2-bis(olato)] phosphate(V) (TRISPHAT, **3**),[21,22] derivatives of tartrates **4** and 10-camphorsulfonate **5**,[23] and enantiopure ammonium salts from natural amines[18] (Figure 3). On the other hand, chiral chelating ligands are also used as auxiliaries to transfer chiral information onto the metal centers. However, it is important to note that in many cases the chiral chelating ligands stay attached to the metal centers and the complexes exist as diastereomers, therefore these complexes do not belong to the category "chiral-at-metal complexes".

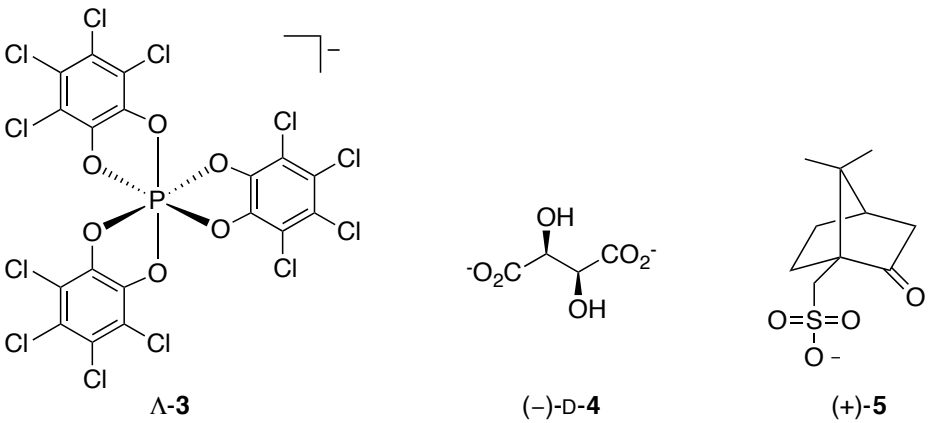

Λ-**3** (−)-D-**4** (+)-**5**

Figure 3: Structures of commonly used enantiopure anions to resolve chiral cationic metal complexes.[21-23]

In the past years, the Meggers group has made significant contributions to the asymmetric synthesis of octahedral chiral-at-metal complexes.[24-26] Initially, the Meggers group was dedicated to employ kinetically inert transition metal complexes (Ru, Ir, Rh, Re, Os) in biological systems, especially as enzyme inhibitors.[27-33] Because a chiral environment is formed at the active site of enzymes, it is reasonable to expect that the potency of one enantiomer should differ from the other one. Indeed, during the development of ruthenium-based kinase inhibitors, the Meggers group synthesized complex **6** as a racemic mixture and separated its enantiomers by chiral HPLC (Figure 4). Subsequent studies revealed that Λ-**6** is a much more potent inhibitor for the PAK1 kinase than inhibitor Δ-**6**.[34] Such chirality-potency correlation has been observed in several other studies as well.[35,36]

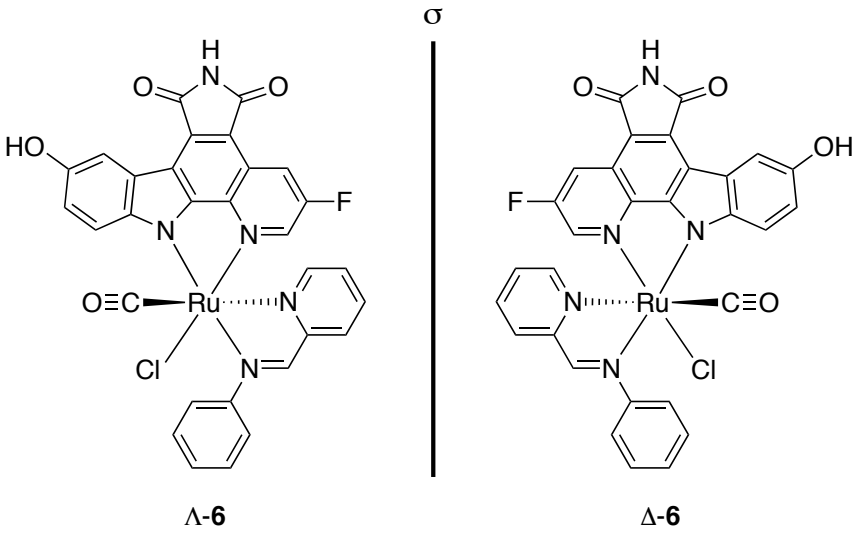

Figure 4: Structures of chiral ruthenium-based kinase inhibitors Λ-**6** and Δ-**6**, Λ-**6** is a significantly more potent inhibitor than Δ-**6** for the PAK1 kinase.[34]

Inspired by these observations, the Meggers group started to develop tools for the asymmetric synthesis of octahedral chiral-at-metal complexes. In this regards, significant progress was achieved in 2009.[37] Initially, commercially available ruthenium(II) dimer **7** is treated with chiral oxazoline (*S*)-**8**. Resulting complex (*S*)-**9** contains a metal-located stereocenter and is obtained as a mixture of diastereomers.[38] The benzene ligand is then substituted by three acetonitrile ligands in the presence of ultraviolet (UV) light to form ruthenium(II) complex (*S*)-**10** containing no metal-located stereocenter. All of the three acetonitrile ligands and the chloride ligand can now be cleaved off and substituted for other ligands (Scheme 1).

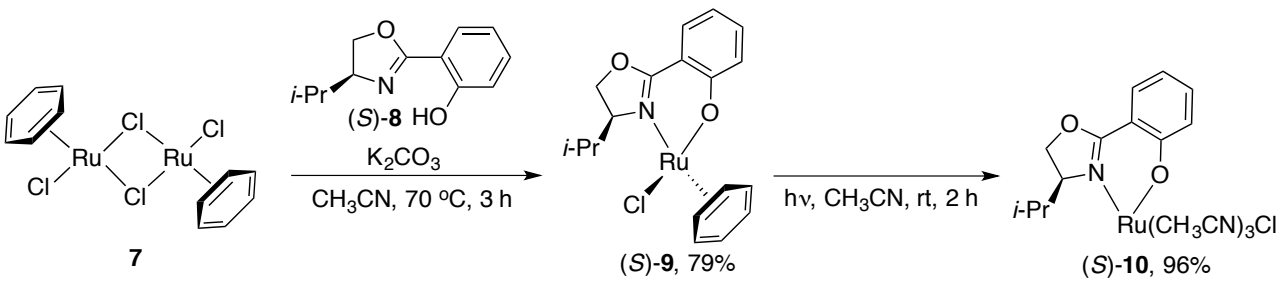

Scheme 1: Introduction of the chiral auxiliary and the formation of the octahedral structure.[37]

The key step to obtain a metal-located stereocenter is the substitution of acetonitrile and chloride ligands with two bidentate ligands [e.g. dtbbpy (**11**) and dmbpy (**12**)], which undergo chiral-auxiliary-controlled diastereoselective coordination to form complex Λ-(*S*)-**13** with high diastereomeric purity (99.6:0.4 dr, Scheme 2).

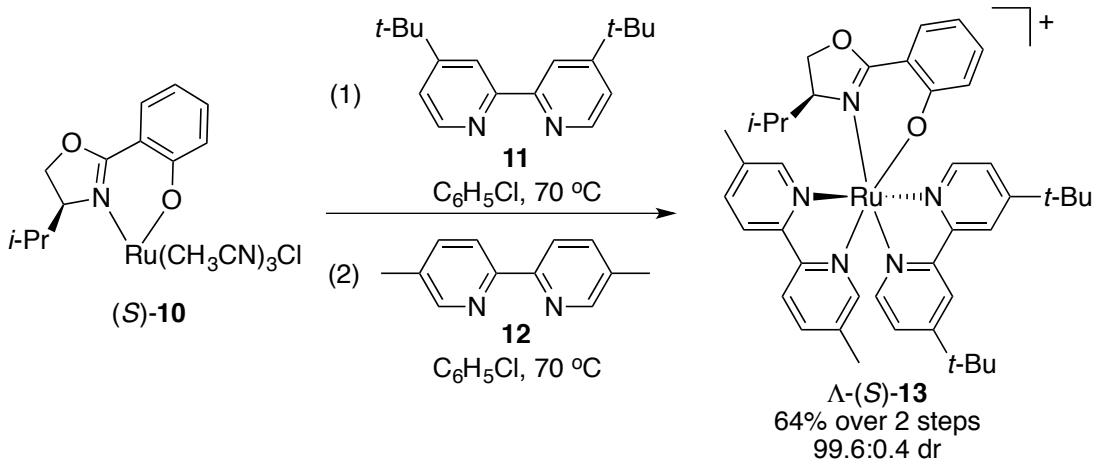

Scheme 2: Formation of a metal-located stereocenter by diastereoselective coordination.[37]

After formation of the metal-located stereocenter, chiral auxiliary (*S*)-**8** could be substituted by acetonitrile ligands under acidic conditions with retention of configuration of the metal-located stereocenter. Then, complex Λ-**14** reacts with 2,2'-bipyridine (bpy, **15**) to yield complex Λ-**16** with high enantiomeric purity (Scheme 3a). A direct transformation of Λ-(*S*)-**13** to Λ-**16** is operable as well (Scheme 3b).

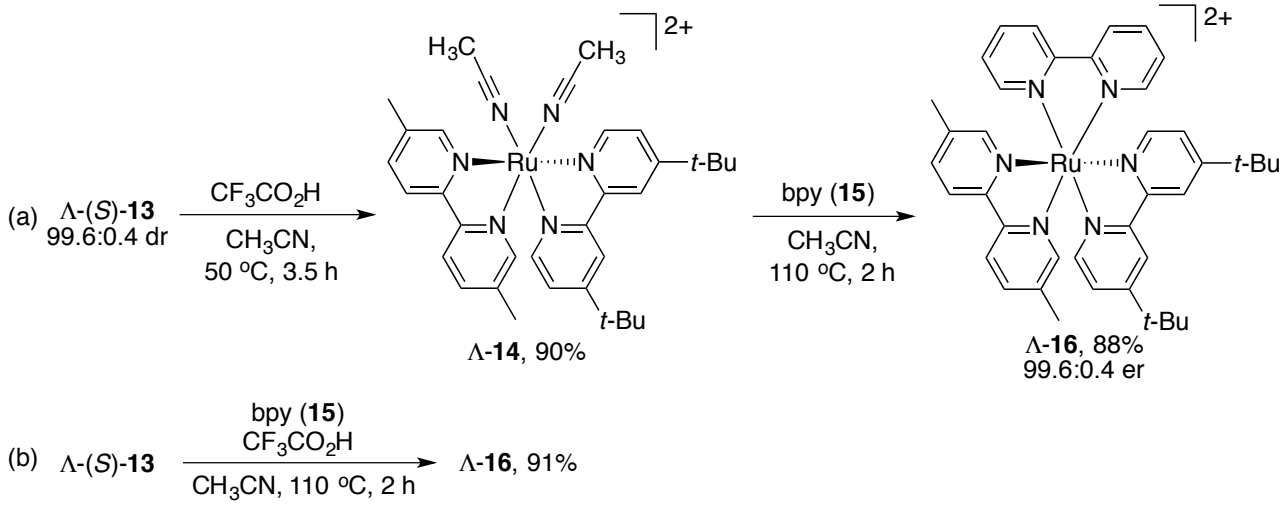

Scheme 3: Substitution of chiral oxazoline (*S*)-**8** by 2,2'-bipyridine (**15**) under retention of configuration.[37]

In a subsequent publication, the performances of several chiral oxazolines with different substituents at their 5-position (instead of *i*-Pr) were investigated. This allowed to expand the scope of the achiral ligands, which led to the first general strategy for the asymmetric synthesis of ruthenium polypyridyl complexes with high enantiopurity.[39] In addition, several other compounds have been identified to be suitable chiral auxiliaries for this class of complexes, such as chiral binaphthyl **17**,[40] sulfinamide **18**,[41] L-proline (**19**),[42] sulfinyl-

phenols **20** and **21** (Figure 5).[43,44] Hence, not only carbon-centered chirality but also sulfur-centered and axial chirality could be exploited to create octahedral complexes with metal-located stereocenter.

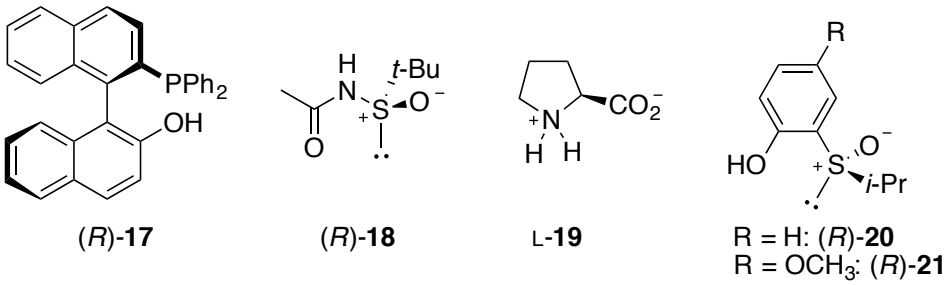

Figure 5: Auxiliaries with axial or sulfur-centered chirality to create octahedral complexes with metal-located stereocenter.[40-44]

Instead of diastereoselective coordination, other strategies have been found operable as well. For example, starting with racemic *cis*-[Ru(bpy)$_3$Cl$_2$] (**22**), a dynamic resolution occurs upon coordination of (*R*)-**18** to form single diastereomer Λ-(*S*)-**23**, whose configuration is thermodynamically favored (Scheme 4).[41] A similar mechanism has been observed in the case of proline (**19**).[42]

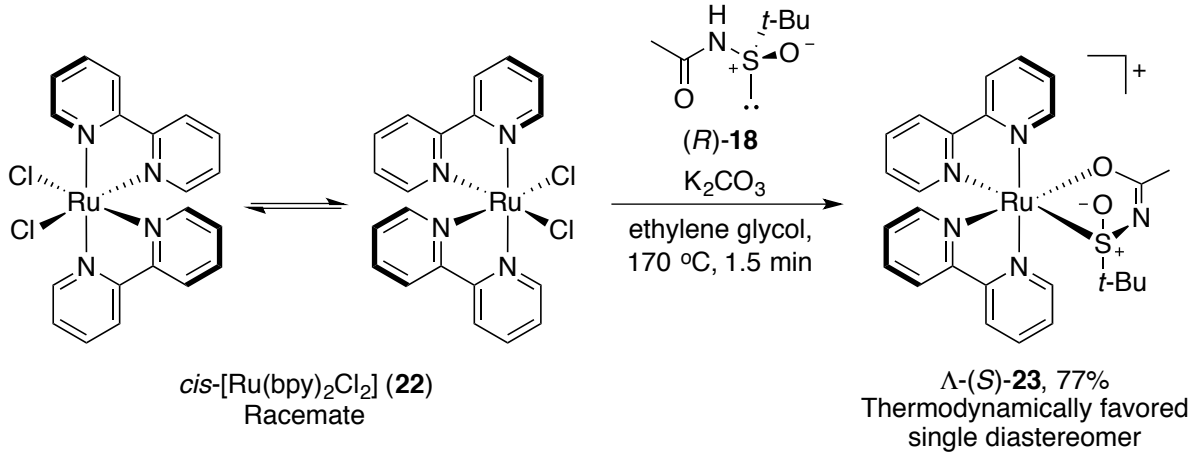

Scheme 4: Dynamic resolution upon coordination of chiral auxiliary (*R*)-**18**.[41]

Furthermore, a method for the achiral precursor *trans*-[Ru(bpy)$_2$(CH$_3$CN)$_2$](CF$_3$SO$_3$)$_2$ (**24**·2OTf) has been developed. Chiral auxiliary (*R*)-**20** is able to induce *trans*−*cis* isomerization under thermodynamic control to form Δ-(*R*)-**25** selectively. Remarkably, with only 20 mol% of auxiliary (*R*)-**21**, chiral-at-metal complex Δ-**26** could still be obtained with 78% *ee* (Scheme 5).[44]

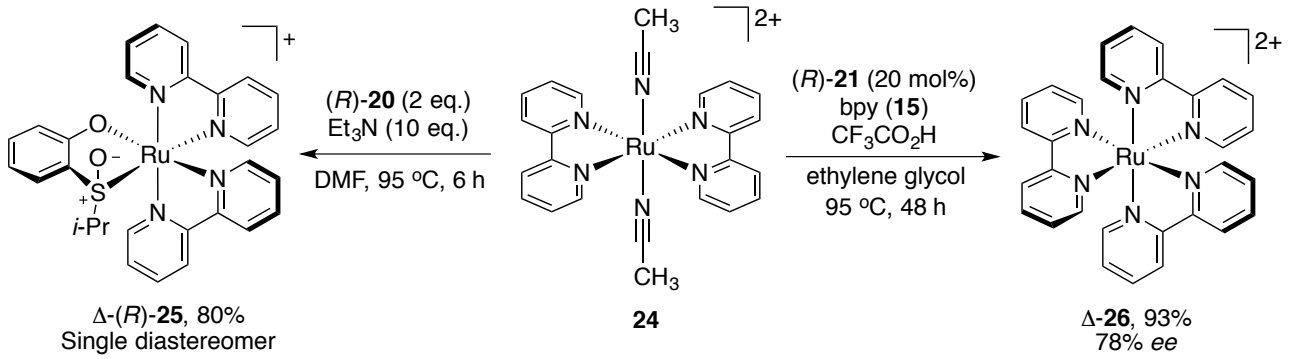

Scheme 5: Preparation of chiral-at-metal ruthenium complexes through isomerization under thermodynamic control.[44]

The Meggers group has also made significant contributions to the preparation of chiral iridium(III) and rhodium(III) complexes. Compared to the asymmetric synthesis of ruthenium(II) polypyridyl complexes, the preparations of chiral iridium and rhodium complexes rely on di-μ-chloro-bridged dimers as precursor, which exist as racemic mixtures of ΛΛ- and ΔΔ-isomers. Splitting of these dimers and introduction of enantiopure auxiliary ligands results in pairs of diastereomers. Resolutions of these diastereomers can be achieved through different techniques. For instance, Marchi and co-worker reported that Λ-(*R*)-**28** and Δ-(*R*)-**28**, which both contain fluorinated phenol oxazoline (*S*)-**27** as chiral auxiliary, are separable by conventional flash column chromatography on silica gel (Scheme 6).[45]

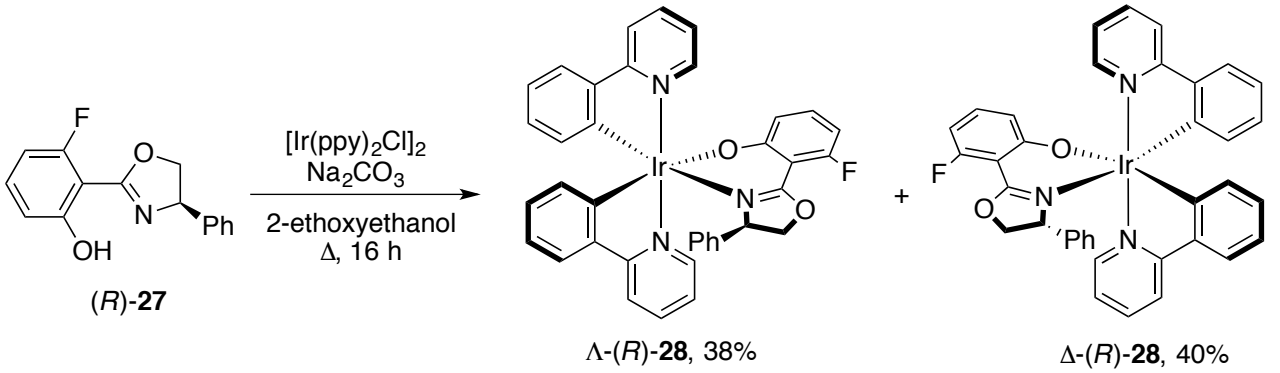

Scheme 6: Preparation of iridium complex **28** with metal-located stereocenter. Separation of diastereomers is achieved through column chromatography on silica gel.[45]

The Meggers group has investigated the performance of more phenol oxazolines (*S*)-**29**–**31** and phenol thiazoline (*S*)-**32** and not only managed to resolve iridium complexes based on 2-phenylpyridine derivatives but also based on 2-phenylbenzothiazole as cyclometalating ligands. Similar to the preparation of chiral-at-metal ruthenium(II) complexes, the chiral auxiliary could be substituted after the resolutions under acidic conditions so that octahedral iridium(III) complexes with metal-centered chirality, such as Λ-**34**, could be obtained with excellent yield and *ee* (Scheme 7).[46]

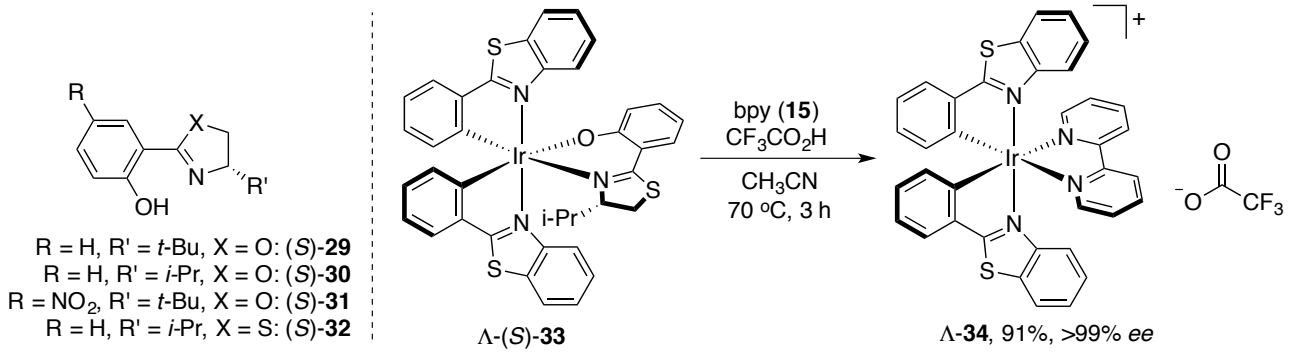

Scheme 7: Structures of further chiral auxiliaries and procedure to prepare chiral-at-metal cyclometalated iridium(III) complexes.[46]

The chiral auxiliary strategy could be applied to rhodium complexes but only few examples have been reported so far. For instance, rhodium dimer complexes **35** and **36** were found to be suitable precursors to prepare the respective enantioenriched rhodium complex (Figure 6).[47,48]

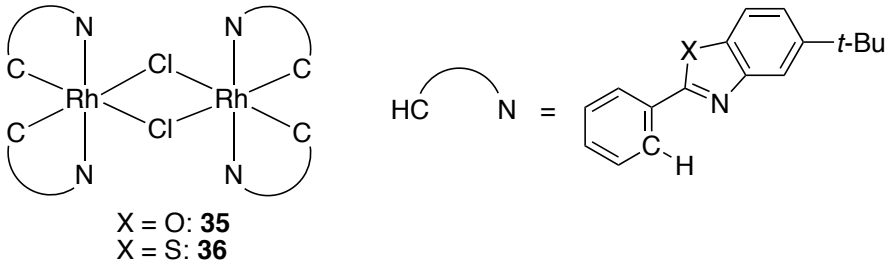

Figure 6: Structure of rhodium dimer complex **35** and **36**.[47,48]

In the case of rhodium dimer complex **35**, proline (**19**) has been employed as chiral auxiliary. Instead by column chromatography, the resolution of the Λ- and Δ-isomers is achieved through diastereoselective precipitation in a well-defined solvent system, where one diastereomer is obtained as precipitates (for example, rhodium complex Λ-L-**37** is obtained when L-proline (**19**) is employed), while the other remains in solution and is subsequently discarded (Scheme 8).[47]

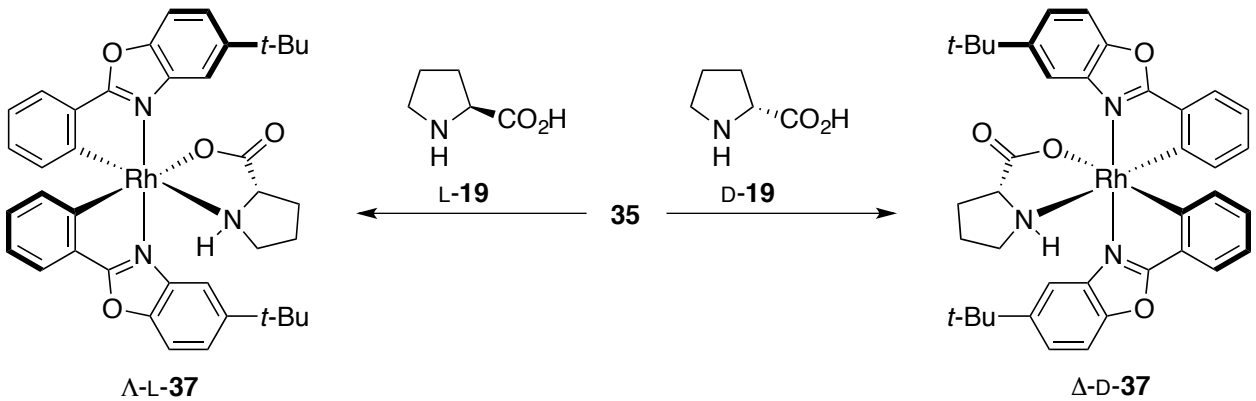

Scheme 8: Preparation of rhodium(III) complex **37** with metal-located stereocenter. Separation of diastereomers is achieved through diastereoselective precipitation.[47]

In the case of rhodium dimer complex **36**, phenol oxazoline (*S*)-**38** has been employed as chiral auxiliary and both Λ-and Δ-isomers of **39** can be isolated at the same time by flash column chromatography on silica gel (Scheme 9).[48]

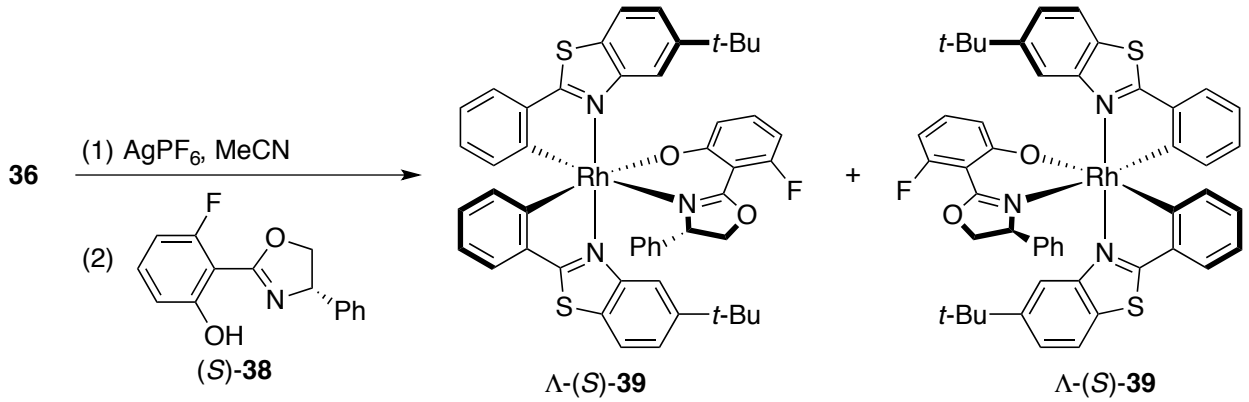

Scheme 9: Preparation of rhodium(III) complex **39** with metal-located stereocenter. Separation of diastereomers is achieved through column chromatography on silica gel.[47]

Both proline (**19**) and (*S*)-**38** can be substituted under acidic conditions, which allows the introduction of further achiral ligands, such as acetonitrile or 2,2'-bipyridine (**15**).

1.2. Applications of Chiral-at-Metal Octahedral Complexes in Asymmetric Catalysis

Having established strategies for the asymmetric synthesis of octahedral complexes with exclusive metal-centered chirality,[26,48,49] the Meggers group wondered whether such complexes could be utilized as chiral catalysts, so that the metal-centered stereoinforamtion would be utilized to enantioselectively generate chiral tetrahedral carbon atoms (Scheme 10).

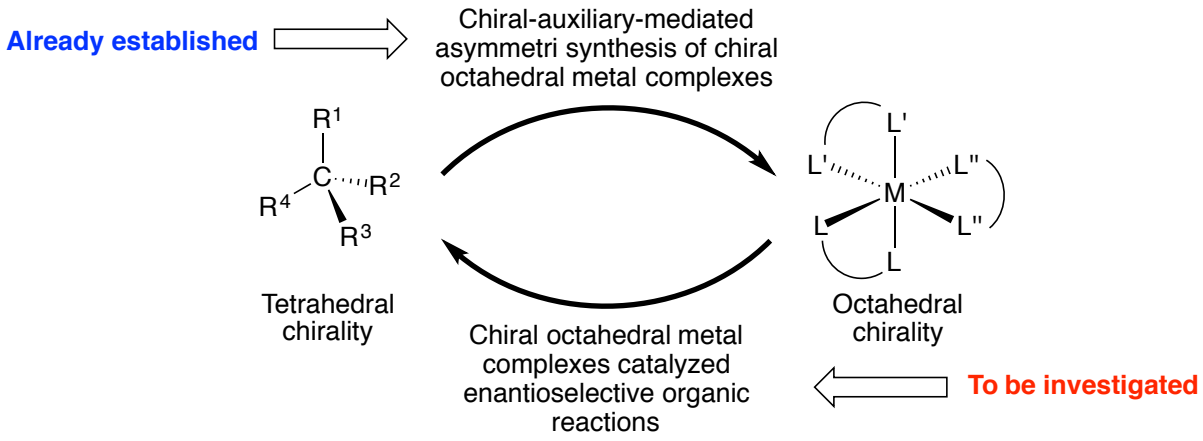

Scheme 10: Chirality transfer between organic small molecules and octahedral metal complexes.

As mentioned, the preparation of enantioenriched organic compounds through asymmetric catalysis has been one of the central topics in organic chemistry in the past decades. To achieve this goal, many different classes of compounds have been investigated to serve as chiral catalysts, such as transition metal complexes with chiral ligands, small organic molecules as organocatalysts, and even enzymes. In contrast, octahedral complexes with exclusive metal-centered chirality remained largely unexplored, in part due to lack of preparation methods. One of the earliest examples has been reported by Gladysz and co-workers in 2008.[51] First, the solubility of the chiral-at-metal cationic complex Δ-$[Co(en)_3]^{3+}$ (**40**) in the organic solvent is increased by a borate (BArF) counterion (Figure 7).

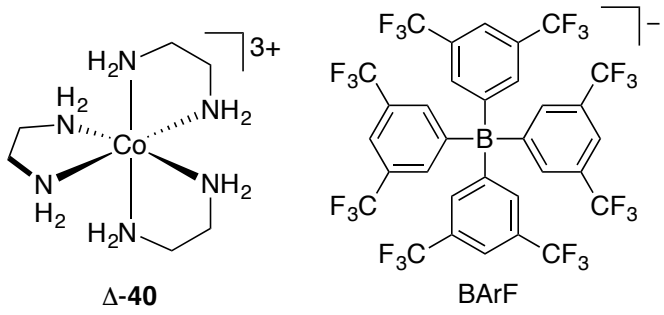

Figure 7: Structures of the chiral cobalt complex Δ-**40** and the borate BArF.[51]

Complex Δ-**40**·3BArF·14H_2O has been found to catalyze the Michael addition between 2-cylcopenten-1-one (**41**) and dimethyl malonate (**42**) giving the product (*R*)-**43** in 78% yield and with only 33% *ee* (Scheme 11). The authors proposed that cation Δ-**40** facilitates the reaction via a second coordinationsphere mechanism.

However, the authors also assume that the lack of a predominant well-defined transition state leads to poor asymmetric induction.[51]

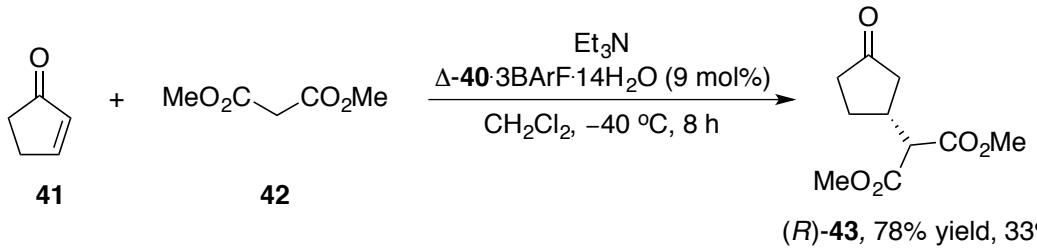

Scheme 11: Chiral-at-metal complex Δ-**40** catalyzes the Michael-addition between **41** and **42**.[51]

As can be seen from Scheme 11 and compound Δ-**40**, the main challenge is it to translate the catalyst's metal-located stereoinformation to the products through effective interactions between both. To address this issue, the Meggers group reported highly sophisticated iridium complex Λ-**44** to catalyze the hydrogen transfer reaction of nitroalkene **45** with Hantzsch ester **46**.[52] By installing 5-amino-3-(2-pyridyl)-1*H*-pyrazole as the catalytically active ligand, complex Λ-**44** carries a double hydrogen bond donor functionality (both NH groups), which enables the catalyst to fixate and activate nitroalkene **45** at the same time. The hydroxyl group (OH) on the benzoxazole ligand is responsible for activation of Hantzsch ester **46** by hydrogen bonding as a hydrogen acceptor and directs the attack from only one prochiral face. The 3,5-dimethylphenyl substituents on the cyclometalated ligands increase the stereoselectivity by blocking the other prochiral face, from which the undesired reaction occurs and further accelerate the reaction by stabilizing the hydrogen bond adduct between catalyst Λ-**44** and nitroalkene **45** (Scheme 12).

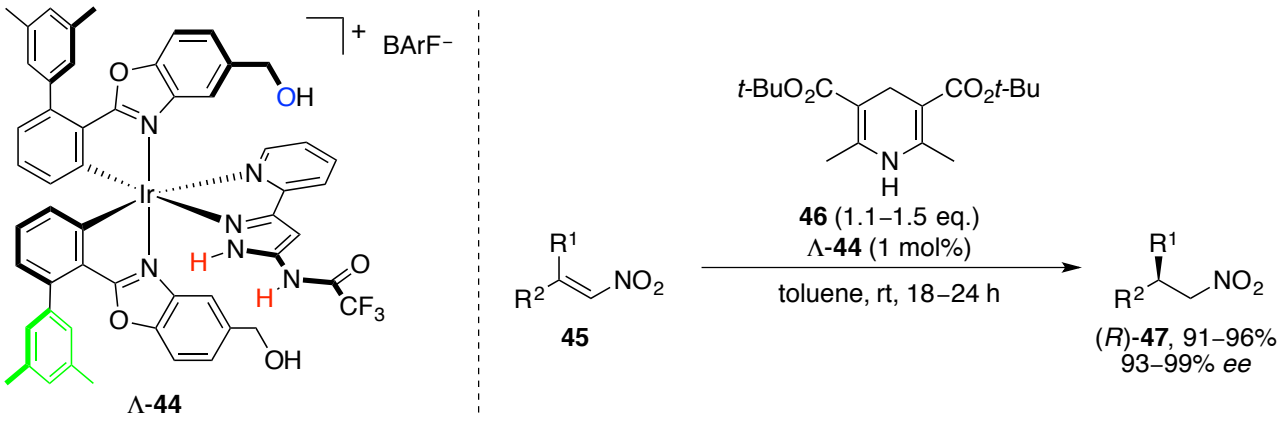

Scheme 12: Chiral-at-metal iridium(III) complex Λ-**44** as bifunctional catalyst for the asymmetric hydrogen transfer reaction between nitroalkene **45** and Hantzsch ester **46**.[52]

The aforementioned mechanistic aspects have been proved through various techniques and have led to the discovery of even more powerful catalyst Λ-**48**.[53] Compared to Λ-**44**, C_2-symmetrical catalyst Λ-**48** bears a bispyrazole ligand and therefore there are two catalytic sites per complex. The hydroxyl groups on Λ-**44** are replaced by carboxamide groups, which are better hydrogen bond acceptors and the 2,6-dimethylphenyl substituents provide stronger steric hindrance than the 3,5-dimethylphenyl substituents. These modifications

have led to excellent catalytic activity, which has allowed catalyst loading as low as 0.005 mol% to still give the products with over 90% yield and *ee* (Scheme 13).

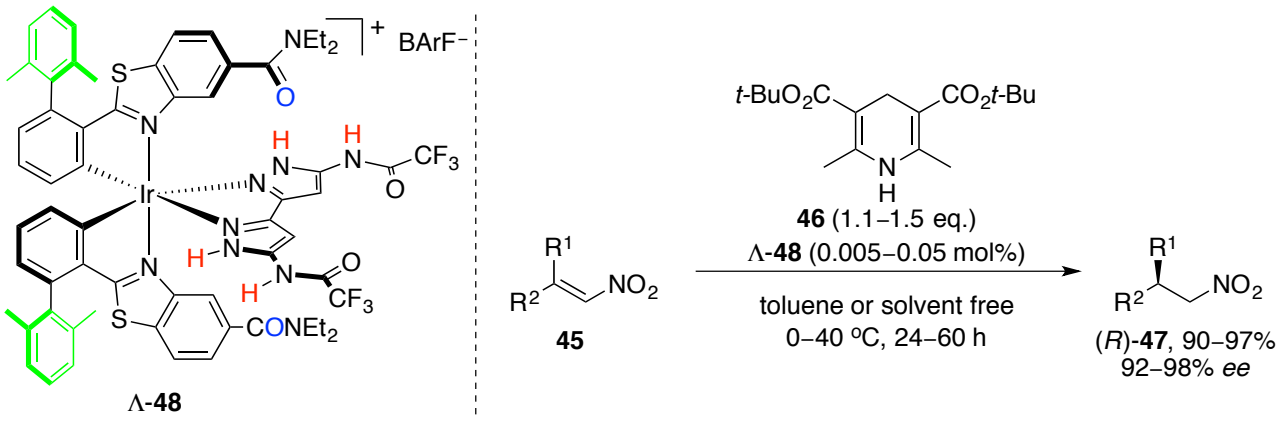

Scheme 13: C_2-symmetrical chiral iridium(III) complex Λ-**48** catalyzed enantioselective hydrogen transfer reaction between nitroalkene **45** and Hantzsch ester **46**.[53]

Based on these results, the Meggers group has moreover developed complexes Λ-**49**,[54] Λ-**50**,[55] and Λ-**51**[56] as very powerful bifunctional catalysts by introduction of different well-tuned ligands. In case of Λ-**49** and Λ-**50**, deprotonation of the pyridyl pyrazole ligands leads to basic nitrogen atoms, which enables the complexes to serve as Brønsted base catalysts and to promote enantioselective sulfa-Michael additions and aza-Henry reactions with high efficiency (Scheme 14).

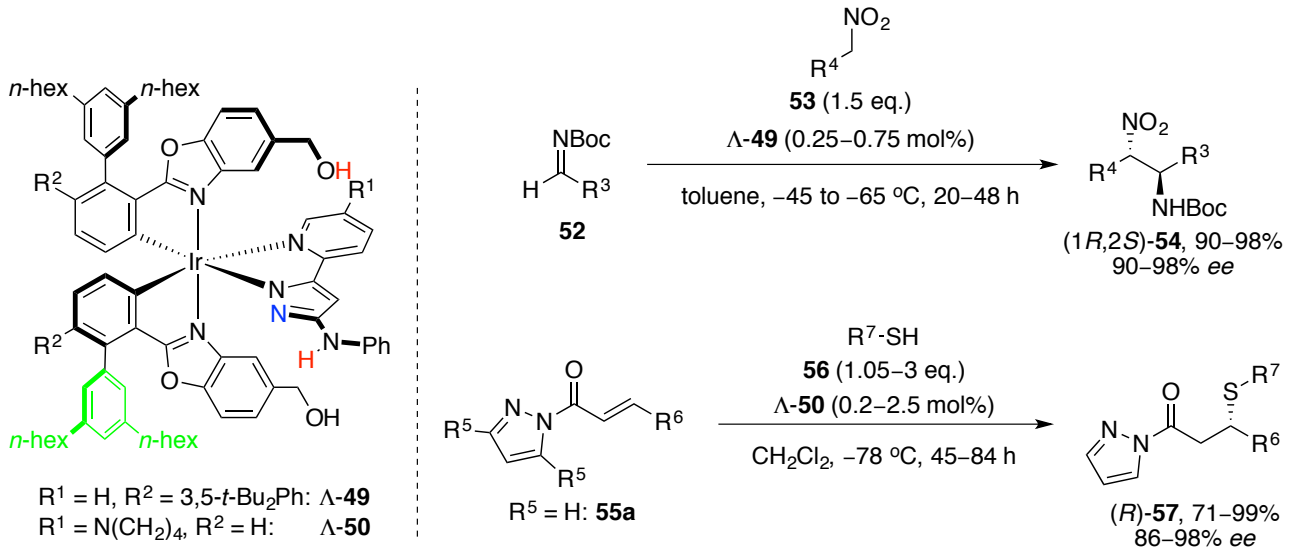

Scheme 14: Chiral iridium(III) complexes as Brønsted base catalysts for asymmetric Michael-addition sand aza-Henry reactions.[54-55]

Installation of a ligand with a secondary amine functionality led to the discovery of enamine/hydrogen-bonding catalyst Λ-**51**, which catalyzes the asymmetric α-amination of aldehydes (**58**) with azo-dicarboxylates.[56] Subsequent reduction and cyclization afford configurationally stable and enantioenriched oxazolidinones (*R*)-**59** with excellent yields and selectivities (Scheme 15).

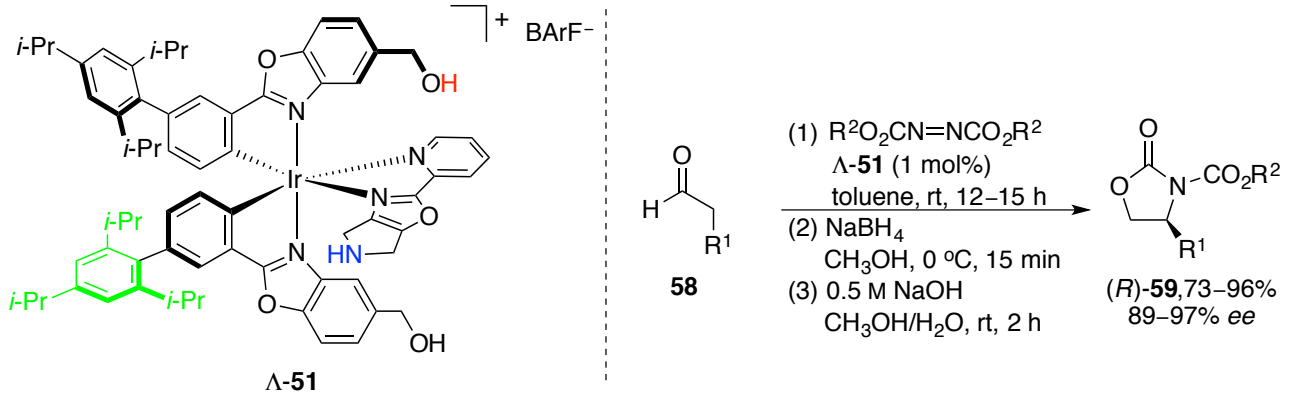

Scheme 15: Chiral iridium complex Λ-**51** serves as an enamine/hydrogen-bonding catalyst.[56]

Compared to organocatalysts, which are based on similar binding and activation modes, such as hydrogen bonding, proton transfer, and enamine formation, chiral octahedral metal complexes **44** and **48**–**51** have proved to be excellent templates for catalyst design and are able to achieve high enantioselectivity at remarkably low catalyst loadings. The good performances of these complexes come from their structural rigidity and globular complexity, which not only provide entropic advantages but also enable the fine tuning of catalyst optimization, so that the catalytically active functional groups can work in a cooperative manner.

In all previous examples (Schemes 12–15), only the metal center's chirality is utilized and the actual catalysis takes place at catalytically active ligands, so in all these examples the metal solely serves as a structural element. Subsequently, the Meggers group has developed C_2-symmetric chiral iridium complex **60** (IrO), whose both labile acetonitrile ligands can be substituted by *α*,*β*-unsaturated 2-acyl imidazole **61aa** to afford Λ-**62aa** (according to ^{1}H-NMR analysis),[57] indicating that complex IrO might be able to function as Lewis acid and activate imidazole substrate **61aa** by increasing its reactivity towards nucleophilic attack (Scheme 16).

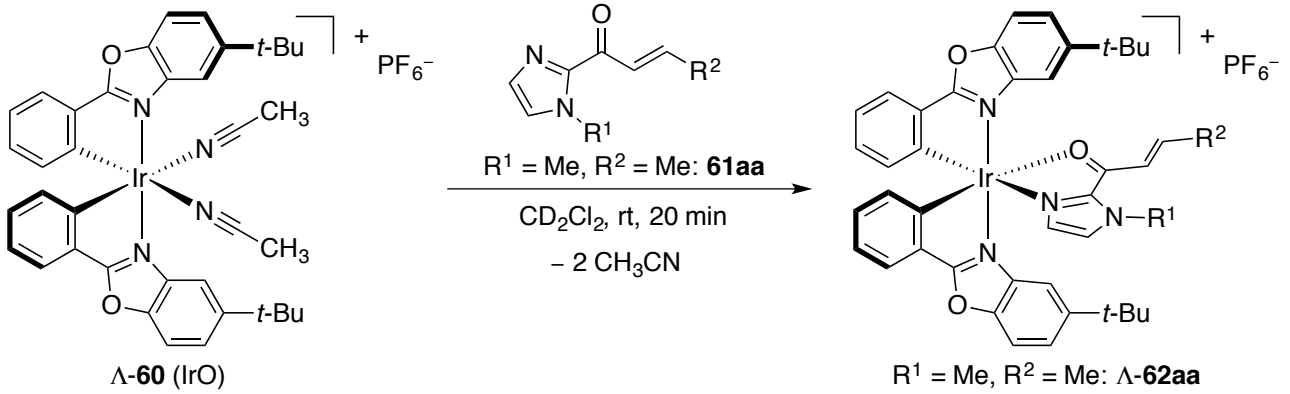

Scheme 16: Substitution of the labile acetonitrile ligands of Λ-**60** by *α*,*β*-unsaturated 2-acyl imidazole **61**.[57]

Indeed, in the presence of only 1 mol% Λ-IrO, Friedel-Crafts alkylation of 1*H*-indole with **61aa** proceeds smoothly to afford product (*S*)-**63** in 97% yield and 96% *ee*. The excellent enantioselectivity of the reaction demonstrates the configurational stability of the catalyst, while both benzoxazole-attached *tert*-butyl groups ensure excellent stereoinduction (Scheme 17).[57]

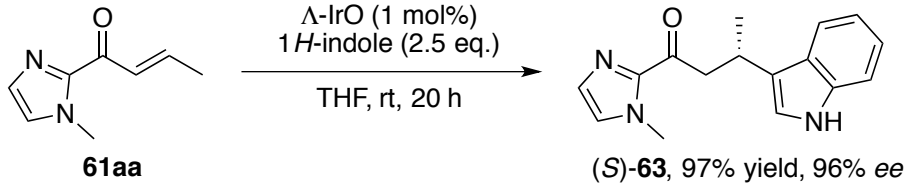

Scheme 17: Iridium(III) Lewis acid with metal-centered chirality catalyzes the asymmetric Friedel-Crafts-alkylation between α,β-unsaturated 2-acyl imidazole **61aa** and 1*H*-indole.[57]

Further research resulted in the discovery of iridium(III) complex **64** (IrS), which has been found to catalyze a wide range of reactions such as Friedel-Crafts alkylations, Michael additions, and cycloadditions to give products with complex structures in high stereoselectivity (Scheme 18).[58]

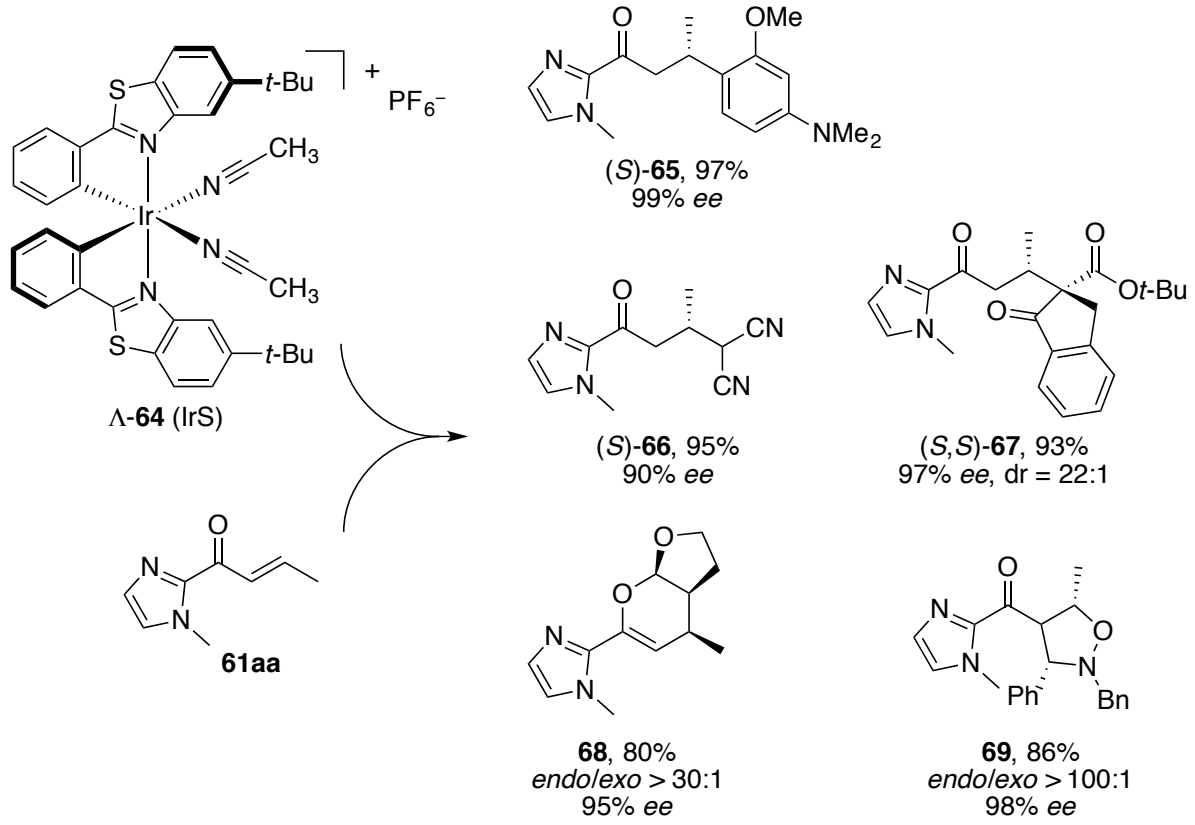

Scheme 18: Chiral-at-metal iridium(III) Lewis acid IrS catalyzes an asymmetric Friedel-Crafts alkylation, Michael additions, and cycloadditions.[58]

The same design principles could be applied to rhodium complexes. As described in chapter 1.1, enantio-enriched rhodium complexes **70** (RhO)[59] and **71** (RhS)[60] can be easily synthesized from their corresponding auxiliary complexes **36** and **39** respectively (Figure 8).

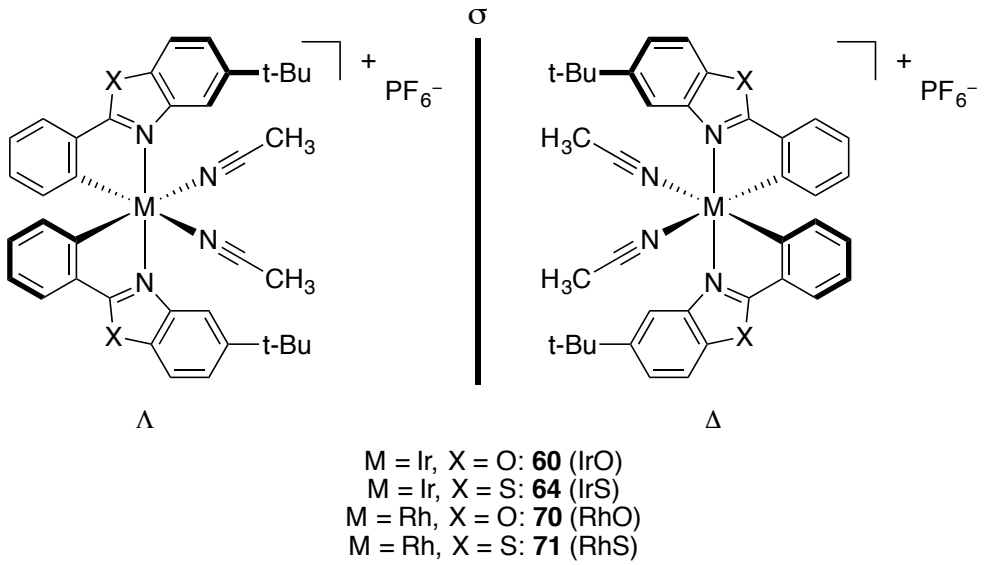

Figure 8: Structures of the chiral-at-metal iridium(III)- and rhodium(III) Lewis acid complexes.

During the evaluation of their catalytic activity as Lewis acids, both rhodium(III) catalysts RhO and RhS proved to be often advantageous over their iridium(III) derivatives. Taking the Michael addition between imidazole substrate **61aa** and Meldrum's acid (**72**) as example: The reactions with iridium catalysts Λ-IrO and Λ-IrS afforded (*S*)-**73** with 81% *ee* and 91% *ee* respectively (Table 1, entries 1 and 2), while product (*R*)-**73** could be obtained with 95% *ee* in the presence of 2 mol% Δ-RhO (entry 3). The superiority of RhO and RhS over IrO and IrS is more obvious when the catalyst loadings are reduced to 1 mol%. Compared to the dramatically lowered enantioselectivities when Δ-IrO and Δ-RhO are employed at such low loadings (entries 4 and 5), Λ-RhS manages to maintain >90% *ee* for (*S*)-**73** (entry 6). Due to a significantly enhanced reaction rates in case of the rhodium catalysts, the enantioselectivity could also be improved by simple reaction temperature reduction (entry 7).

Table 1: Chiral-at-metal Lewis acid catalyzed Michael addition between **72** and **61aa**.

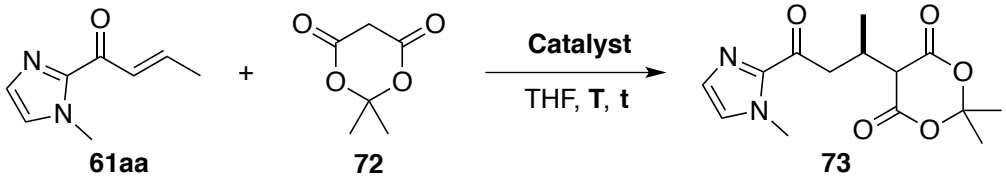

Entry	Catalyst	T	t	Product
1	Λ-IrO (2 mol%)	rt	6 h	(*S*)-**73**, 93% yield, 81% *ee*[58]
2	Λ-IrS (2 mol%)	rt	6 h	(*S*)-**73**, 94% yield, 91% *ee*[58]
3	Δ-RhO (2 mol%)	rt	6 h	(*R*)-**73**, 96% yield, 95% *ee*[58]
4	Δ-IrO (1 mol%)	rt	16 h	(*R*)-**73**, 99% yield, 68% *ee*[59]
5	Δ-RhO (1 mol%)	rt	16 h	(*R*)-**73**, 99% yield, 85% *ee*[59]
6	Λ-RhS (1 mol%)	rt	16 h	(*S*)-**73**, 99% yield, 93% *ee*[60]
7	Δ-RhO (1 mol%)	5 °C	16 h	(*R*)-**73**, 97% yield, 94% *ee*[59]

In addition to electrophile activation, the iridium and rhodium Lewis acids have also demonstrated their ability to activate nucleophiles by catalyzing an asymmetric α-amination of 2-acyl imidazoles.[59] Upon coordination of **74aa** to the metal center, the acidity of the α-proton increases and therefore an enolization is possible in the protic solvent *iso*-propanol. The metal enolate then attacks dibenzyl azodicarboxylate (**75**) to afford the amination product (*R*)-**76** with good selectivity. Again, the rhodium catalyst RhO furnishes the product with higher *ee* and furthermore at a lower catalyst loading than catalyst IrO (Scheme 19).

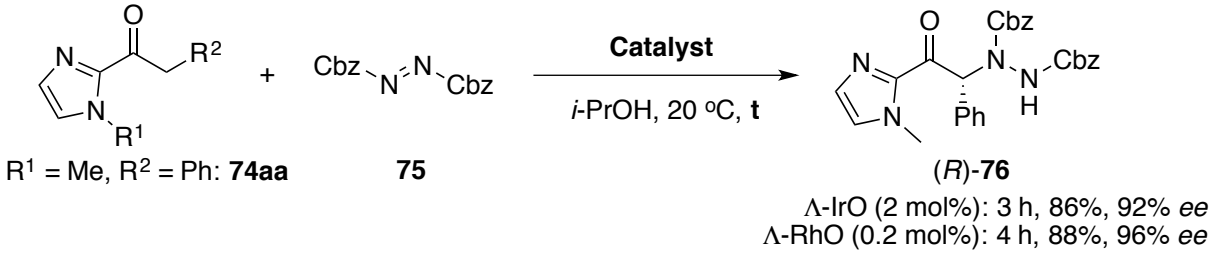

Scheme 19: Lewis acid catalyzed asymmetric α-amination of 2-acyl imidazoles with chiral-at-metal-rhodium(III) and iridium(III) complexes.[59]

To prove this mechanistic proposal, iridium enolate complex **77aa** was crystallized and studied by X-ray diffraction analysis. As illustrated in Figure 9, 2-acyl imidazole **74aa** coordinates to the iridium center in a bidentate fashion and the nucleophilicity of the α-position is increased through enolization. The *tert*-butyl groups provide steric hindrance and the chirality of the metal center determines which of both enantiomers of **76** is predominantly obtained.

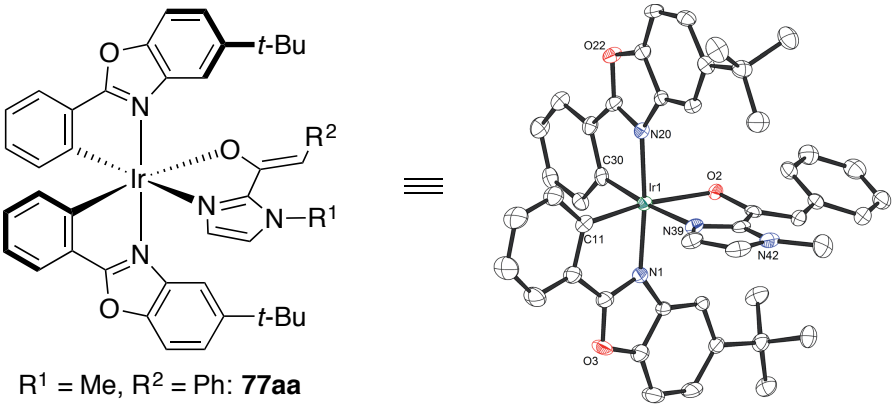

Figure 9: Crystal structure of iridium enolate complex **77aa**.[59]

In summary, the Meggers group has employed octahedral chiral-at-metal complexes in asymmetric catalysis by installing functional groups on the ligands in order to mimic binding and activating modes of the well-established organocatalysts. Due to their rigid nature and structural complexity, such complexes are able to achieve remarkably high levels of asymmetric induction at very low catalyst loadings. In order to fully grasp the potential of such chiral-at-metal catalysts, complexes with labile ligands and yet stable configurations have been developed to activate both electrophiles and nucleophiles. Recently, the Lewis acid catalysts have been successfully employed in visible-light driven reactions, in which the metal center provides chirality, catalytic activity, and photoredox property simultaneously, which is discussed in detail in the subsequent section.

1.3. Visible-Light Driven Asymmetric Photocatalysis

As early as 1912, the idea of photochemistry was proposed by Giacomo Ciamician. He envisioned that mankind would one day be able to utilize sunlight as a direct indefinite source of energy for chemical process, just like plants absorb sunlight and convert carbon dioxide and water to glucose and oxygen.[61] Thinking along these lines, industrial syntheses could be carried out in an environmentally friendly manner and no more rely on fossil fuels, which not only create pollutions but could be completely exhausted as well. Despite recent progress of photochemistry in organic synthesis,[62,63] chemistry companies have only slowly adopted this approach for fine chemicals production. One fundamental limitation in photochemistry is that most organic molecules absorb light only in the UV region, which is not abundant in the solar spectrum. And to perform photochemical reactions, special photoreactors are often required to generate high-energy UV radiation, which raises safety and cost concerns. Furthermore, UV photons have energy in the energy range of C,C-bonds. While activating substrates and promoting desired transformations, UV radiation can therefore easily lead to non-productive side-reactions, especially when complex structure or sensitive functional groups are present in the substrate.

One strategy to circumvent these problems is it to employ photocatalysts that are able to absorb visible light and form excited states to initiate chemical transformations.[64,65] Thanks to the great efforts devoted to the development of photovoltaic cells, organic light emitting devices (OLED), water splitting, and carbon dioxide reduction using visible light, the photochemical properties of various inorganic compounds[66,67] and organometallic complexes[68-70] have been well studied. Among these photoactive species, polypyridyl ruthenium(II)[71,72] and cyclometalated iridium(III)[73,74] complexes are especially attractive due to their straightforward preparations, long lifetime of their excited states, ability to luminescence emission, redox properties, and their structural and chemical stability.

Taking $[Ru(bpy)_3]^{2+}$ (**26**) as an example, it exhibits broad, strong absorbance in the visible spectrum (λ_{max} = 452 nm). Upon irradiation with visible light, the complex is raised to excited states and then rapidly undergo radiationless deactivation and intersystem crossing (ISC) to the lowest excited state - the first triplet metal-to-ligand-charge-transfer excited state ($^3MLCT_1$). As return of the triplet excited state to the singlet ground state is spin-forbidden, the lifetime of this triplet excited state can be as long as 1.1 μs in acetonitrile solution at room temperature.[75] Compared to the ground state, excited $*[Ru(bpy)_3]^{2+}$ is both easier to oxidize and easier to reduce. In the presence of an oxidant, photoexcited complex $*[Ru(bpy)_3]^{2+}$ can be oxidized (oxidative quenching) through a single electron transfer (SET) to generate $[Ru(bpy)_3]^{3+}$, which itself is also a strong oxidant (Scheme 20, path a). Analogously, reduced species $[Ru(bpy)_3]^{+}$ can also be formed depending on the reaction conditions (Scheme 20, path b). Therefore, various chemical reactions can be initiated by generating these redox-active species. Finally, $*[Ru(bpy)_3]^{2+}$ can be deactivated through sensitized energy transfer, in which the excited complex transfers its triplet energy to an acceptor (A) so that the acceptor is raised to triplet excited state (Scheme 20, path c).[76] This process is of high interest because triplet energy transfer triggered reactions with organic UV-absorbing photosensitizers have been well established, replacing UV-light by visible light is highly desired in this area.[77]

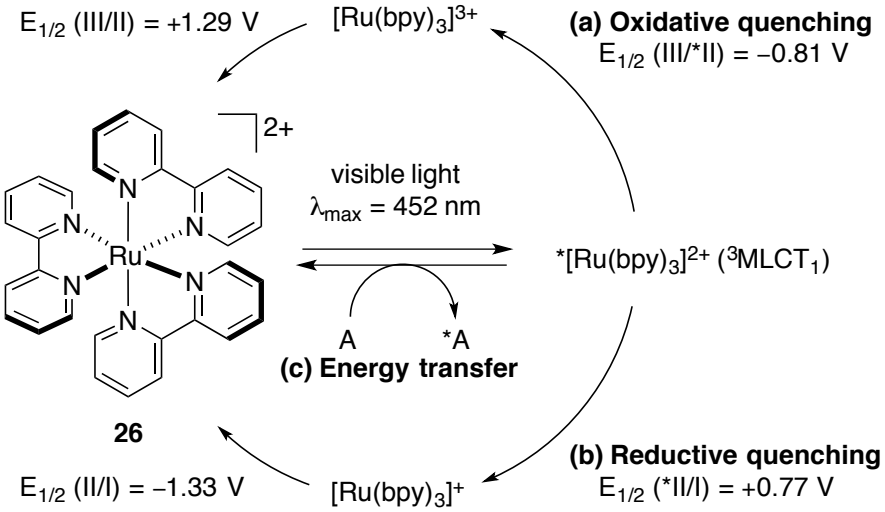

Scheme 20: Major deactivation pathways of $*[Ru(bpy)_3]^{2+}$, potentials are given with respect to saturated calomel electrode (SCE).[76-77]

One of the earliest examples where a visible light absorbing photocatalyst was employed to promote an organic reaction was reported by Cano-Yelo and Deronzier in 1984. They reported about a photocatalytic Pschorr reaction to synthesize substituted phenanthrenes.[78] The authors proposed that diazonium salt **78** is reduced by excited $*[Ru(bpy)_3]^{2+}$ through a SET and the subsequent release of nitrogen produces aryl radical **79**, which undergoes intramolecular cyclization. Radical **81** is then oxidized by $[Ru(bpy)_3]^{3+}$ to form cation **81** and the deprotonation affords phenanthrene **82** (Scheme 21).

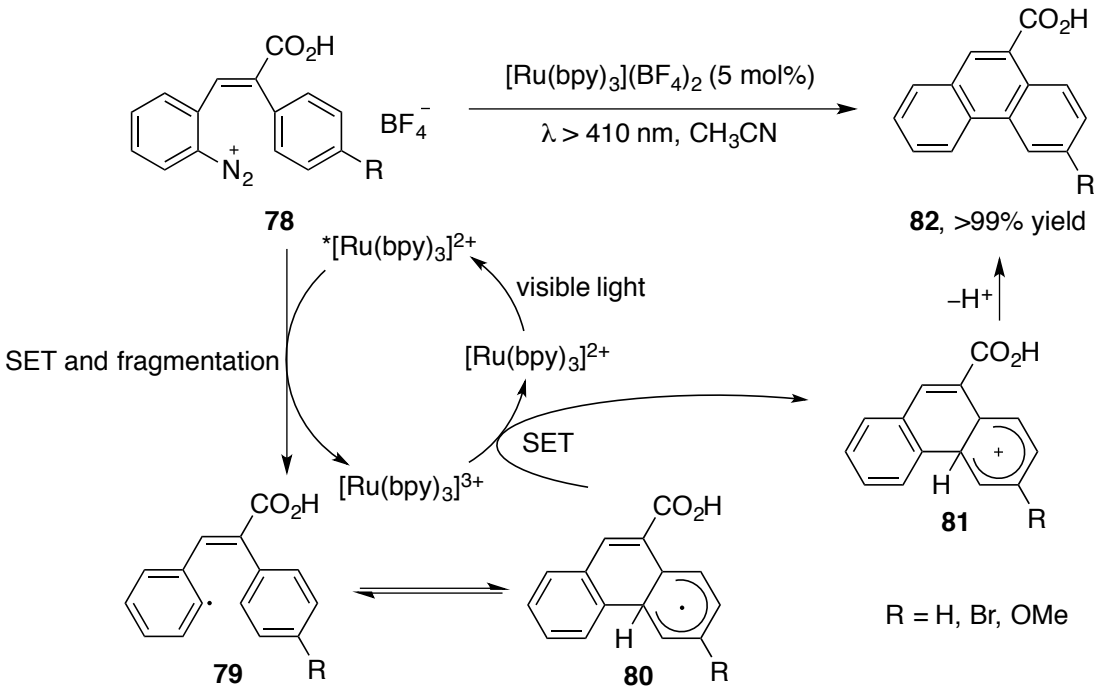

Scheme 21: Photocatalytic Pschorr reaction with visible light and its proposed mechanism.[78]

Although several studies dealing with photocatalysis with visible light have been published following Cano-Yelo and Deronzier's initial report,[79-82] it was not until recent years that the utilization of visible light has

truly gained a lot of attentions from the organic chemists. In 2001, Krische and co-workers reported a cobalt catalyzed intramolecular [2+2]-cycloaddition of tethered bis(enone) **83**.[83] The authors proposed that the reaction proceeds via anionic radical intermediate **84**, which is formed through single electron reduction by cobalt complex **86** (Table 2, entry 1). In order to prove this mechanistic proposal, Krische employed different techniques to achieve this single electron reduction by other means, for example chrysene radical anion **87** (entry 2) or cathodic reduction (entry 3) and still managed to obtain cyclobutane **85**.[84,85] Yoon and co-workers successfully combined the photoredox abilities of $[Ru(bpy)_3]^{2+}$ and Krische's radical [2+2]-cycloaddition, in which photocatalysis is responsible for the reduction of bis(enones) (entry 4).[86]

Table 2: Intramolecular [2+2]-cycloaddition of tethered bis(enone) **83** via radical anion intermediate.[83-86]

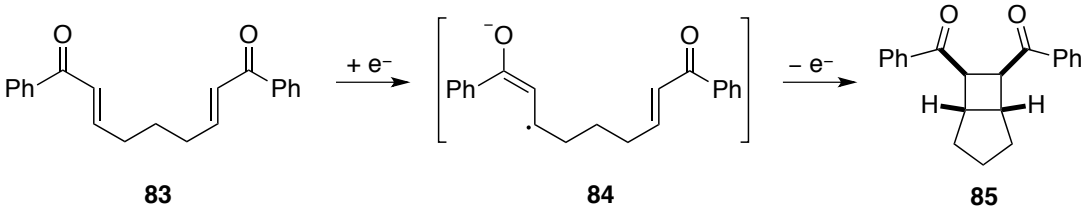

83 **84** **85**

Entry	Catalyst, Reagent	Product
1[83]	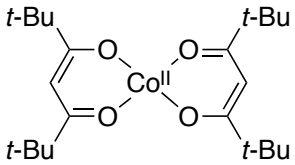 **86** (10 mol%), $PhMeSiH_2$ (4 eq.)	*cis*-**85** (72%)
2[84]	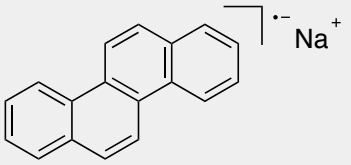 **87** (70 mol%)	*cis*-**85** (32%)
3[85]	Cathodic reduction (−0.90 V, $LiClO_4$)	*cis*-**85** (17%); *trans*-**85**, (20%)
4[86]	$[Ru(bpy)_3]Cl_2$ (5 mol%), $LiBF_4$ (2 eq.) *i*-Pr_2NEt (2 eq.), visible light	**85** (89%), *cis*:*trans* > 10:1

After proving the necessity of each component of the reaction, Yoon and co-workers proposed that the photoexcited ruthenium complex is deactivated through reductive quenching by *i*-Pr_2NEt to generate stronger reductant $[Ru(bpy)_3]^+$, which transfers an electron to activated bis(enone) (**83**·Li^+). The lithium ion acts as a Lewis acid to facilitate the reduction and the tetrafluoroborate increases the solubility of $[Ru(bpy)_3]^{2+}$ (Scheme 22).

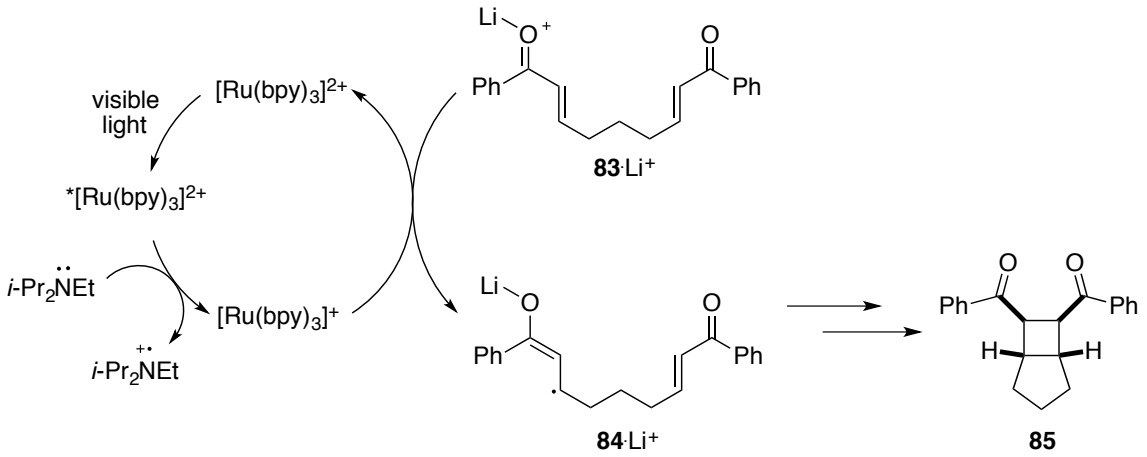

Scheme 22: Proposed mechanism of the photocatalytic intramolecular [2+2]-cycloaddition of tethered bis(enone) **83** with visible light.[86]

Among all the methods developed for this particular intramolecular [2+2]-cycloaddition, photoredox catalysis is clearly superior to the others in terms of catalyst loading, yield, and selectivity. Furthermore, Yoon and co-workers developed an intermolecular version of this reaction (*vide infra*) and demonstrated that the reaction can be performed on a gram scale using sunlight instead of light bulb as irradiation source without compromising the yields and diastereomeric ratios of the products.[87]

Triggered by pioneering works from Yoon, MacMillan,[88] Stephenson,[89] and many others, photocatalysis has experienced a real boom over the last decade. The ability of visible-light-absorbing chromophores of single electron transfers at excited states can not only be applied to established radical transformations but can also be exploited to develop new unique transformations. In addition, further metal complexes such as $[Ru(bpz)_3]^{2+}$ (**88**), $[Ir(ppy)_2(dtbbpy)]^+$ (**89**), $[Ir\{dF(CF_3)ppy\}_2(dtbbpy)]^+$ (**90**) and *fac*-$[Ir(ppy)_3]$ (**91**) have been discovered as catalysts, which have different redox properties (Figure 10).[90-95]

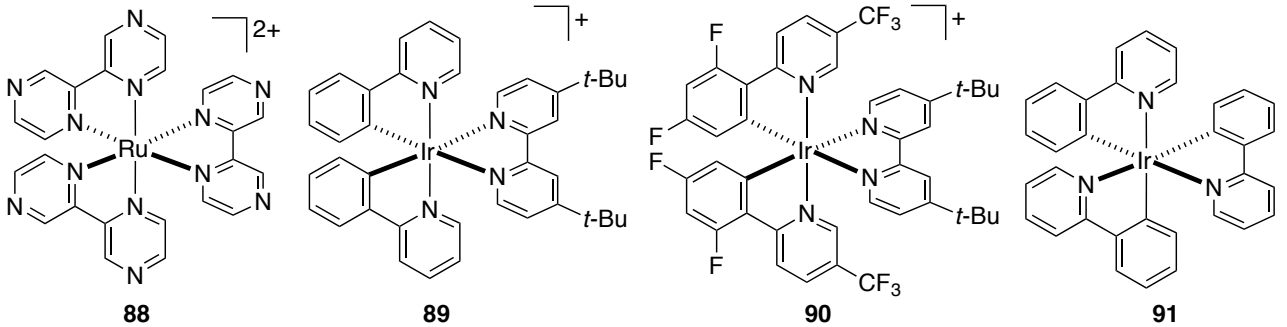

88

$E_{1/2}$ (III/*II) = −0.26 V
$E_{1/2}$ (*II/I) = +1.45 V
$E_{1/2}$ (III/II) = +1.86 V
$E_{1/2}$ (II/I) = −0.80 V

89

$E_{1/2}$ (IV/*III) = −0.96 V
$E_{1/2}$ (*III/II) = +0.66 V
$E_{1/2}$ (IV/III) = +1.21 V
$E_{1/2}$ (III/II) = −1.51 V

90

$E_{1/2}$ (IV/*III) = −0.89 V
$E_{1/2}$ (*III/II) = +1.21 V
$E_{1/2}$ (IV/III) = +1.69 V
$E_{1/2}$ (III/II) = −1.37 V

91

$E_{1/2}$ (IV/*III) = −1.73 V
$E_{1/2}$ (*III/II) = +0.31 V
$E_{1/2}$ (IV/III) = +0.77 V
$E_{1/2}$ (III/II) = −2.19 V

Figure 10: Common photoredox catalysts with visible light, potentials are presented with respect to saturated calomel electrode (SCE).[90-95]

As mentioned above, photocatalysis can ben an efficient tool to develop economic and ecologic processes. Therefore, it is no surprise that there is large interest in enantioselective photocatalytic reactions. A number of reactions have been reported to achieve this goal in the past few years.[96,97] In general, most of these reactions fall into three categories: (1) By employing substrate-activating chiral co-catalysts, the photo-catalysis-generated reactive radicals or ions are captured under stereocontrol; (2) By interacting with chiral co-catalysts, the substrate's photophysical properties are altered and hence the subsequent photocatalyzed reactions proceed enantioselectively; (3) By employing chiral photocatalysts, which provide photoactivation and stereocontrol at the same time.

The first of these three approaches is also the most widely adopted approach. As one of the earliest examples for photocatalysis with visible light, the MacMillan group successfully combined chiral imidazolidinone organocatalyst **92** and photoredox catalysis in order to perform asymmetric α-alkylation of aldehydes. A number of electron-deficient alkyl halides have been found to be suitable and these include bromo malonate **93,** phenacyl bromides **94**,[88] α-cyanoalkyl bromides **95**,[98] benzyl bromides **96**,[99] trifluoromethyl- and perfluoroalkyl iodides **97**.[100] In these reactions, alkyl halides are reduced through photoredox catalysis to radical anions, which rapidly decompose to halides and carbon-centered radicals **100**. C,C-bond formation and the chiral induction are achieved through addition of electron-deficient radicals **100** to the electron-rich double bond of chiral enamine **99**, which is generated from aldehyde **58** and chiral imidazolidione **92**. After oxidation and hydrolysis α-amino radical **101** is converted to enantioenriched alkylated product **98**. Meanwhile, **92** is released to initiate the next catalytic cycle (Scheme 23).

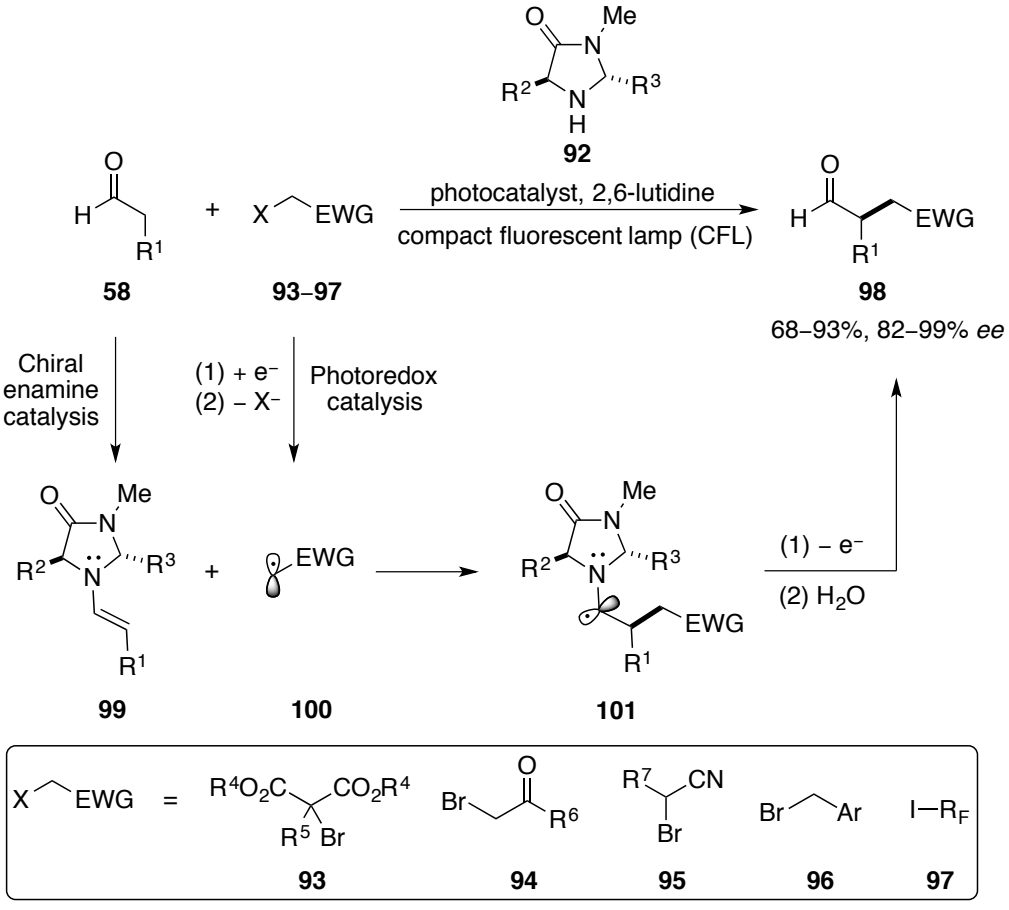

Scheme 23: Merger of photoredox catalysis with asymmetric enamine catalysis by MacMillan.[88,98-100]

Depending on the reaction partners, different photocatalysts can be employed for these reactions. In case of $[Ru(bpy)_3]Cl_2$ and $[Ir(ppy)_2(dtbbpy)]PF_6$ as photocatalysts, it is supposed that photoexcited complexes are first deactivated by a sacrificial amount of enamine **99** to afford the reactive reductants $[Ru(bpy)_3]^+$ and $[Ir(ppy)_2(dtbbpy)]$, which then transfer an electron to the alkyl halides **93–97** to initiate the first catalytic cycle and are reproduced by oxidizing the α-amino radical **101** from excited state (Scheme 24a). On the other hand, when neutral photocatalyst *fac*-$[Ir(ppy)_3]$ is employed as photocatalyst, no sacrificial amount of enamine **99** is required to initiate the reaction. Because *fac*-$[Ir(ppy)_3]$ should be able to reduce the alkyl halides directly from excited state ($E_{1/2}$ (V/*III) = −1.73 V) (Scheme 24b).

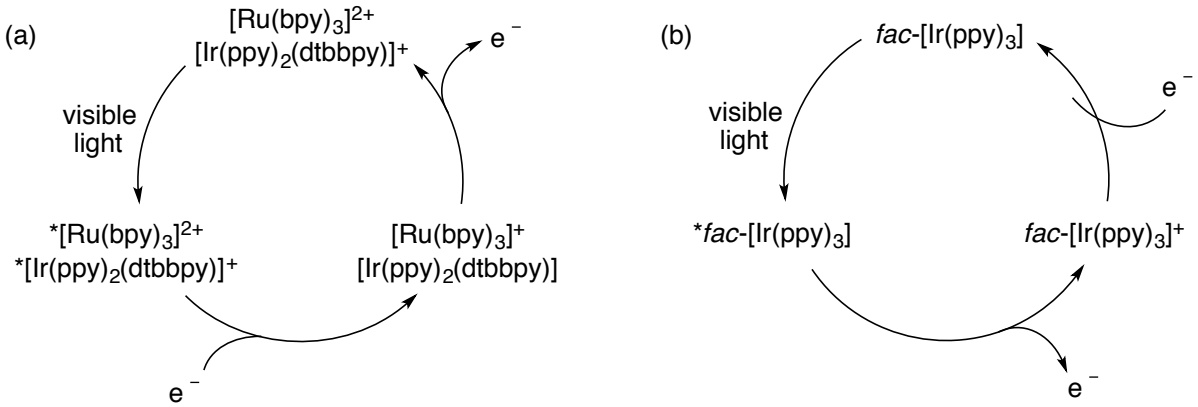

Scheme 24: Photoredox catalytic cycles of MacMillan's asymmetric α-alkylation of aldehydes.[88,98-100]

MacMillan's success has prompted the search for other enantioselective catalytic reactions using this dual catalysis strategy. Zeitler and Ferroud identified eosin Y (**102**) and rose bengal (**103**) as suitable organic photosensitizers, which allow it to perform MacMillan's asymmetric alkylation of aldehydes under metal-free conditions (Figure 11).[101,102]

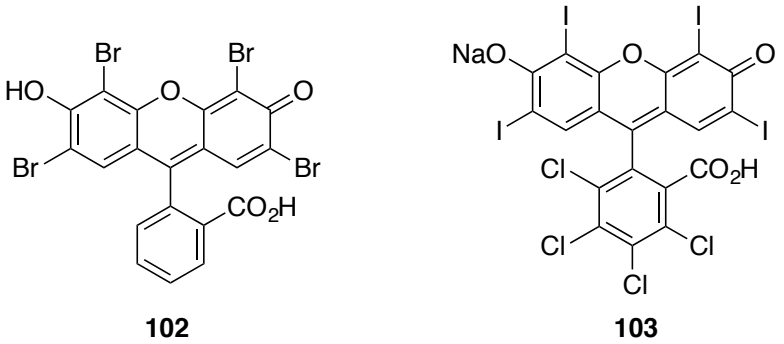

102 **103**

Figure 11: Structures of organic photosensitizes eosin Y (**102**) and rose bengel (**103**).[101,102]

Inspired by MacMillan's catalysis design principle, Luo and co-workers reported an enantioselective alkylation of β-ketocarbonyls **104** with phenacyl bromides **94** by employing chiral primary amine **105** and achiral $[Ru(bpy)_3]Cl_2$ as catalysts. Chiral primary amine **105** activates β-ketocarbonyls **104** by forming enamines **106** and electron-deficient radicals **107** are generated through photoredox catalysis. The products **108** could be obtained in modest to excellent yields with high *ee* (Scheme 25).[103]

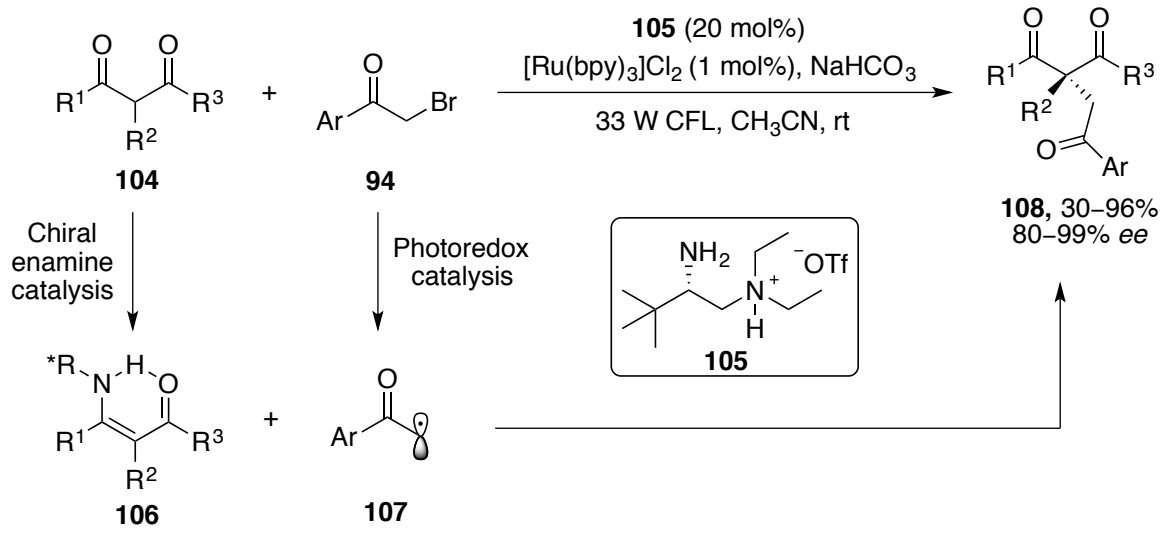

Scheme 25: Chiral primary amine (enamine catalyst) and achiral ruthenium complex catalyzed asymmetric alkylation of β-ketocarbonyls.[103]

Photoredox catalysis is also able to produce ionic electrophiles: Oxidation of *N*-aryl-tetrahydroisoquinolines **109** to iminium ions **110** via photoredox catalysis has been reported by Stephenson, which can be denoted as visible-light driven *aza*-Henry reaction with nitroalkanes **112** as nucleophiles.[104] Based on this report, the addition of other nucleophiles such as cyanide anion,[105] enol silane **113**,[106] and indoles **114**[107] have been subsequently reported as well (Scheme 26).

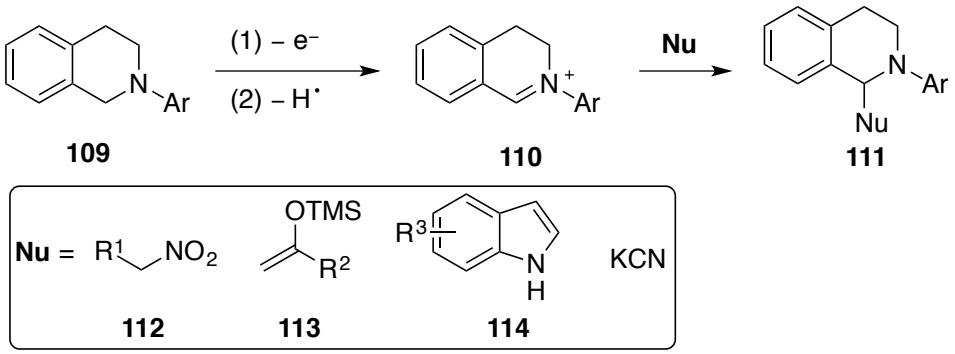

Scheme 26: Visible-light driven photooxidation of **109** and subsequent trapping of iminium ion **110** with various nucleophiles.[104-107]

To fully explore the potential of **109** in enantioselective photoredox catalysis, several groups have attempted to combine chiral, nucleophile-activating catalysts with photooxidation of **109** but have faced significant issues. In some cases, the chiral nucleophiles have to be introduced after the photooxidation is completely finished in order to achieve satisfactory enantioselectivities. Therefore, such reactions are actually the combination of two consecutive reactions in one pot instead of merging catalysis.[108-110] The Rovis group reported the first successful example of an asymmetric photoredox reaction with tetrahydroisoquinoline **109** and chiral *N*-heterocyclic carbene (NHC) catalyst **115**. Aldehydes (**58**) first react with NHC catalyst **115** to Breslow intermediates **117** and then with photocatalytically generated iminium ions **110** to products **116**, which are obtained with modest to very good enantioselectivities (Scheme 27).[111]

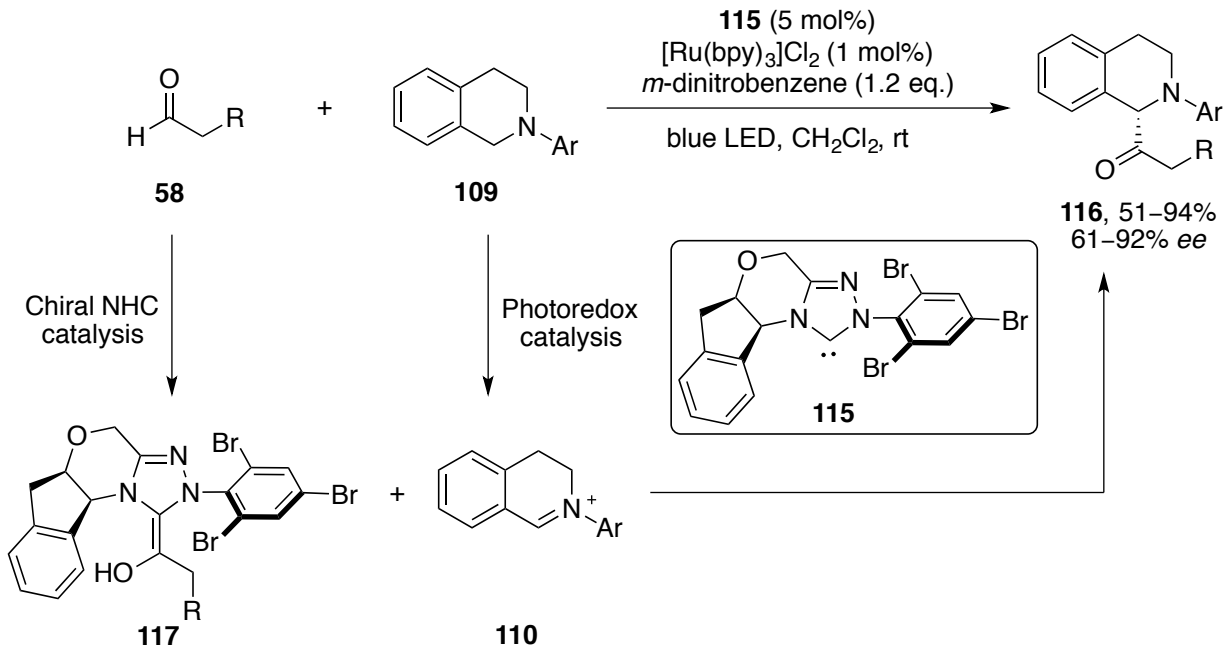

Scheme 27: Combination of photoredox catalysis with chiral NHC catalysis.[111]

Chiral copper catalysis has been successfully combined with visible-light driven oxidation of tetrahydroisoquinolines **109**. An asymmetric cross-dehydrogenative-coupling reaction with alkynes (**118**) was developed, in which the copper salt and chiral ligand **119** are responsible for alkyne activation and chiral induction (Scheme 28).[112]

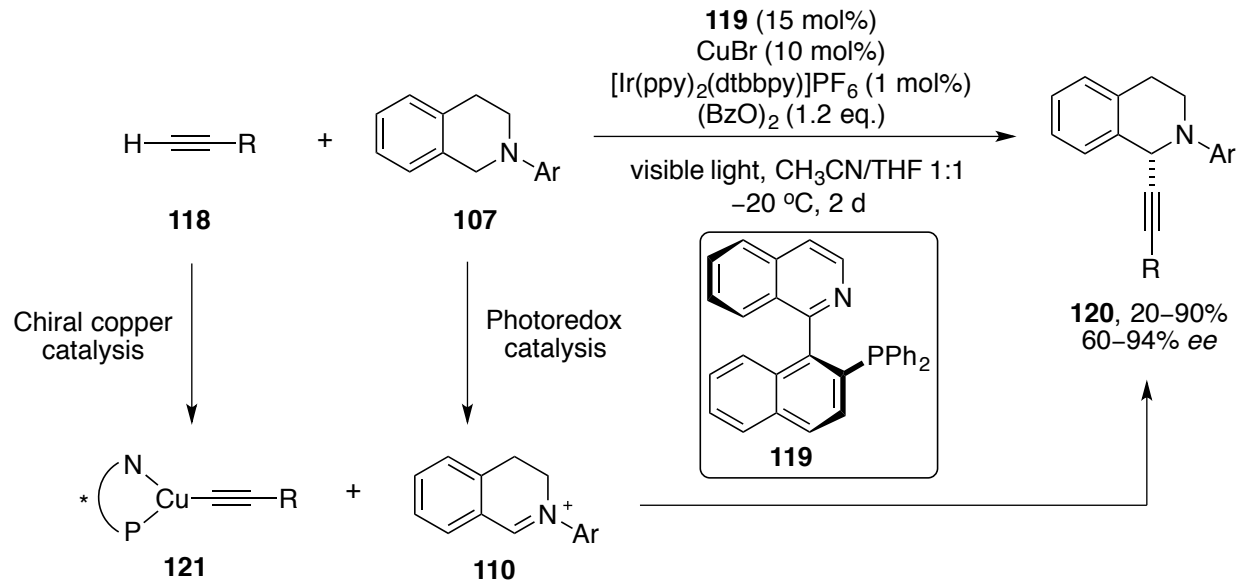

Scheme 28: Combination of photoredox catalysis with chiral copper catalysis.[112]

Chiral Lewis acids are also capable of activating nucleophiles to react with electron-deficient radicals and ions, which are produced through photocatalysis. In this context, Liu and co-workers first reported the photoreduction of aryl azides **122**.[113] After being reduced to anion radical, molecular nitrogen is released and subsequent protonation results in the nitrogen-centered radical **123**, which undergoes hydride radical abstraction to produce the aniline **124** (Scheme 29).

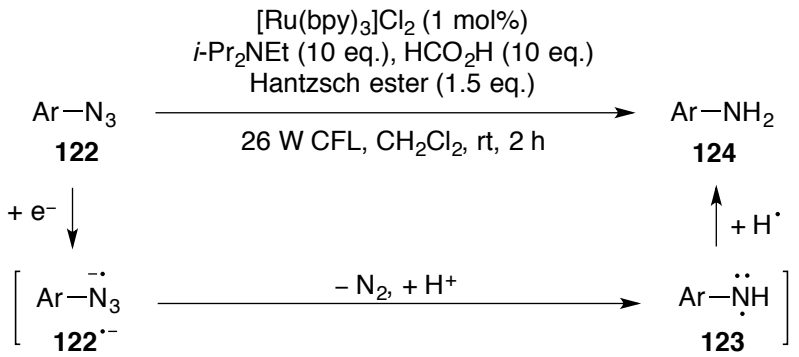

Scheme 29: Visible-light driven photoreduction of aryl azides to anilines.[113]

Similarly, Gryko and co-workers have employed α-diazoacetates **125** to produce carbon-centered electron-deficient radicals **128** under photoredox conditions. Radical **128** reacts with enamine **127** to afford racemic α-alkylated aldehydes **126** (Scheme 30).[114]

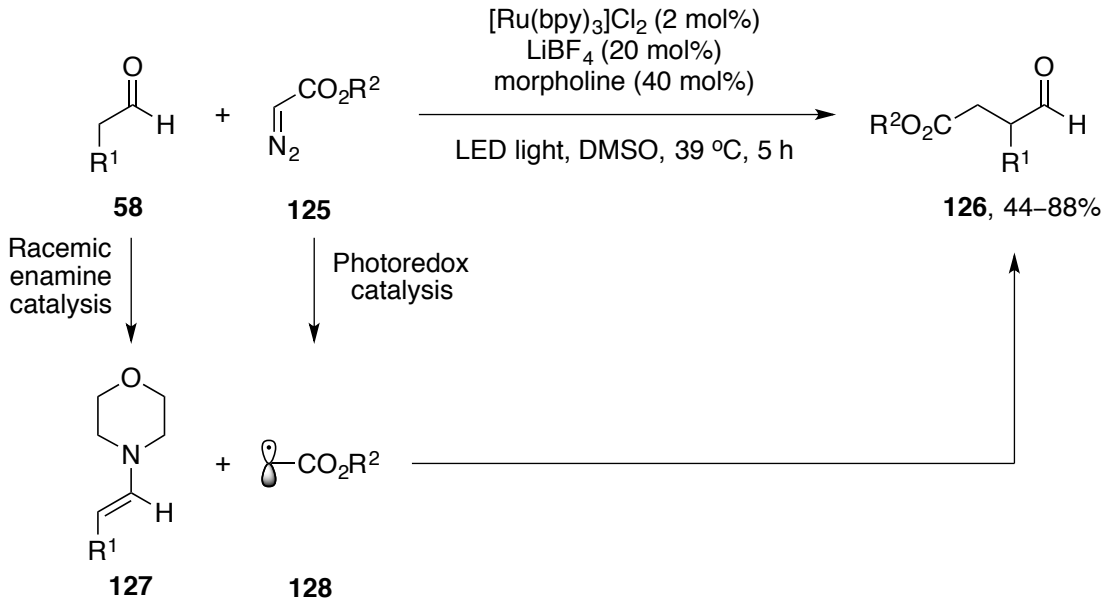

Scheme 30: Visible-light driven racemic α-alkylation of aldehydes with α-diazoacetate.[114]

Thinking along these lines, Meggers envisioned that radicals **123** and **128** could enantioselectively add to electron-rich double bond of chiral metal enolate complexes. Indeed, with chiral-at-metal Lewis acid Λ/Δ-RhS, enantioselective α-alkylation and α-amination of 2-acyl imidazoles **74** could be achieved to afford alkylation or amination products **129** with excellent enantioselectivities (Scheme 31).[115]

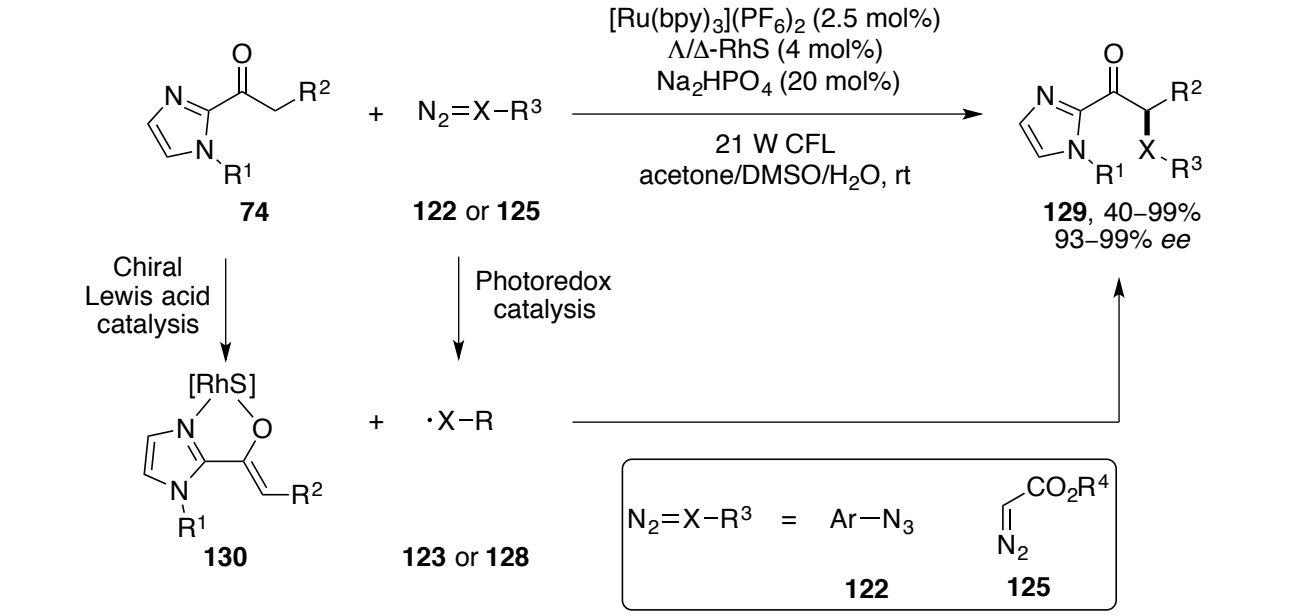

Scheme 31: Visible-light driven asymmetric α-alkylation and α-amination of 2-acyl imidazoles.[115]

Apart from nucleophile activation through enolization, Lewis acids can enhance the electrophilicity of carbonyl compounds upon coordination as well, such as *α,β*-unsaturated carbonyl compounds, which allows them to be attacked by nucleophilic radicals. However, many established reactions in this category are performed with triethylborane and a stoichiometric amount of tributyltin hydride as radical initiator and hydrogen source, the first being highly flammable and the second highly toxic.[116] Visible-light driven photocatalysis is an approach to produce nucleophilic radicals which avoids these disadvantages.

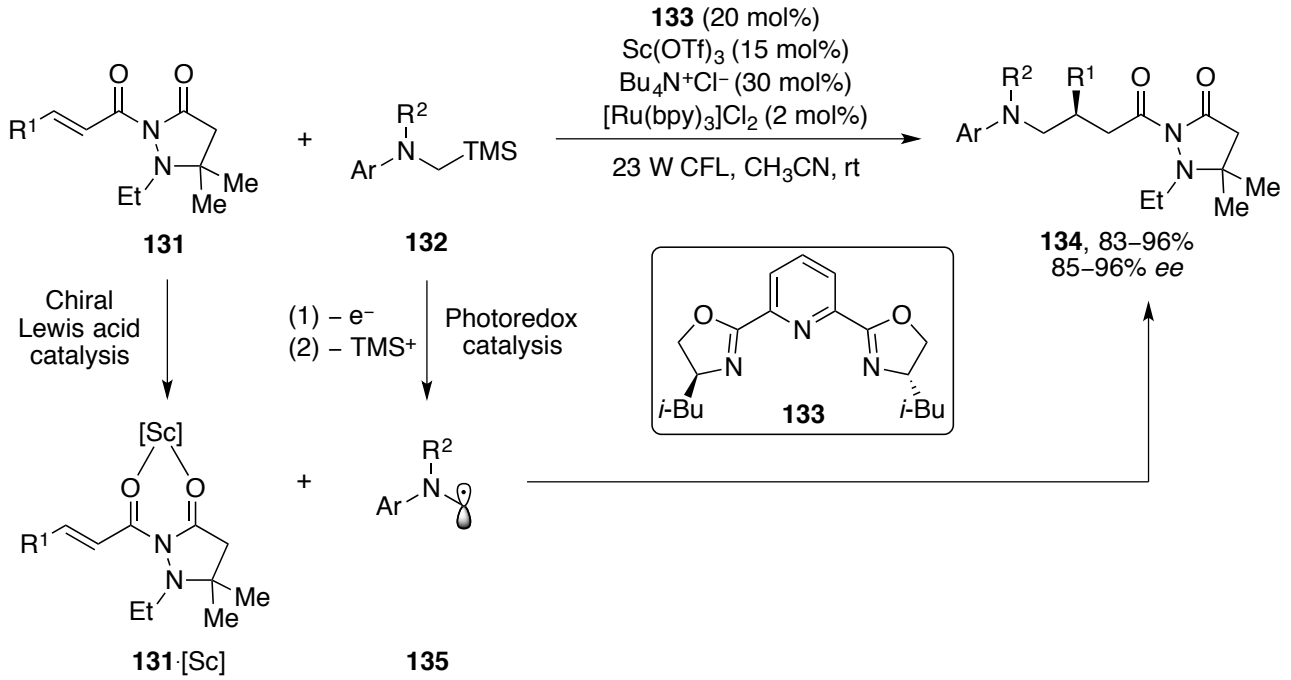

Scheme 32: Chiral Lewis acid catalyzed radical addition to *α,β*-unsaturated carbonyl compounds.[121]

Photoinitiated oxidation of α-silylamines **132** to produce nucleophilic α-amino radicals **135** has been known for a long time[117] and racemic addition of them to electron-deficient alkenes has been demonstrated by several groups recently.[118-120] Yoon employed scandium(III) trifluoromethanesulfonate (OTf) and PyBOX ligand **133** as a chiral Lewis acid to achieve an enantioselective conjugate addition reaction of α-amino radicals **135**, which are generated through photoredox catalysis (Scheme 32).[121]

Meggers' chiral-at-metal Lewis acid catalyst RhS has proven to be a superior catalyst for this type of reaction.[122] With organic photosensitizer **136**, alkyl radicals **140** are produced from organotrifluoroborate precursor **137** and add to *N*-acyl pyrazoles **55b** or 2-acyl imidazoles **61**, which are activated by chiral Lewis acid catalyst Λ-RhS. Compared to Yoon's catalytic system, Λ-RhS acts as a highly efficient catalyst and furnishes products **138** with excellent *ee* at even lower catalyst loading (4 mol%, Scheme 33).

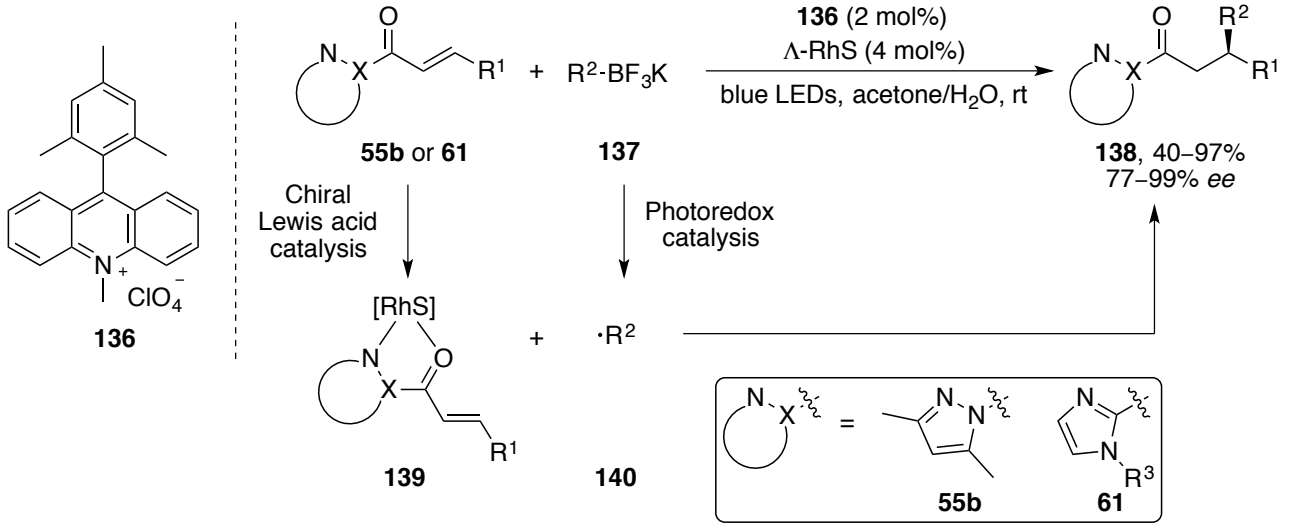

Scheme 33: Visible-light driven asymmetric conjugate addition of alkyl radicals to alkenes.[122]

The second approach to achieve visible-light driven enantioselective catalysis is to employ chiral co-catalysts to alter the substrates' photophysical properties such as redox potentials and triplet energy, so that they become capable of getting activated by photocatalysts and the following stereogenic steps occur under stereocontrol. A representative example has been published by Yoon and co-workers, they were able to design an intermolecular and enantioselective version of their aforementioned radical [2+2]-cycloaddition reaction (see Table 2). As mentioned, Lewis acid $LiBF_4$ enables single electron reduction of enones by $[Ru(bpy)_3]^+$. Therefore, a chiral Lewis acid should in principle provide stereocontrol, in case cyclization is much faster than substrate dissociation. Yoon and co-workers found out that combining $Eu(OTf)_3$ with chiral peptide ligand **143** gives diastereomer *trans*-**145** whereas slightly different ligand **144** gives the opposite diastereomer *cis*-**145** (Scheme 34).[123]

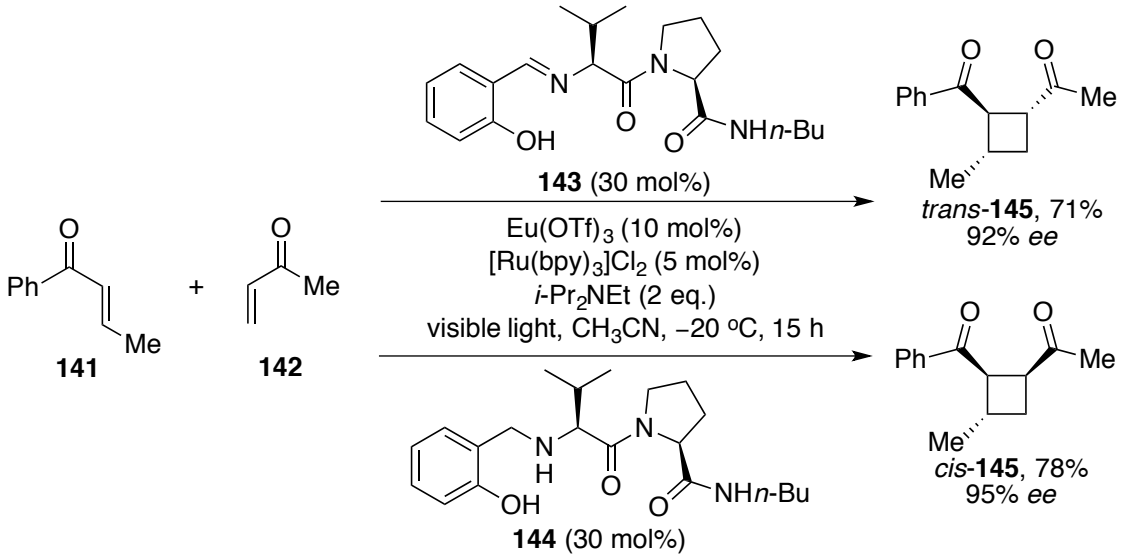

Scheme 34: Chiral Lewis acid catalyzed asymmetric radical intermolecular [2+2]-cycloaddition.[123]

This strategy has been successfully applied to an intermolecular radical [3+2]-cycloaddition as well.[124] Similar to the radical [2+2]-cycloaddition, chiral Lewis acid **148** facilitates single electron reduction of substrate **146** under photoredox conditions, the reduced substrate undergoes first a reversible ring-opening and then a cycloaddition with alkene **147** to yield cyclopentane product **149** with up to 99% *ee* (Scheme 35).

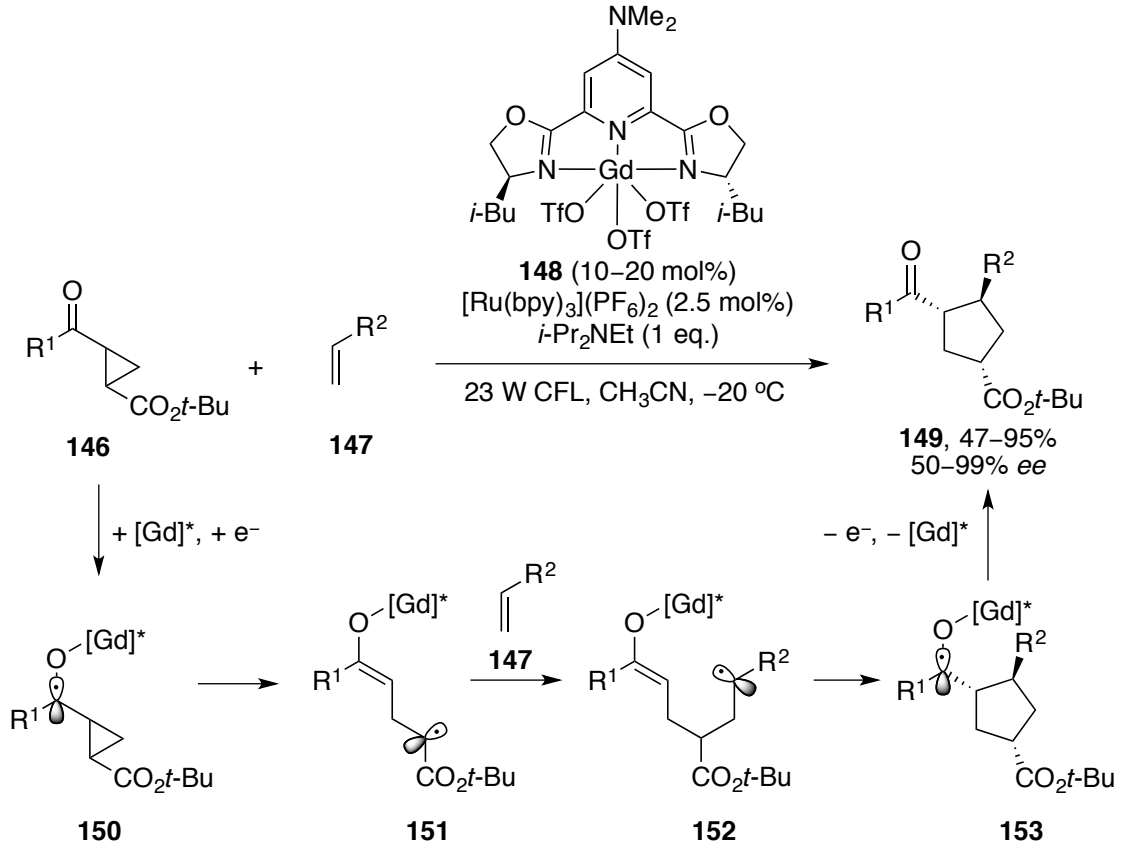

Scheme 35: Chiral Lewis acid catalyzed asymmetric intermolecular radical [3+2]-cycloaddition.[124]

Yoon and co-workers have also employed a chiral Lewis acid to enable an enantioselective [2+2]-cycloaddition through triplet energy transfer (see Scheme 20, path c).[125] One of the requirements for triplet energy transfer is that the sensitizer's triplet energy state is higher in energy than the one of the acceptor.[126] 2'-Hydroxychalcones **154** and $[Ru(bpy)_3]^{2+}$ have triplet energy (E_T) of 54 kcal/mol and 46 kcal/mol respectively. Therefore, direct triplet energy transfer from excited photocatalyst $*[Ru(bpy)_3]^{2+}$ to **154** is not possible. However, the triplet energy of **154** is lowered to 33 kcal/mol upon coordinating to $Sc(OTf)_3$. In combination with chiral PyBOX ligand **156**, 2'-hydroxychalcones **154** and dienes **155** are transformed to cyclobutanes **157** with excellent *ee*, in which only activated substrate **154**·[Sc] is able to receive triplet energy from photoexcited catalyst $*[Ru(bpy)_3]^{2+}$ (Scheme 36). This mechanistic suggestion was proved with several experiments and more importantly, an SET-pathway could be ruled out for the reaction as no cyclobutane product **157** could be obtained, neither in the presence of an oxidant nor in the presence of a reductant.

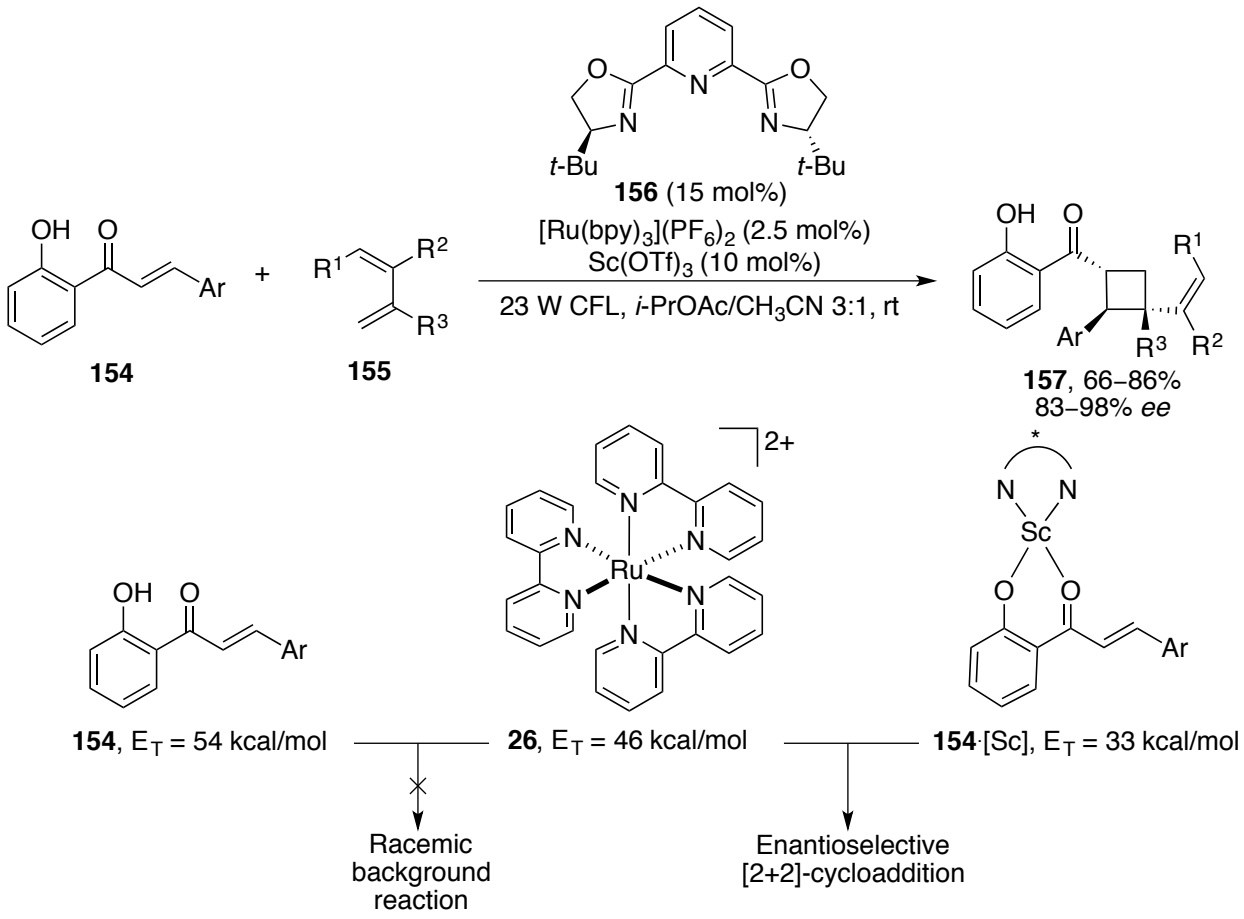

Scheme 36: Chiral Lewis acid catalyzed [2+2]-cycloaddition through triplet energy transfer.[125]

The third approach is to employ a chiral photosensitizer as single catalyst to promote enantioselective transformations. The first attempt to adopt this approach was reported in 1993 by Ohkubo and co-workers, they employed chiral photocatalyst Δ-$[Ru(menbpy)_3]^{2+}$ (**158**) and oxidant cobalt(III) acetylacetonate [$Co(acac)_3$] to catalyze the oxidative dimerization of 2-naphthol (**159**) (Scheme 37).[127] However, product **160** was obtained with only 16% *ee* presumably due to the lack of strong covalent or non-covalent bonds between chiral catalyst Δ-**158** and substrate **159** apart from weak van-der-Waals interactions. Furthermore, it

is not clear whether the enantioselectivity of the resulting product derives from the chiral ligand sphere or the metal-centered chirality of catalyst Δ-**158**. Finally, the racemization of catalyst Δ-**158** under the reaction conditions (25 ºC, 16 h, λ > 400 nm from a 500 W xenon lamp) should also be taken into consideration. Nonetheless, this example points out the challenge to design a single chiral catalyst which is at the same time the photocatalyst. Because in "classic" photochemistry, the photocatalyst's exclusive task is it to generate radicals whereas another catalyst or catalytic system is responsible for stereocontrol.

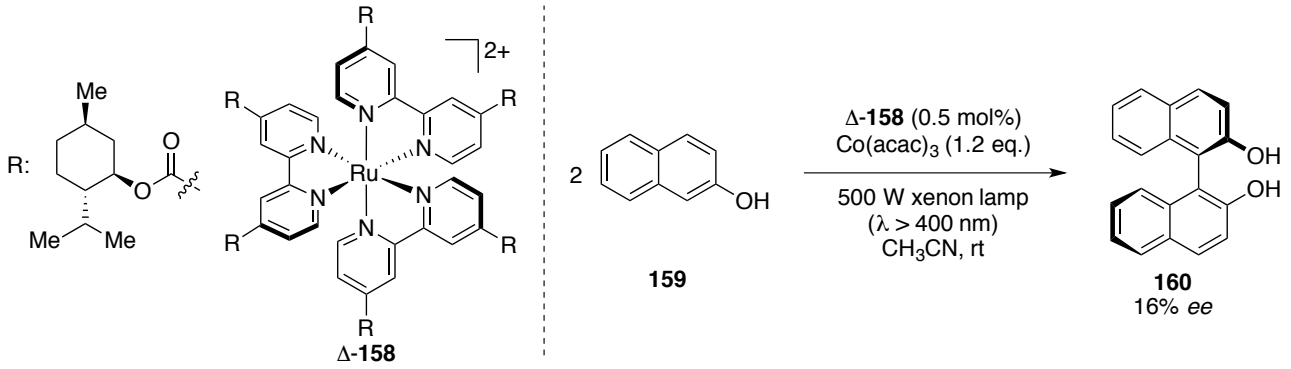

Scheme 37: Oxidative dimerization of 2-naphthol with a chiral photosensitizer and visible light.[127]

Bach and co-workers were able to obtain more promising results with catalyst **162**, in which they fused an organic photosensitizer to a chiral spirocyclic pyrrolizidine. The photosensitizing element, a benzophenone derivative, provides photocatalytic activity and steric hindrance. The lactam functionality of catalyst **162** recognizes and fixates substrate **161** in the catalyst's chiral environment through hydrogen bonding. In this chiral environment an intramolecular radical cyclization takes place, which affords product **163** with modest 70% *ee* at 30 mol% catalyst loading. A drawback of this reaction is that it requires UV-irradiation (λ > 300 nm) instead of visible light (λ = 380−750 nm) (Scheme 38).[128]

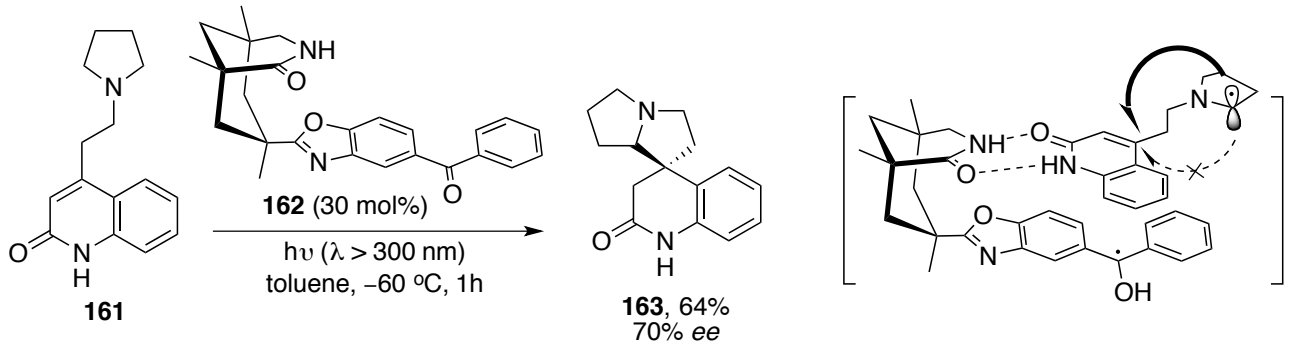

Scheme 38: Chiral spirocyclic pyrrolizidine catalyzed enantioselective intramolecular cyclization.[128]

Bach and co-workers continued to work on this system and could significantly improve it: First, they replaced the flexible benzophenone moiety by a xanthone moiety, which serves in catalyst **164** as a triplet photosensitizer and catalyzes the intramolecular [2+2]-cycloaddition of **166** via a triplet energy transfer mechanism. Although UV-light (λ = 366 nm) is still required, higher yield and enantioselectivity could be obtained.[129,130] Finally, a visible light version (λ = 400−700 nm) of this reaction could be established by

employing thioxanthone catalyst **165** (Scheme 39).[131] The overall insights gained from this work have led to successful developments of several other asymmetric intra- and intermolecular [2+2]-cycloaddition reactions of quinolones and pyridones derivatives.[132-134]

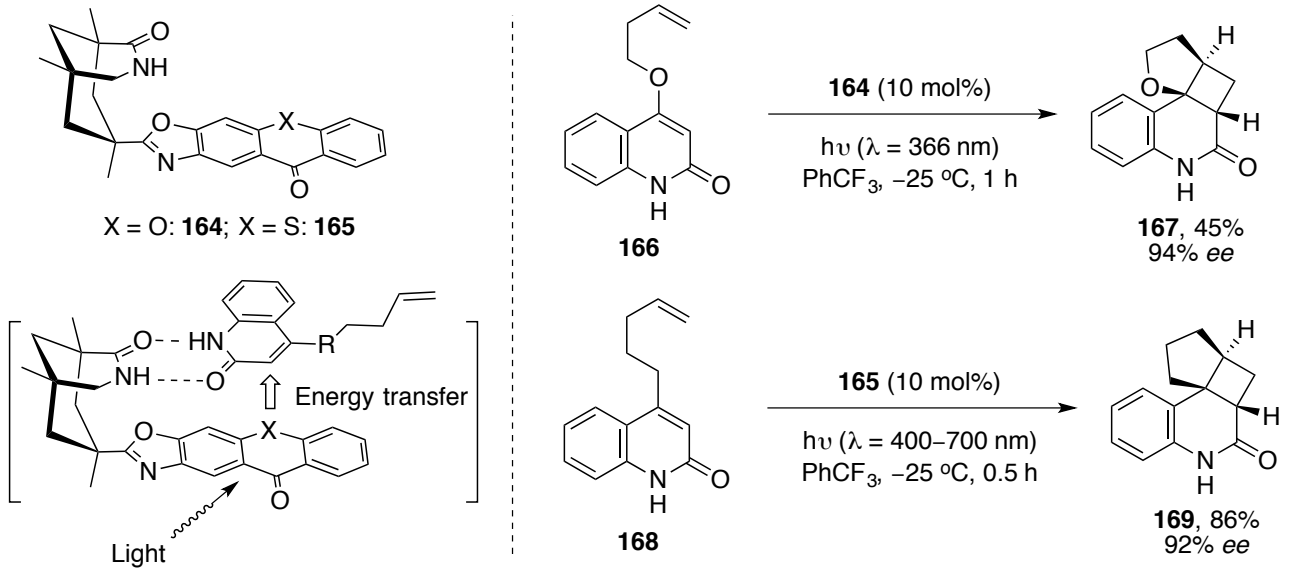

Scheme 39: Chiral spirocyclic pyrrolizidine catalyzed enantioselective [2+2]-cycloaddition.[129-131]

Although Bach's system poses a new concept in asymmetric photocatalysis, its limited substrate scope and the tedious catalyst synthesis remain significant drawbacks of this system. A more elegant strategy has been realized by Meggers and co-workers with chiral-at-metal iridium(III) Lewis acids. Meggers and co-workers reasoned that the metal centers of the chiral Lewis acids IrO and IrS could provide chirality, Lewis acidity, and photoredox functionality at the same time. Inspired by the excellent results that addition of electron-deficient radicals to chiral electron-rich double bonds has achieved (see Scheme 23 and 25), the radical α-alkylation of 2-acyl imidazoles **74** with phenacyl bromides **94** and substituted benzyl bromides **96** was chosen as a model reaction. In the presence of only 2 mol% chiral catalyst Λ-IrS and the weak base Na_2HPO_4, irradiation with visible light affords **170** with excellent results (>99% yield and 99% *ee*). As there is no reductant present in the system, bromides **94** and **96** are presumably reduced by a photoexcited iridium(III) species through an oxidative quenching cycle (see Scheme 20, path a and Scheme 24b). From all the presumably formed iridium species, it is most probable that iridium enolate complex **171** functions not only as the nucleophilic intermediate to capture the electrophilic radicals **100**, but also as the actual photosensitizer. As **171** is a neutral species, it probably transfers an electron more readily to bromides **94** and **96**. Several mechanistic experiments have confirmed these mechanistic suggestions (Scheme 40).[135]

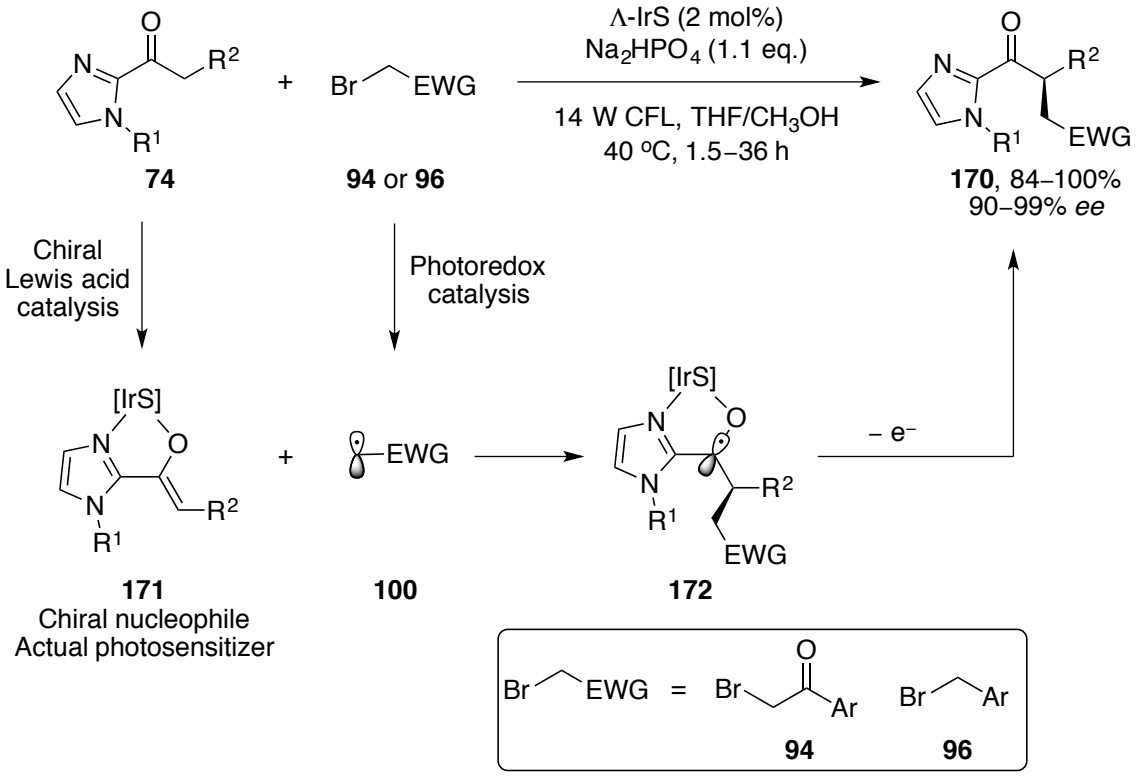

Scheme 40: Chiral-at-metal iridium catalyzed enantioselective α-alkylation of 2-acyl imidazoles with and phenacyl bromides **94** and substituted benzyl bromides **96**.[135]

Meggers and co-workers have found that other electron-deficient halides as alkylation reagents are suitable for this photocatalytic system: By utilizing perfluoroalkyl iodides **97** (R_F-I) and trichloromethyl bromide, asymmetric α-perfluoroalkylation[136] and α-trichloromethylation[137] of 2-acyl imidazoles **74** could be established. Moreover, they discovered that 2-acyl pyridines, apart from 2-acyl imidazoles, are suitable substrates as well (Scheme 41).

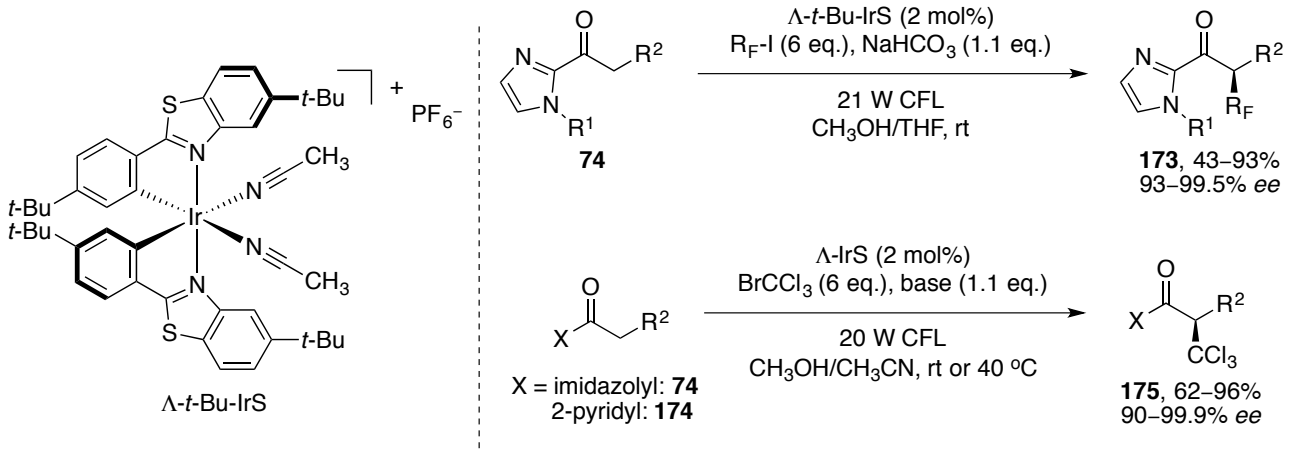

Scheme 41: Chiral-at-metal iridium catalyzed asymmetric α-perfluoroalkylation and α-trichloro-methylation of 2-acyl imidazoles and 2-acyl pyridines with visible light.[136,137]

The Meggers group further demonstrated the versatility of their chiral iridium catalysts with an asymmetric α-alkylation of 2-acyl imidazoles with α-silylamines via a net oxidative pathway. Similar to an afore-

mentioned study from Yoon and co-workers (see Scheme 32),[121] α-silylamines **132** are first photocatalytically oxidized to the according radical cations which then fragments into α-amino radicals **135** and trimethylsilyl cations. However, instead of adding to electron-deficient double bonds, α-amino radicals **135** are further oxidized to iminium ions **177**. Combining the photoredox property and the enolate chemistry of catalyst Λ-IrO, alkylation products **176** are obtained with excellent *ee* in the presence of air. According to photo-luminescence quenching and other control experiments, it is supposed that the reaction is initiated by cationic iridium species **178** (Scheme 42).[138]

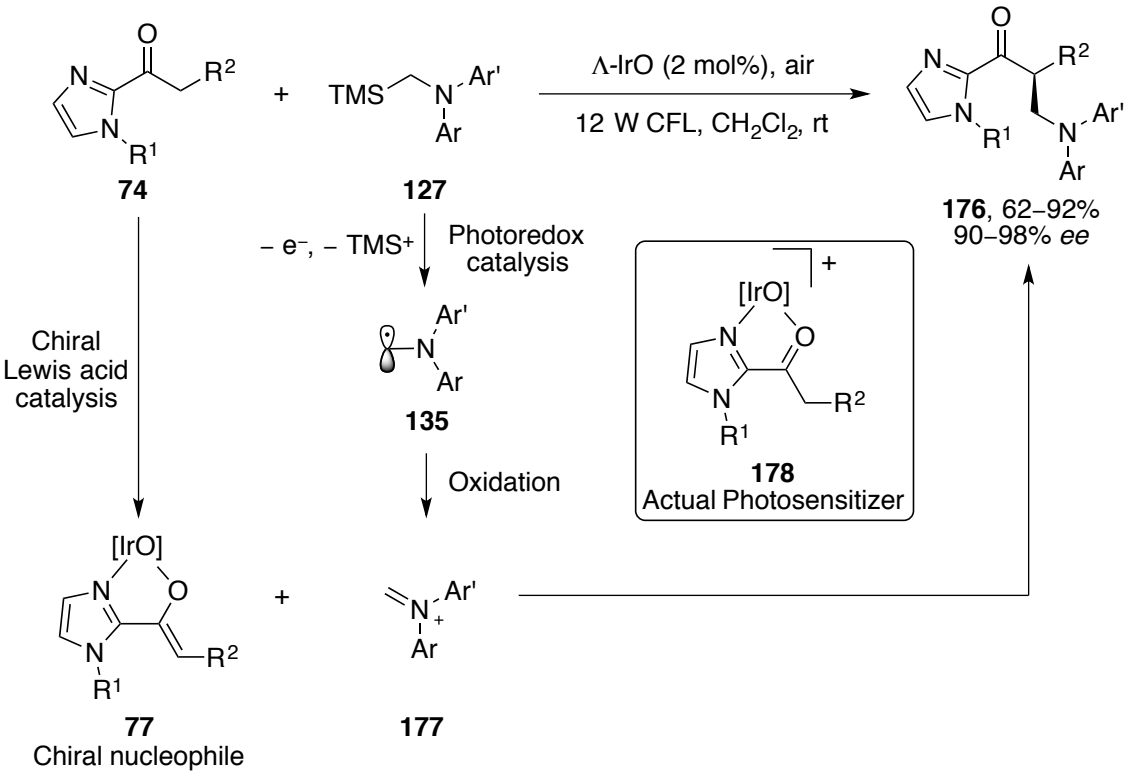

Scheme 42: Asymmetric photocatalysis with chiral-at-metal iridium complexes by a net oxidative mechanism.[138]

Furthermore, chiral-at-metal iridium complex Λ-IrS is able to catalyze the enantioselective radical-radical cross-coupling reaction between trifluoromethyl ketones **179**–**180** and diarylamines **181**.[139] Electron-rich α-amino radical **184** forms by reducing the photoexcited iridium-substrate complex to an electro-neutral species, which can be interpreted as an electron-deficient iridium-coordinated ketyl radical **183**. The C,C-bond is then formed by radical-radical cross-coupling to give 2-amino alcohols **182** enantioselectively (Scheme 43).

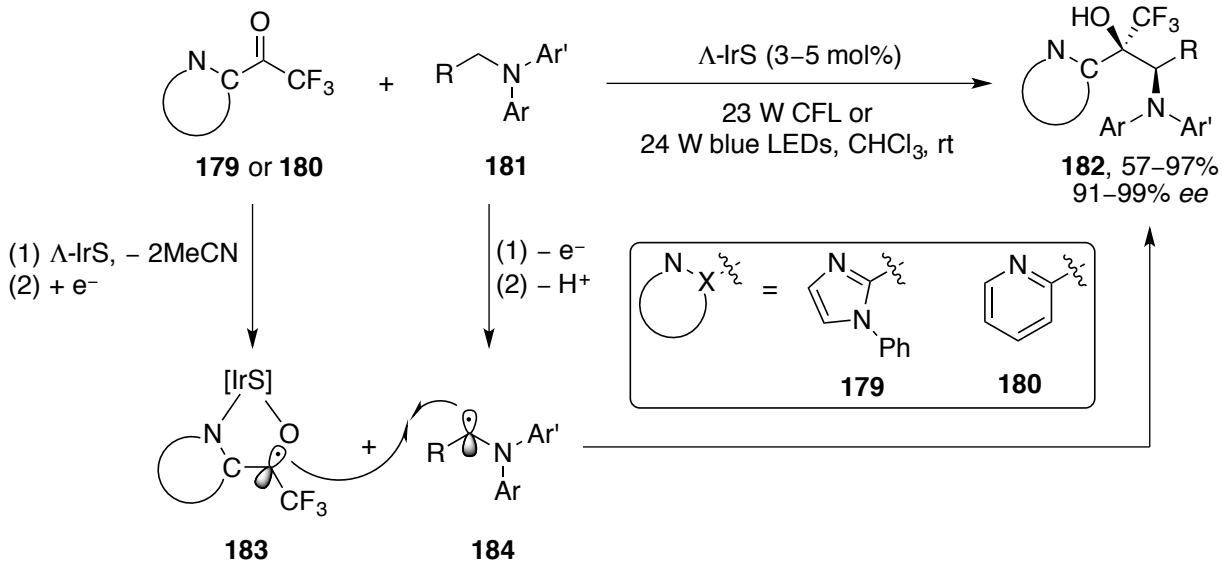

Scheme 43: Asymmetric photocatalysis with chiral-at-metal iridium complexes by a radical-radical cross-coupling mechanism.[139]

Apart from the three aforementioned general approaches, Bach's and Melchiorre's groups have disclosed other interesting concepts to perform enantioselective photocatalysis: The Bach group successfully employed chiral Lewis acid catalysts to facilitate the enantioselective intramolecular [2+2]-cycloaddition of enones, in which the coordination by the catalyst leads to a bathochromic shift of the substrate so that the catalyst-substrate-complex is selectively photoexcited resulting in enantioselective formation of the products.[140-142] Melchiorre and co-workers utilized chiral amines to activate carbonyl compounds by enamine formation, which are able to form electron donor-acceptor (EDA) complexes with electron-deficient alkyl halides. In case of the formed EDA complexes exhibit significant light absorption within the visible range, irradiation with visible light results in excitation of the EDA complexes which then reduce the alkyl halides to initiate the reactions.[143-146] Despite the success of Bach and Melchiorre, these concepts greatly depend on the photophysical properties of the reaction partners and therefore they do not serve as a general approach for the development of visible-light driven asymmetric catalysis.

Chapter 2. Aim of this Work

As mentioned in the first chapter of this thesis, Meggers' transition metal complexes with metal-centered chirality have well proven their applicability as versatile chiral catalysts.[147,148] These complexes effectively catalyze a wide range of reactions and their applications in asymmetric photocatalysis are especially impressive.

The aim of this work was to further explore the potential of these chiral Lewis acid catalysts in enantioselective transformations, particularly in photocatalysis. Because the visible-light driven asymmetric α-alkylation reactions of 2-acyl imidazoles via enolate intermediates are closely related to the catalytic system developed by the MacMillan group (trapping photocatalytically generated electron-deficient radicals with electron-rich chiral enolates and enamines, see Schemes 23 and 40), it is reasonable to suppose that electron-deficient alkyl halides **93–97** (see Schemes 23) should also be proper alkylation reagents for reactions catalyzed by the chiral-at-metal Lewis acid catalysts. Inspired by MacMillan's results and previous results from the Meggers group, one aim of this work was it to investigate the reactivity of bromo malonates **93** and α-cyanoalkyl bromides **95** towards 2-acyl imidazoles **74** with a chiral-at-metal iridium complex as photocatalyst (Scheme 44).

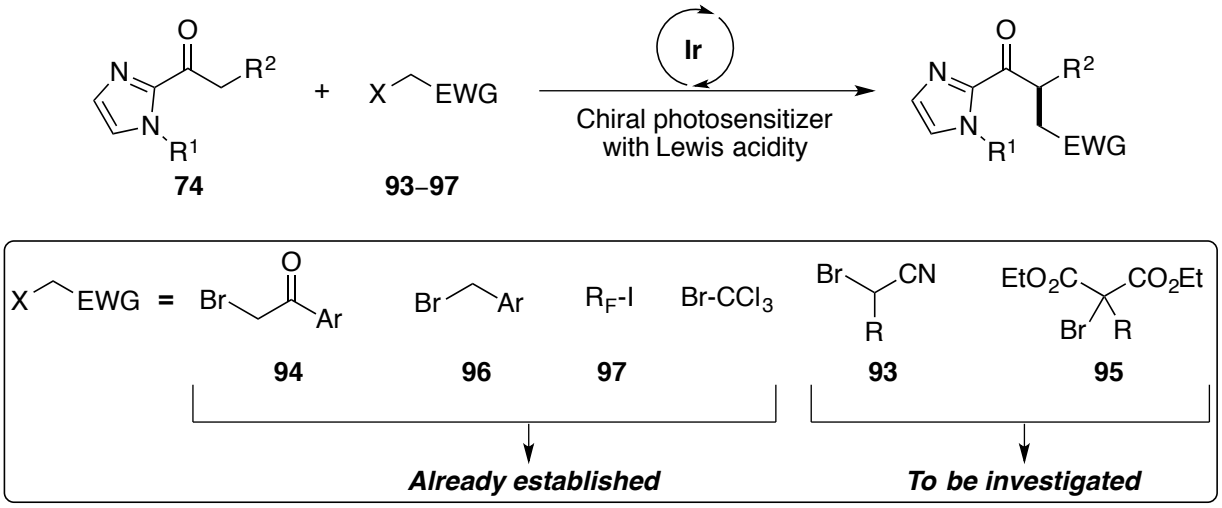

Scheme 44: Aim of this work.

Another aim of this work was it to develop further radical precursors apart from alkyl halides **93–97**, which generate electron-deficient radicals photocatalytically and then react with chiral iridium or rhodium enolate complexes.

Chapter 3. Results and Discussions

3.1. Combining Photoredox Catalysis with Chiral-Rhodium(III)-Complex Directed Lewis Acid Catalysis: Asymmetric α-Alkylation of 2-Acyl Imidazoles with α-Cyanoalkyl Bromides

3.1.1. Introduction

After the chiral iridium Lewis acids IrO and IrS had been successfully applied in a series of enantioselective α-alkylation reactions by utilizing iridium's photoredox property, Lewis acidity, and chirality at the same time (see Schemes 40 and 41),[135-137] we wondered whether α-cyanoalkyl bromides **95** are suitable alkylation reagents for this system as well. The introduction of the nitrile group renders the resulting products highly valuable as building blocks for organic synthesis, because the nitrile group can be conveniently transformed into various functional groups, such as carboxylic acids, amides, amines, and others.[149] To demonstrate the value of introduction of a nitrile group, MacMillan and co-workers described an efficient total synthesis of (−)-bursehernin (**188**) based on their enantioselective α-cyanoalkylation of aldehydes.[98] As illustrated in Scheme 45, aldehyde **58a** reacts with bromoacetonitrile (**95a**) under photocatalysis conditions to afford chiral α-alkylated product **185** with 94% *ee*. Reduction of the aldehyde group and hydrolysis of the nitrile group result in lactone **186** in 86% yield. Lactone **186** is then enolized by lithium diisopropylamide (LDA) and reacts with benzyl bromide **187** in the presence of hexamethylphosphoramide (HMPA). This alkylation step proceeds diastereoselectively and (−)-bursehernin (**188**) is obtained without any loss of *ee* (Scheme 45).

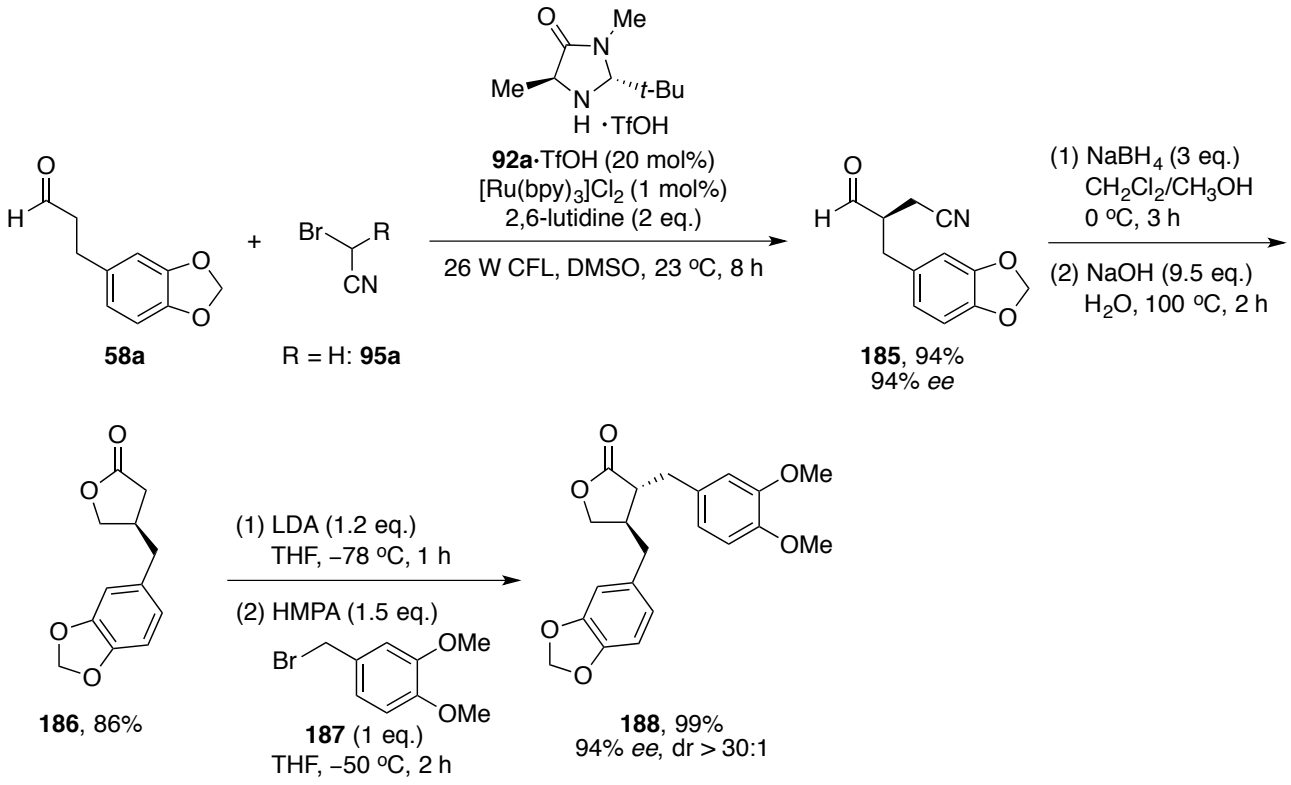

Scheme 45: Total synthesis of (−)-bursehernin with enantioselective α-alkylation of aldehyde **58a** with bromoacenitrile (**95a**) as key step.

In order to develop synthetically useful transformations with our chiral-at-metal Lewis acid catalysts, we decided to investigate the reactivity of α-cyanoalkyl bromides **95** in the visible-light driven enantioselective α-alkylation reactions of 2-acyl imidazoles.

3.1.2. Preliminary Results

Initially, 2-acyl imidazole substrate **74aa** and bromoacetonitrile (**95a**) were chosen as standard substrates. The reaction was performed in the presence of Λ-IrS (2 mol%) and Na_2HPO_4 in a mixture of methanol and tetrahydrofuran (THF) (v/v, 4:1), which had been identified in previous studies as well-suited reaction conditions.[135] To our delight, irradiation with two 13-Watt compact fluorescent lamps (CFL) at room temperature for 24 h afforded product (*R*)-**189aaa**[150] in 24% yield with 58% *ee*. The conversion of the reaction was calculated to be 31% based on re-isolation of starting material **74aa** (Table 3, entry 1). Switching catalyst from Λ-IrS to Λ-IrO resulted in higher conversion, better yield, and improved enantioselectivity (Table 3, entry 2).

Table 3: Results of the catalyst optimization.

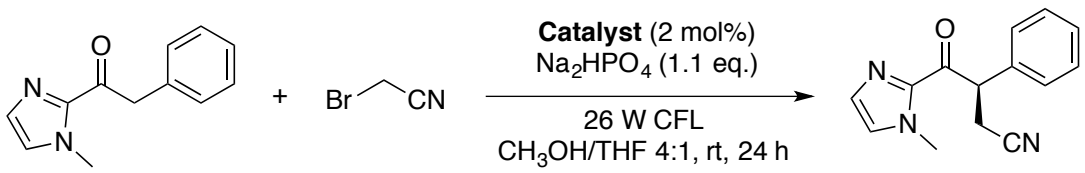

74aa **95a**, 3 eq. (*R*)-**189aaa**

Entry	Catalyst	Conversion	Yield	*ee*
1	Λ-IrS	31 %	24 %	58 %
2	Λ-IrO	50 %	49 %	63 %
3	Λ-RhO	24 %	21 %	74 %

In a previously reported visible-light driven asymmetric α-amination of 2-acyl imidazoles with ODN-carbamates **190** (ODN=2,4-dinitrophenylsulfonyloxy), Δ-RhO was found to be a suitable catalyst for this reaction.[151] Mechanistic studies suggest that neutral rhodium(III) enolate complex **192** absorbs photons and then transfers an electron to **190**, which then fragments to 2,4-dinitrophenylsulfonate and electron-deficient aminyl radical **193** (Scheme 46). Inspired by this work, the α-alkylation of 2-acyl imidazole **74aa** with bromoacetonitrile (**95a**) was performed with chiral rhodium catalyst Λ-RhO. While a significant improvement of the enantioselectivity (74% *ee*) for (*R*)-**189aaa** was observed, only 24% of the starting material **74aa** was consumed resulting in low yield (21% yield, Table 3, entry 3). In consideration of the promising enantioselectivity with Λ-RhO, we decided to further optimize the reaction conditions with this catalyst.

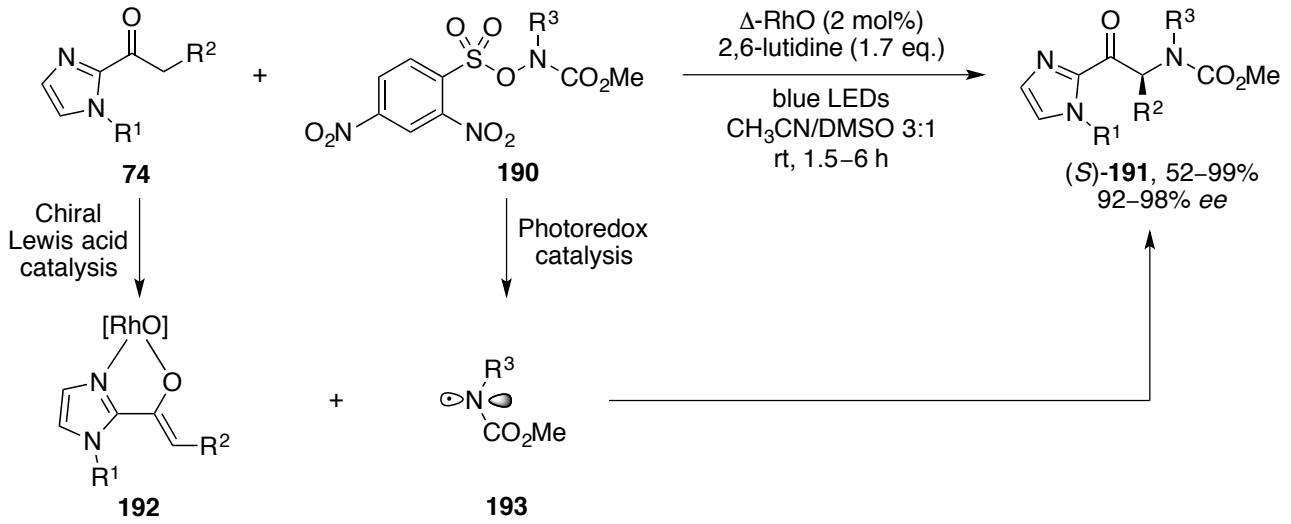

Scheme 46: Chiral rhodium(III) Lewis acid catalyzed asymmetric α-amination of 2-acyl imidazoles.[151]

3.1.3. Optimization of the Reaction Conditions - Single Catalyst

The optimization efforts began with the evaluation of various solvents. By removing THF from the solvent system, higher conversion and yield were obtained, albeit with decreased *ee* (38% conv., 29% yield, 60% *ee*, Table 4, entry 2). Replacement of methanol by *N*-methyl-2-pyrrolidone (NMP), dimethylacetamide (DMA), acetonitrile, and THF led to no or very low conversion (entries 3–6). However, it was encouraging to discover that acetonitrile as solvent afforded product (*R*)-**189aaa** with higher *ee* than THF (54% and 46% *ee*, entries 5 and 6). Therefore, it seemed probable that replacement of THF by CH_3CN in a combination with methanol could lead to an improved *ee*. Indeed, when the reaction was carried out in CH_3OH/CH_3CN 4:1, a slight improvement of *ee* was observed, but the yield remained unsatisfactory (28% yield, 77% *ee*, entry 7).

Table 4: Results of solvent optimizations.

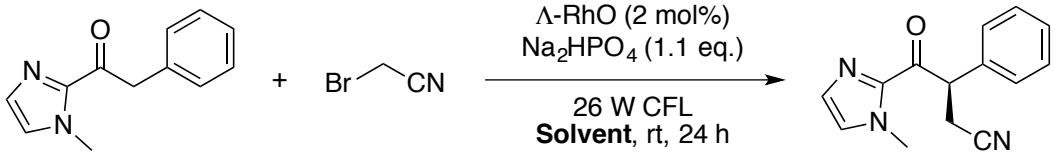

Entry	Solvent	Result
1	CH_3OH/THF 4:1	24% conv., 21% yield, 74% *ee*
2	CH_3OH	38% conv., 29% yield, 60% *ee*
3	NMP	no conversion
4	DMA	no conversion
5	CH_3CN	traces, 54% *ee*
6	THF	traces, 46% *ee*
7	CH_3OH/CH_3CN 4:1	28% yield, 77% *ee*

Previous studies from our lab had revealed that the choice of the base can be crucial in certain cases,[135-137,150] Use of $NaHCO_3$ or sodium acetate (NaOAc) led to lower yield and *ee* (40% and 15% *ee*, Table 5, entries 2 and 3). Cs_2CO_3 greatly enhanced the rate of the reaction but the reaction proceeded with almost no enantioselectivity (70% yield, 5% *ee*, entry 4), presumably because 2-acyl imidazole substrate **74aa** is deprotonated without coordination to the rhodium center, which leads to a racemic background reactions. Moreover, strong bases can facilitate racemization of enantioenriched product (*R*)-**189aaa** by enolization as well. As inorganic bases had not given promising results, organic 2,6-lutidine was employed but also failed to improve the results (30% conv., 12% yield, 31% *ee*, entry 5).

Table 5: Results of base optimizations.

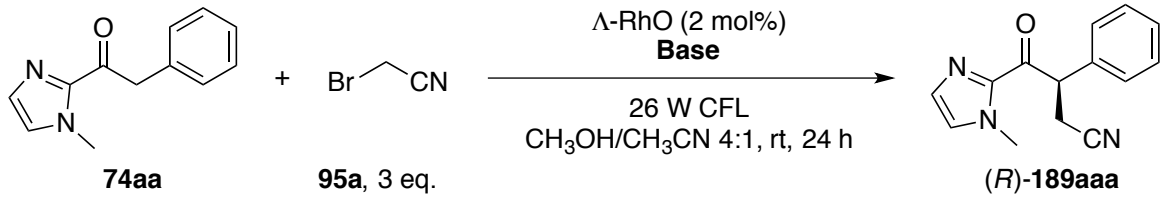

Entry	Base	Result
1	Na_2HPO_4 (1.1 eq.)	28% yield, 76.5% *ee*
2	$NaHCO_3$ (1.1 eq.)	traces, 40% *ee*
3	NaOAc (1.1 eq.)	traces, 15% *ee*
4	Cs_2CO_3 (1.1 eq.)	70% yield, 5% *ee*
5	2,6-lutidine (1.1 eq.)	30% conv., 12% yield, 31% *ee*
6	*i*-Pr_2NEt (2.0 eq.)	53% conv., 44% yield, 35% *ee*
7	no base	no conversion

As illustrated in Scheme 47, addition of α-cyanoalkyl radical **194** to rhodium enolate complex **192** results in ketyl radical **195**. The oxidation of **195** to rhodium-product-complex **196** is generally achieved either by catalyst turnover (**192**$^+$ → **192**) or by chain propagation (**95** → **194**), both of which are crucial for radical production. We suggest that the inefficient production of **194** might be responsible for the low conversion.

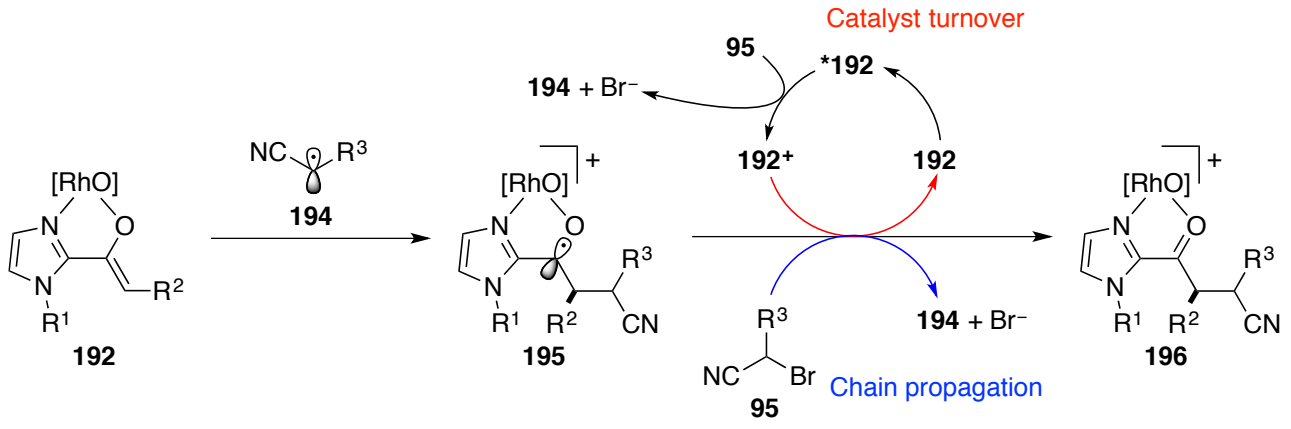

Scheme 47: Conversion of ketyl radical **195** to rhodium-product-complex **196** through catalyst turnover or chain propagation, both processes are crucial for production of α-cyanoalkyl radical **194**.

Stephenson addressed the issue of catalyst-turnover by adding trialkylamine which serves as reducing agents to regenerate the photocatalyst (Scheme 48),[152] which inspired us to use two equivalents of *i*-Pr_2NEt instead of non-reducing bases. While conversion and yield indeed improved (53% conv., 44% yield), product (*R*)-**189aaa** was obtained with only 35% *ee* (Table 5, entry 6). It is worth noting that no conversion of **74aa** was observed in the absence of base, which indicates that the formation of the rhodium enolate complex **192** is crucial for the reaction (entry 7).

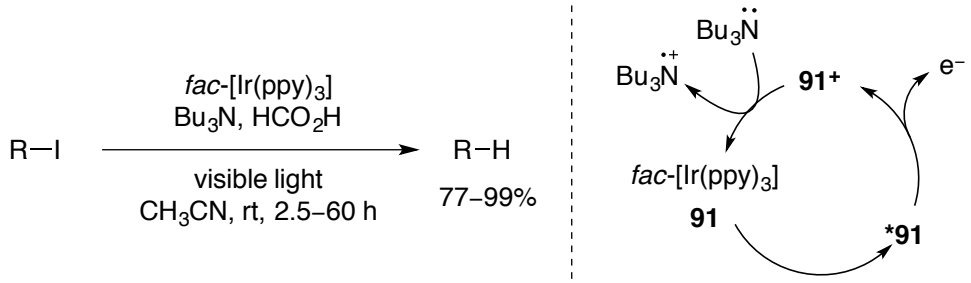

Scheme 48: Stephenson's photochemical reduction of alkyl and aryl iodides, the catalysis benefits from employing a trialkylamine.[152]

3.1.4. Optimization of the Reaction Conditions - Dual Catalysis Strategy

Having only limited success with the single catalyst system, we decided to test a dual catalysis system, in which the chiral-at-metal Lewis acid catalyst activates 2-acyl imidazole substrates **74** by facilitating enolization whereas generation of α-cyanoalkyl radicals **194** is achieved by a separate photocatalyst. We started with Λ-RhO as Lewis acid catalyst and *fac*-[$Ir(ppy)_3$] as photocatalyst due to its strong ability to donate an electron in its excited state among the common photoredox catalysts (see Figure 10 for comparison). To our delight, full conversion of **74aa** was achieved and product (*R*)-**189aaa** was obtained in 85% yield with 58% *ee* after 24 h irradiation (Table 6, entry 1). By repeating this reaction, we found that the reaction was actually finished after 17 h and (*R*)-**189aaa** was isolated with both higher yield and *ee* (92% yield, 64% *ee*, entry 2), which indicates that racemization of (*R*)-**189aaa** occurred under the reaction conditions. To address this issue, the methyl group on the imidazolyl moiety was substituted by more bulky groups to prevent racemization of the alkylated product. The enantioselectivity of the reaction was improved by employing *N*-phenyl substrate **74ba** but a prolonged reaction duration was required in order to achieve complete conversion of the starting material (36 h, 72% yield, 70% *ee*, entry 3), which is disadvantageous as a long reaction time apparently favors racemization. Therefore, we decided to accelerate the reaction by increasing the amount of bromoacetonitrile (**95a**) to 6 equivalents and the required reaction time was successfully shortened to 12 h to afford (*R*)-**189baa** in 88% yield with 72% *ee* (entry 4). A brief solvent screening was conducted with the main goal to completely dissolve the photoredox catalyst *fac*-[$Ir(ppy)_3$]. By increasing the amount of acetonitrile of the binary solvent system the reaction was slowed down and gave a slightly better enantioselectivity (24 h, 58% yield, 74% *ee*, entry 5). Replacing acetonitrile with dichloromethane partially increased the solubility of *fac*-[$Ir(ppy)_3$] and the yield but the *ee* remained basically unchanged (71% yield, 73% *ee*, entry 6). A major improvement was observed when the steric hindrance was further increased by employing **74ca** as substrate (81% yield and 80% *ee*, entry 7). Compared to *fac*-

[Ir(ppy)$_3$], soluble complex [Ir(ppy)$_2$(dtbbpy)]PF$_6$ (**89**·PF$_6$) proved to be a better photoredox catalyst for the reaction giving product (*R*)-**189caa** with 84% *ee* (entry 8). Finally, a sufficiently satisfactory result was achieved by switching the catalyst from Λ-RhO to Λ-RhS. Surprisingly, product (*R*)-**189caa** was obtained with this catalyst in 99% yield and 94% *ee* after only 1.5 h photolysis (entry 9). Furthermore, the amount of bromoacetonitrile (**95a**) could be reduced to 3 equivalents without adverse effects on yield and *ee* of the product (entry 10).

Table 6: Reaction optimization with the dual catalysis approach.

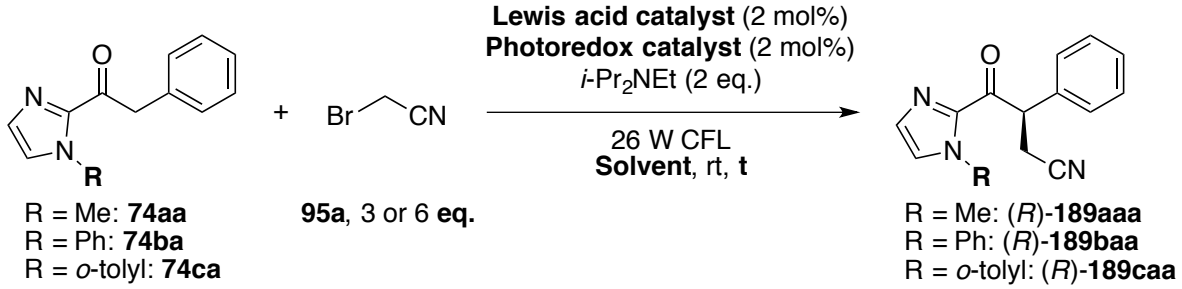

Entry	Lewis acid catalyst	Photoredox catalyst	R	eq.	Solvent	t	Result
1	Λ-RhO	*fac*-[Ir(ppy)$_3$]	Me	3	CH_3OH/CH_3CN 4:1	24 h	85% yield, 58% *ee*
2	Λ-RhO	*fac*-[Ir(ppy)$_3$]	Me	3	CH_3OH/CH_3CN 4:1	17 h	92% yield, 64% *ee*
3	Λ-RhO	*fac*-[Ir(ppy)$_3$]	Ph	3	CH_3OH/CH_3CN 4:1	36 h	72% yield, 70% *ee*
4	Λ-RhO	*fac*-[Ir(ppy)$_3$]	Ph	6	CH_3OH/CH_3CN 4:1	12 h	88% yield, 72% *ee*
5	Λ-RhO	*fac*-[Ir(ppy)$_3$]	Ph	6	CH_3OH/CH_3CN 1:1	24 h	58% yield, 74% *ee*
6	Λ-RhO	*fac*-[Ir(ppy)$_3$]	Ph	6	CH_3OH/CH_2Cl_2 1:1	24 h	71% yield, 73% *ee*
7	Λ-RhO	*fac*-[Ir(ppy)$_3$]	*o*-tolyl	6	CH_3OH/CH_2Cl_2 1:1	24 h	81% yield, 80% *ee*
8	Λ-RhO	[Ir(ppy)$_2$(dtbbpy)]PF$_6$	*o*-tolyl	6	CH_3OH/CH_2Cl_2 1:1	24 h	81% yield, 84% *ee*
9	Λ-RhS	[Ir(ppy)$_2$(dtbbpy)]PF$_6$	*o*-tolyl	6	CH_3OH/CH_2Cl_2 1:1	1.5 h	99% yield, 94% *ee*
10	Λ-RhS	[Ir(ppy)$_2$(dtbbpy)]PF$_6$	*o*-tolyl	3	CH_3OH/CH_2Cl_2 1:1	5 h	99% yield, 94% *ee*

3.1.5. Evaluation of the Substrate Scope

With optimized reaction conditions in hand, we now evaluated the substrate scope of the reaction. Several 2-acyl imidazoles **74cb–f** were synthesized using a literature-known procedure[136,151] and to test the reactivity of branched α-cyanoalkyl bromides *rac*-2-bromo-3,3-diethoxypropanenitrile (**95b**) was synthesized according to MacMillan's procedure.[98] Because the synthesis of RhO is easier than the synthesis of RhS, racemic references were synthesized with *rac*-RhO and 6 equivalents of **95a**. After 24 h photolysis, racemic references *rac*-**189cba–cfa** were obtained in modest to very good yield. In most cases the starting materials were not completely consumed (Table 7, entry 1–4). The results of substrate scope evaluation revealed that electron-donating substituents on the phenyl ring are well-tolerated. Excellent results were achieved with **74cb** giving product (*S*)-**189cba** in >99% yield with 95% *ee* (entry 1). However, electron-withdrawing

substituents gave lower enantioselectivities (entries 2−4) and in the case of **74cd**, product (*S*)-**189cda** was obtained almost as a racemic mixture (entry 3). To our delight, 2-acyl imidazole with alkyl moiety **74cf** worked well in the system to give (*S*)-**189cfa** with very high *ee* (92% yield, 96% *ee*, entry 5).

Table 7: Evaluation of the substrate scope: 2-acyl imidazoles

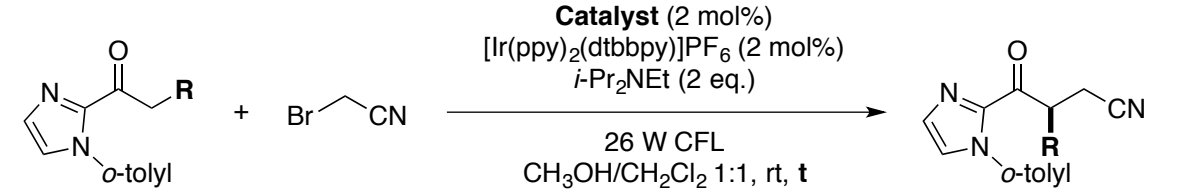

74
R = *p*-Me-Ph: **74cb**
R = *p*-Br-Ph: **74cc**
R = *p*-NO_2-Ph: **74cd**
R = *o*-Cl-Ph: **74ce**
R = Et: **74cf**

95a, 3 or 6 **eq.**

189
R = *p*-Me-Ph: **189cba**
R = *p*-Br-Ph: **189cca**
R = *p*-NO_2-Ph: **189cda**
R = *o*-Cl-Ph: **189cea**
R = Et: **189cfa**

Entry	2-Acyl imidazole	with *rac*-RhO[a]	with Δ-RhS[b]
1	**74cb**	*rac*-**189cba**, 24 h, 54% yield[c]	(*S*)-**189cba**, 12 h, 100% yield, 95% *ee*
2	**74cc**	*rac*-**189cca**, 24 h, 64% yield[c]	(*S*)-**189cca**, 12 h, 91% yield, 88% *ee*
3	**74cd**	*rac*-**189cda**, 24 h, 77% yield	(*S*)-**189cda**, 24 h, 81% yield, 1% *ee*
4	**74ce**	*rac*-**189cea**, 24 h, 63% yield[c]	(*S*)-**189cea**, 12 h, 100% yield, 84% *ee*
5	**74cf**	*rac*-**189cfa**, 24 h, 100% yield	(*S*)-**189cfa**, 24 h, 92% yield, 96% *ee*

[a] With 6 eq. **95a**; [b] With 3 eq. **95a**; [c] Incomplete conversion.

The reaction with branched α-cyanoalkyl bromide **95b** was conducted with standard substrate **74ca**. Similar to the reactions above (see Table 7), the reaction was first performed with *rac*-RhO as catalyst. Product *rac*-**189cab** was obtained in 81% yield as a mixture of diastereomers, which were resolved by silica gel flash column chromatography (Scheme 49) and both analytically characterized.

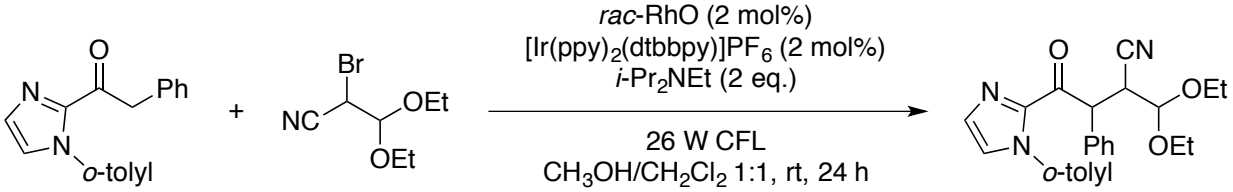

74ca

95b, 6 eq.

rac-**189cab**, 81%

Scheme 49: Reaction with branched α-cyanoalkyl bromide **95b** and catalyst *rac*-RhO.

With the necessary analytical data in hand, the reaction was now performed with Δ-RhS. The diastereomeric ratio of (*S*)-**189cab** was determined as 2.5:1 by ^{1}H-NMR analysis of the crude reaction mixture (see experimental section, p.107, the configuration of the β-position was not determined). After purification, (*S*)-**189cab** was isolated in quantitative yield and both diastereomers were obtained with 98% *ee* in the presence of only 3 equivalents **95b** after 15 h (Scheme 50).

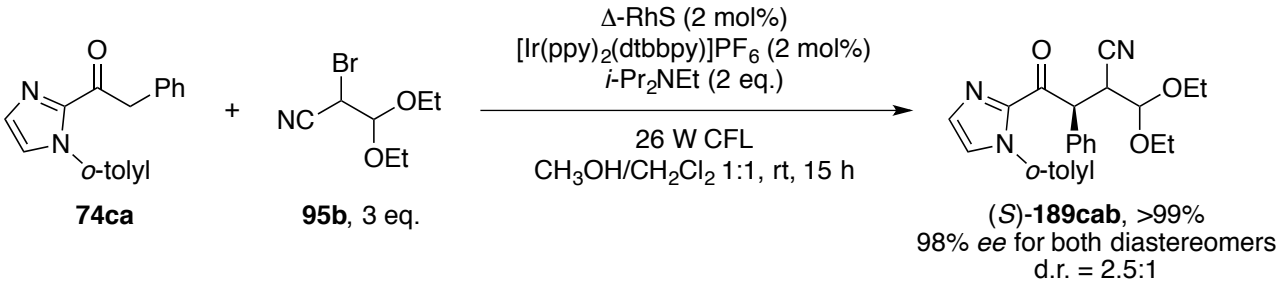

Scheme 50: Evaluation of the substrate scope: a branched α-cyanoalkyl bromide.

3.1.6. Mechanistic Investigations

First, alkylated product **189cca** resulted from the reaction with **74cc** and Δ-RhS (Table 7, entry 2) was crystallized and characterized by X-ray diffraction. The absolute configuration of the chiral center is assigned to be *S*, which supports the mechanistic proposal that the reaction proceeds via a rhodium enolate complex **197** (Scheme 51).

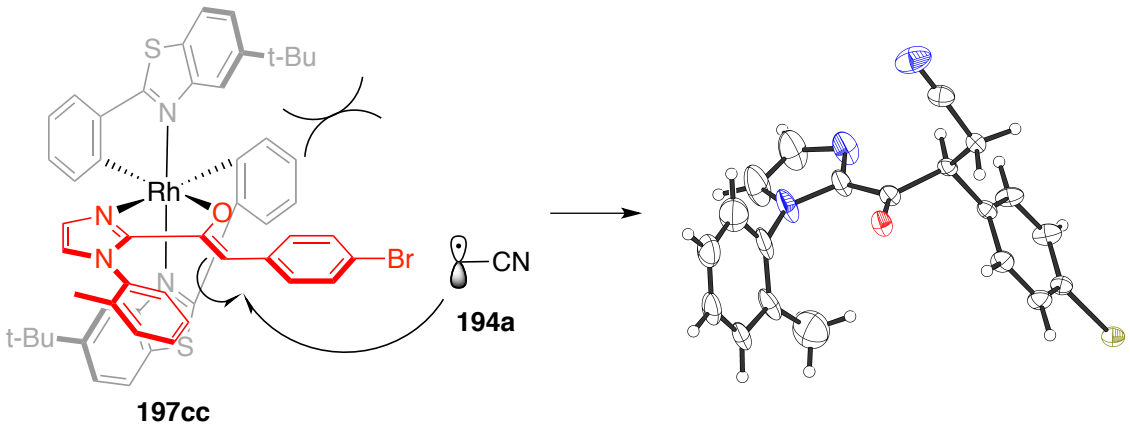

Scheme 51: Crystal structure of (*S*)-**189cca** and mechanistic proposal.

Several experiments were performed to gain more insights into the mechanism of the reaction. As mentioned, after only 1.5 h photolysis under optimized reaction conditions, product (*R*)-**189caa** was obtained in 99% yield with 94% *ee* (Table 8, entry 1). Within the same span of time, reactions both in the absence of light and in the presence of air failed to afford detectable amounts of desired product (*R*)-**189caa** according to ^{1}H-NMR analysis of the crude reaction mixtures (entries 2 and 4, see experimental section, Figure 17 and 18, p. 109−110). However, (*R*)-**189caa** could be obtained after a prolonged reaction time with 4% and 60% *ee* respectively (entries 3 and 5). Similarly, the absence of [Ir(ppy)$_2$(dtbbpy)]PF$_6$ resulted in no detectable conversion of **74ca** after 1.5 h photolysis (entry 6) while (*R*)-**189caa** was obtained in 97% yield with 79% *ee* after 24 h photolysis (entry 7). Finally, (*R*)-**189caa** was formed in the absence of Lewis acid catalyst (31% yield, entry 8).

Table 8: Results of experiments to investigate the reaction's mechanism.

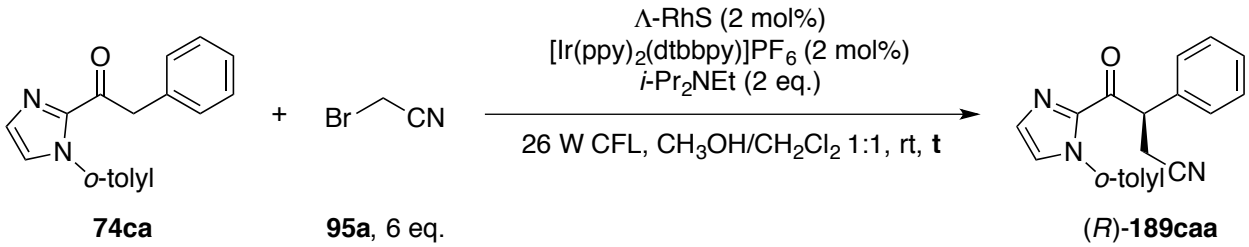

Entry	Variation of the conditions	t	Yield [%], (*ee* [%])
1	-	1.5 h	99, (94)
2	In the absence of light	1.5 h	<5, (n.d.)
3	In the absence of light	48 h	72, (4)
4	In the presence of air	1.5 h	<5, (n.d.)
5	In the presence of air	48 h	23, (60)
6	Without $[Ir(ppy)_2(dtbbpy)]PF_6$	1.5 h	<5, (n.d.)
7	Without $[Ir(ppy)_2(dtbbpy)]PF_6$	24 h	97, (79)
8	Without Λ-RhS	48 h	31, (n.d.)

The fact that there is some reaction in the absence of light and in the presence of air, indicates the existence of a non-radical background reaction, for example an S_N2-type nucleophilic substitution reaction, in which the rhodium enolate complex attacks bromoacetonitrile (**95a**) directly, but apparently at a much slower rate. Due to its relatively strong basicity, *i*-Pr_2NEt is able to promote the enolization of 2-acyl imidazoles **74** without the assistance of RhS, which then react with **95a** in a racemic background reaction. Indeed, when **74ca** was mixed with 2 equivalents *i*-Pr_2NEt in CD_2Cl_2/CD_3OD (v/v 1:1) no signal for the methylene group of **74ca** was observed by ^{1}H-NMR (see experimental section, Figure 19−21, p.111−112). Hence, there might be racemic and enantioselective variants for the assumed S_N2-pathway (Scheme 52). The racemic variant of the S_N2-pathway might significantly contribute to the lower *ee* of **189**, especially in case of the reactions which were carried out in the absence of light (see Table 8, entries 2 and 3). As a radical pathway can be ruled out in the absence of light, the fact that (*R*)-**189caa** was obtained with only 4% *ee* suggests that the rhodium enolate complex **197** is highly reactive towards α-cyanoalkyl radicals **194** but not towards α-cyanoalkyl bromides **95**.

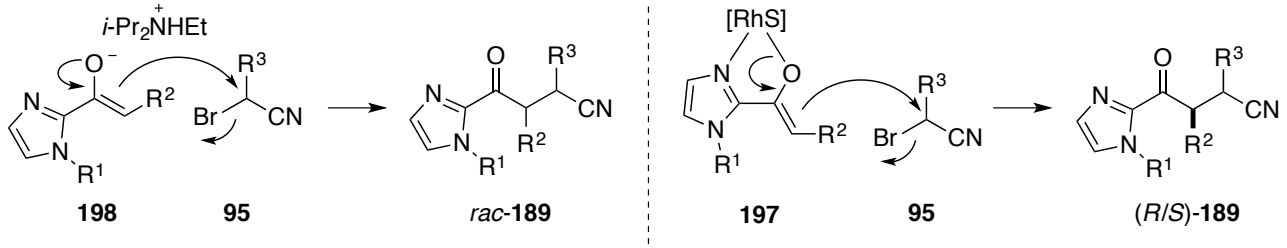

Scheme 52: Assumed non-radical S_N2-pathways to form alkylated product **189**.

As can be seen in Table 8, the radical pathway seems to be not completely suppressed by atmospheric oxygen, as (*R*)-**189caa** was obtained in 23% yield with 60% *ee* (entry 5). A literature search[90] revealed that air or oxygen is commonly employed either as oxidant to convert the reduced photoredox catalyst to its ground state or as oxidative quencher. In consideration of the cationic nature of the photocatalyst $[Ir(ppy)_2(dtbbpy)]^+$ and the presence of excessive reductive quencher *i*-Pr_2NEt in the reaction mixture, it is reasonable to assume that the photocatalyst is first reduced from its excited state. The reduced photocatalyst could then be converted to the ground state either by transferring an electron to α-cyanoalkyl bromides **95** or by getting oxidized by air. Both pathways are competitive to each other and the latter one inhibits the production of α-cyanoalkyl radicals **194** to a certain degree, which might be crucial for the enantioselectivity of the reaction (Scheme 53). Therefore, (*R*)-**189caa** was presumably obtained with a lower but still significantly higher *ee* than the product from the dark reaction (compare with entries 3 and 5).

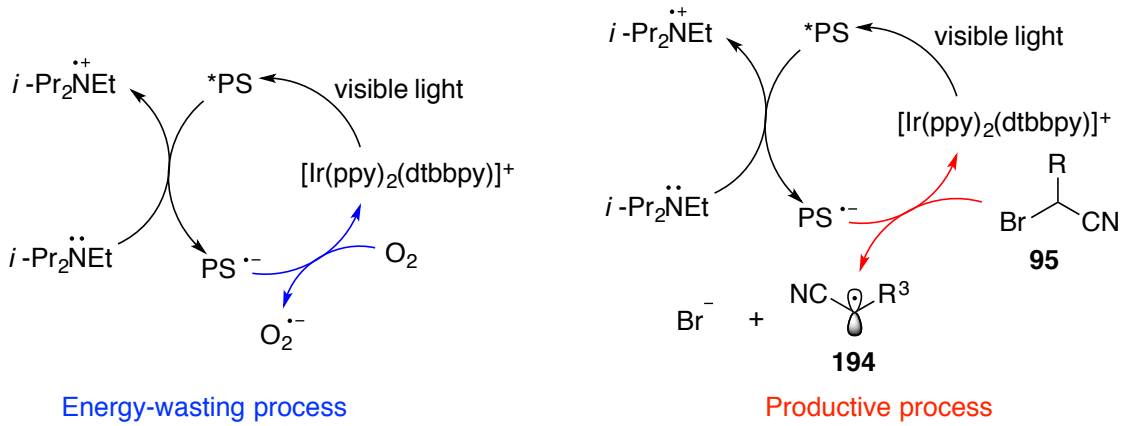

Scheme 53: Possible mechanism of regeneration of photocatalyst:.

Similarly, the absence of $[Ir(ppy)_2(dtbbpy)]PF_6$ resulted in basically no conversion of **74ca** after 1.5 h photolysis (Table 8, entry 6) while (*R*)-**189caa** was obtained in 97% yield with 79% *ee* after prolonged reaction time (entry 7), which indicates that the rhodium enolate complex **197** can also absorb photons and then reduce α-cyanoalkyl bromides **95** to initiate the reaction (compare with Scheme 46). At last, because RhS is not required for the enolization of **74ca**, *rac*-**189caa** was formed in the absence of Lewis acid catalyst (31% yield, entry 8) presumably through the aforementioned non-radical S_N2-pathway (see Scheme 52). The low yield demonstrates the low reactivity of ammonium enolates **198** towards α-cyanoalkyl radicals **194**.

In another study from the Meggers group, RhS is also employed as chiral Lewis acid to activate 2-acyl imidazoles **74** through enolization to react with alkyl and aminyl radicals which were generated by photoreduction of azides **122** and α-diazoacetates **125** (see Scheme 31).[115] Given the similarity of these two reactions to our current study, the mechanistic investigations of these two reactions might provide further useful informations. First, the authors performed reactions with various Lewis acid catalysts such as $Sc(OTf)_3$, $FeCl_3$, and $Cu(OAc)_2$ and none of them was capable of catalyzing the reaction, which shows the unique reactivity of rhodium enolate complex **197** towards radical addition. Next, the authors performed Stern-Volmer quenching experiments with photocatalyst $[Ru(bpy)_3]^{2+}$ and they discovered that the excited

photoredox catalyst is reduced by rhodium enolate complex **197** to initiate the reaction and at the same time generates α-carbonyl radical **199** (Scheme 54).

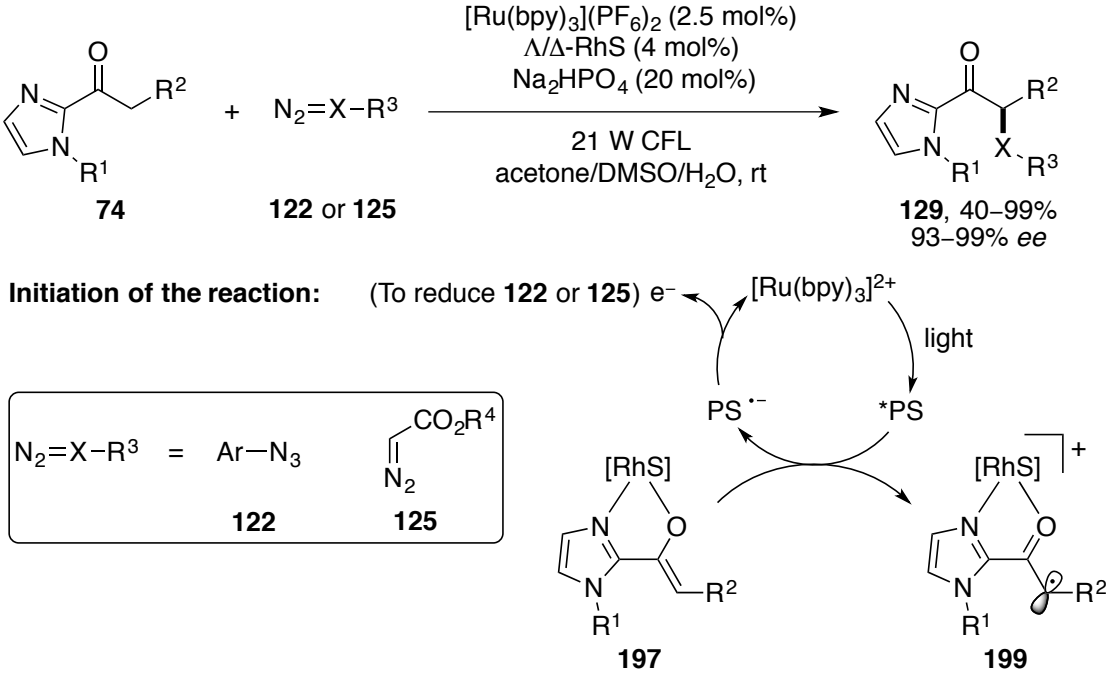

Scheme 54: Rhodium enolate complex **197** acts as reductive quencher and is oxidized by the excited photoredox catalyst to produce α-carbonyl radical **199**.[115]

α-Carbonyl radical **199** could be captured either by silyl enol ether **200** or by oxygen to afford alkylated product **201** or oxygenation product **202** (Scheme 55). In the current study, oxygenation product **202** was not observed in the presence of air (Table 8, entry 4 and 5), which indicates that the excited photocatalyst *$[Ir(ppy)_2(dtbbpy)]^+$ is probably not deactivated by rhodium enolate complex **197** and this is consistent with the proposal that *i*-Pr_2NEt acts as both base and reductive quencher.

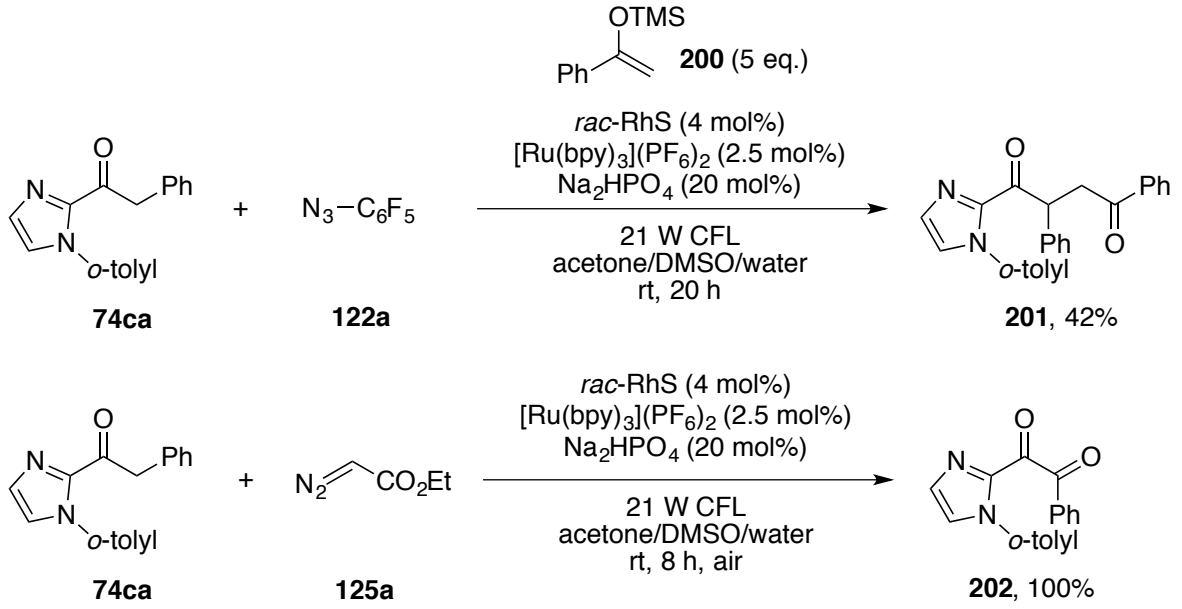

Scheme 55: α-Carbonyl radical **199** is captured by silyl enol ether **186** and oxygen.[115]

With these informations in hand, a mechanistic picture for the asymmetric α-alkylation of 2-acyl imidazoles with α-cyanoalkyl bromides can be drawn: In consideration of the basicity and the amount of *i*-Pr_2NEt in the reaction mixture, we propose that substrate **74** is deprotonated directly without coordination to RhS. The resulting ammonium enolate **198** then substitutes the acetonitrile ligands to form rhodium enolate complex **197**. On the other hand, the reaction is triggered by photoexcitation of $[Ir(ppy)_2(dtbbpy)]PF_6$. The excited photocatalyst is then deactivated by the second equivalent *i*-Pr_2NEt through reductive quenching to afford strong reductant $[Ir]^{II}$, which transfers an electron to electron-deficient α-cyanoalkyl bromide **95**. In the course of the fragmentation of reduced **95**, α-cyanoalkyl radical **194** is formed and reacts with rhodium enolate complex **197** under stereocontrol. The resulting rhodium ketyl radical **203** is then readily oxidized to rhodium product complex **204** either by the excited photocatalyst (pathway A) or α-cyanoalkyl bromide **95** (pathway B). The latter pathway is known as chain propagation. Finally, product **189** is released and a second equivalent ammonium enolate **198** coordinates to the rhodium center to initiate the next catalytic cycle (Scheme 56). In the previous studies utilizing chiral-at-metal Lewis acid catalysts to activate substrates through enolization, it is common to employ weak bases in order to ensure that substrate enolization only occurs upon coordination. In the current study, it appears that rhodium enolate complex **197** so preferentially reacts with electrophilic radicals that possible racemic pathways (non-radical S_N2 pathway and radical addition to ammonium enolate **198**) are effectively suppressed, which ultimately results in a high level of enantioselectivity.

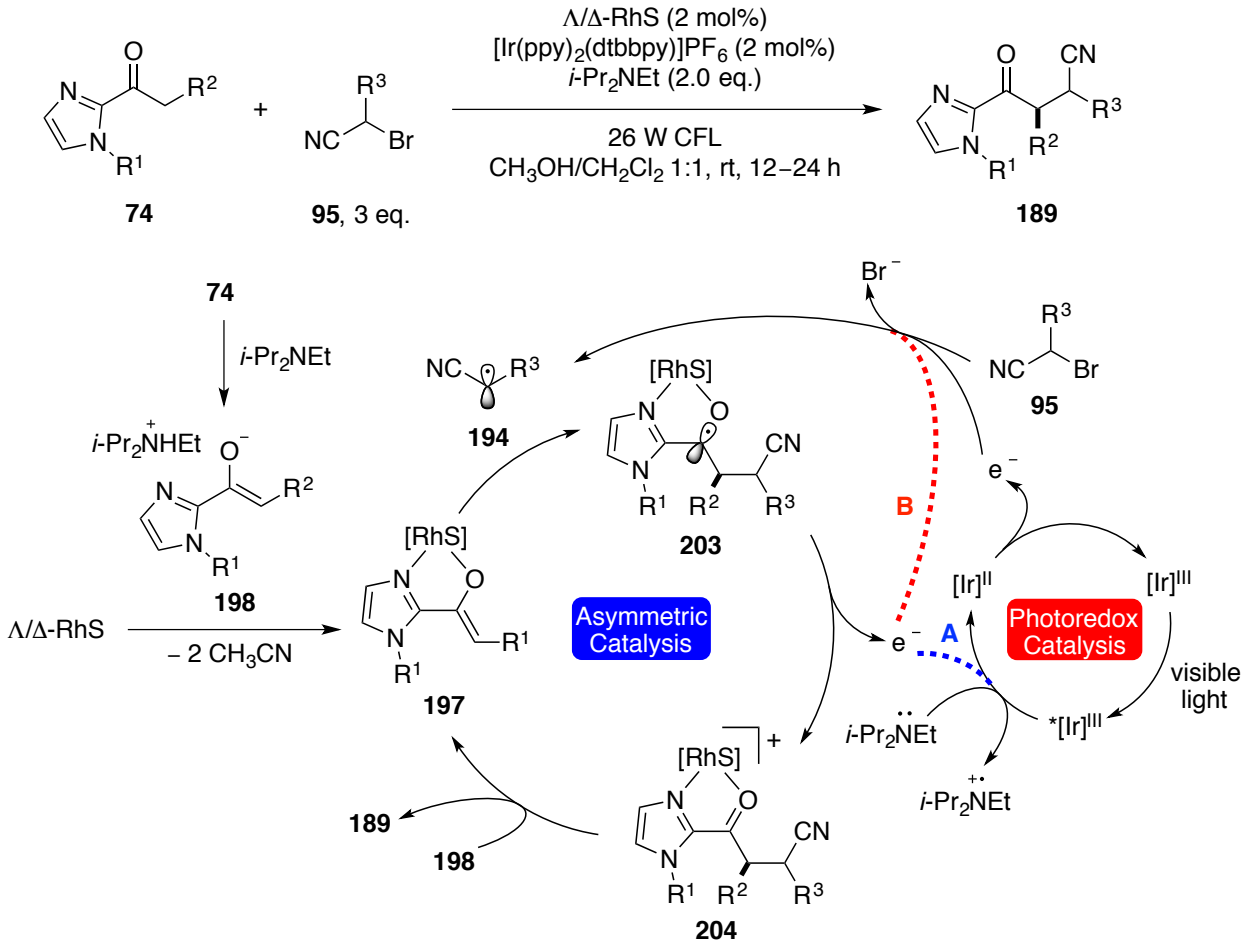

Scheme 56: Proposed mechanism for the visible-light driven enantioselective α-alkylation of 2-acyl imidazoles with α-cyanoalkyl bromides.

With additional mechanistic experiments, the proposed mechanism from Scheme 56 could be further confirmed. For instance, Stern-Volmer quenching experiments with $[Ir(ppy)_2(dtbbpy)]^+$ could determine whether *i*-Pr_2NEt indeed serves as reductive quencher instead of rhodium enolate complex **197**. In addition, experiments could be performed to capture α-cyanoalkyl radical **194** to confirm that the reaction proceeds via a radical pathway.

3.1.7. Conclusion and Future Perspectives

An asymmetric α-alkylation of 2-acyl imidazoles with α-cyanoalkyl bromides has been successfully established by combining photoredox catalysis with Lewis acid catalysis with chiral-at-metal octahedral rhodium(III) complexes. Under optimized conditions the products could be obtained with up to >99% yield and 98% *ee* (Scheme 57).

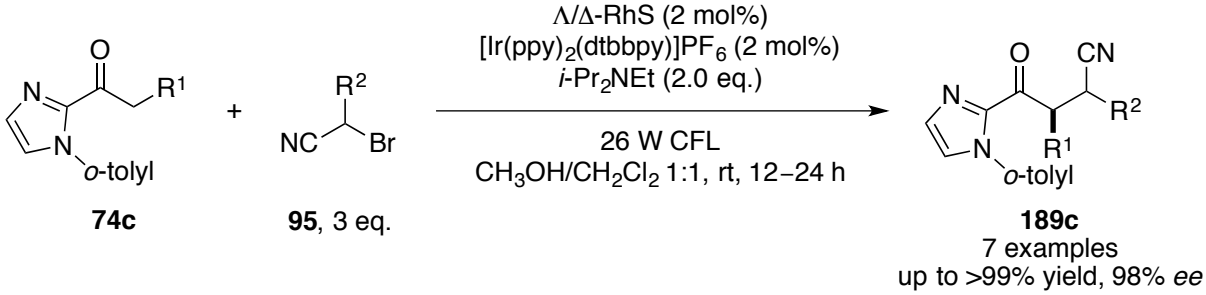

Scheme 57: α-Alkylation of 2-acyl imidazoles with α-cyanoalkyl bromides under optimized reaction conditions.

The substrate scope seems to be somewhat limited as imidazole substrates with electron-withdrawing aryl groups result in lower *ee* of the products presumably due to product racemization (see Table 7). However, branched α-cyanoalkyl bromide **95b** could be employed as alkylation reagent to afford the corresponding products with excellent *ee* (see Scheme 50). To the best of our knowledge, this is the first example where the chiral-at-metal iridium(III) or rhodium(III) enolate complexes react with secondary carbon-centered radicals. Future efforts might be spent on mechanistic investigations as mentioned above. In case this project is continued, the evaluation of various branched α-cyanoalkyl bromides and imidazole substrates with alkyl functionalization are highly promising (see Table 7, entry 5 and Scheme 50) and should therefore have a high priority.

3.2. Enantioselective α-Benzoyloxylation of 2-Acyl Imidazoles Catalyzed by Chiral-at-Metal Rhodium Lewis Acid

3.2.1. Introduction

The enantioselective α-oxygenation of carbonyl compounds has been intensely investigated due to the importance of the resulting products in organic synthesis. However, most catalytic strategies rely on pre-formed enolates, either (silyl) enol ethers, or ketene acetals.[153,154] Recently, chiral amine catalysts have been used to facilitate direct asymmetric α-oxygenation reactions by activating aldehydes and ketones through enamine formation. Several groups have successfully employed nitrosobenzene (**205**) as electrophile to achieve an asymmetric α-aminoxylation of carbonyl compounds.[155-160] Despite good yields and enantio-selectivities, the high reactivity of nitrosobenzene (**205**) often led to inseparable bis-aminoxylation products or in some cases only to modest *N*,*O*-selectivity (Scheme 58). To address these issues, several-fold excess of carbonyl compounds or a slow addition of nitrosobenzene (**205**) is required, which limits the practical value of this strategy.

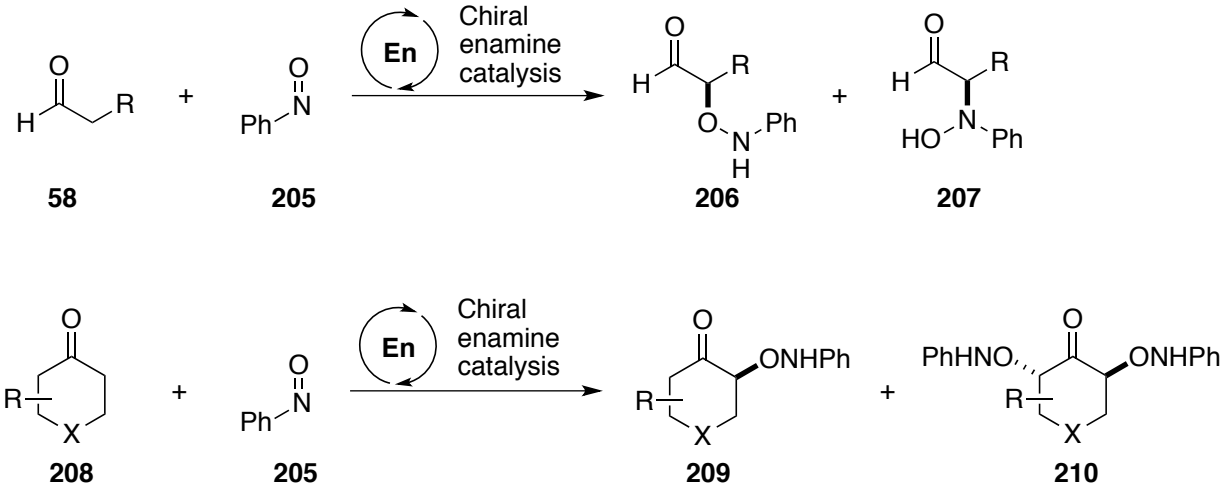

Scheme 58: Direct α-aminoxylation of aldehydes and ketones with nitrosobenzene catalyzed by chiral amines.[155-160]

On the other hand, benzoyl peroxide (**211**, BPO) seems to be a good alternative oxygen source to achieve this asymmetric α-oxygenation because it is inexpensive, readily available, and easy to handle. Indeed, chiral imidazolidinone **92b**,[162] pyrrolidine **213**,[161] and silylated prolinol **124**[163] have been reported to facilitate the enantioselective α-benzoyloxylation of aldehydes with BPO (**211**). After subsequent *in situ* reduction, enantioenriched β-benzoyl alcohol **212** could be obtained with excellent *ee* (Scheme 59).

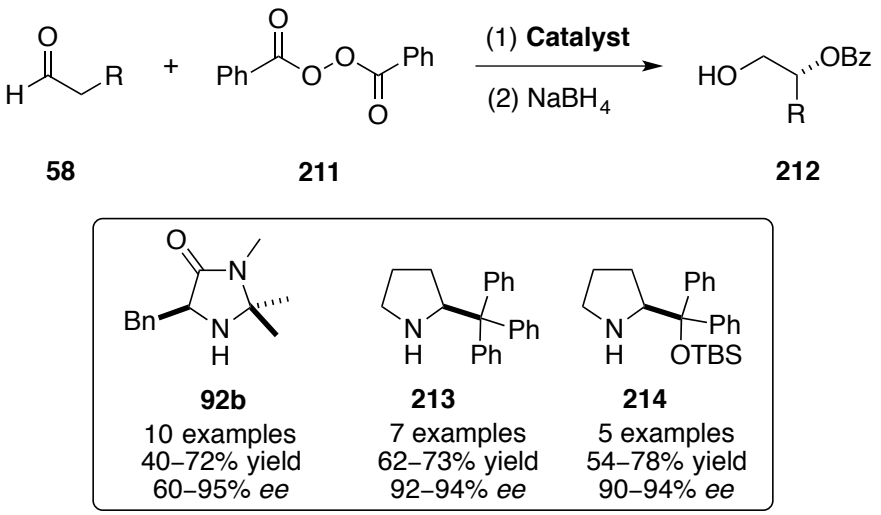

Scheme 59: Direct α-benzoyloxylation of aldehydes through chiral enamine catalysis.[161-163]

In terms of ketones, the List group discovered that chiral primary amine **215** promotes the asymmetric α-benzoyloxylation of cyclic ketones **208**.[164] Trichloroacetic acid is employed as co-catalyst in order to enhance the electrophilicity of BPO (**211**) and substoichiometric amounts of 2,6-di-*tert*-butyl-4-methyl-phenol (BHT) are added to suppress an undesired radical process, which would otherwise result in side reactions and lower yields (Scheme 60).

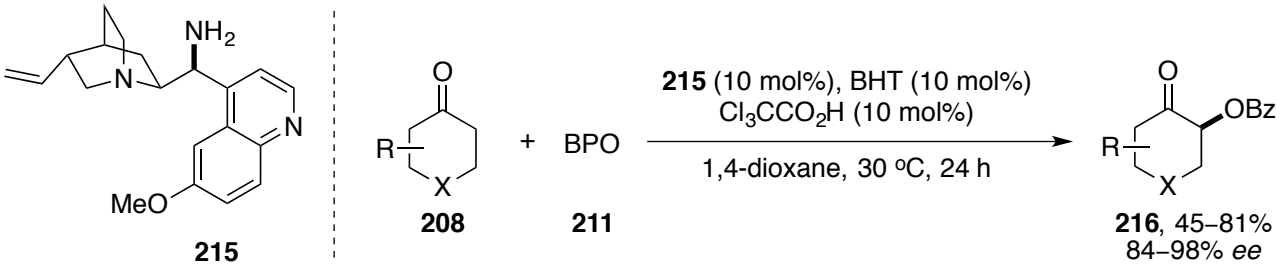

Scheme 60: Direct α-benzoyloxylation of cyclic ketones by chiral enamine catalysis.[164]

Despite the success of enamine catalysis, significant limitations of it should be addressed in the future. For instance, the substrate scope is limited, only aldehydes with alkyl, benzyl, and allyl moieties have been successfully employed, and the yields of the products remain to be improved. In the case of ketones, the reaction requires anhydrous BPO (**211**) instead of the more common hydrate to ensure satisfactory yields, which raises safety and cost concerns. Furthermore, to the best of our knowledge, a direct enantioselective α-benzoyloxylation of acyclic ketones has not been developed yet.

Recently, BPO (**211**) has been used in photoredox reactions as well. In a visible-light driven direct benzoyl-oxylation of electron-rich arenes,[165] BPO (**211**) accepts an electron from photoexcited $*[Ru(bpy)_3]^{2+}$ and undergoes fragmentation to produce a benzoyl radical, which is an electrophilic radical and reacts with electron-rich arenes **217** to afford product **218** (Scheme 61).

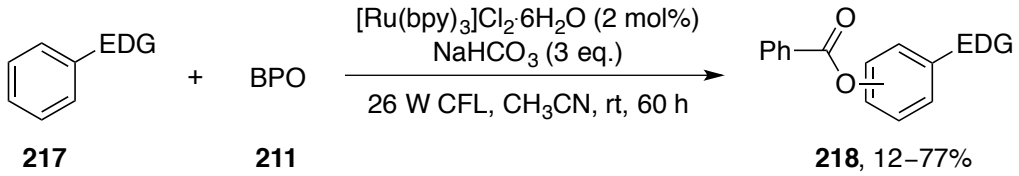

217 **211** **218**, 12–77%

Scheme 61: Visible light triggered direct benzoyloxylation of electron-rich arenes.[165]

We became curious whether chiral-at-metal Lewis acid catalysts could catalyze the asymmetric α-benzoyloxylation of 2-acyl imidazoles via either a polar or a radical pathway to address the limitations of the existing methods for the α-benzoyloxylation of carbonyl compounds.

3.2.2. Preliminary Results

We started our investigation by adopting the photoredox conditions[165] and 2-acyl imidazole **74ag** was chosen as model substrate. To our delight, in the presence of 1.5 equivalents BPO (**211**), 3 equivalents $NaHCO_3$, 2 mol% $[Ru(bpy)_3]Cl_2·6H_2O$, and 3 mol% *rac*-RhO, imidazole substrate **74ag** was converted to **219ag** in 72% yield after only 2 h photolysis with visible light. A control experiment revealed that visible light is not necessary for the reaction, which indicates that the reaction most likely proceeds via a polar pathway (similar to enamine catalysis, see Scheme 59 and 60). The reaction was repeated in the absence of visible light and photocatalyst and enantioenriched product **219ag** was obtained in 96% yield with 40% *ee* (Scheme 62). It is worth noting that the absolute configuration of the enantioenriched product was not determined due to the relatively low selectivity.

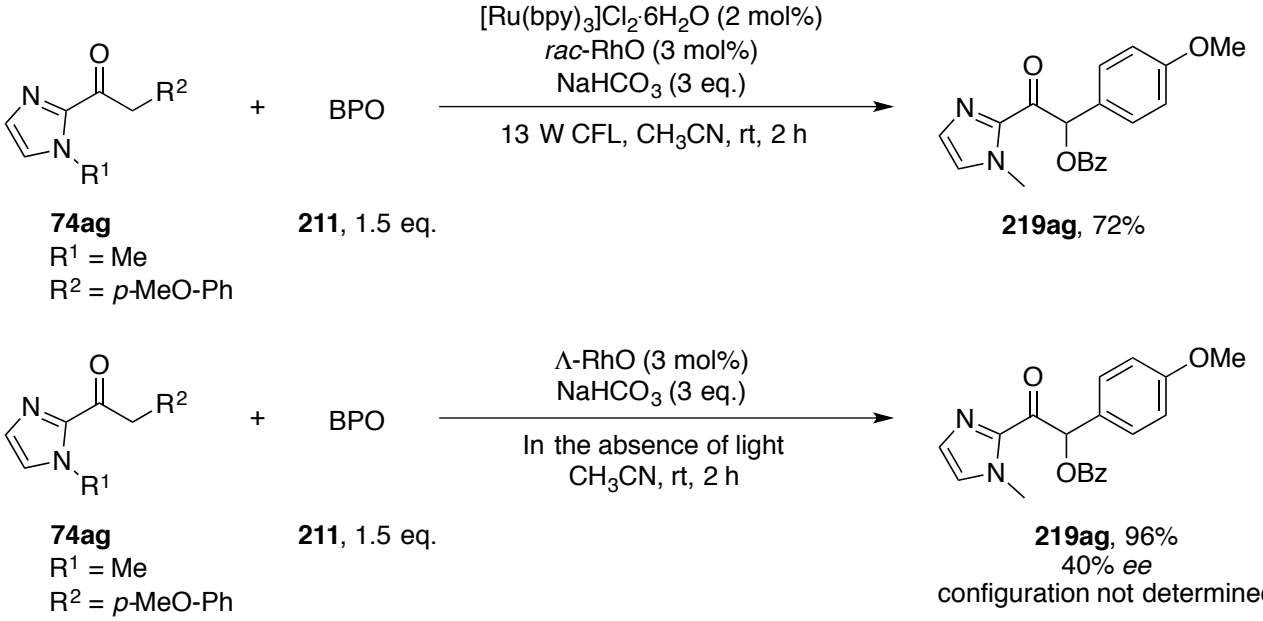

Scheme 62: Preliminary results of the α-benzoyloxylation of 2-acyl imidazoles with BPO.

3.2.3. Optimization of the Reaction Conditions

First, various solvents were screened. It is worth noting that substrate **74ag** was smoothly converted to product **219ag** and that side products are basically not formed, which allows to monitor the reactions directly by HPLC-analysis. While CH_2Cl_2 and CH_3NO_2 did not provide any improvement (40% *ee* and 20% *ee*, Table 9, entry 2 and 3), the absence of $NaHCO_3$ led to an improved enantioselectivity (47% *ee* and 52% *ee* in THF, entry 4 and 5).

Table 9: Solvent evaluation in the presence of $NaHCO_3$.

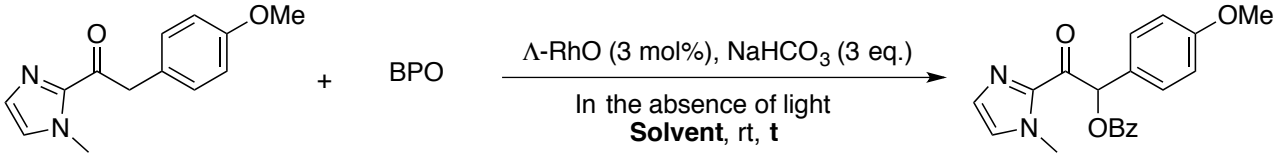

74ag **211**, 1.5 eq. **219ag**

Entry	Solvent	t	Result
1	CH_3CN	1.5 h	40% *ee*
2	CH_2Cl_2	12 h	40% *ee*
3	CH_3NO_2	12 h	20% *ee*
4	THF	12 h	47% *ee*
5[a]	THF	2.5 h	52% *ee*

[a] Reaction was performed in the absence of $NaHCO_3$.

Hence, further solvents were screened in the absence of base. Among all evaluated solvents, toluene and 1,2-dimethoxyethane (DME) afforded the best results and reactions in these solvents were finished after 1.5 h to give product **219ag** with 56% *ee* (Table 10, entry 3 and 7). Finally, a control experiment was performed in acetonitrile without the catalyst. According to HPLC analysis of the crude reaction mixture no product was formed, which indicates that catalyst RhO drastically accelerated the reaction.

Table 10: Solvent evaluation in the absence of base.

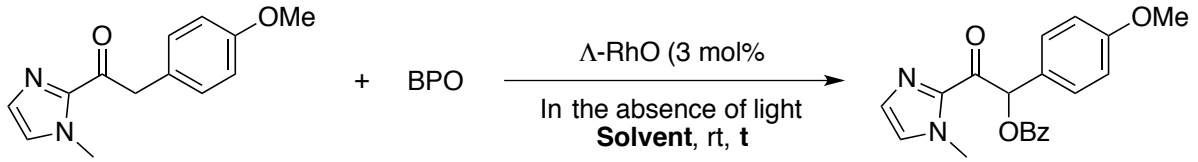

74ag **211**, 1.5 eq. **219ag**

Entry	Solvent	t	Results
1	THF	2.5 h	52 % *ee*
2	1,4-dioxane	1.5 h	53 % *ee*
3	toluene	1.5 h	56 % *ee*
4[a]	$CHCl_3$	1.5 h	48 % *ee*

Entry	Solvent	t	Results
5	acetone	3 h	45 % *ee*
6[a,b]	DMSO	3 h	45 % *ee*
7	DME	1.5 h	56 % *ee*
8	EtOH	1.5 h	44 % *ee*
9	*i*-PrOH	1.5 h	51 % *ee*
10[c]	CH_3CN	1.5 h	no conversion

[a] Incomplete conversion; [b] Side products were observed; [c] In the absence of catalyst.

Next, we screened different catalysts and variated the molar ratio of the reactants. Excess of imidazole substrate **74ag** failed to improve the results in terms of both reaction rate and enantioselectivity (Table 11, entry 1; compare with Table 9, entry 5), while iridium catalysts significantly lowered the *ee* of the product (entry 2 and 3).

Table 11: Influence of molar ratio and catalysts.

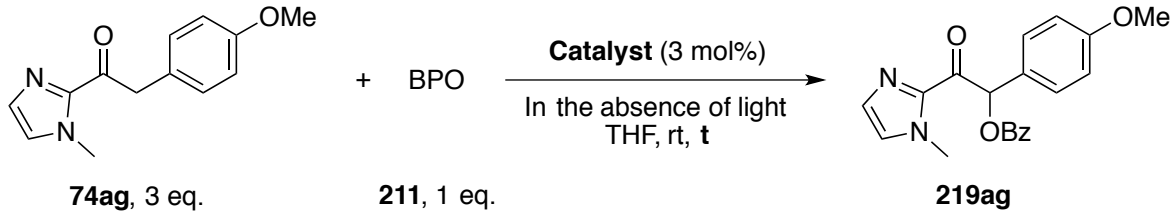

74ag, 3 eq. **211**, 1 eq. **219ag**

Entry	Catalyst	t	Result
1	Λ-RhO	3 h	52% *ee*
2[a]	Λ-IrO	20 h	25% *ee*
3[a]	Λ-IrS	20 h	27% *ee*

[a] Incomplete conversion

Sticking to RhO as catalyst and toluene or DME as solvent, we went on evaluating the influences of concentration, temperature, and different additives on the reaction. Lower temperature and lower concentration of substrate **74ag** resulted in a slower reaction rate while little or no improvement of product's *ee* was observed (56% *ee* and 58% *ee*, Table 12, entries 2 and 3). To accelerate the reaction, 10 mol% of tifluoroacetic acid (TFA) were added with the intention to enhance the electrophilicity of BPO (**211**). However, substrate **74ag** still was not fully consumed and the *ee* of **219ag** was decreased (54% *ee*, entry 4). Radical scavengers hydroxyquinone (HQ) and BHT were also not able to improve product's *ee* (52% and 56% *ee*, entries 5 and 6).

Table 12: Optimization of reaction conditions.

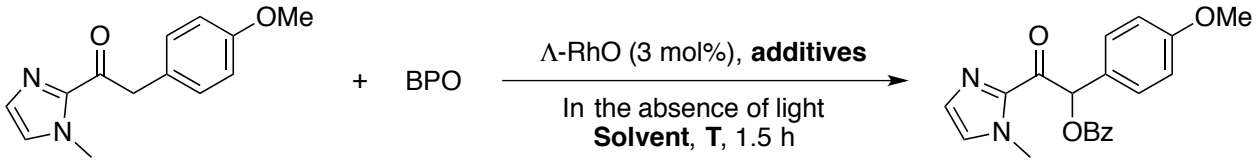

74ag **211**, 1.5 eq. **219ag**

Entry	Concentration of 74ag	Solvent	T	Additives	*ee*
1	0.4 M	DME or toluene	rt	none	56 %
2[a]	0.4 M	toluene	0 °C	none	56 %
3[a]	0.1 M	toluene	rt	none	58 %
4[a]	0.1 M	toluene	rt	TFA (10 mol%)	54 %
5[a]	0.4 M	DME	rt	HQ (10 mol%)	52 %
6[a]	0.4 M	DME	rt	BHT (10 mol%)	56 %

[a] Incomplete conversion.

Significant improvement was achieved with substrate **74aa**, as product **219aa** was obtained in promising 85% yield with 72% *ee*. Replacement of the imidazolyl moiety's methyl group by *iso*-propyl led to further improvement of the enantioselectivity to 79% *ee* (Scheme 63).

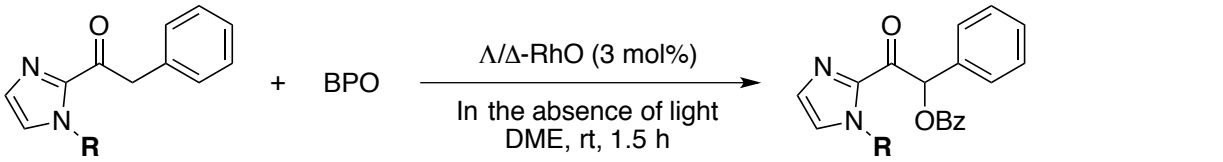

R = Me: **74aa** **211**, 1.5 eq. R = Me: **219aa**, 85%, –72% *ee* with Δ-RhO
R = *i*-Pr: **74da** R = *i*-Pr: **219da**, 97%, 79% *ee* with Λ-RhO

Scheme 63: Influence of the substrate, lacking methoxy group and *N*-*iso*-propyl group led to improved *ee*.

By increasing the catalyst loading to 6 mol%, product **219da** was formed with 82% ee after 1.5 h according to HPLC analysis of the crude reaction mixture. However, when **205da** was isolated after a total reaction time of 22 h the *ee* of the isolated product was found to be only 52%, which indicates racemization of the product under the applied reaction conditions (Scheme 64).

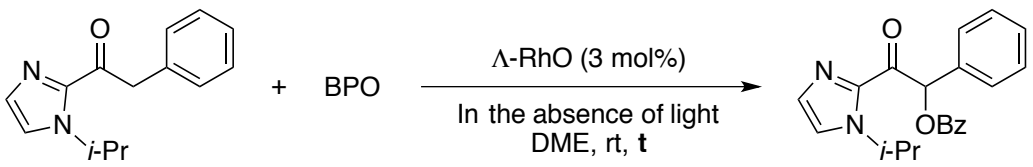

74da **211**, 1.5 eq. **219da**, 82% *ee* after 1.5 h
52% *ee* after 22 h

Scheme 64: Indication for product racemization under the applied reaction conditions.

Being aware that α-aryl substituted 2-acyl imidazoles are especially prone to undesired enolization and thus racemization, we now switched over to an alkyl substituted 2-acyl imidazole **74dh**. However, no conversion of substrate **74dh** was observed under identical reaction conditions after 24 h (Scheme 65).

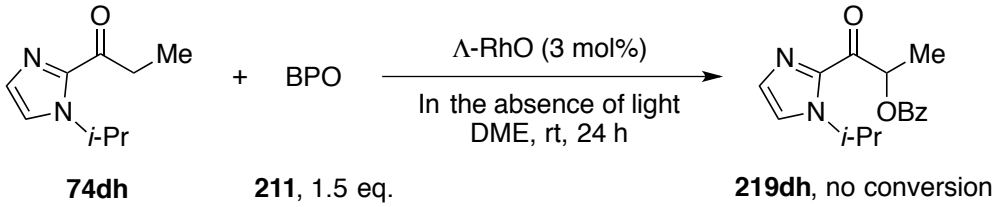

74dh **211**, 1.5 eq. **219dh**, no conversion

Scheme 65: Reaction with the imidazole substrate **74dh**.

In consideration that in the absence of base **74dh** might not be enolized. At the same time, the low electrophilicity of BPO (**211**) might prevent conversion, the reaction was now performed in the presence of 1.1 equivalents of various bases or acids. Among all tested additives, which included Na_2HPO_4, NaOAc, Na_2CO_3, K_2HPO_4, K_2CO_3, Cs_2CO_3, *i*-Pr_2NEt, *i*-Pr_2NH, Et_3N, *n*-Bu_3N, 2,6-lutidine, and benzoic acid ($PhCO_2H$), trifluoroacetic acid (TFA), *p*-toluenesulfonic acid mono hydrate (*p*-$TsOH{\cdot}H_2O$), trifluoromethane-sulfonic acid (TfOH), only both bases Na_2CO_3 and *i*-Pr_2NH were able to promote the reaction to afford product **219dh** in 26% and 29% yield after 24 h. It is worth noting that imidazole substrate **74dh** was not fully consumed in both reactions, which also proceeded with unsatisfactory enantioselectivities (Scheme 66).

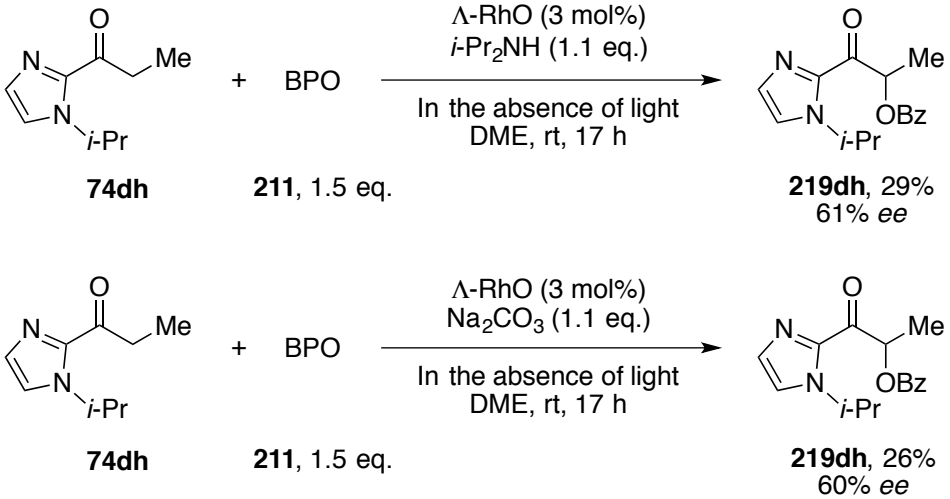

74dh **211**, 1.5 eq. **219dh**, 29% 61% *ee*

74dh **211**, 1.5 eq. **219dh**, 26% 60% *ee*

Scheme 66: Reaction with substrate **74dh** in the presence of *i*-Pr_2NH and Na_2CO_3.

In an alternative approach, the reaction was performed under the photoredox conditions and it seems that the benzoyl radical prefers to react with the imidazolyl ring instead of with the enolate's double bond as the ^1H NMR analysis of the resulting product indicated intact methylene signals (Scheme 67, ^1H-NMR spectrum of the product in the experimental section, Figure 22, p.118).

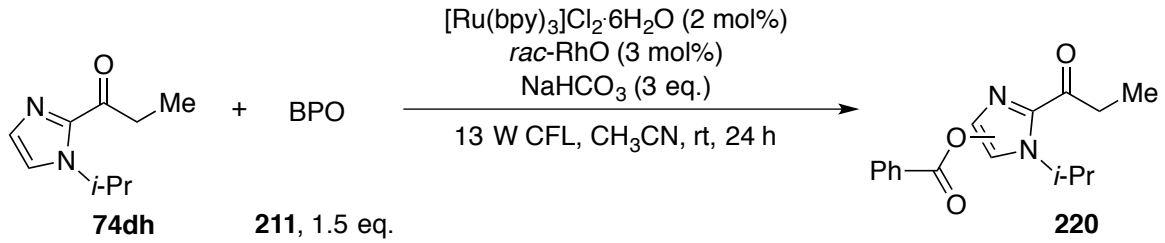

74dh **211**, 1.5 eq. **220**

Scheme 67: Reaction with imidazole substrate **74dh** under photoredox conditions.

3.2.4. Conclusion and Further Perspectives

Despite single encouraging results (97% yield and 79% *ee* for **219da**, Scheme 64), the development of enantioselective α-benzoyloxylation of 2-acyl imidazoles was not successful. To address the current issues regarding product racemization and scope, the reaction with 2-acyl imidazole **74ca** as substrate and RhS as catalyst should be investigated.

3.3. Iridium and Rhodium Lewis Acids Promoted Direct α-Arylation of 2-Acyl Imidazoles

3.3.1. Introduction

Great efforts have been spent on developing strategies to achieve α-arylations of carbonyl compounds due to the importance of the resulting products in pharmaceutical and biological chemistry. The non-catalytic traditional synthesis methods mostly rely on nucleophilic aromatic substitutions between enolates and highly activated aryl halides and therefore the substrate scope of these methods is limited.[166] On the other hand, metal catalyzed cross-coupling reactions are well-established, which may follow two pathways depending on the coupling partners (Scheme 68). In most cases, palladium, nickel, and copper complexes are employed as catalysts which first undergo oxidative addition to activate aryl halides or pseudo aryl halides **222**. Next, transmetalation with **226** and enolates **221** leads to formation of the second metal-carbon bond. Finally, reductive elimination affords arylation products **223** (pathway A).[167-169] The other pathway has been less exploited so far as it requires pre-activation of both the carbonyl and the aryl compounds. Here, the oxidative addition step takes place with racemic α-halo carbonyl compounds **225** and various arylmetal reagents **224** may be used as aryl source (pathway B).[170-173]

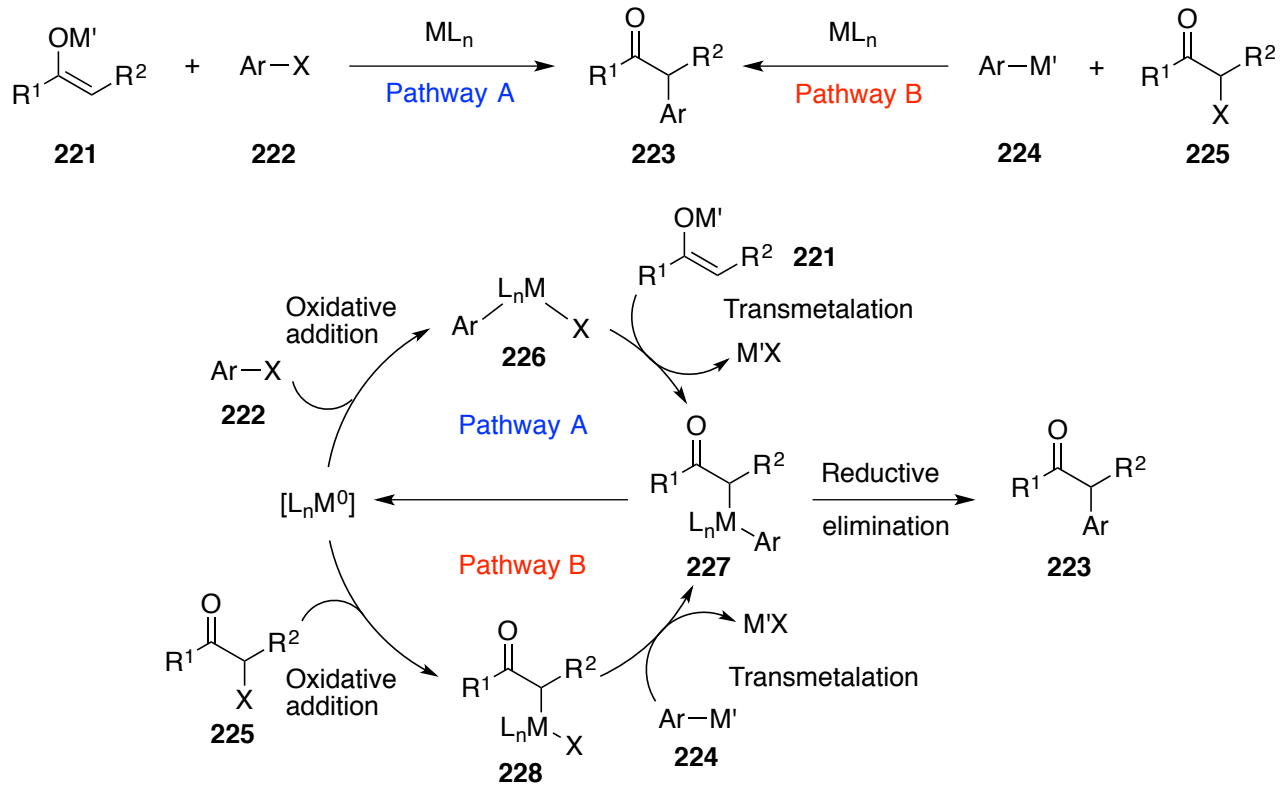

Scheme 68: General catalytic cycles for the metal-catalyzed α-arylation of carbonyl compounds.[167-173]

Apart from the cross-coupling reactions above, other methods have been developed as well. Chi and coworkers reported the α-arylation of α-functionalized ketones with non-activated indoles via oxyallyl cation intermediates **230**.[174] The MacMillan group further expanded the substrate scope of this reaction by employing various *N*-, *O*-, *F*-nucleophiles (Scheme 69a).[175] Another method which enables the utilization of arenes without pre-activation is to employ α-diazo carbonyl compounds **211** as substrates. Various metal

catalysts have been proved to catalyze the degradation of diazo compounds effectively. The resulting carbenoids undergo C,H-insertions to give arylated products **233** (Scheme 69b).[176-180]

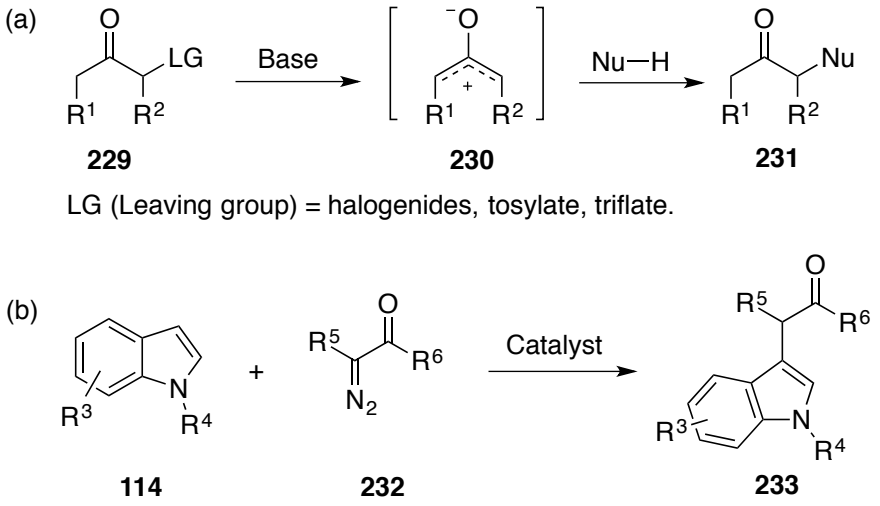

Scheme 69: α-Arylation of α-functionalized ketones and α-diazo carbonyl compounds.[174-180]

In spite of the eligibility of the aforementioned methods, pre-activation of at least one of both reaction partners is always required. Ideally, a direct method for the α-arylation of carbonyl compounds would be desired. However, an obvious challenge is that both the α-postion of a carbonyl compound and most arenes are nucleophiles in nature and therefore a direct coupling requires an umpolung process. One pioneering example has been by MacMillan and co-workers with their SOMO catalysis (single occupied molecular orbital)[181] and is demonstrated in Scheme 70. In this reaction, octanal (**58b**) is coupled with *N*-Boc pyrrole (**234**) to afford enantioenriched product **235** with good result (85% yield, 84% *ee*). The authors propose that the key electrophilic intermediate is formed by removal of one electron from the nucleophilic enamine by ceric ammonium nitrate (CAN).

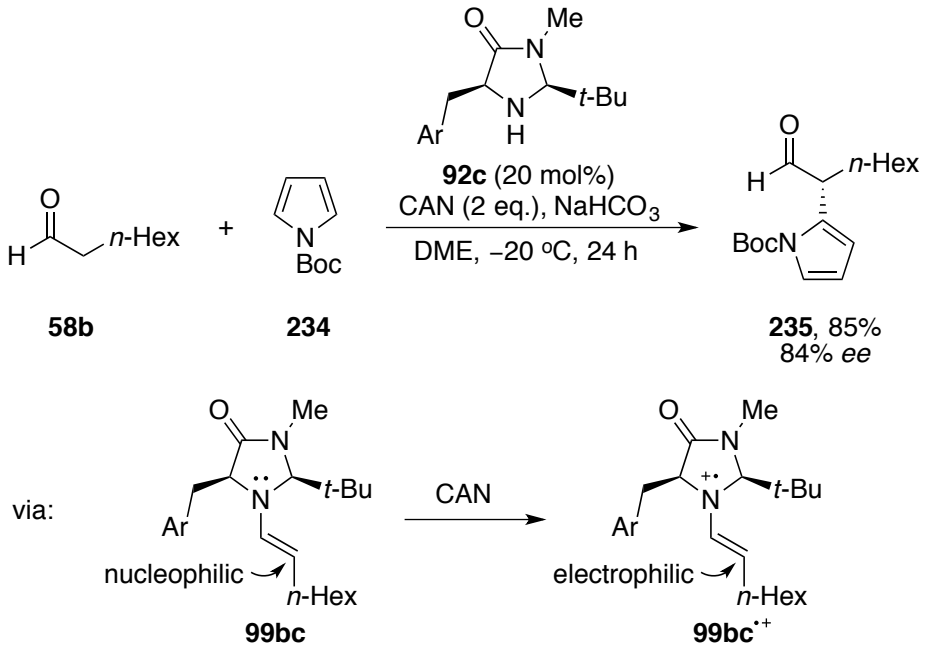

Scheme 70: Enantioselective intermolecular α-arylation of aldehydes via organo-SOMO catalysis.[181]

Further investigations by MacMillan and co-workers have resulted in the development of an enantioselective intramolecular α-arylation of aldehydes, similar chemistry has been reported by the Nicolaou group a little earlier as well (Scheme 71).[182,183]

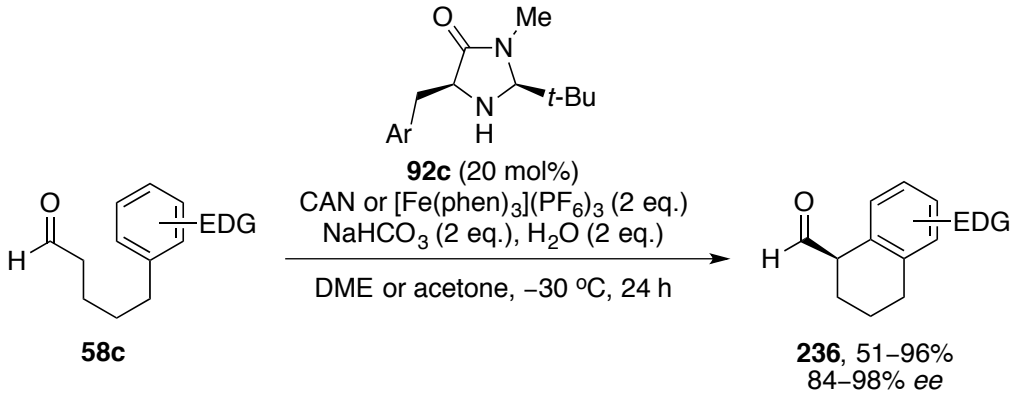

Scheme 71: Enantioselective intramolecular α-arylation of aldehydes via organo-SOMO catalysis.[182,183]

Direct C-3 alkylation of indoles with ketones has been developed using $Ce(OAc)_3$ as catalyst and *tert*-butyl-hydroperoxide (TBHP) as stoichiometric oxidant in the presence of β-cyclodextrin (β-CD) and water.[184] The authors propose that the catalyst is oxidized by TBHP to active species Ce(IV)=O, which then reacts with indoles **114** and ketones **237** to afford products **233** through oxidative C,H-activation (Scheme 72). This method is atom-economical and the catalytic system can be recycled and reused.

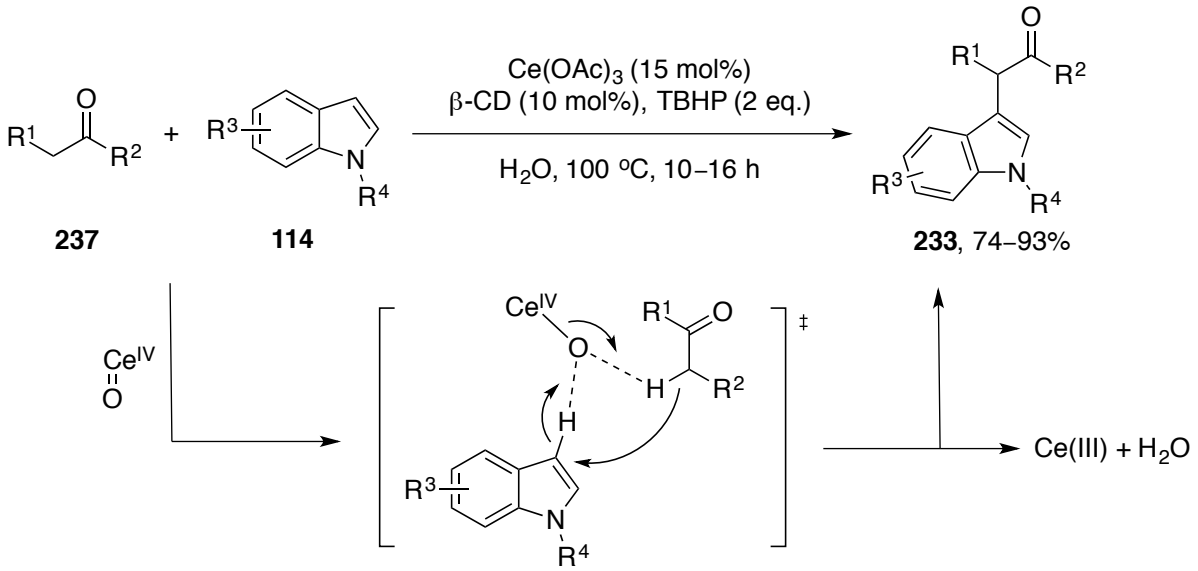

Scheme 72: Direct C-3 alkylation of indoles with ketones via oxidative C,H-bond activation.[184]

An aerobic, transition-metal-free direct α-arylation of ketones **237a** has been reported as well.[185] However, this method is only suited for substituted nitrobenzenes **238** as the C,C-bond formation relies on direct attack of the *in situ* generated enolates onto electron-deficient arenes **238**, which is then followed by O_2-mediated C-H oxidation to give products **239** in modest yields (Scheme 73).

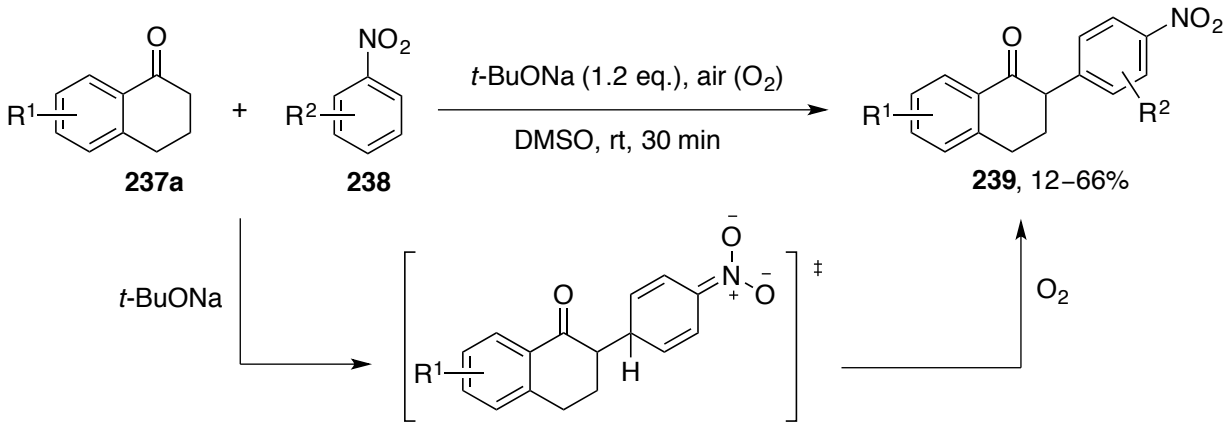

Scheme 73: Oxidative direct α-arylation of ketones with substituted nitrobenzenes via aerobic oxidation.[185]

3.3.2. Preliminary Results

After the visible-light driven enantioselective α-alkylation of 2-acyl imidazoles with substituted benzyl and phenyl bromides had been successfully established (see Scheme 40), Haohua Huo investigated the reactions with diethyl bromomalonate (**93a**) as alkylation reagent.

Table 13: Huo's results of the reactions with diethyl bromomalonate (**93a**) as alkylation reagent.

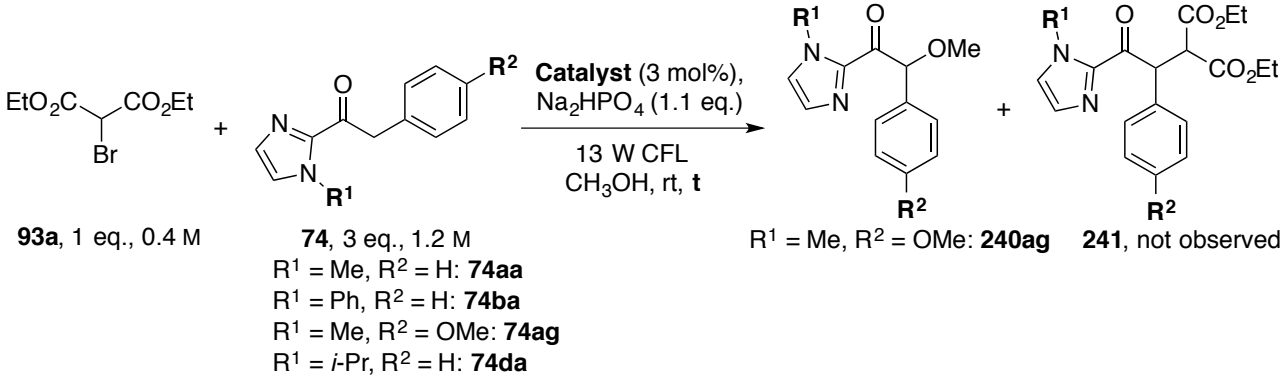

Entry	Catalyst	2-Acyl imidazole	t	Result
1	Λ-IrO	**74ag**	6 h	**240ag**, 88%, 0% *ee*
2	Λ-IrS	**74ag**	6 h	**240ag**, 67%, 18% *ee*
3[a]	*rac*-IrO	**74ag**	22 h	No conversion
4	*rac*-IrO	**74aa**	22 h	No conversion
5	*rac*-IrO	**74ba**	22 h	No conversion
6	*rac*-IrO	**74da**	22 h	No conversion

[a] Reaction was performed without **93a**.

Surprisingly, α-methoxy product **240ag** was obtained as a racemic mixture (88% yield, 0% *ee*, Table 13, entry 1) instead of expected alkylated product **241**. Switching to catalyst Λ-IrS resulted in **240ag** with 18% *ee* (entry 2). Further experiments revealed that both diethyl bromomalonate (**93a**) and the methoxy substituent on the substrate's phenyl ring are crucial for the formation of α-methoxy product **240**, as the

absence of diethyl bromomalonate (**93a**) or use of substrates **74aa**, **74ba**, and **74da** resulted in no conversion of the imidazole substrates (entries 3−6).

The formation of α-methoxy product **240ag** is an intriguing observation because it indicates that the α-position of the imidazole's carbonyl group undergoes an umpolung process and is attacked by the nucleophilic solvent methanol. Based on previous studies from our lab where chiral-at-metal Lewis acids are employed in asymmetric photoredox catalysis,[135-137] we reasoned that malonyl radical **242** does not, as initially expected, add to the double bond of iridium enolate complex **77ag** but oxidizes **77ag** to afford α-keto radical intermediate **244ag**, which is further oxidized to α-keto carbocation **245**, presumably by the oxidized photocatalyst (Scheme 74). This suggestion also provides a reasonable explanation for the importance of the methoxy substituent attached to imidazole substrate **74ag**, which stabilizes α-keto carbocation **245ag**. However, due to its positive charge, carbocation **245ag** is very likely attacked by methanol without coordination to the chiral catalyst and therefore only low enantioselectivities are observed.

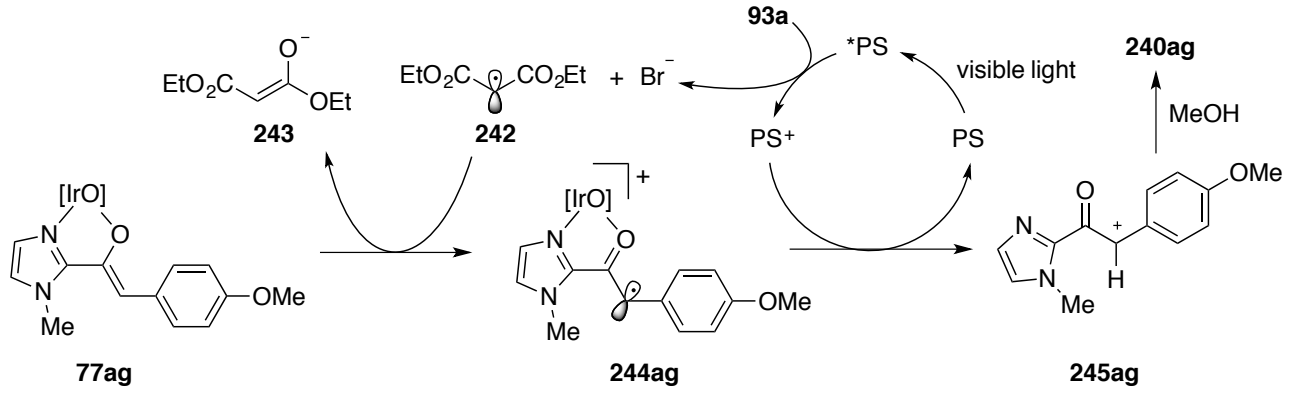

Scheme 74: Proposed mechanism for the formation of methoxy product **240**.

In order to achieve better results with this transformation, we decided to explore the potential of other nucleophiles to capture α-keto radical **244ag** under stereocontrol. Among the evaluated nucleophiles, all of which are known to react with α-keto radicals,[90-95] only the reaction with 1*H*-indole (**114a**) yielded the desired product while methoxy product **240ag** was obtained in 30−74% yield in the presence of 2-(trimethyl-siloxy)furan (**246**), silyl enol ether **200**, and 1,1-diphenylethylene (**249**). No conversion of imidazole substrate **74ag** was observed in the reactions with allylsilane **246** and enamine **248** (Scheme 75).

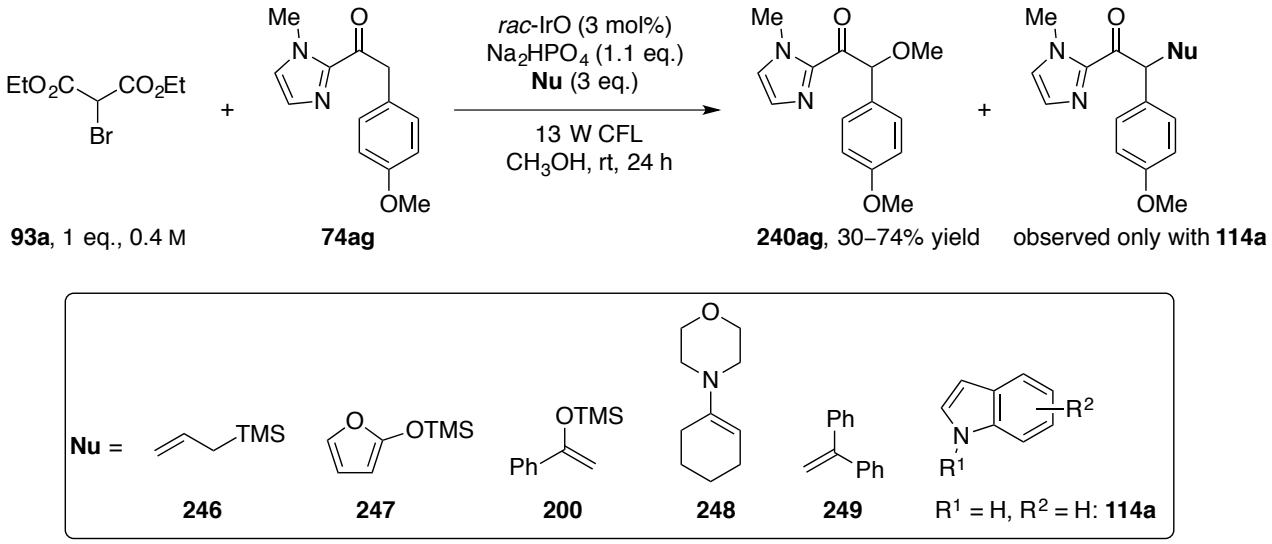

Scheme 75: Evaluation of nucleophiles to couple with 2-acyl imidazole **74ag**.

Repetition of the experiment 1*H*-indole (**114a**) and enantiopure catalyst Λ-IrO afforded product **250aga** in 68% yield with 20% *ee*. Due to the commercial availability of diethyl bromomalonate (**93a**) we also tested the reaction with excess of **93a** and to our delight, the desired product was obtained with slightly improved selectivity (28% *ee*, Scheme 76). It is worth to mention that it was not clear at the time whether the indole moiety was attached via its 2- or 3-position and the absolute configuration of the enantioenriched product was not determined. Although **250aga** was the major product, a small amount of methoxy product **240ag** was also formed.

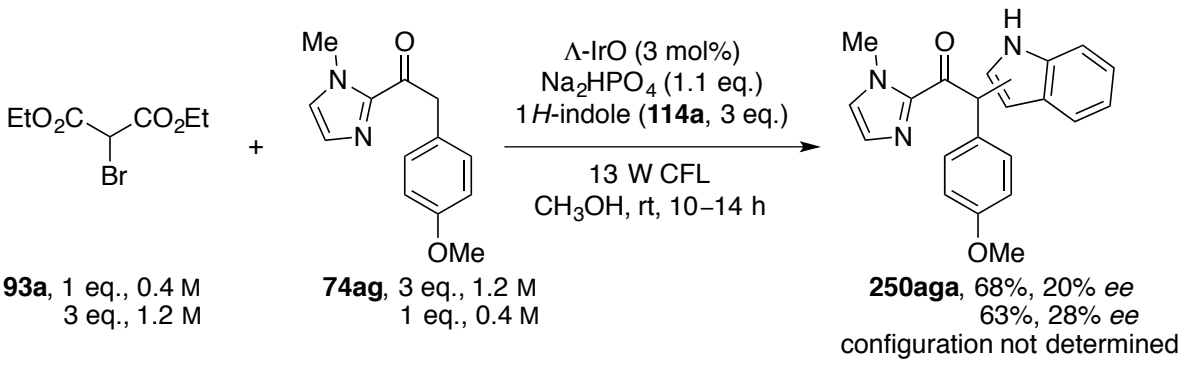

Scheme 76: Investigation of the reaction with 1*H*-indole.

In order to suppress formation of methoxy product **240ag**, we performed a short solvent screening, which revealed that *iso*-propanol is the solvent of choice as no alkoxyl products were formed with it and a higher yield for **250aga** could be obtained (79% conv. and 72% yield after 40 h, Scheme 77).

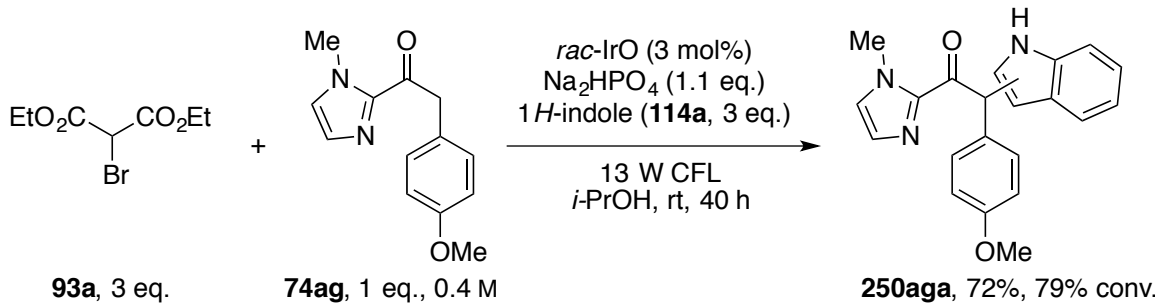

Scheme 77: Investigation of the reaction in *iso*-propanol.

3.3.3. Mechanistic Investigations

Before further optimization of the reaction conditions, we wanted to gain more insights into the mechanism of the reaction, because our initial mechanistic suggestions (see Scheme 74) was apparently not consistent with the aforementioned observations (see Scheme 75). First, it seems to be unlikely that in the presence of excess nucleophiles α-keto radical complex **244ag** would be further oxidized to carbocation **245ag**, which then reacts with methanol to give methoxy product **240ag**. Second, in case of the reactions where no conversion of imidazole substrate **74ag** was observed, malonyl radical **242** still did not react with the mentioned nucleophiles in Scheme 75. All of these observations indicate that α-keto radical complex **244ag** and malonyl radical **242** are not formed as initially proposed.

As mentioned, it was initially not clear whether the indolyl residue of product **250aga** was connected to 2-acyl imidazolyl moiety via its 2- or its 3-position. An two-dimensional NMR analysis of **250aga** revealed that the indolyl residue is connected to the rest of the product via its 3-position as we observed a correlation signal between the NH proton and the adjacent proton in the ^{1}H,^{1}H-COSY spectrum (Figure 12).

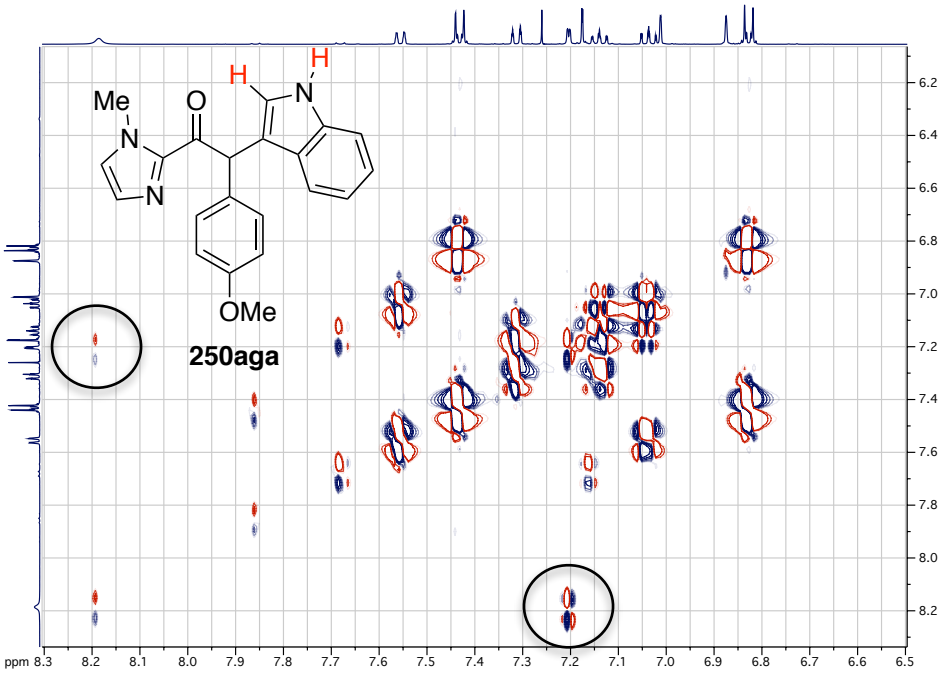

Figure 12: ^{1}H,^{1}H-COSY spectrum of compound **250aga**.

Additional evidence for the proposed structure was provided by reactions with 2- and 3-substituted indoles. While imidazole substrate **74ag** and 1,2-dimethyl-1*H*-indole (**114b**) were smoothly converted to α-arylated product **250agb** in 69% yield only 54% conversion for **74ag** was observed and methoxy product **240ag** was obtained in 33% yield when the reaction was carried out with 3-methyl-1*H*-indole (**114c**) (Scheme 78). By proving the structure of product **250** we were able to conclude that it can not be a radical intermediate **244** which reacts with 1*H*-indole (**114a**) as the 2-position would be the preferred coupling position in this case. [186,187] In other words, it is unlikely that radical **244ag** is formed in the course of the reaction.

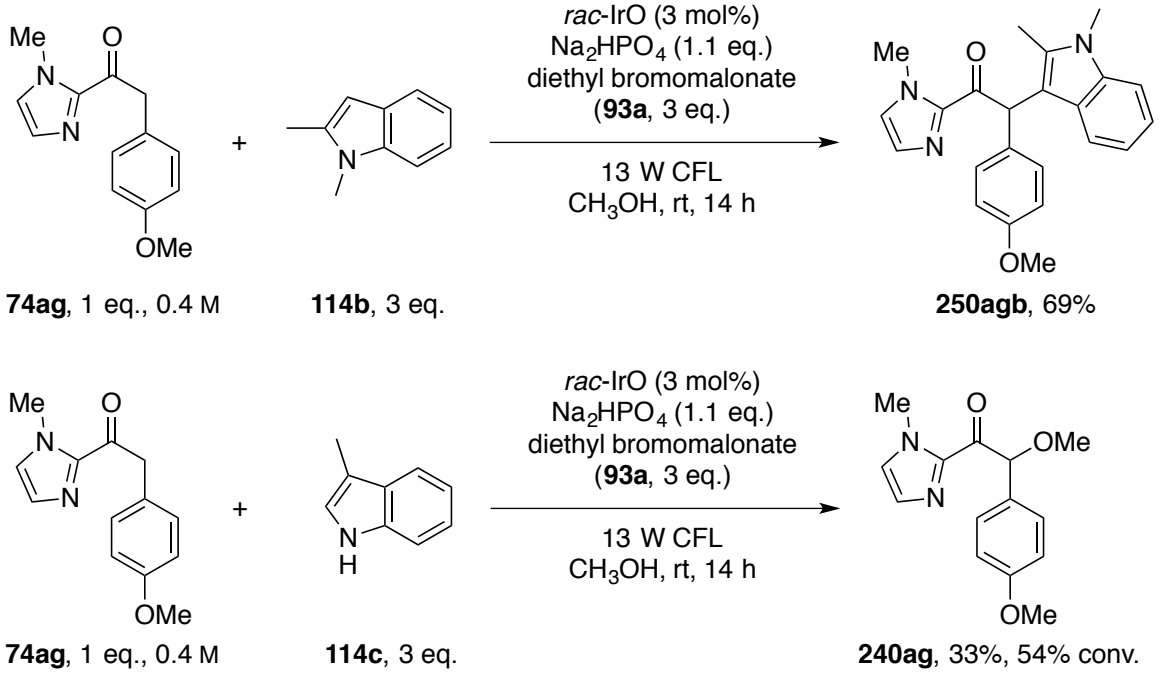

Scheme 78: Reactions with 2- and 3-substituted indoles.

Next, control experiments were performed in the absence of light and we found out that visible light was not necessary for the reaction as enantioenriched product **250aga** was obtained after 15 h even with higher yield and *ee* (82% yield, 33% *ee*, Scheme 79). This experiment further confirms that the reaction does not proceed via a radical pathway as single electron transfer (SET) is hardly able to take place in the absence of light.

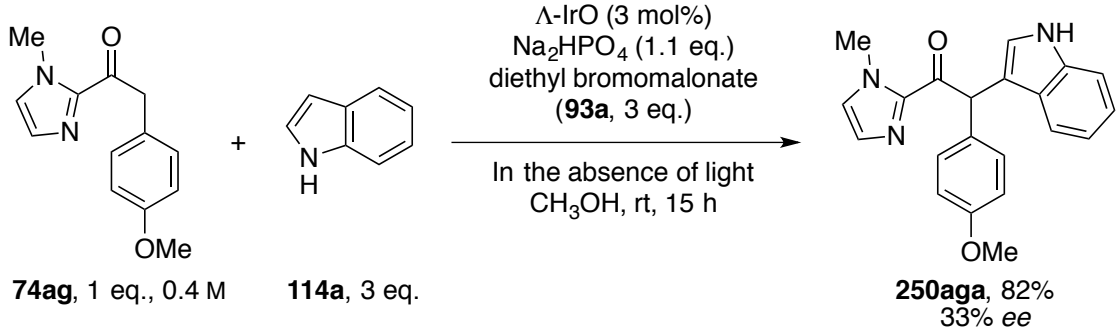

Scheme 79: Control experiment in the absence of light, the reaction gave improved yield and *ee* for **250aga**.

A hint about the reaction mechanism was given by the reaction with imidazole substrate **74aa** lacking a methoxy substituent. After 20 h in the absence of light, substrate **74aa** was converted to a mixture of arylated, methoxylated, and brominated products (Scheme 80).

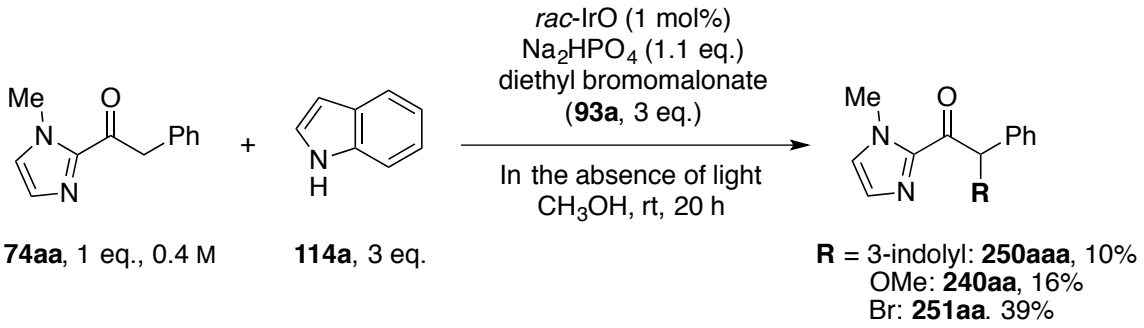

Scheme 80: Reaction with imidazole substrate **74aa** lacking a methoxy substituent.

The formation and isolation of brominated product **251aa** is intriguing because it might be an intermediate during the formation of **250aaa** and **240aa**. Indeed, when reaction was carried out with imidazole substrate **74ag** in *iso*-propanol in the absence of 1*H*-indole (**114a**), brominated product **251ag** was again observed according to thin layer chromatography (TLC) of the reaction mixture after 48 h. By adding 1*H*-indole (**114a**) to the reaction mixture, brominated product **251ag** disappeared after 7 h and arylated product **250aga** was formed (Scheme 81 and see experimental section, Figure 25, p.125). A literature survey revealed that mono- or dibromo-1,3-dicarbonyl compounds are known as brominating agents.[188,189]

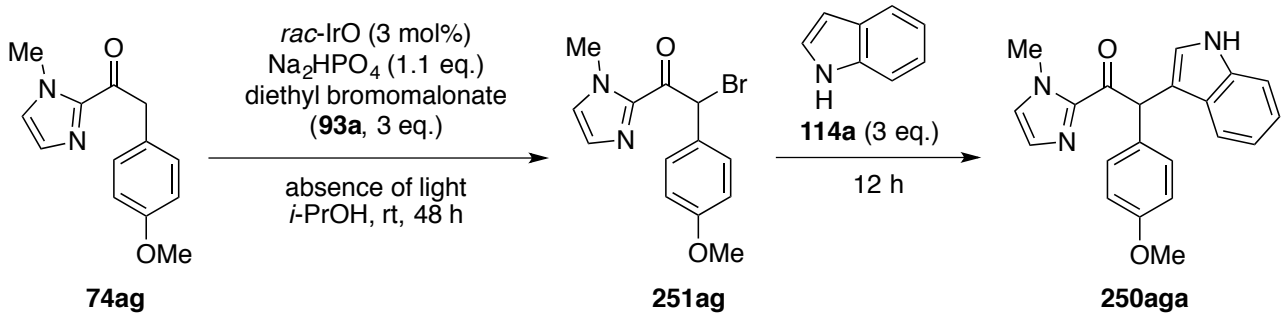

Scheme 81: Mechanism investigation by adding 1*H*-indole stepwise, α-brominated product is the intermediate for the formation of **250aga**.

With these informations in hand, a more accurate mechanism can be proposed: imidazole substrate **74ag** first coordinates to the iridium center of catalyst IrO in a bidentate fashion and two acetonitrile molecules are released, which results in enhanced acidity of the α-proton and enolization in the presence of Na_2HPO_4. Iridium enolate complex **77ag** then attacks the electrophilic bromine of diethyl bromomalonate (**93a**) and brominated product **251ag** is presumably released before the Friedel-Crafts alkylation occurs. Non-coordinating brominated product **251ag** undergoes fragmentation to form α-keto cation **245ag**, whose stability explains the reactivity difference between the substrates with and without methoxy substituent (**74ag** and **74aa**) as the methoxy substituent is able to effectively stabilize the positive charge on **245ag**. Finally, Friedel-Crafts alkylation between **245ag** and **114a** gives arylated product **250aga** (Scheme 82).

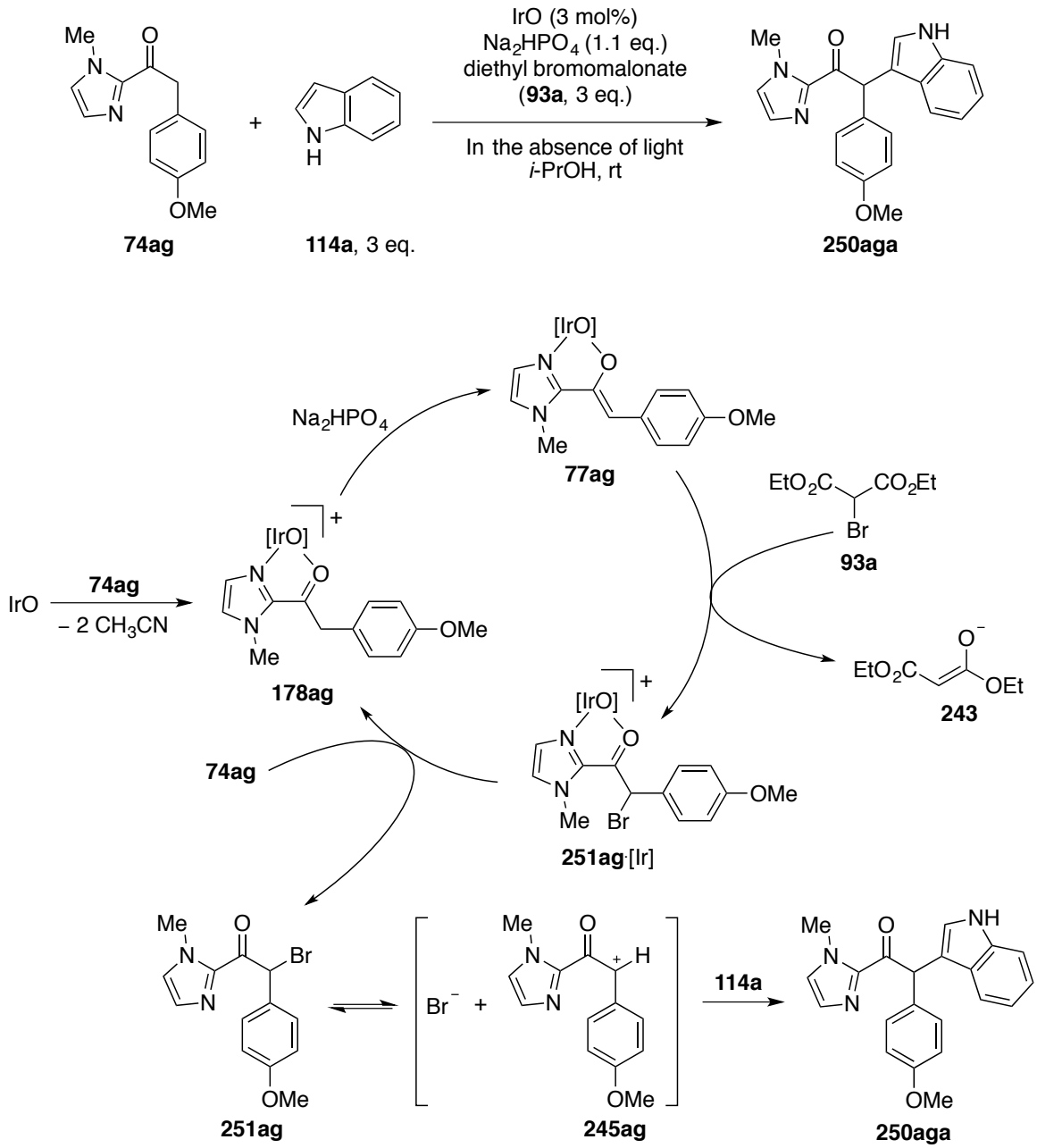

Scheme 82: Mechanistic studies and proposal: iridium Lewis acid catalyzes the α-bromination of 2-acyl imidazole, which is followed by a Friedel-Crafts alkylation

According to the low but still significant *ee* of the arylated product **250aga** (33% *ee*, see Scheme 79), we suggest that although the aforementioned mechanism via α-keto cation **245ag** is the dominant pathway for the conversion of **251ag** to **250aga**, an enantioselective pathway should exist as well. For instance, the bromination step should in principle proceed enantioselectively and a subsequent S_N2-like Friedel-Crafts alkylation with enantioenriched bromide **251ag** would then result in enantioenriched arylated product **250aga** going along with an inversion of the stereocenter of **251ag**. Hence, it is important to determine the absolute configuration of enantioenriched product **250aga**, in order to fully understand the reactions mechanism, which would allow to rationally develop asymmetric variant of this reaction.

3.3.4. Optimization of the Reaction Conditions

Having revealed that the α-keto cation **245ag** is the key intermediate of the racemic pathway, we now focused on optimizing the reaction conditions to develop a racemic variant of the direct α-arylation of 2-acyl imidazoles. As mentioned, *iso*-propanol as solvent is able to effectively prevent the formation of the alkoxy product. However, in this solvent the reaction proceeded slower and did not run to completion (see Scheme 77). Therefore, we synthesized 3,3-dibromopetane-2,4-dione (**252**) in the hope that it would be a stronger bromination reagent. Indeed, employing dibromide **252** led to complete conversion of **74ag** in *iso*-propanol to give arylated product **250aga** in 86% yield (Table 14, entry 1). It is worth mentioning that substrate **74aa** required quantitative amounts of AgOTf to furnish **250aaa** in 51% yield (entry 2). Notably, substrate with alkyl moiety **74bh** could not be coupled with 1*H*-indole (**114a**) even in the presence of AgOTf and instead brominated product **251bh** was obtained in 99% yield (entry 3).

Table 14: Evaluation of **252** as brominating reagent with different imidazole substrates.

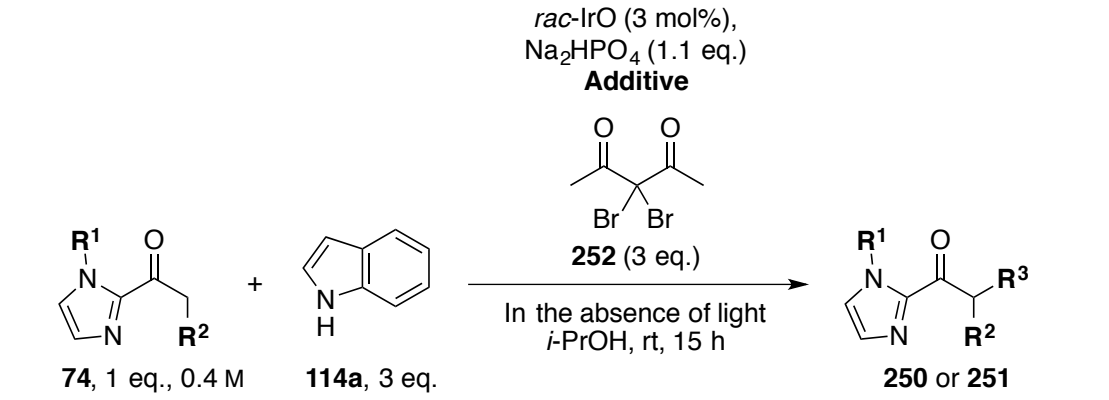

Entry	Imidazole substrate	Additive	Product (yield)
1	**74ag**	none	**250aga** (86%)
2	**74aa**	AgOTf (1.1 eq,)	**250aaa** (51%)
3	**74bh**	AgOTf (1.1 eq,)	**251bh** (99%)

Catalyst RhO was tested in this reaction as well. However, replacement of IrO against RhO resulted in a lower yield (59% yield). Among all the tested solvents, which included CH_3NO_2, acetone, THF, DMF, toluene, chloroform, 1,4-dioxane, DMSO, diethyl ether, and DME, only reactions in THF and DMF led to complete conversion of **74ag** to arylated product **250aga** in 76% and 28% yield respectively (Scheme 83).

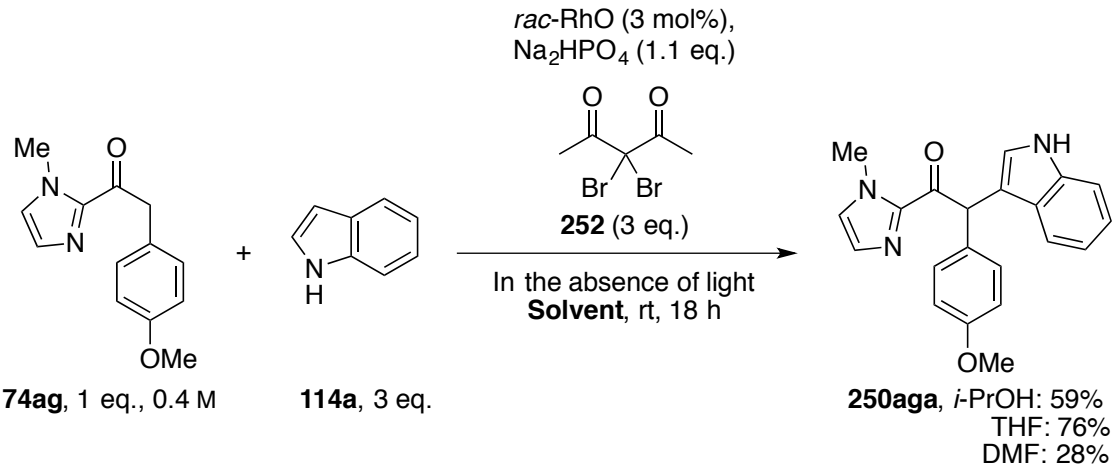

Scheme 83: Solvent screening with RhO as catalyst.

Next, we evaluated the influence of different bases in THF and found out that 2,6-lutidine gave highest yield (89%, Table 15, entry 3), while cesium carbonate and amines gave low yields of **250aga** (43% and 42%, entries 2, 4, and 5).

Table 15: Results of base screening.

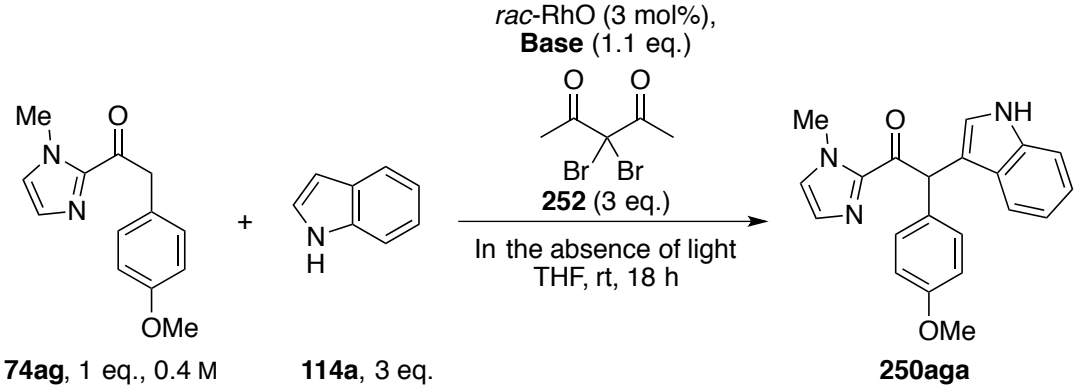

Entry	Base	Yield
1	Na_2HPO_4	76 %
2	Cs_2CO_3	67 %
3	2,6-Lutidine	89 %
4	2,2,6,6-Tetramethylpiperidine	43 %
5	Triethylamine	42 %

3.3.5. Evaluation of the Arene Scope

We then explored the arene scope of the reaction using 2-acyl imidazole substrate **74ag**. To our delight, the yield of **250agb** was improved to 81% by using rhodium catalyst RhO compared to 69% with iridium catalyst IrO (see Scheme 78). Substituents on the 5- and 6- position of the indole ring are well-tolerated and both electron-rich and electron-deficient indoles could be coupled with **74ag** to give products **250agd**,

250age, and **250agf** in good yields. Notably, apart from indoles, other electron-rich arenes such as benzenes and pyrroles are suitable arenes for the reaction (**253** and **254**) (Scheme 84).

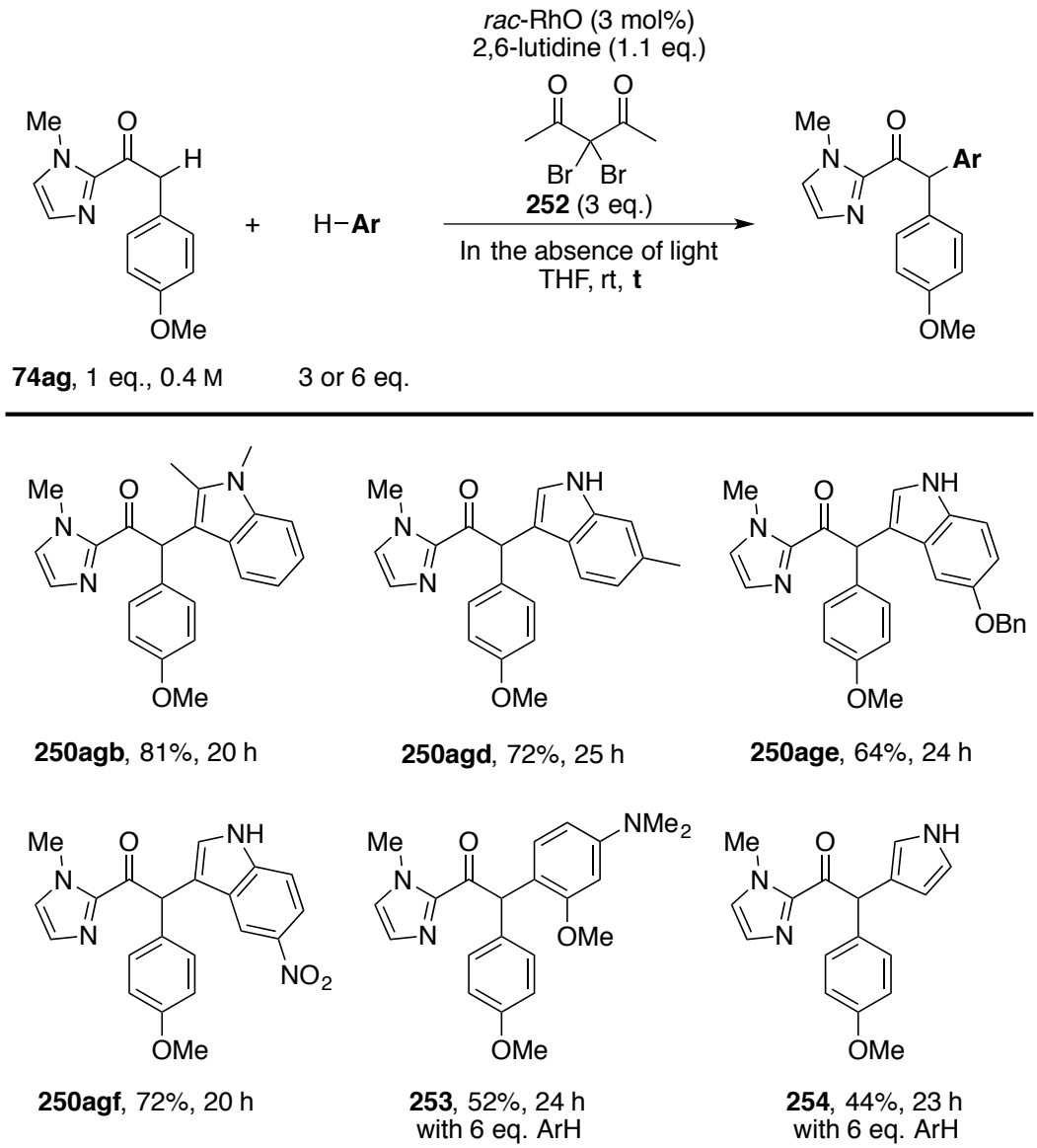

Scheme 84: Arene scope of the direct α-arylation of 2-acyl imidazoles.

3.3.6. Conclusion and Future Perspectives

With the initial goal to use diethyl bromomalonate (**93a**) in a photocatalyzed asymmetric α-alkylation of 2-acyl imidazoles, we developed a racemic variant of the rhodium Lewis acid catalyzed direct α-arylation of 2-acyl imidazoles. According to our mechanistic studies, the reaction proceeds through a Lewis acid catalyzed bromination and a subsequent Friedel-Crafts alkylation. While electron-rich imidazole substrates (e.g. **74ag**) could be used in the reaction without any problems, electron-neutral imidazoles (e.g. **74aa**) already required the addition of a silver(I) salt to proceed the formation of the corresponding carbocation **245**. The reaction does not work with alkyl substituted 2-acyl imidazole (e.g. **74bh**), which only give brominated intermediate **251** as product.

In order to make the method more attractive, further optimizations could be done in the future. As the method gives racemic product, the *tert*-butyl substituents on the catalyst are no longer necessary. The means that rhodium complexes **255** and **256** are probably able to catalyze the reaction as well, whose synthesis is much easier (Figure 13).

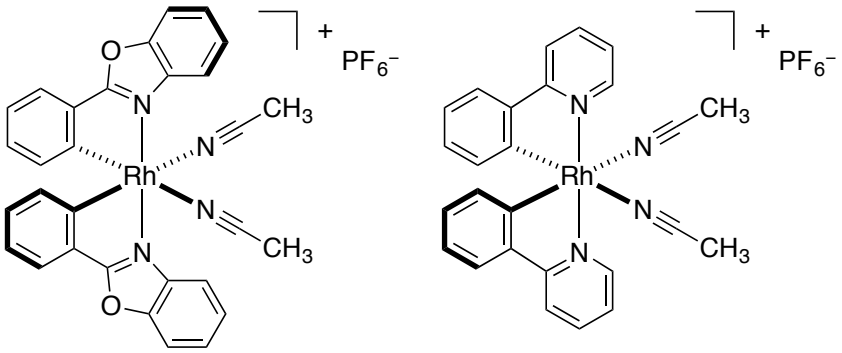

255 **256**

Figure 13: Rhodium complexes with less-complicated structure are probably able to catalyze the reaction as well.

Second, the amounts of the bromination reagent and the arenes might be reduced by increase of reaction concentration and temperature. In addition, the synthetic value of this method could be demonstrated by performing the syntheses of the two endothelia antagonists UK-350,926 (**257**) and UK-349,862 (**258**).[190] 2-Acyl imidazole **74ai** seems to be a suitable substrate for the direct α-arylation method due to the electron-rich nature of the phenyl substituent. Direct conversion of arylated products **250aig** and **250aih** to endothelia antagonists **257** and **258** should be feasible due to the existence of well-established procedures to remove the imidazolyl group and introduce other groups such as sulfonamide **259** (Scheme 85).[115,122,151,191,192]

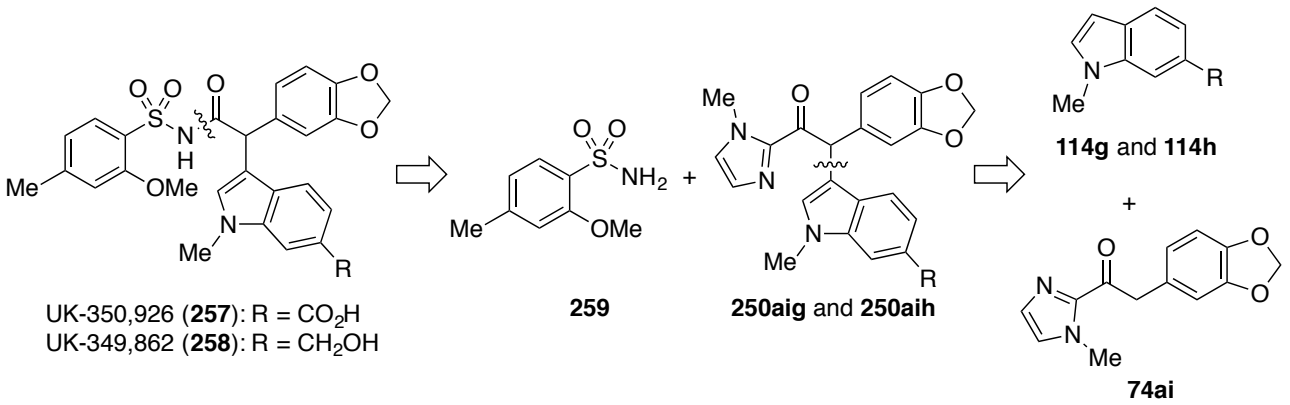

Scheme 85: Retrosynthesis of UK-350,926 and UK-349,862 based on the chiral-at-metal Lewis acid catalyzed direct α-arylation of 2-acyl imidazoles.

Chapter 4. Summary and Outlook

In conclusion, the chiral-at-metal iridium(III) and rhodium(III) Lewis acids have demonstrated their excellent configurational stability and their capacity to facilitate the enolization of 2-acyl imidazoles. Based on this, various α-functionalization methods for 2-acyl imidazoles could be developed with high efficiency in terms of both yield and enantioselectivity. In this thesis, the successful development of an asymmetric α-alkylation with α-cyanoalkyl bromides and a racemic direct α-arylation have been described. In addition, an asymmetric α-benzoyloxylation has been developed which remains to be further improved (Scheme 86). As mechanistic studies of all these three reactions revealed, the nucleophilic metal enolate complexes are capable of reacting with various electrophiles directly without pre-activation.

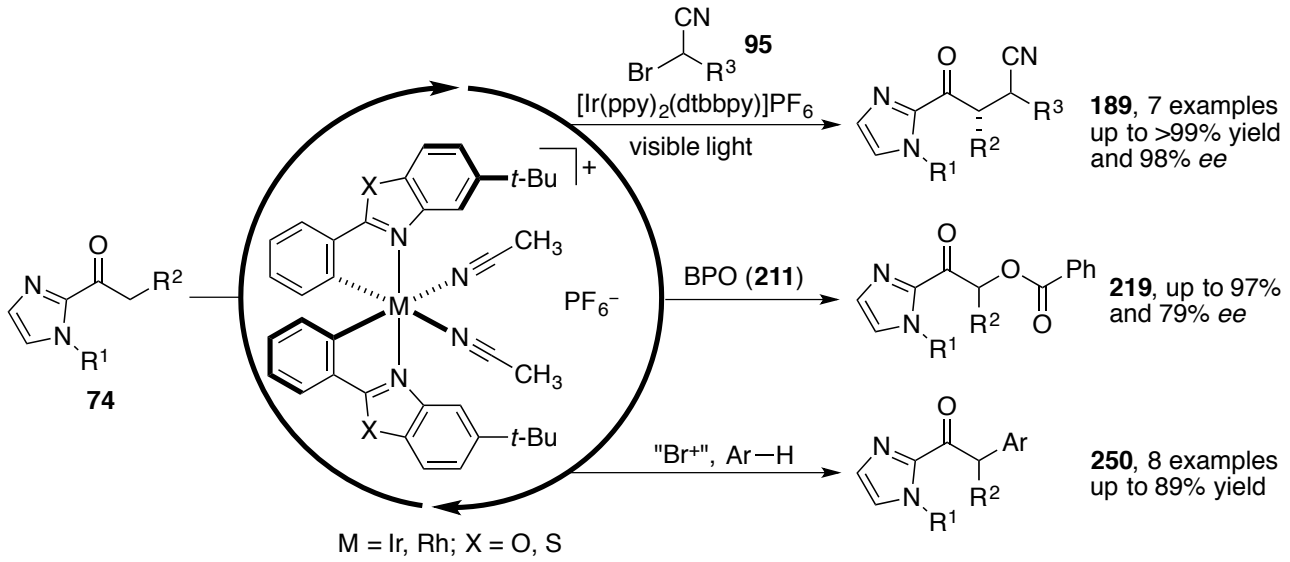

Scheme 86: Chiral-at-metal iridium(III) and rhodium(III) catalyzed α-functionalization of 2-acyl imidazoles.

Besides the future perspectives for these three processes which have been discussed beforehand, further efforts should be spent on expanding the substrate scope, especially on replacing imidazolyl by other readily accessible groups, in order to enable a more convenient substrate synthesis and product derivatization. For instance, *N*-acyl pyrazoles are promising as they have already been successfully employed in several reactions[122,138,193,194] and the reactivity of this class of compounds remains to be explored.

As mentioned in Chapter 3.1.6 (p. 45), the mechanistic investigations of the asymmetric α-alkylation of 2-acyl imidazoles **74** with azides **122** and α-diazoacetates **125** from the Meggers group[115] has provided useful informations to our current studies. Furthermore, it is impressive to see that it is actually rhodium enolate complex **197** that acts as a reductive quencher to initiate the reaction (Scheme 87a) and the resulting α-keto radical **199** was successfully captured by silyl enol ether **200** (Scheme 87b).

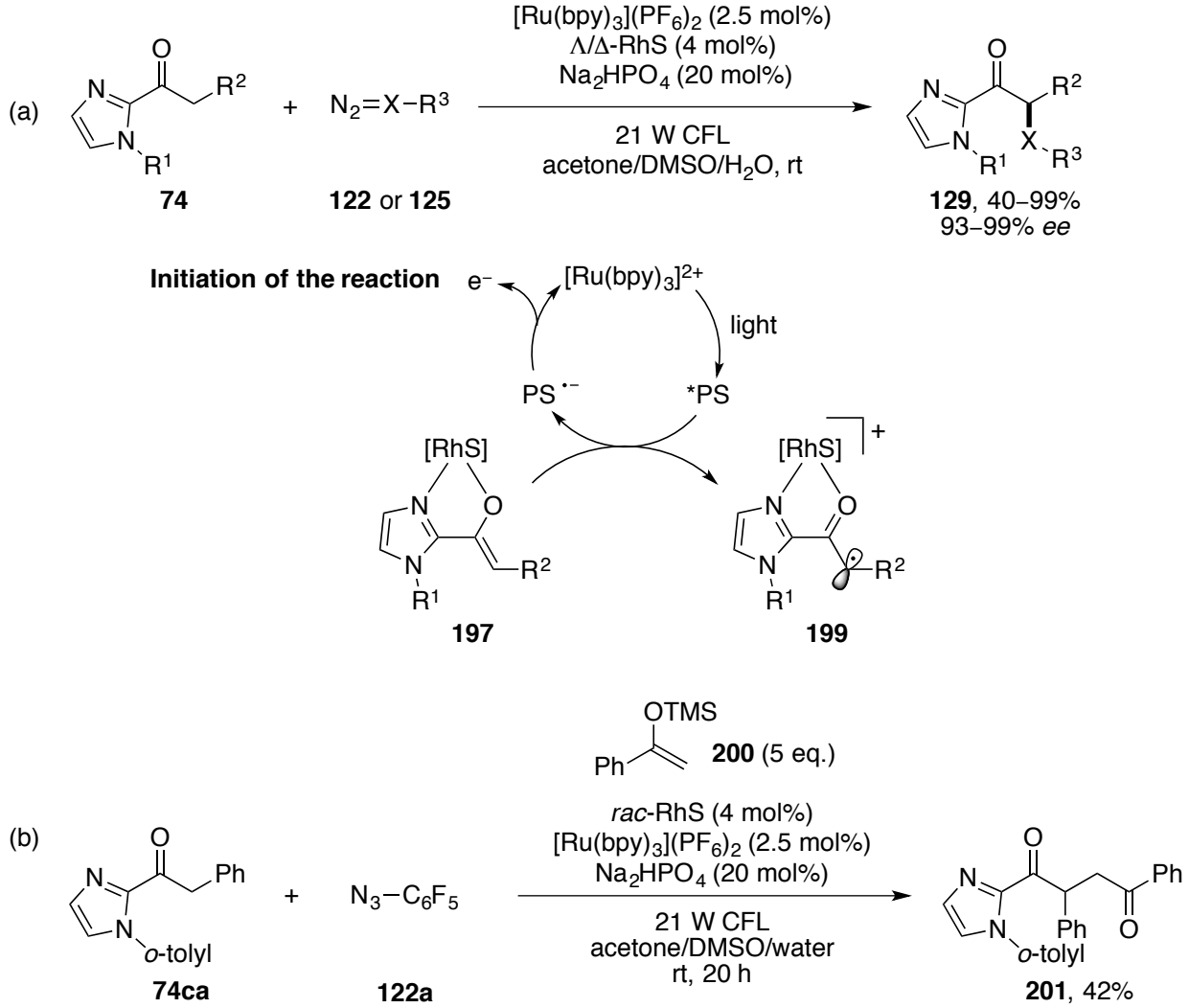

Scheme 87: Asymmetric α-alkylation of 2-acyl imidazoles with azides or diazoacetates and the experimental support for the existence of the α-keto radical.[115]

This observation has the potential to lead to further applications of our chiral-at-metal Lewis acids in enantioselective photoredox catalysis with visible light. It will be intriguing to see whether compound **201** is formed with any selectivity in the presence of an enantiopure catalyst. From a mechanistic perspective, the formation of compound **201** is highly similar to MacMillan's SOMO-organocatalysis instead of the photoredox catalysis with chiral imidazolidinones. Although these two processes share several similarities, such as the radical nature, the resulting products (enantioenriched α-alkylated aldehydes), and the chiral imidazolidinone catalysts, the photoredox catalysis should not be considered as the visible-light version of the SOMO-organocatalysis. In case of photoredox catalysis, the active chiral intermediate is the enamine, which reacts with with electron-deficient radicals under stereocontrol, whereas the enamine gets oxidized in SOMO-organocatalysis to form a radical intermediate and reacts with various SOMO-philes (Figure 14).

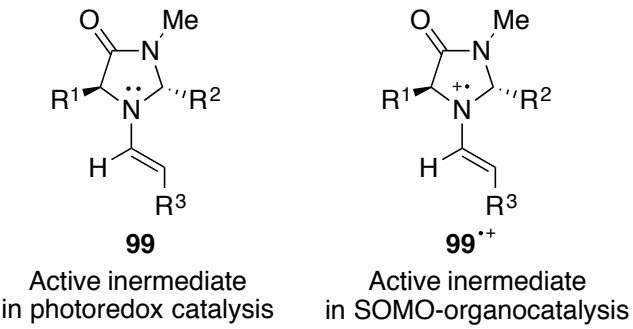

Figure 14: Structures of the active intermediates for MacMillan's photoredox catalysis and SOMO-organocatalysis.

MacMillan and co-workers noted this difference regarding intermediate in the asymmetric α-nitroalkylation of aldehydes via oxidative organocatalysis.[195] They discovered that depending on the reaction conditions, product **261** was formed with different diastereoselectivity (Table 16).

Table 16: Asymmetric α-nitroalkylation of aldehydes via oxidative organocatalysis, diastereoselectivity varies from the reaction conditions.[195]

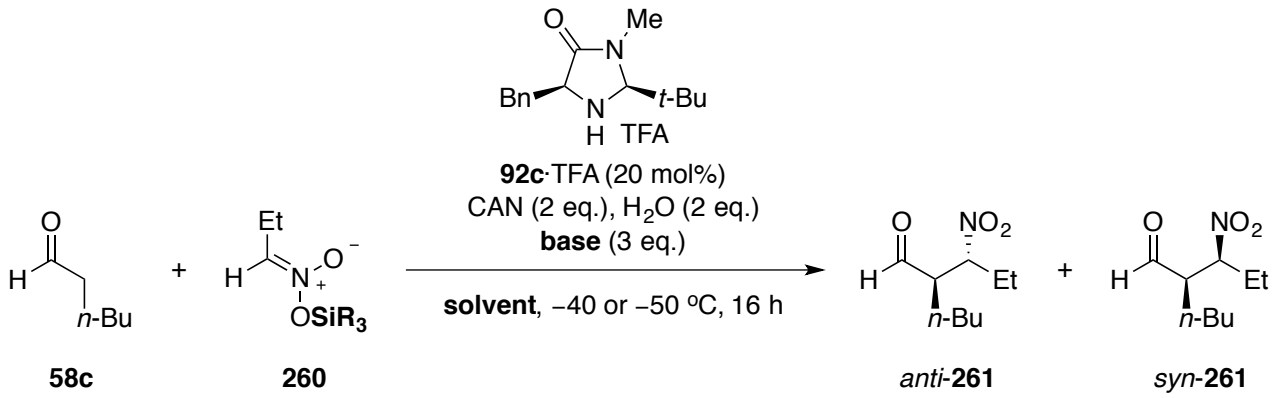

Entry	SiR_3	Base	Solvent	Yield	*ee*	*anti*/*syn*
1	TBS	NaO_2CCF_3	Acetone	68 %	94 %	1:6
2	TIPS	$NaHCO_3$	THF	84 %	90 %	5:1

The authors suggested that the difference of the diastereoselectivity arises from whether enamine **99cc** or nitronate **260** gets oxidized by ceric ammonium nitrate and through variation of the silyl protective group and reaction conditions, a selective oxidation can be achieved (Scheme 88).

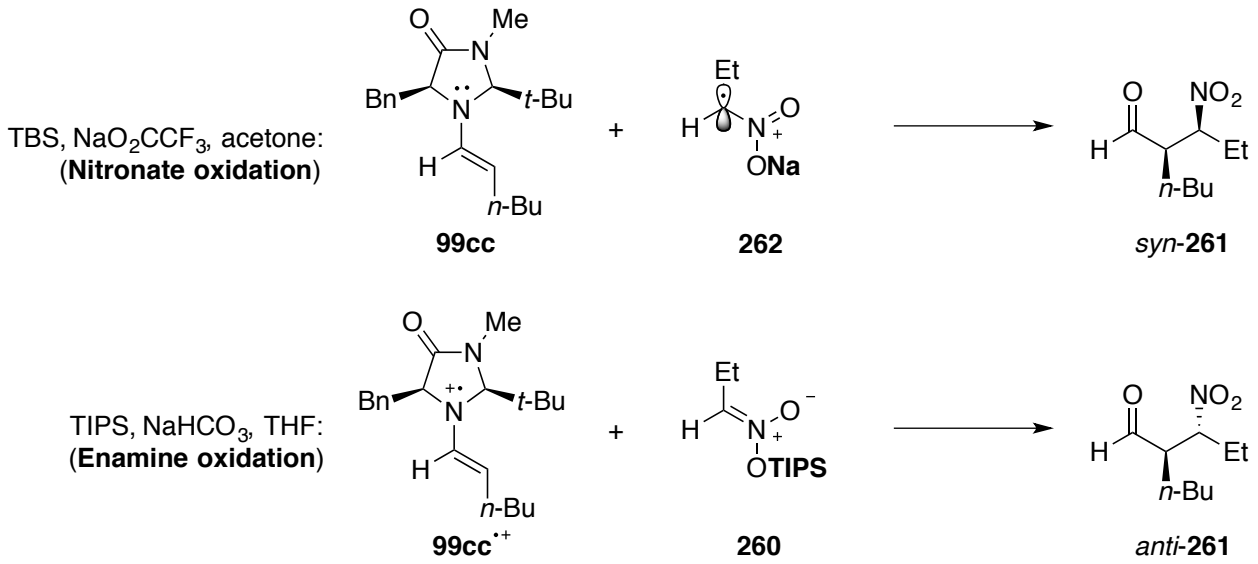

Scheme 88: MacMillan and co-workers proposed that the diastereoselectivity of the reaction is determined by whether nitronate or enamine gets oxidized.[195]

Although both SOMO-organocatalysis[181,195-198] and photoredox catalysis [88,98-100] with chiral imidazolidinones have been well-established, it is not until very recently that MacMillan and co-workers have successfully employed enamine radical cation in asymmetric photoredox catalysis,[199] where alkenes were employed as SOMO-philes to react with the enamine radical cation, the following hydrogen-atom transfer (HAT) with a thiolphenol catalyst and hydrolysis afforded enantioenriched alkylated aldehydes **262** (Scheme 89).[199]

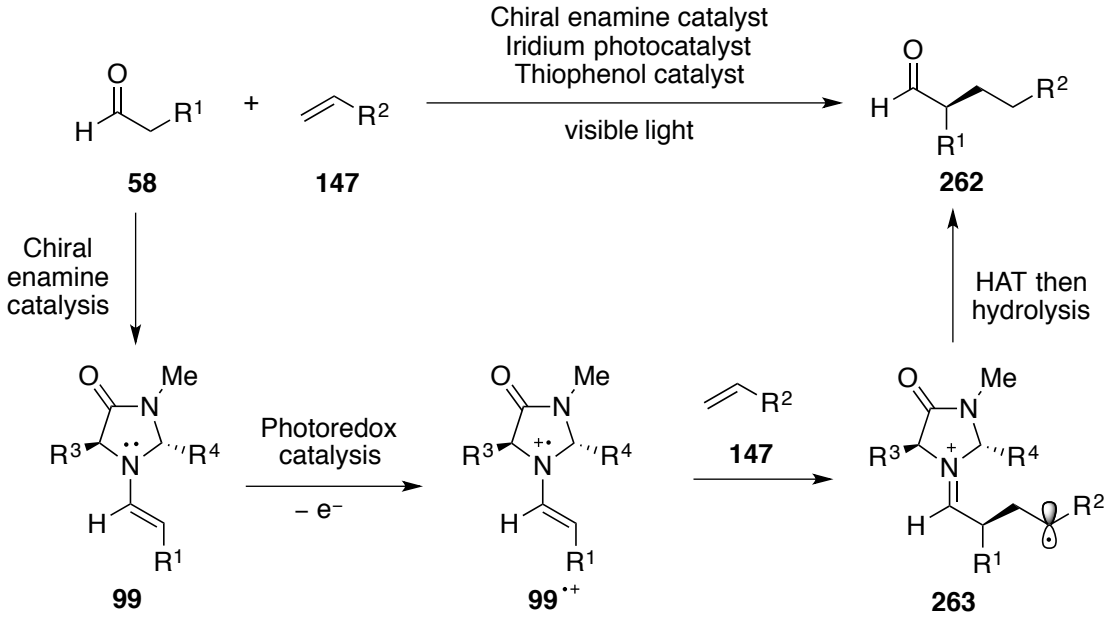

Scheme 89: MacMillan's enantioselective α-alkylation of aldehydes by merging photoredox, enamine, and HAT-catalysis.[199]

Due to the similarity between α-keto radical **199** of the enamine radical cation, the combination our chiral-at-metal rhodium Lewis acid catalyst RhS and the photoredox catalyst $[Ru(bpy)_3]^{2+}$ could potentially disclose a

series of interesting enantioselective transformations according to MacMillan's SOMO-organo-catalysis and the aforementioned reaction (see Scheme 87b) serves as an excellent starting point for further investigations. One obvious challenge is that the chiral rhodium catalyst is not required for the bond formation step and α-keto radical **264** could be captured without coordinating to the metal center (Scheme 90). However, this should be overcome by employing excess amounts of silyl enol ether **200**.

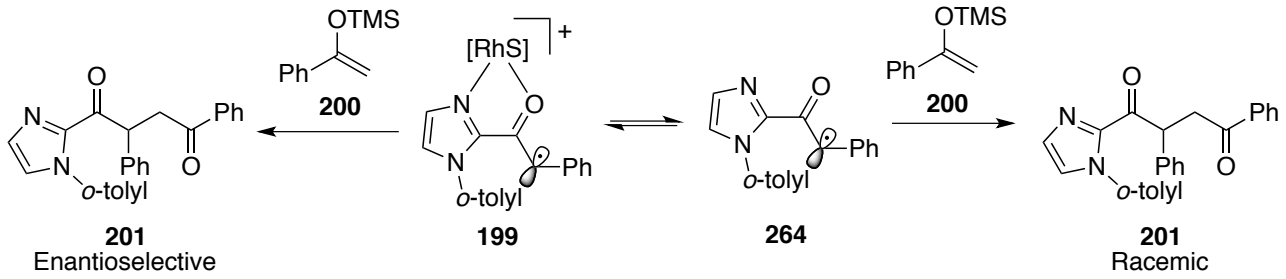

Scheme 90: As the chiral rhodium catalyst is not required for the bond formation step and the possible release of α-keto radical **264** results in racemic reaction.

Chapter 5. Experimental Section

5.1. Methods and Materials

General Methods for Syntheses: All air- and moisture sensitive reactions were carried out under nitrogen atmosphere. Glassware was heated to 630 ºC with a heat gun for 10 min under vacuum and refilled with moisture-free nitrogen prior to use. Room Temperature is defined as 20−22 ºC. Reactions with visible-light were performed by placing one or two 13-Watt Osram DULUXSTAR TWIST compact fluorescent lamps (CFL, 13W/840 E27, 850 Lumens) in front of the Schlenk-tubes. The distance between the lamps and the Schlenk-tubes was approximately 10 cm as shown in Figure 15. In the cases that reactions were performed in the absence of light, the Schlenk-tubes or flasks were wrapped up with aluminum foil, before the reactions were carried out.

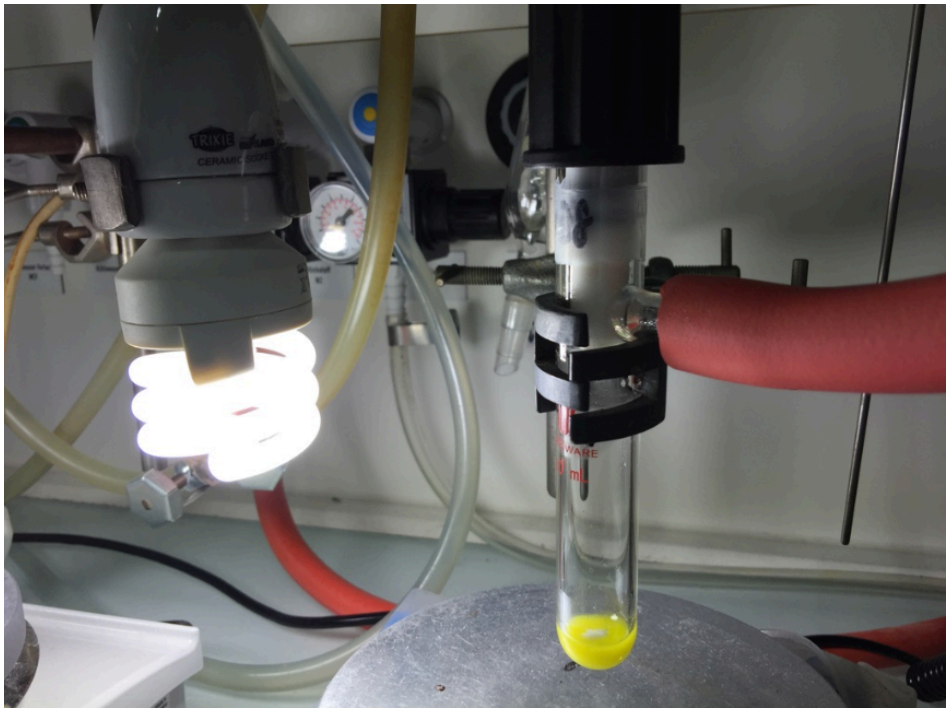

Figure 15: Exemplary setup of the photoreactions with visible light.

Solvents: The solvents for reactions were distilled from sodium/benzophenone (THF, Et_2O) or calcium hydride (CH_3CN, CH_2Cl_2, $CHCl_3$, toluene, DMF). *N*-methyl-2-pyrrolidone (NMP) and methanol were dried over molecular sieves and stored under nitrogen atmosphere. HPLC-grade ethanol, *iso*-propanol, acetone and reagent grade *N*,*N*-dimethyl-acetamide (DMA), xylene, 1,2-dimethoxyethane, nitromethane, 1,4-dioxane, and dimethylsulfoxide (DMSO) were purchased and used without further purification. The solvents for extraction and chromatography were distilled on rotary evaporator at 40 °C prior to use.

Materials: All reagents were purchased from commercial suppliers and used directly. The synthesized reagents were either employed directly or stored in sealed vessels at 4 ºC prior to use.

Thin Layer Chromatography: Thin layer chromatography (TLC) was performed with aluminum TLC plates coated with silica gel (Merck DC Kieselgel 60 F_{254}). The visualization of the compounds was achieved by either using a UV lamp (λ = 254 or 366 nm) or by immersing the developed plates in iodine stain or potassium permanganate dip.

Column Chromatography: Column chromatography was performed with silica gel 60 M from Machery-Nagel as stationary phase. Compressed air was used in order to build up pressure for flash column chromatography.

Centrifugation: Centrifugation was performed on an Eppendorf Centrifuge 5810R.

Nuclear Magnetic Resonance Spectroscopy: NMR spectra were recorded on Bruker DRX 500 (^{1}H-NMR: 500 MHz, ^{13}C-NMR: 125 MHz) or Bruker AV 300 (^{1}H-NMR: 300 MHz, ^{13}C-NMR: 75.5 MHz) at room temperature. The chemical shifts δ are given in ppm (parts per million) relative to tetramethylsilane (TMS, δ = 0 ppm) and NMR standards for calibration are as follows: ^{1}H-NMR: δ = 7.26 ($CDCl_3$), 5.31 (CD_2Cl_2), 3.31 (CD_3OD), 2.50 (DMSO-*d*$_6$); ^{13}C-NMR: δ = 77.16 ($CDCl_3$), 53.80 (CD_2Cl_2), 39.52 (DMSO-d_6). Coupling constants *J* are calculated according to the recorded spectra in hertz (Hz). The multiplicities of the signals are described as s = single, d = doublet, t = triplet, q = quartet, m = multiplet and combinations thereof.

Mass Spectrometry: High-resolution mass spectra (HRMS) were recorded on a Brusker En Apex Ultra 7.0 TFT-MS(ESI+) instrument using ESI technique by the staffs of the department for mass spectrometry on the chemistry faculty, Philipps-University of Marburg.

Chiral HPLC Analysis: Chiral HPLC analysis was carried out with Agilent 1200 HPLC system. Daicel Chiralpak AD-H column (internal diameter: 4.60 mm, length = 250 mm) and Daicel Chiralpak IC column (internal diameter: 4.60 mm, length = 250 mm) were used as stationary phase. As mobile phase, commercially available HPLC grade hexanes and *i*-PrOH were used directly.

Single-Crystal X-Ray Diffraction Studies: X-ray data were collected with a Bruker D8 QUEST area Detektor. Measurement and evaluation of the data were performed by the staffs of the department for crystal structure analysis on the chemistry faculty, Philipps-University of Marburg. The obtained crystal structure was refined by Dr. Klaus Harms.

5.2. Synthesis of Catalysts

The catalysts were synthesized according to literature. To determine the absolute configuration and the enantiopurity of the catalysts, ^{1}H-NMR spectra of the metal auxiliary complexes with literature.

5-(*tert*-Butyl)-2-phenylbenzo[*d*]oxazole (265)[57]

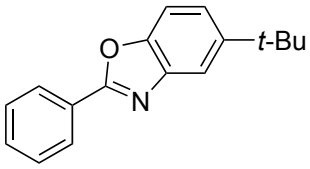

2-Amino-4-(*tert*-butyl)phenol (1.65 g, 10.0 mmol) and benzaldehyde (1.00 mL, 10.0 mmol) were added to *m*-xylene (33 mL). After stirring for 0.5 h at 120 ºC, 4-methoxy-TEMPO (93.0 mg, 500 μmol) was added and reaction mixture was stirred at 120 ºC for 20 h in the presence of air. The mixture was cooled to rt and concentrated under vacuum, the residue was purified through flash column chromatography on silica gel (*n*-hexane:EtOAc 20:1) to afford the product (2.04 g, 8.12 mmol, 81%) as white solid.

^{1}H-NMR (300 MHz; $CDCl_3$): δ 8.26 (ddd, *J* = 5.4, 2.9, 1.4 Hz, 2H), 7.84 (dd, *J* = 1.9, 0.5 Hz, 1H), 7.52−7.47 (m, 4H), 7.41 (dd, *J* = 8.6, 1.9 Hz, 1H), 1.41 (s, 9H, 3CH_3);

^{13}C-NMR (75.5 MHz; $CDCl_3$): δ 163.2 (N=*C*-O), 148.9 (O*C*CN), 148.1 (*C*-*t*-Bu), 142.2 (OC*C*N), 131.3 (C_{Ph}), 128.9 (2C_{Ph}), 127.6 (2C_{Ph}), 127.5 (C_{Ph}), 122.9 (OC*C*HC-*t*-Bu), 116.6 (NC*C*HC-*t*-Bu), 109.8 (O*C*CHC-*t*-Bu), 35.0 (*C*Me_3), 31.9 (3*C*H_3);

HRMS(ESI+) calcd. for $C_{17}H_{18}NO$ $(M + H)^+$ 252.1383, found: 252.1392.

1-(Bromo)-4-(*tert*-butyl)-2-nitrobenzene (266)[58]

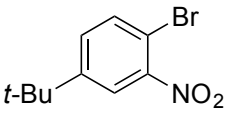

A mixture of HNO_3 (1.40 mL, 65% in H_2O) and H_2SO_4 (2.10 mL, 98%) was added dropwise to 1-bromo-4-(*tert*-butyl)benzene (2.00 mL, 11.7 mmol) at 0 ºC. After warming to rt, the mixture was stirred at rt for 18 h, then quenched with ice, and extracted with *n*-hexane (3 × 20 mL). The organic layers were combined, dried over Na_2SO_4, and concentrated under vacuum to afford the product (3.02 g, 11.7 mmol, >99%) as pale yellow oil.

^{1}H-NMR (300 MHz; $CDCl_3$): δ 7.83 (d, *J* = 2.3 Hz, 1H, *t*-BuCC*H*CNO_2), 7.64 (d, *J* = 8.5 Hz, 1H, BrCC*H*), 7.44 (dd, *J* = 8.5, 2.4 Hz, 1H, CHC*H*C-*t*-Bu), 1.34 (s, 9H, 3CH_3).

5-(*tert*-Butyl)-2-phenylbenzo[*d*]thiazole (267)[200]

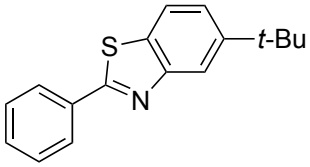

1-Bromo-4-(*tert*-butyl)-2-nitrobenzene (3.02 g, 11.7 mmol), benzyl amine (3.20 mL, 29.3 mmol) and sulfur (562 mg, 17.6 mmol) were added to pyridine (2.4 mL) under nitrogen atmosphere. The mixture was stirred at 100 ºC for 18 h, cooled to rt, and concentrated under vacuum. The residue was diluted with CH_2Cl_2 and then filtered over celite. The filtrate was concentrated under vacuum and the residue was purified through flash column chromatography on silica gel (*n*-hexane then *n*-hexane:EtOAc 40:1) to afford the product (2.12 g, 7.93 mmol, 68%) as yellow solid.

^{1}H-NMR (300 MHz; $CDCl_3$): δ 8.13 (dd, *J* = 1.9, 0.5 Hz, 1H), 8.10−8.08 (m, 2H), 7.84−7.81 (m, 1H), 7.51−7.48 (m, 4H), 1.43 (s, 9H, 3C*H*$_3$);

^{13}C-NMR (75.5 MHz; $CDCl_3$): δ 168.3 (N=*C*-S), 154.5 (S*C*CN), 150.3 (*C*-*t*-Bu), 133.9 (SC*C*N), 132.1 (C_{Ph}), 131.0 (C_{Ph}), 129.1 (2C_{Ph}), 127.6 (2C_{Ph}), 123.6 (SC*C*HC-*t*-Bu), 121.1 (NC*C*HC-*t*-Bu), 119.8 (S*C*CHC-*t*-Bu), 35.1 (*C*Me$_3$), 31.7 (3*C*H$_3$);

HRMS(ESI+) calcd. for $C_{17}H_{18}NS$ $(M + H)^+$ 268.1154, found: 268.1157.

Iridium(III) dimer derived from 5-(*tert*-butyl)-2-phenylbenzo[*d*]oxazole (268)[57]

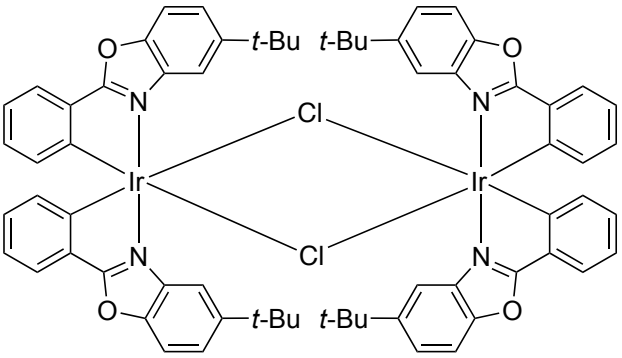

Iridium(III) chloride trihydrate (580 mg, 1.64 mmol) and 5-(*tert*-butyl)-2-phenylbenzo[*d*]oxazole (909 mg, 3.62 mmol) were added to 2-ethoxyethanol (56.0 mL) and water (18.7 mL) under nitrogen atmosphere. The mixture was heated to 120 ºC under reflux for 24 h. After cooling to rt, the yellow precipitates were obtained through filtration and then washed with water and diethyl ether. The yellow solid (1.23 g, 844 μmol, >99%) were dried under air and used without further purification.

^{1}H-NMR (300 MHz; CD_2Cl_2): δ 8.31 (dd, *J* = 1.7, 0.7 Hz, 4H), 7.58−7.55 (m, 4H), 7.28−7.21 (m, 8H), 6.86 (td, *J* = 7.4, 1.0 Hz, 4H), 6.65−6.59 (m, 4H), 6.07 (dd, *J* = 7.8, 0.3 Hz, 4H), 1.23 (s, 36H, 9C*H*$_3$);

^{13}C-NMR (75.5 MHz; CD_2Cl_2): δ 177.0, 149.1, 148.1, 144.4, 139.8, 132.9, 131.6, 130.5, 125.7, 123.6, 121.8, 115.1, 110.6, 35.3, 31.7.

Iridium(III) dimer derived from 5-(*tert*-butyl)-2-phenylbenzo[*d*]thiazole (269)[58]

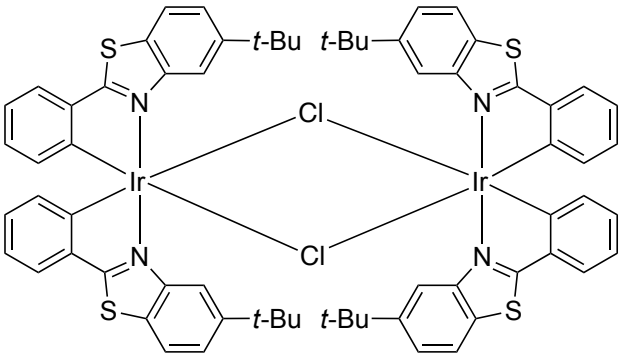

Iridium(III) chloride trihydrate (500 mg, 1.42 mmol) and 5-(*tert*-butyl)-2-phenylbenzo[*d*]thiazole (834 mg, 3.12 mmol) were added to 2-ethoxyethanol (48.0 mL) and water (16.0 mL) under nitrogen atmosphere. The mixture was heated to 120 ºC under reflux for 24 h and then cooled to rt. The orange precipitates were obtained through filtration and then washed with water and diethyl ether. The orange solid (637 mg, 419 μmol, 59%) were dried under air and used without further purification.

^{1}H-NMR (300 MHz; CD_2Cl_2): δ 8.88 (d, *J* = 1.7 Hz, 4H), 7.48 (dd, *J* = 7.6, 1.2 Hz, 4H), 7.43 (d, *J* = 8.5 Hz, 4H), 7.29 (dd, *J* = 8.6, 1.8 Hz, 4H), 6.76 (td, *J* = 7.4, 1.0 Hz, 4H), 6.39 (td, *J* = 7.5, 1.1 Hz, 4H), 5.94 (d, *J* = 7.8 Hz, 4H), 1.22 (s, 36H, 12C*H*$_3$);

^{13}C-NMR (75.5 MHz; CD_2Cl_2): δ 179.3, 151.8, 150.3, 145.9, 142.2, 133.9, 129.2, 127.9, 125.4, 122.7, 121.75, 121.67, 120.3, 35.6 (4*C*Me$_3$), 31.8 (12*C*H$_3$).

Rhodium(III) dimer derived from 5-(*tert*-butyl)-2-phenylbenzo[*d*]oxazole (35)[59]

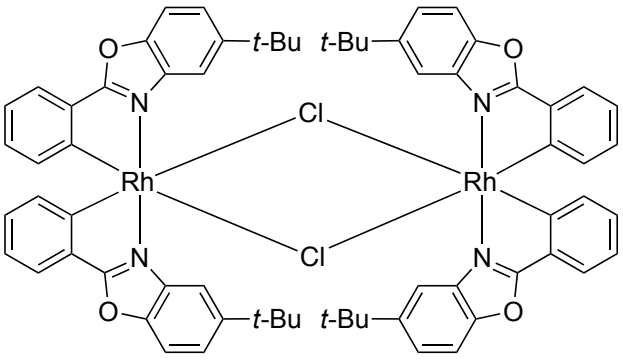

Rhodium(III) chloride trihydrate (419 mg, 2.00 mmol) and 5-(*tert*-butyl)-2-phenylbenzo[*d*]oxazole (1.03 g, 4.10 mmol) were added to 2-ethoxyethanol (69.0 mL) and water (23.0 mL) under nitrogen atmosphere. The mixture was heated to 120 ºC under reflux for 24 h and then cooled to rt. The black precipitates were collected through centrifuge, washed with CH_3OH and extracted with CH_2Cl_2. Evaporation of the solvent under vacuum afforded the product as pale yellow solid (746 mg, 584 μmol, 58%).

^{1}H-NMR (300 MHz; CD_2Cl_2): δ 8.39 (t, *J* = 1.2 Hz, 4H), 7.66 (dd, *J* = 7.6, 1.2 Hz, 4H), 7.22 (d, *J* = 1.0 Hz, 8H), 6.97 (td, *J* = 7.4, 1.0 Hz, 4H), 6.77 (td, *J* = 7.6, 1.5 Hz, 4H), 6.13 (d, *J* = 7.8 Hz, 4H), 1.23 (s, 36H, 12C*H*$_3$);

^{13}C-NMR (75.5 MHz; CD_2Cl_2): δ 170.4, 170.3, 164.8, 164.3, 148.9, 147.9, 139.6, 139.5, 133.5, 131.20, 131.18, 131.1, 125.4, 123.9, 123.0, 115.8, 110.4, 35.3 (4*C*Me$_3$), 31.7 (12*C*H$_3$).

Racemic iridium(III) Lewis acid catalyst derived from 5-(*tert*-butyl)-2-phenylbenzo[*d*]oxazole (*rac*-IrO, 60)

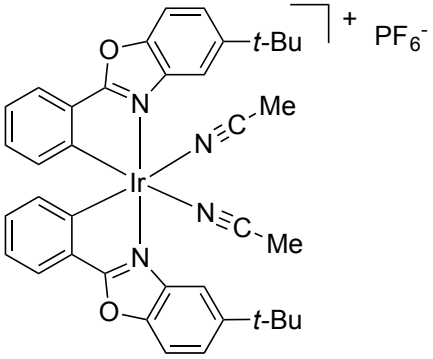

Iridium dimer **268** (500 mg, 343 mmol) and $AgPF_6$ (191 mg, 755 mmol) were added to acetonitrile (114 mL) under nitrogen atmosphere. The mixture was stirred at 50 ºC for 18 h and then cooled to rt. After evaporating the solvent under vacuum, the residue was purified through flash column chromatography on silica gel (CH_2Cl_2:CH_3CN 30:1) to afford the product as yellow solid (630 mg, 685 μmol, >99%).

^{1}H-NMR (300 MHz; CD_2Cl_2): δ 7.77 (dd, *J* = 1.8, 0.6 Hz, 2H), 7.69−7.60 (m, 6H), 6.92 (td, *J* = 7.5, 1.1 Hz, 2H), 6.76 (td, *J* = 7.5, 1.5 Hz, 2H), 6.30−6.27 (m, 2H), 2.35 (s, 6H, 2CNC*H*$_3$), 1.38 (s, 18H, 2C(C*H*)$_3$);

^{13}C-NMR (75.5 MHz; CD_2Cl_2): δ 177.3, 151.1, 148.7, 142.0, 138.3, 132.9, 132.6, 130.0, 126.2, 125.0, 123.6, 120.8, 112.9, 111.9, 35.6, 31.7, 3.8;

HRMS(ESI+) calcd. for $C_{38}H_{38}IrN_4O_2$ (M^+) 775.2621, found: 775.2659.

Racemic rhodium(III) Lewis acid catalyst derived from 5-(*tert*-butyl)-2-phenylbenzo[*d*]oxazole (*rac*-RhO, 70)

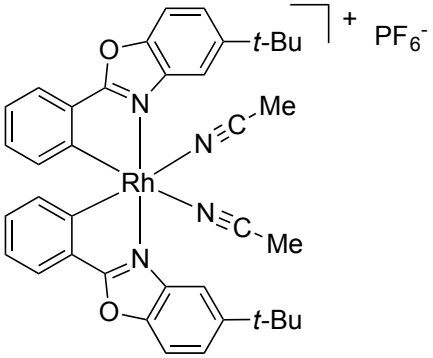

Rhodium dimer **35** (128 mg, 100 μmol) and $AgPF_6$ (55.6 mg, 220 μmol) were added to CH_3CN (33.3 mL) under nitrogen atmosphere. The mixture was stirred at 50 ºC for 18 h and then cooled to rt. After evaporating the solvent under vacuum, the residue was purified through column chromatography on silica gel (CH_2Cl_2 then CH_2Cl_2:CH_3CN 20:1) to afford the product as pale yellow solid (167 mg, 201 μmol, >99%).

^{1}H-NMR (300 MHz; CD_2Cl_2): δ 7.88 (s, 2H), 7.77−7.67 (m, 6H), 7.08 (td, *J* = 7.5, 1.0 Hz, 2H), 6.93 (td, *J* = 7.6, 1.5 Hz, 2H), 6.39 (d, *J* = 7.9 Hz, 2H), 2.30 (s, 6H), 1.46 (s, 18H);

^{13}C-NMR (75 MHz; CD_2Cl_2): δ 168.8, 148.4, 146.1, 135.4, 130.73, 130.69, 129.63, 129.62, 127.9, 123.6, 122.5, 121.9, 110.7, 109.2, 33.0, 29.1.

Racemic rhodium(III) Lewis acid catalyst derived from 5-(*tert*-butyl)-2-phenylbenzo[*d*]thiazole (*rac*-RhS, 71)[60]

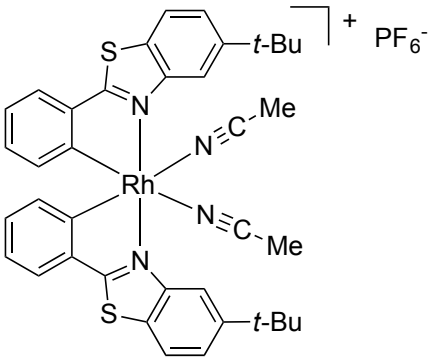

Rhodium(III) chloride trihydrate (100 mg, 478 μmol) and 5-(*tert*-butyl)-2-phenylbenzo[*d*]thiazole (307 mg, 478 μmol) were added to 2-ethoxyethanol (4.80 mL) under nitrogen atmosphere. The mixture was stirred at 125 ºC. A dark red solution was formed after 2 h and yellow precipitates were observed after 15 h. The mixture was cooled to rt and filtered. The residue was washed with water, dried under air to afford orange solid (177 mg), which were then added to acetonitrile (41.0 mL) and $AgPF_6$ (73.4 mg, 290 μmol). After stirring at 50 ºC for 18 h, the mixture was concentrated under vacuum and the residue was purified through flash column chromatography on silica gel (CH_2Cl_2 then CH_2Cl_2:CH_3CN 20:1) to afford the product as pale yellow solid (50.0 mg, 58.0 μmol, 12% over 2 steps).

^{1}H-NMR (300 MHz; CD_2Cl_2): δ 8.49 (s, 2H), 8.01 (d, *J* = 8.6 Hz, 2H), 7.71 (dd, *J* = 8.6, 1.8 Hz, 2H), 7.66 (dd, *J* = 7.6, 1.2 Hz, 2H), 7.03 (td, *J* = 7.5, 0.9 Hz, 2H), 6.83 (td, *J* = 7.6, 1.3 Hz, 2H), 6.20 (d, *J* = 7.7 Hz, 2H), 2.17 (s, 6H), 1.45 (s, 18H);

^{13}C-NMR (75.5 MHz; CD_2Cl_2): δ 176.8, 152.9, 150.0, 140.4, 133.5, 131.3, 129.1, 126.2, 125.5, 124.5, 122.9, 117.0, 35.6, 31.6, 3.6;

MS(ESI+) found: 635.7626, $C_{34}H_{32}N_2RhS_2$ $(M - 2CH_3CN)^+$.

Λ/Δ-(*S*)-Iridium auxiliary complex derived from 5-(*tert*-butyl)-2-phenylbenzo[*d*]oxazole (270)[57]

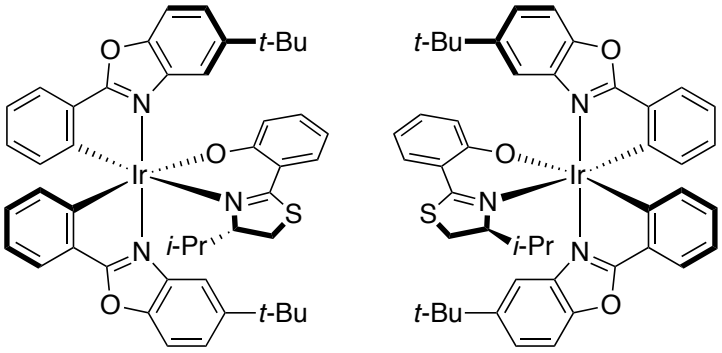

Iridium dimer **268** (250 mg, 172 μmol) and (*S*)-2-(4-isopropyl-4,5-dihydrothiazol-2-yl)phenol (102 mg, 429 μmol) were added to ethanol (17.2 mL) under nitrogen atmosphere. After adding triethylamine (238 μL, 1.72 mmol), the mixture was stirred at 95 ºC for 24 h. The homogeneous solution was cooled to rt and kept at rt without stirring for further 24 h, during which yellow precipitates were formed. The precipitates were obtained through filtration and identified as complex Δ-(*S*)-**270** (109 mg, 119 μmol, 35%) by comparing its ^{1}H-NMR data to literature.[57] The filtrate was concentrated under vacuum and purified through column

chromatography on silica gel (CH_2Cl_2:*n*-hexane 2:1) to afford complexes Δ-(*S*)-**270** (41.0 mg, 44.9 μmol, 13%) and Λ-(*S*)-**265** (153 mg, 168 μmol, 49%) respectively.

Λ-(*S*)-**270**:

^{1}H-NMR (300 MHz; CD_2Cl_2): δ 7.96 (d, *J* = 1.5 Hz, 1H), 7.70 (dd, *J* = 7.6, 0.8 Hz, 1H), 7.65−7.55 (m, 3H), 7.52−7.47 (m, 3H), 7.44 (dd, *J* = 1.8, 0.5 Hz, 1H), 7.14 (ddd, *J* = 8.6, 6.8, 1.8 Hz, 1H), 6.97−6.82 (m, 3H), 6.79−6.73 (m, 2H), 6.70−6.67 (m, 1H), 6.37 (dd, *J* = 7.6, 0.5 Hz, 1H), 6.28 (s, 1H), 4.72 (ddd, *J* = 9.8, 2.6, 1.7 Hz, 1H), 3.38 (dd, *J* = 11.6, 9.8 Hz, 1H), 3.01 (dd, *J* = 11.7, 1.6 Hz, 1H), 1.45 (s, 9H), 1.19 (s, 9H), 0.23 (d, *J* = 7.0 Hz, 3H), 0.15 (d, *J* = 7.0 Hz, 3H).

Δ-(*S*)-**270**:

^{1}H-NMR (300 MHz; CD_2Cl_2): δ 7.96 (d, *J* = 1.9 Hz, 1H), 7.73−7.60 (m, 3H), 7.55−7.49 (m, 2H), 7.44 (dd, *J* = 7.1, 1.7 Hz, 2H), 7.37 (dd, *J* = 8.0, 1.7 Hz, 1H), 7.02 (ddd, *J* = 8.5, 7.0, 1.6 Hz, 1H), 6.95−6.88 (m, 2H), 6.84−6.73 (m, 3H), 6.60 (dd, *J* = 8.5, 0.6 Hz, 1H), 6.47−6.44 (m, 1H), 6.32−6.27 (m, 1H), 3.63 (dd, *J* = 8.3, 1.6 Hz, 1H), 2.91 (dd, *J* = 11.3, 1.9 Hz, 1H), 2.68 (t, *J* = 10.6 Hz, 1H), 2.14 (dtd, *J* = 13.7, 6.8, 1.4 Hz, 1H), 1.27 (s, 9H), 1.19 (s, 9H), 1.06 (d, *J* = 6.8 Hz, 3H), 0.05 (d, *J* = 7.0 Hz, 3H).

Λ-L-Rhodium prolinate complex derived from 5-(*tert*-butyl)-2-phenylbenzo[*d*]oxazole (37)[59]

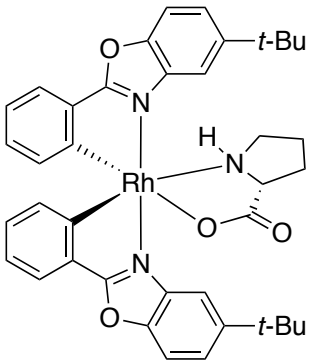

Sodium methoxide (16.2 mg, 300 μmol) was dissolved in CH_3OH (16.0 mL) and L-proline (34.5 mg, 300 μmol) was added in one portion. The mixture was stirred at rt under nitrogen atmosphere for 10 min and then rhodium dimer **35** (201 mg, 150 μmol) was added. The mixture was stirred at 50 ºC for 12 h and then cooled to rt. CH_2Cl_2 (16.0 mL) was added and the reaction mixture was stirred at rt for further 12 h. The solvent was removed by evaporation and the residue was taken up with CH_2Cl_2/Et_2O (5.00 mL, v/v 1:6), the precipitates were obtained through centrifuge and then washed with CH_2Cl_2/Et_2O (3 × 5.00 mL, v/v 1:6) to afford the product (87.2 mg, 112 μmol, 42%) as pale yellow solid.

^{1}H-NMR (300 MHz; CD_2Cl_2): δ 8.09 (d, *J* = 1.9 Hz, 1H), 7.76 (dd, *J* = 7.5, 1.5 Hz, 2H), 7.72−7.69 (m, 1H), 7.66−7.54 (m, 3H), 7.29 (d, *J* = 1.6 Hz, 1H), 7.02 (tdd, *J* = 7.4, 2.8, 1.1 Hz, 2H), 6.93−6.87 (m, 2H), 6.69 (d, *J* = 7.7 Hz, 1H), 6.42 (d, *J* = 7.6 Hz, 1H), 4.23−4.10 (m, 2H), 2.68 (s, 1H), 2.18−1.95 (m, 4H), 1.34 (s, 9H), 1.37 (s, 9H).

Λ/Δ-(*S*)-Rhodium auxiliary complex derived from 5-(*tert*-butyl)-2-phenylbenzo[*d*]thiazole (39)[60]

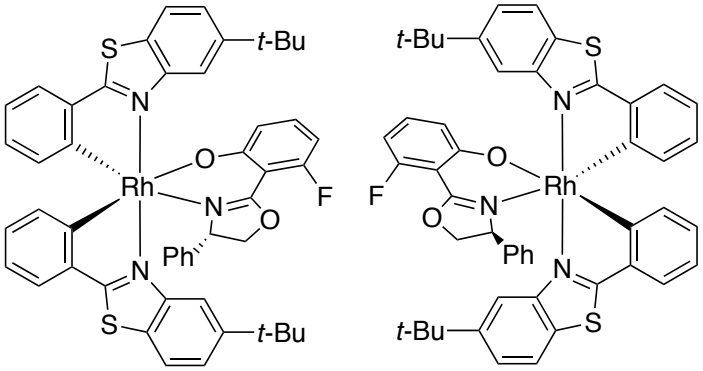

rac-RhS (230 mg, 267 μmol), (*S*)-3-fluoro-2-(4-phenyl-4,5-dihydrooxazol-2-yl)phenol (75.4 mg, 293 μmol), and K_2CO_3 (73.7 mg, 533 μmol) were added to ethanol (13.4 mL) under nitrogen atmosphere and the mixture was stirred at 70 ºC for 18 h. After cooling to rt, the reaction mixture was filtered over celite and the precipitates were washed with CH_2Cl_2. The filtrate was concentrated under vacuum and the residue was taken up with EtOH/*n*-hexane (30.0 mL, v/v 1:1). The precipitates were obtained through centrifuge and washed with EtOH/*n*-hexane (4 × 15.0 mL, v/v 1:1) to afford complex Λ-(*S*)-**39** as yellow solid (120 mg, 135 μmol, 50%). The filtrate was purified through column chromatography on silica gel (*n*-hexane:EtOAc 5:1) to give complex Δ-(*S*)-**39** complex as yellow solid (115 mg, 130 μmol, 48%).

Λ-(*S*)-**39**:

^{1}H-NMR (300 MHz; CD_2Cl_2): δ 8.89 (d, *J* = 1.9 Hz, 1H), 7.96 (d, *J* = 1.8 Hz, 1H), 7.79 (d, *J* = 8.6 Hz, 1H), 7.60 (d, *J* = 8.6 Hz, 2H), 7.52 (dd, *J* = 8.6, 1.8 Hz, 1H), 7.45 (dd, *J* = 8.6, 1.9 Hz, 1H), 7.41−7.38 (m, 1H), 6.99−6.68 (m, 9H), 6.37−6.30 (m, 3H), 5.87 (d, *J* = 7.7 Hz, 1H), 5.79 (dd, *J* = 12.3, 7.3 Hz, 1H), 4.85 (d, *J* = 4.7 Hz, 2H), 3.99 (d, *J* = 4.4 Hz, 1H), 1.44 (s, 9H), 1.27 (s, 9H).

Δ-(*S*)-**39**:

^{1}H-NMR (300 MHz; CD_2Cl_2): δ 9.06 (s, 1H), 8.37 (s, 1H), 7.92 (dd, *J* = 8.5, 1.8 Hz, 1H), 7.78 (dd, *J* = 8.3, 1.9 Hz, 1H), 7.59 (t, *J* = 8.5 Hz, 2H), 7.50 (d, *J* = 8.6 Hz, 1H), 7.18 (d, *J* = 7.6 Hz, 1H), 6.97−6.70 (m, 8H), 6.56 (t, *J* = 7.4 Hz, 1H), 6.40 (t, *J* = 7.4 Hz, 1H), 6.26 (dd, *J* = 14.0, 8.4 Hz, 2H), 6.15 (d, *J* = 7.3 Hz, 1H), 5.80 (t, *J* = 9.8 Hz, 1H), 4.32−4.27 (m, 1H), 4.07−4.00 (m, 1H), 3.92 (dd, *J* = 11.5, 8.3 Hz, 1H), 1.37 (s, 9H), 1.23 (s, 9H);

^{13}C-NMR (75.5 MHz; CD_2Cl_2): δ 176.6, 167.1, 152.6, 151.3, 140.6, 138.8, 135.3, 133.5, 132.9, 132.7, 130.1, 129.5, 128.2, 127.7, 127.4, 126.0, 125.7, 124.5, 124.4, 123.1, 122.2, 122.1, 122.0, 119.3, 118.9, 117.4, 98.7, 98.4, 75.0, 70.3, 35.6, 35.4, 31.6, 31.5.

Cleavage of the Chiral Auxiliary

General procedure 1

To the auxiliary complex (1.00 eq.) solution in acetonitrile (10.0 mM) was added trifluoroacetic acid (5.0 eq.) under nitrogen atmosphere. The reaction mixture was stirred at rt in the absence of light for 2 h and then concentrated under vacuum. The residue was taken up with CH_2Cl_2 and then NH_4PF_6 (30.0 eq.) was added. The mixture was stirred at rt and the anion exchange was monitored by TLC analysis. After complete

conversion, solvent was evaporated under vacuum and the residue was purified through flash column chromatography on silica gel to afford the enantiomeric pure Lewis acid catalysts.

Λ-Iridium Lewis acid catalyst derived from 5-(*tert*-butyl)-2-phenylbenzo[*d*]oxazole (Λ-IrO, 60)[57]

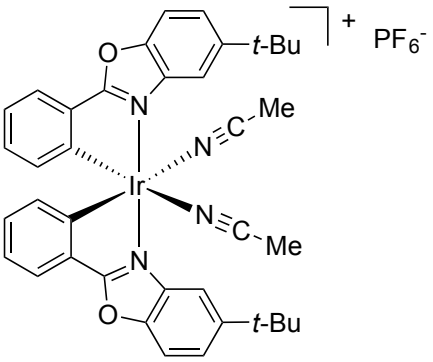

Iridium auxiliary complex Λ-(*S*)-**270** (227 mg, 249 μmol) was converted to Λ-IrO (203 mg, 222 μmol, 89%) according to general procedure 1. The ^{1}H-NMR data was consistent with the racemic compound.

Λ-Iridium Lewis acid catalyst derived from 5-(*tert*-butyl)-2-phenylbenzo[*d*]thiazole (Λ-IrS, 64)[58]

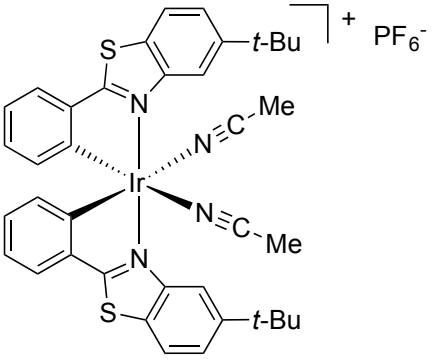

Λ-(*S*)-Iridium auxiliary complex (217 mg, 230 μmol) was converted to Λ-IrS (215 mg, 225 μmol, 98%) according to general procedure 1.

^{1}H-NMR (300 MHz; CD_2Cl_2): δ 8.41 (d, *J* = 1.7 Hz, 2H), 8.01 (d, *J* = 8.6 Hz, 2H), 7.72 (dd, *J* = 8.6, 1.8 Hz, 2H), 7.66 (dd, *J* = 7.7, 0.9 Hz, 2H), 6.95 (td, *J* = 7.5, 1.0 Hz, 2H), 6.73 (td, *J* = 7.5, 1.4 Hz, 2H), 6.17 (dd, *J* = 7.7, 0.4 Hz, 2H), 2.34 (s, 6H), 1.46 (s, 18H);

^{13}C-NMR (75.5 MHz; CD_2Cl_2): δ 181.3, 153.0, 150.3, 142.7, 141.1, 132.9, 131.5, 128.7, 126.1, 125.4, 123.6, 123.1, 121.6, 116.7, 35.6, 31.7, 4.0;

HRMS(ESI+) calcd. for $C_{38}H_{38}IrN_4S_2$ (M^+) 807.2160, found: 807.2184.

Λ-Rhodium Lewis acid catalyst derived from 5-(*tert*-butyl)-2-phenylbenzo[*d*]oxazole (Λ-RhO, 70)[59]

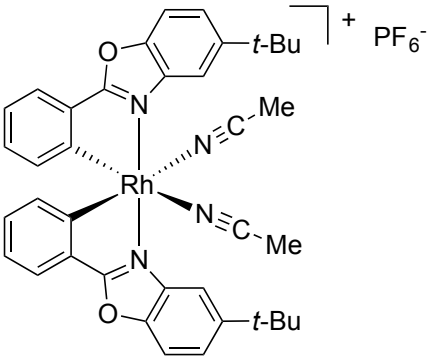

Rhodium prolinate complex Λ-L-**37** (146 mg, 204 μmol) and NH_4PF_6 (333 mg, 2.04 mmol) were added to acetonitrile (41.0 mL) under nitrogen atmosphere and stirred at 50 ºC in the absence of light for 18 h. After cooling to rt, the mixture was concentrated under vacuum and the residue was purified through flash column chromatography on silica gel (CH_2Cl_2 then CH_2Cl_2:CH_3CN 20:1) to afford the product as pale yellow solid (154 mg, 175 μmol, 86%). The ^{1}H-NMR data was consistent with the racemic compound.

Λ-Rhodium Lewis acid catalyst derived from 5-(*tert*-butyl)-2-phenylbenzo[*d*]thiazole (Λ-RhS, 71)[60]

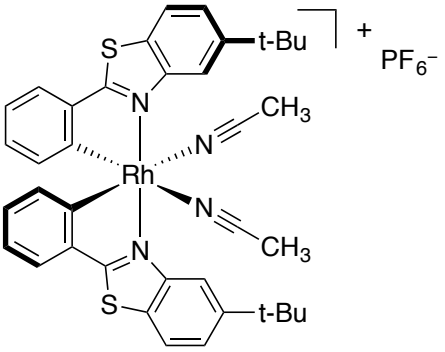

Rhodium auxiliary complex Λ-(*S*)-**39** (120 mg, 135 μmol) were dissolved in acetonitrile (7.00 mL) and then trifluoroacetic acid (51.5 μL, 673 μmol) was added in one portion. The reaction mixture was stirred at rt for 1 h. Excess NH_4PF_6 was added. The mixture was stirred at rt for further 10 min and then filtered over a silica pad (CH_2Cl_2:CH_3CN 20:1). The filtrate was concentrated under vacuum and dissolved in CH_2Cl_2. Excess NH_4PF_6 was added again and the anion exchange was monitored by TLC-analysis. After complete conversion, the mixture was concentrated under vacuum and the residue was purified through flash column chromatography on silica gel (CH_2Cl_2:CH_3CN 20:1) to afford the catalysts Λ-RhS (47.1 mg, 54.6 μmol, 40%).

Δ-Rhodium Lewis acid catalyst derived from 5-(*tert*-butyl)-2-phenylbenzo[*d*]thiazole (Δ-RhS, 71)[60]

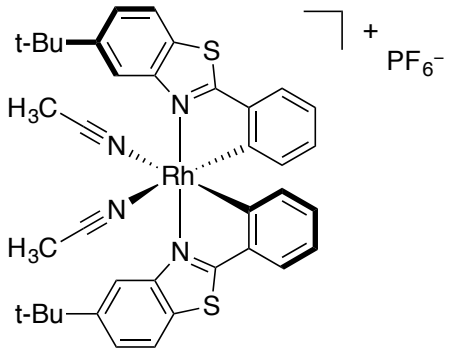

Rhodium auxiliary complex Δ-(*S*)-**39** (115 mg, 129 μmol) were dissolved in acetonitrile (6.50 mL) and then trifluoroacetic acid (49.4 μL, 645 μmol) was added in one portion. The reaction mixture was stirred at rt for 1 h. Excess NH_4PF_6 was added. The mixture was stirred at rt for further 10 min and then filtered over a silica pad (CH_2Cl_2:CH_3CN 20:1). The filtrate was concentrated under vacuum and dissolved in CH_2Cl_2. Excess NH_4PF_6 was added again and the anion exchange was monitored by TLC-analysis. After complete conversion, the mixture was concentrated under vacuum and the residue was purified through flash column chromatography on silica gel (CH_2Cl_2:CH_3CN 20:1) to afford the catalysts Δ-RhS (62.8 mg, 72.8 μmol, 56%).

Iridium dimer derived from 2-phenylpyridine (271)[201]

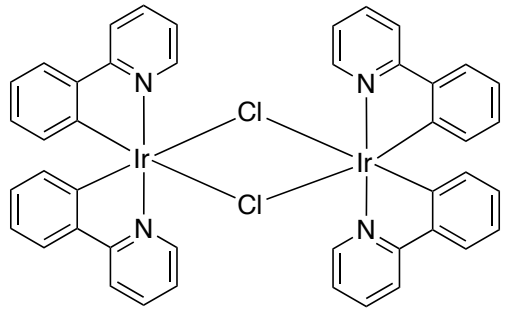

Iridium(III) chloride trihydrate (500 mg, 1.42 mmol) and 2-phenylpyridine (446 μL, 3.12 mmol) were added to 2-ethoxyethanol (48.0 mL) and water (16.0 mL) under nitrogen atmosphere. The mixture was heated to 120 ºC under reflux for 24 h and then cooled to rt. The precipitates were obtained through filtration and then washed with water and diethyl ether. The yellow solid (480 mg, 451 μmol, 63%) were dried under air and used without further purification.

^{1}H-NMR (300 MHz; CD_2Cl_2): δ 9.25 (ddd, *J* = 5.8, 1.5, 0.7 Hz, 4H), 7.93 (d, *J* = 7.8 Hz, 4H), 7.79 (ddd, *J* = 8.1, 7.4, 1.6 Hz, 4H), 7.55 (dd, *J* = 7.8, 1.3 Hz, 4H), 6.84−6.78 (m, 8H), 6.60 (td, *J* = 7.5, 1.2 Hz, 4H), 5.87 (dd, *J* = 7.8, 0.8 Hz, 4H);

^{13}C-NMR (75.5 MHz; CD_2Cl_2): δ 168.5, 151.9, 145.3, 144.4, 137.0, 130.8, 129.5, 124.1, 123.0, 121.8, 119.1.

***fac*-Tris(2-phenylpyridinato-C^2,*N*)iridium(III) [*fac*-Ir(ppy)$_3$] (91)[201]**

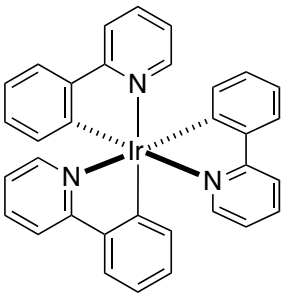

Iridium dimer **271** (216 mg, 201 μmol) and 2-phenylpyridine (144 μL, 1.01 mmol) were added to 2-ethoxyethanol (38.8 mL) under nitrogen atmosphere. After adding $AgPF_6$ (104 mg, 403 μmol), the mixture was heated to 200 ºC for 24 h and then cooled to rt. Water was added and precipitates were collected through filtration, washed with CH_3OH, diethyl ether and *n*-hexane. The residue was purified through flash column chromatography on silica gel (CH_2Cl_2:CH_3OH 10:1) to afford the product (201 mg, 307 μmol, 76%) as yellow solid.

^{1}H-NMR (300 MHz; CD_2Cl_2): δ 7.91 (d, *J* = 8.2 Hz, 3H), 7.68−7.61 (m, 6H), 7.56 (ddd, *J* = 5.5, 1.6, 0.9 Hz, 3H), 6.94−6.85 (m, 6H), 6.81−6.72 (m, 6H);

^{13}C-NMR (75.5 MHz; CD_2Cl_2): δ 166.9, 161.4, 147.6, 144.2, 137.2, 136.6, 130.1, 124.4, 122.5, 120.3, 119.3;

HRMS(ESI+) calcd. for $C_{33}H_{24}IrN_3Na$ $(M + Na)^+$ 678.1493, found: 678.1501.

Iridium photoredox catalyst [Ir(ppy)$_2$(dtbbpy)]PF$_6$ (89·PF$_6$)[202]

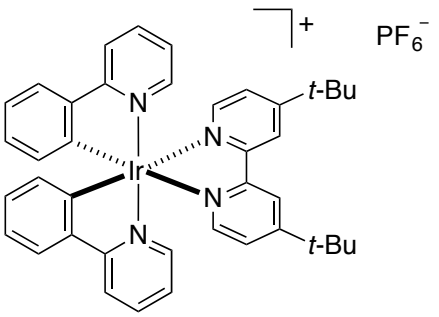

Iridium dimer **271** (200 mg, 187 μmol), $AgPF_6$ (104 mg, 410 μmol), and 4,4'-di-*tert*-butyl-2,2'-bipyridine (125 mg, 466 μmol) were added to CH_2Cl_2 (18.7 mL) under nitrogen atmosphere. The mixture was stirred at rt for 4 h. After evaporating the solvent under vacuum, the residue was purified through flash column chromatography on silica gel (CH_2Cl_2:CH_3CN 20:1) to afford the product as yellow solid (311 mg, 340 μmol, 91%).

^{1}H-NMR (300 MHz; CD_2Cl_2): δ 8.28 (d, *J* = 1.7 Hz, 2H), 7.95 (dd, *J* = 7.8, 0.6 Hz, 2H), 7.90 (d, *J* = 5.8 Hz, 2H), 7.79 (ddd, *J* = 8.2, 7.4, 1.5 Hz, 2H), 7.73 (dd, *J* = 7.7, 1.2 Hz, 2H), 7.51 (ddd, *J* = 5.8, 1.5, 0.7 Hz, 2H), 7.43 (dd, *J* = 5.9, 1.9 Hz, 2H), 7.09−6.99 (m, 4H), 6.93 (td, *J* = 7.4, 1.4 Hz, 2H), 6.30 (dd, *J* = 7.6, 0.8 Hz, 2H), 1.42 (s, 18H);

^{13}C-NMR (75.5 MHz; CD_2Cl_2): δ 168.3, 164.5, 156.0, 150.7, 149.0, 144.1, 138.5, 132.0, 131.1, 126.0, 125.2, 123.6, 123.0, 121.3, 120.2, 36.0, 30.4;

HRMS(ESI+) calcd. for $C_{40}H_{40}IrN_4$ (M^+) 769.2879. found: 769.2909.

5.3. Synthesis of Catalysis Substrates

1-Methyl-1*H*-imidazole (**272a**) and 1-isopropyl-1*H*-imidazole (**272d**) are commercially available and were employed directly, whereas 1-phenyl-1*H*-imidazoles (**272b**) and 1-(*o*-tolyl)-1*H*-imidazole (**272c**) were synthesized according to literature.[203] Weinreb-amides **273** and 2-acyl imidazoles **74** were synthesized according to the procedures published by our group recently.[137,138,151]

5.3.1. Synthesis of 1*H*-Imidazoles

1-Phenyl-1*H*-imidazole (272b)

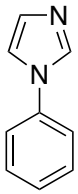

1*H*-Imidazole (1.02 g, 15 mmol), phenyl iodide (897 µL, 10.0 mmol), Cu_2O (143 mg. 1.00 mmol), and KOH (1.32 g, 20.0 mmol, 85% w/w) were added to DMSO (20.0 mL). The mixture was bubbled with argon at rt for 30 min. Under argon atmosphere, the degassed mixture was stirred at 130 ºC for 24 h. After cooling to rt, the dark blue reaction mixture was filtered over silica gel and washed with ethyl acetate. The filtrate was then taken up by water (100 mL) and ethyl acetate (100 mL). The aqueous layer was extracted with ethyl acetate (3 × 50 mL). The organic layers were combined, dried over Na_2SO_4, filtered, and concentrated under vacuum. The residue was purified through flash column chromatography on silica gel (*n*-hexane:EtOAc 1:2) to afford the product (1.20 g, 8.32 mmol, 83%) as pale yellow oil.

^{1}H-NMR (300 MHz; $CDCl_3$): δ 7.89 (s, 1H, N=C*H*N), 7.52−7.47 (m, 2H, H_{Ph}), 7.42−7.35 (m, 3H, H_{Ph}), 7.29−7.30 (m, 1H, C*H*N=C), 7.22 (s, 1H, C*H*NPh);

^{13}C-NMR (75.5 MHz; $CDCl_3$): δ 137.4 (CHN*C*), 135.5 (N*C*HNPh), 130.4 (*C*HN=C), 129.8 ($2C_{Ph}$), 127.4 (C_{Ph}), 121.4 ($2C_{Ph}$), 118.2 (*C*HNPh);

HRMS(ESI+) calcd. for $C_9H_9N_2$ $(M + H)^+$ 145.0760, found: 145.0764.

1-(*o*-Tolyl)-1*H*-imidazole (272c)

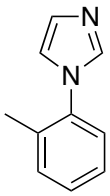

1*H*-Imidazole (3.06 g, 45.0 mmol), *o*-tolyl iodide (3.80 mL, 30.0 mmol), KOH (4.36 g, 66.0 mmol, 85% w/w), and Cu_2O (429 mg, 3.00 mmol) were added to DMSO (60.0 mL). The reaction mixture was degassed by being bubbled with argon for 30 min at rt. After stirring at 130 ºC for 18 h and then cooling to rt, the mixture was poured onto water and extracted with ethyl acetate (3 × 100 mL). The combined organic layers were dried over Na_2SO_4 and filtered over celite. The solvent was evaporated under vacuum and the residue was

purified through flash column chromatography on silica gel (*n*-hexane:EtOAc 2:1) to afford the product (3.85 g, 24.3 mmol, 81%) as yellow oil.

^{1}H-NMR (300 MHz; $CDCl_3$): δ 7.62 (s, 1H, N=C*H*-N), 7.36−7.34 (m, 3H, C*H*=N-CH + 2H$_{o\text{-tolyl}}$), 7.24−7.22 (m, 2H, 2H$_{o\text{-tolyl}}$), 7.07 (s, 1H, C*H*N-*o*-tolyl), 2.19 (s, 3H, CH_3).

5.3.2. Synthesis of Weinreb-Amides

Depending on the commercially available starting materials, Weinreb-amides **273** were synthesized through two different procedures.

General Procedure 2A

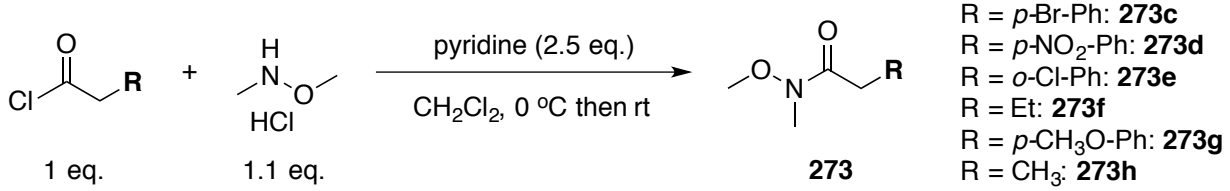

R = Ph: **273a**
R = *p*-CH_3-Ph: **273b**
R = *p*-Br-Ph: **273c**
R = *p*-NO_2-Ph: **273d**
R = *o*-Cl-Ph: **273e**
R = Et: **273f**
R = *p*-CH_3O-Ph: **273g**
R = CH_3: **273h**

N,O-Dimethylhydroxylamine hydrochloride (537 mg. 5.50 mmol) and pyridine (1.00 mL, 12.5 mmol) were dissolved in CH_2Cl_2 (10.0 mL) and cooled to 0 ºC. Acyl chloride (5.00 mmol) was added dropwise under nitrogen atmosphere. The solution was stirred at 0 ºC for 30 min and then at rt for 1 h. The solution was diluted with ethyl acetate (50.0 mL) and washed with aq. HCl (1 M, 3 × 10.0 mL), saturated aq. $NaHCO_3$ solution (3 × 10.0 mL), and brine (1 × 20.0 mL). The organic layer was dried over Na_2SO_4 and concentrated under vacuum. The residue was purified through flash column chromatography on silica gel (*n*-hexane:EtOAc) to afford the product.

General Procedure 2B

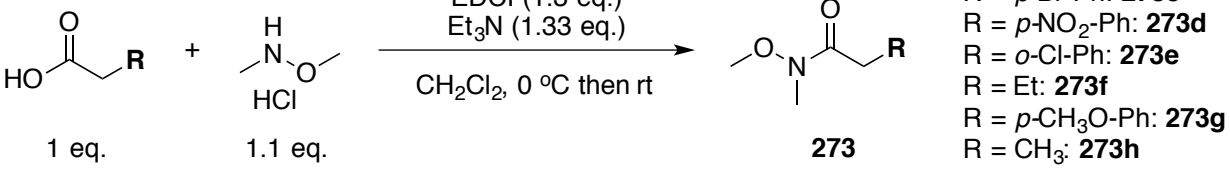

R = Ph: **273a**
R = *p*-CH_3-Ph: **273b**
R = *p*-Br-Ph: **273c**
R = *p*-NO_2-Ph: **273d**
R = *o*-Cl-Ph: **273e**
R = Et: **273f**
R = *p*-CH_3O-Ph: **273g**
R = CH_3: **273h**

N,O-Dimethylhydroxylamine hydrochloride (537 mg. 5.50 mmol), carboxylic acid (5.00 mmol), and 4-dimethylaminopyridine (61.1 mg, 500 μmol) were dissolved in CH_2Cl_2 (25.0 mL) and cooled to 0 ºC. Triethylamine (927 μL, 6.65 mmol) and ethylcarbodiimide hydrochloride (1.25 g, 6.50 mmol) were added at 0 ºC successively. After being stirred at 0 ºC for 1 h under nitrogen atmosphere, the reaction solution was warmed to rt and stirred for further 16 h. The solution was diluted with ethyl acetate (50.0 mL) and washed with aq. HCl (1 M, 3 × 10.0 mL), saturated aq. $NaHCO_3$ solution (3 × 10.0 mL), and brine (1 × 20.0 mL). The organic layer was dried over Na_2SO_4 and concentrated under vacuum. The residue was purified through flash column chromatography on silica gel (*n*-hexane:EtOAc) to afford the product.

***N*-Methoxy-*N*-methyl-2-phenylacetamide (273a)**

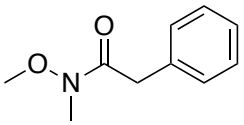

Following general procedure 2A, 2-phenylacetyl chloride (3.00 mL, 22.7 mmol) was converted to Weinreb-amide **273a** (4.04 g, 22.5 mmol, 99%).

^{1}H-NMR (300 MHz; $CDCl_3$): δ 7.30−7.17 (m, 5H, 5H$_{Ph}$), 3.73 (s, 2H, O=CC*H*$_2$), 3.54 (t, *J* = 1.1 Hz, 3H, OC*H*$_3$), 3.14−3.13 (m, 3H, NC*H*$_3$);

^{13}C-NMR (75.5 MHz; $CDCl_3$): δ 172.2 (O=*C*), 134.9, (O=CCH$_2$*C*), 129.2 (2C$_{Ph}$), 128.3 (2C$_{Ph}$), 126.6 (C$_{Ph}$), 61.1 (O*C*H$_3$), 39.3 (O=C*C*H$_2$), 32.1 (N*C*H$_3$);

HRMS(ESI+) calcd. for $C_{10}H_{13}NO_2Na$ $(M + Na)^+$ 202.0838, found: 202.0839.

***N*-Methoxy-*N*-methyl-2-(*p*-tolyl)acetamide (273b)**

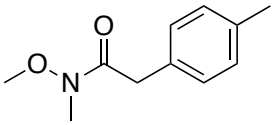

Following general procedure 2B, 2-(*p*-tolyl)acetic acid (751 mg, 5.00 mmol) was converted to Weinreb-amide **273b** (948 mg, 4.91 mmol, 98%).

^{1}H-NMR (300 MHz; $CDCl_3$): δ 7.17 (d, *J* = 8.1 Hz, 2H, 2H$_{p\text{-tolyl}}$), 7.11 (d, *J* = 8.0 Hz, 2H, 2H$_{p\text{-tolyl}}$), 3.71 (s, 2H, O=CC*H*$_2$), 3.57 (s, 3H, OC*H*$_3$), 3.16 (s, 3H, NC*H*$_3$), 2.31 (s, 3H, CC*H*$_3$);

^{13}C-NMR (75.5 MHz; $CDCl_3$): δ 172.3 (O=*C*), 136.0 (*C*CH$_3$), 131.7 (O=CCH$_2$*C*), 129.0 (4C$_{p\text{-tolyl}}$), 61.0 (O*C*H$_3$), 38.8 (O=C*C*H$_2$), 32.1 (N*C*H$_3$), 20.8 (C*C*H$_3$);

HRMS(ESI+) calcd. for $C_{11}H_{16}NO_2$ $(M + H)^+$ 194.1176, found: 194.1176.

2-(4-Bromophenyl)-*N*-methoxy-*N*-methylacetamide (273c)

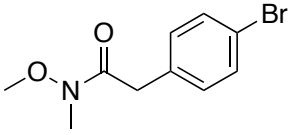

Following general procedure 2B, 2-(4-bromophenyl)acetic acid (1.08 g, 5.00 mmol) was converted to Weinreb-amide **273c** (1.29 g, 5.00 mmol, >99%).

^{1}H-NMR (300 MHz; $CDCl_3$): δ 7.43−7.38 (m, 2H, 2H$_{p\text{-Br-Ph}}$), 7.16−7.12 (m, 2H, 2H$_{p\text{-Br-Ph}}$), 3.69 (s, 2H, O=CC*H*$_2$), 3.60 (s, 3H, OC*H*$_3$), 3.16 (s, 3H, NC*H*$_3$);

^{13}C-NMR (75.5 MHz; $CDCl_3$): δ 171.7 (O=*C*), 133.9 (*C*Br), 131.5 (2C$_{p\text{-Br-Ph}}$), 131.1 (2C$_{p\text{-Br-Ph}}$), 120.7 (O=CCH$_2$*C*), 61.3 (O*C*H$_3$), 38.7 (O=C*C*H$_2$), 32.3 (N*C*H$_3$);

HRMS(ESI+) calcd. for $C_{10}H_{12}BrNO_2Na$ $(M + Na)^+$ 281.9924, found: 281.9927.

***N*-Methoxy-*N*-methyl-2-(4-nitrophenyl)acetamide (273d)**

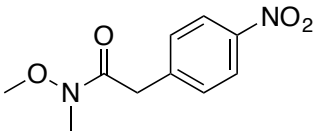

Following general procedure 2B, 2-(4-nitrophenyl)acetic acid (906 mg, 5.00 mmol) was converted to Weinreb-amide **273d** (1.11 g, 4.95 mmol, 99%).

^{1}H-NMR (300 MHz; $CDCl_3$): δ 8.12−8.07 (m, 2H, 2H$_{p\text{-nitro-Ph}}$), 7.43−7.38 (m, 2H, 2H$_{p\text{-nitro-Ph}}$), 3.83 (s, 2H, O=CC*H*$_2$), 3.65 (s, 3H, OC*H*$_3$), 3.15 (s, 3H, NC*H*$_3$);

^{13}C-NMR (75.5 MHz; $CDCl_3$): δ 170.6 (O=*C*), 146.9 (*C*NO$_2$), 142.6 (O=CCH$_2$*C*), 130.4 (2C$_{p\text{-nitro-Ph}}$), 123.5 (2C$_{p\text{-nitro-Ph}}$), 61.4 (O*C*H$_3$), 38.8 (O=C*C*H$_2$), 32.2 (N*C*H$_3$);

HRMS(ESI+) calcd. for $C_{10}H_{12}N_2O_4Na$ $(M + Na)^+$ 247.0689, found: 247.0691.

2-(2-Chlorophenyl)-*N*-methoxy-*N*-methylacetamide (273e)

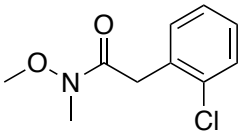

Following general procedure 2B, 2-(2-chlorophenyl)acetic acid (853 mg, 5.00 mmol) was converted to Weinreb-amide **273e** (1.06 g, 4.96 mmol, 99%).

^{1}H-NMR (300 MHz; $CDCl_3$): δ 7.34−7.31 (m, 1H, H$_{o\text{-Cl-Ph}}$), 7.26−7.23 (m, 1H, H$_{o\text{-Cl-Ph}}$), 7.20−7.13 (m, 2H, 2H$_{o\text{-Cl-Ph}}$), 3.86 (s, 2H, O=CC*H*$_2$), 3.63 (t, *J* = 1.6 Hz, 3H, OC*H*$_3$), 3.16 (t, *J* = 1.3 Hz, 3H, NC*H*$_3$);

^{13}C-NMR (75.5 MHz; $CDCl_3$): δ 171.1 (O=*C*), 134.2 (*C*Cl), 133.1 (O=CCH$_2$*C*), 131.3 (C$_{o\text{-Cl-Ph}}$), 129.2 (C$_{o\text{-Cl-Ph}}$), 128.1 (C$_{o\text{-Cl-Ph}}$), 126.6 (C$_{o\text{-Cl-Ph}}$), 61.1 (O*C*H$_3$), 36.8 (O=C*C*H$_2$), 32.2 (N*C*H$_3$);

HRMS(ESI+) calcd. for $C_{10}H_{12}ClNO_2Na$ $(M + Na)^+$ 236.0449, found: 236.0450.

***N*-Methoxy-*N*-methylbutyramide (273f)**

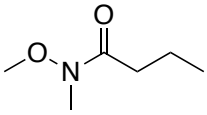

Following general procedure 2A, butyric chloride (522 µL, 5.00 mmol) was converted to Weinreb-amide **273f** (386 mg, 2.94 mmol, 59%). The product is volatile.

^{1}H-NMR (300 MHz; $CDCl_3$): δ 3.60 (t, *J* = 0.6 Hz, 3H, OC*H*$_3$), 3.09 (s, 3H, NC*H*$_3$), 2.31 (t, *J* = 7.5 Hz, 2H, O=CC*H*$_2$), 1.64−1.51 (m, 2H, C*H*$_2$CH$_3$), 0.88 (td, *J* = 7.4, 0.7 Hz, 3H, CH$_2$C*H*$_3$);

^{13}C-NMR (75.5 MHz; $CDCl_3$): δ 174.5 (O=*C*), 61.1 (O*C*H$_3$), 33.8 (O=C*C*H$_2$), 32.2 (N*C*H$_3$), 18.0 (*C*H$_2$CH$_3$), 13.9 (CH$_2$*C*H$_3$);

HRMS(ESI+) calcd. for $C_6H_{13}NO_2Na$ $(M + Na)^+$ 154.0838, found: 154.0839.

***N*-Methoxy-2-(4-methoxyphenyl)-*N*-methylacetamide (273g)**

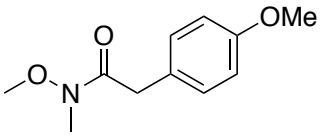

Following general procedure 2A, 2-(4-methoxyphenyl)acetyl chloride (3.00 mL, 19.6 mmol) was converted to Weinreb-amide **273g** (3.99 g, 19.1 mmol, 97%).

^{1}H-NMR (300 MHz; $CDCl_3$): δ 7.20 (d, *J* = 8.7 Hz, 2H, $H_{p\text{-MeO-Ph}}$), 6.84 (d, *J* = 8.7 Hz, 2H, $H_{p\text{-MeO-Ph}}$), 3.76 (d, *J* = 1.4 Hz, 3H, C*H*$_3$ON), 3.69 (s, 2H, O=CC*H*$_2$), 3.59 (d, *J* = 1.2 Hz, 3H, C*H*$_3$OC), 3.16 (d, *J* = 1.2 Hz, 3H, C*H*$_3$N);

^{13}C-NMR (75.5 MHz; $CDCl_3$): δ 172.7 (*C*=O), 156.5 (*C*OCH$_3$), 130.3 (2C$_{p\text{-MeO-Ph}}$), 127.0 (O=CCH$_2$*C*), 114.0 (2C$_{p\text{-MeO-Ph}}$), 61.3 (*C*H$_3$ON), 55.3 (*C*H$_3$OC), 38.5 (O=C*C*H$_2$), 32.3 (*C*H$_3$N);

HRMS(ESI+) calcd. for $C_{11}H_{15}NO_3Na$ $(M + Na)^+$ 232.4953, found: 232.0948.

***N*-Methoxy-*N*-methylpropionamide (273h)**

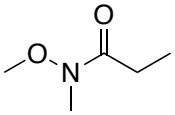

Following general procedure 2B, propionic acid (748 µL, 10.0 mmol) was converted to Weinreb-amide **273h** (837 mg, 7.14 mmol, 71%). The product is volatile.

^{1}H-NMR (300 MHz; $CDCl_3$): δ 3.68 (s, 3H, OC*H*$_3$), 3.18 (s, 3H, NC*H*$_3$), 2.45 (q, *J* = 7.5 Hz, 2H, O=CC*H*$_2$), 1.14 (t, *J* = 7.5 Hz, 3H, O=CCH$_2$C*H*$_3$).

5.3.3. Synthesis of 2-Acyl Imidazoles

General Procedure 3

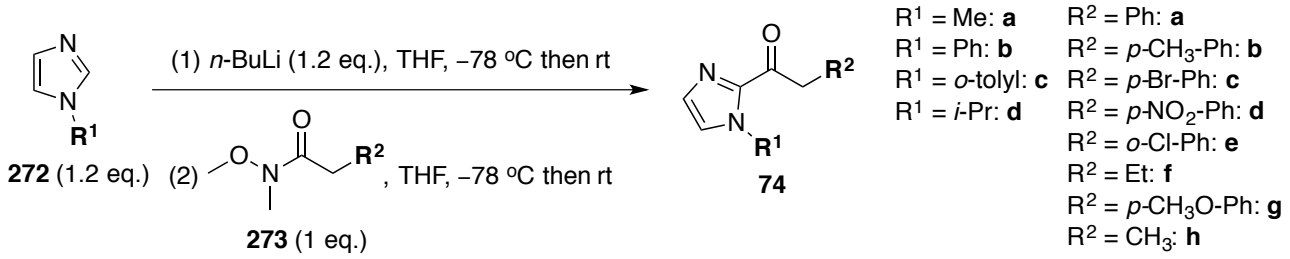

N-Substituted 1*H*-imidazole **272** (1.20 eq.) was dissolved in THF (400 mM) and cooled to −78 °C. *n*-Butyl-lithium (1.20 eq., 1.60 M or 2.50 M in hexane) was added dropwise. The reaction mixture was stirred at −78 °C for 30 min and then at rt for 30 min. The mixture was cooled to −78 °C and Weinreb-amide **273** (1.00 eq.) was added. The mixture was allowed to warm to rt and stirred for further 18 h. The reaction was quenched by adding acetic acid (6.00 eq.) and then diluted with ethyl acetate. The organic layer was washed with saturated aq. $NaHCO_3$ solution (3×), water (3×), and brine (1×). After drying over Na_2SO_4, the solvent was removed under vacuum and the residue was purified through flash column chromatography on silica gel (*n*-hexane: EtOAc) to afford the product.

1-(1-Methyl-1*H*-imidazol-2-yl)-2-phenylethan-1-one (74aa)

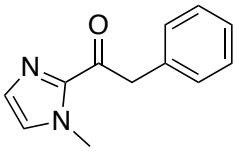

Following general procedure 3, 1*H*-imidazole **272a** (2.16 g, 26.3 mmol) and Weinreb-amide **273a** (3.93 g, 21.9 mmol) were converted to 2-acyl imidazole **74aa** (3.25 g, 16.2 mmol, 74%).

^{1}H-NMR (300 MHz; $CDCl_3$): δ 7.38−7.24 (m, 5H, $5H_{Ph}$), 7.22 (d, *J* = 1.0 Hz, 1H, C*H*N=C), 7.06 (d, *J* = 0.5 Hz, 1H, C*H*NCH_3), 4.47 (s, 2H, O=CC*H*$_2$), 3.98 (s, 3H, C*H*$_3$);

HRMS(ESI+) calcd. for $C_{12}H_{13}N_2O$ $(M + H)^+$ 201.1022, found: 201.1023.

2-(4-Methoxyphenyl)-1-(1-methyl-1*H*-imidazol-2-yl)ethan-1-one (74ag)

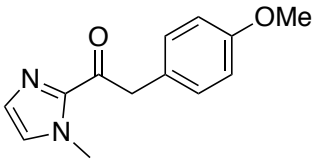

Following general procedure 3, 1*H*-imidazole **272a** (706 mg, 8.60 mmol) and Weinreb-amide **273g** (1.50 g, 7.17 mmol) were converted to 2-acyl imidazole **74ag** (1.33 g, 5.78 mmol, 81%).

^{1}H-NMR (300 MHz; $CDCl_3$): δ 7.28−7.23 (m, 2H, $2H_{p\text{-MeO-Ph}}$), 7.16 (d, *J* = 0.9 Hz, 1H, C*H*N=C), 7.01 (s, 1H, C*H*NCH_3), 6.87−6.82 (m, 2H, $H_{p\text{-MeO-Ph}}$), 4.35 (s, 2H, C*H*$_2$), 3.94 (s, 3H, OC*H*$_3$), 3.76 (s, 3H, NC*H*$_3$);

^{13}C-NMR (75.5 MHz; $CDCl_3$): δ 190.5 (*C*=O), 158.6 (*C*OCH_3),142.9 (N=*C*NCH_3), 130.9 ($2C_{p\text{-MeO-Ph}}$), 129.3 (O=CCH_2*C*), 127.4(*C*HN), 126.7 (*C*HNCH_3), 114.0 ($2C_{p\text{-MeO-Ph}}$), 55.3 (O*C*H_3), 44.6 (O=C*C*H_2), 36.2 (N*C*H_3);

HRMS(ESI+) calcd. for $C_{13}H_{15}N_2O_2$ $(M + H)^+$ 231.1128, found: 232.1134.

2-Phenyl-1-(1-phenyl-1*H*-imidazol-2-yl)ethan-1-one (74ba)

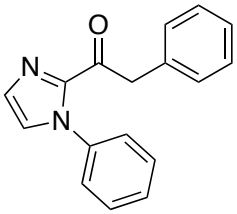

Following general procedure 3, 1*H*-imidazole **272b** (966 mg, 6.70 mmol) and Weinreb-amide **273a** (1.00 g, 5.58 mmol) were converted to 2-acyl imidazole **74ba** (782 mg, 2.98 mmol, 53%).

^{1}H-NMR (300 MHz; $CDCl_3$): δ 7.40−7.35 (m, 3H, $3H_{Ph}$), 7.31−7.17 (m, 8H, $7H_{Ph}$ + C*H*N=C), 7.15 (d, *J* = 1.0 Hz, 1H, C*H*NPh), 4.43 (s, 2H, O=CC*H*$_2$);

^{13}C-NMR (75.5 MHz; $CDCl_3$): δ 188.6 (O=*C*), 142.9 (N=*C*NPh), 138.4 (N*C*), 134.5 (O=CCH_2*C*), 130.1 ($2C_{Ph}$), 129.9 (*C*HN=C), 129.0 ($2C_{Ph}$), 128.8 (*C*HNPh), 128.5 ($2C_{Ph}$), 127.5 (C_{Ph}), 126.9 (C_{Ph}), 126.0 ($2C_{Ph}$), 45.7 (O=C*C*H_2);

HRMS(ESI+) calcd. for $C_{17}H_{15}N_2O$ $(M + H)^+$ 263.1179, found: 263.1181.

2-Phenyl-1-(1-(*o*-tolyl)-1*H*-imidazol-2-yl)ethan-1-one (74ca)

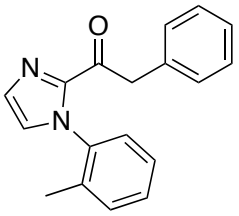

Following general procedure 3, 1*H*-imidazole **272c** (802 mg, 5.07 mmol) and Weinreb-amide **273a** (757 mg, 4.22 mmol) were converted to 2-acyl imidazole **74ca** (831 mg, 3.01 mmol, 71%).

^{1}H-NMR (300 MHz; $CDCl_3$): δ 7.33 (d, *J* = 1.0 Hz, 1H, C*H*N=C), 7.3−7.17 (m, 8H, $5H_{Ph}$ + $3H_{o\text{-tolyl}}$), 7.06−7.04 (m, 2H, C*H*N-*o*-tolyl), 4.41 (q, *J* = 15.2 Hz, 2H, O=CCH_2), 1.86 (s, 3H, CH_3);

^{13}C-NMR (75.5 MHz; $CDCl_3$): δ 188.4 (O=*C*), 143.4 (CHN=*C*), 137.9 (CHN*C*), 134.6 (*C*HN=C), 134.5 (O=CCH_2*C*), 130.8 ($C_{o\text{-tolyl}}$), 130.1 ($C_{o\text{-tolyl}}$), 129.98 ($2C_{Ph}$), 129.1 ($C_{o\text{-tolyl}}$), 128.5 ($2C_{Ph}$), 126.9 (CH_3*C*), 126.8 (C_{Ph}), 126.6 ($C_{o\text{-tolyl}}$), 126.3 (C*H*N-*o*-tolyl), 45.5 (O=C*C*H_2), 17.1 (*C*H_3);

HRMS(ESI+) calcd. for $C_{18}H_{17}N_2O$ $(M + H)^+$ 277.1335, found: 277.1338.

2-(*p*-Tolyl)-1-(1-(*o*-tolyl)-1*H*-imidazol-2-yl)ethan-1-one (74cb)

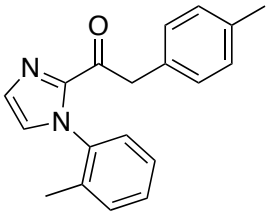

Following general procedure 3, 1*H*-imidazole **272c** (261 mg, 1.65 mmol) and Weinreb-amide **273b** (290 mg, 1.50 mmol) were converted to 2-acyl imidazole **74cb** (291 mg, 1.00 mmol, 67%).

^{1}H-NMR (300 MHz; $CDCl_3$): δ 7.34 (d, *J* = 0.9 Hz, 1H, C*H*N=C), 7.31−7.05 (m. 8H, $4H_{p\text{-tolyl}}$ + $3H_{o\text{-tolyl}}$ + C*H*N-*o*-tolyl), 7.01 (d, *J* = 7.5 Hz, 1H, $H_{o\text{-tolyl}}$), 4.41 (d, *J* = 15.2 Hz, 1H, O=CCH_2), 4.35 (d, *J* = 15.2 Hz, 1H, O=CCH_2), 2.28 (s, 3H, *p*-CH_3-Ph), 1.89 (s, 3H, *o*-CH_3-Ph);

^{13}C-NMR (75.5 MHz; $CDCl_3$): δ 188.6 (O=*C*), 143.4 (CHN=*C*), 138.1 (*C*CH_3), 138.0 (CHN*C*), 134.6 (*C*HN=C), 134.3 (O=CCH_2*C*), 130.82 ($C_{o\text{-tolyl}}$), 130.76 ($C_{p\text{-tolyl}}$), 130.1 ($C_{o\text{-tolyl}}$), 129.1 ($C_{o\text{-tolyl}}$), 128.4 ($C_{p\text{-tolyl}}$), 127.6 ($C_{p\text{-tolyl}}$), 127.03 ($C_{p\text{-tolyl}}$), 126.9 (NC*C*CH_3), 126.6 ($C_{o\text{-tolyl}}$), 126.4 (*C*HN-*o*-tolyl), 45.4 (O=C*C*H_2), 21.5 (*C*H_3), 17.2 (NCC*C*H_3);

HRMS(ESI+) calcd. for $C_{19}H_{19}N_2O$ $(M + H)^+$ 291.1492, found: 291.1495.

2-(4-Bromophenyl)-1-(1-(*o*-tolyl)-1*H*-imidazol-2-yl)ethan-1-one (74cc)

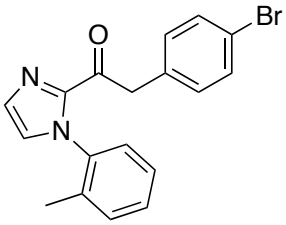

Following general procedure 3, 1*H*-imidazole **272c** (261 mg, 1.65 mmol) and Weinreb-amide **273c** (387 mg, 1.50 mmol) were converted to 2-acyl imidazole **74cc** (459 mg, 1.29 mmol, 86%).

^{1}H-NMR (300 MHz; $CDCl_3$): δ 7.40−7.35 (m, 2H, 2H$_{p\text{-Br-Ph}}$), 7.34 (d, *J* = 1.0 Hz, 1H, C*H*N=C), 7.32−7.19 (m, 3H, 3H$_{o\text{-tolyl}}$), 7.18−7.13 (m, 2H, 2H$_{p\text{-Br-Ph}}$), 7.09−7.04 (m, 2H, C*H*N-*o*-tolyl + H$_{o\text{-tolyl}}$), 4.41 (d, *J* = 15.3 Hz, 1H, O=CC*H*$_2$), 4.33 (d, *J* = 15.3 Hz, 1H, O=CC*H*$_2$), 1.88 (s, 3H, C*H*$_3$);

^{13}C-NMR (75.5 MHz; $CDCl_3$): δ 187.8 (O=*C*), 143.1 (CHN=*C*), 137.8 (CHN*C*), 134.5 (*C*HN=C), 133.5 (O=CCH$_2$*C*), 131.7 (2C$_{p\text{-Br-Ph}}$), 131.6 (2C$_{p\text{-Br-Ph}}$), 130.8 (C$_{o\text{-tolyl}}$), 130.2 (C$_{o\text{-tolyl}}$), 129.2 (C$_{o\text{-tolyl}}$), 127.1 (*C*CH$_3$), 126.7 (C$_{o\text{-tolyl}}$), 126.3 (*C*HN-*o*-tolyl), 121.0 (*C*Br), 44.8 (O=C*C*H$_2$), 17.2 (*C*H$_3$);

HRMS(ESI+) calcd. for $C_{18}H_{16}BrN_2O$ $(M + H)^+$ 355.0441, found: 355.0445.

2-(4-Nitrophenyl)-1-(1-(*o*-tolyl)-1*H*-imidazol-2-yl)ethan-1-one (74cd)

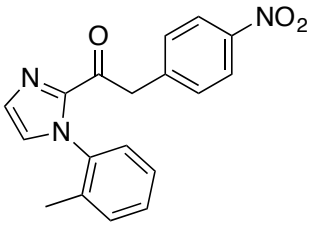

Following general procedure 3, 1*H*-imidazole **272c** (261 mg, 1.65 mmol) and Weinreb-amide **273d** (336 mg, 1.50 mmol) were converted to 2-acyl imidazole **74cd** (141 mg, 439 µmol, 29%).

^{1}H-NMR (300 MHz; $CDCl_3$): δ 8.16−8.11 (m, 2H, 2H$_{p\text{-nitro-Ph}}$), 7.49−7.45 (m, 2H, 2H$_{p\text{-nitro-Ph}}$), 7.38 (d, *J* = 1.0 Hz, 1H, C*H*N=C), 7.35−7.22 (m, 3H, 3H$_{o\text{-tolyl}}$), 7.14 (d, *J* = 1.0 Hz, 1H, C*H*N-*o*-tolyl), 7.09 (dd, *J* = 7.6, 1.0 Hz, 1H, H$_{o\text{-tolyl}}$), 4.55 (q, *J* = 13.7 Hz, 2H, O=CC*H*$_2$), 1.90 (s, 3H, CH_3);

^{13}C-NMR (75.5 MHz; $CDCl_3$): δ 186.8 (O=*C*), 147.2 (*C*NO$_2$), 142.9 (CHN=*C*), 142.1 (O=CCH$_2$*C*), 137.7 (C$_{o\text{-tolyl}}$), 134.5 (*C*HN=C), 130.97 (2C$_{p\text{-nitro-Ph}}$), 130.95 (C$_{o\text{-tolyl}}$), 130.5 (C$_{o\text{-tolyl}}$), 129.4, (C$_{o\text{-tolyl}}$) 127.5 (*C*CH$_3$), 126.8 (C$_{o\text{-tolyl}}$), 126.3 (*C*HN-*o*-tolyl), 123.7 (2C$_{p\text{-nitro-Ph}}$), 45.2 (O=C*C*H$_2$), 17.2 (*C*H$_3$);

HRMS(ESI+) calcd. for $C_{16}H_{15}N_3O_3Na$ $(M + Na)^+$ 344.1006, found: 344.1009.

2-(2-Chlorophenyl)-1-(1-(*o*-tolyl)-1*H*-imidazol-2-yl)ethan-1-one (74ce)

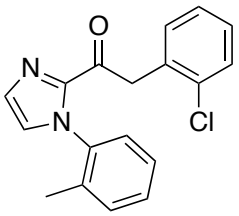

Following general procedure 3, 1*H*-imidazole **272c** (261 mg, 1.65 mmol) and Weinreb-amide **273e** (320 mg, 1.50 mmol) were converted to the 2-acyl imidazole **74ce** (371 mg, 1.19 mmol, 80%).

^{1}H-NMR (300 MHz; $CDCl_3$): δ 7.36−7.09 (m, 10H, 4H$_{o\text{-tolyl}}$ + 4H$_{o\text{-Cl-Ph}}$ + 2H$_{\text{imidazolyl}}$), 4.73 (d, *J* = 17.6 Hz, 1H, O=CC*H*$_2$), 4.54 (d, *J* = 17.6 Hz, 1H, O=CC*H*$_2$), 1.96 (s, 3H, C*H*$_3$);

^{13}C-NMR (75.5 MHz; $CDCl_3$): δ 187.1 (O=*C*), 143.2 (CHN=*C*), 137.9 (CHN*C*), 134.8 (*C*Cl), 134.6 (*C*HN=C), 133.1 (O=CCH$_2$*C*), 132.3 (C$_{o\text{-Cl-Ph}}$), 130.8 (C$_{o\text{-tolyl}}$), 130.1 (C$_{o\text{-Cl-Ph}}$), 129.4 (C$_{o\text{-tolyl}}$), 129.1 (C$_{o\text{-tolyl}}$), 128.5 (C$_{o\text{-Cl-Ph}}$), 126.8 (C$_{o\text{-tolyl}}$ + C$_{o\text{-Cl-Ph}}$), 126.7 (CH$_3$*C*), 126.3 (*C*HN-*o*-tolyl), 43.7 (O=C*C*H$_2$), 17.2 (*C*H$_3$);

HRMS(ESI+) calcd. for $C_{18}H_{16}ClN_2O$ $(M + H)^+$ 311.0946, found: 311.0949.

1-(1-(*o*-Tolyl)-1*H*-imidazol-2-yl)butan-1-one (74cf)

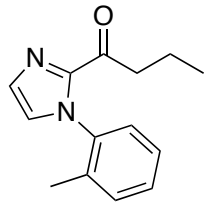

Following general procedure 3, 1*H*-imidazole **272c** (261 mg, 1.65 mmol) and Weinreb-amide **273f** (197 mg, 1.50 mmol) were converted to 2-acyl imidazole **74cf** (290 mg, 1.27 mmol, 85%).

^{1}H-NMR (300 MHz; $CDCl_3$): δ 7.38−7.23 (m, 4H, C*H*N=C + $3H_{o\text{-tolyl}}$), 7.12−7.09 (m, 1H, $H_{o\text{-tolyl}}$), 7.05 (d, *J* = 1.0 Hz, 1H, C*H*N-*o*-tolyl), 3.19−3.00 (m, 2H, O=CCH_2), 1.96 (s, 3H, CCH_3), 1.67 (dq, *J* = 14.7 Hz, 7.4 Hz, 2H, CH_2CH$_3$), 0.94 (t, *J* = 7.4 Hz, 3H, CH_2CH_3);

^{13}C-NMR (75.5 MHz; $CDCl_3$): δ 191.6 (O=*C*), 143.7 (N=*C*N-*o*-tolyl), 138.2 (CHN*C*), 134.6 (*C*HN=C), 130.8 ($C_{o\text{-tolyl}}$), 129.7 ($C_{o\text{-tolyl}}$), 129.1 ($C_{o\text{-tolyl}}$), 126.7 ($C_{o\text{-tolyl}}$), 126.4 (*C*HN-*o*-tolyl), 126.3 (*C*CH$_3$), 41.0 (O=C*C*H$_2$), 17.6 (*C*H$_2$CH$_3$), 17.2 (C*C*H$_3$), 13.9 (CH$_2$*C*H$_3$);

HRMS(ESI+) calcd. for $C_{14}H_{17}N_2O$ $(M + H)^+$ 229.1335, found: 229.1337.

1-(1-*iso*-Propyl-1*H*-imidazol-2-yl)-2-phenylethan-1-one (74da)

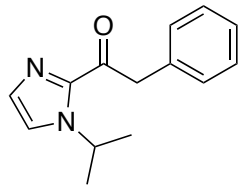

Following general procedure 3, 1*H*-imidazole **272d** (760 µL, 6.70 mmol) and Weinreb-amide **273a** (1.00 g, 5.58 mmol) were converted to 2-acyl imidazole **74da** (888 mg, 3.89 mmol, 70%).

^{1}H-NMR (300 MHz; $CDCl_3$): δ 7.36−7.21 (m, 7H, $5H_{Ph}$ + $2H_{imidazolyl}$), 5.49 (dt, *J* = 13.4 Hz, 6.7 Hz, 1H, NC*H*Me$_2$), 4.45 (s, 2H, O=CCH_2), 1.39 (d, *J* = 6.7 Hz, 6H, 2CH_3);

^{13}C-NMR (75.5 MHz; $CDCl_3$): δ 190.3 (O=*C*), 142.3 (N=*C*N), 134.9 (C_{Ph}), 130.0 ($2C_{Ph}$), 129.8 (*C*HN=C), 128.5 ($2C_{Ph}$), 126.8 (*C*HN*i*-Pr), 121.6 (C_{Ph}), 49.4 (N*C*HMe$_2$), 46.1 (O=C*C*H$_2$), 23.7 (2*C*H$_3$);

HRMS(ESI+) calcd. for $C_{14}H_{17}N_2O$ $(M + H)^+$ 229.1335, found: 229.1345.

1-(1-*iso*-Propyl-1*H*-imidazol-2-yl)propan-1-one (74dh)

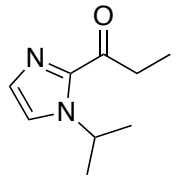

Following general procedure 3, 1*H*-imidazole **272d** (973 µL, 8.57 mmol) and Weinreb-amide **273h** (837 mg, 7.14 mmol) were converted to 2-acyl imidazole **74dh** (899 mg, 5.41 mmol, 76%). The product is volatile.

^{1}H-NMR (300 MHz; $CDCl_3$): δ 7.24 (d, *J* = 0.9 Hz, 1H, C*H*N=C), 7.15 (d, *J* = 0.6 Hz, 1H, C*H*N*i*Pr), 5.55 (dt, *J* = 13.4, 6.7 Hz, 1H, C*H*Me$_2$), 3.15 (q, *J* = 7.4 Hz, 2H, O=CCH_2), 1.43 (d, *J* = 6.7 Hz, 6H, CH(CH_3)$_2$), 1.17 (t, *J* = 7.4 Hz, 3H, O=CCH$_2$CH$_3$);

^{13}C-NMR (75.5 MHz; $CDCl_3$): δ 194.0 (O=*C*), 142.2 (N=*C*N*i*-Pr), 129.3 (*C*HN=C), 120.9 (*C*HN*i*-Pr), 49.3 (N*C*H), 33.1 (O=C*C*H_2), 23.7 (NCH(*C*H_3)$_2$), 8.3 (O=CCH$_2$*C*H_3).

5.3.4. Synthesis of Other Reagents

Both branched α-cyanoalkyl bromide **95b** and dibromo-1,3-dicarbonyl compound **252** were synthesized according to published literature.[98,204]

rac-2-Bromo-3,3-diethoxypropanenitrile (95b)[98]

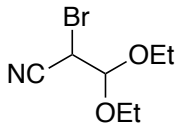

3-Ethoxyacrylonitrile (1.00 mL, 9.72 mmol, *E,Z*-mixture) was dissolved in ethanol (10.0 mL) under nitrogen atmosphere. *N*-bromosuccinimid (1.73 g, 9.72 mmol) was added in 5 portions every 5 min. The mixture was stirred at rt for further 2 h and then filtered. The filtrate was concentrated under vacuum and then taken up with CH_2Cl_2 and water. After layer separation, the aqueous layer was extracted with CH_2Cl_2. The combined organic layers were dried over $MgSO_4$ and concentrated under vacuum. The residue was purified through flash column chromatography on silica gel (*n*-hexane:EtOAc 25:1) to afford the product as colorless oil (926 mg, 4.17 mmol, 43%).

^{1}H-NMR (300 MHz; $CDCl_3$): δ 4.68 (dd, *J* = 5.7, 0.5 Hz, 1H, C*H*(OEt)$_2$), 4.29 (d, *J* = 5.7 Hz, 1H, C*H*CNBr), 3.84−3.57 (m, 4H, 2CH_2), 1.23 (q, *J* = 6.9 Hz, 6H, 2CH_3);

^{13}C-NMR (75.5 MHz; $CDCl_3$): δ 115.2 (*C*N), 101.2 (*C*H(OEt)$_2$), 65.1 (O*C*H$_2$CH$_3$), 64.1 (O*C*H$_2$CH$_3$), 29.3 (Br*C*CN), 14.98 (OCH$_2$*C*H$_3$), 14.96 (OCH$_2$*C*H$_3$);

HRMS(ESI+) calcd. for $C_7H_{12}BrNO_2Na$ $(M + Na)^+$ 243.9944, found: 243.9945.

3,3-Dibromopentane-2,4-dione (252)[204]

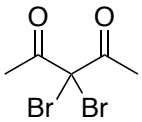

Pentane-2,4-dione (1.00 mL, 9.74 mmol) and *N*-bromosuccinimid (4.33 g, 24.4 mmol) were dissolved in 1,2-dichloroethane (25.0 mL) under nitrogen atmosphere. The mixture was stirred at 60 ºC for 18 h and then cooled to rt. The white precipitates were removed by filtration and the yellow filtrate was concentrated under vacuum. The residue was purified through flash column chromatography on silica gel (*n*-hexane:EtOAc 25:1) to afford the product as pale yellow oil (2.04 g, 7.92 mmol, 81%).

^{1}H-NMR (300 MHz; $CDCl_3$): δ 2.61 (s, 6H, 2CH_3);

^{13}C-NMR (75.5 MHz; $CDCl_3$): δ 193.4 (2O=*C*), 68.4 (*C*Br$_2$), 24.7 (2*C*H$_3$).

5.4. Asymmetric α-Alkylation of 2-Acyl Imidazoles with α-Cyanoalkyl Bromides

As mentioned, the absolute configuration of enantioenriched product **189cca** was assigned to be *S* through X-ray diffraction (see Chapter 3.1.6, p.42). According to this result and the absolute configuration of the catalyst, which was employed in this reaction, the absolute configurations of other enantioenriched alkylated products **189** can be extrapolated.

5.4.1. Optimizations of the Reaction Conditions - Single Catalyst

General Procedure 4

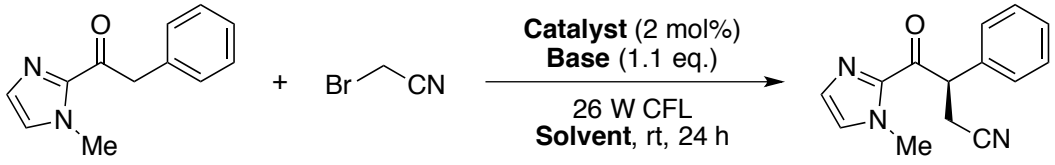

74aa **95a**, 3 eq. (*R*)-**189aaa**

To a Schlenk-tube were added 2-acyl imidazole substrate **74aa** (200 μmol), base (220 μmol), and catalyst (4.00 μmol) under nitrogen atmosphere. Solvent (500 μL) was added and the reaction mixture was stirred at rt for 5 min. After adding bromoacetonitrile (41.8 μL, 600 μmol), the Schlenk-tube was sealed with a screw-cap and reaction mixture was frozen by immersing the tube in liquid nitrogen. The frozen mixture was evacuated for 15 min and then warmed to rt under nitrogen atmosphere. This freeze-pump-thaw degassing procedure was repeated for further two cycles and the reaction mixture was stirred at rt under irradiation with two 13- Watt compact fluorescent lamps (CFL) for 24 h. After evaporating the solvent under vacuum, the residue was purified through flash column chromatography on silica gel (*n*-hexane:EtOAc 5:1 then 2:1) to afford remaining starting material **74aa** and product (*R*)-**189aaa**. The conversion was calculated according to recovered **74aa** and the enantiomeric purity was determined through HPLC analysis of (*R*)-**189aaa** on chiral stationary phase.

Catalyst Screening (Table 3, p.36)

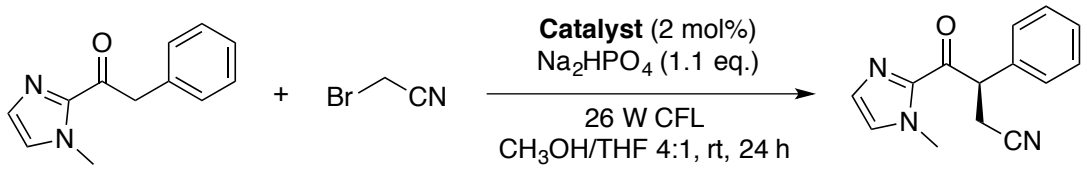

74aa **95a**, 3 eq. (*R*)-**189aaa**

Following general procedure 4, 2-acyl imidazole substrate **74aa** (40.0 mg, 200 μmol) was converted to (*R*)-1**89aaa** with Na_2HPO_4 (31.2 mg, 220 μmol) as base in CH_3OH/THF (500 μL, v/v 4:1) as solvent. The reaction with Λ-IrS (3.80 mg, 4.00 μmol) as catalyst afforded **74aa** (27.7 mg, 138 μmol, 31% conv.) and (*R*)-**189aaa** (11.3 mg, 47.2 μmol, 24%) with 58% *ee* (entry 1). The reaction with Λ-IrO (3.70 mg, 4.00 μmol) as catalyst afforded **74aa** (20.0 mg, 100 μmol, 50% conv.) and (*R*)-**189aaa** (23.6 mg, 98.6 μmol, 49%) with 63% *ee* (entry 2). The reaction with Λ-RhO (3.30 mg, 4.00 μmol) as catalyst afforded **74aa** (30.2 mg, 151 μmol, 24% conv.) and (*R*)-**189aaa** (10.0 mg, 41.8 μmol, 21%) with 73% *ee* (entry 3).

(*R*)-4-(1-Methyl-1*H*-imidazol-2-yl)-4-oxo-3-phenylbutanenitrile (189aaa)

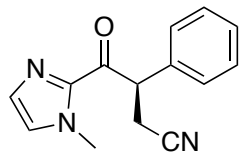

^{1}H-NMR (300 MHz; $CDCl_3$): δ 7.42−7.39 (m, 2H, $2H_{Ph}$), 7.33−7.20 (m, 3H, $3H_{Ph}$), 7.10 (d, *J* = 0.7 Hz, 1H, C*H*N=C), 6.98 (s, 1H, C*H*NCH_3), 5.47 (t, *J* = 7.7 Hz, 1H, O=CC*H*), 3.92 (s, 3H, CH_3), 3.06 (dd, *J* = 16.7, 7.9 Hz, 1H, CH_2CN), 2.86 (dd, *J* = 16.7, 7.5 Hz, 1H, CH_2CN);
^{13}C-NMR (75.5 MHz; $CDCl_3$): δ 188.2 (O=*C*), 141.8 (CHN=*C*), 136.4 (O=CCH*C*), 130.0 (*C*HN=C), 129.1 ($2C_{Ph}$), 128.3 ($2C_{Ph}$), 128.2 (*C*HNCH_3), 128.0 (C_{Ph}), 118.2 (*C*N), 49.1 (O=C*C*H), 36.1 (*C*H_3), 20.7 (*C*H_2CN);
HRMS(ESI+) calcd. for $C_{14}H_{13}N_3ONa$ $(M + Na)^+$ 263.0980, found: 262.0953;
HPLC Daicel Chiralpak AD-H column, 25 ºC, 1.0 mL/min, hexanes:*i*-PrOH 70:30, isocratic flow, t_R(major) = 6.7 min, t_R(minor) = 11.1 min.

Solvent Screening (Table 4, p.37)

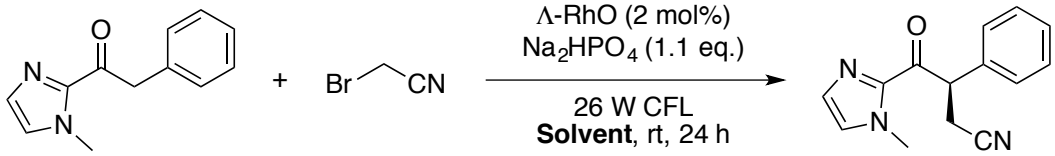

74aa **95a**, 3 eq. (*R*)-**189aaa**

Following general procedure 4, 2-acyl imidazole substrate **74aa** (40.0 mg, 200 μmol) was converted to (*R*)-**189aaa** with Na_2HPO_4 (31.2 mg, 220 μmol) as base and Λ-RhO (3.30 mg, 4.00 μmol) as catalyst. The reaction in CH_3OH (500 μL) afforded **74aa** (25.0 mg, 125 μmol, 38% conv.) and (*R*)-**189aaa** (13.7 mg, 57.3 μmol, 29%) with 60% *ee* (entry 2). No product formation was observed in *N*-methyl-2-pyrrolidone (500 μL) and dimethyl acetamide (500 μL) (entry 3 and 4). The reaction in CH_3CN and THF afforded only traces amount of (*R*)-**189aaa** with 54% *ee* (entry 5) and 46% *ee* (entry 6) respectively. The reaction in CH_3OH/CH_3CN (500 μL, v/v 4:1) afforded (*R*)-**189aaa** (13.5 mg, 56.4 μmol, 28%) with 77% *ee* (entry 7).

Base Screening (Table 5, p.38)

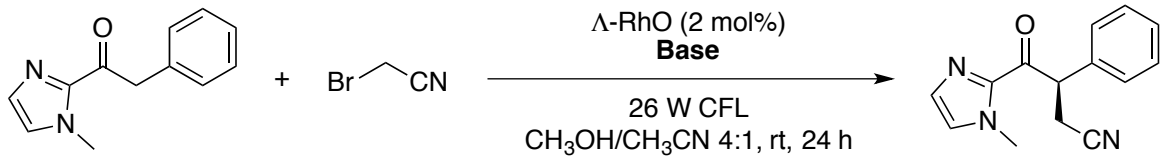

74aa **95a**, 3 eq. (*R*)-**189aaa**

Following general procedure 4, 2-acyl imidazole substrate **74aa** (40.0 mg, 200 μmol) was converted to (*R*)-**189aaa** with and Λ-RhO (3.30 mg, 4.00 μmol) as catalyst in CH_3OH/CH_3CN (500 μL, v/v 4:1) as solvent. The reactions with $NaHCO_3$ (9.20 mg, 220 μmol) and sodium acetate (9.00 mg, 220 μmol) afforded (*R*)-**189aaa** only in traces of amount with 40% *ee* (entry 2) and 15% *ee* (entry 3) respectively. The reaction with Cs_2CO_3 (35.8 mg, 220 μmol) afforded (*R*)-**189aaa** (33.5 mg, 140 μmol, 70%) with 5% *ee* (entry 4). The reaction with 2,6-lutidine (25.5 μL, 220 μmol) afforded **74aa** (28.1 mg, 140 μmol, 30% conv.) and (*R*)-**189aaa** (5.80 mg, 24.2 μmol, 12%) with 31% *ee* (entry 5). The reaction with *i*-Pr_2NEt (69.2 μL,

400 μmol) afforded **74aa** (18.8 mg, 93.9 μmol, 53% conv.) (*R*)-**189aaa** (17.4 mg, 72.7 μmol, 36%) with 31% *ee* (entry 6). The reaction in the absence of base didn't afford any product after 24 h according to TLC analysis of the reaction mixture (entry 7).

5.4.2. Optimizations of the Reaction Conditions - Dual Catalysis Strategy

General Procedure 5

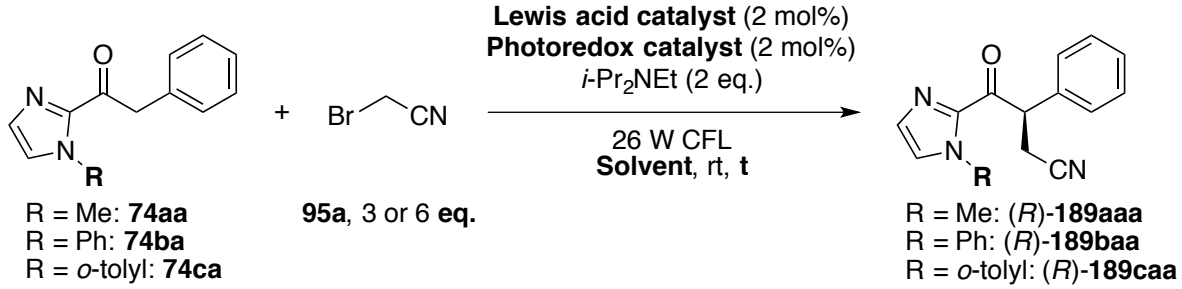

To a Schlenk-tube were added 2-acyl imidazole substrate **74** (200 μmol), *i*-Pr$_2$NEt (69.2 μL, 400 μmol), chiral Lewis acid catalyst (4.00 μmol), photoredox catalyst (4.00 μmol), and solvent (500 μL) under nitrogen atmosphere. The reaction mixture was stirred at rt for 5 min. After adding bromoacetonitrile, the Schlenk-tube was sealed with a screw-cap and reaction mixture was degassed through the freeze-pump-thaw procedure for three cycles and stirred at rt under irradiation with two 13-Watt CFL for the given duration. After evaporating the solvent under vacuum, the residue was purified through column chromatography on silica gel (*n*-hexane:EtOAc 5:1 then 2:1) to afford the product. The enantiomeric purity was determined through HPLC analysis of the product on chiral stationary phase.

Optimization of Dual Catalysis Strategy (Table 6, p.40)

Entries 1−2:

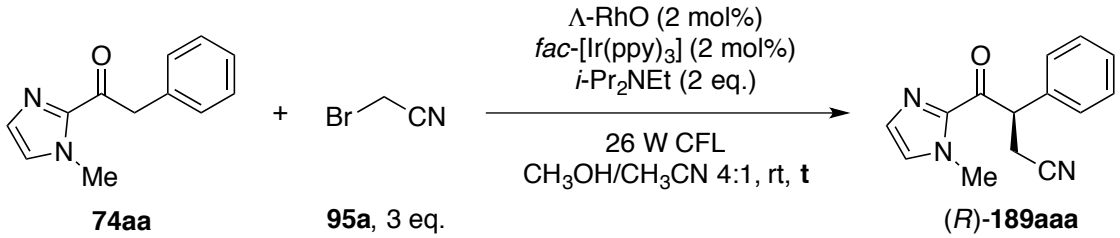

Following general procedure 5, the 2-acyl imidazole substrate **74aa** (40.0 mg, 200 μmol) and bromoacetonitrile (41.8 μL, 600 μmol) were converted to (*R*)-**189aaa** with Λ-RhO (3.30 mg, 4.00 μmol) and *fac*-[Ir(ppy)$_3$] (2.60 mg, 4.00 μmol) in CH_3OH/CH_3CN (500 μL, v/v 4:1). 24 h photolysis and the following purification yielded (*R*)-**189aaa** (40.6 mg, 170 μmol, 85%) with 58% *ee* (entry 1), while 17 h photolysis afforded (*R*)-**189aaa** (44.2 mg, 185 μmol, 92%) with 64% *ee* (entry 2).

Entries 3–6:

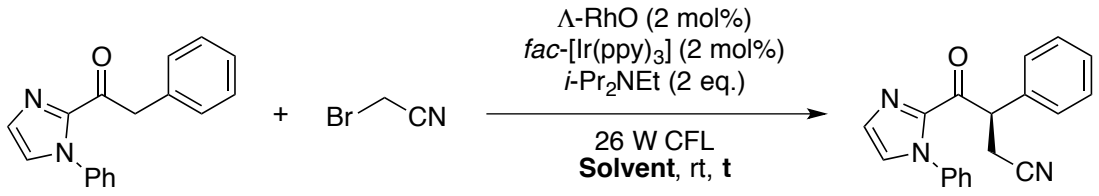

74ba **95a**, 3 or 6 **eq.** (*R*)-**189baa**

Following general procedure 5, 2-acyl imidazole substrate **74ba** (52.5 mg, 200 μmol) and bromoacetonitrile (41.8 μL, 600 μmol) were converted to (*R*)-**189baa** with Λ-RhO (3.30 mg, 4.00 μmol) and *fac*-[Ir(ppy)$_3$] (2.60 mg, 4.00 μmol) in CH_3OH/CH_3CN (500 μL, v/v 4:1). (*R*)-**189baa** (43.5 mg, 144 μmol, 72%) was obtained with 70% *ee* after 36 h photolysis (entry 3). Increasing the amount of the bromoacetonitrile (83.6 μL, 1.20 mmol) yielded (*R*)-**189baa** (53.2 mg, 177 μmol, 88%) with 72% *ee* and the duration of the reaction was shortened to 12 h (entry 4). Switching the solvent system to CH_3OH/CH_3CN (500 μL, v/v 1:1) and CH_3OH/CH_2Cl_2 (500 μL, v/v 1:1) yielded (*R*)-**189baa** (34.7 mg, 115 μmol, 58% and 42.7 mg, 142 μmol, 71%) with 74% *ee* and 73% *ee* after 24 h photolysis respectively (entry 5 and 6).

(*R*)-4-Oxo-3-phenyl-4-(1-phenyl-1*H*-imidazol-2-yl)butanenitrile (189baa)

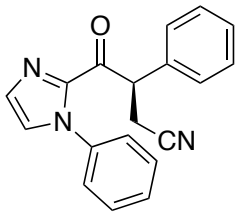

^{1}H-NMR (300 MHz; $CDCl_3$): δ 7.46–7.24 (m, 9H, 8H$_{Ph}$ + H$_{imidazolyl}$), 7.18–7.14 (m, 3H, 2H$_{Ph}$ + H$_{imidazolyl}$), 5.48 (t, *J* = 7.7 Hz, 1H, O=CC*H*), 2.98 (dd, *J* = 16.8, 7.7 Hz, 1H, C*H*$_2$CN), 2.79 (dd, *J* = 16.8, 7.7 Hz, 1H, C*H*$_2$CN);

^{13}C-NMR (75.5 MHz; $CDCl_3$): δ 186.9 (O=*C*), 141.8 (CHN=*C*), 138.0 (CHN*C*), 136.2 (O=CCH*C*), 130.5 (*C*HN=C), 129.3 (2C$_{Ph}$), 129.2 (2C$_{Ph}$), 129.1 (C$_{Ph}$), 128.4 (2C$_{Ph}$), 128.3 (C$_{Ph}$), 127.9 (*C*HNPh), 125.8 (2C$_{Ph}$), 118.1 (*C*N), 49.6 (O=C*C*H), 20.7, (*C*H$_2$CN);

HRMS(ESI+) calcd. for $C_{19}H_{15}N_3ONa$ $(M + Na)^+$ 324.1107, found: 324.1110;

HPLC Daicel Chiralpak AD-H column, 25 ºC, 1.0 mL/min, hexanes:*i*-PrOH 70:30, isocratic flow, t_R(major) = 7.9 min, t_R(minor) = 23.5 min.

Entries 7–10:

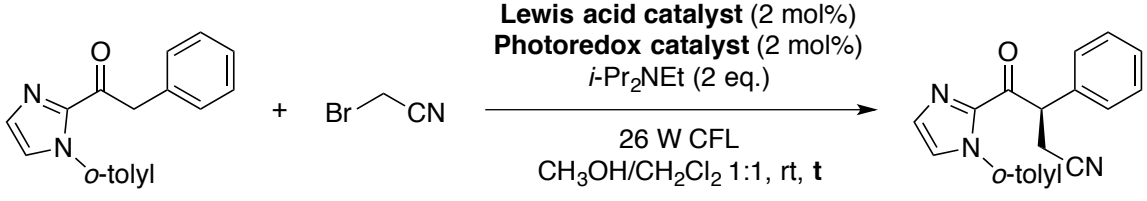

74ca **95a**, 3 or 6 **eq.** (*R*)-**189caa**

Following general procedure 5, 2-acyl imidazole substrate **74ca** (55.3 mg, 200 μmol) and bromoacetonitrile (83.6 μL, 1.20 mmol) were converted to (*R*)-**189caa** with Λ-RhO (3.30 mg, 4.00 μmol) and *fac*-[Ir(ppy)]$_3$

(2.60 mg, 4.00 μmol) in CH_3OH/CH_2Cl_2 (500 μL, v/v 1:1) after 24 h photolysis. Product (*R*)-**189caa** (51.2 mg, 162 μmol, 81%) was obtained with 80% *ee* (entry 7). Replacing *fac*-[Ir(ppy)]$_3$ with [Ir(ppy)$_2$(dtbbpy)]PF_6 (3.70 mg, 4.00 μmol) resulted in (*R*)-**189caa** (51.3 mg, 163 μmol, 81%) with 84% *ee* (entry 8). The combination of Λ-RhS (3.80 mg, 4.00 μmol) and [Ir(ppy)$_2$(dtbbpy)]PF_6 (3.70 mg, 4.00 μmol) yielded (*R*)-**189caa** (62.7 mg, 199 μmol, 99%) with 94% *ee* after 1.5 h photolysis (entry 9). The same result (62.7 mg, 199 μmol, 99% yield, 94% *ee*) was achieved after 5 h photolysis, when the amount of acetonitrile (41.8 μL, 600 μmol) was reduced (entry 10).

(*R*)-4-Oxo-3-phenyl-4-(1-(o-tolyl)-1*H*-imidazol-2-yl)butanenitrile (177caa)

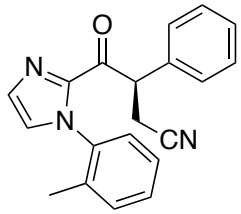

^{1}H-NMR (300 MHz; $CDCl_3$): δ 7.39−6.86 (m, 11H, 5H$_{Ph}$ + 4H$_{o\text{-tolyl}}$ + 2H$_{imidazolyl}$), 5.46 (t, *J* = 7.8 Hz, 1H, O=CC*H*), 2.97 (dt, *J* = 16.5, 8.1 Hz, 1H, C*H*$_2$CN), 2.77 (td, *J* = 17.4, 7.5 Hz, 1H, C*H*$_2$CN), 2.04 and 1.58 (s,, 3H, C*H*$_3$), contained rotamers;

^{13}C-NMR (75.5 MHz; $CDCl_3$): δ 186.9 (O=*C*), 142.3 (CHN=*C*), 137.52 and 137.50 (d, J = 2.0 Hz, CHN*C*), 136.2 and 136.1 (O=CCH*C*), 134.9 and 134.3 (*C*HN=C), 130.9 and 130.8 (C$_{o\text{-tolyl}}$), 130.69 and 130.64 (C$_{o\text{-tolyl}}$), 129.44 and 129.39 (C$_{o\text{-tolyl}}$), 129.2 (d, J = 4.2 Hz, 2C$_{Ph}$), 128.41 and 128.38 (2C$_{Ph}$), 128.3 (C$_{Ph}$), 127.3 (C$_{o\text{-tolyl}}$), 126.8 and 126.7 (*C*CH$_3$), 126.6 and 126.2 (*C*HN-*o*-tolyl), 118.1 (*C*N), 49.6 and 49.4 (O=C*C*H), 20.7 and 20.4 (*C*H$_2$CN), 17.3 and 16.6 (*C*H$_3$), contained rotamers;

HRMS(ESI+) calcd. for $C_{20}H_{17}N_3ONa$ $(M + Na)^+$ 338.1264, found: 338.1267;

HPLC Daicel Chiralpak AD-H column, 25 ºC, 1.0 mL/min, hexanes:*i*-PrOH 70:30, isocratic flow, t_R(major) = 6.3 min, t_R(minor) = 21.3 min.

5.4.3. Evaluation of the Substrate Scope

General Procedure 6

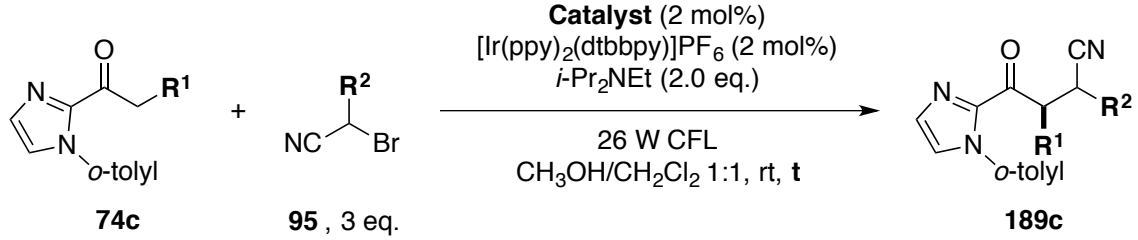

To a Schlenk-tube were added 2-acyl imidazole substrate **74c** (200 μmol), *i*-Pr$_2$NEt (69.2 μL, 400 μmol), [Ir(ppy)$_2$(dtbbpy)]PF_6 (3.70 mg, 4.00 μmol), and Δ-RhS (3.50 mg, 4.00 μmol) under nitrogen atmosphere. CH_3OH/CH_2Cl_2 (500 μL, v/v 1:1) was added and the reaction mixture was stirred at rt for 5 min. After adding α-cyanoalkyl bromide **95** (600 μmol), the Schlenk-tube was sealed with a screw-cap and reaction mixture was degassed through the freeze-pump-thaw procedure for three cycles and stirred at rt under irradiation with two 13-Watt CFL for the given duration. After evaporating the solvent under vacuum, the

residue was purified through flash column chromatography on silica gel (*n*-hexane:EtOAc 5:1 then 2:1) to afford the product. The enantiomeric purity was determined through HPLC analysis of the product on chiral stationary phase. The preparations of the racemic references were carried out with 6 equivalents α-cyanoalkyl bromide and *rac*-RhO as catalyst on 100 μmol scale.

Scope of the 2-Acyl Imidazoles (Table 7, p.41)

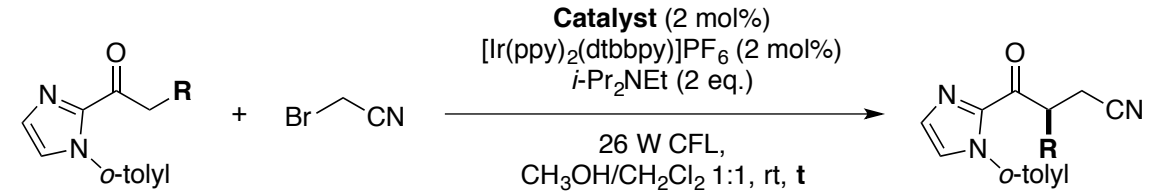

R = *p*-Me-Ph: **74cb**
R = *p*-Br-Ph: **74cc**
R = *p*-NO_2-Ph: **74cd**
R = *o*-Cl-Ph: **74ce**
R = Et: **74cf**

95a, 3 or 6 **eq.**

R = *p*-Me-Ph: **189cba**
R = *p*-Br-Ph: **189cca**
R = *p*-NO_2-Ph: **189cda**
R = *o*-Cl-Ph: **189cea**
R = Et: **189cfa**

(*S*)-4-Oxo-3-(*p*-tolyl)-4-(1-(*o*-tolyl)-1*H*-imidazol-2-yl)butanenitrile (189cba)

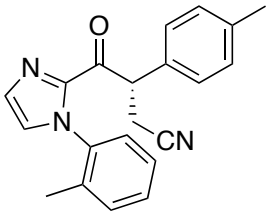

Following general procedure 6, 2-acyl imidazole substrate **74cb** (29.0 mg, 100 μmol) and bromoacetonitrile (41.8 μL, 600 μmol) were converted to *rac*-**189cba** (17.9 mg, 54.3 μmol, 54%) with *rac*-RhO (1.70 mg, 2.00 μmol) as catalyst after 24 h photolysis. The conversion of **74cb** was incomplete. With Δ-RhS (3.50 mg, 4.00 μmol) as catalyst, **74cb** (58.1 mg, 200 μmol) and bromoacetonitrile (41.8 μL, 600 μmol) were converted to (*S*)-**189cba** (66.7 mg, 200 μmol, >99%, 95% *ee*) as pale yellow solid. The conversion of **74cb** was complete after 12 h (entry 1).

^{1}H-NMR (300 MHz; $CDCl_3$): δ 7.42−6.89 (m, 10H, $8H_{o\text{-tolyl}}$ + $2H_{imidazolyl}$), 5.43 (t, *J* = 7.7 Hz, 1H, O=CC*H*), 2.97 (ddd, *J* = 16.8, 9.0, 7.9 Hz, 1H, CH_2CN), 2.76 (td, *J* = 16.5, 7.4 Hz, 1H, CH_2CN), 2.32 (d, *J* = 1.9 Hz, 3H, CH_3), 2.05 and 1.63 (s, 3H, NCCCH_3), contained rotamers;

^{13}C-NMR (75.5 MHz; $CDCl_3$): δ 187.1 (O=*C*), 142.4 (CHN=*C*), 139.0 and 138.9 (*C*HNC), 137.60 and 137.55 (*C*CH_3), 136.10 and 136.06 (O=CCH*C*), 134.9 and 134,4 (*C*HN=C), 130.97 and 130.86 ($C_{o\text{-tolyl}}$), 130.70 and 130.66 ($C_{o\text{-tolyl}}$), 129.46 and 129.41 ($C_{o\text{-tolyl}}$), 129.1 ($4C_{p\text{-tolyl}}$), 128.98 and 128.96 ($C_{o\text{-tolyl}}$), 127.23 and 126.68 (*C*HN-*o*-tolyl), 126.84 and 126.19 (NC*C*CH_3), 125.51 and 125.44 ($C_{o\text{-tolyl}}$), 118.2 (*C*N), 49.57 and 49.44 (O=C*C*H), 21.5 (*C*H_3), 20.8 and 20.6 (d, J = 20.7 Hz, *C*H_2CN), 17.4 and 16.6 (NCC*C*H_3), contained rotamer;

HRMS(ESI+) calcd. for $C_{21}H_{19}N_3ONa$ $(M + Na)^+$ 352.1420, found: 352.1424;

HPLC Daicel Chiralpak AD-H column, 25 ºC, 1.0 mL/min, hexanes:*i*-PrOH 70:30, isocratic flow, t_R(minor) = 5.9 min, t_R(major) = 26.8 min.

(*S*)-3-(4-Bromophenyl)-4-oxo-4-(1-(*o*-tolyl)-1*H*-imidazol-2-yl)butanenitrile (189cca)

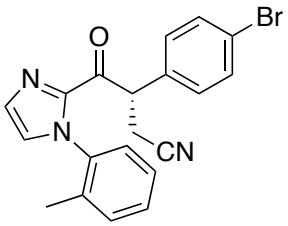

Following general procedure 6, 2-acyl imidazole substrate **74cc** (35.5 mg, 100 μmol) and bromoacetonitrile (41.8 μL, 600 μmol) were converted to *rac*-**189cca** (25.3 mg, 64.2 μmol, 64%) with *rac*-RhO (1.70 mg, 2.00 μmol) as catalyst after 24 h photolysis. The conversion of **74cc** was incomplete. With Δ-RhS (3.50 mg, 4.00 μmol) as catalyst, **74cc** (71.0 mg, 200 μmol) and bromoacetonitrile (41.8 μL, 600 μmol) were converted to (*S*)-**189caa** (72.0 mg, 183 μmol, 91%, 88% *ee*) as white solid. The conversion of **74cc** was complete after 12 h (entry 2).

^{1}H-NMR (300 MHz; $CDCl_3$): δ 7.48−7.44 (m, 2H, $2H_{p\text{-Br-Ph}}$), 7.40−6.90 (m, 8H, $4H_{o\text{-tolyl}}$ + $2H_{p\text{-Br-Ph}}$ + $2H_{\text{imidazolyl}}$), 5.44 (t, *J* = 7.8 Hz, 1H, O=CC*H*), 3.00−2.89 (m, 1H, C*H*$_2$CN), 2.85−2.71 (m, 1H, C*H*$_2$CN), 2.03 and 1.64 (s, 3H, C*H*$_3$), contained rotamers;

^{13}C-NMR (75.5 MHz; $CDCl_3$): δ 186.4 (O=*C*), 142.0 (CHN=*C*), 137.43 and 137.39 (CHN*C*), 135.2 (*C*Br), 134.8 and 134.3 (*C*HN=C), 132.44 and 132.39 (O=CCH*C*), 131.0 and 130.9 ($C_{o\text{-tolyl}}$), 130.87 and 130.83 ($C_{o\text{-tolyl}}$), 130.1 ($2C_{p\text{-Br-Ph}}$), 129.55 and 129.51 ($C_{o\text{-tolyl}}$), 127.6 ($C_{o\text{-tolyl}}$), 126.9 and 126.8 (*C*CH$_3$), 126.6 and 126.1 (*C*HN-*o*-tolyl), 122.6 ($2C_{p\text{-Br-Ph}}$), 117.8 (*C*N), 48.97 and 48.83 (O=CC*H*), 20.6 and 20.4 (*C*H$_2$CN), 17.3 and 16.8 (*C*H$_3$), contained rotamers;

HRMS(ESI+) calcd. for $C_{20}H_{16}BrN_3ONa$ $(M + Na)^+$ 416.0369, found: 416.0372;

HPLC Daicel Chiralpak AD-H column, 25 ºC, 1.0 mL/min, hexanes:*i*-PrOH 70:30, isocratic flow, t_R(minor) = 7.7 min, t_R(major) = 24.3 min.

(*S*)-3-(4-nitrophenyl)-4-oxo-4-(1-(*o*-tolyl)-1*H*-imidazol-2-yl)butanenitrile (189cda)

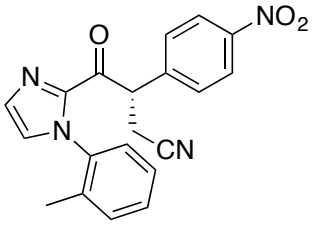

Following general procedure 6, 2-acyl imidazole substrate **74cd** (32.1 mg, 100 μmol) and bromoacetonitrile (41.8 μL, 600 μmol) were converted to *rac*-**189cda** (27.7 mg, 76.9 μmol, 77%) with *rac*-RhO (1.70 mg, 2.00 μmol) as catalyst after 24 h photolysis. The conversion of **74cd** was complete. With Δ-RhS (3.50 mg, 4.00 μmol) as catalyst, **74cd** (64.3 mg, 200 μmol) and bromoacetonitrile (41.8 μL, 600 μmol) were converted to (*S*)-**189cda** (58.5 mg, 162 μmol, 81%, 1% *ee*) as white solid. The conversion of **74cd** was complete after 24 h (entry 3).

^{1}H-NMR (300 MHz; $CDCl_3$): δ 8.20 (dd, *J* = 8.7, 1.8 Hz, 2H, $2H_{p\text{-nitro-Ph}}$), 7.61−7.54 (m, 2H, $2H_{p\text{-nitro-Ph}}$), 7.44−6.91 (m, 6H, $2H_{\text{imidazolyl}}$ + $4H_{o\text{-tolyl}}$), 5.61 (t, *J* = 7.7 Hz, 1H, O=CC*H*), 3.07−2.80 (m, 2H, C*H*$_2$CN), 2.03 and 1.65 (s, 3H, C*H*$_3$), contained rotamers;

^{13}C-NMR (75.5 MHz; $CDCl_3$): δ 185.3 (O=*C*), 147.8 (*C*NO_2), 143.26 and 143.19 (CHN=*C*), 141.6

(O=CCH*C*), 137.11 and 137.10 (CHN*C*), 134.7 and 134.1 (*C*HN=C), 131.04 and 131.00 ($C_{o\text{-tolyl}}$), 130.99 and 130.88 ($2C_{p\text{-nitro-Ph}}$), 129.59 and 129.56 ($C_{o\text{-tolyl}}$), 129.4 ($C_{o\text{-tolyl}}$), 127.9 ($C_{o\text{-tolyl}}$), 126.89 and 126.76 (*C*CH_3), 126.41 and 125.98 (*C*HN-*o*-tolyl), 124.31 and 124.27 ($2C_{p\text{-nitro-Ph}}$), 117.30 and 117.28 (*C*N), 49.13 and 49.03 (O=C*C*H), 20.41 and 20.25 (*C*H_2CN), 17.2 and 16.7 (*C*H_3), contained rotamers;

HRMS(ESI+) calcd. for $C_{20}H_{16}N_4O_3Na$ $(M + Na)^+$ 383.1115, found: 383.1118;

HPLC Daicel Chiralpak AD-H column, 25 ºC, 1.0 mL/min, hexanes:*i*-PrOH 70:30, isocratic flow, t_R(minor) = 10.6 min, t_R(major) = 41.1 min.

(*S*)-3-(2-chlorophenyl)-4-oxo-4-(1-(o-tolyl)-1H-imidazol-2-yl)butanenitrile (189cea)

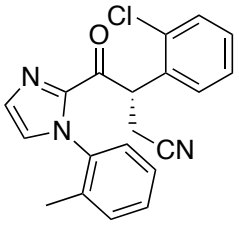

Following general procedure 6, 2-acyl imidazole substrate **74ce** (31.1 mg, 100 μmol) and bromoacetonitrile (41.8 μL, 600 μmol) were converted to *rac*-**189cea** (22.1 mg, 63.3 μmol, 63%) with *rac*-RhO (1.70 mg, 2.00 μmol) as catalyst after 24 h photolysis. The conversion of **74ce** was incomplete. With Δ-RhS (3.50 mg, 4.00 μmol) as catalyst, **74ce** (62.2 mg, 200 μmol) and bromoacetonitrile (41.8 μL, 600 μmol) were converted to (*S*)-**189cea** (70.1 mg, 200 μmol, >99%, 84% *ee*) as pale yellow solid. The conversion of **74ce** was complete after 12 h (entry 4).

HRMS(ESI+) calcd. for $C_{20}H_{17}ClN_3O$ $(M + H)^+$ 350.1055, found: 350.1056;

HPLC Daicel Chiralpak AD-H column, 25 ºC, 1.0 mL/min, hexanes:*i*-PrOH 70:30, isocratic flow, t_R(minor) = 5.4 min, t_R(major) = 13.0 min.

(*R*)-3-(1-(*o*-tolyl)-1*H*-imidazole-2-carbonyl)pentanenitrile (189cfa)

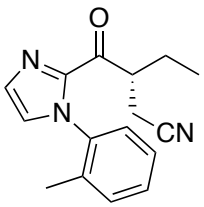

Following general procedure 6, 2-acyl imidazole substrate **74cf** (22.8 mg, 100 μmol) and bromoacetonitrile (41.8 μL, 600 μmol) were converted to *rac*-**189cfa** (26.7 mg, 100 μmol, >99%) with *rac*-RhO (1.70 mg, 2.00 μmol) as catalyst after 24 h photolysis. The conversion of **74cf** was complete. With Δ-RhS (3.50 mg, 4.00 μmol) as catalyst, **74cf** (45.7 mg, 200 μmol) and bromoacetonitrile (41.8 μL, 600 μmol) were converted to (*S*)-**189cfa** (49.4 mg, 185 μmol, 92%, 96% *ee*) as yellow oil. The conversion of **74cf** was complete after 24 h (entry 5).

^{1}H-NMR (300 MHz; $CDCl_3$): δ 7.42−7.26 (m, 4H, $3H_{imidazolyl}$ + H_{PhMe}), 7.17−7.07 (m, 2H, $H_{imidazolyl}$ + $H_{o\text{-tolyl}}$), 4.15 (quintet, *J* = 6.8 Hz, 1H, O=CC*H*), 2.69−2.50 (m, 2H, C*H*$_2$CN), 2.00−1.73 (m, 5H, C*H*$_3$ + C*H*$_2$CH$_3$), 0.92 (q, *J* = 7.7 Hz, 3H, CH$_2$C*H*$_3$);

^{13}C-NMR (75.5 MHz; $CDCl_3$): δ 190.5 (O=*C*), 142.51 and 142.49 (CHN=*C*), 137.8 and 137.7 (CHN*C*), 134.9 and 134.2 (*C*HN=C), 131.0 and 130.9 ($C_{o\text{-tolyl}}$), 130.49 and 130.46 ($C_{o\text{-tolyl}}$), 129.4 ($C_{o\text{-tolyl}}$), 127.34 and 127.30 ($C_{o\text{-tolyl}}$), 126.9 and 126.75 *C*CH_3), 126.6 and 126.2 (*C*HN-*o*-tolyl), 118.41 and 118.38 (*C*N), 44.8 and 44.65 (O=C*C*H), 25.1 (*C*H_2CH_3), 18.16 and 18.12 (*C*H_2CN), 17.32 and 17.15 (*C*H_3), 10.93 and 10.86 CH_2*C*H_3);

HRMS(ESI+) calcd. for $C_{16}H_{17}N_3ONa$ $(M + Na)^+$ 290.1264, found: 290.1266;

HPLC Daicel Chiralpak AD-H column, 25 ºC, 1.0 mL/min, hexanes:*i*-PrOH 70:30, isocratic flow, t_R(minor) = 5.7 min, t_R(major) = 6.5 min.

Scope of the α-Cyanoalkyl bromides (Scheme 49, p.41 and Scheme 50, p.42)

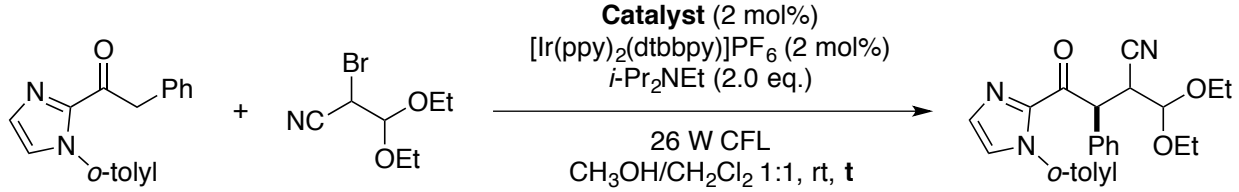

74ca **95b**, 3 or 6 **eq.** **189cab**

(3*S*)-2-(Diethoxymethyl)-4-oxo-3-phenyl-4-(1-(*o*-tolyl)-1*H*-imidazol-2-yl)butanenitrile (177cab)

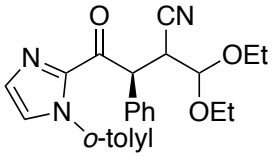

Following general procedure 6, 2-acyl imidazole **74ca** (55.3 mg, 200 μmol) and branched α-cyanoalkyl bromide **95b** (200 μL, 1.20 mmol) were converted to *rac*-**189cab** (67.6 mg, 81%) with *rac*-RhO (3.30 mg, 4.00 μmol) as catalyst. The conversion of **74ca** was incomplete after 24 h photolysis. The diastereomers of *rac*-**189cab** were separated from each other through flash column chromatography on silica gel (*n*-hexane:EtOAc 3:1 then 1.5:1) to obtain the necessary analytical data for respective diastereomer of **189cab**. With Δ-RhS (3.50 mg, 4.00 μmol) as catalyst, **74ca** (55.3 mg, 200 μmol) and branched α-cyanoalkyl bromide **95b** (104 μL, 600 μmol) were converted to (*S*)-**189cab** (83.2 mg, 199 μmol, >99%). The conversion of **74ca** was complete after 15 h. According to the earlier obtained analytical data and ^{1}H-NMR spectra of the crude reaction mixture, the diastereomeric ratio was determined as 2.5:1 (Figure 16). The HPLC analysis on chiral stationary phase of the product revealed 98% *ee* for both diastereomers of (*S*)-**189cab**.

^{1}H-NMR (300 MHz; $CDCl_3$): **major diastereomer**: δ 7.43−6.79 (m, 10H, $4H_{o\text{-tolyl}}$ + $5H_{Ph}$ + $H_{imidazolyl}$), 7.03 (d, *J* = 0.9 Hz, 1H, C*H*N-*o*-tolyl), 5.51 (dd, *J* = 11.7, 9.8 Hz, 1H, O=CC*H*), 4.57 (dd, *J* = 7.7, 5.8 Hz, 1H, C*H*$(OEt)_2$), 3.87 (ddd, *J* = 9.6, 8.5, 5.8 Hz, 1H, NCC*H*), 3.74−3.64 (m, 2H, OC*H*$_2$$CH_3$), 3.57−3.46 (m, 2H, OC*H*$_2$$CH_3$), 2.05 and 1.51 (s, 3H, C*H*$_3$), 1.20−1.05 (m, 6H, 2OCH_2C*H*$_3$), contained rotamers; **minor diastereomer**: δ 7.41−6.91 (m, 10H, $4H_{o\text{-tolyl}}$ + $5H_{Ph}$ + $H_{imidazolyl}$), 7.04 (d, *J* = 0.4 Hz, 1H, C*H*N-*o*-tolyl), 5.57 (dd, *J* = 10.5, 6.3 Hz, 1H, O=CC*H*), 4.08 (dd, *J* = 14.8, 3.6 Hz, 1H, C*H*$(OEt)_2$), 3.80−3.69 (m, 1H, NCC*H*), 3.56−3.48 (m, 2H, OC*H*$_2$$CH_3$), 3.42−3.32 (m, 2H, OC*H*$_2$$CH_3$), 2.05 and 1.63 (s, 3H, C*H*$_3$), 1.26−1.20 (m, 3H, OCH_2C*H*$_3$), 1.10 (td, *J* = 7.0, 2.0 Hz, 3H, OCH_2C*H*$_3$), contained rotamers;

^{13}C-NMR (75.5 MHz; $CDCl_3$): δ 186.8, 186.5, 186.4, 142.53, 142.46, 142.43, 142.33, 137.70, 137.67, 137.61, 137.55, 135.12, 135.08, 134.98, 134.66, 134.56, 134.49, 134.2, 130.92, 130.84, 130.79, 130.69, 130.63, 130.57, 130.49, 130.41, 129.37, 129.32, 129.26, 129.13, 129.08, 129.03, 128.96, 128.2, 127.20, 127.17, 127.11, 127.02, 126.80, 126.69, 126.63, 126.53, 126.29, 126.26, 126.1, 118.22, 118.14, 118.05, 118.00, 100.71, 100.54, 99.7, 64.2, 63.95, 63.91, 63.70, 63.60, 63.57, 52.22, 52.06, 51.1, 50.7, 40.13, 39.94, 39.77, 39.63, 17.41, 17.28, 16.7, 16.5, 15.19, 15.14, 15.11, 14.93, contained rotamers, mixture of both diasteromers;

HRMS(ESI+) calcd. for $C_{25}H_{28}N_3O_3$ $(M + H)^+$ 419.2125, found: 418.2130;

HPLC Daicel Chiralpak AD-H column, 25 ºC, 1.0 mL/min, hexanes:*i*-PrOH 70:30, isocratic flow, **major diastereomer**: t_R(minor) = 4.6 min, t_R(major) = 6.1 min; **minor diastereomer**: t_R(minor) = 4.0 min, t_R(major) = 6.0 min.

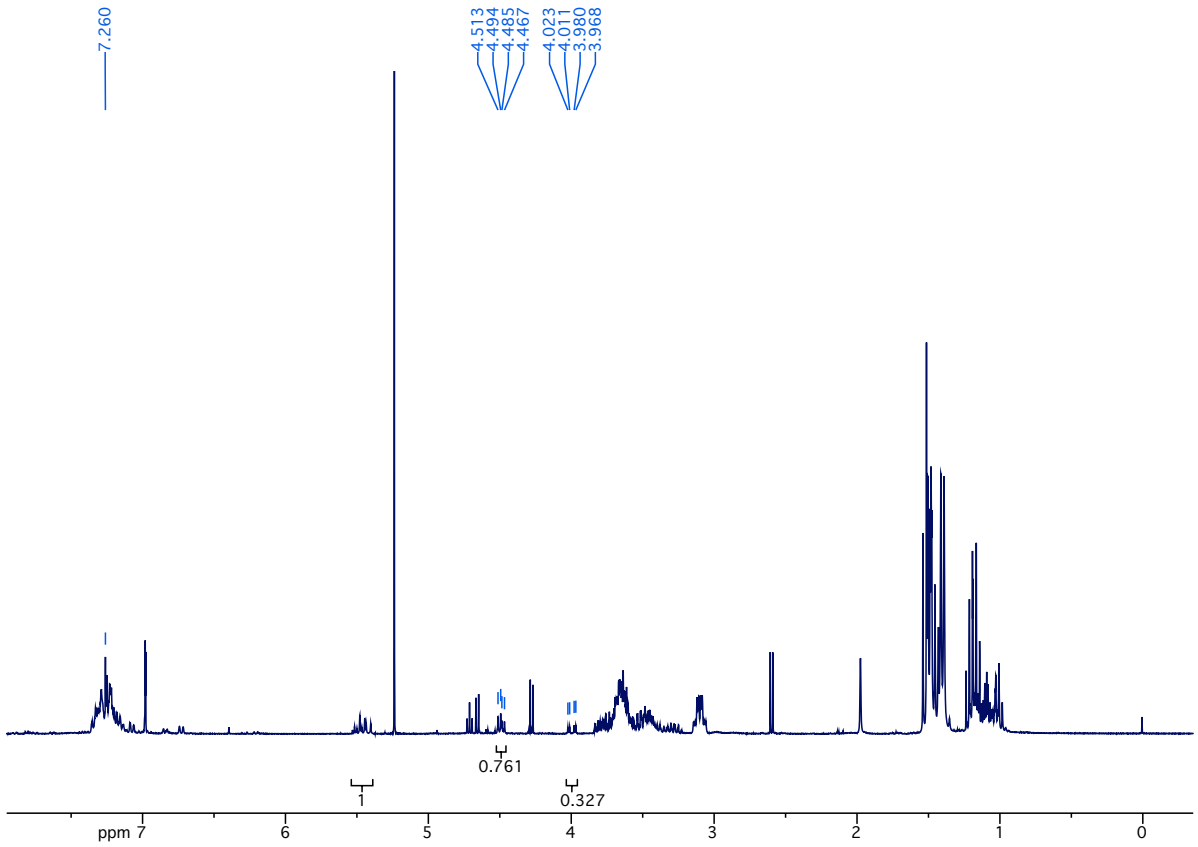

Figure 16: ^{1}H-NMR spectrum of the crude reaction mixture to determine the diastereomeric ratio of (*S*)-**189cab**.

5.4.4. Mechanistic Investigations (Table 8, p.43)

General Procedure 7 (Reaction Conditions without Variations)

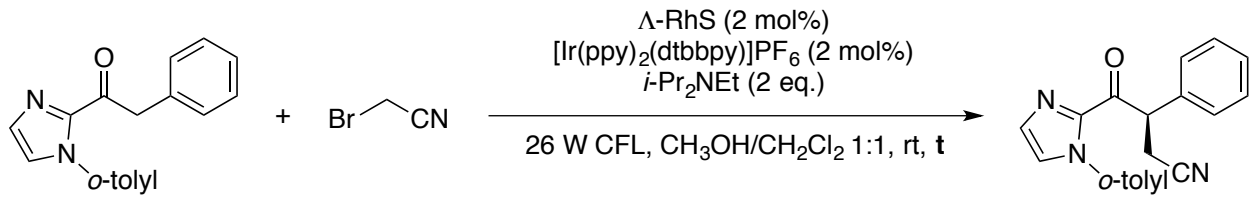

74ca **95a**, 6 eq. (*R*)-**189caa**

To a Schlenk-tube were added 2-acyl imidazole substrate **74ca** (55.3 mg, 200 µmol), *i*-Pr_2NEt (69.2 µL, 400 µmol), $[Ir(ppy)_2(dtbbpy)]PF_6$ (3.70 mg, 4.00 µmol), Λ-RhS (3.50 mg, 4.00 µmol), and CH_3OH/CH_2Cl_2 (500 µL, v/v 1:1) under nitrogen atmosphere. The mixture was stirred at rt for 5 min. After adding bromo-acetonitrile (83.6 µL, 1.20 mmol), the Schlenk-tube was sealed with a screw-cap and reaction mixture was degassed through the freeze-pump-thaw procedure for three cycles and stirred at rt under irradiation with two 13-Watt CFL for the given duration. After evaporating the solvent under vacuum, the residue was purified through flash column chromatography on silica gel (*n*-hexane:EtOAc 5:1 then 2:1) to afford the product. The enantiomeric purity was determined through HPLC analysis of the product on chiral stationary phase as described (see Chapter 5.4.2, p.103).

Entries 2 and 3:

Following general procedure 7, the reaction was performed in the absence of light. The reaction mixture was submitted to ^{1}H-NMR analysis after 1.5 h and no product formation could be detected (Figure 17). The reaction was repeated and worked up after 48 h. The purification afforded remaining substrate **74ca** (12.4 mg, 44.9 µmol, 78% conv.) and product (*R*)-**189caa** (45.6 mg, 145 µmol, 72%) with 4% *ee*.

Entries 4 and 5:

Following general procedure 7, the reaction was performed without being degassed. An air balloon was connected to the Schlenk-tube during the reaction. The reaction mixture was submitted to ^{1}H-NMR analysis after 1.5 h and no product formation could be detected (Figure 18). The reaction was repeated and worked up after 48 h. The purification afforded remaining substrate **74ca** (32.9 mg, 119 µmol, 41% conv.) and product (*R*)-**189caa** (14.5 mg, 46.0 µmol, 23%) with 60% *ee*.

Entries 6 and 7:

Following general procedure 7, the reaction was performed in the absence of $[Ir(ppy)_2(dtbbpy)]PF_6$. The reaction mixture was submitted to ^{1}H-NMR analysis after 1.5 h and no product formation could be detected. The reaction was repeated and the TLC analysis of crude reaction mixture indicated a complete conversion of 2-acyl imidazole substrate **74ca** after 24 h photolysis. The purification afforded product (*R*)-**177caa** (61.2 mg, 194 µmol, 97%) with 79% *ee*.

Entry 8:

Following general procedure 7, the reaction was performed in the absence of Λ-RhS and worked up after 48 h to afford product *rac*-**189caa** (19.8 mg, 62.8 μmol) in 31% yield.

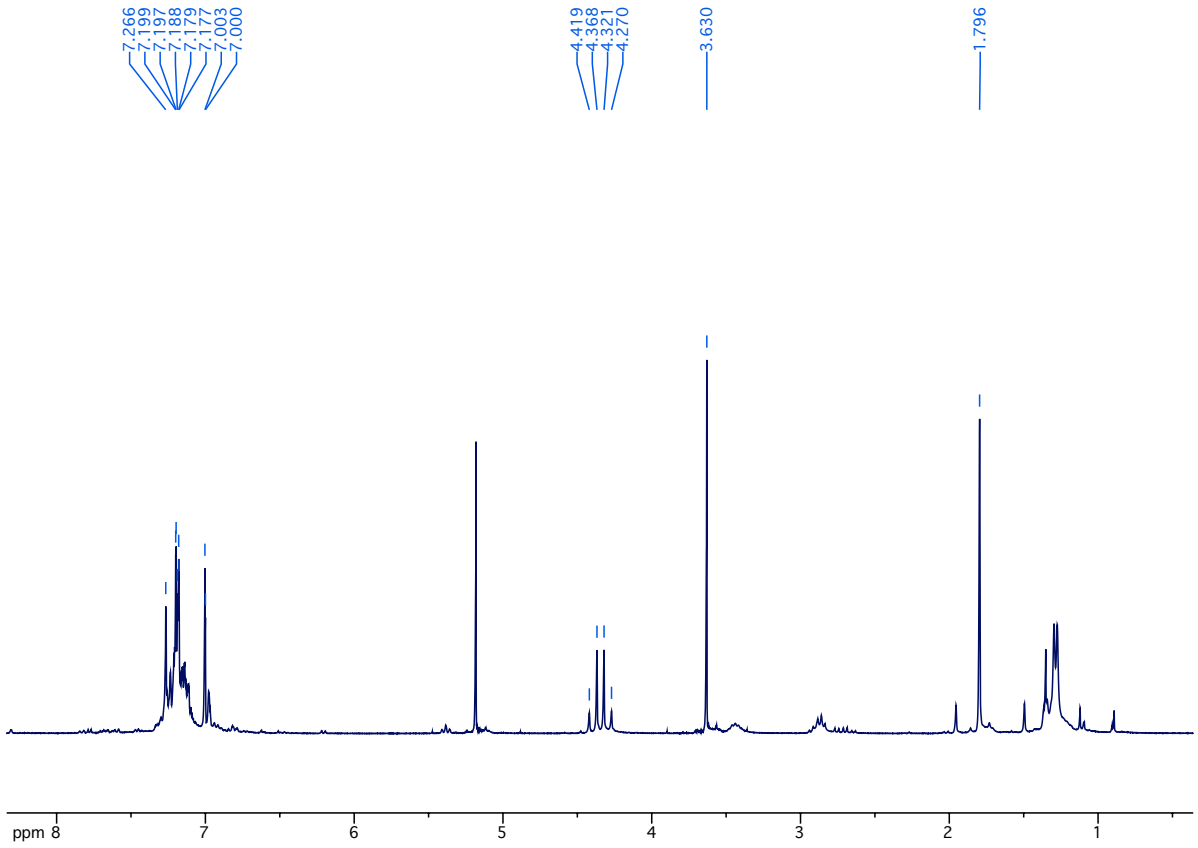

Figure 17: ^{1}H-NMR spectrum of the crude reaction mixture from Table 8, entry 2 (p.43).

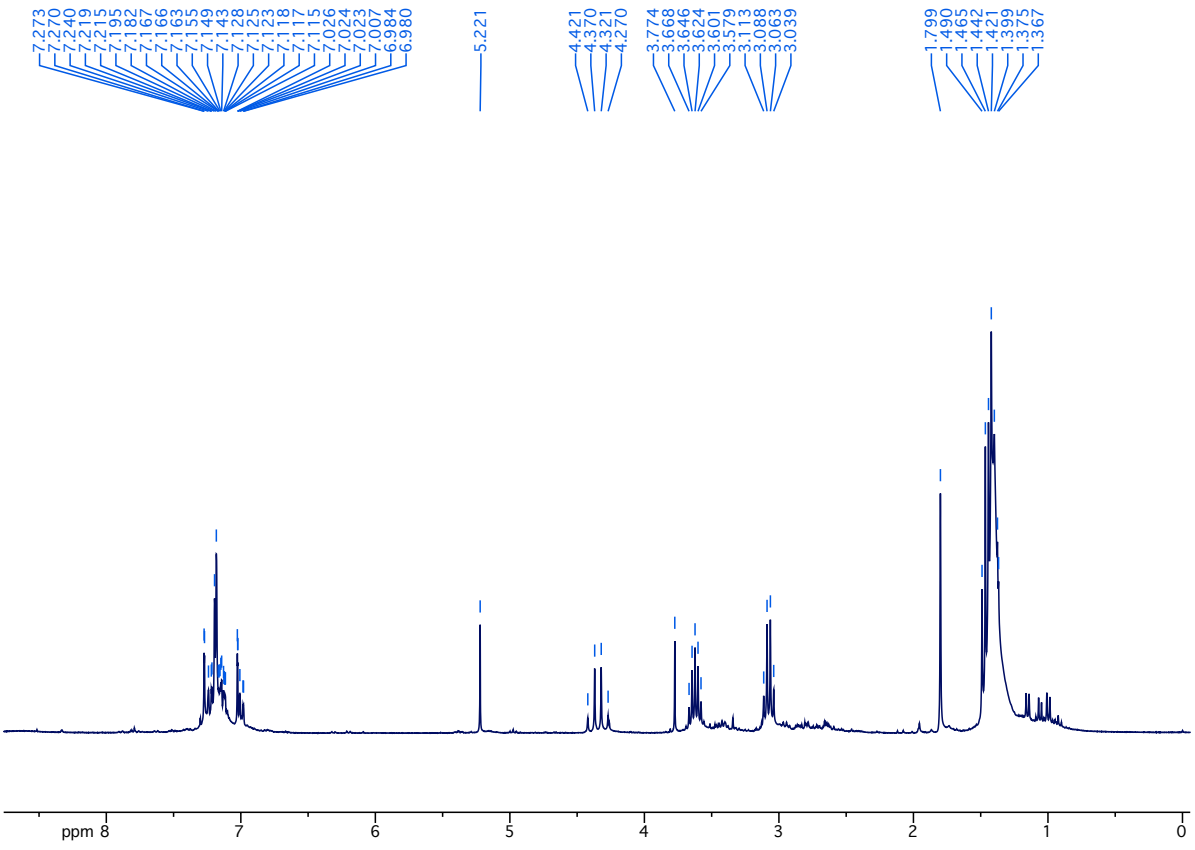

Figure 18: ^{1}H-NMR spectrum of the crude reaction mixture from Table 8, entry 4 (p.43).

^{1}H-NMR Analysis of Enolization (p.43)

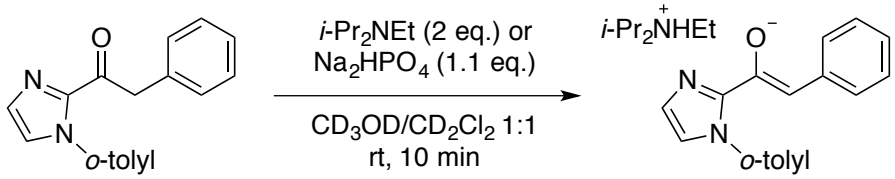

As reference, 2-acyl imidazole substrate **74ca** was dissolved in CD_2Cl_2/CD_3OD (v/v 1:1) at rt and submitted to ^{1}H-NMR analysis (Figure 19). 2-acyl imidazole substrate **74ca** (55.3 mg, 200 µmol) was dissolved in CD_3OD/CD_2Cl_2 (500 µL, v/v 1:1) under nitrogen atmosphere in a Schlenk-tube. After adding *i*-Pr_2NEt (69.2 µL, 400 µmol) and Na_2HPO_4 (56.8 mg, 400 µmol) respectively, the mixtures were degassed through the freeze-pump-thaw procedure for three cycles and stirred at rt for 10 min. The mixtures were submitted to ^{1}H-NMR analysis and the methylene signal of **74ca** could be observed with Na_2HPO_4 (Figure 20) and vanished in the presence of *i*-Pr_2NEt (Figure 21), indicating that **74ca** was enolized by *i*-Pr_2NEt in the absence of Lewis acid catalyst.

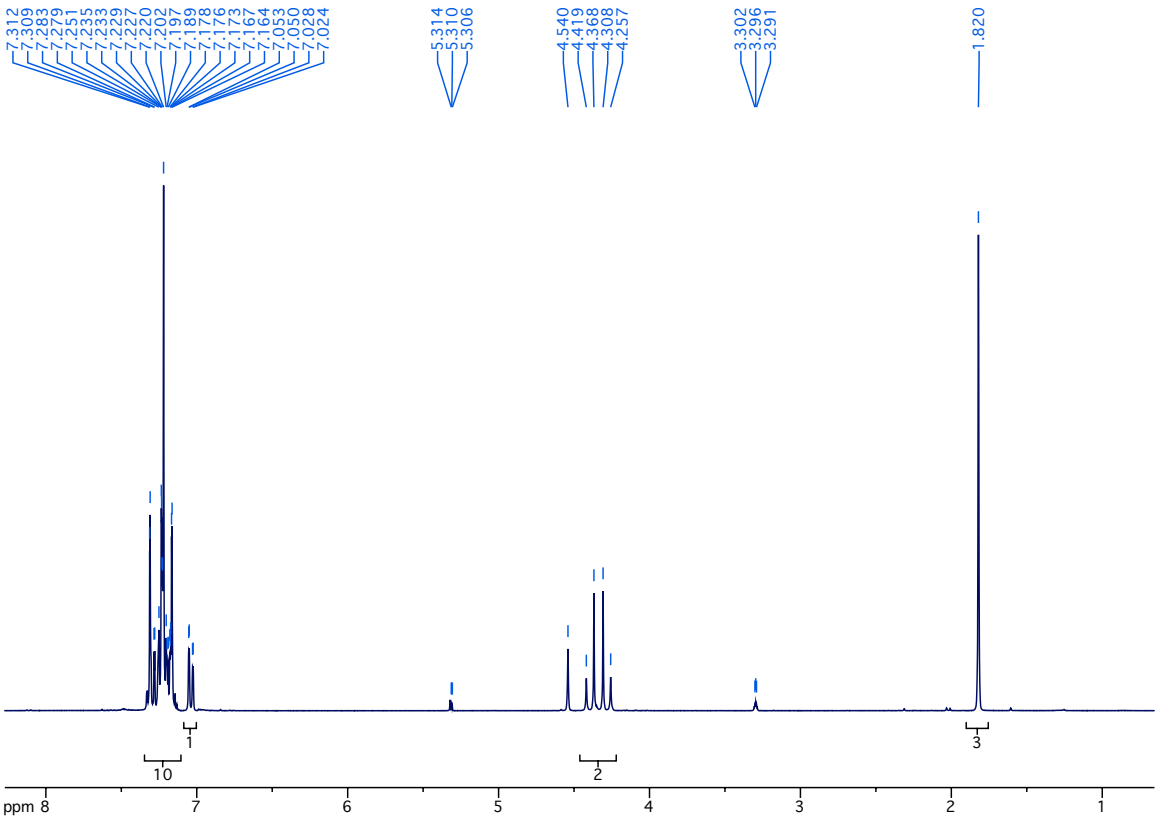

Figure 19: ^{1}H-NMR spectrum **74ca** in CD_2Cl_2/CD_3OD.

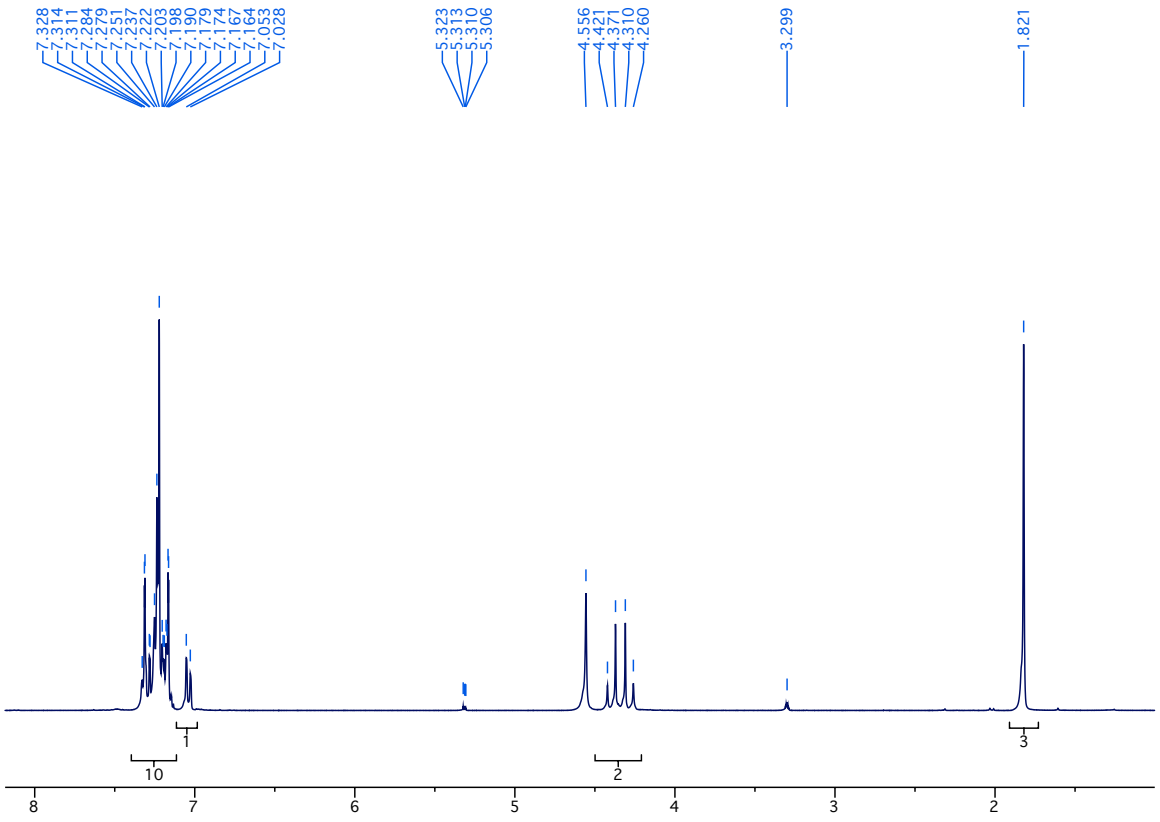

Figure 20: ^{1}H-NMR spectrum of **74ca** and Na_2HPO_4 in CD_2Cl_2/CD_3OD.

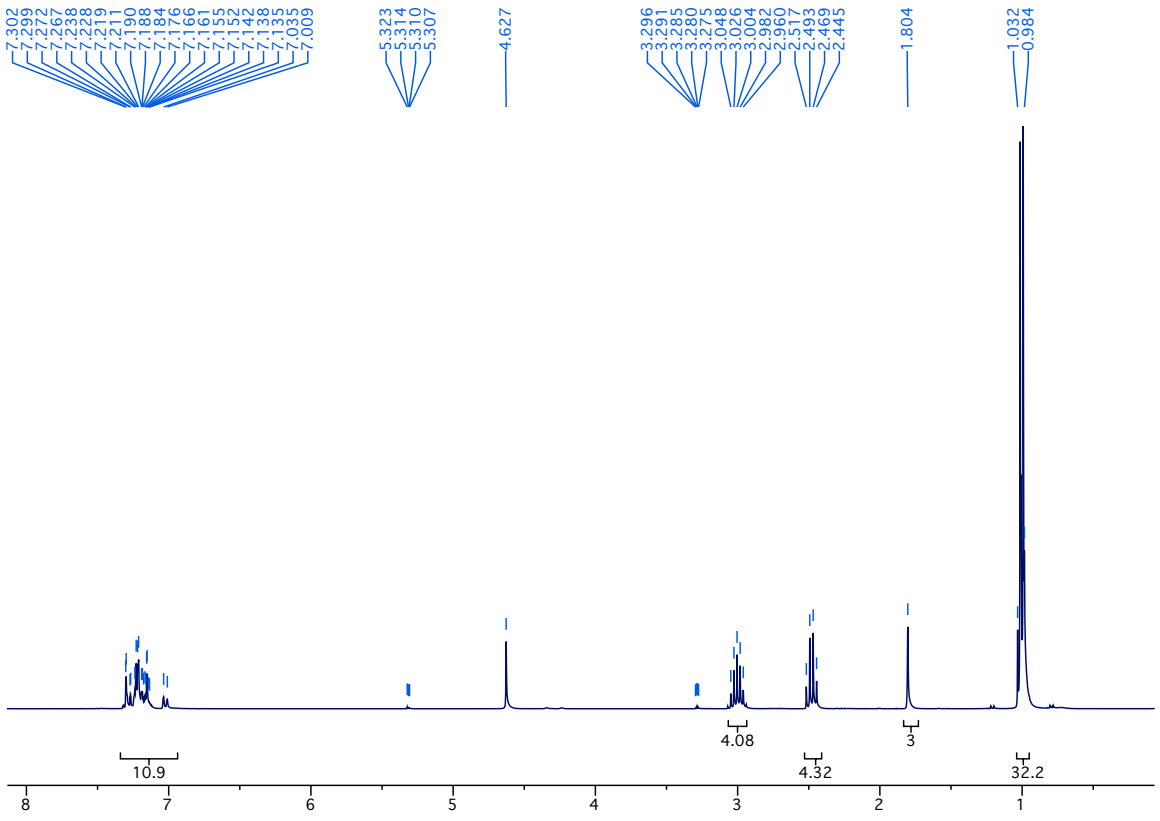

Figure 21: ^{1}H-NMR spectrum of **74ca** and *i*-Pr_2NEt in CD_3OD/CD_2Cl_2.

5.5. Asymmetric α-Benzoyloxylation of 2-Acyl Imidazoles

5.5.1. Preliminary Results (Scheme 62, p.50)

Procedure with Photocatalyst:

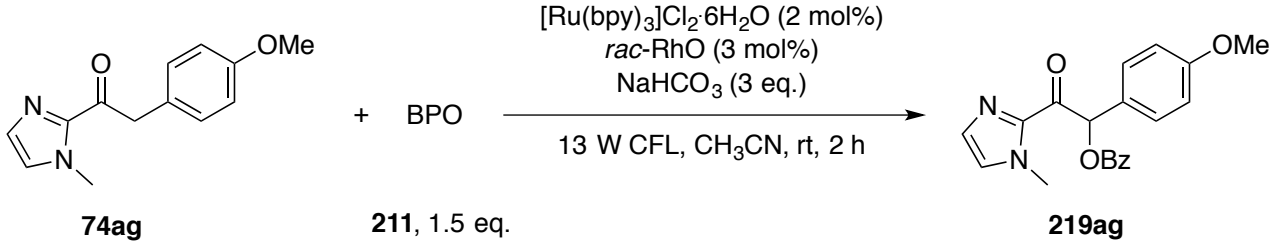

74ag **211**, 1.5 eq. **219ag**

To a Schlenk-tube were added 2-acyl imidazole substrate **74ag** (46.0 mg, 200 µmol), benzoyl peroxide (96.8 mg, 300 µmol, 75%), $NaHCO_3$ (50.4 mg, 600 µmol), $[Ru(bpy)_3]Cl_2 \cdot 6H_2O$ (3.00 mg, 4.00 µmol), and *rac*-RhO (5.00 mg, 6.00 µmol). After adding acetonitrile (500 µL), the tube was sealed with a screw-cap. The reaction mixture was degassed through the freeze-pump-thaw procedure for three cycles and stirred at rt under irradiation with a 13-Watt CFL. The TLC analysis of the reaction mixture revealed a complete conversion of imidazole substrate **74ag** after 2 h. After evaporating the solvent in vacuum, the residue was purified through flash column chromatography on silica gel (*n*-hexane:EtOAc 3:1) to afford **219ag** (50.4 mg, 144 µmol, 72%) as pale yellow oils. The reaction was repeated in absence of light and finished in 2 h to give a similar result, demonstrating that visible light was not necessary for the reaction.

Procedure without Photocatalyst:

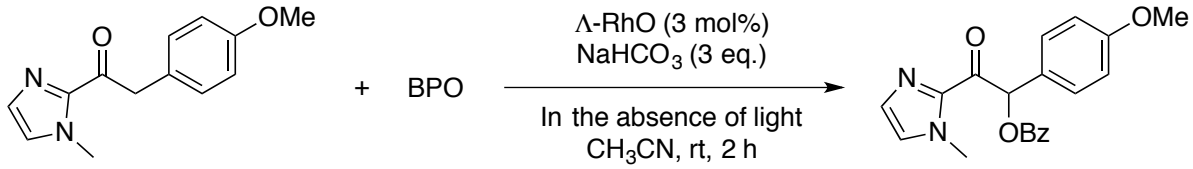

74ag **211**, 1.5 eq. **219ag**

To a Schlenk-tube were added 2-acyl imidazole substrate **74ag** (46.0 mg, 200 µmol), benzoyl peroxide (96.8 mg, 300 µmol, 75%), $NaHCO_3$ (50.4 mg, 600 µmol), Λ-RhO (5.00 mg, 6.00 µmol), and acetonitrile (500 µL) under nitrogen atmosphere. The tube was sealed with a screw-cap and the reaction mixture was stirred at rt for 2 h in the absence of light. After evaporating the solvent in vacuum, the residue was purified through flash column chromatography on silica gel (*n*-hexane:EtOAc 3:1) to afford **219ag** (67.4 mg, 192 µmol, 96%) with 40% *ee* as pale yellow oil. The absolute configuration of **219ag** was not determined

1-(4-Methoxyphenyl)-2-(1-methyl-1H-imidazol-2-yl)-2-oxoethyl benzoate (219ag)

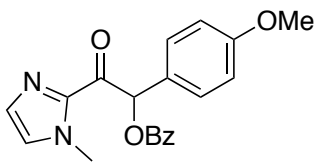

^{13}C-NMR (75.5 MHz, $CDCl_3$): δ 185.5 (O=*C*), 166.1 (O=*C*Ph), 160.2 (*C*OCH_3), 141.0 (N=*C*NCH_3), 133.5 (C_{Ph}), 133.3, 130.2, 130.0, 129.9, 129.7, 128.50, 128.45, 127.4, 126.1, 114.3, 55.4 (O*C*H_3), 36.0 (N*C*H_3);

HPLC Daicel Chiralpak AD-H column, 25 ºC, 0.5 mL/min, hexanes:*i*-PrOH 70:30, isocratic flow, t_R(major) = 23.9 min, t_R(minor) = 29.0 min.

5.5.2. Optimization of the Reaction Conditions

Solvent Screening (Table 9 and Table 10, p.51−52)

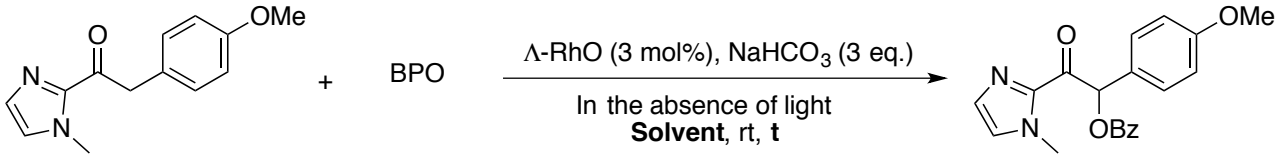

74ag **211**, 1.5 eq. **219ag**

To a Schlenk-tube were added 2-acyl imidazole substrate **74ag** (23.0 mg, 100 μmol), benzoyl peroxide (48.4 mg, 150 μmol, 75%), $NaHCO_3$ (25.2 mg, 300 μmol), Λ-RhO (2.50 mg, 3.00 μmol), and the solvent (250 μL) under nitrogen atmosphere. The tube was sealed with a screw-cap and the mixture was stirred at rt in absence of light for the given reaction duration. A small amount reaction mixture was taken out and diluted with HPLC-grade hexanes. The samples were filtered through a syringe filter and analyzed through chiral HPLC to determine the enantiomeric excess of **219ag**. The results of the reactions with $NaHCO_3$ as base are given in Table 9 (p.51). The results of the reactions in the absence of base are given in Table 10 (p. 51−52).

Influences of Molar Ratio and Catalysts (Table 11, p.52)

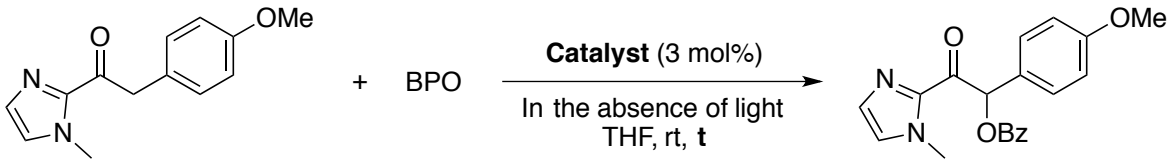

74ag, 3 eq. **211**, 1 eq. **219ag**

To a Schlenk-tube were added 2-acyl imidazole substrate **74ag** (69.0 mg, 300 μmol), benzoyl peroxide (32.3 mg, 100 μmol, 75%), chiral Lewis acid catalyst (3.00 μmol), and THF (250 μL) under nitrogen atmosphere. The tube was sealed with a screw-cap and the mixture was stirred at rt in absence of light. A small amount reaction mixture was taken out and diluted with HPLC-grade hexanes. The samples were filtered through a syringe filter and analyzed through chiral HPLC to determine the enantiomeric excess of the product. While the reaction with Λ-RhO (2.50 mg, 3.00 μmol) revealed a complete conversion of **74ag** after 3 h to give **219ag** with 52% *ee* (entry 1). The reactions with Λ-IrO (2.80 mg, 3.00 μmol) and Λ-IrS (2.90 mg, 3.00 μmol) afforded **219ag** with 25% *ee* and 27% *ee* respectively. Imidazole substrate **74ag** was not completely consumed after 20 h in both reactions with iridium catalyst (entries 2 and 3). The absolute configuration of **219ag** was not determined.

Influences of Concentration, Temperature, and Additives (Table 12, p.53)

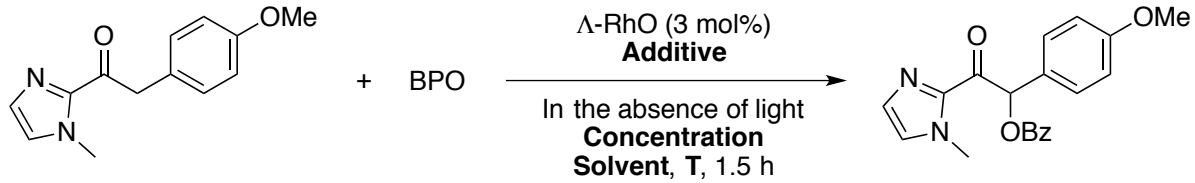

74ag **211**, 1.5 eq. **219ag**

Entry 2:

To a Schlenk-tube were added 2-acyl imidazole substrate **74ag** (23.0 mg, 100 μmol), benzoyl peroxide (48.4 mg, 150 μmol, 75%), Λ-RhO (2.50 mg, 3.00 μmol), and toluene (250 μL) under nitrogen atmosphere. The tube was sealed with a screw-cap and the mixture was stirred at 0 °C in absence of light for 1.5 h. A small amount reaction mixture was taken out and diluted with HPLC-grade hexanes. The sample was filtered through a syringe filter and analyzed through HPLC to reveal that **74ag** was not completely consumed and **219ag** was formed with 56% *ee*. The absolute configuration of **219ag** was not determined.

Entry 3:

To a Schlenk-tube were added 2-acyl imidazole substrate **74ag** (23.0 mg, 100 μmol), benzoyl peroxide (48.4 mg, 150 μmol, 75%), Λ-RhO (2.50 mg, 3.00 μmol), and toluene (1.00 mL) under nitrogen atmosphere. The tube was sealed with a screw-cap and the mixture was stirred at rt in absence of light for 1.5 h. A small amount reaction mixture was taken out and diluted with HPLC-grade hexanes. The sample was filtered through a syringe filter and analyzed through HPLC to reveal that **74ag** was not completely consumed and **219ag** was formed with 58% *ee*. The absolute configuration of **219ag** was not determined.

Entry 4:

To a Schlenk-tube were added 2-acyl imidazole substrate **74ag** (23.0 mg, 100 μmol), benzoyl peroxide (48.4 mg, 150 μmol, 75%), trifluoroacetic acid (765 nL, 10.0 μmol) Λ-RhO (2.50 mg, 3.00 μmol), and toluene (1.00 mL) under nitrogen atmosphere. The tube was sealed with a screw-cap and the mixture was stirred at rt in absence of light for 1.5 h. A small amount reaction mixture was taken out and diluted with HPLC-grade hexanes. The sample was filtered through a syringe filter and analyzed through HPLC to reveal that **74ag** was not completely consumed and **219ag** was formed with 54% *ee*. The absolute configuration of **219ag** was not determined.

Entry 5:

To a Schlenk-tube were added 2-acyl imidazole substrate **74ag** (23.0 mg, 100 μmol), benzoyl peroxide (48.4 mg, 150 μmol, 75%), hydroxyquinone (1.10 mg, 10.0 μmol), Λ-RhO (2.50 mg, 3.00 μmol) and 1,2-dimethoxyethane (250 μL) under nitrogen atmosphere. The tube was sealed with a screw-cap and the mixture was stirred at rt in absence of light for 1.5 h. A small amount reaction mixture was taken out and diluted with HPLC-grade hexanes. The sample was filtered through a syringe filter and analyzed through HPLC to reveal that **74ag** was completely consumed and **219ag** was formed with 52% *ee*. The absolute configuration of **219ag** was not determined.

Entry 6:

The procedure from entry 5 was repeated with 2,6-di-*tert*-butyl-4-methylphenol (2.20 mg, 10.0 µmol) instead of hydroxyquinone. The HPLC analysis of the crude reaction mixture revealed that **74ag** was completely consumed and **219ag** was formed with 56% *ee*. The absolute configuration of **219ag** was not determined.

Influences of Substrate, Catalyst Loading, and Racemization (Scheme 63 and Scheme 64, p.53)

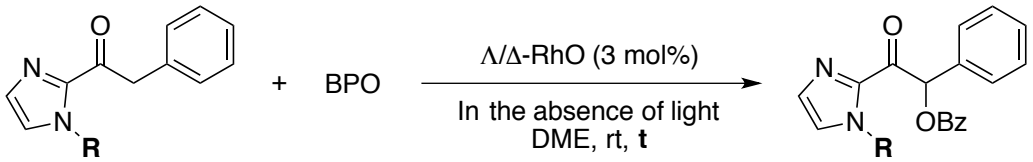

R = Me: **74aa**
R = *i*-Pr: **74da**

211, 1.5 eq.

R = Me: **219aa**
R = *i*-Pr: **219da**

To a Schlenk-tube were added 2-acyl imidazole substrate **74** (200 µmol), benzoyl peroxide (96.7 mg, 300 µmol, 75%), RhO (5.00 mg, 3.00 µmol), and DME (500 µL) under nitrogen atmosphere. The tube was sealed with a screw-cap and the mixture was stirred at rt in absence of light. After evaporating the solvent in vacuum, the residue was purified through flash column chromatography on silica gel (*n*-hexane:EtOAc 3:1) to afford the product **219**.

The reaction with substrate **74aa** (34.0 µL, 200 µmol) was performed with the catalyst Δ-RhO to afford the product **219aa** (54.7 mg, 171 µmol, 85%) with −72% *ee*. The reaction with substrate **74da** (41.4 µL, 200 µmol) was performed with the catalyst Λ-RhO to afford the product **219da** (67.8 mg, 195 µmol, 97%) with 79% *ee* (scheme 63, p.53). With Λ-RhO (10.0 mg, 6.00 µmol) as catalyst, the reaction was repeated with **74da** (41.4 µL, 200 µmol). After 1.5 h, HPLC analysis of the crude reaction mixture revealed 82% *ee* for **219da**. The solvent was evaporated in vacuum after 22 h and the residue was purified through flash column chromatography on silica gel to afford **219da** (72.1 mg, 207 µmol, >99%) with 52% *ee* (scheme 64, p.53). The absolute configurations of **219aa** and **219da** were not determined.

2-(1-Methyl-1*H*-imidazol-2-yl)-2-oxo-1-phenylethyl benzoate (219da)

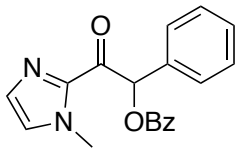

^{1}H-NMR (300 MHz; $CDCl_3$): δ 8.16−8.13 (m, 2H, $2H_{O=CPh}$), 7.80−7.76 (m, 2H, $2H_{Ph}$), 7.60−7.54 (m, 1H, $1H_{O=CPh}$), 7.49−7.34 (m, 6H, $2H_{O=CPh}$ + $3H_{Ph}$ + O=CC*H*), 7.22 (d, *J* = 0.8 Hz, 1H, C*H*N=C), 7.01 (s, 1H, C*H*NCH_3), 3.93 (s, 3H, NCH_3);

^{13}C-NMR (75.5 MHz; $CDCl_3$): δ 185.4 (O=C), 166.0 (O=*C*Ph), 141.1 (N=*C*NCH3), 134.2 (C_{Ph}), 133.4 (C_{Ph}), 130.1 ($2C_{Ph}$), 130.0 (*C*HN=C), 129.7 (C_{Ph}), 128.9 (*C*HNCH_3), 128.8 ($2C_{Ph}$), 128.5 ($2C_{Ph}$), 127.6 (C_{Ph}), 77.5 (O=C*C*H), 36.0 (N*C*H_3);

HPLC Daicel Chiralpak AD-H column, 25 ºC, 2.0 mL/min, hexanes:*i*-PrOH 90:10, isocratic flow, t_R(minor) = 10.6 min, t_R(major) = 11.3 min.

2-(1-*iso*-Propyl-1*H*-imidazol-2-yl)-2-oxo-1-phenylethyl benzoate (219da)

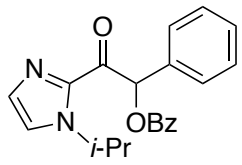

^{1}H-NMR (300 MHz; $CDCl_3$): δ 8.17−8.13 (m, 2H, $2H_{O=CPh}$), 7.78−7.74 (m, 2H, $2H_{O=CPh}$), 7.60−7.54 (m, 1H, $H_{O=CPh}$), 7.52 (s, 1H, O=CC*H*), 7.47−7.33 (m, 5H, $3H_{Ph}$ + $2H_{imidazolyl}$), 7.25−7.23 (m, 2H, $2H_{Ph}$), 5.44 (dt, *J* = 13.3, 6.7 Hz, 1H, C*H*Me$_2$), 1.44 (d, *J* = 6.7 Hz, 3H, C*H*$_3$), 1.32 (d, *J* = 6.7 Hz, 3H, C*H*$_3$);
^{13}C-NMR (75.5 MHz; $CDCl_3$): δ 185.4 (O=*C*), 166.0 (O=*C*Ph), 140.6 (N=*C*N-*i*-Pr), 134.5 (C_{Ph}), 133.3 ($C_{O=CPh}$), 130.5 (*C*HN=C), 130.1 ($2C_{Ph}$), 129.8 ($C_{O=CPh}$), 128.84 (*C*HN-*i*-Pr), 128.76 ($2C_{Ph}$), 128.73 ($2C_{O=CPh}$), 128.5 ($2C_{O=CPh}$), 121.8 (C_{Ph}), 77.9 (O=C*C*H), 49.4 (*C*HMe$_2$), 23.6 (*C*H$_3$), 23.5 (*C*H$_3$);
HRMS(ESI+) calcd. for $C_{21}H_{21}N_2O_3$ $(M + H)^+$ 349.1547, found: 349.1547;
HPLC Daicel Chiralpak AD-H column, 25 ºC, 2.0 mL/min, hexanes:*i*-PrOH 90:10, isocratic flow, t_R(major) = 3.6 min, t_R(minor) = 4.7 min.

Reactions with Substrate 74dh In the Absence of Light (Scheme 66, p.54)

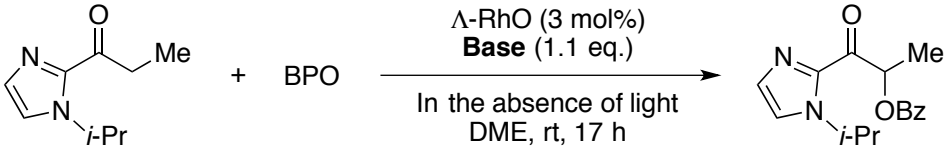

74dh **211**, 1.5 eq. **219dh**

To a Schlenk-tube were added 2-acyl imidazole substrate **74dh** (32.5 μL, 200 μmol), benzoyl peroxide (96.7 mg, 300 μmol, 75%), Λ-RhO (5.00 mg, 3.00 μmol), base (220 μmol), and DME (500 μL) under nitrogen atmosphere. The tube was sealed with a screw-cap and the mixture was stirred at rt in absence of light for 17 h. After evaporating the solvent in vacuum, the residue was purified through flash column chromatography on silica gel (*n*-hexane:EtOAc 3:1) to afford a mixture of **74dh** and **219dh**. The yield of **219dh** was calculated according to the ^{1}H-NMR spectra of the mixture. The reaction with *i*-Pr$_2$NH (31.0 μL, 220 μmol) afforded **219dh** in 29% yield with 61% *ee* and the reaction with Na_2CO_3 (23.4 mg, 220 μmol) afforded **219dh** in 26% yield with 60% *ee*.

1-(1-*iso*-Propyl-1*H*-imidazol-2-yl)-1-oxopropan-2-yl benzoate (219dh)

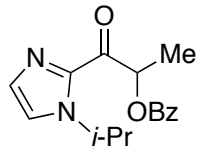

^{1}H-NMR (300 MHz; $CDCl_3$): δ 8.11−8.08 (m, 2H, $2H_{Ph}$), 7.57−7.52 (m, 1H, H_{Ph}), 7.45−7.40 (m, 2H, $2H_{Ph}$), 7.28 (d, *J* = 1.0 Hz, 1H, $H_{imidazolyl}$), 7.21 (d, *J* = 0.9 Hz, 1H, $H_{imidazolyl}$), 6.39 (q, *J* = 7.0 Hz, 1H, O=CC*H*), 5.50−5.44 (m, 1H, C*H*Me$_2$), 1.74 (d, *J* = 7.0 Hz, 3H, O=CCHC*H*$_3$), 1.42 (d, *J* = 6.7 Hz, 6H, 2C*H*$_3$).

Reactions with Substrate 74dh in the Presence of Light (Scheme 67, p.55)

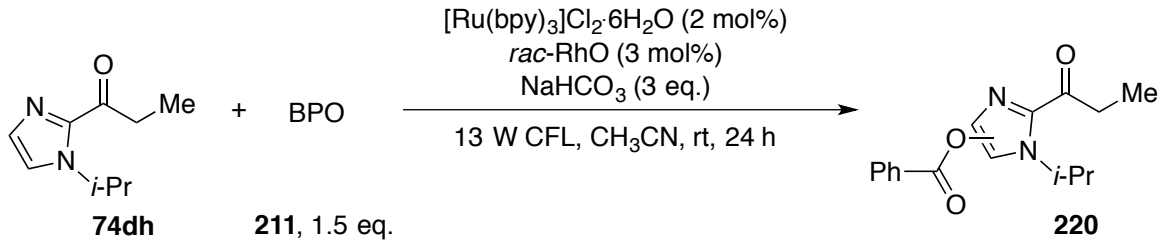

74dh **211**, 1.5 eq. **220**

To a Schlenk-tube were added 2-acyl imidazole substrate **74dh** (16.6 mg, 100 µmol), benzoyl peroxide (48.4 mg, 150 µmol, 75%), $NaHCO_3$ (25.4 mg, 300 µmol), $[Ru(bpy)_3]Cl_2·6H_2O$ (1.50 mg, 2.00 µmol), *rac*-RhO (2.50 mg, 3.00 µmol), and acetonitrile (250 µL). The tube was sealed with a screw-cap. and the reaction mixture was degassed through the freeze-pump-thaw procedure for three cycles. After irradiating with a 13-Watt CFL at rt for 24 h, the solvent was evaporated under vacuum. The residue was purified through flash column chromatography on silica gel (*n*-hexane:EtOAc 3:1) to afford **220** that contained intact methylene group (Figure 22).

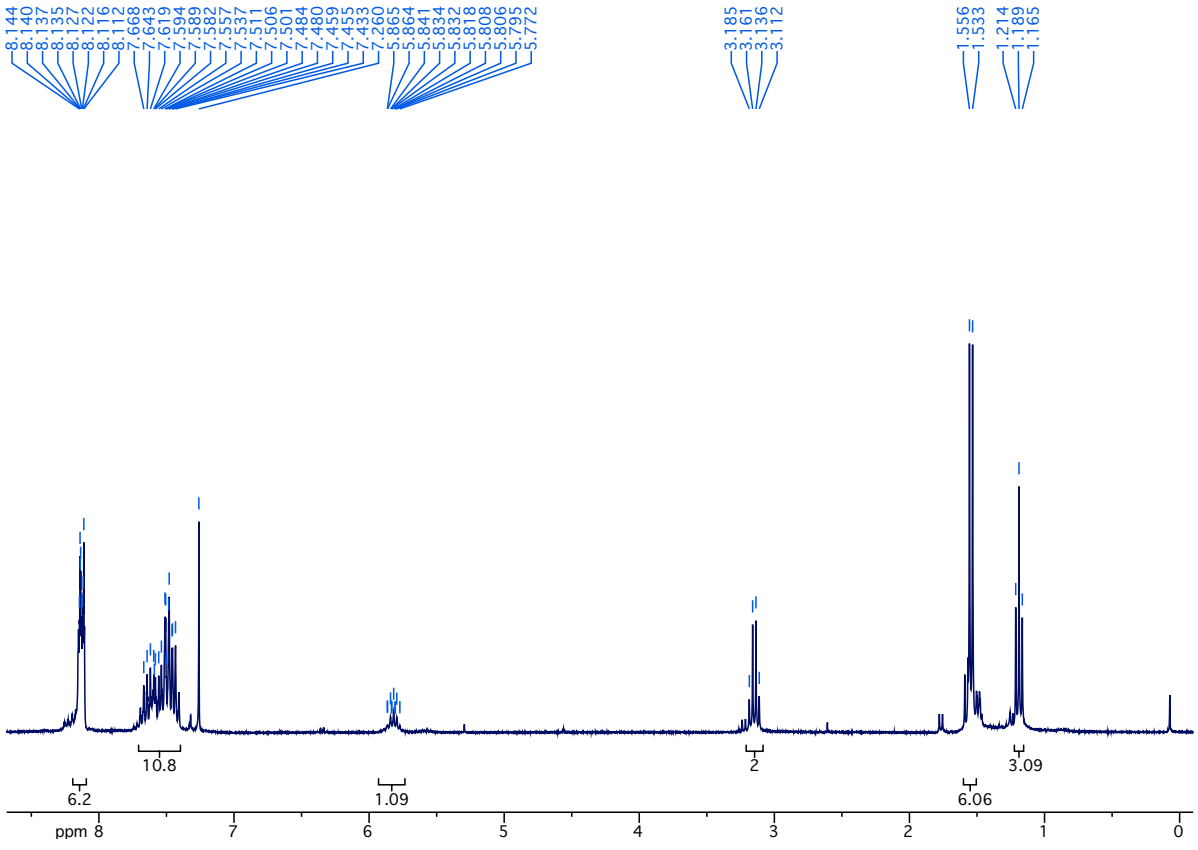

Figure 22: ^{1}H-NMR spectrum of **220** from the reaction illustrated in Scheme 67 (p.55).

5.6. Direct α-Arylation of 2-Acyl Imidazoles

5.6.1. Preliminary Results

Investigation of Nucleophiles (Scheme 75, p.61)

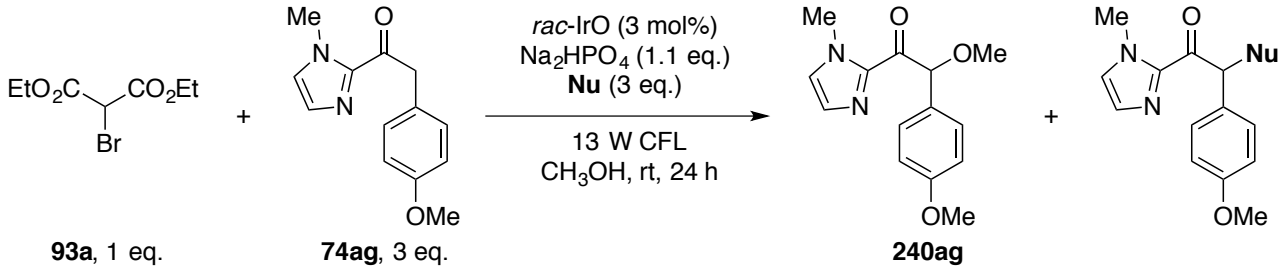

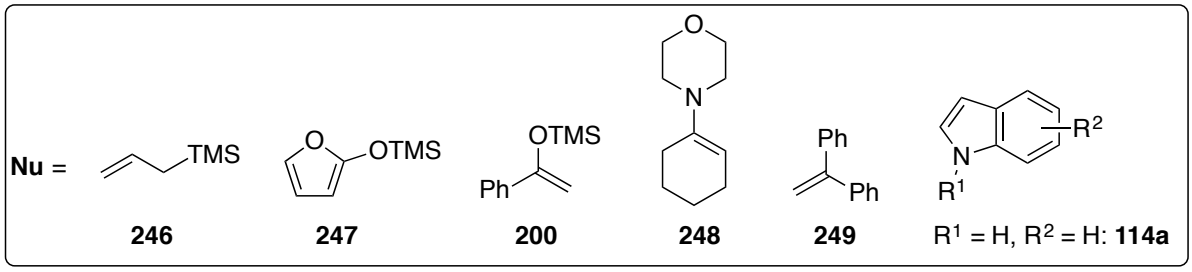

To a Schlenk-tube were added 2-acyl imidazole **74ag** (138 mg, 600 µmol), diethyl bromomalonate (37.1 µL, 200 µmol, 92%), nucleophile **114a**, **200**, **246**–**249** (600 µmol), Na_2HPO_4 (31.2 mg, 220 µmol), and *rac*-IrO (5.50 mg, 6.00 µmol). After adding methanol (500 µL), the tube was sealed with a screw-cap. The reaction mixture was degassed through the freeze-pump-thaw procedure for three cycles and irradiated with a 13-Watt CFL at rt for 24 h. The TLC analysis revealed that the reactions with the allylsilane **246** (47.6 µL, 300 µmol) and the enamine **248** (98.4 µL, 600 µmol) resulted in no conversion of imidazole substrate **74ag**. After purification through flash column chromatography on silica gel (*n*-hexane:EtOAc 2:1), the reactions with 2-(trimethylsiloxy)furan (**247**, 101 µL, 600 µmol), silyl enol ether **200** (123 µL, 600 µmol), and 1,1-diphenylethylene (**249**, 106 µL, 600 µmol) afforded methoxy product **240ag** (32.4 mg, 124 µmol, 62%; 15.8 mg, 60.7 µmol, 30%; 38.5 mg, 148 µmol, 74%).

2-Methoxy-2-(4-methoxyphenyl)-1-(1-methyl-1*H*-imidazol-2-yl)ethan-1-one (240ag)

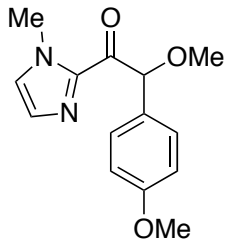

^{1}H-NMR (300 MHz; $CDCl_3$): δ 7.51–7.48 (m, 2H, $2H_{p\text{-MeO-Ph}}$), 7.12 (s, 1H, C*H*N=C), 6.98 (s, 1H, C*H*NCH_3), 6.85–6.82 (m, 2H, $2H_{p\text{-MeO-Ph}}$), 6.11 (s, 1H, O=CC*H*OCH_3), 3.92 (s, 3H, $COCH_3$), 3.74 (s, 3H, NCH_3), 3.39 (s, 3H, $CHOCH_3$);

^{13}C-NMR (75.5 MHz; $CDCl_3$): δ 188.4 (*C*=O), 159.8 (*C*OCH_3), 141.9 (N=*C*N), 129.7 ($2C_{p\text{-MeO-Ph}}$), 129.6

(O=CCH$_2$*C*), 128.4 (*C*HN=C), 127.4 (*C*HNCH$_3$), 114.1 (2C$_{p\text{-MeO-Ph}}$), 83.2 (O=C*C*HOCH$_3$), 57.0 (O=CCHO*C*H$_3$), 55.3 (O*C*H$_3$), 36.0 (N*C*H$_3$);

HRMS(ESI+) calcd. for $C_{14}H_{17}N_2O_3$ $(M + H)^+$ 261.1234, found: 261.1235.

Reactions with 1*H*-Indole (Scheme 76, p.61 and Scheme 77, p.62)

General Procedure 8

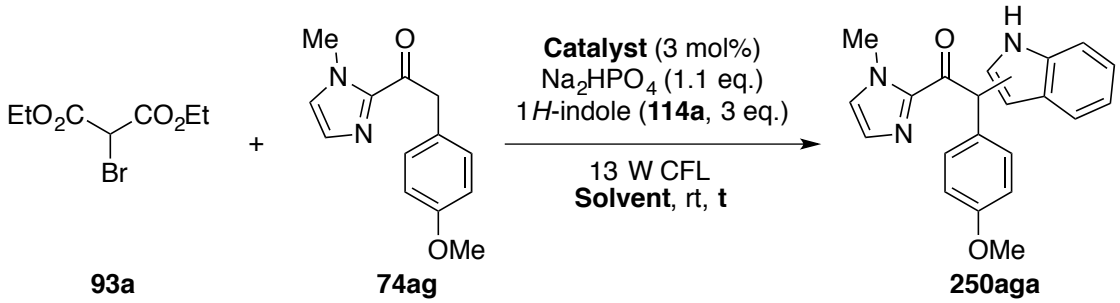

93a **74ag** **250aga**

To a Schlenk-tube were added 2-acyl imidazole **74ag**, diethyl bromomalonate (**93a**), 1*H*-indole (70.3 mg, 600 µmol), Na_2HPO_4 (31.2 mg, 220 µmol), and IrO (5.50 mg, 6.00 µmol). After adding solvent (500 µL), the tube was sealed with a screw-cap. The reaction mixture was degassed through the freeze-pump-thaw procedure for three cycles and irradiated with a 13-Watt CFL at rt. After evaporating the solvent in vacuum, the residue was purified through flash column chromatography (*n*-hexane:ethyl acetate 3:1) to afford the arylated product **250aga**. The absolute configuration of enantioenriched **250aga** was not determined.

Following general procedure 8, the reaction was performed with 2-acyl imidazole **74ag** (138 mg, 600 µmol), diethyl bromomalonate (37.1 µL, 200 µmol, 92%), and Λ-IrO (5.50 mg, 6.00 µmol) in methanol (500 µL) to afford **250aga** (47.3 mg, 137 µmol, 68%) with 20% *ee* after 14 h photolysis (Scheme 76, p.61).

Following general procedure 8, the reaction was performed with 2-acyl imidazole **74ag** (46.0 mg, 200 µmol), diethyl bromomalonate (111 µL, 600 µmol, 92%), and Λ-IrO (5.50 mg, 6.00 µmol) in methanol (500 µL) to afford **250aga** (43.2 mg, 125 µmol, 63%) with 28% *ee* after 10 h photolysis (Scheme 76, p.61).

Following general procedure 8, the reaction was performed with 2-acyl imidazole **74ag** (23.0 mg, 100 µmol), diethyl bromomalonate (55.6 µL, 300 µmol, 92%), 1*H*-indole (35.1 mg, 300 µmol), Na_2HPO_4 (15.6 mg, 110 µmol), and *rac*-IrO (2.80 mg, 3.00 µmol) in *iso*-propanol (250 µL) to afford **250aga** (24.9 mg, 72.1 µmol, 72%) after 40 h photolysis. The conversion of **74ag** was not complete according to the TLC analysis of the crude reaction mixture (Scheme 77, p.62).

2-(1*H*-Indol-3-yl)-2-(4-methoxyphenyl)-1-(1-methyl-1*H*-imidazol-2-yl)ethan-1-one (250aga)

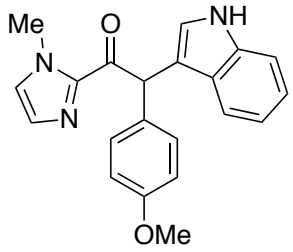

^{1}H-NMR (500 MHz; $CDCl_3$): δ 8.19 (s, 1H, N*H*), 7.56 (dd, *J* = 7.8, 0.8 Hz, 1H, $1H_{indolyl}$), 7.45−7.42 (m, 2H, $H_{p\text{-MeO-Ph}}$), 7.31 (dt, *J* = 8.1, 0.8 Hz, 1H, $H_{indolyl}$), 7.20 (dd, *J* = 2.4, 0.5 Hz, 1H, NHC*H*), 7.18 (d, *J* = 0.9 Hz, 1H, C*H*N=C), 7.14 (ddd, *J* = 8.1, 7.1, 1.1 Hz, 1H, $H_{indolyl}$), 7.04 (ddd, *J* = 8.0, 7.1, 1.0 Hz, 1H, $H_{indolyl}$), 7.01 (s, 1H, C*H*NCH_3), 6.87 (s, 1H, O=CC*H*), 6.84−6.81 (m, 2H, $H_{p\text{-MeO-Ph}}$), 3.98 (s, 3H, NCH_3), 3.75 (s, 3H, OCH_3);

^{13}C-NMR (75.5 MHz; $CDCl_3$): δ 191.3 (*C*=O), 158.7 (*C*OCH_3), 143.0 (N=*C*NCH_3), 136.4 ($C_{indolyl}$), 131.3 (O=CCH*C*), 130.2 ($2C_{p\text{-MeO-Ph}}$), 129.4 (*C*HN=C), 127.7 (*C*HNCH_3), 127.0 ($C_{indolyl}$), 123.6 ($C_{indolyl}$), 122.3 ($C_{indolyl}$), 119.7 ($C_{indolyl}$), 119.6 ($C_{indolyl}$), 114.7 ($C_{indolyl}$), 114.0 ($2C_{p\text{-MeO-Ph}}$), 111.2 ($C_{indolyl}$), 55.3 (O*C*H_3);

HRMS(ESI+) calcd. for $C_{21}H_{20}N_3O_2$ $(M + H)^+$ 346.1550, found: 346.1559;

HPLC Daicel Chiralpak IC column, 25 ºC, 0.5 mL/min, hexanes:*i*-PrOH 70:30, isocratic flow, t_R(major) = 14.7 min, t_R(minor) = 17.1 min.

5.6.2. Mechanistic Investigations

General Procedure 9

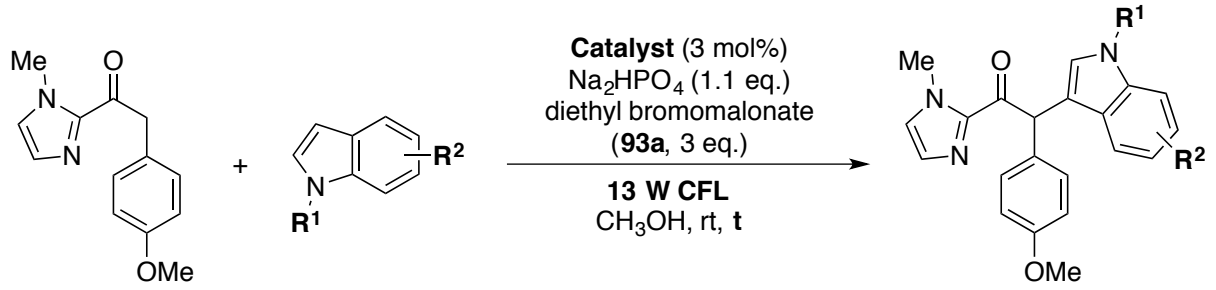

To a Schlenk-tube were added 2-acyl imidazole **74ag** (46.0 mg, 200 μmol), diethyl bromomalonate (111 μL, 600 μmol), indole **114** (600 μmol), Na_2HPO_4 (31.2 mg, 220 μmol), and *rac*-IrO (5.50 mg, 6.00 μmol). After adding methanol (500 μL), the tube was sealed with a screw-cap. The reaction mixture was degassed through the freeze-pump-thaw procedure for three cycles and then either irradiated with a 13-Watt CFL at rt or stirred at rt in the absence of light. After evaporating the solvent in vacuum, the residue was purified through flash column chromatography (*n*-hexane: ethyl acetate 3:1) to afford the products.

Reactions with 2- and 3-Substituted Indoles (Scheme 78, p.63)

Following general procedure 9, the reaction with 1,2-dimethyl-1*H*-indole (**114b**, 87.1 mg, 600 µmol) and *rac*-IrO (5.50 mg, 6.00 µmol) afforded α-arylated product **250agb** (51.3 mg, 137 µmol, 69%) after 14 h photolysis. The reaction with 3-methyl-1*H*-indole (**114c**, 78.7 mg, 600 µmol) afforded remaining substrate **74ag** (21.2 mg, 92.1 µmol, 54% conv.) and methoxy product **240ag** (17.4 mg, 66.8 µmol, 33%) after 14 h photolysis, while no α-arylated product was formed.

2-(1,2-Dimethyl-1*H*-indol-3-yl)-2-(4-methoxyphenyl)-1-(1-methyl-1*H*-imidazol-2-yl)ethan-1-one (250agb)

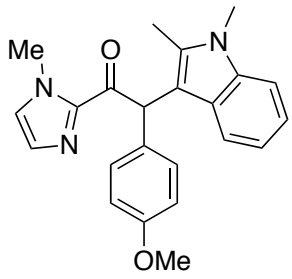

^{1}H-NMR (300 MHz; $CDCl_3$): δ 7.63 (d, *J* = 7.9 Hz, 1H, $H_{indolyl}$), 7.25−7.22 (m, 3H, $2H_{p\text{-MeO-Ph}}$ + $H_{indolyl}$), 7.15−7.09 (m, 2H, $H_{indolyl}$ + C*H*N=C), 7.02 (ddd, *J* = 8.0, 7.0, 1.1 Hz, 1H, $H_{indolyl}$), 6.93 (d, *J* = 0.5 Hz, 1H, C*H*NCH_3), 6.84 (s, 1H, O=CC*H*), 6.84−6.79 (m, 2H, $2H_{p\text{-MeO-Ph}}$), 3.91 (s, 3H, OCH_3), 3.76 (s, 3H, $CHNCH_3$), 3.65 (s, 3H, CH_3CNCH_3), 2.51 (s, 3H, CH_3CNCH_3);
^{13}C-NMR (75.5 MHz; $CDCl_3$): δ 191.3 (O=*C*), 158.2 (*C*OCH_3), 143.7 (N=*C*NCH_3), 136.9 ($C_{indolyl}$), 136.1 ($C_{indolyl}$), 131.9 ($C_{indolyl}$), 130.0 ($2C_{p\text{-MeO-Ph}}$), 129.0 (*C*HN=C), 127.4 (O=CCH*C*), 127.2 (*C*$HNCH_3$), 120.5 ($C_{indolyl}$), 120.4 ($C_{indolyl}$), 119.3 ($C_{indolyl}$), 113.7 ($2C_{p\text{-MeO-Ph}}$), 108.6 ($C_{indolyl}$), 107.5 ($C_{indolyl}$), 55.3 (OCH_3), 49.1 (O=C*C*H), 36.2 ($CHNCH_3$), 29.7 (CH_3CNCH_3), 11.0 (CH_3CNCH_3);
HRMS(ESI+) calcd. for $C_{23}H_{24}N_3O_2$ $(M + H)^+$ 374.1863, found: 374.1874.

Control Experiment in the Absence of Visible Light (Scheme 79, p.63)

Following general procedure 9, the reaction was performed with 1*H*-indole (**114a**, 70.3 mg, 600 µmol) and Λ-IrO (5.50 mg, 6.00 µmol). After stirring at rt in the absence of light for 15 h, **74ag** was completely consumed and yielded a white solid (62.9 mg), which is a mixture of arylated product **250aga** (82% yield, 33% *ee*) and methoxy product **240ag** (12% yield) according to ^{1}H-NMR spectrum (Figure 23). The absolute configuration of enantioenriched product was not determined.

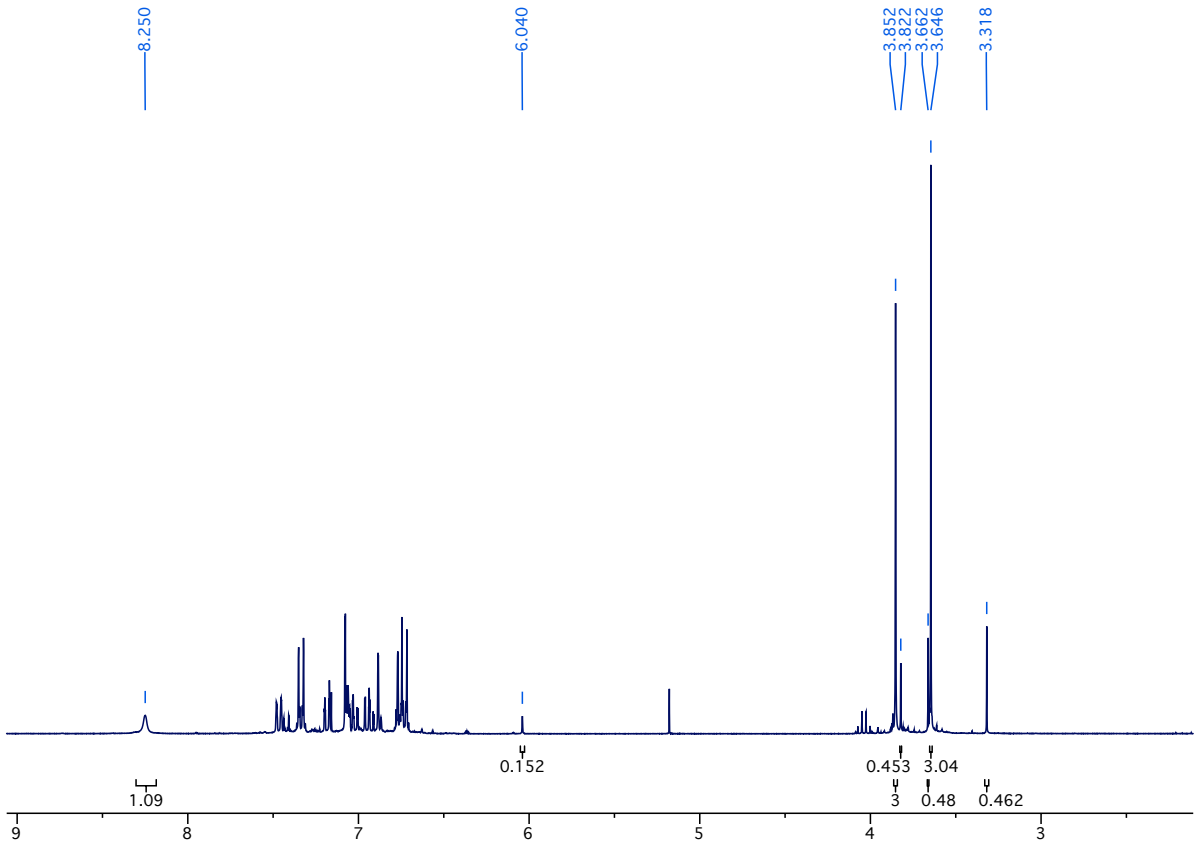

Figure 23: ^{1}H-NMR spectrum of a mixture of **250aga** and **240ag**.

Reaction with Imidazole Substrate 74aa (Scheme 80, p.64)

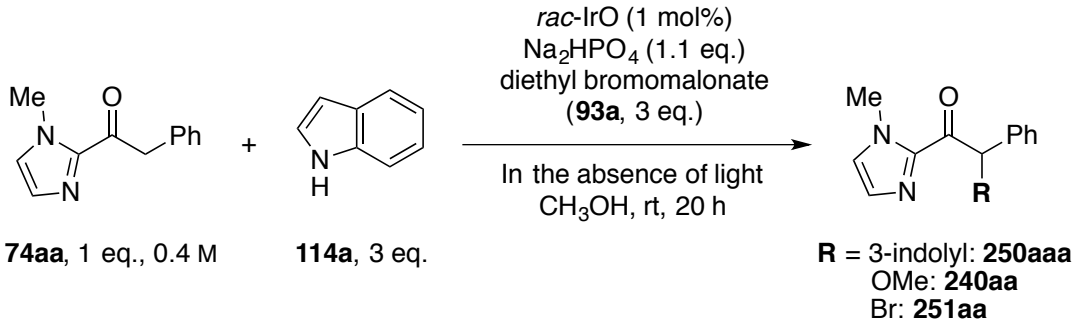

To a Schlenk-tube were added 2-acyl imidazole substrate **74aa** (16.9 µL, 100 µmol), diethyl bromomalonate (55.6 µL, 300 µmol), 1*H*-indole (35.1 mg, 300 µmol), Na_2HPO_4 (15.6 mg, 110 µmol), *rac*-IrO (1.00 mg, 1.00 µmol), and methanol (250 µL) under nitrogen atmosphere. The tube was sealed with a screw-cap and the reaction mixture was stirred at rt for 15 h in absence of light. TLC analysis revealed a complete conversion of **74aa**. The solvent was evaporated in vacuum and residue was purified through flash column chromatography on silica gel (*n*-hexane:EtOAc 3:2) to afford brominated product **251aa** (11.0 mg, 39%) and a mixture (6.70 mg) of arylated product **250aaa** (10%) and methoxy product **240aa** (16%) (Figure 24).

2-Bromo-1-(1-methyl-1*H*-imidazol-2-yl)-2-phenylethan-1-one (251aa)

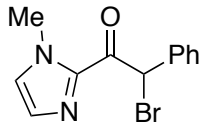

^{1}H-NMR (300 MHz; $CDCl_3$): δ 7.68−7.64 (m, 2H, $2H_{Ph}$), 7.37−7.29 (m, 3H, $3H_{Ph}$), 7.20 (d, *J* = 0.9 Hz, 1H, C*H*N=C), 7.09 (s, 1H, C*H*NCH_3), 6.99 (s, 1H, O=CC*H*Br), 3.99 (s, 3H, CH_3);

^{13}C-NMR (75.5 MHz; $CDCl_3$): δ 183.5 (O=*C*), 140.5 (N=*C*NCH_3), 135.8 (O=CCH*C*), 129.8 (*C*HN=C), 129.6 ($2C_{Ph}$), 129.0 (*C*HNCH_3), 128.8 ($2C_{Ph}$), 128.5 (C_{Ph}), 49.3 (O=C*C*H), 36.4 (N*C*H_3);

HRMS(ESI+) calcd. for $C_{12}H_{11}BrN_2ONa$ $(M + Na)^+$ 300.9947, found: 300.9973.

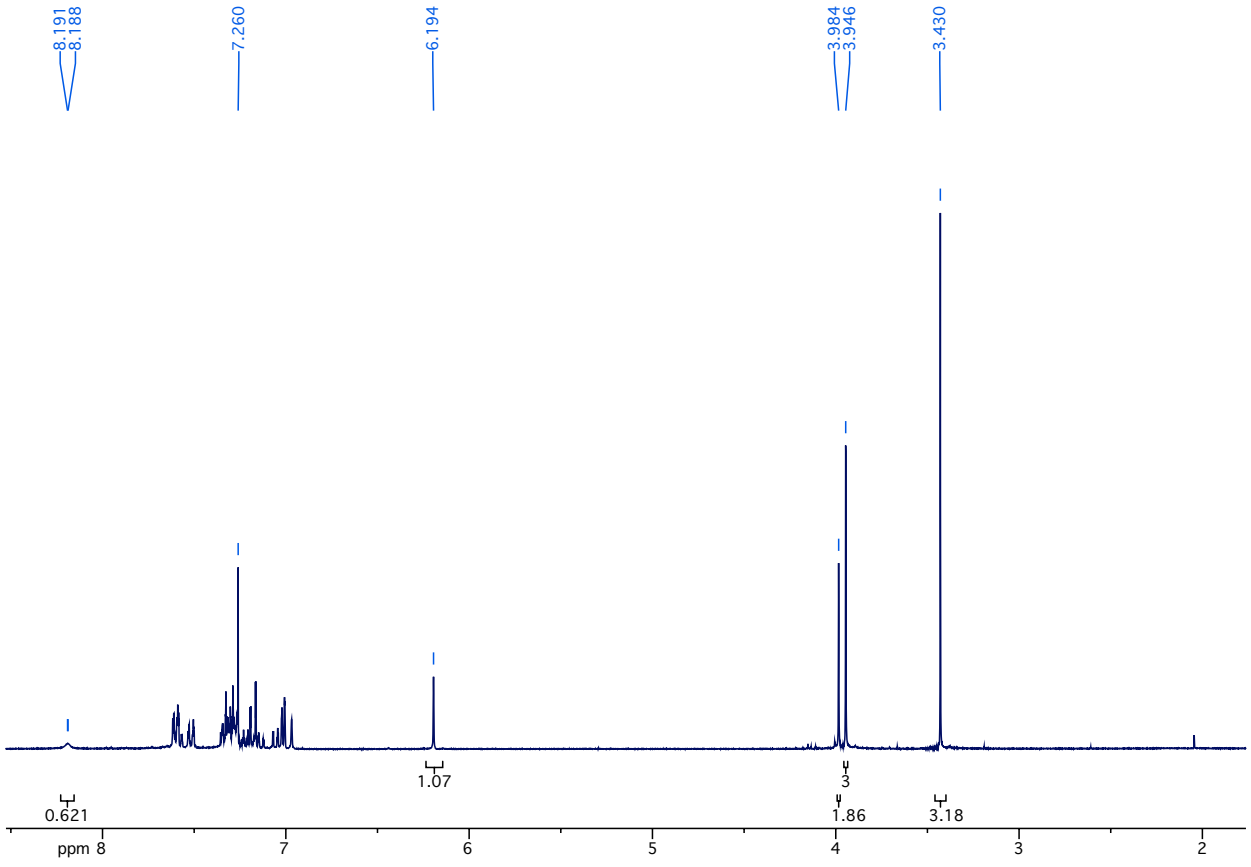

Figure 24: ^{1}H-NMR spectrum of a mixture of **250aaa** and **240aa**.

Mechanism Investigation through Stepwise Addition of 1*H*-indole (Scheme 81, p.64)

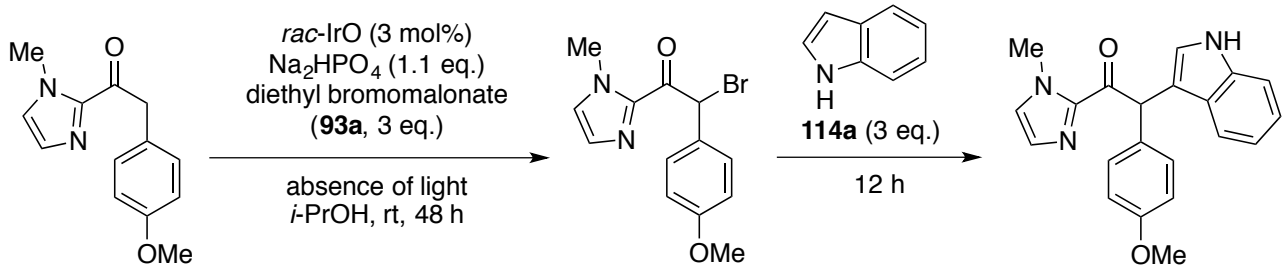

To a Schlenk-tube were added 2-acyl imidazole substrate **74ag** (46.0 mg, 200 µmol), diethyl bromomalonate (111 µL, 600 µmol), Na_2HPO_4 (31.2 mg, 220 µmol), *rac*-IrO (5.50 mg, 6.00 µmol), and *iso*-propanol (500 µL) under nitrogen atmosphere. The tube was sealed with a screw-cap and the reaction mixture was stirred at rt for 48 h in absence of light. TLC analysis revealed an incomplete conversion of **74ag** and the formation of brominated product **251ag** (Figure 25, spot 1). 1*H*-indole (70.2 mg, 600 µmol) was then added and the reaction mixture was stirred for 12 h. TLC analysis revealed that brominated product **251ag** was consumed and arylated product **250aga** was formed (spot 2). A complete conversion of **74ag** could not be achieved, when the mixture was stirred for further 24 h (spot 3).

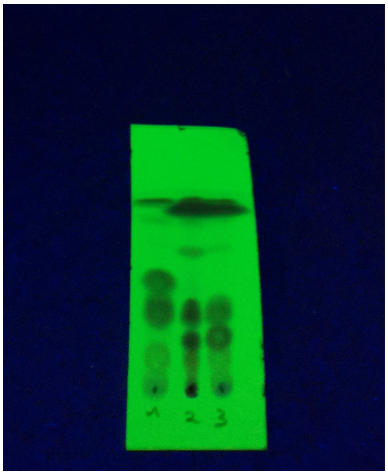

Figure 25: TLC analysis of the reaction from scheme 81 (p.64).

5.6.3. Optimization of the Reaction Conditions

General Procedure 10

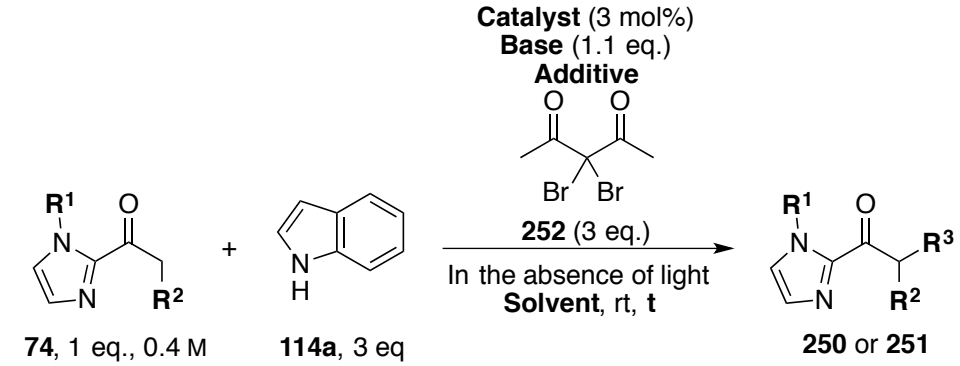

R^1 = Me, R^2 = Ph: **74aa**
R^1 = Me, R^2 = *p*-MeO-Ph: **74ag**
R^1 = Ph, R^2 = Me: **74bh**

R^1 = Me, R^2 = Ph, R^3 = 3-indolyl: **250aaa**
R^1 = Me, R^2 = *p*-MeO-Ph, R^3 = 3-indolyl: **250aga**
R^1 = Ph, R^2 = Me, R^3 = Br: **251bh**

To a Schlenk-tube were added 2-acyl imidazole substrate **74** (200 µmol), 3,3-dibromopetane-2,4-dione (**252**, 81.7 µL, 600 µmol), 1*H*-indole (70.3 mg, 600 µmol), base (220 µmol), catalyst (6.00 µmol), and solvent (500 µL) under nitrogen atmosphere. The tube was sealed with a screw-cap and the reaction mixture was stirred at rt for the given duration in the absence of light. The solvent was evaporated in vacuum and the residue was purified through flash column chromatography on silica gel (*n*-hexane:EtOAc) to afford the product **250** or **251**.

Evaluation of 3,3-Dibromopetane-2,4-dione (252) as Brominating Reagent with different 2-Acyl Imidazoles (Table 14, p.66)

Following general procedure 10, the reaction was performed with 2-acyl imidazole substrate **74ag** (46.0 mg, 200 µmol), Na_2HPO_4 (31.2 mg, 220 µmol), and *rac*-IrO (5.50 mg, 6.00 µmol) in *iso*-propanol (500 µL). The TLC analysis of the crude reaction mixture revealed a complete conversion of imidazole substrate **74ag** after 15 h and the purification afforded arylated product **250aga** (59.6 mg, 173 µmol, 86%) as white solid (entry 1).

Following general procedure 10, the reaction was performed with 2-acyl imidazole substrate **74aa** (33.8 µL, 200 µmol), Na_2HPO_4 (31.2 mg, 220 µmol), *rac*-IrO (5.50 mg, 6.00 µmol), and AgOTf (56.5 mg, 220 µmol) in *iso*-propanol (500 µL). The TLC analysis of the crude reaction mixture revealed a complete conversion of imidazole substrate **74aa** after 17 h and the purification afforded arylated product **250aaa** (32.2 mg, 102 µmol, 86%) as pale brown solid (entry 2).

2-(1*H*-Indol-3-yl)-1-(1-methyl-1*H*-imidazol-2-yl)-2-phenylethan-1-one (250aaa)

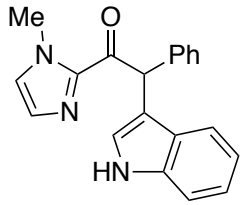

^{1}H-NMR (300 MHz; $CDCl_3$): δ 8.14 (s, br, 1H, N*H*), 7.58 (dd, *J* = 7.9, 0.4 Hz, 1H, $H_{indolyl}$), 7.54−7.51 (m, 2H, $2H_{indolyl}$), 7.33−7.26 (m, 3H, $3H_{Ph}$), 7.24−7.12 (m, 4H, $2H_{Ph}$ + $H_{indolyl}$ + C*H*N=C), 7.07−7.01 (m, 2H, $H_{indolyl}$ + C*H*NCH_3), 6.95 (s, 1H, O=CC*H*), 3.98 (s, 3H, NC*H*$_3$);
^{13}C-NMR (75.5 MHz; $CDCl_3$): δ 191.1 (O=*C*), 143.1 (N=*C*NCH_3), 139.3 (O=CCH*C*), 136.4 ($C_{indolyl}$), 129.5 (*C*HN=C), 129.2 ($2C_{Ph}$), 128.6 ($2C_{Ph}$), 127.8 (*C*HNCH_3), 127.1 ($C_{indolyl}$), 127.0 (C_{Ph}), 123.7 ($C_{indolyl}$), 122.3 ($C_{indolyl}$), 119.8 ($C_{indolyl}$), 119.6 ($C_{indolyl}$), 114.6 ($C_{indolyl}$), 111.2 ($C_{indolyl}$), 49.7 (O=C*C*H), 36.5 (N*C*H_3);
HRMS(ESI+) calcd. for $C_{20}H_{16}N_3O$ $(M)^+$ 314.1288, found: 314.1291.

Following general procedure 10, the reaction was performed with 2-acyl imidazole substrate **74bh** (40.0 mg, 200 µmol), Na_2HPO_4 (31.2 mg, 220 µmol), *rac*-IrO (5.50 mg, 6.00 µmol), and AgOTf (56.5 mg, 220 µmol) in *iso*-propanol (500 µL). The TLC analysis of the crude reaction mixture revealed a complete conversion of the imidazole substrate **74bh** after 17 h and the purification afforded brominated product **251bh** (55.5 mg, 199 µmol, 99%) as yellow oil (entry 3).

2-Bromo-1-(1-phenyl-1*H*-imidazol-2-yl)propan-1-one (231bh)

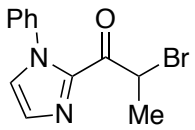

^{1}H-NMR (300 MHz; $CDCl_3$): δ 7.49−7.45 (m, 3H, $3H_{Ph}$), 7.33−7.29 (m, 3H, $2H_{Ph}$ + C*H*NPh), 7.25 (d, *J* = 1.0 Hz, 1H, C*H*N=C), 5.87 (q, *J* = 6.8 Hz, 1H, O=CC*H*), 1.80 (d, *J* = 6.8 Hz, 3H, C*H*$_3$);
^{13}C-NMR (75.5 MHz; $CDCl_3$): δ 184.3 (O=*C*), 140.8 (N=*C*NPh), 137.9 (C_{Ph}), 130.0 (*C*HN=C), 129.3 ($2C_{Ph}$), 129.1 (C_{Ph}), 127.9 (*C*HNPh), 125.6 ($2C_{Ph}$), 43.4 (O=C*C*H), 19.7 (*C*H_3).

Solvent Screening with RhO as Catalyst (Scheme 83, p.67)

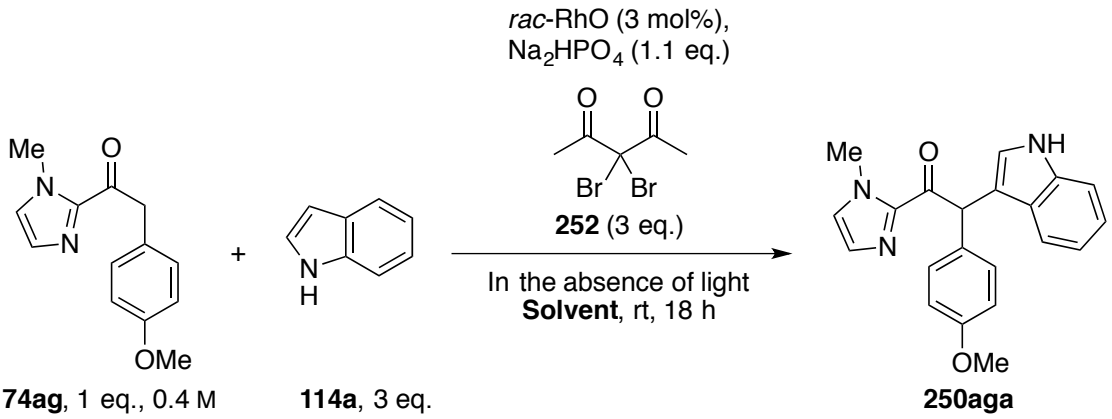

74ag, 1 eq., 0.4 M **114a**, 3 eq. **250aga**

Following general procedure 10, the reactions were performed with 2-acyl imidazole substrate **74ag** (46.0 mg, 200 μmol), Na_2HPO_4 (31.2 mg, 220 μmol), and *rac*-RhO (5.00 mg, 6.00 μmol). The reactions were worked up after 18 h. The reaction in *iso*-propanol (500 μL) afforded arylated product **250aga** (41.0 mg, 119 μmol, 59%) as white solid. The reaction in THF (500 μL) afforded **250aga** (52.2 mg, 151 μmol) in 76% yield. The reaction in DMF (500 μL) afforded **250aga** (19.0 mg, 55.0 μmol) in 28% yield.

Base Screening (Table 15, p.67)

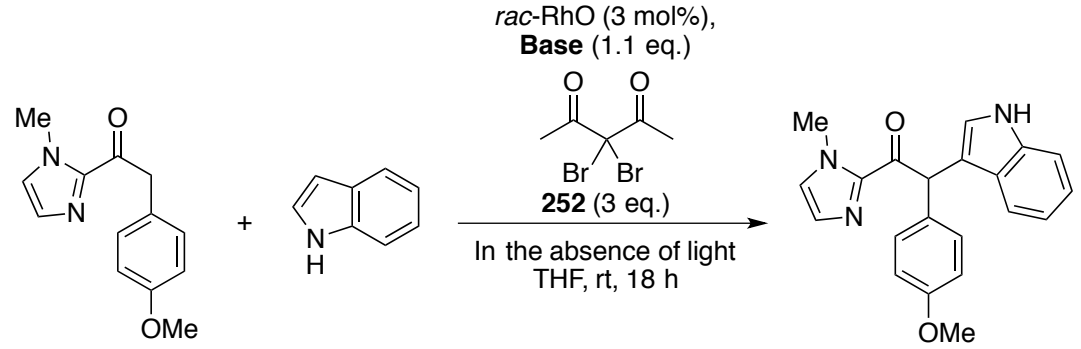

74ag, 1 eq., 0.4 M **114a**, 3 eq. **250aga**

Following general procedure 10, the reactions were performed with 2-acyl imidazole substrate **74ag** (92.0 mg, 400 μmol), dibromide **252** (163 μL, 1.20 mmol), 1*H*-indole (141 mg, 1.20 mmol), and *rac*-RhO (10.0 mg, 12.0 μmol) in THF (1.00 mL). The reactions were worked up after 18 h. The reaction with Cs_2CO_3 (143 mg, 440 μmol) afforded arylated product **250aga** (93.7 mg, 271 μmol) in 67% yield (entry 2). The reaction with 2,6-lutidine (51.2 μL, 440 μmol) afforded **250aga** (123 mg, 356 μmol) in 89% yield (entry 3). The reaction with 2,2,6,6-tetramethylpiperidine (74.3 μL, 440 μmol) afforded **250aga** (60.2 mg, 174 μmol) in 43% yield (entry 4). The reaction with triethylamine (61.3 μL, 440 μmol) afforded **250aga** (57.4 mg, 166 μmol) in 42% yield (entry 5).

5.6.4. Evaluation of the Arene Scope (Scheme 84, p.68)

General Procedure 11

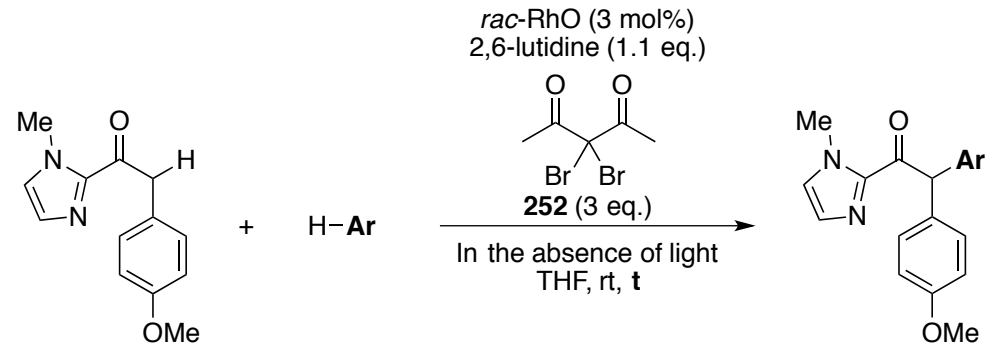

74ag, 1 eq., 0.4 M 3 or 6 eq.

To a Schlenk-tube were added 2-acyl imidazole substrate **74ag** (92.0 mg, 400 μmol), dibromide **252** (163 μL, 1.20 mmol), arene (1.20 or 2.40 mmol), 2,6-lutidine (51.2 μL, 440 μmol), *rac*-RhO (10.0 mg, 12.0 μmol), and THF (1.00 mL) under nitrogen atmosphere. The tube was sealed with a screw-cap and the reaction mixture was stirred at rt for the given duration in absence of light. The solvent was evaporated under vacuum and the residue was purified through flash column chromatography on silica gel (*n*-hexane:EtOAc) to afford the product.

2-(1,2-Dimethyl-1*H*-indol-3-yl)-2-(4-methoxyphenyl)-1-(1-methyl-1*H*-imidazol-2-yl)ethan-1-one (250agb)

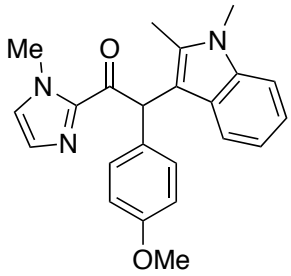

Following general procedure 11, the reaction was performed with 2-acyl imidazole substrate **74ag** (92.0 mg, 400 μmol) and 1,2-dimethyl-1*H*-indole (174 mg, 1.20 mmol) to afford arylated product **250agb** (131 mg, 351 μmol, 81%) after 20 h. The NMR data are consistent with the afore-presented data (p.122).

2-(4-Methoxyphenyl)-1-(1-methyl-1*H*-imidazol-2-yl)-2-(6-methyl-1*H*-indol-3-yl)ethan-1-one (250agd)

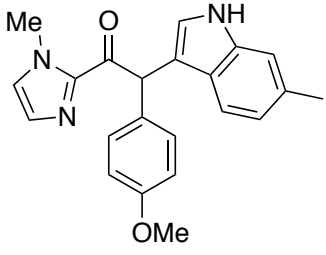

Following general procedure 11, the reaction was performed with 2-acyl imidazole substrate **74ag** (92.0 mg, 400 μmol) and 6-methyl-1*H*-indole (157 mg, 1.20 mmol) to afford arylated product **250agd** (104 mg, 289 μmol, 72%) after 25 h.

^{1}H-NMR (300 MHz; $CDCl_3$): δ 8.22 (s, br, 1H, N*H*), 7.46−7.41 (m, 3H, $2H_{p\text{-MeO-Ph}}$ + $1H_{indolyl}$), 7.17 (d, *J* = 0.9 Hz, 1H, C*H*N=C), 7.07−7.05 (m, 2H, $2H_{indolyl}$), 6.97 (s, 1H, C*H*NCH_3), 6.90−6.82 (m, 4H, $2H_{p\text{-MeO-Ph}}$ + $1H_{indolyl}$ + O=CC*H*), 3.95 (s, 3H, OCH_3), 3.75 (s, 3H, NCH_3), 2.41 (s, 3H, CH_3);

^{13}C-NMR (75.5 MHz; $CDCl_3$): δ 191.4 (O=*C*), 158.6 (*C*OCH_3), 143.0 (N=*C*NCH_3), 136.9 ($C_{indolyl}$), 131.9 ($C_{indolyl}$), 131.4 (O=CCH*C*), 130.2 ($2C_{p\text{-MeO-Ph}}$), 129.3 (*C*HN=C), 127.7 (*C*HNCH_3), 124.8 ($C_{indolyl}$), 123.1 ($C_{indolyl}$), 121.4 ($C_{indolyl}$), 119.2 ($C_{indolyl}$), 114.3 ($C_{indolyl}$), 114.0 ($2C_{p\text{-MeO-Ph}}$), 111.2 ($C_{indolyl}$), 55.3 (O*C*H_3), 49.0 (O=C*C*H), 36.3 (N*C*H_3), 21.7 (*C*H_3);

HRMS(ESI−) calcd. for $C_{22}H_{20}N_3O_2$ (M − H)−, 358.1550, found: 358.1553.

2-(5-(Benzyloxy)-1*H*-indol-3-yl)-2-(4-methoxyphenyl)-1-(1-methyl-1*H*-imidazol-2-yl)ethan-1-one (250age)

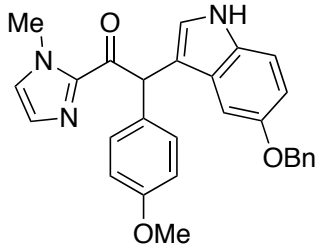

Following general procedure 11, the reaction was performed with 2-acyl imidazole substrate **74ag** (92.0 mg, 400 μmol) and 5-(benzyloxy)-1*H*-indole (268 mg, 1.20 mmol) to afford arylated product **250age** (115 mg, 255 μmol, 64%) after 24 h.

^{1}H-NMR (300 MHz; $CDCl_3$): δ 8.11 (s, 1H, N*H*), 7.43−7.28 (m, 7H, $2H_{p\text{-MeO-Ph}}$ + $5H_{Ph}$), 7.20−7.17 (m, 3H, $2H_{indolyl}$ + C*H*N=C), 7.11 (d, *J* = 2.3 Hz, 1H, $H_{indolyl}$), 7.00 (s, 1H, C*H*NCH_3), 6.89−6.82 (m, 4H, $2H_{p\text{-MeO-Ph}}$ + $1H_{indolyl}$ + O=CC*H*), 5.00 (s, 2H, CH_2), 3.95 (s, 3H, OCH_3), 3.76 (s, 3H, NCH_3);

^{13}C-NMR (75.5 MHz; $CDCl_3$): δ 191.1 (O=*C*), 158.7 (*C*OCH_3), 153.3 (*C*OBn), 142.9 (N=*C*NCH_3), 137.9 ($C_{indolyl}$), 131.8 ($C_{indolyl}$), 131.2 (O=CCH*C*), 130.2 ($2C_{p\text{-MeO-Ph}}$), 129.2 (*C*HN=C), 128.6 (C_{Ph}), 128.5 ($2C_{Ph}$), 127.8 ($2C_{Ph}$), 127.7 (C_{Ph}), 127.4 (*C*HNCH_3), 124.5 ($C_{indolyl}$), 114.4 ($C_{indolyl}$), 114.1 ($2C_{p\text{-MeO-Ph}}$), 113.2 ($C_{indolyl}$), 111.9 ($C_{indolyl}$), 103.1 ($C_{indolyl}$), 70.9 (O*C*H_2Ph), 55.3 (O*C*H_3), 49.0 (O=C*C*H), 36.5 (N*C*H_3);

2-(4-Methoxyphenyl)-1-(1-methyl-1*H*-imidazol-2-yl)-2-(5-nitro-1*H*-indol-3-yl)ethan-1-one (250agf)

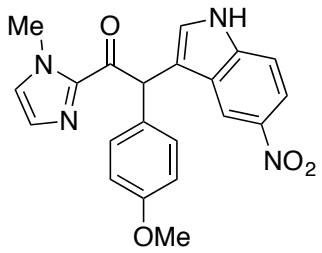

Following general procedure 11, the reaction was performed with the 2-acyl imidazole substrate **74ag** (92.0 mg, 400 μmol) and 5-nitro-1*H*-indole (195 mg, 1.20 mmol) to afford arylated product **250agf** (113 mg, 289 μmol, 72%) after 20 h.

^{1}H-NMR (300 MHz; $CDCl_3$): δ 9.20 (s, br, 1H, N*H*), 8.47 (d, *J* = 2.1 Hz, 1H, $H_{indolyl}$), 7.95 (dd, *J* = 9.0, 2.2 Hz, 1H, $H_{indolyl}$), 7.42−7.38 (m, 2H, $2H_{p\text{-MeO-Ph}}$), 7.28 (d, *J* = 2.1 Hz, 1H, $H_{indolyl}$), 7.23 (d, *J* = 9.0 Hz, 1H,

$H_{indolyl}$), 7.19 (d, *J* = 0.8 Hz, 1H, C*H*N=C), 7.06 (s, 1H, C*H*NCH$_3$), 6.85 (s, 1H, O=CC*H*), 6.84−6.80 (m, 2H, 2H$_{p\text{-MeO-Ph}}$), 3.98 (s, 3H, OC*H*$_3$), 3.73 (s, 3H, NC*H*$_3$);

^{13}C-NMR (75.5 MHz; $CDCl_3$): δ 190.5 (O=*C*), 158.9 (*C*OCH$_3$), 142.6 (N=*C*NCH$_3$), 141.6 ($C_{indolyl}$), 139.5 ($C_{indolyl}$), 130.4 ($C_{indolyl}$), 130.1(2C$_{p\text{-MeO-Ph}}$), 129.6 ($C_{indolyl}$), 128.2 (*C*HN=C), 126.9 (*C*HNCH$_3$), 126.3 (O=CCH*C*), 117.8 ($C_{indolyl}$), 117.3 ($C_{indolyl}$), 116.8 ($C_{indolyl}$), 114.3 (2C$_{p\text{-MeO-Ph}}$), 111.3 ($C_{indolyl}$), 55.3 (O*C*H$_3$), 48.6 (O=C*C*H), 36.4 (N*C*H$_3$).

2-(4-(Dimethylamino)-2-methoxyphenyl)-2-(4-methoxyphenyl)-1-(1-methyl-1*H*-imidazol-2-yl)ethan-1-one (253)

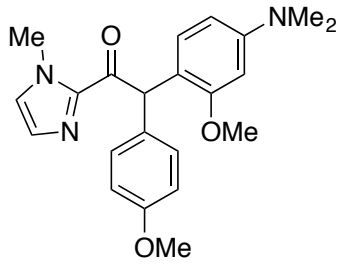

Following general procedure 11, the reaction was performed with 2-acyl imidazole substrate **74ag** (92.0 mg, 400 µmol) and 3-methoxy-*N*,*N*-dimethylaniline (352 µL, 2.40 mmol) to afford arylated product **253** (78.8 mg, 208 µmol, 52%) after 24 h.

^{1}H-NMR (300 MHz; $CDCl_3$): δ 7.31−7.28 (m, 2H, 2H$_{p\text{-MeO-Ph}}$), 7.11 (d, *J* = 0.9 Hz, 1H, C*H*N=C), 6.95 (s, 1H, C*H*NCH$_3$), 6.90−6.81 (m, 3H, 2H$_{p\text{-MeO-Ph}}$ + H$_{Ar}$), 6.67 (s, 1H, O=CC*H*), 6.29 (td, *J* = 8.5, 2.4 Hz, 2H, 2H$_{Ar}$), 3.97 (s, 3H, OC*H*$_3$), 3.77 (s, 3H, OC*H*$_3$), 3.75 (s, 3H, NC*H*$_3$), 2.93 (s, 6H, N(C*H*$_3$)$_2$);

^{13}C-NMR (75.5 MHz; $CDCl_3$): δ 192.2 (O=*C*), 158.6 (*C*OCH$_3$), 157.8 (*C*OCH$_3$), 150.7(*C*N(CH$_3$)$_2$), 143.3 (N=*C*NCH$_3$), 130.9 (2C$_{p\text{-MeO-Ph}}$), 130.6 (O=CCH*C*), 130.0 (*C*HN=C), 129.2 (*C*HNCH$_3$), 126.8 (C$_{Ar}$), 118.4 (C$_{Ar}$), 114.1 (2C$_{p\text{-MeO-Ph}}$), 105.1 (C$_{Ar}$), 97.2 (C$_{Ar}$), 55.8 (O*C*H$_3$), 55.3 (O*C*H$_3$), 51.2 (O=C*C*H), 41.2 (N(*C*H$_3$)$_2$), 36.3 (N*C*H$_3$).

2-(4-Methoxyphenyl)-1-(1-methyl-1*H*-imidazol-2-yl)-2-(1*H*-pyrrol-3-yl)ethan-1-one (254)

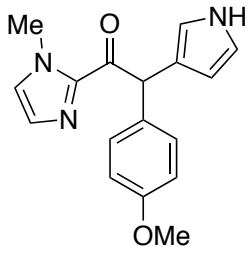

Following general procedure 11, the reaction was performed with 2-acyl imidazole substrate **74ag** (92.0 mg, 400 µmol) and 1*H*-pyrrole (167 µL, 2.40 mmol) to afford the arylated product **254** (52.4 mg, 177 µmol, 44%) after 23 h.

^{1}H-NMR (300 MHz; $CDCl_3$): δ 9.13 (s, br, 1H, N*H*), 7.36−7.33 (m, 2H, 2H$_{p\text{-MeO-Ph}}$), 7.20 (s, 1H, C*H*N=C), 7.04 (s, 1H, C*H*NCH$_3$), 6.85−6.82 (m, 2H, 2H$_{p\text{-MeO-Ph}}$), 6.75 (s, 1H, O=CC*H*), 6.56 (s, 1H, H$_{pyrrole}$), 6.14 (dd, *J* = 5.2, 2.3 Hz, 2H, 2H$_{pyrrole}$), 3.97 (s, 3H, OC*H*$_3$), 3.76 (s, 3H, NC*H*$_3$);

^{13}C-NMR (75.5 MHz; $CDCl_3$): δ 190.4 (O=*C*), 158.8 (*C*OCH_3), 142.7 (N=*C*NCH_3), 131.1 (O=CCH*C*), 129.8 (2$C_{p\text{-MeO-Ph}}$), 129.6 ($C_{pyrrole}$), 128.6 (*C*HN=C), 128.0 (*C*HNCH_3), 117.8 ($C_{pyrrole}$), 114.1 (2$C_{p\text{-MeO-Ph}}$), 108.4 ($C_{pyrrole}$), 107.7 ($C_{pyrrole}$), 55.4 (O*C*H_3), 50.5 (O=C*C*H), 36.5 (N*C*H_3).

Chapter 6. References

[1] V. Prelog, *Science* **1976**, *193*, 17−24.

[2] G. P. Moss, *Pure Appl. Chem.* **1996**, *68*, 2193−2222.

[3] J.-A. Le Bel, *Bull. Soc. Chim. Paris* **1874**, *22*, 337.

[4] J. H. van't Hoff, *Bull. Soc. Chim. Fr.* **1875**, *23*, 295.

[5] H. D. Flack, *Acta Cryst.* **2009**, *A65*, 371−389.

[6] L. A. Nguyen, H. He, C. Pham-Huy, *Int. J. Biomed. Sci.* **2006**, *2*, 85−100.

[7] S. C. Stinson, *Chem. Eng. News* **2000**, *78*, 55−79.

[8] E. L. Eliel, S. H. Wilen, *Stereochemistry of Organic Compounds*, J. Wiley& Sons, New York, **1994**.

[9] J. Halpern, B. M. Trost, *Proc. Natl. Acad. Sci. USA* **2004**, *101*, 5347.

[10] S. Borman, *Chem. Eng. News* **2001**, *79*, 5.

[11] W. S. Knowles, *Angew. Chem. Int. Ed.* **2002**, *41*, 1998−2007.

[12] R. Noyori, *Angew. Chem. Int. Ed.* **2002**, *41*, 2008−2022.

[13] K. B. Sharpless, *Angew. Chem. Int. Ed.* **2002**, *41*, 2024−2032.

[14] *Privileged Chiral Ligands and Catalysts* (Ed.: Q.-L. Zhou,), Wiley-VCH, Weinheim, **2011**.

[15] A. Werner, A. Vilmos, *Z. Anorg. Allg. Chem.* **1899**, *21*, 145−158.

[16] A. Werner, *Ber. Dtsch. Chem. Ges.* **1911**, *44*, 1887.

[17] J. Jacques, A. Collet, S. H. Wilen, *Enatiomers, Racemates and Resolutions*, J. Wiley & Sons, Chichester, **1996**.

[18] H. Amouri, M. Gruselle, *Chirality in Transition Metal Chemistry: Molecules, Supramolecular Assemblies and Materials*, J. Wiley & Sons, Chichester, **2008**, ch. 2, p. 57.

[19] J. Crassous, *Chem. Soc. Rev.* **2009**, *38*, 830−845.

[20] J. Crassous, *Chem. Commun.* **2012**, *48*, 9684−9692.

[21] J. Lacour, C. Ginglinger, C. Grivet, G. Bernardinelli, *Angew. Chem. Int. Ed.* **1997**, *36*, 608−610.

[22] M. Chavarot, S. Menage, O. Hamelin, F. Charnay, J. Pecaut, M. Fontecave, *Inorg. Chem.* **2003**, *42*, 4810−4816.

[23] J. Lacour, V. Hebbe-Viton, *Chem. Soc. Rev.* **2003**, *32*, 373−382.

[24] E. Meggers, *Chem. Eur. J.* **2010**, *16*, 752−758.

[25] E. Meggers, *Eur. J. Inorg. Chem.* **2011**, 2911−2926.

[26] L. Gong, M. Wenzel, E. Meggers, *Acc. Chem. Res.* **2013**, *46*, 2635−2644.

[27] E. Meggers, *Curr. Opin. Chem. Biol.* **2007**, *11*, 287−292.

[28] E. Meggers, *Chem. Commun.* **2009**, 1001−1010.

[29] S. P. Mulcahy, E. Meggers, *Topics Organomet. Chem.* **2010**, *32*, 141−153.

[30] M. Dörr, E. Meggers, *Curr. Opin. Chem. Biol.* **2014**, *19*, 76−81.

[31] L. Zhang, P. Carroll, E. Meggers, *Org. Lett.* **2004**, *6*, 521−523.

[32] H. Bregman, D. S. Williams, G. E. Atilla, P. J. Carroll, E. Meggers, *J. Am. Chem. Soc.* **2004**, *126*, 13594−13595.

[33] H. Bregman, P. J. Carroll, E. Meggers, *J. Am. Chem. Soc.* **2006**, *128*, 877−884.

[34] J. Maksimoska, L. Feng, K. Harms, C. Yi, J. Kissil, R. Marmorstein, E. Meggers, *J. Am. Chem. Soc.* **2008**, *130*, 15764−15765.

[35] J. E. Debreczeni, A. N. Bullock, G. E. Atilla, D. S. Williams, H. Bregman, S. Knapp, E. Meggers, *Angew. Chem. Int. Ed.* **2006**, *45*, 1580−1585.

[36] H. Bregman, E. Meggers, *Org. Lett.* **2006**, *8*, 5465−5468.

[37] L. Gong, S. P. Mulcahy, K. Harms, E. Meggers, *J. Am. Chem. Soc.* **2009**, *131*, 9602−9603.

[38] A. J. Davenport, D. L. Davies, J. Fawatt, D. R. Russell, *Dalton Trans.* **2004**, 1481−1492.

[39] L. Gong, S. P. Mulcahy, D. Devarajan, K. Harms, G. Frenking, E. Meggers, *Inorg. Chem.* **2010**, *49*, 7692−7699.

[40] L. Gong, C. Müller, M. A. Celik, G. Frenking, E. Meggers, *New J. Chem.* **2011**, *35*, 788−793.

[41] Z. Lin, M. A. Celik, C. Fu, K. Harms, G. Frenking, E. Meggers, *Chem. Eur. J.* **2011**, *17*, 12602−12605.

[42] C. Fu, M. Wenzel, E. Treutlein, K. Harms, E. Meggers, *Inorg. Chem.* **2012**, *51*, 10004−10011.

[43] Z. Lin, L. Gong, M. A. Celik, K. Harms, G. Frenking, E. Meggers, *Chem. Asian J.* **2011**, *6*, 474−481.

[44] L. Gong, Z. Lin, K. Harms, E. Meggers, *Angew. Chem. Int. Ed.* **2010**, *49*, 7955−7957.

[45] E. Marchi, R. Sinisi, G. Bergamini, M. Tragni, M. Monari, M. Bandini, P. Ceroni, *Chem. Eur. J.* **2012**, *18*, 8765−8773.

[46] M. Helms, Z. Lin, L. Gong, K. Harms, E. Meggers, *Eur. J. Inorg. Chem.* **2013**, 4164−4172.

[47] C. Wang, L.-A. Chen, H. Huo, X. Shen, K. Harms, L. Gong, E. Meggers, *Chem. Sci.* **2015**, 1094−1100.

[48] E. Meggers, *Chem. Eur. J.* **2010**, *16*, 752−758.

[49] E. Meggers, *Eur. J. Inorg. Chem.* **2011**, 2911−2926.

[50] L. Gong, L.-A. Chen, E. Meggers, *Angew. Chem. Int. Ed.* **2014**, *53*, 10868−10874.

[51] C. Ganzmann, J. A. Gladysz, *Chem. Eur. J.* **2008**, *14*, 5397−5400.

[52] L.-A. Chen, W. Xu, B. Huang, J. Ma, L. Wang, J. Xi, K. Harms, L. Gong, E. Meggers, *J. Am. Chem. Soc.* **2013**, *135,* 10598−10601.

[53] W. Xu, M. Arieno, H. Löw, K. Huang, X. Xie, T. Cruchter, Q. Ma, J. Xi, B. Huang, O. Wiest, L. Gong, E. Meggers, *J. Am. Chem. Soc.* **2016**, *138*, 8774−8780.

[54] J. Ma, X. Ding, Y. Hu, Y. Huang, L. Gong, E. Meggers, *Nat. Commun.* **2014**, *5*, 4531.

[55] X. Ding, C. Tian, Y. Hu, L. Gong, E. Meggers, *Eur. J. Org. Chem.* **2016**, 887−890.

[56] H. Huo, C. Fu, C. Wang, K. Harms, E. Meggers, *Chem. Commun.* **2014**, *50*, 10409−10411.

[57] H. Huo, C. Fu, K. Harms, E. Meggers, *J. Am. Chem. Soc.* **2014**, *136*, 2990−2993.

[58] X. Shen, H. Huo, C. Wang, B. Zhang, K. Harms, E. Meggers, *Chem. Eur. J.* **2015**, *21*, 9720−9726.

[59] C. Wang, L.-A. Chen, H. Huo, X. Shen, K. Harms, L. Gong, E. Meggers, *Chem. Sci.* **2015**, *6*, 1094−1100.

[60] J. Ma, X. Shen, K. Harms, E. Meggers, *Dalton Trans.* **2016**, *45*, 8320−8323.

[61] G. Ciamician, *Science* **1912**, *36*, 385−394.

[62] N. Hoffmann, *Chem. Rev.* **2008**, *108*, 1052−1103.

[63] T. Bach, J. P. Hehn, *Angew. Chem. Int. Ed.* **2011**, *50*, 1000−1045.

[64] K. Zeitler, *Angew. Chem. Int. Ed.* **2009**, *48*, 9785−9789.

[65] M. A. Ischay, J. Du, T. P. Yoon, *Nature Chem.* **2010**, *2*, 527−532.

[66] A. Kudo, Y. Miseki, *Chem. Soc. Rev.* **2009**, *38*, 253−278.

[67] J. L. White, M. F. Baruch, J. E. Pander III, Y. Hu, I. C. Fortmeyer, J. E. Park, T. Zhang, K. Liao, Y. Yan, T. W. Shaw, E. Abelev, A. B. Bocarsly, *Chem. Rev.* **2015**, *115*, 12888−12935.

[68] M. K. Nazeeruddin, M. Grätzel, *Photofunctional Transition Metal Complexes* (Ed.: V. W. W. Yam), Springer Berlin Heidelberg, **2007**, *123*, p. 113−175.

[69] R. Reithmeier, C. Bruckmeier, B. Rieger, *Catalysts* **2012**, *2*, 544−571.

[70] M. D. Kärkäs, O. Verho, E. V. Johnson, B. Åkermark, *Chem. Rev.* **2014**, *114*, 11863−12001.

[71] A. Juris, V. Balzani, *Coord. Chem. Rev.* **1988**, *84*, 85−277.

[72] S. Campagna, F. Puntoriero, F. Nastasi, G. Bergamini, V. Balzani, *Top. Curr. Chem.* **2007**, *280*, 117−214.

[73] L. Flamigni, A. Barbieri, C. Sabatini, B. Ventura, F. Barigelletti, *Top. Curr. Chem.* **2007**, *281*, 143−203.

[74] Y. You, W. Nam, *Chem. Soc. Rev.* **2012**, *41*, 7061−7084.

[75] A. Juris, V. Balzani, P. Belser, A. von Zelewsky, *Helv. Chim. Acta* **1981**, *64*, 2175−2182.

[76] M. Wrighton, J. Markham, *J. Phys. Chem.* **1973**, *77*, 3042−3044.

[77] A. Albini, *Synthesis* **1981**, *4*, 249−264.

[78] H. Cano-Yelo, A. Deronzier, *J. Chem. Soc. Perkin Trans. 2* **1984**, 1093−1098.

[79] H. Cano-Yelo, A. Deronzier, *Tetrahedron Lett.* **1984**, *25*, 5517−5520.

[80] J. M. Zen, S. L. Liou, A. S. Kumar, M. S. Hsia, *Angew. Chem. Int. Ed.* **2003**, *42*, 577−579.

[81] K. Okada, K. Okamoto, N. Morita, M. Oda, *J. Am. Chem. Soc.* **1991**, *113*, 9401−9402.

[82] E. Hasegawa, S. Takizawa, T. Seida, A. Yamaguchi, N. Yamaguchi, N. Chiba, T. Takahashi, H. Ikeda, K. Akiyama, *Tetrahedron* **2006**, *62*, 6581−6588.

[83] T.-G. Baik, A. L. Luis, L.-C. Wang, M. J. Krische, *J. Am. Chem. Soc.* **2001**, *123*, 6716−6717.

[84] Y. Roh, H.-Y. Jang, V. Lynch, N. L. Bauld, M. J. Krische, *Org. Lett*. **2002**, *4*, 611−613.

[85] J. Yang, G. A. N. Felton, N. L. Bauld, M. J. Krische, *J. Am. Chem. Soc.* **2004**, *126*, 1634−1635.

[86] M. A. Ischay, M. E. Anzovino, J. Du, T. P. Yoon, *J. Am. Chem. Soc.* **2008**, *130*, 12886−12887.

[87] J. Du, T. P. Yoon, *J. Am. Chem. Soc.* **2009**, *131*, 14604−14605.

[88] D. A. Nicewicz, D. W. C. MacMillan, *Science* **2008**, *322*, 77−80.

[89] J. M. R. Narayanam, J. W. Tucker, C. R. J. Stephenson, *J. Am. Chem. Soc.* **2009**, *131*, 8756−8757.

[90] C. K. Prier, D. A. Rankic, D. W. C. MacMillan, *Chem. Rev.* **2013**, *113*, 5322−5363.

[91] J. M. R. Narayanam, C. R. J. Stephenson, *Chem. Soc. Rev.* **2011**, *40*, 102−113.

[92] J. Xuan, W.-J. Xiao, *Angew. Chem. Int. Ed.* **2012**, *51*, 6828−6838.

[93] Y. Xi, H. Yi, A. Lei, *Org. Biomol. Chem.* **2013**, *11*, 2387−2403.

[94] M. Reckenthäler, A. G. Griesbeck, *Adv. Synth. Catal.* **2013**, *355*, 2727−2744.

[95] M. H. Shaw, J. Twilton, D. W. C. MacMillan, *J. Org. Chem.* **2016**, *81*, 6898−6926.

[96] E. Meggers, *Chem. Commun.* **2015**, *51*, 3290−3301.

[97] C. Wang, Z. Lu, *Org. Chem. Front.* **2015**, *2*, 179−190.

[98] E. R. Welin, A. A. Warkentin, J. C. Conrad, D. W. C. MacMillan, *Angew. Chem. Int. Ed.* **2015**, *54*, 9668−9672.

[99] H.-W. Shih, M. N. V. Wal, R. L. Grange, D. W. C. MacMillan, *J. Am. Chem. Soc.* **2010**, *132*, 13600−13603.

[100] D. A. Nagib, M. E. Scott, D. W. C. MacMillan, *J. Am. Chem. Soc.* **2009**, *131*, 10875−10877.

[101] M. Neumann, S. Füldner, B. König, K. Zeitler, *Angew. Chem. Int. Ed.* **2011**, *50*, 951-954.

[102] K. Fidaly, C. Ceballos, A. Falguières, M. S.-I. Veitia, A. Guy, C. Ferroud, *Green Chem.* **2012**, *14*, 1293−12973.

[103] Y. Zhu, L. Zhang, S. Luo, *J. Am. Chem. Soc.* **2014**, *136*, 14642−14645.

[104] A. G. Condie, J. C. Gonzáles-Gómez, C. R. J. Stephenson, *J. Am. Chem. Soc.* **2010**, *132*, 1464−1465.

[105] M. Rueping, S. Zhu, R. M. Königs, *Chem. Commun.* **2011**, *47*, 12709−12711.

[106] G. Zhao, C. Yang, L. Guo, H. Sun, C. Chen, W. Xia, *Chem. Commun.* **2012**, *48*, 2337−2339.

[107] D. B. Freeman, L. Furst, A. G. Condie, C. R. J. Stephenson, *Org. Lett.* **2012**, *14*, 94−97.

[108] M. Rueping, C. Vila, R. M. Königs, K. Poscharny, D. C. Fabry, *Chem. Commun.* **2011**, *47*, 2360−2362.

[109] Z.-J. Feng, J. Xuan, S.-D. Xia, W. Ding, W. Guo, J.-R. Chen, Y.-Q. Zou, L.-Q. Lu, W.-J. Xiao, *Org. Biomol. Chem.* **2014**, *12*, 2037−2040.

[110] G. Bergonzini, C. S. Schindler, C.-J. Wallentin, E. N. Jacobsen, C. R. J. Stephenson, *Chem. Sci.* **2014**, *5*, 112−116.

[111] D. A. DiRocco, T. Rovis, *J. Am. Chem. Soc.* **2012**, *134*, 8094−8097.

[112] I. Perepichka, S. Kundu, Z. Hearne, C.-J. Li, *Org. Biomol. Chem.* **2015**, *13*, 447−451.111

[113] Y. Chen, A. S. Kamlet, J. B. Steinman, D. R. Liu, *Nat. Chem.* **2011**, *3*, 146−153.

[114] K. Rybicka-Jasińska, Ł. W. Ciszewski, D. Gryko, *Adv. Synth. Catal.* **2016**, *358*, 1671−1678.

[115] X. Huang, R. D. Webster, K. Harms, E. Meggers, *J. Am. Chem. Soc.* **2016**, *138*, 12636−12642.

[116] M. P. Sibi, S. Manyem, J. Zimmerman, *Chem. Rev.* **2003**, *103*, 3263−3295.

[117] M. A. Brumfield, S. L. Quillen, U. C. Yoon, P. S. Mariano, *J. Am. Chem. Soc.* **1984**, *106*, 6855−6856.

[118] P. Kohls, D. Jadhav, G. Pandey, O. Reiser, *Org. Lett.* **2012**, *14*, 672−675.

[119] Y. Miyake, K. Nakajima, Y. Nishibayashi, *J. Am. Chem. Soc.* **2012**, *134*, 3338−3341.

[120] L. R. Espelt, E. M. Wiensch, T. P. Yoon, *J. Org. Chem.* **2013**, *78*, 4107−4114.

[121] L. R. Espelt, I. S. McPherson, E. M. Wiensch, T. P. Yoon, *J. Am. Chem. Soc.* **2015**, *137*, 2452−2455.

[122] H. Huo, K. Harms, E. Meggers, *J. Am. Chem. Soc.* **2016**, *138*, 6936−6939.

[123] J. Du, K. L. Skubi, D. M. Schultz, T. P. Yoon, *Science* **2014**, *344*, 392−396.

[124] A. G. Amador, E. M. Sherbrook, T. P. Yoon, *J. Am. Chem. Soc.* **2016**, *138*, 4722−4725.

[125] T. R. Blum, Z. D. Miller, D. M. Bates, I. A. Guzei, T. P. Yoon, *Science* **2016**, *354*, 1391−1395.

[126] T. N. Singh-Rachford, F. N. Castellano, *Coord. Chem. Rev.* **2010**, *254*, 2560−2573.

[127] T. Hamada, H. Ishida, S. Usui, Y. Watanabe, K. Tsumura, K. Ohkubo, *J. Chem. Soc., Chem. Commun.* **1993**, 909−911.

[128] A. Bauer, F. Westkämpfer, S. Grimme, T. Bach, *Nature* **2005**, *436*, 1139−1140.

[129] C. Müller, A. Bauer, T. Bach, *Angew. Chem. Int. Ed.* **2009**, *48*, 6640−6642.

[130] C. Müller, A. Bauer, M. M. Maturi, M. C. Cuquerella, M. A. Miranda, T. Bach, *J. Am. Chem. Soc.* **2011**, *133*, 16689−16697.

[131] R. Alonso, T. Bach, *Angew. Chem. Int. Ed.* **2014***, 53,* 4368−4371.

[132] M. M. Maturi, M. Wenninger, R. Alonso, A. Bauer, A. Pöthig, E. Riedle, T. Bach, *Chem. Eur. J.* **2013**, *19*, 7461−7472.

[133] M. M. Maturi, T. Bach, *Angew. Chem. Int. Ed.* **2014**, *53*, 7661−7664.

[134] A. Tröster, R. Alonso, A. Bauer, T. Bach, *J. Am. Chem. Soc.* **2016**, *138*, 7808−7811.

[135] H. Huo, X. Shen, C. Wang, L. Zhang, P. Röse, G. Hilt, E. Meggers, *Nature* **2014**, *515*, 100−103.

[136] H. Huo, X. Huang, X. Shen, K. Harms, E. Meggers, *Synlett.* **2016**, *27*, 749−753.

[137] H. Huo, C. Wang, K. Harms, E. Meggers, *J. Am. Chem. Soc.* **2015**, *137*, 9551−9554.

[138] C. Wang, Y. Zheng, H. Huo, P. Röse, L. Zhang, K. Harms, G. Hilt, E. Meggers, *Chem. Eur. J.* **2015**, *21*, 7355−7359.

[139] C. Wang, J. Qin, X. Shen, R. Riedel, K. Harms, E. Meggers, *Angew. Chem. Int. Ed.* **2016**, *55*, 685−688.

[140] H. Guo, E. Herdtweck, T. Bach, *Angew. Chem. Int. Ed.* **2010**, *49*, 7782−7785.

[141] R. Brimioulle, T. Bach, *Science* **2013**, *342*, 840−843.

[142] R. Brimioulle, A. Bauer, T. Bach, *J. Am. Chem. Soc.* **2015**, *137*, 5170−5176.

[143] E. Arceo, I. D. Jurberg, A. Álvarez-Fernández, P. Melchiorre, *Nat. Chem.* **2013**, *5*, 750−756.

[144] E. Arceo, A. Bahamonde, G. Bergonzini, P. Melchiorre, *Chem. Sci.* **2014**, *5*, 2438−-2442.

[145] M. Silvi, E. Arceo, I. Jurberg, C. Cassani, P. Melchiorre, *J. Am. Chem. Soc.* **2015**, *137*, 6120−6123.

[146] A. Bahamonde, P. Melchiorre, *J. Am. Chem. Soc.* **2016**, *138*, 8019−8030.

[147] T. P. Yoon, E. N. Jacobsen, *Science* **2003**, *299*, 1691−1693.

[148] A. G. Amador, T. P. Yoon, *Angew, Chem. Int. Ed.* **2016**, *55*, 2304−2306.

[149] *The Organic Chemistry of Aliphatic Nitrogen Compounds* (ED.: B. R. Brown), Oxford University Press, Oxford, **1994**, p. 217, 342.

[150] The number **189** represents the general number of the alkylated 2-acyl imidazoles **74** with α-cyano-alkyl bromides **95**. In case of product **189aaa**, the first and the second **a** represent the *N*-methyl and the phenyl substituents of 2-acyl imidazole **74** respectively. The third **a** represents the hydrogen substituent of α-cyanoalkyl bromides **95**. Therefore, the exact number of the product resulted from the 2-acyl imidazole **74aa** and bromoacetonitrile (**95a**) is **189aaa**. Similar numbering is to be seen in the following parts of the thesis as well.

[151] X. Shen, K. Harms, M. Marsch, E. Meggers, *Chem. Eur. J.* **2016**, *22*, 9102−9105.

[152] J. D. Nguyen, E. M. D'Amato, J. M. R. Narayanam, C. R. J. Stephenson, *Nat. Chem.* **2012**, *4*, 854−859.

[153] J. M. Janey, *Angew. Chem. Int. Ed.* **2005**, *44*, 4292−4300.

[154] A. M. R. Smith, K. K. Hii, *Chem. Rev.* **2011**, *111*, 1637−1656.

[155] G. Zhong, *Angew. Chem. Int. Ed.* **2003**, *42*, 4247−4250.

[156] S. P. Brown, M. P. Brochu, C. J. Sinz, D. W. C. MacMillan, *J. Am. Chem. Soc.* **2003**, *125*, 10808−10809.

[157] Y. Hayashi, J. Yamaguchi, K. Hibino, M. Shoji, *Tetrahedron Lett.* **2003**, *44*, 8293−8296.

[158] A. Bøgevig, H. Sunden, A. Cordova, *Angew. Chem. Int. Ed.* **2004**, *43*, 1109−1112.

[159] Y. Hayashi, J. Yamaguchi, T. Sumiya, M. Shoji, *Angew. Chem. Int. Ed.* **2004**, *43*, 1112−1115.

[160] A. Cordova, H. Sunden, A. Bøgevig, M. Johansson, F. Himo, *Chem. Eur. J.* **2004**, *10*, 3673−3684.

[161] M. J. P. Vaismaa, S. C. Yau, N. C. O. Tomkinson, *Tetrahedron Lett.* **2009**, *50*, 3625−3627.

[162] T. Kano, H. Mii, K. Maruoka, *J. Am. Chem. Soc.* **2009**, *131*, 3450−3451.

[163] H. Gotoh, Y. Hayashi, *Chem. Commun.* **2009**, 3083−3085.

[164] O. Lifchits, N. Demoulin, B. List, *Angew. Chem. Int. Ed.* **2011**, *50*, 9680−9683.

[165] H. Rao, P. Wang, C.-J. Li, *Eur. J. Org. Chem.* **2012**, 6503−6507.

[166] *Comprehensive Organic Synthesis Vol. 4* (Ed.: B. M. Trost, I. Flemming, M. F. Semmelhack), Pergamon, New York, **1991**, chapter 2.2.

[167] J. M. Fox, X. Huang, A. Chieffi, S. L. Buchwald, *J. Am. Chem. Soc.* **2000**, *122*, 1360−1370.

[168] D. A. Culkin, J. F. Hartwig, *Acc. Chem. Res.* **2003**, *36*, 234−245.

[169] C. C. C. Johansson, T. J. Colacot, *Angew. Chem. Int. Ed.* **2010**, *49*, 676−707.

[170] C. Fischer, G. C. Fu, *J. Am. Chem. Soc.* **2005**, *127*, 4594−4595.

[171] N. A. Strotman, S. Sommer, G. C. Fu, *Angew. Chem. Int. Ed.* **2007**, *46*, 3556−3558.

[172] C. Liu, C. He, W. Shi, M. Chen, A. Lei, *Org. Lett.* **2007**, *9*, 5601−5604.

[173] P. M. Lundin, J. Esquivias, G. C. Fu, *Angew. Chem. Int. Ed.* **2008**, *48*, 154−156.

[174] Q. Tang, X. Chen, B. Tiwari, Y. R. Chi, *Org. Lett.* **2012**, *14* 1922−1925.

[175] M. N. Vander Wal, A. K. Dinger, D. W. C. MacMillan, *Chem. Sci.* **2013**, *4*, 3075−3079.

[176] S. Muthusamy, C. Gunanathan, S. A. Babu, E. Suresh, P. Dastidar, *Chem. Commun.* **2002**, 824−825.

[177] R. Gibe, M. A. Kerr, *J. Org. Chem.* **2002**, *67*, 6247−6249.

[178] A. DeAngelis, V. W. Shurtleff, O. Dmitrenko, J. M. Fox, *J. Am. Chem. Soc.* **2011**, *133*, 1650−1653.

[179] Y. Cai, S.-F. Zhu, G.-P. Wang, Q.-L. Zhou, *Adv. Synth. Catal.* **2011**, *353*, 2939−2944.

[180] J. M. Fracile, K. L. Jeune, J. A. Mayoral, N. Ravasio, F. Zaccheria, *Org. Biomol. Chem.* **2013**, *11*, 4327−4332.

[181] T. D. Beeson, A. Mastracchio, J.-B. Hong, K. Ashton, D. W. C. MacMillan, *Science* **2007**, *316*, 582−585.

[182] J. C. Conrad, J. Kong, B. N. Laforteza, D. W. C. MacMillan, *J. Am. Chem. Soc.* **2009**, *131*, 11640−11641.

[183] K. C. Nicolaou, R. Reingruber, D. Sarlah, S. Bräse, *J. Am. Chem. Soc.* **2009**, *131*, 2086−2087.

[184] Y. L. Hu, H. Jiang, M. Lu, *Green Chem.* **2011**, *13*, 3079−3087.

[185] Q.-L. Xu, H. Gao, M. Yousufuddin, D. H. Ess, L. Kürti, *J. Am. Chem. Soc.* **2013**, *135*, 14048−14051.

[186] Y. M. Osornio, R. Cruz-Almanza, V. Jiménez-Montaño, L. D. Miranda, *Chem. Commun.* **2003**, 2316−2317.

[187] L. Furst, B. S. Matsuura, J. M. R. Narayanam, J. W. Tucker, C. R. J. Stephenson, *Org. Lett.* **2010**, *12*, 3104−3107.

[188] G. S. Coumbarides, M. Dingjan, J. Eames, N. Weerasooriya, *Bull. Chem. Soc. Jpn.* **2001**, *74*, 179−180.

[189] X.-M. Cui, Y.-H. Guan, N. Li, H. Lv, L.-A. Fu, K. Guo, X. Fan, *Tetrahedron Lett.* **2014**, *55*, 90−93.

[190] C. P. Ashcroft, S. Challenger, D. Clifford, A. M. Derrick, Y. Hajikarimian, K. Slucock, T. V. Silk, M. Thomson, N. M. Thomson, J. R. Williams, *Org. Process Res. Dev.* **2005**, *9*, 663−669.

[191] D. A. Evans, K. R. Fandrick, H.-J. Song, *J. Am. Chem. Soc.* **2005**, *127*, 8942−8943.

[192] E. L. Tyson, E. P. Farney, T. P. Yoon, *Org. Lett.* **2012**, *14*, 1110−1113.

[193] Y. Tan, W. Yuan, L. Gong, E. Meggers, *Angew. Chem. Int. Ed.* **2015**, *54*, 13045−13048.

[194] C. Wang, K. Harms, E. Meggers, *Angew. Chem. Int. Ed.* **2016**, *55*, 13495−13498.

[195] J. E. Wilson, A. D. Casarez, D. W. C. MacMillan, *J. Am. Chem. Soc.* **2009**, *113*, 11332−11334.

[196] H.-Y. Jang, J.-B. Hong, D. W. C. MacMillan, *J. Am. Chem. Soc.* **2007**, *129*, 7004−7005.

[197] H. Kim, D. W. C. MacMillan, *J. Am. Chem. Soc.* **2008**, *130*, 398−399.

[198] D. W. C. MacMillan, *Nature* **2008**, *455*, 304−308.

[199] A. G. Capacci, J. T. Malinowski, N. J. McAlpine, J. Kuhne, D. W. C. MacMillan, *Nat. Chem.* **2017**, published online, DOI: 10.1038/NCHEM.2797.

[200] T. B. Nguyen, L. Ermolenko, P. Retailleau, A. Al-Mourabit, *Angew. Chem. Int. Ed.* **2014**, *53*, 13808−13812.

[201] M. G. Colombo, T. C. Brunold, T. Riedener, H. U. Güdel, *Inorg. Chem.* **1994**, *33*, 545−550.

[202] J. D. Slinker, A. A. Gorodetsky, M. S. Lowry, J. Wang, S. Parker, R. Rohl, S. Bernhard, G. G. Malliaras, *J. Am. Chem. Soc.* **2004**, *126*, 2763−2767.

[203] F. Xue, C. Cai, H. Sun, Q. Shen, J. Rui, *Tetrahedron Lett.* **2008**, *49*, 4386−4389.

[204] J. Yoshida, S. Yano, T. Ozawa, N. Kawabata, *J. Org. Chem.* **1985**, *50*, 3467−3473.

Chapter 7. Appendices

7.1. NMR-Spectra

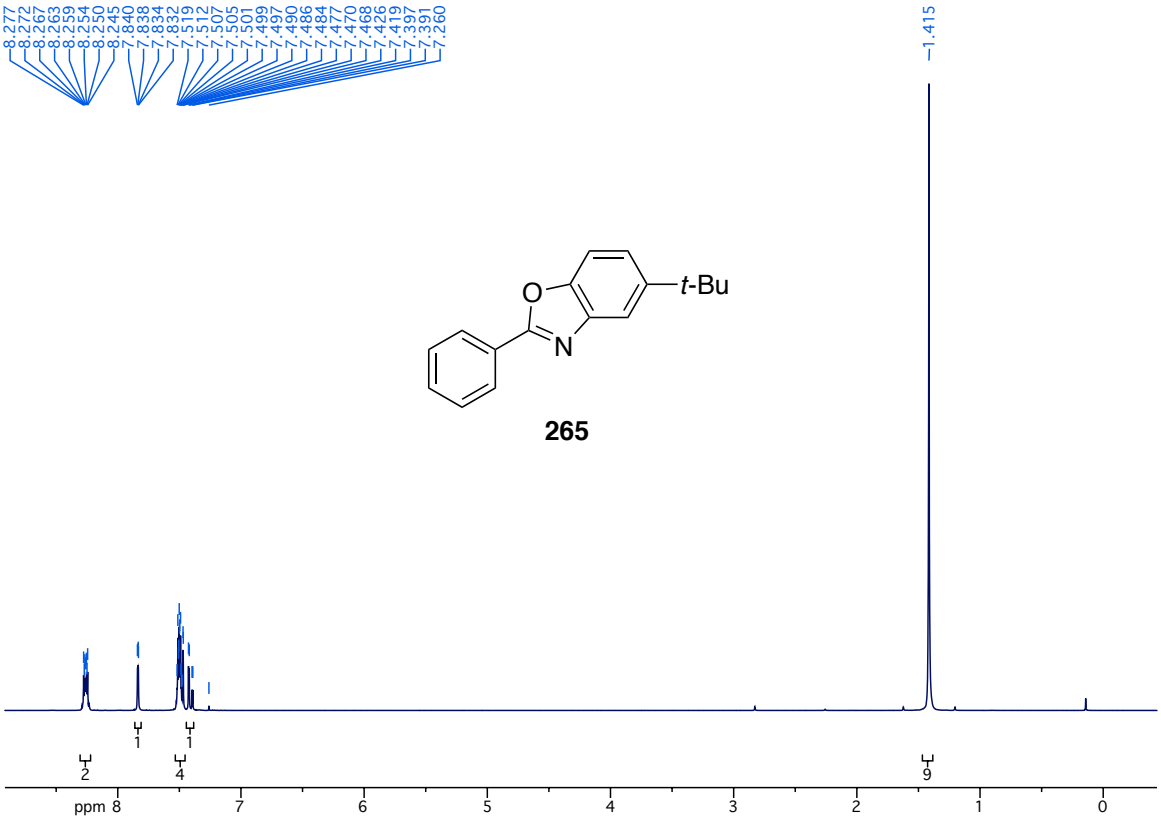

^{1}H-NMR spectrum of compound **265** (300 MHz, $CDCl_3$)

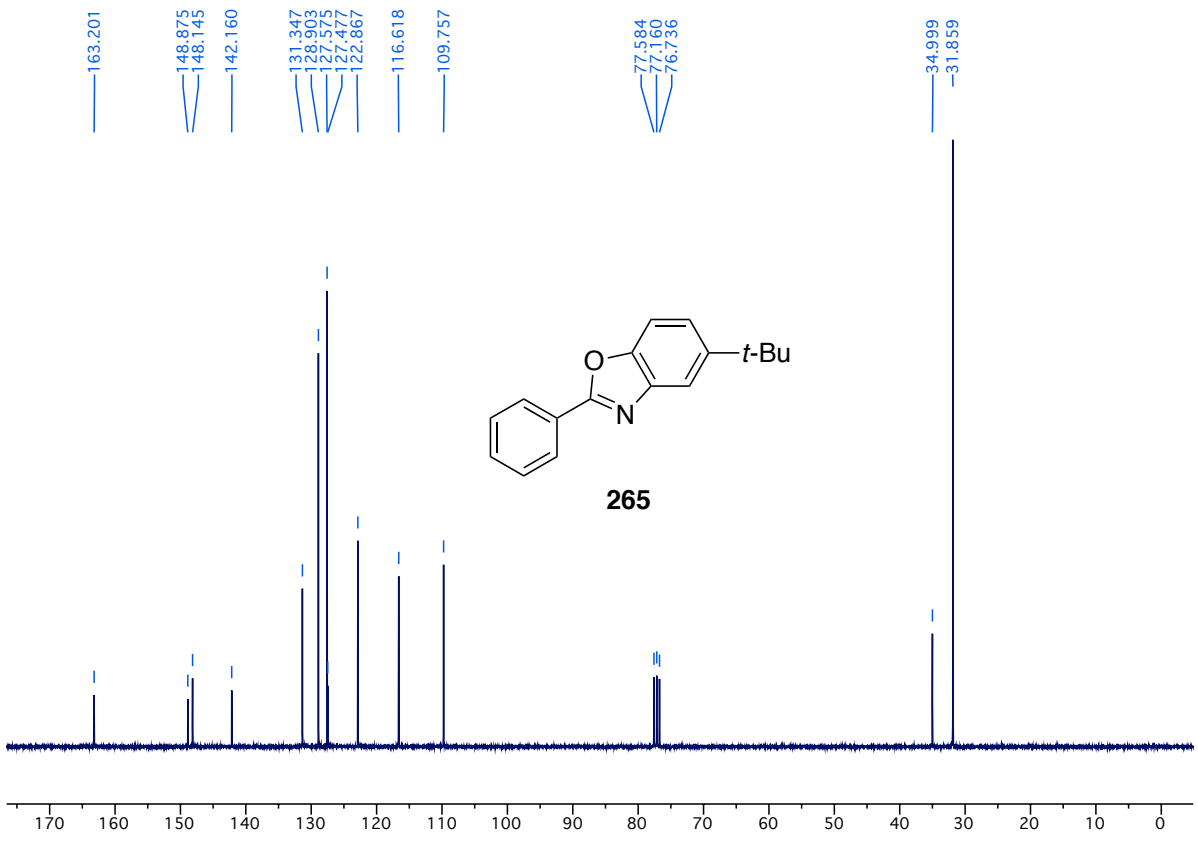

^{13}C-NMR spectrum of compound **265** (75.5 MHz, $CDCl_3$)

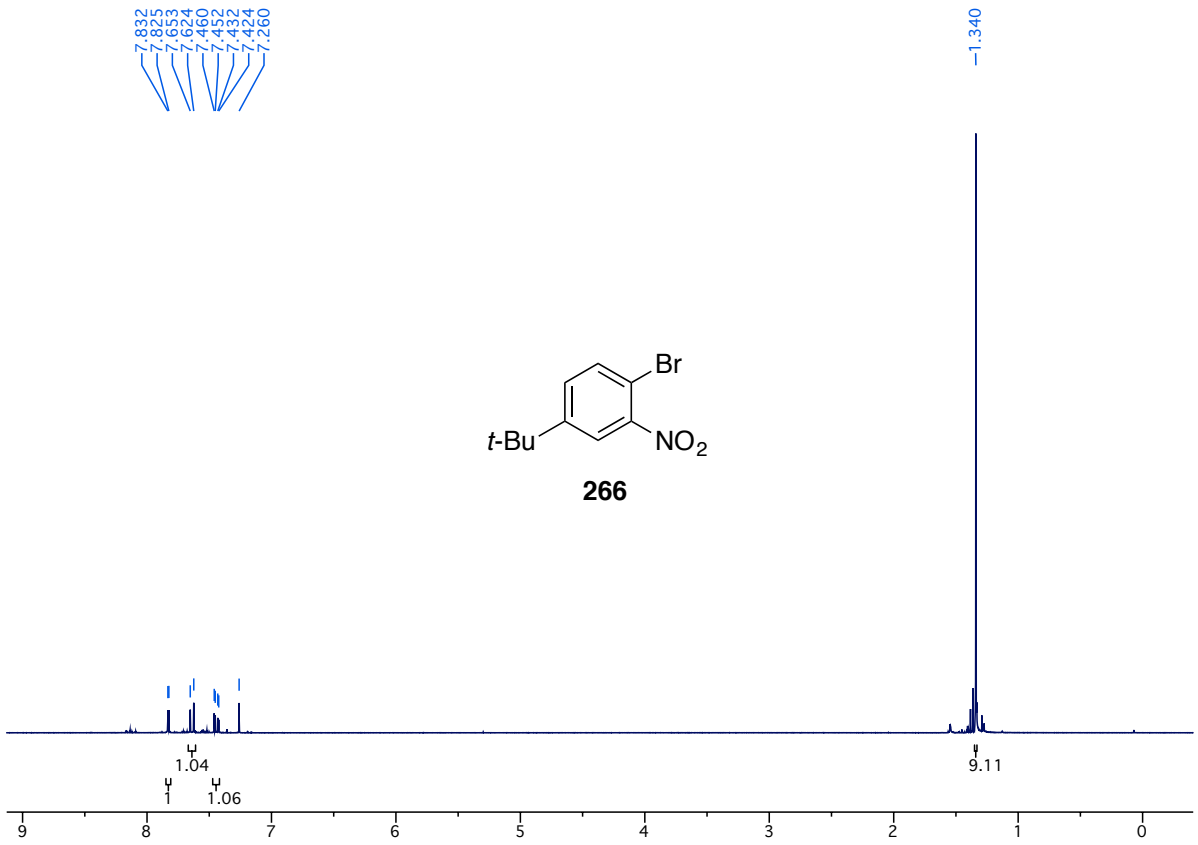

^{1}H-NMR spectrum of compound **266** (300 MHz, $CDCl_3$)

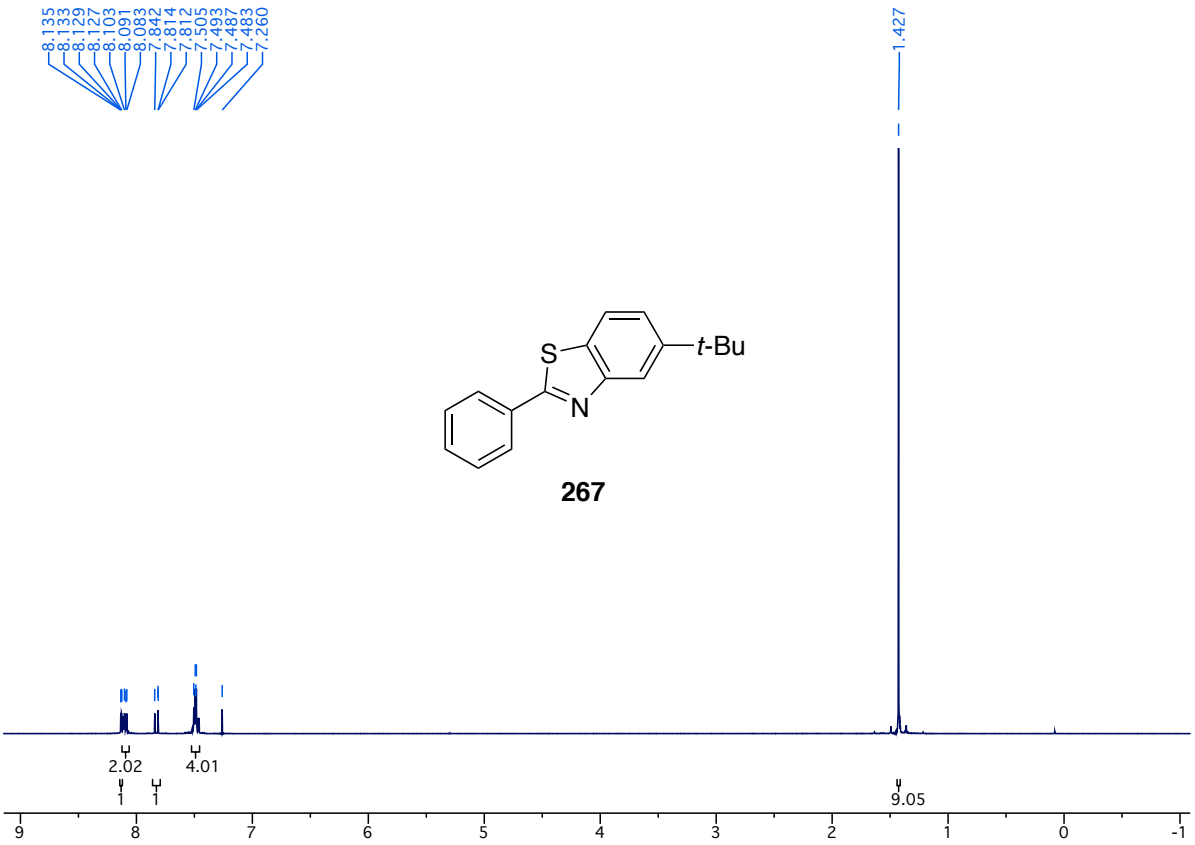

^{1}H-NMR spectrum of compound **267** (300 MHz, $CDCl_3$)

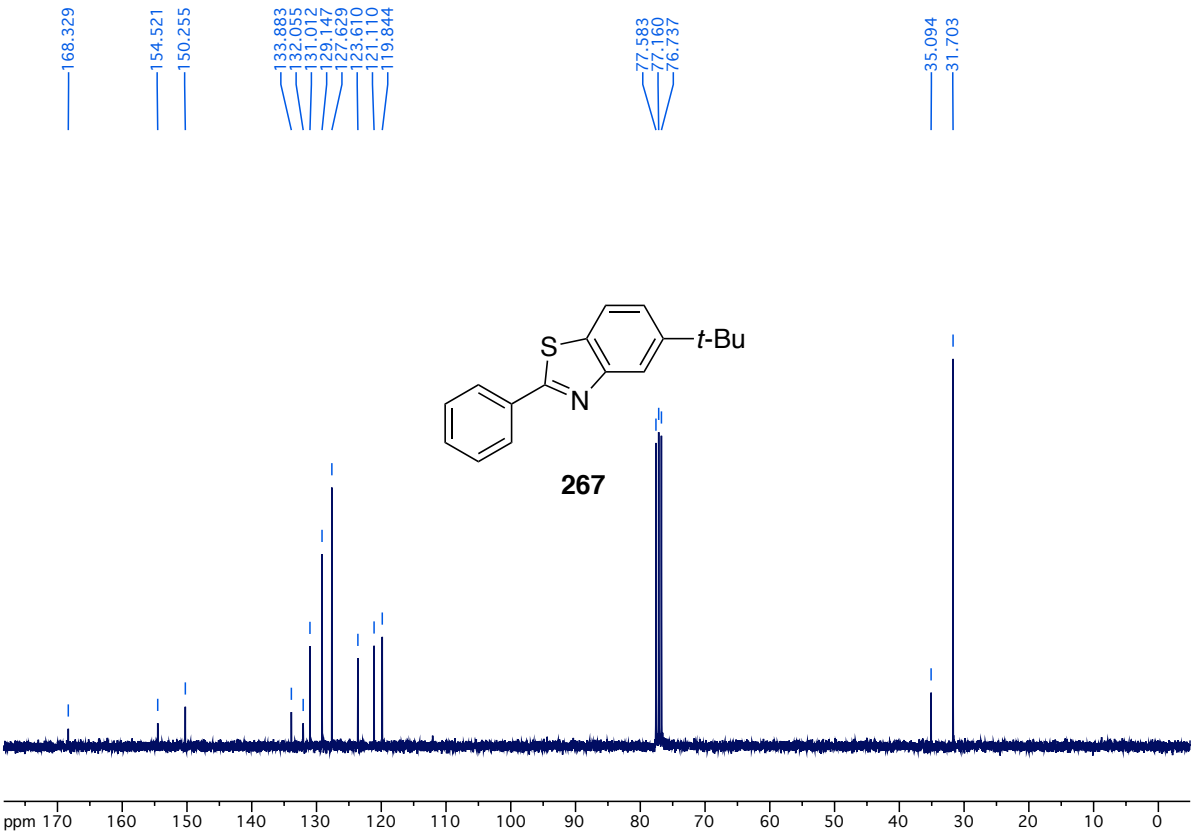

^{13}C-NMR spectrum of compound **267** (75.5 MHz, $CDCl_3$)

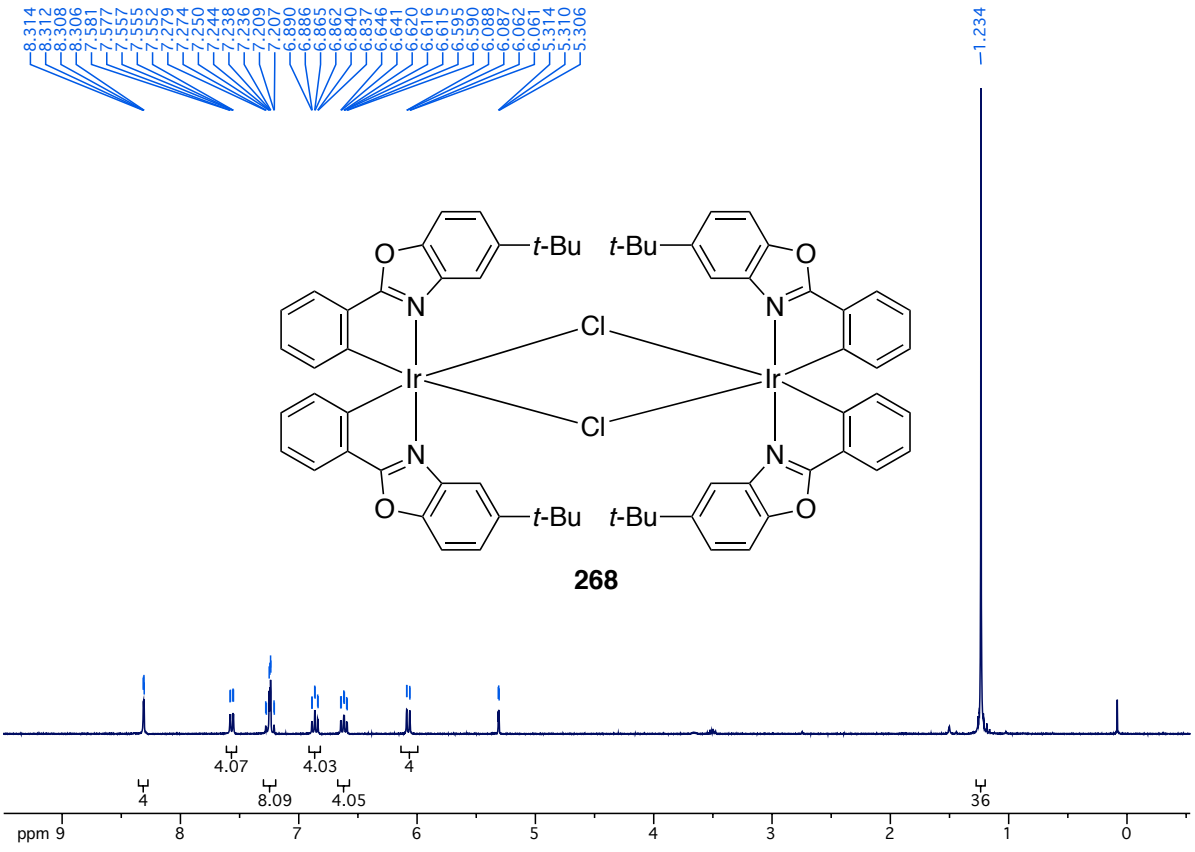

^{1}H-NMR spectrum of compound **268** (300 MHz, CD_2Cl_2)

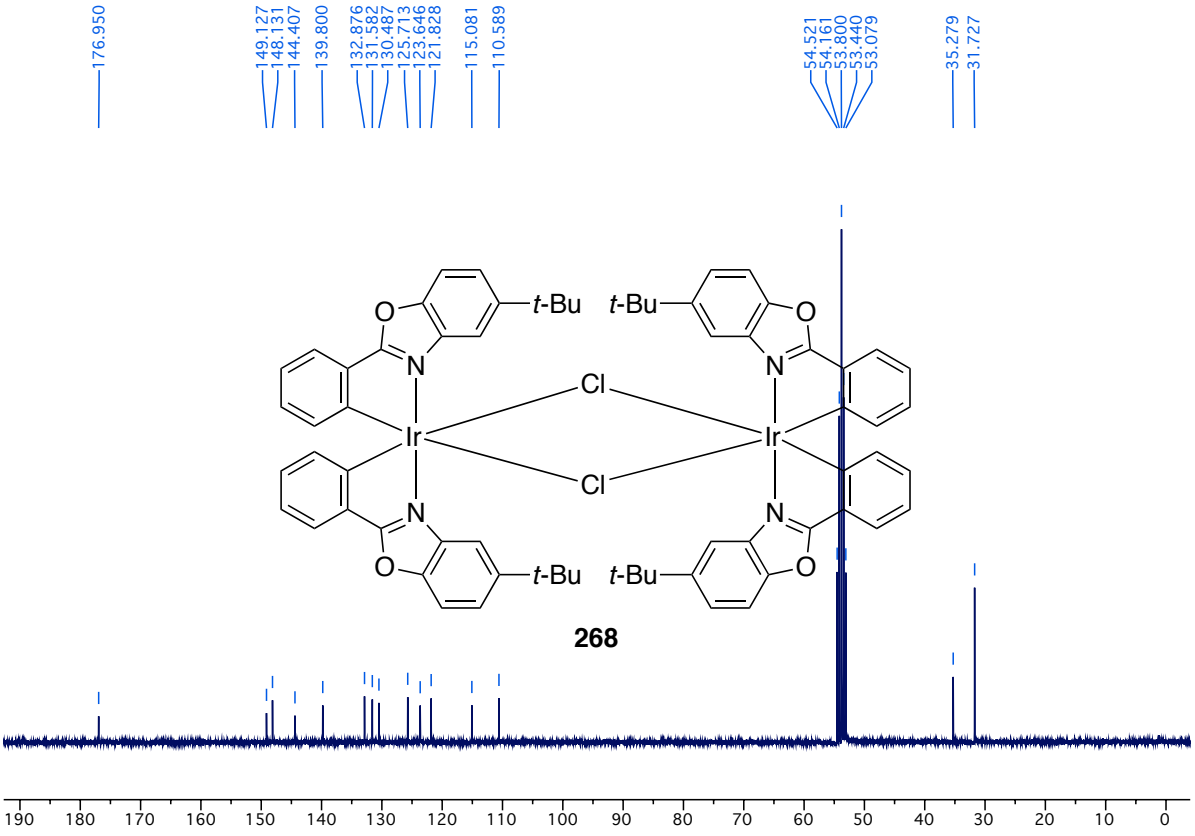

^{13}C-NMR spectrum of compound **268** (75.5 MHz, CD_2Cl_2)

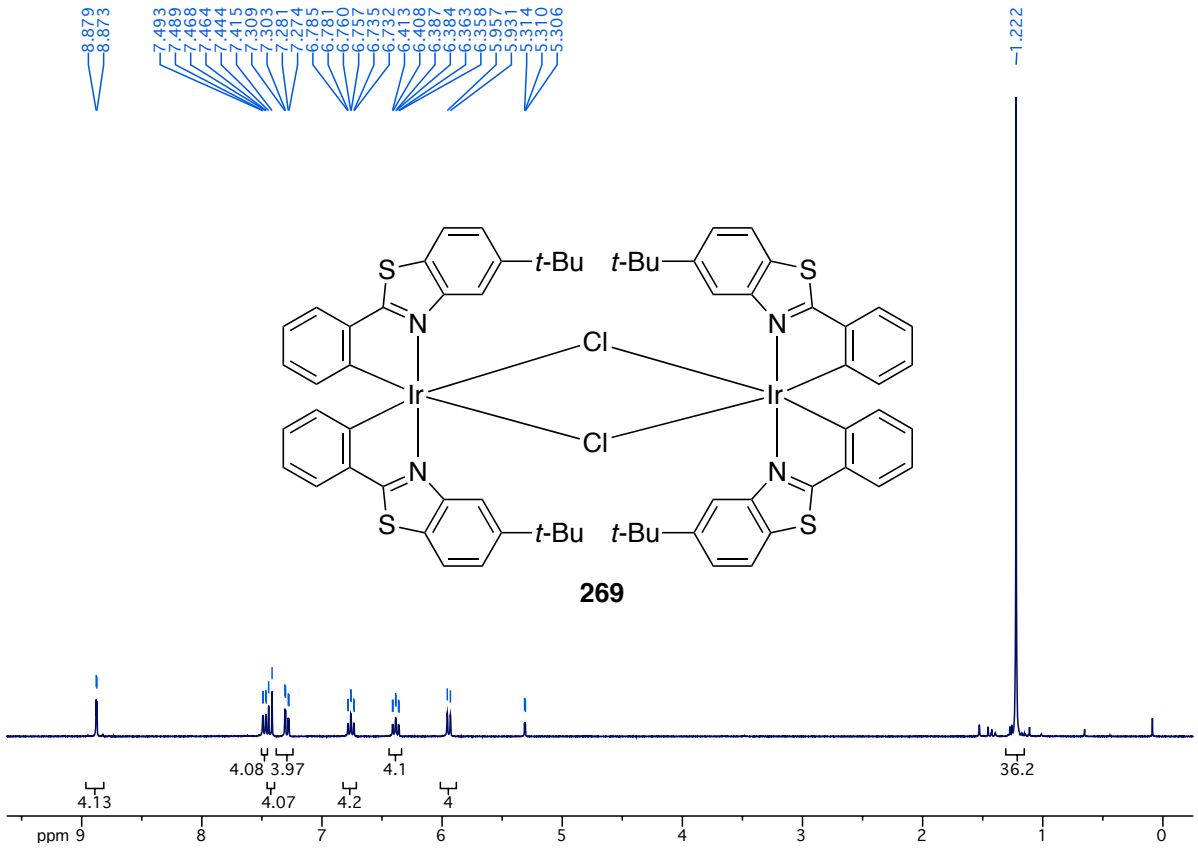

^{1}H-NMR spectrum of compound **269** (300 MHz, CD_2Cl_2)

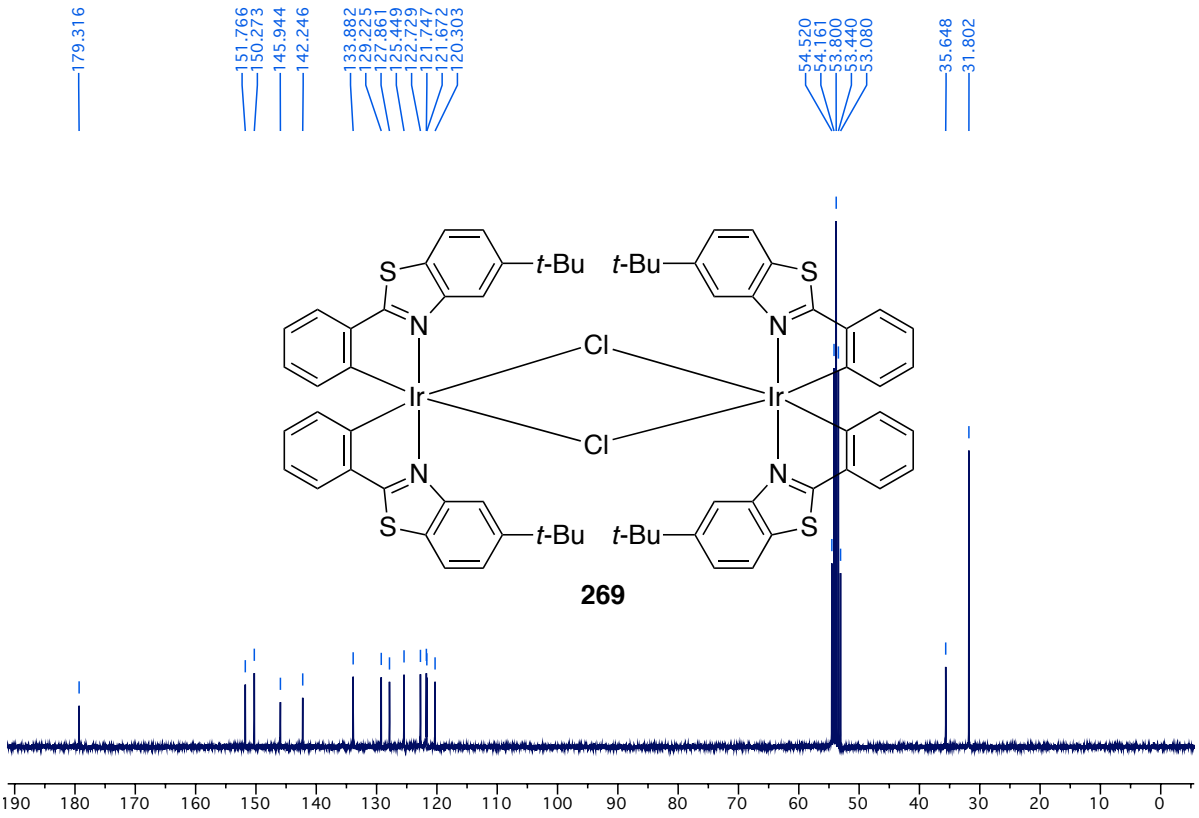

^{13}C-NMR spectrum of compound **269** (75.5MHz, CD_2Cl_2)

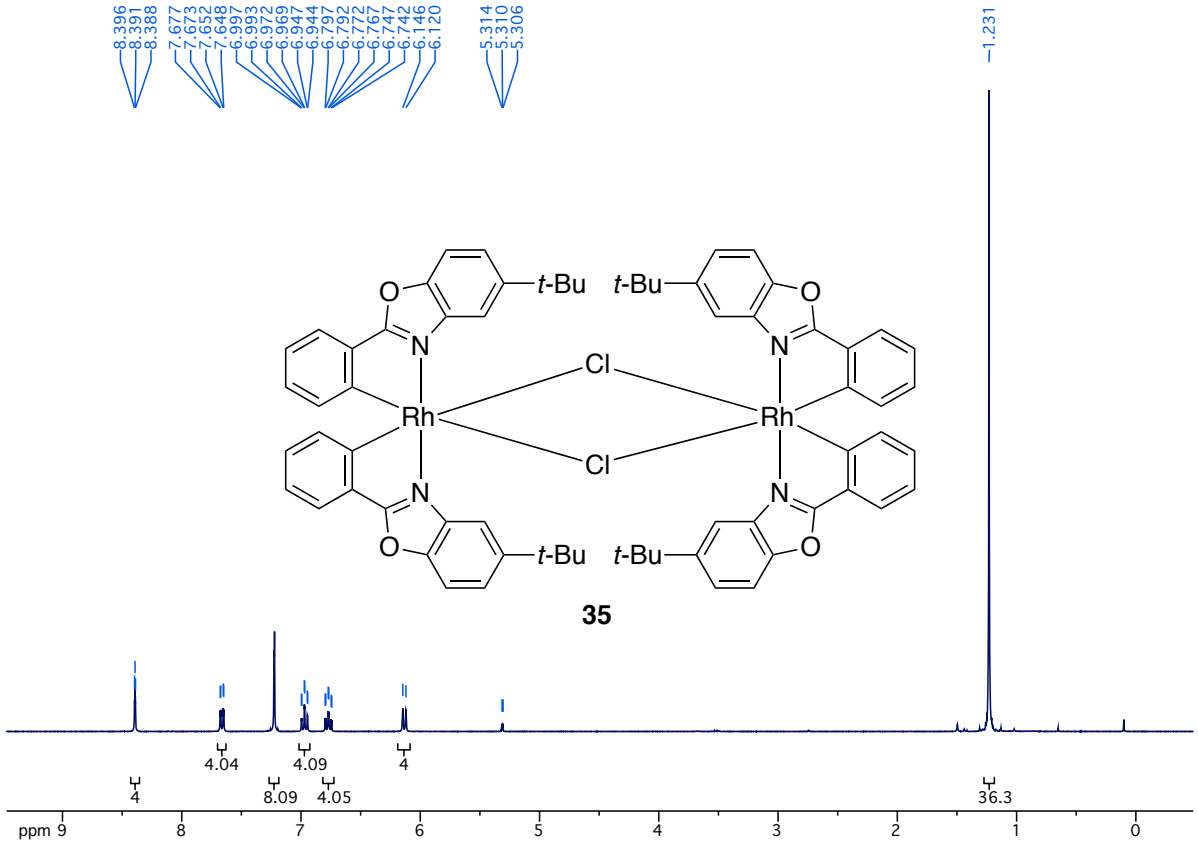

^{1}H-NMR spectrum of compound **35** (300 MHz, CD_2Cl_2)

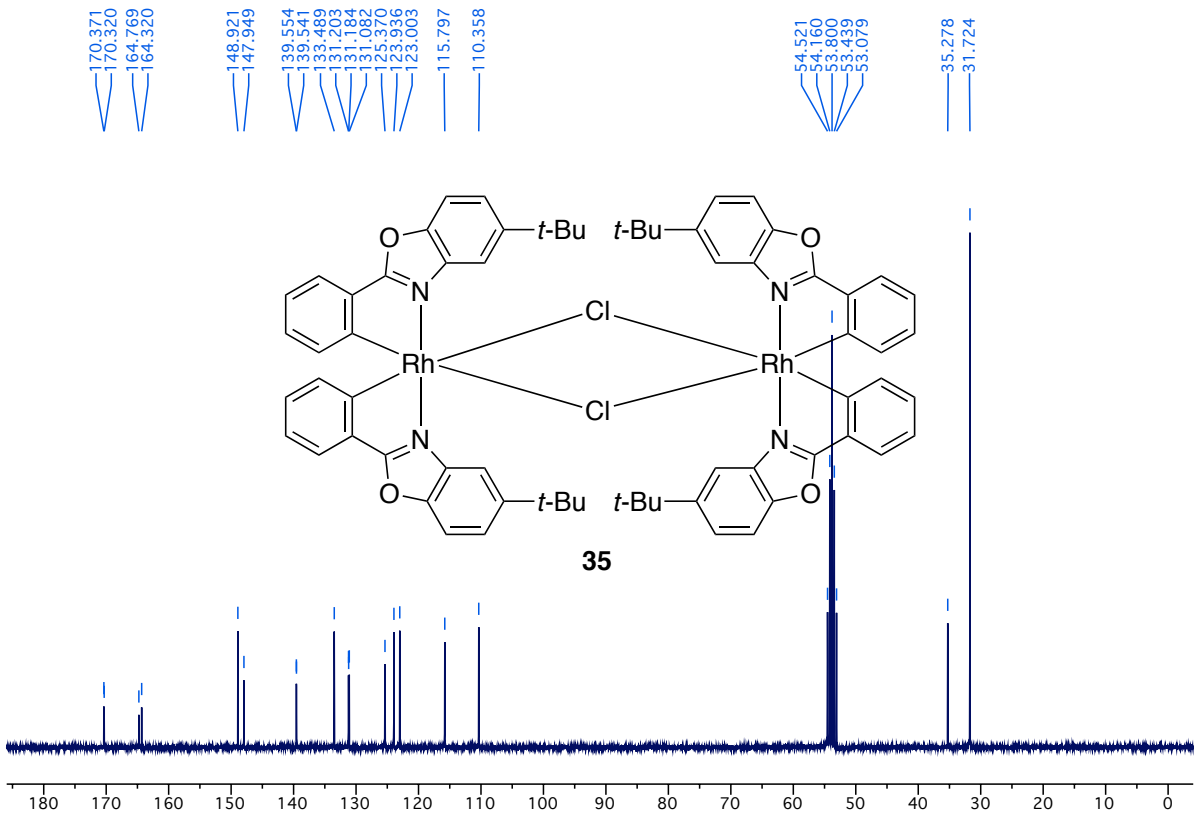

^{13}C-NMR spectrum of compound **35** (75.5 MHz, CD_2Cl_2)

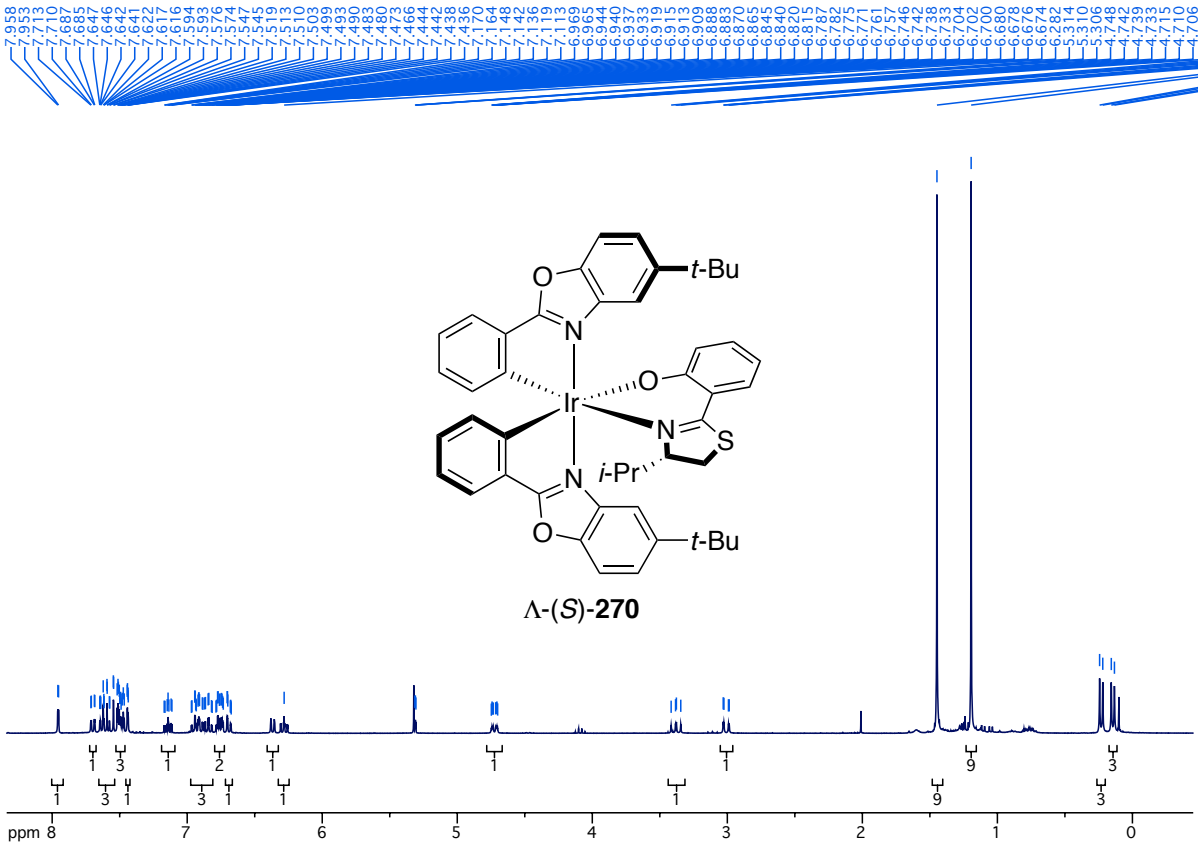

^{1}H-NMR spectrum of compound Λ-(*S*)-**270** (300 MHz, CD_2Cl_2)

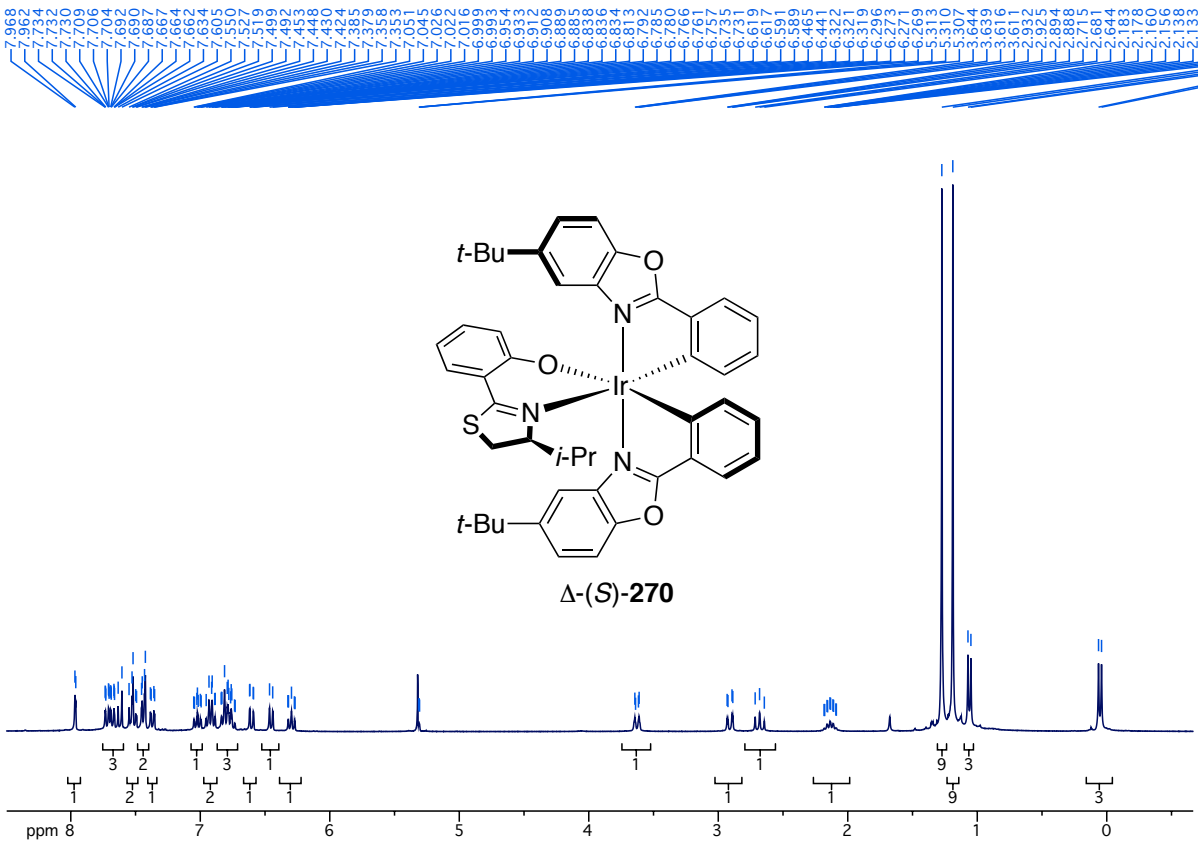

^{1}H-NMR spectrum of compound Δ-(*S*)-**270** (300 MHz, CD_2Cl_2)

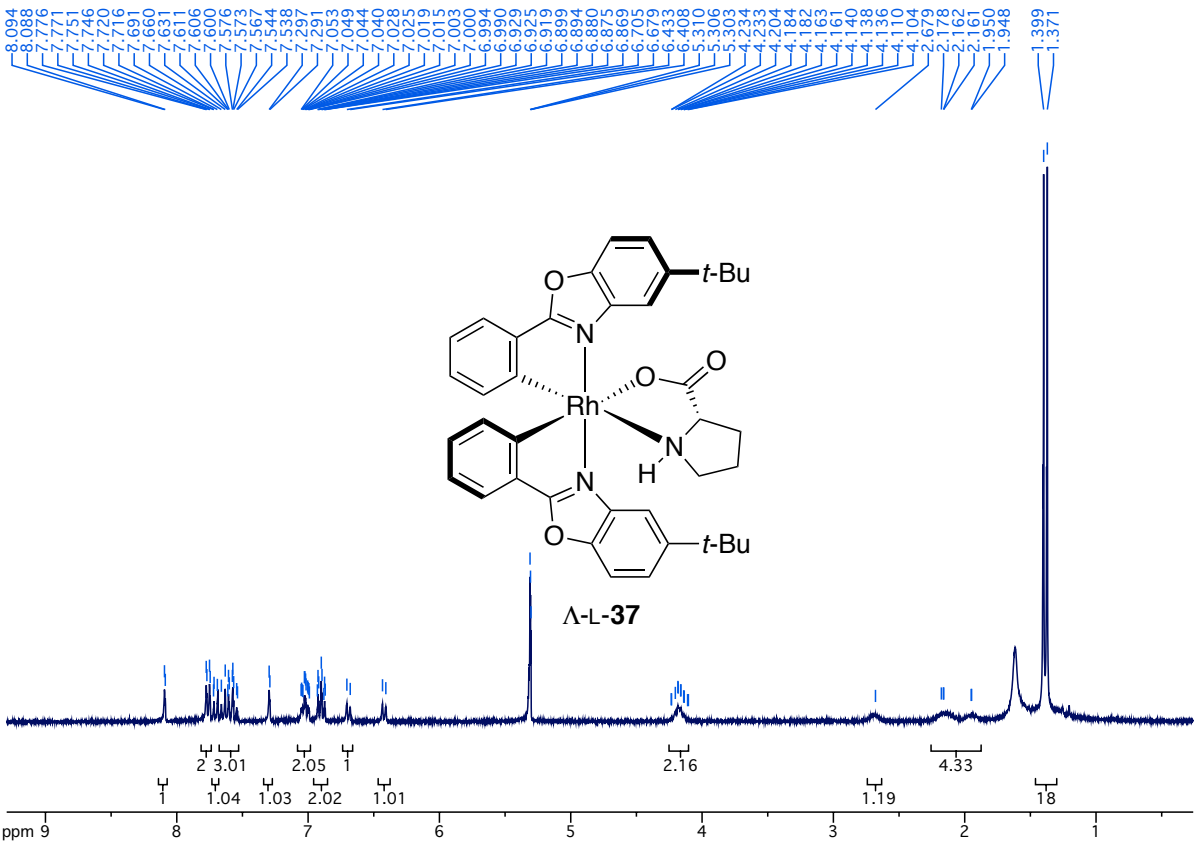

^{1}H-NMR spectrum of compound Λ-L-**37** (300 MHz, CD_2Cl_2)

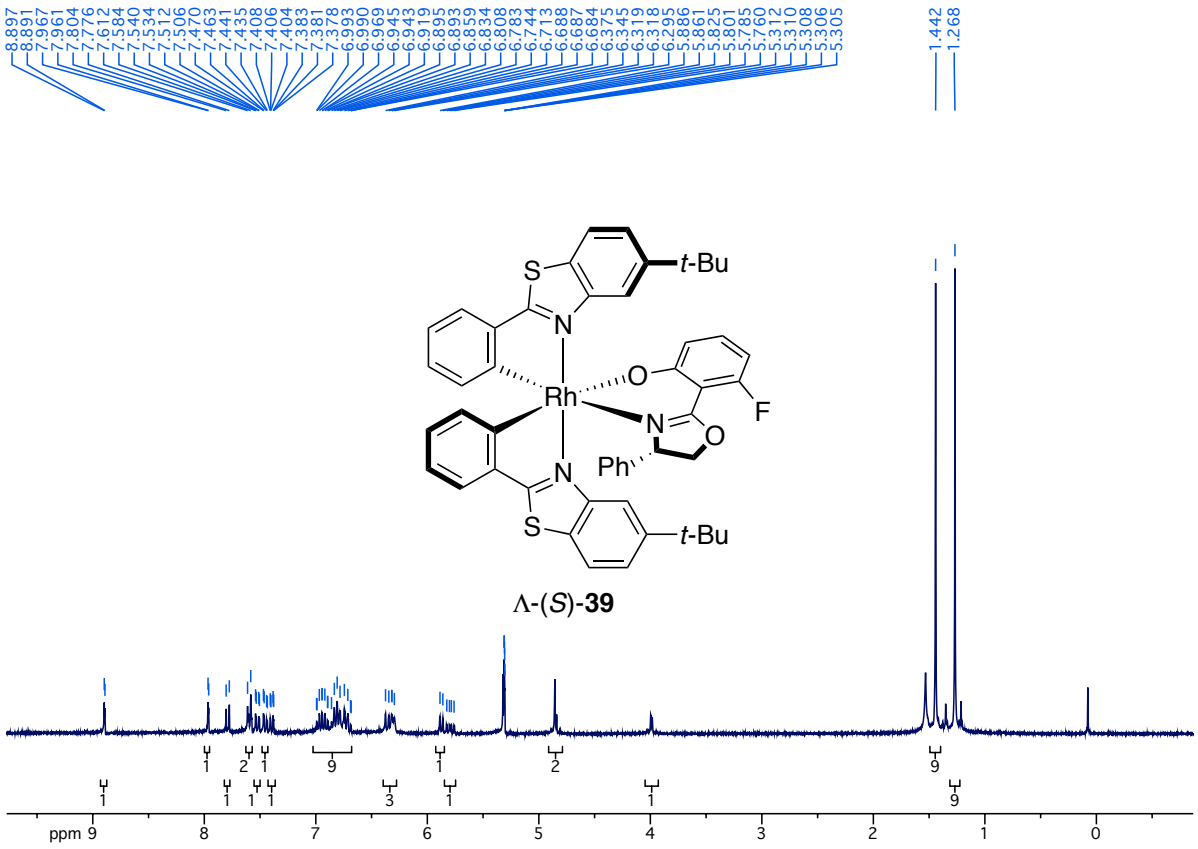

^{1}H-NMR spectrum of compound Λ-(*S*)-**39** (300 MHz, CD_2Cl_2)

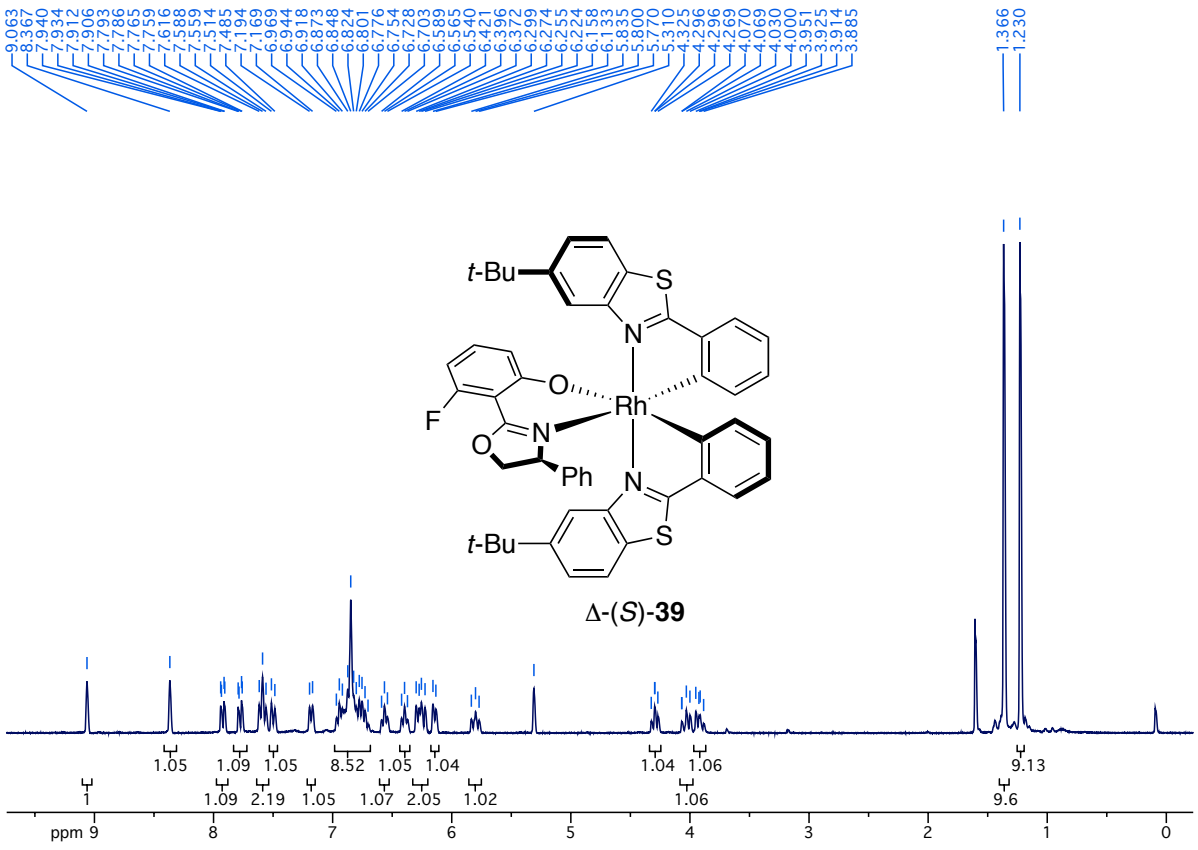

^{1}H-NMR spectrum of compound Δ-(*S*)-**39** (300 MHz, CD_2Cl_2)

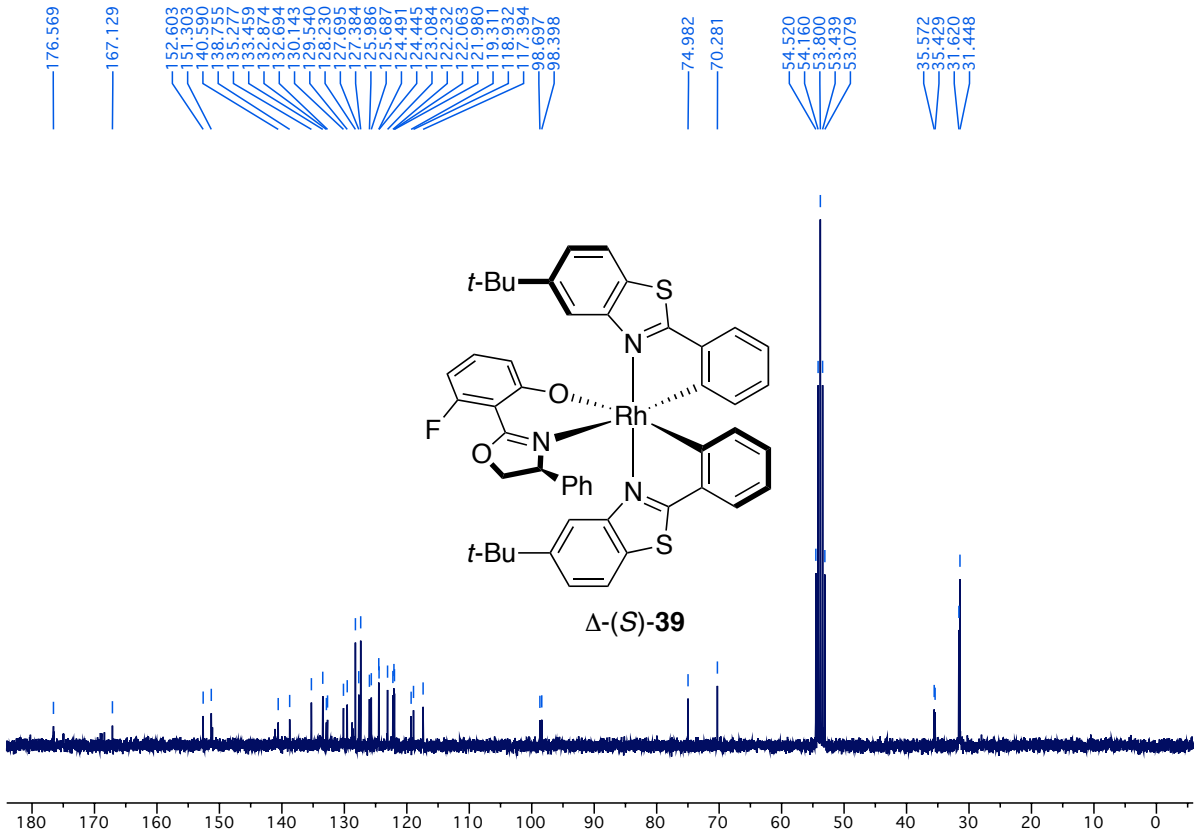

^{13}C-NMR spectrum of compound Δ-(*S*)-**39** (75.5 MHz, CD_2Cl_2)

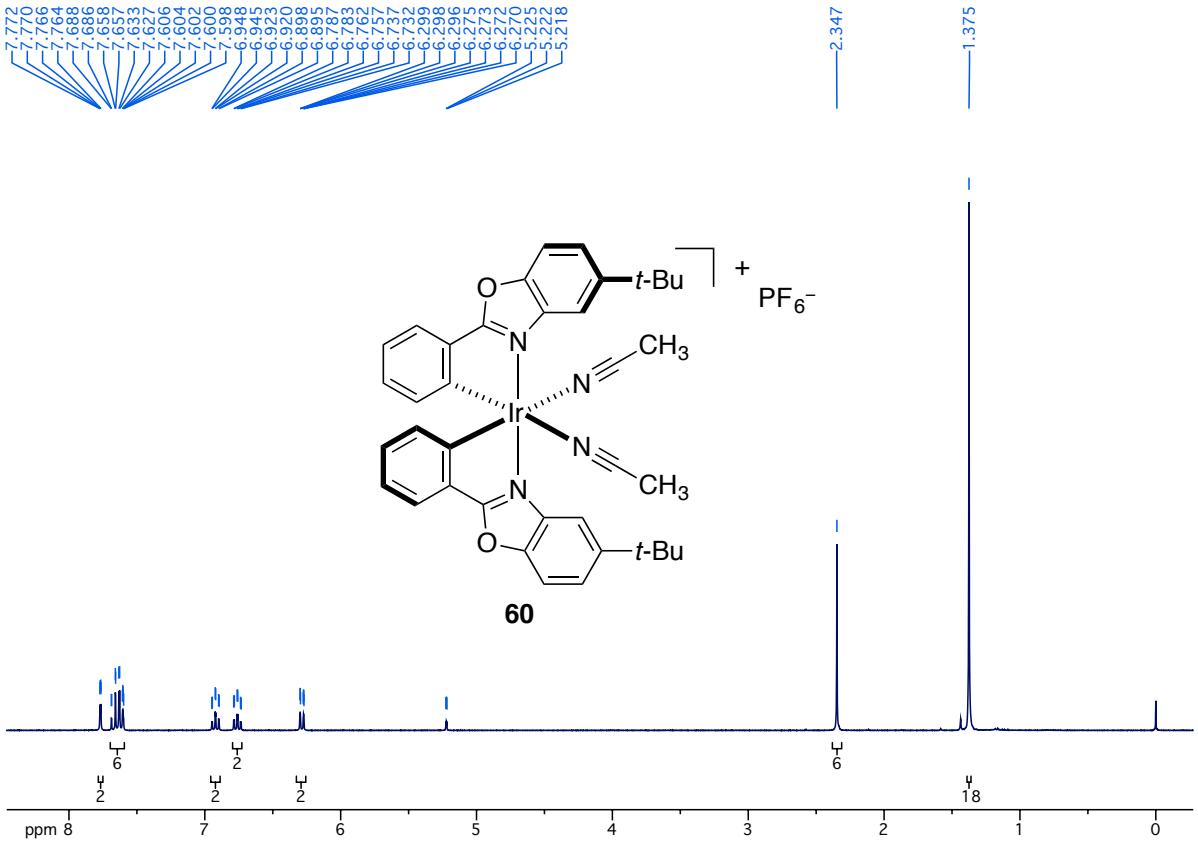

^{1}H-NMR spectrum of compound **60** (IrO) (300 MHz, CD_2Cl_2)

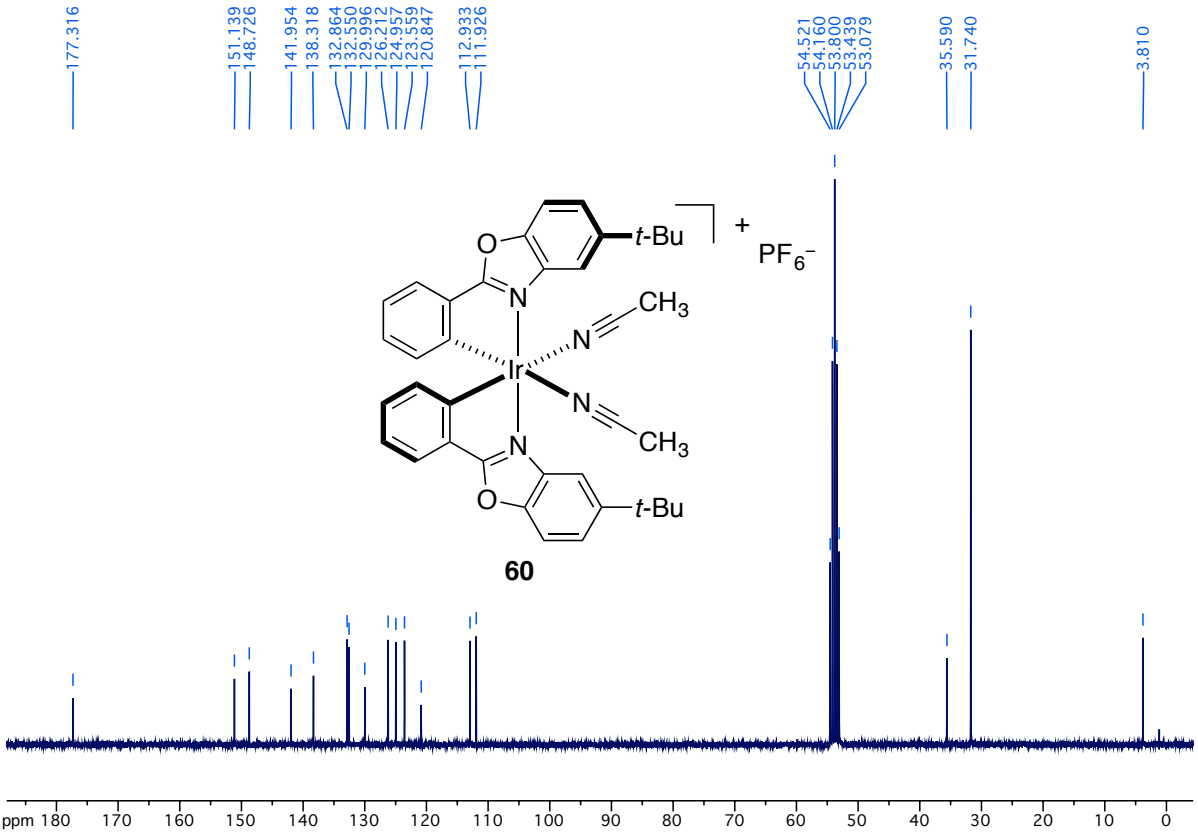

^{13}C-NMR spectrum of compound **60** (IrO) (75.5 MHz, CD_2Cl_2)

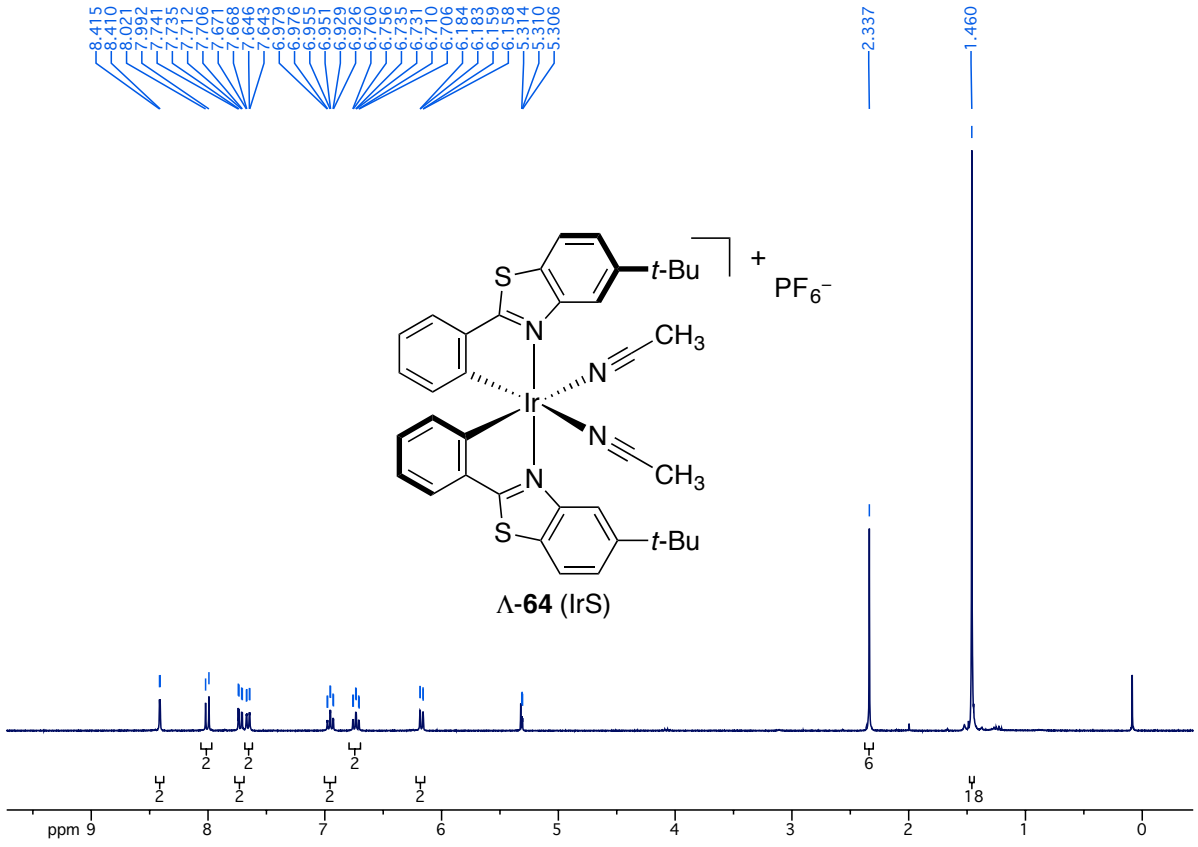

^{1}H-NMR spectrum of compound Λ-**64** (IrS) (300 MHz, CD_2Cl_2)

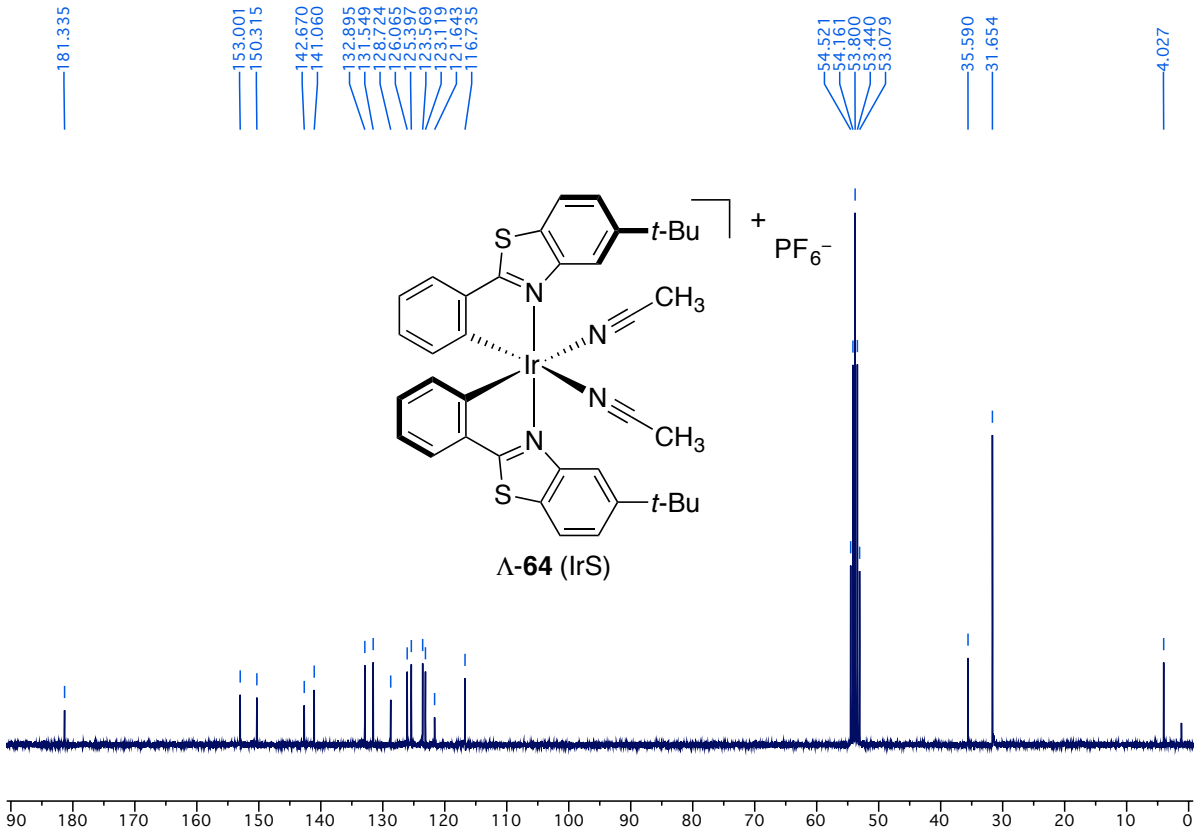

^{13}C-NMR spectrum of compound Λ-**64** (IrS) (75.5 MHz, CD_2Cl_2)

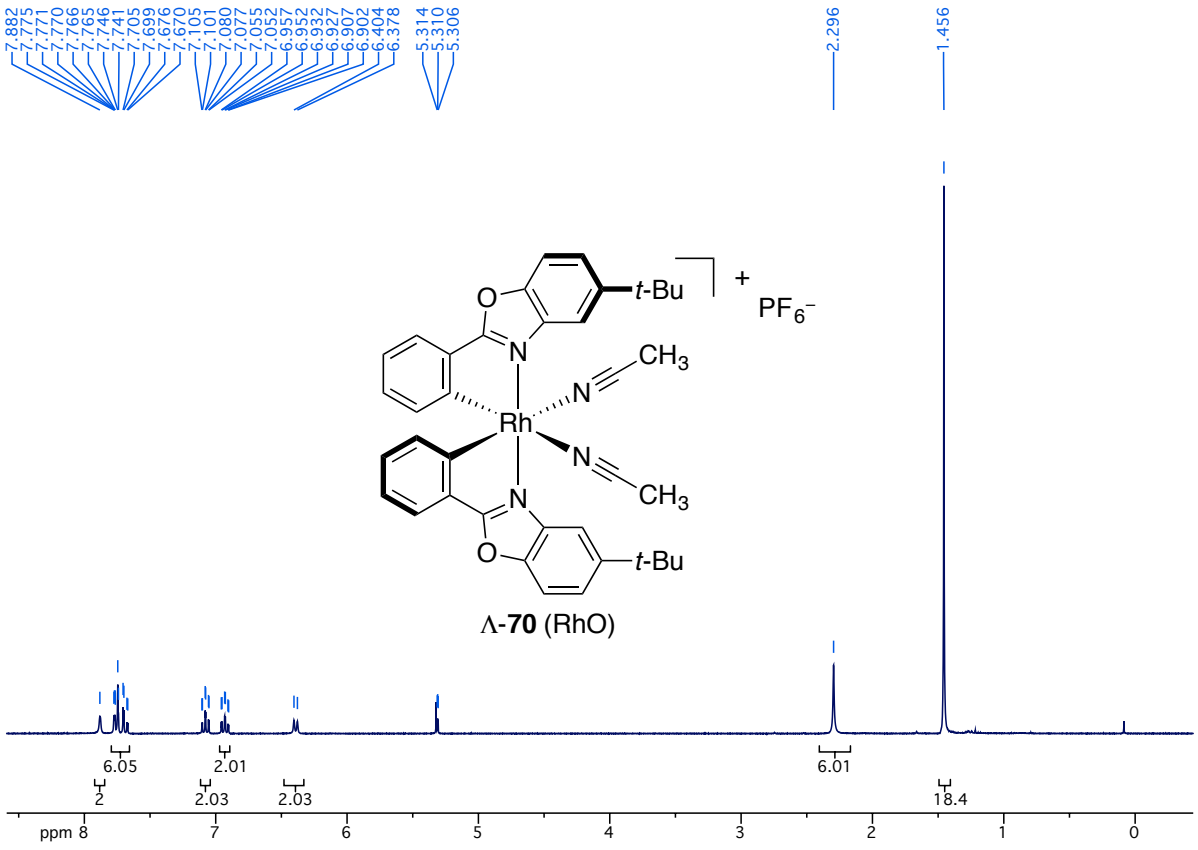

^{1}H-NMR spectrum of compound Λ-**70** (RhO) (300 MHz, CD_2Cl_2)

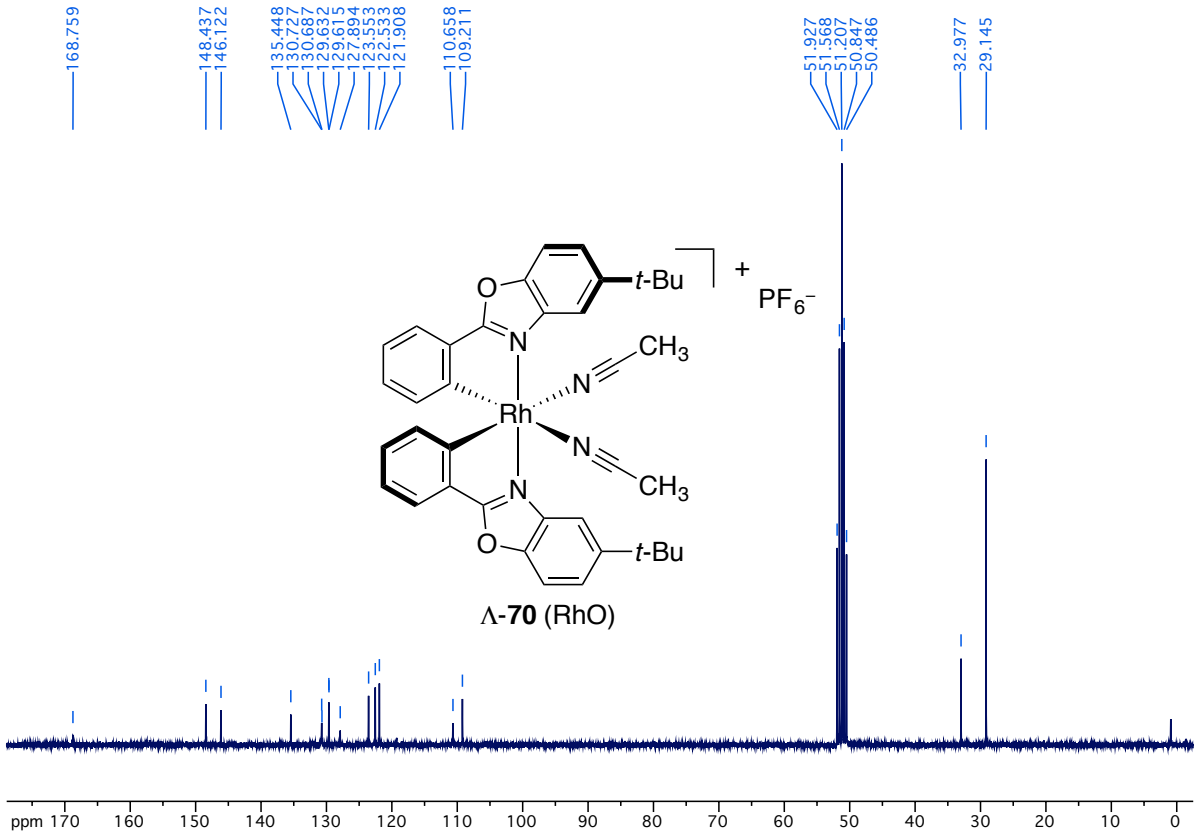

^{13}C-NMR spectrum of compound Λ-**70** (RhO) (75.5 MHz, CD_2Cl_2)

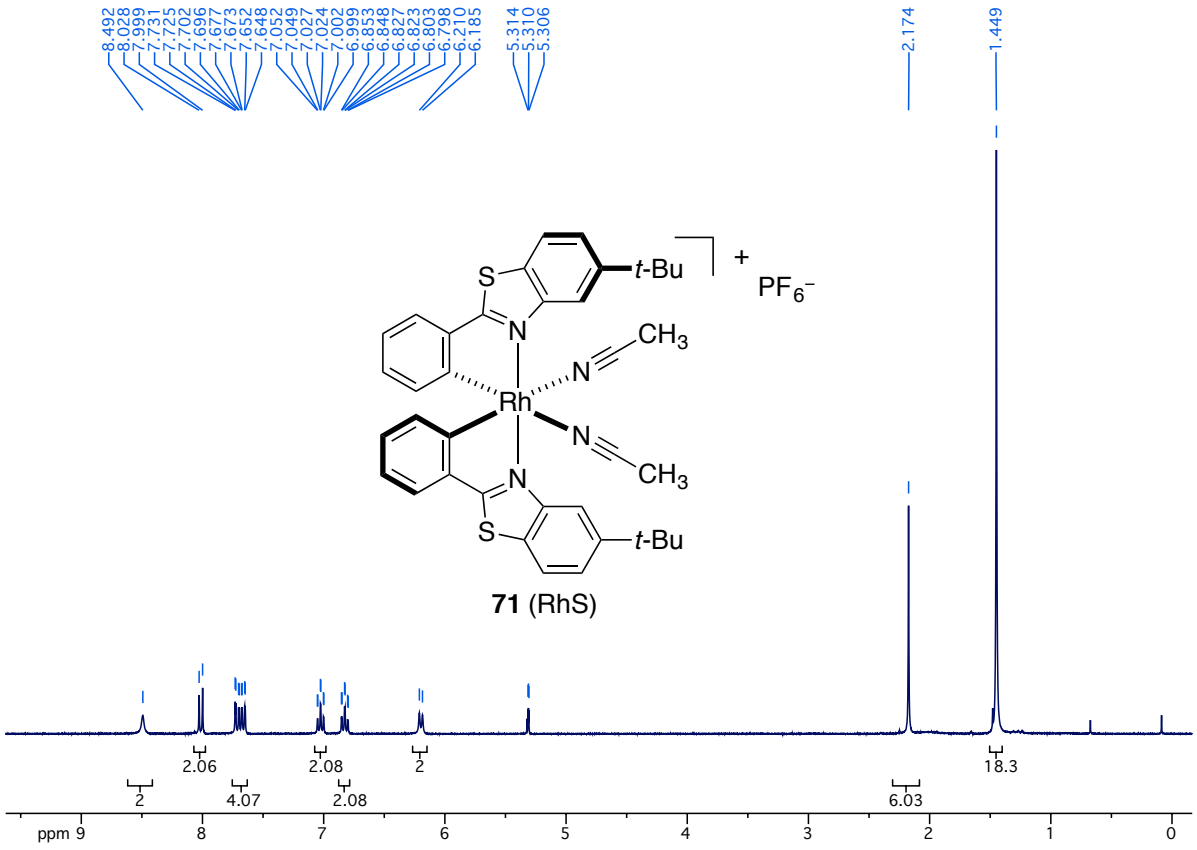

^{1}H-NMR spectrum of compound **71** (RhS) (300 MHz, CD_2Cl_2)

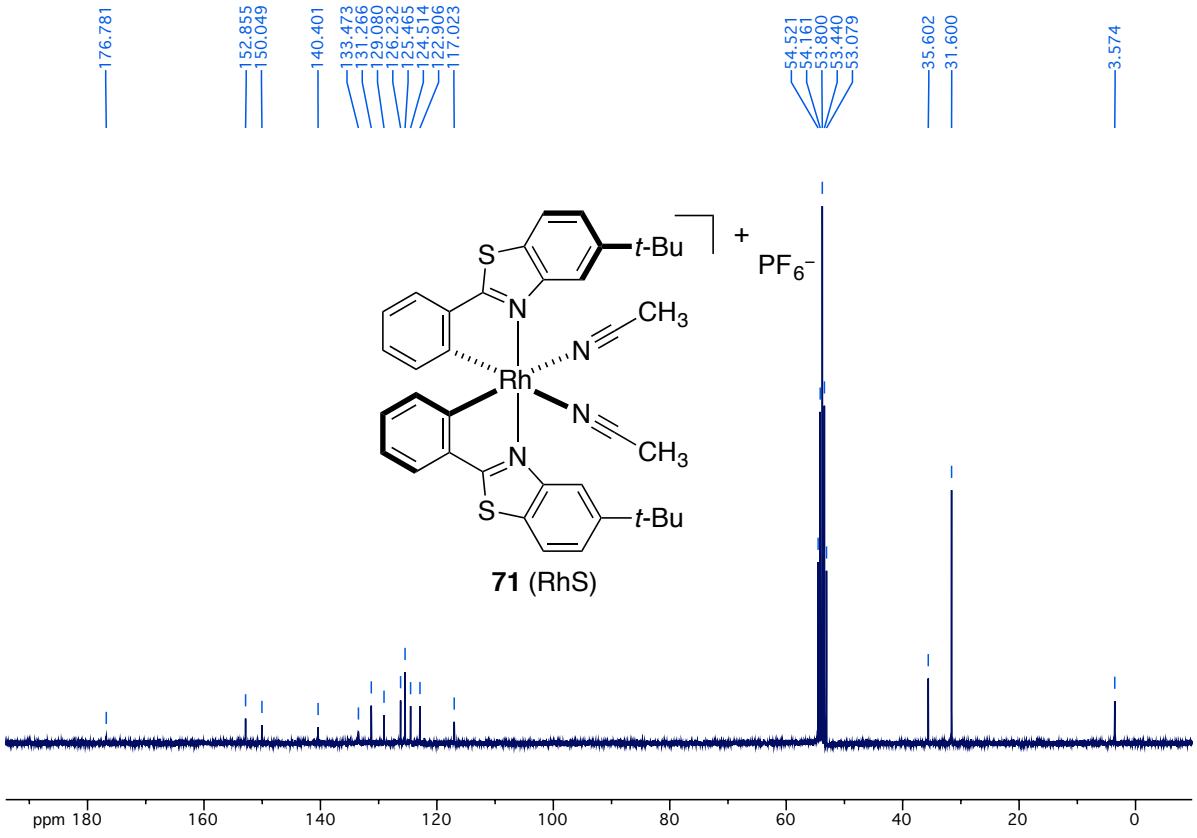

^{13}C-NMR spectrum of compound **71** (RhS) (75.5 MHz, CD_2Cl_2)

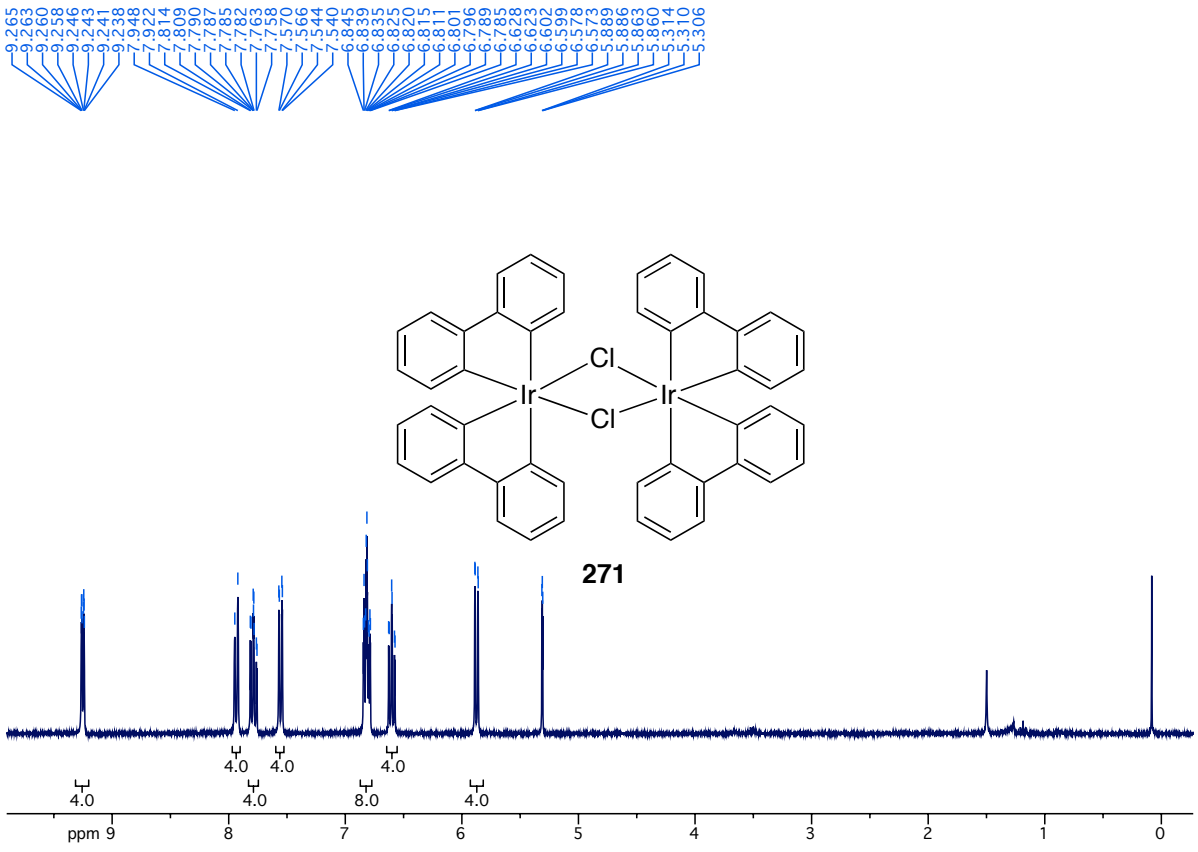

^{1}H-NMR spectrum of **271** (300 MHz, CD_2Cl_2)

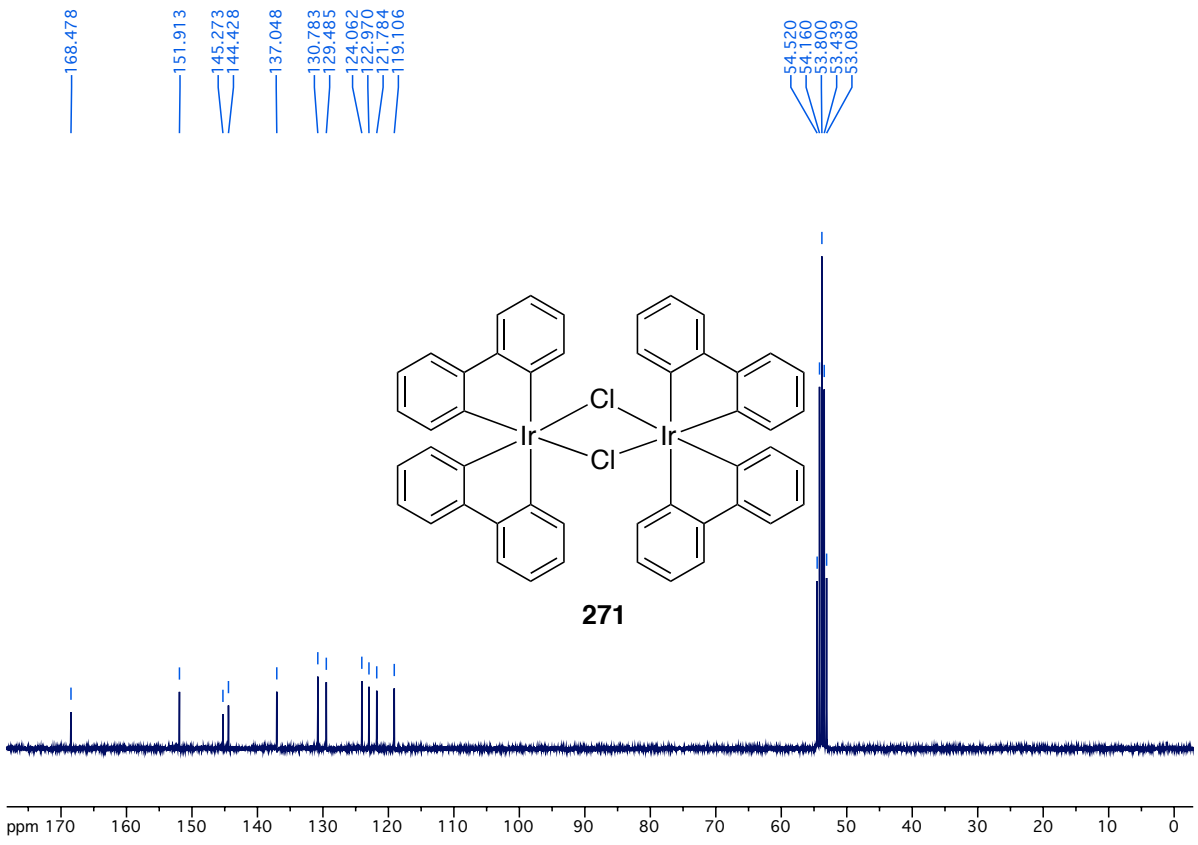

^{13}C-NMR spectrum of **271** (75.5 MHz, CD_2Cl_2)

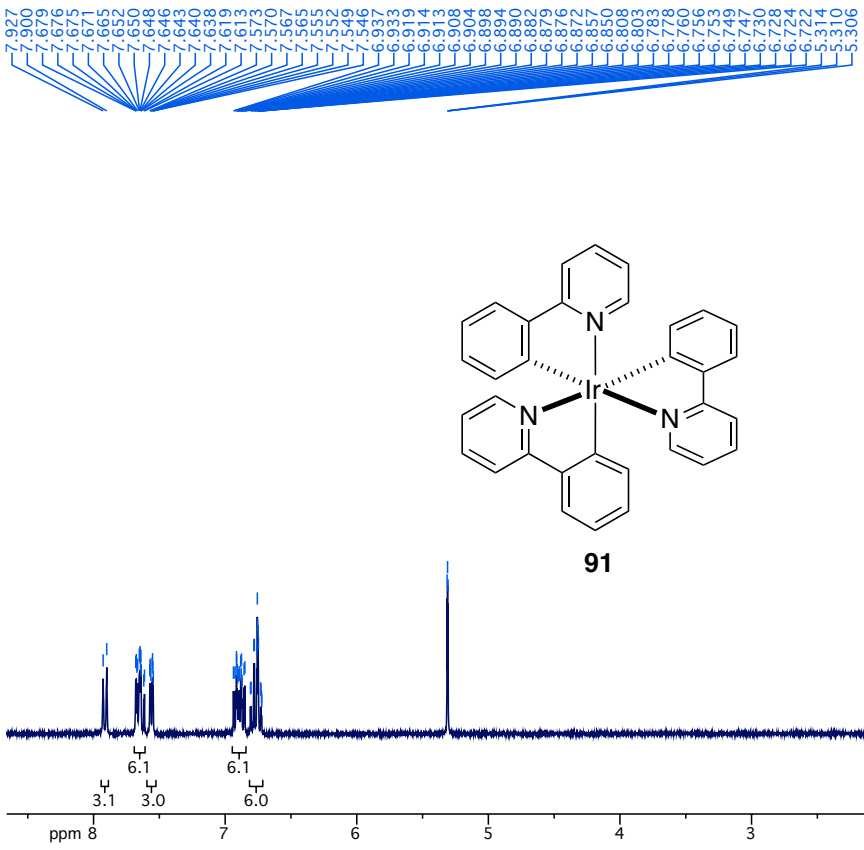

^{1}H-NMR spectrum of **91** (300 MHz, CD_2Cl_2)

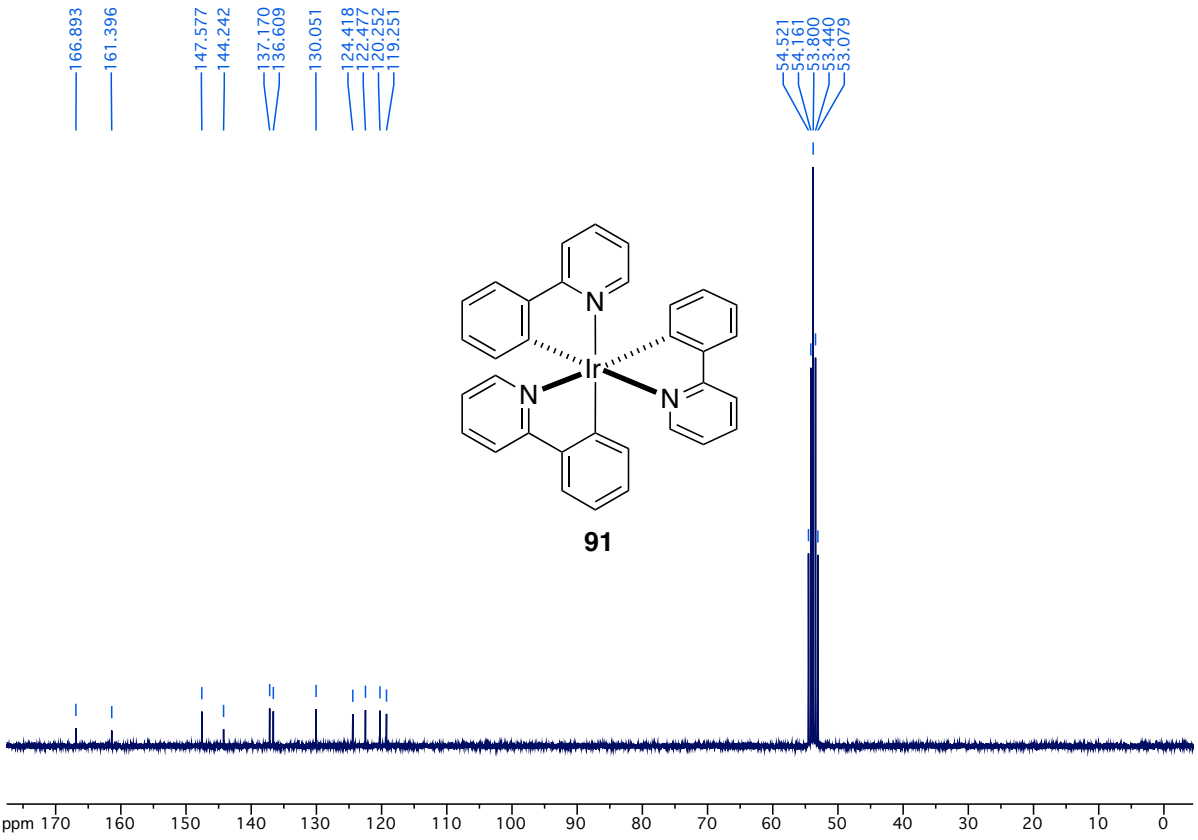

^{13}C-NMR spectrum of **91** (75.5 MHz, CD_2Cl_2)

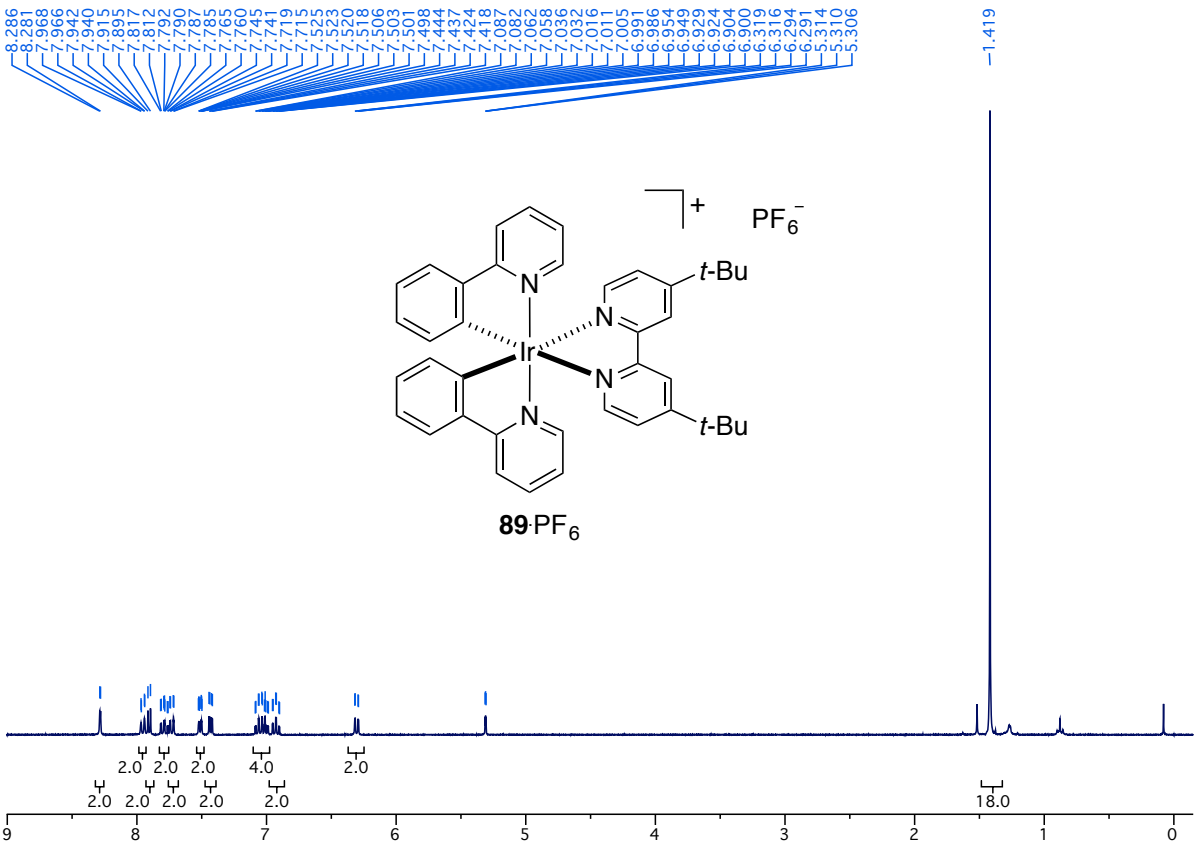

^{1}H-NMR spectrum of **89**·PF_6 (300 MHz, CD_2Cl_2)

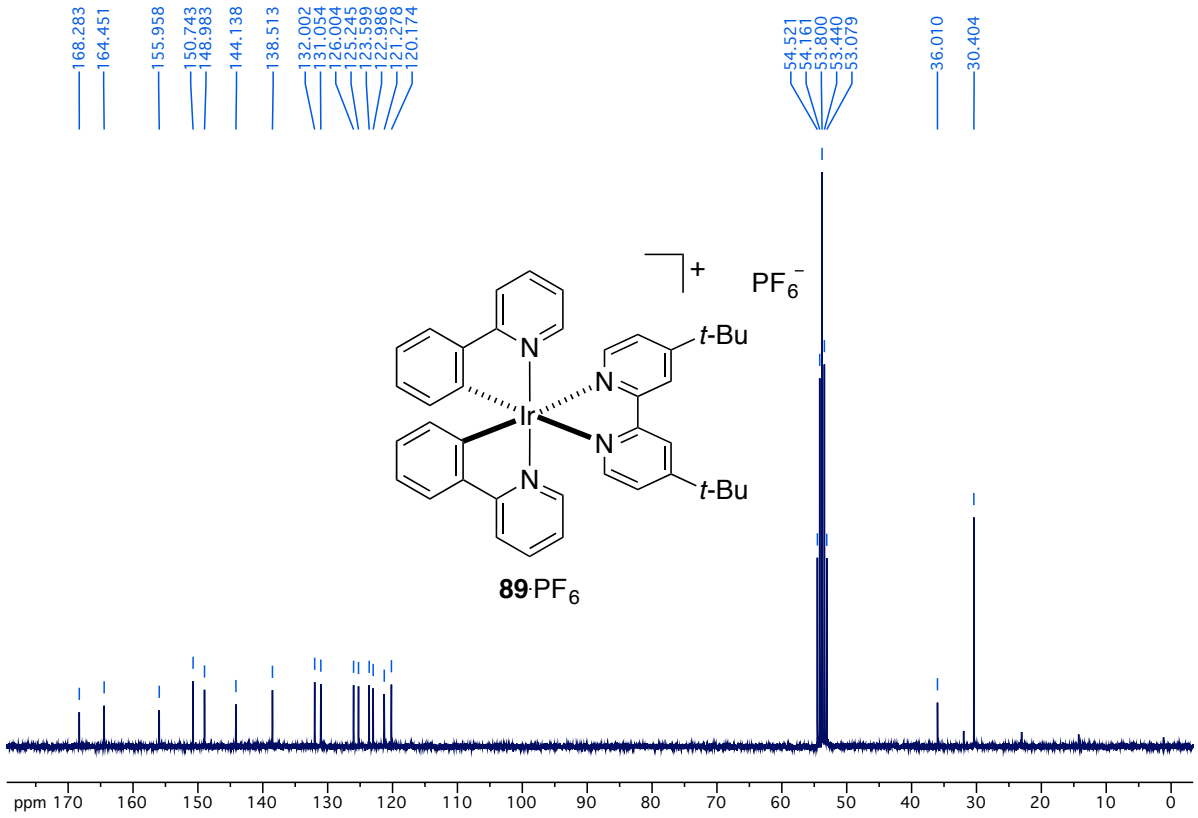

^{13}C-NMR spectrum of **89**·PF_6 (75.5 MHz, CD_2Cl_2)

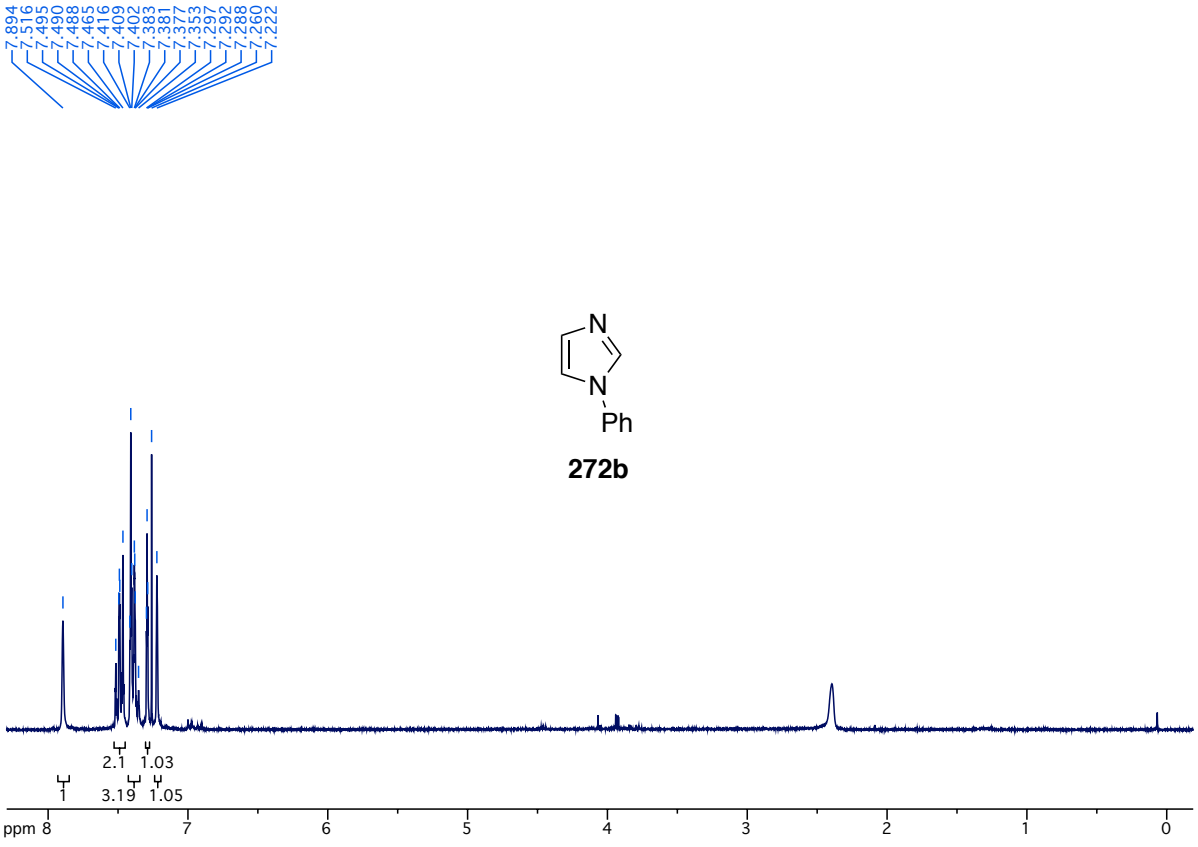

^{1}H-NMR spectrum of compound **272b** (300 MHz, $CDCl_3$)

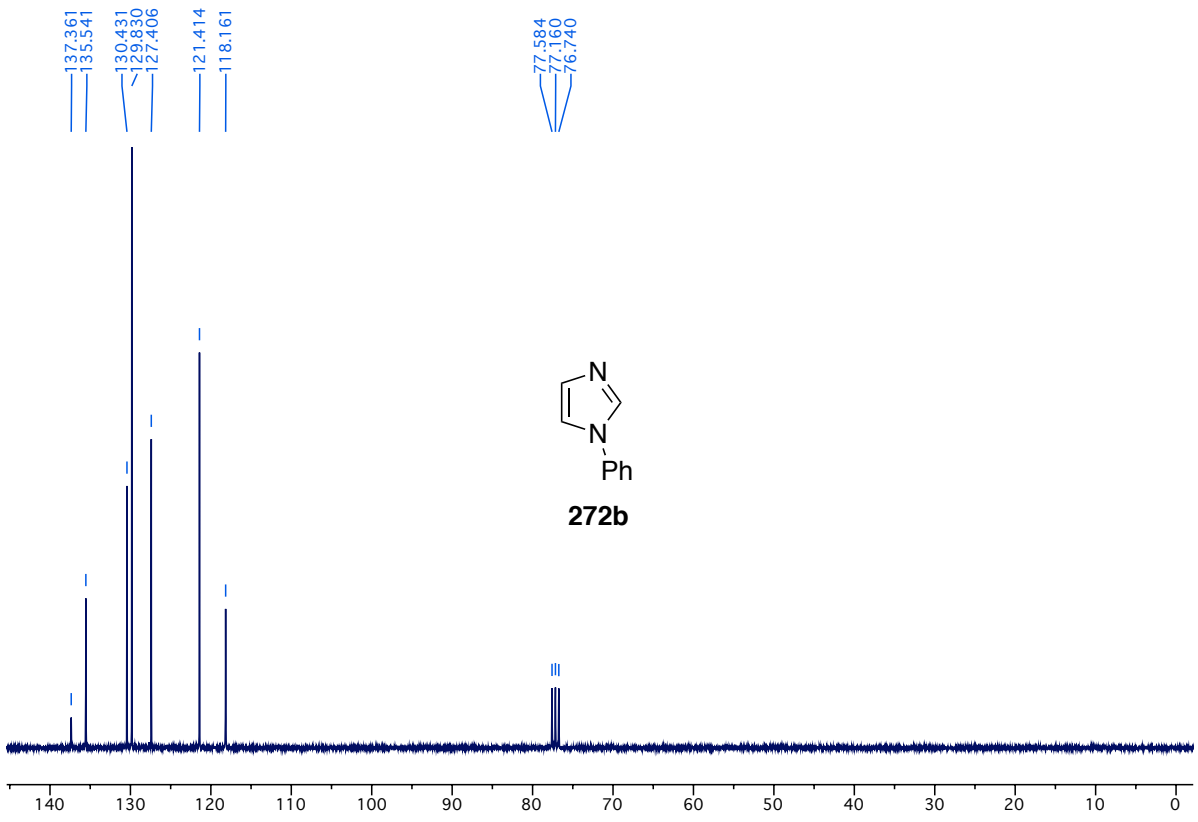

^{13}C-NMR spectrum of compound **272b** (75.5 MHz, $CDCl_3$)

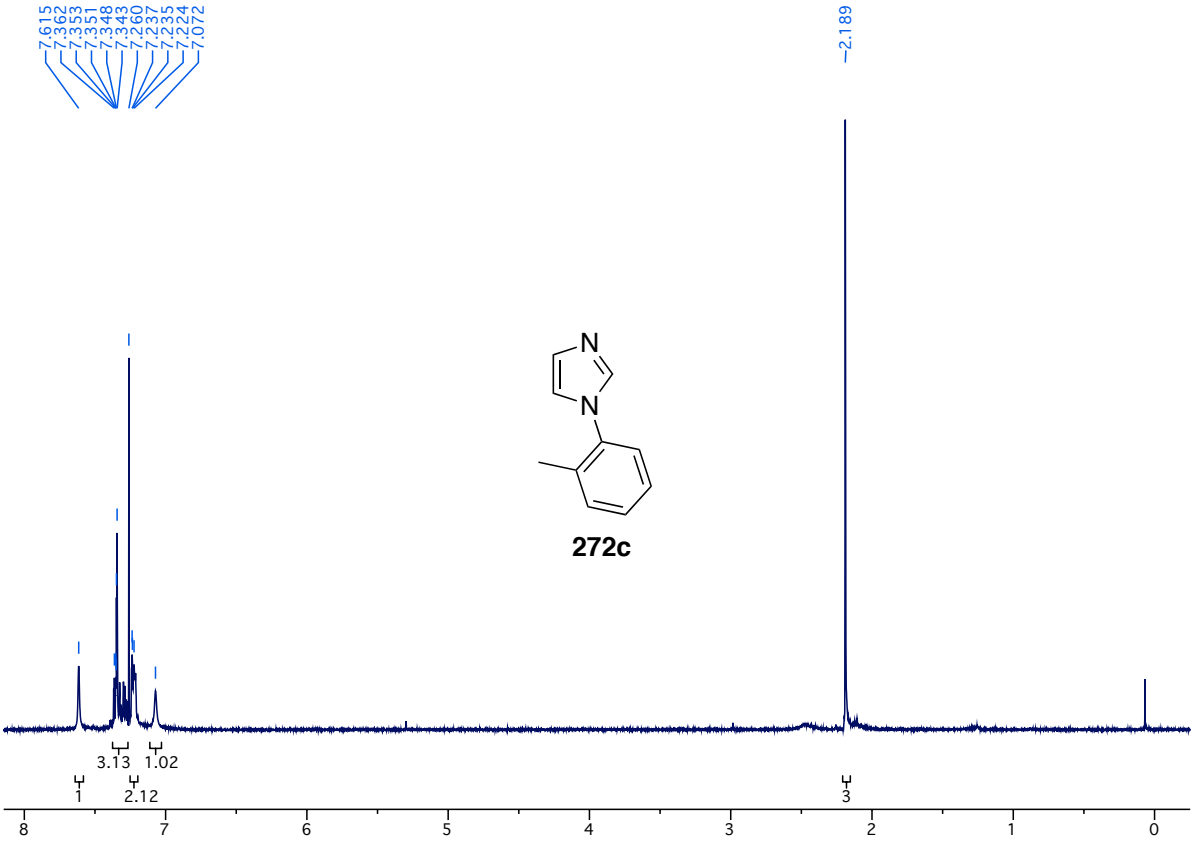

^{1}H-NMR spectrum of compound **272c** (300 MHz, $CDCl_3$)

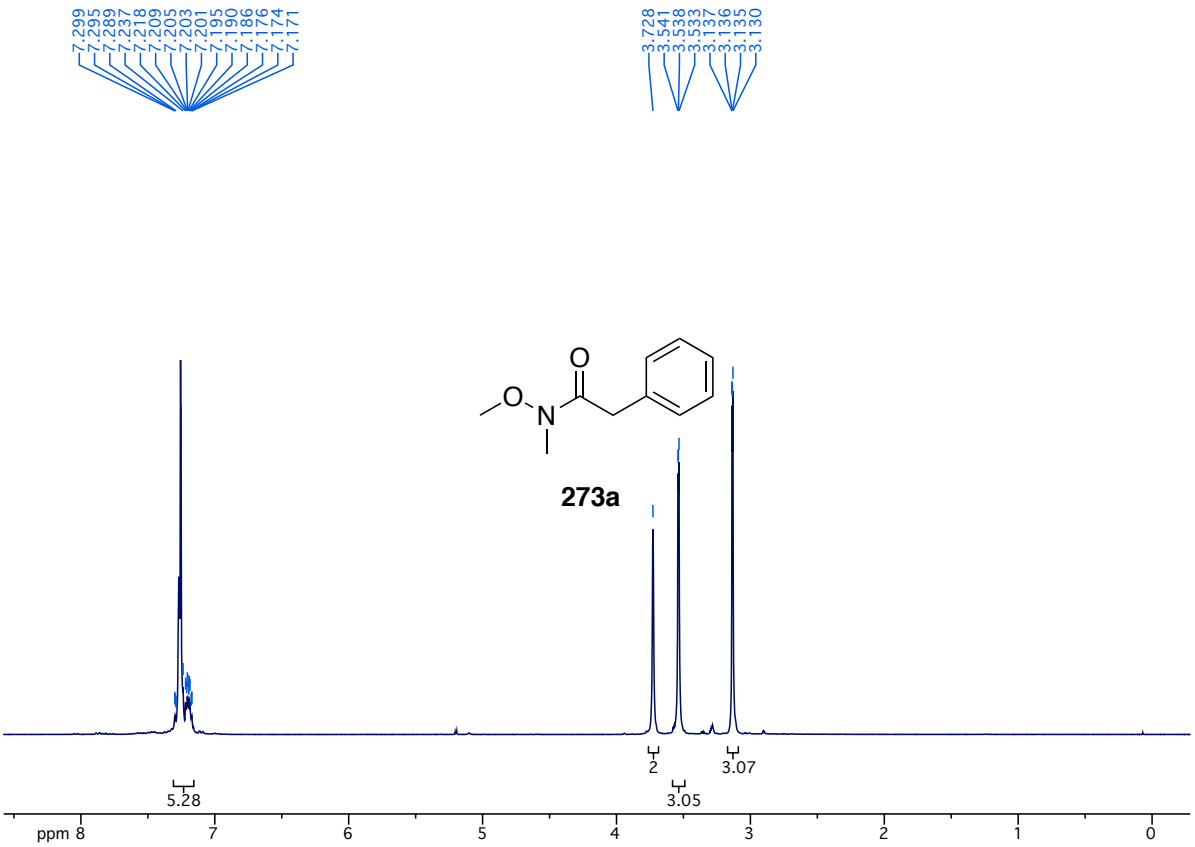

^{1}H-NMR spectrum of compound **273a** (300 MHz, $CDCl_3$)

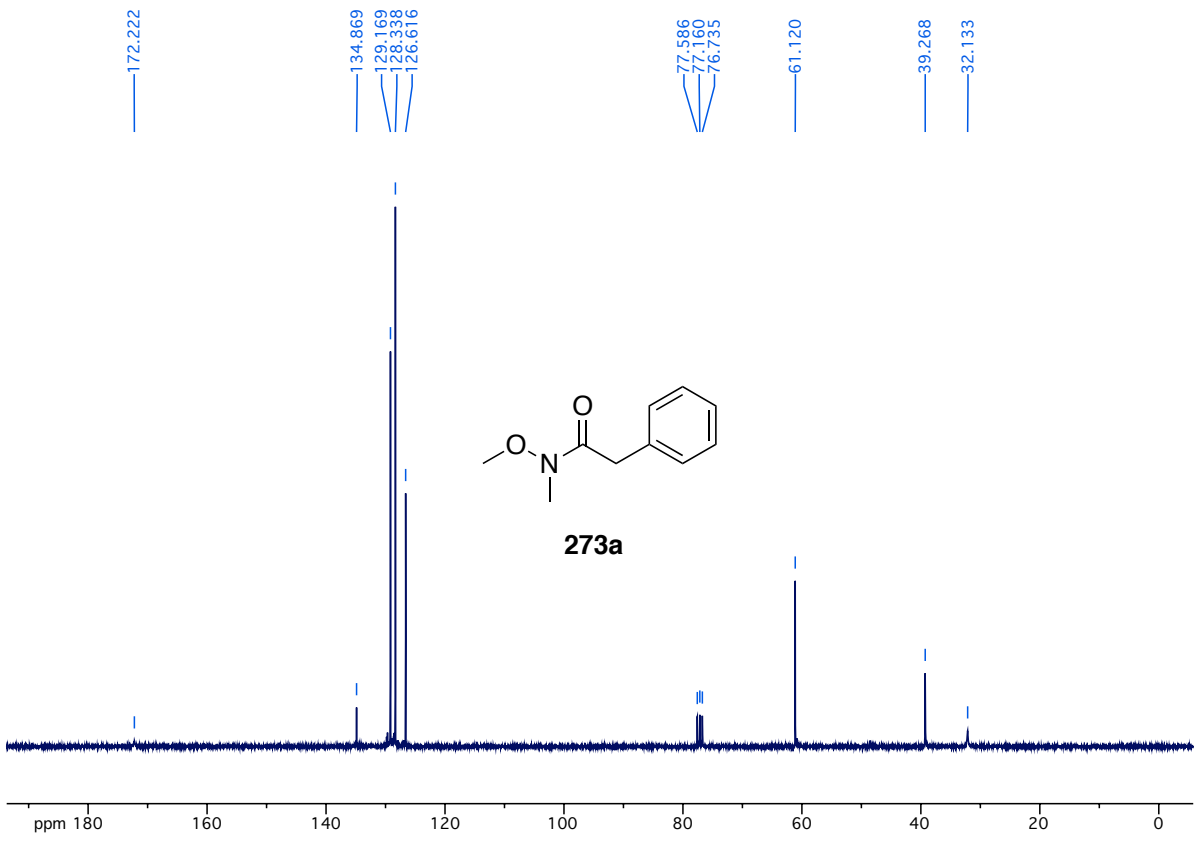

^{13}C-NMR spectrum of compound **273a** (75.5 MHz, $CDCl_3$)

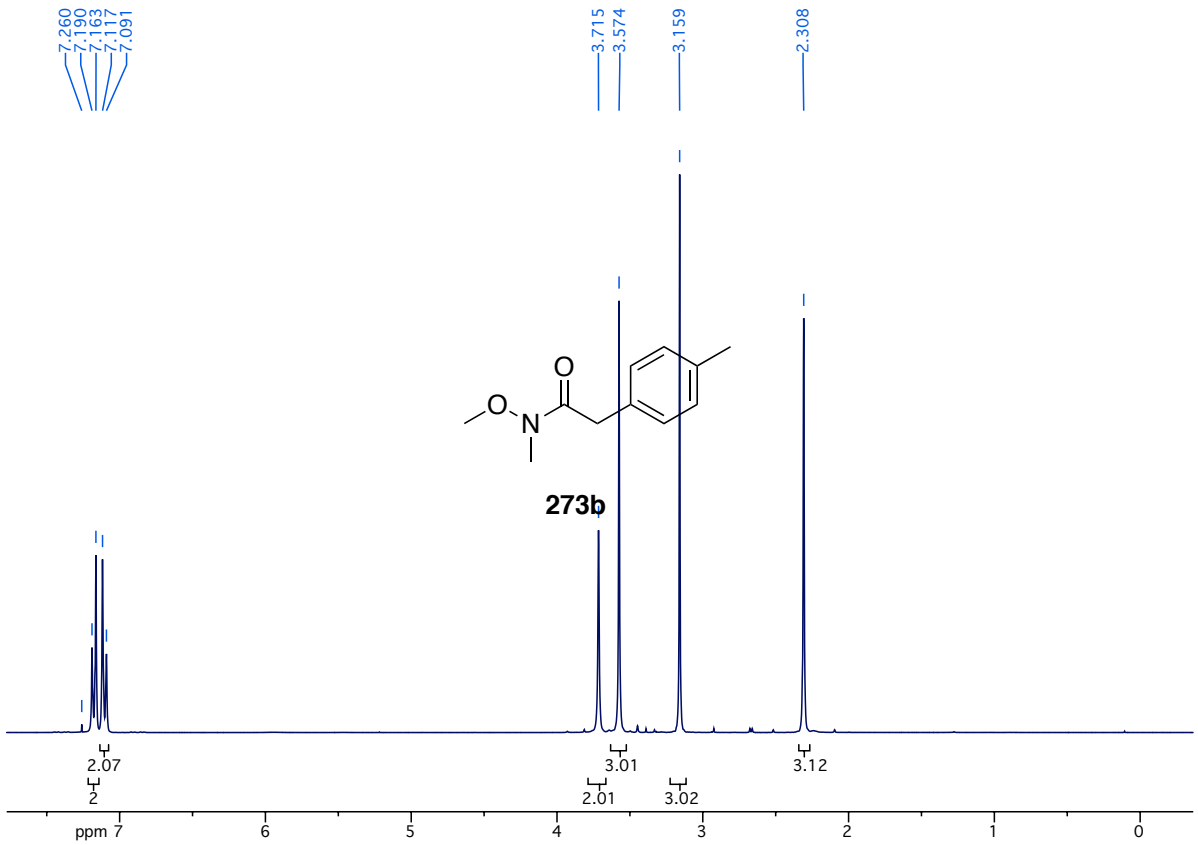

^{1}H-NMR spectrum of compound **273b** (300 MHz, $CDCl_3$)

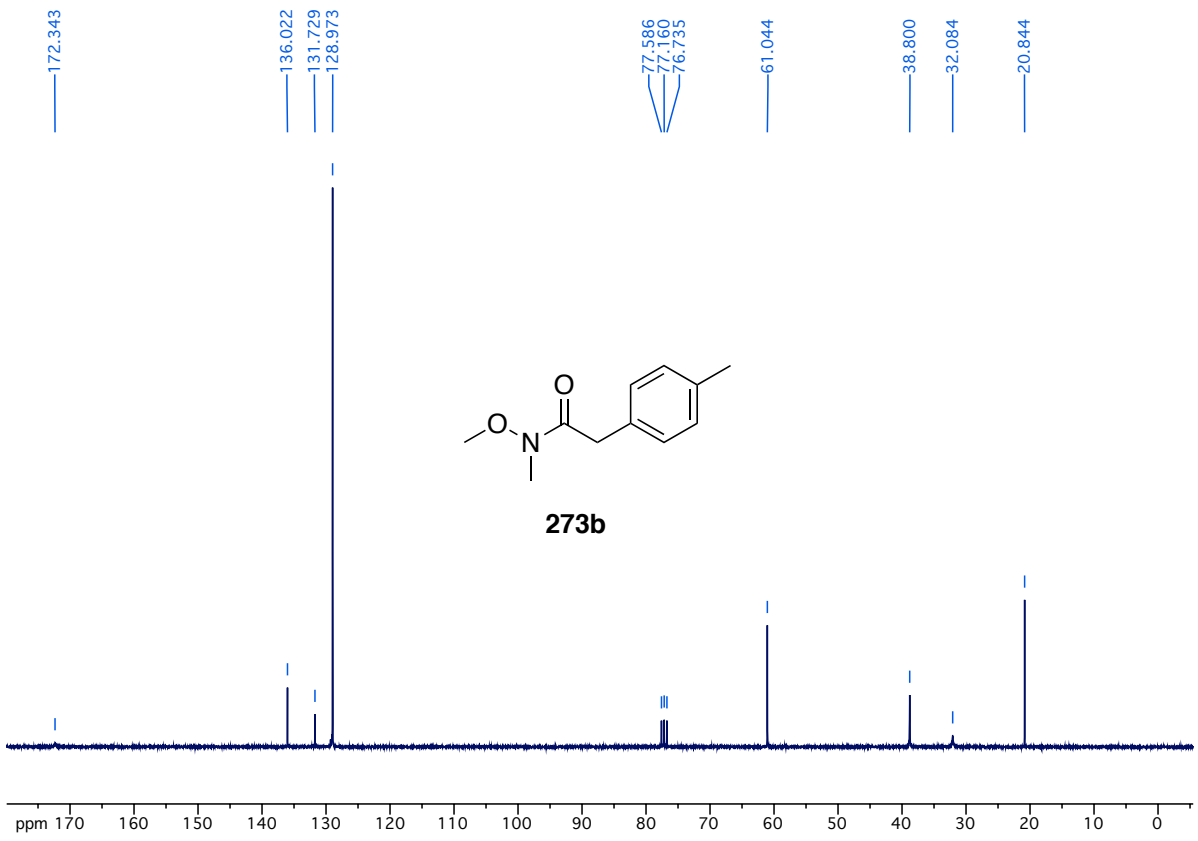

^{13}C-NMR spectrum of compound **273b** (75.5 MHz, $CDCl_3$)

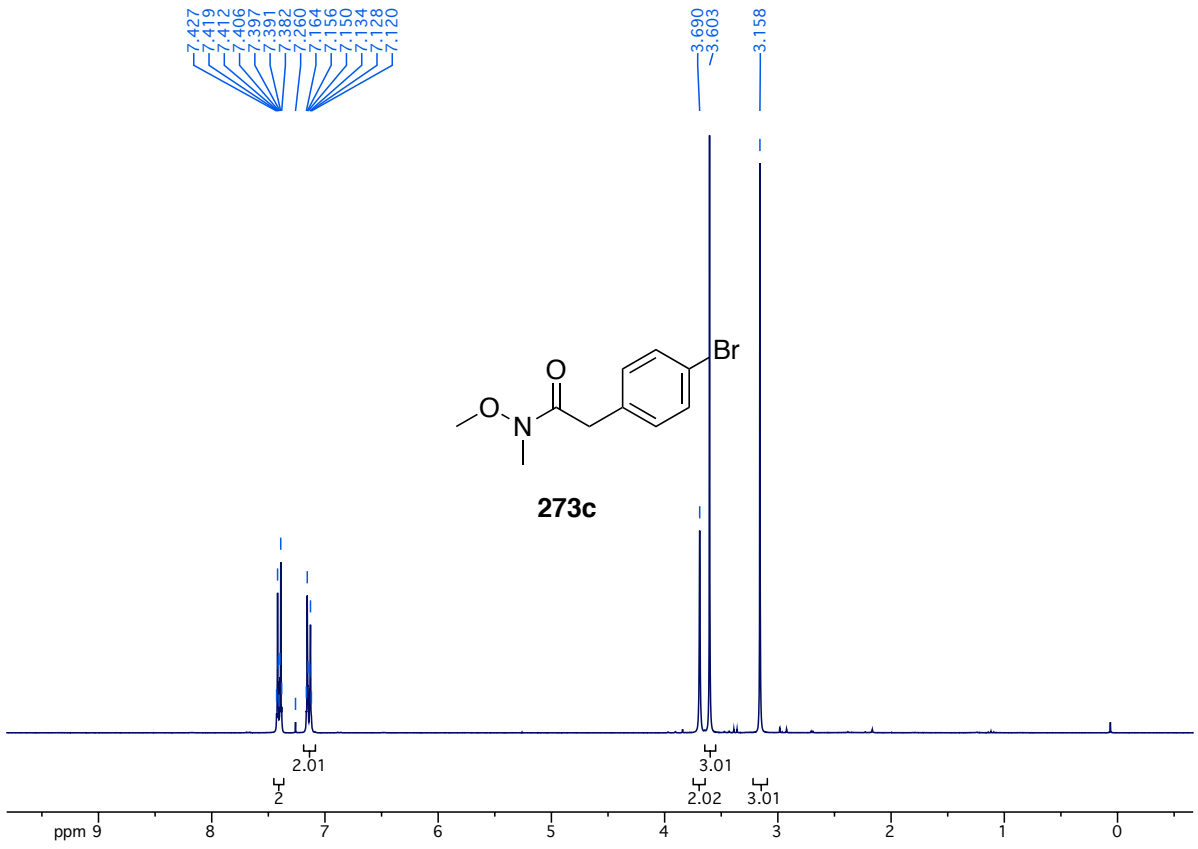

^{1}H-NMR spectrum of compound **273c** (300 MHz, $CDCl_3$)

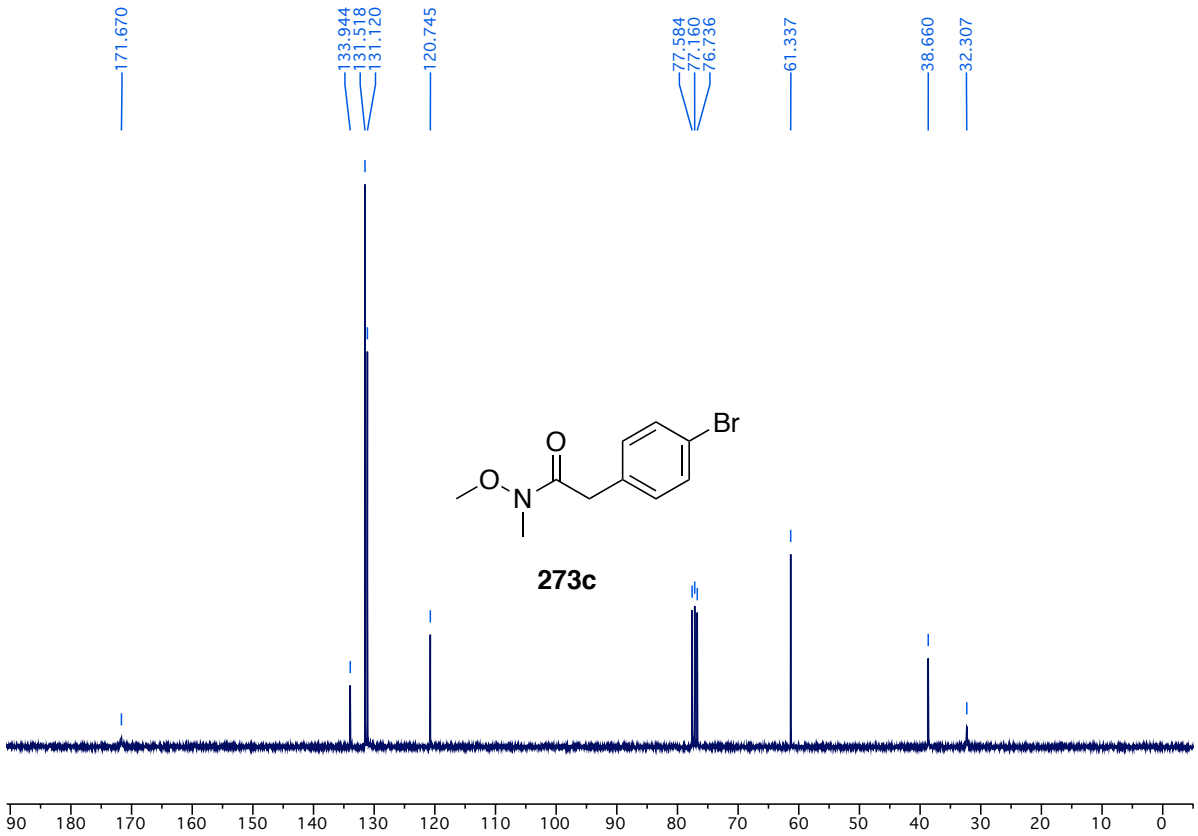

^{13}C-NMR spectrum of compound **273c** (75.5 MHz, $CDCl_3$)

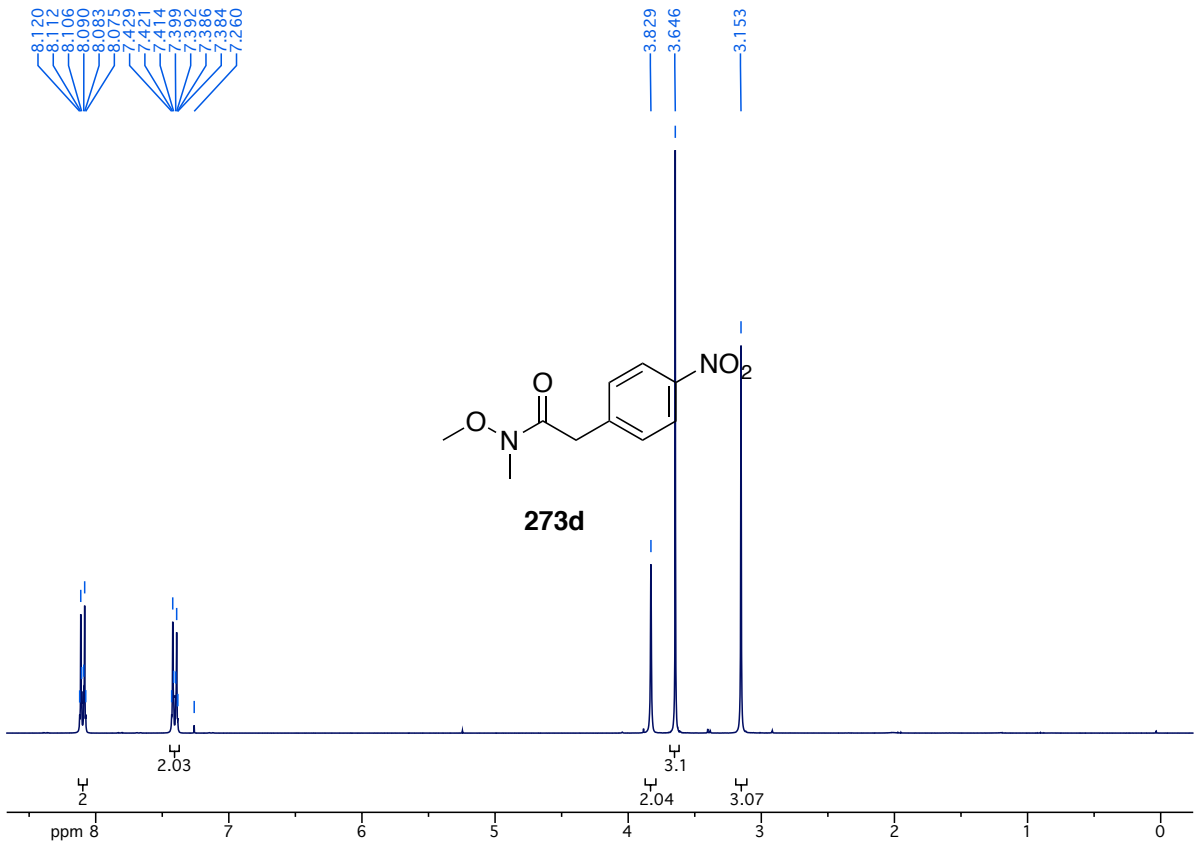

^{1}H-NMR spectrum of compound **273d** (300 MHz, $CDCl_3$)

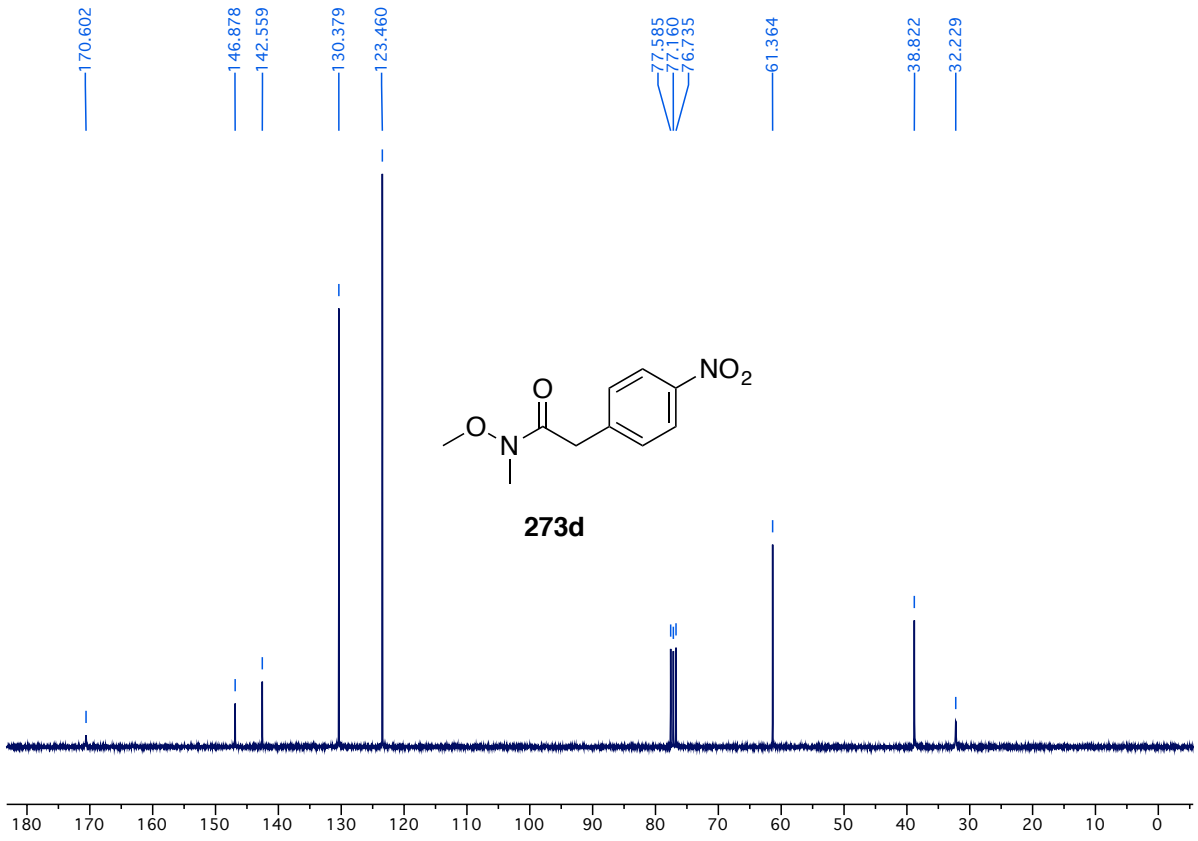

^{13}C-NMR spectrum of compound **273d** (75.5 MHz, $CDCl_3$)

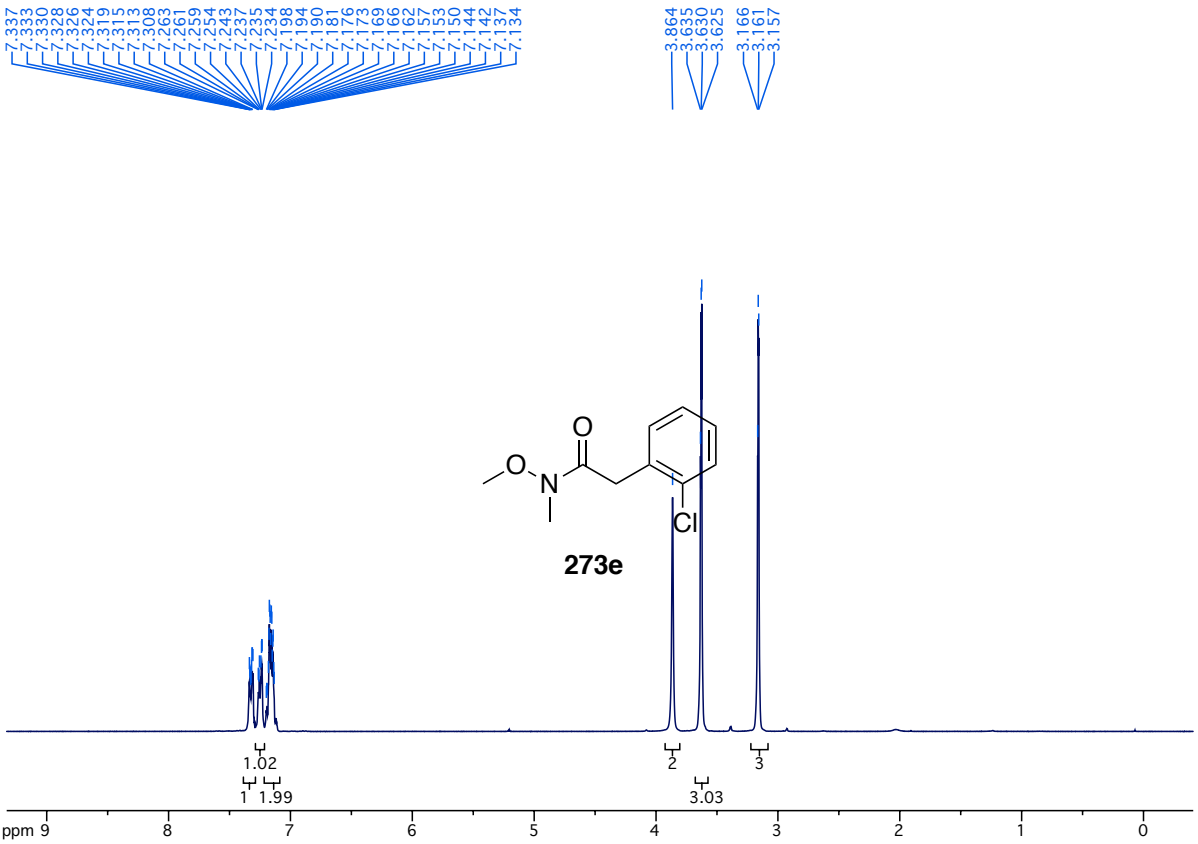

^{1}H-NMR spectrum of compound **273e** (300 MHz, $CDCl_3$)

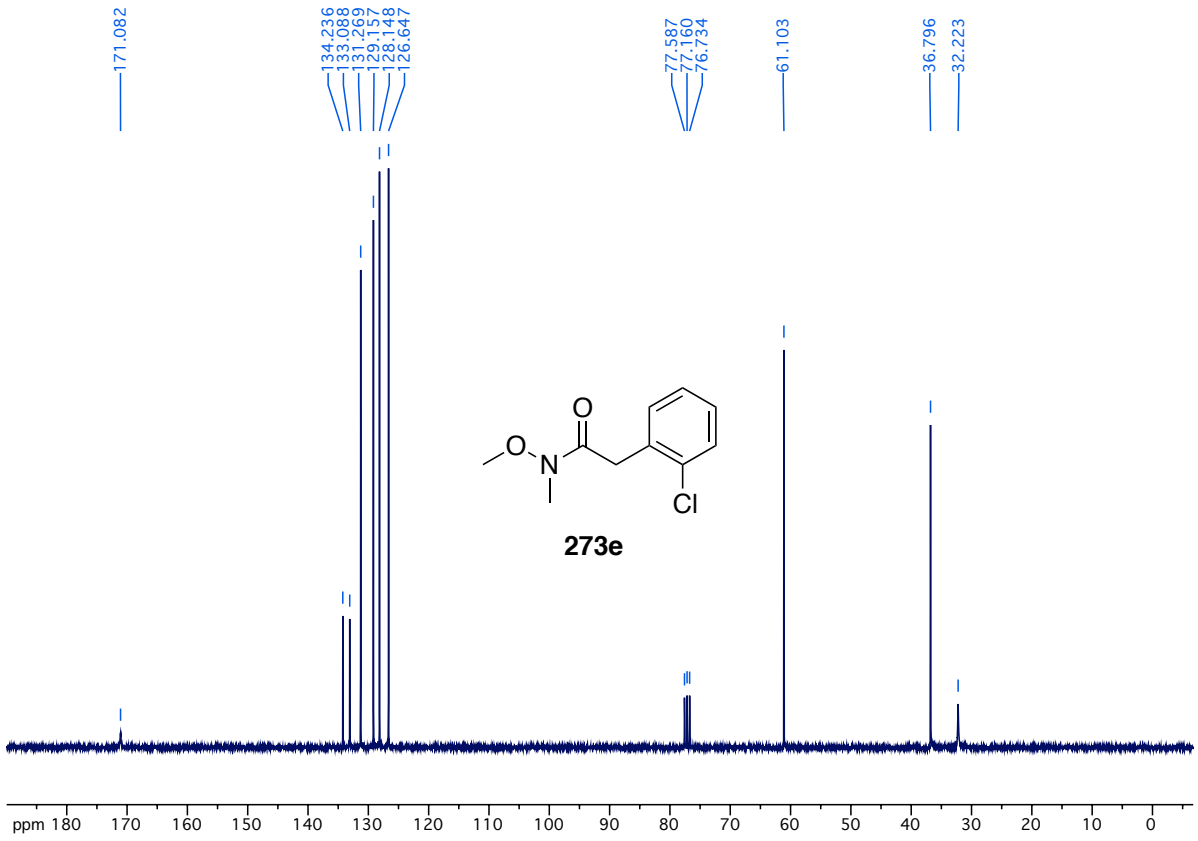

^{13}C-NMR spectrum of compound **273e** (75.5 MHz, $CDCl_3$)

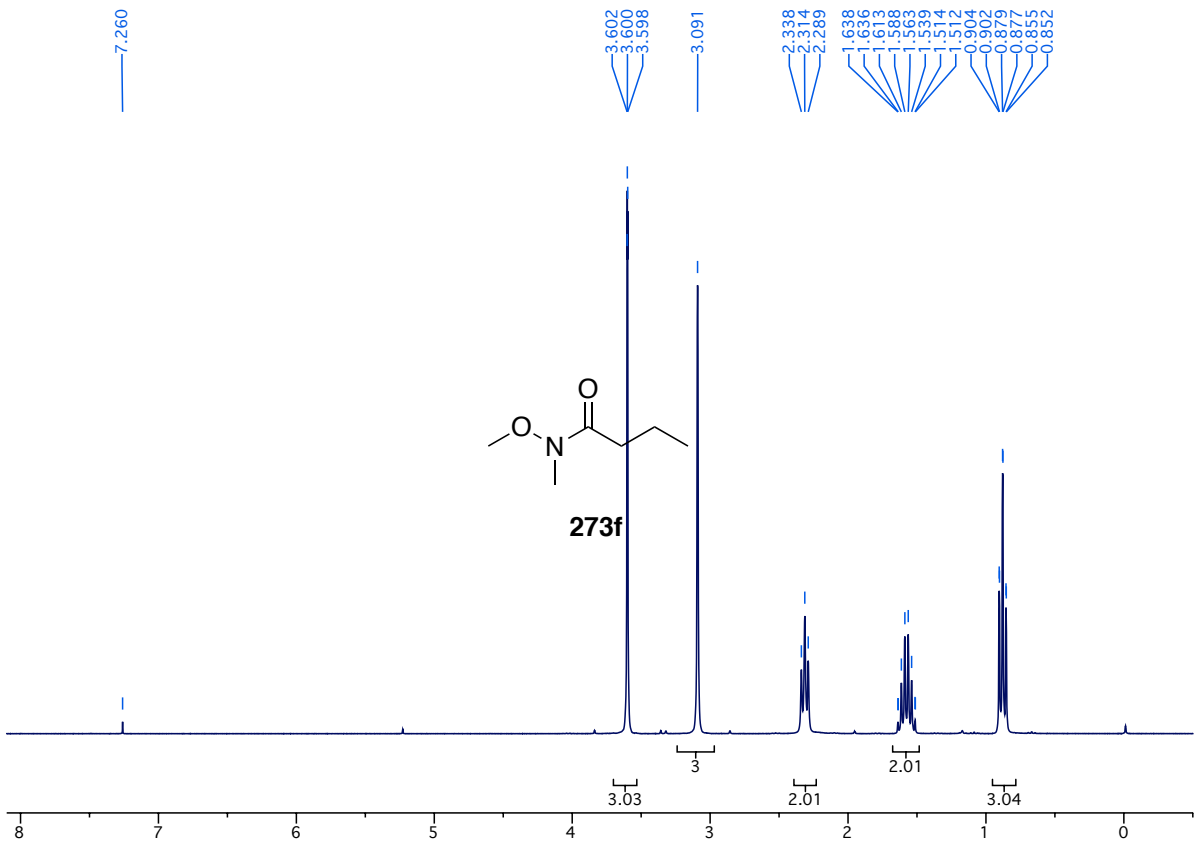

^{1}H-NMR spectrum of compound **273f** (300 MHz, $CDCl_3$)

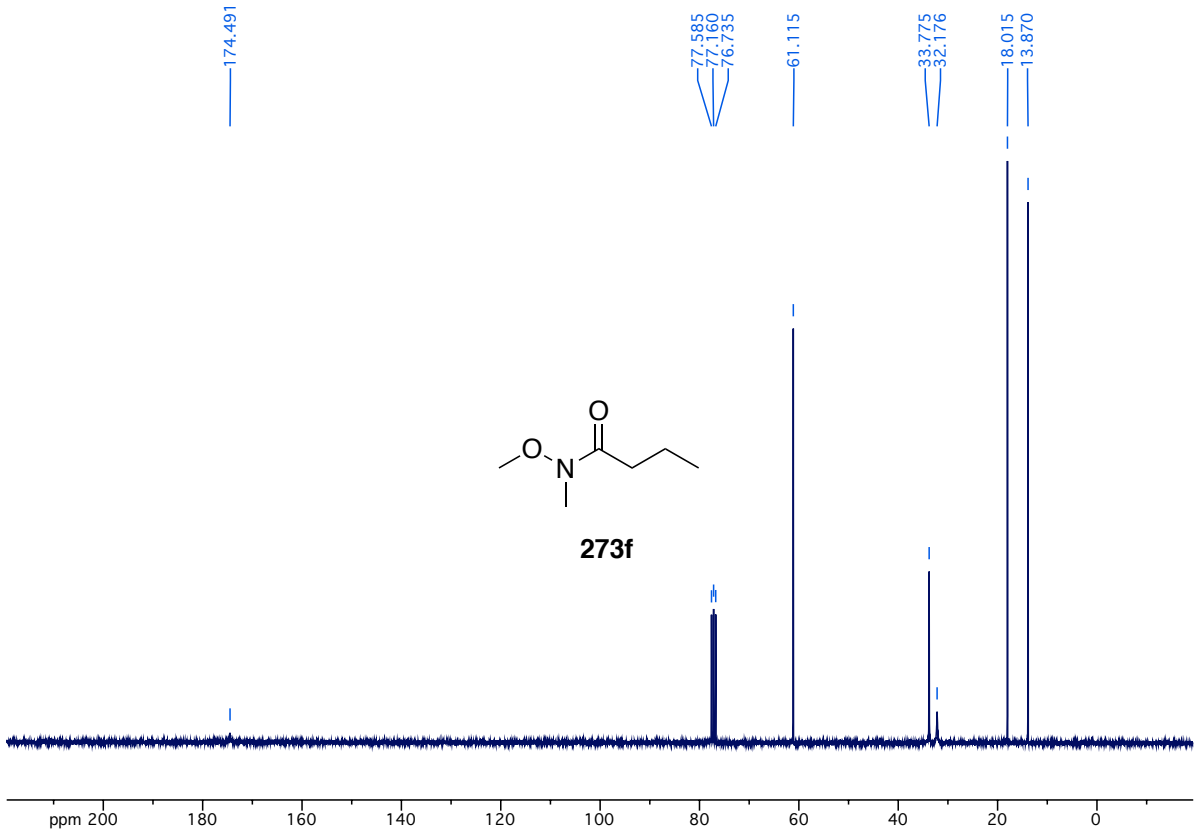

^{13}C-NMR spectrum of compound **273f** (75.5 MHz, $CDCl_3$)

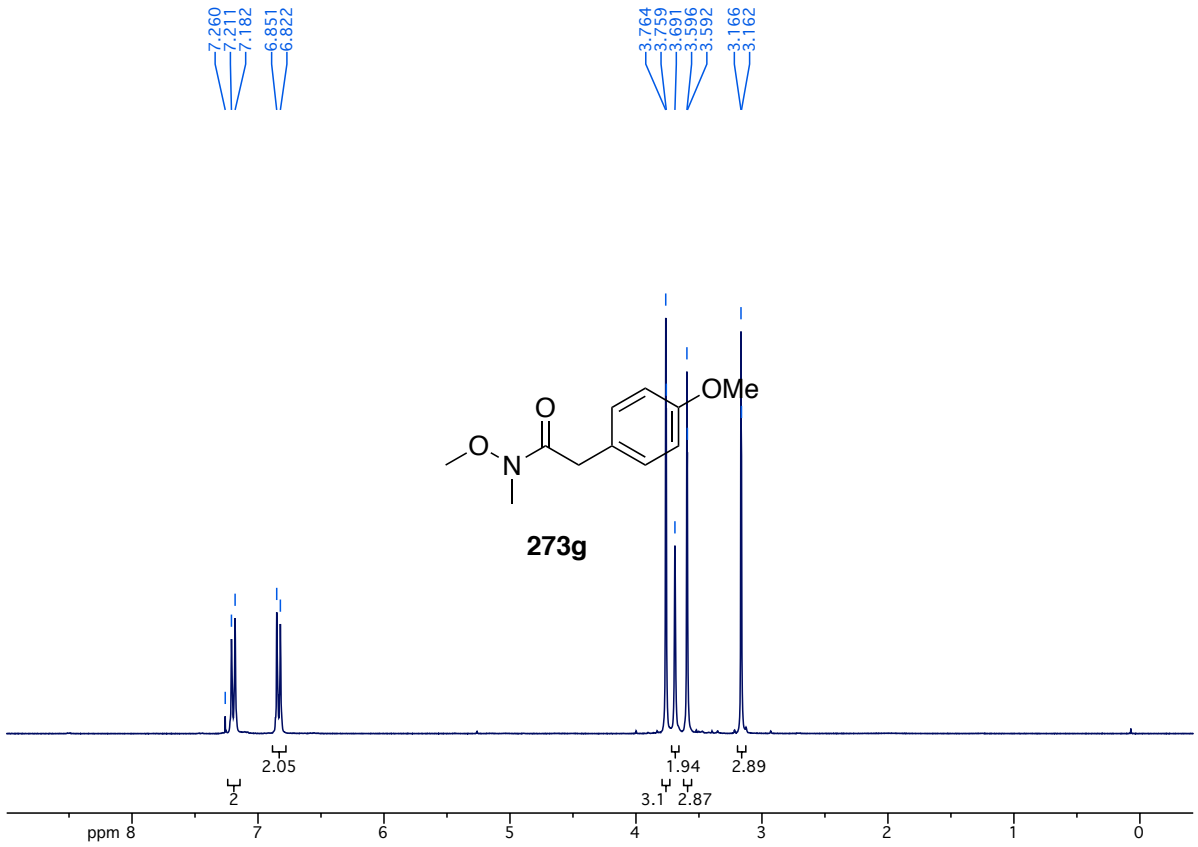

^{1}H-NMR spectrum of compound **273g** (300 MHz, $CDCl_3$)

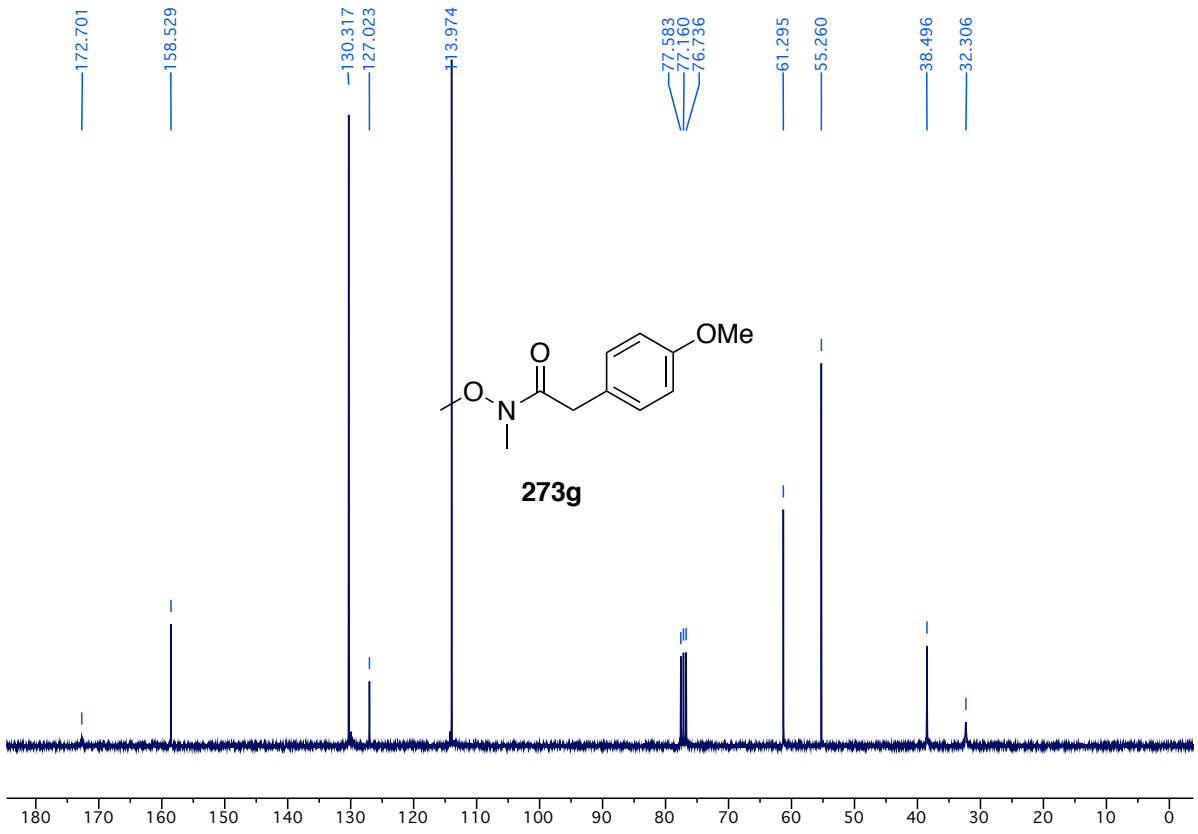

^{13}C-NMR spectrum of compound **273g** (75.5 MHz, $CDCl_3$)

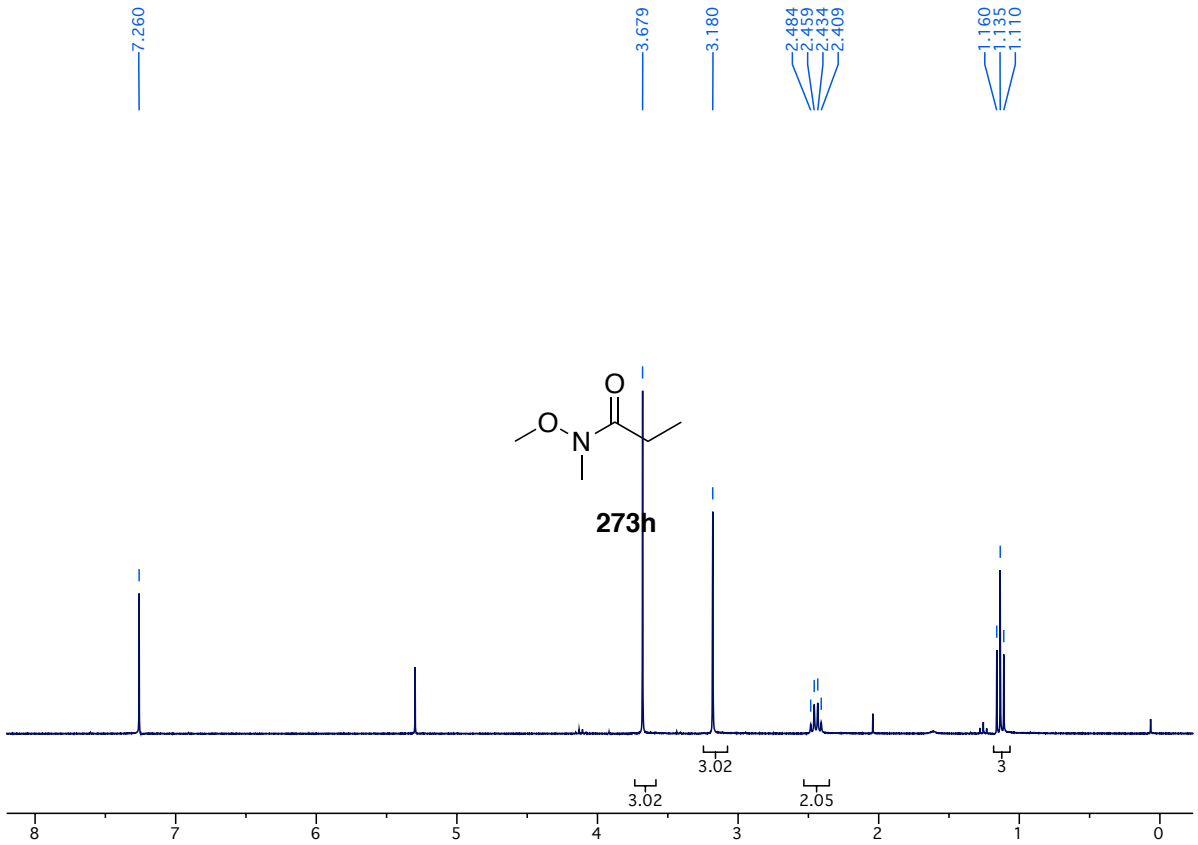

^{1}H-NMR spectrum of compound **273h** (300 MHz, $CDCl_3$)

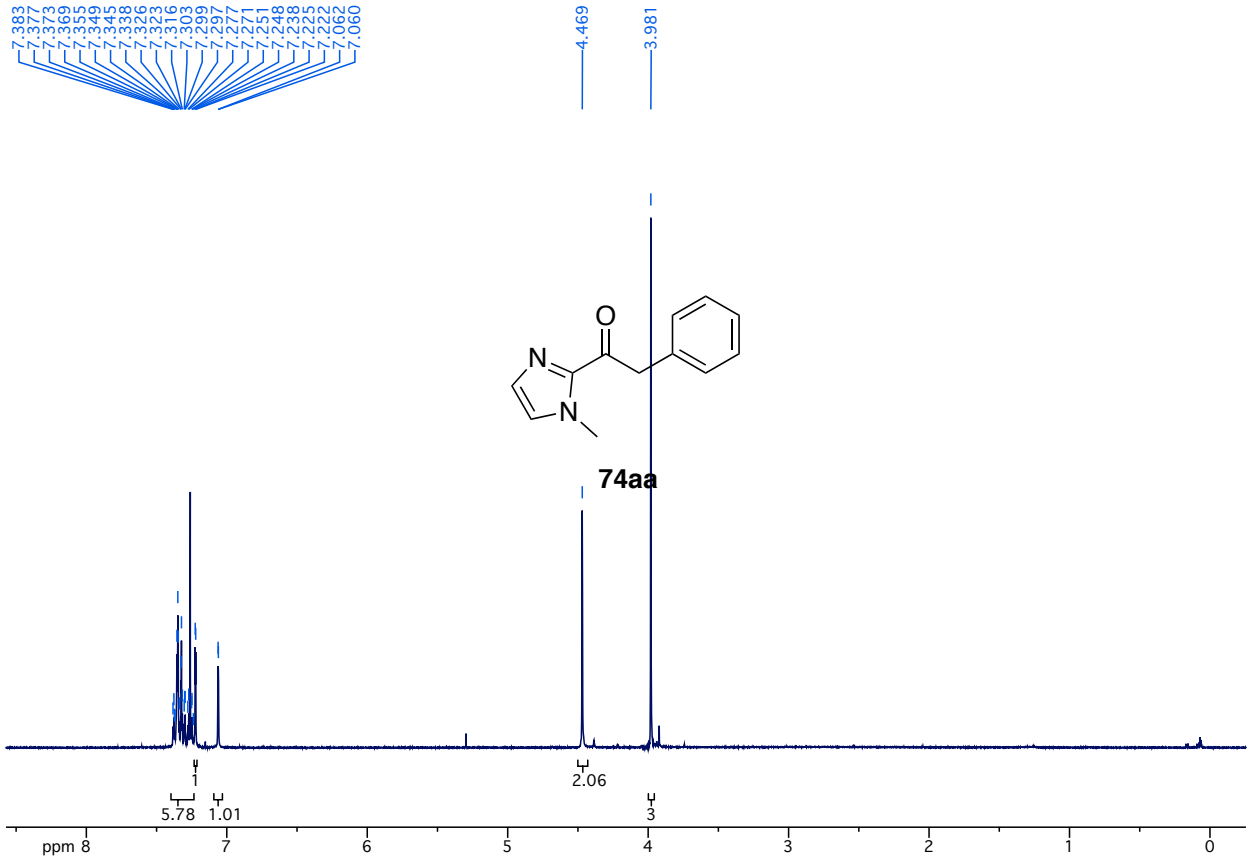

^{1}H-NMR spectrum compound **74aa** (300 MHz, $CDCl_3$)

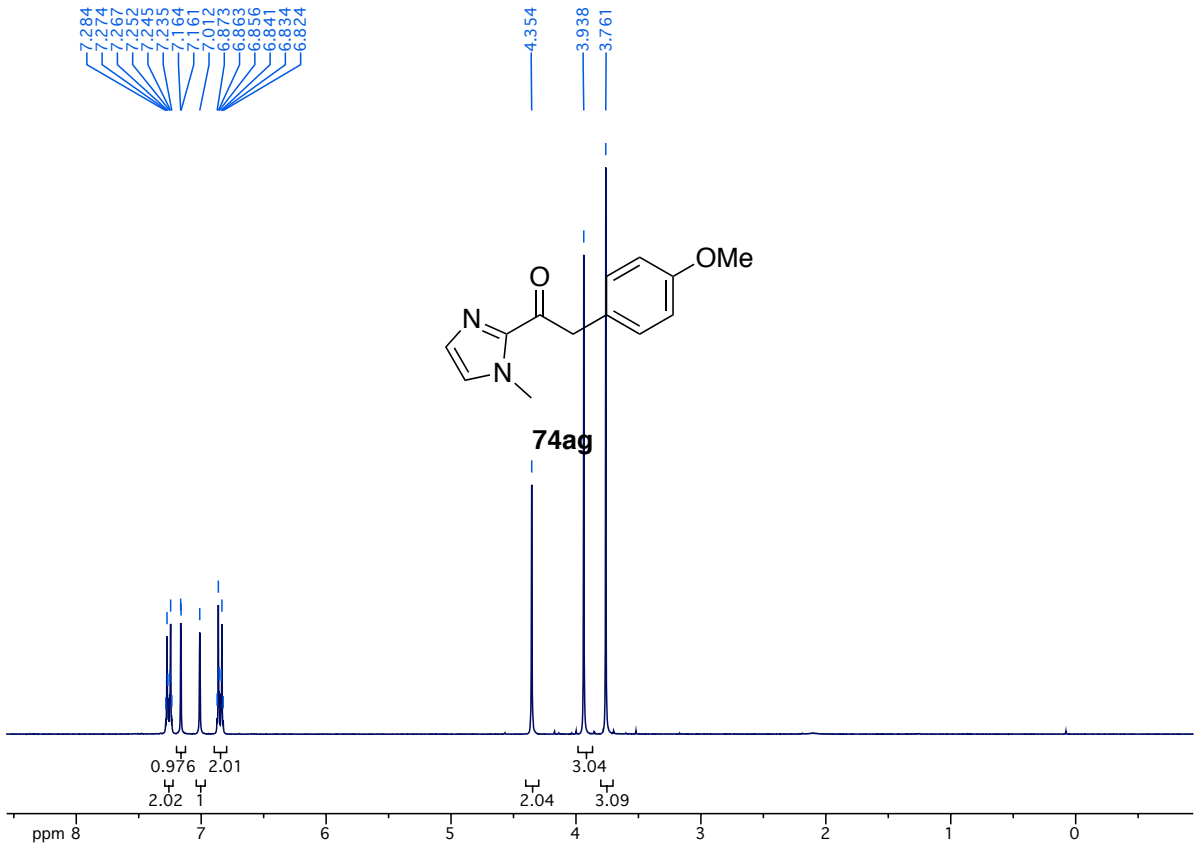

^{1}H-NMR spectrum of compound **74ag** (300 MHz, $CDCl_3$)

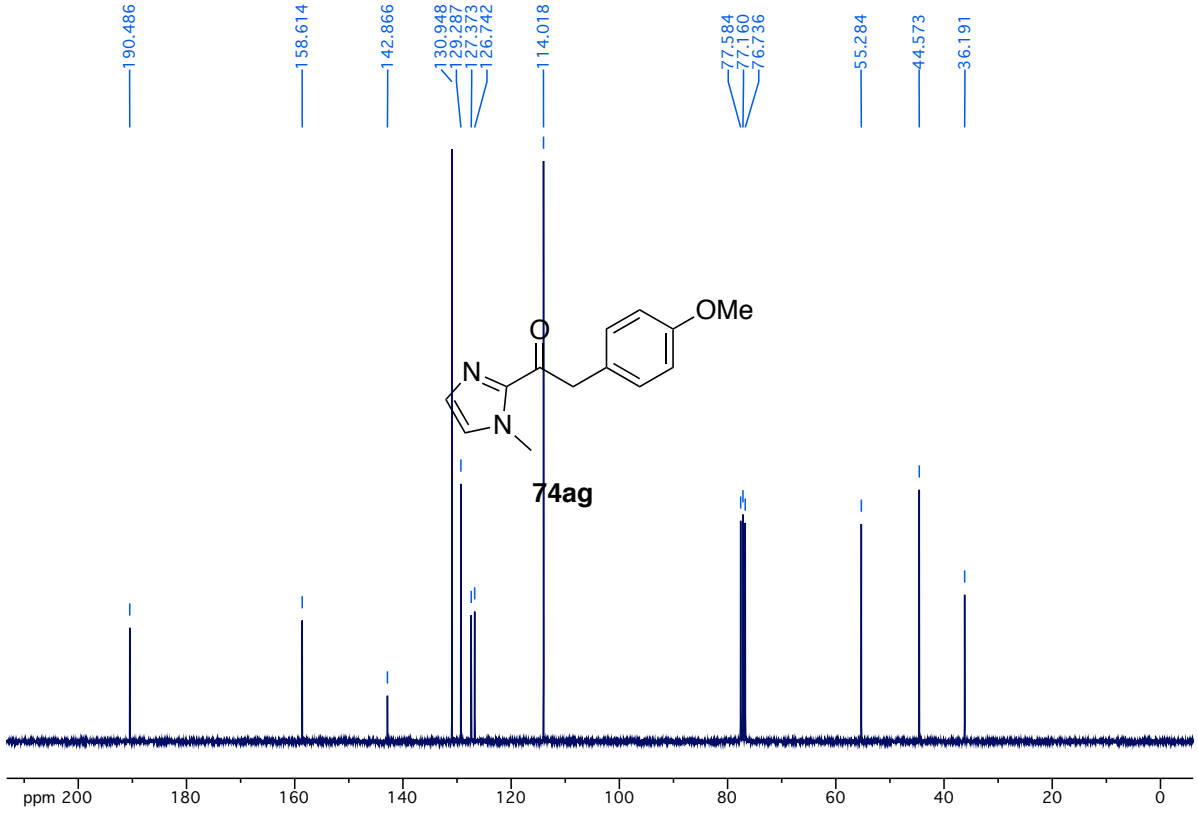

^{13}C-NMR spectrum of compound **74ag** (75.5 MHz, $CDCl_3$)

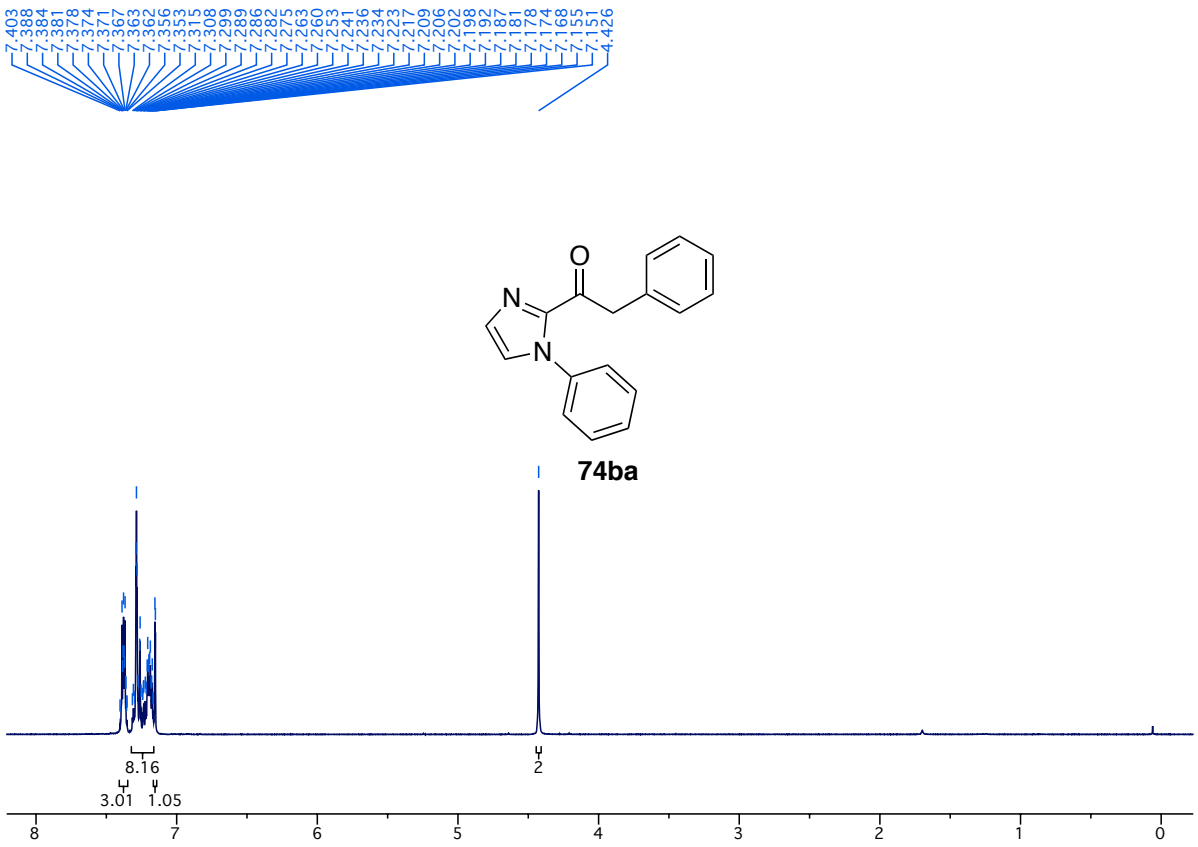

^{1}H-NMR spectrum of compound **74ba** (300 MHz, $CDCl_3$)

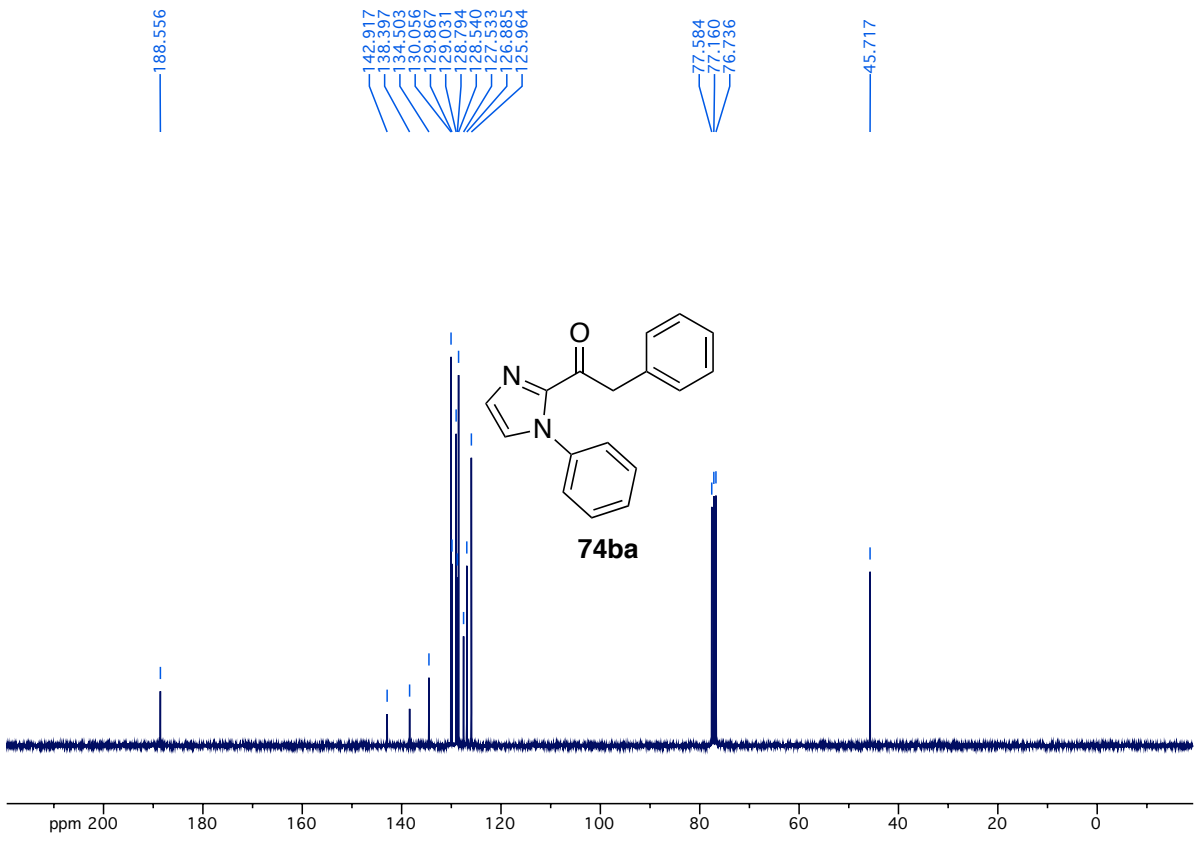

^{13}C-NMR spectrum of compound **74ba** (75.5 MHz, $CDCl_3$)

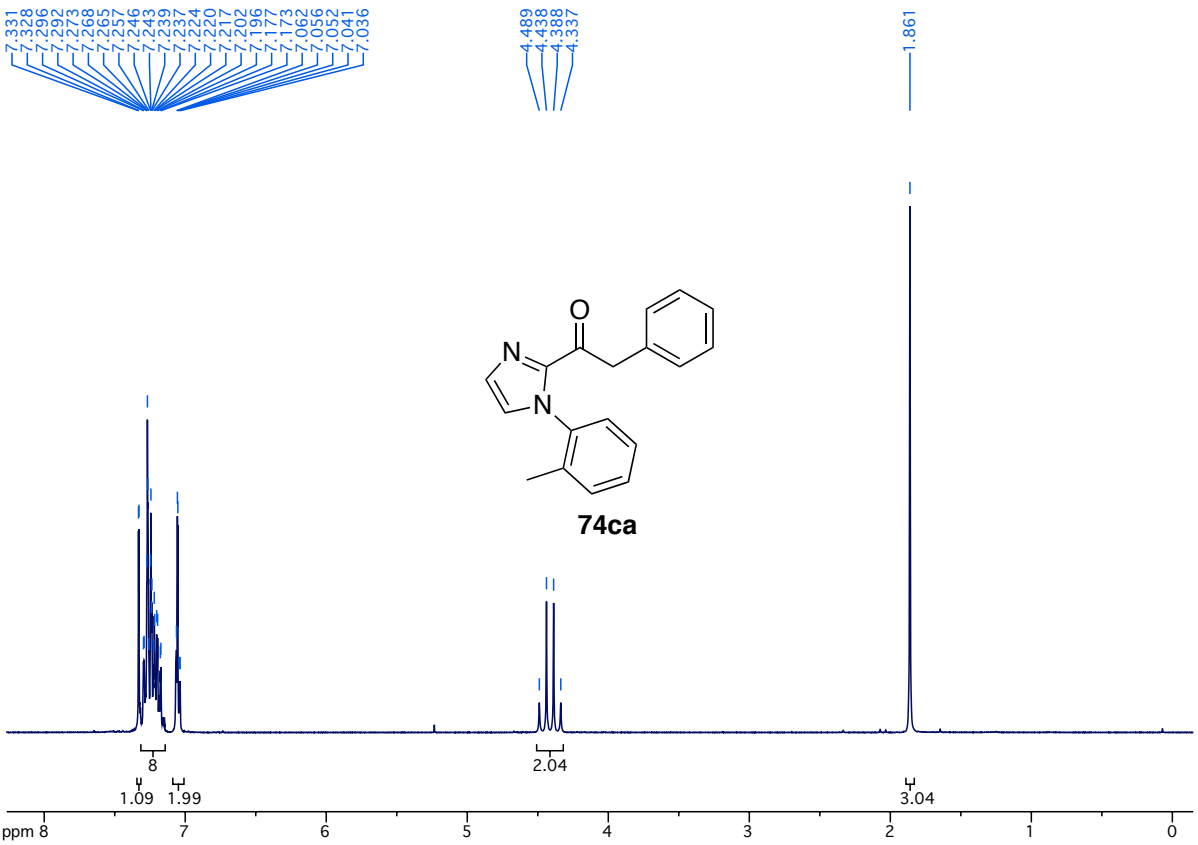

^{1}H-NMR spectrum of compound **74ca** (300 MHz, $CDCl_3$)

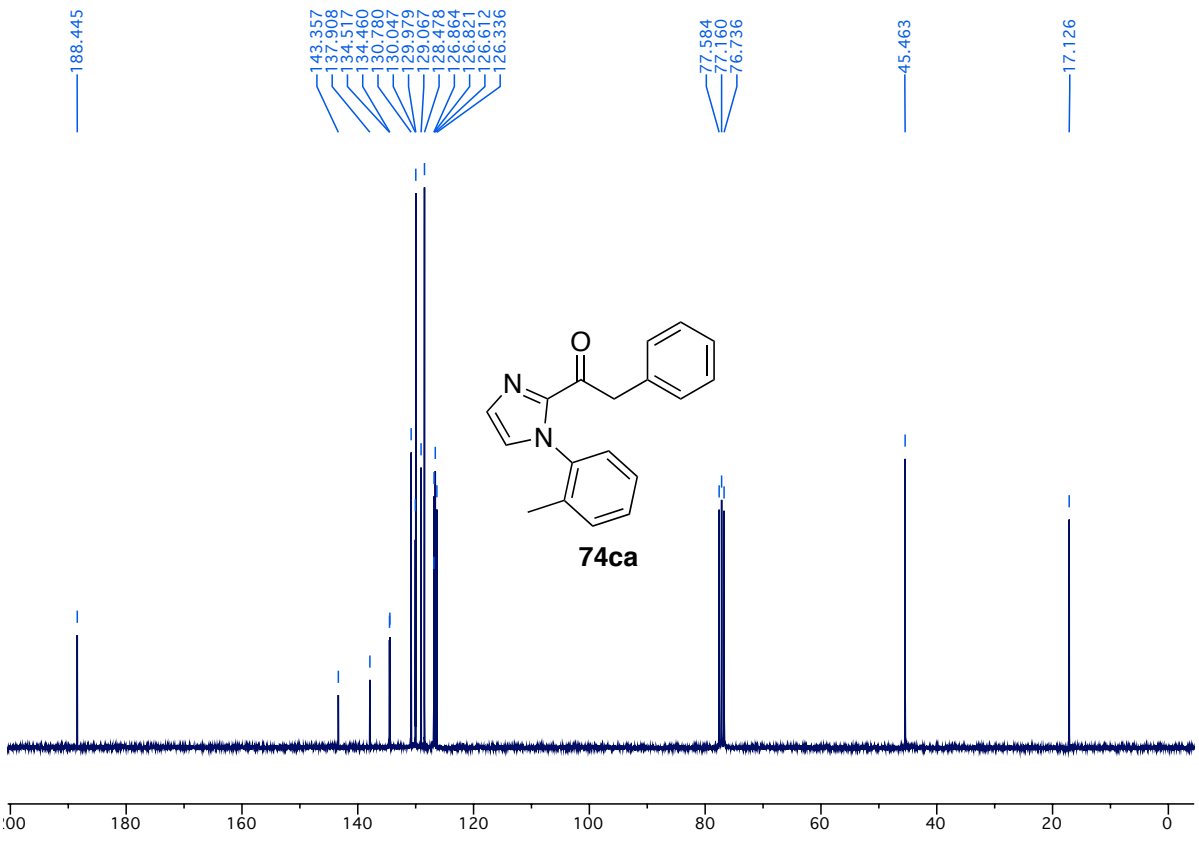

^{13}C-NMR spectrum of compound **74ca** (75.5 MHz, $CDCl_3$)

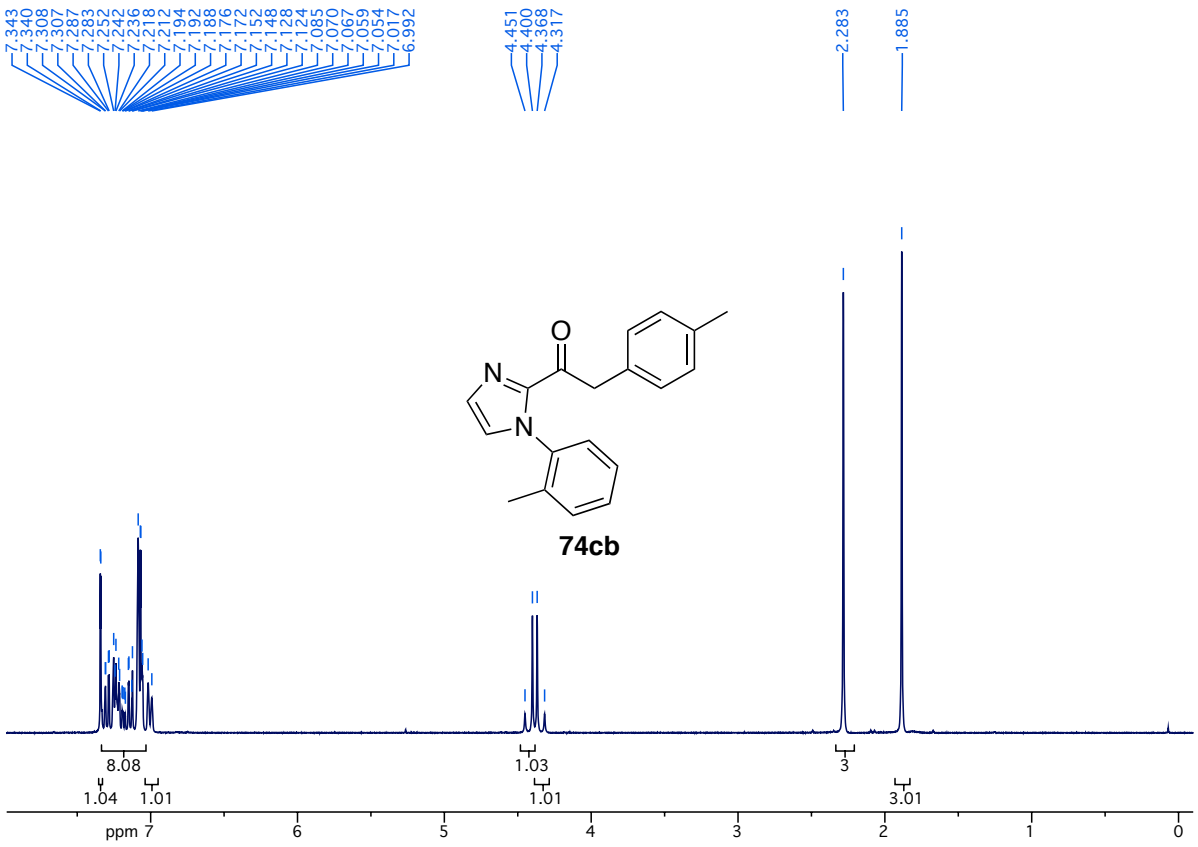

^{1}H-NMR spectrum of compound **74cb** (300 MHz, $CDCl_3$)

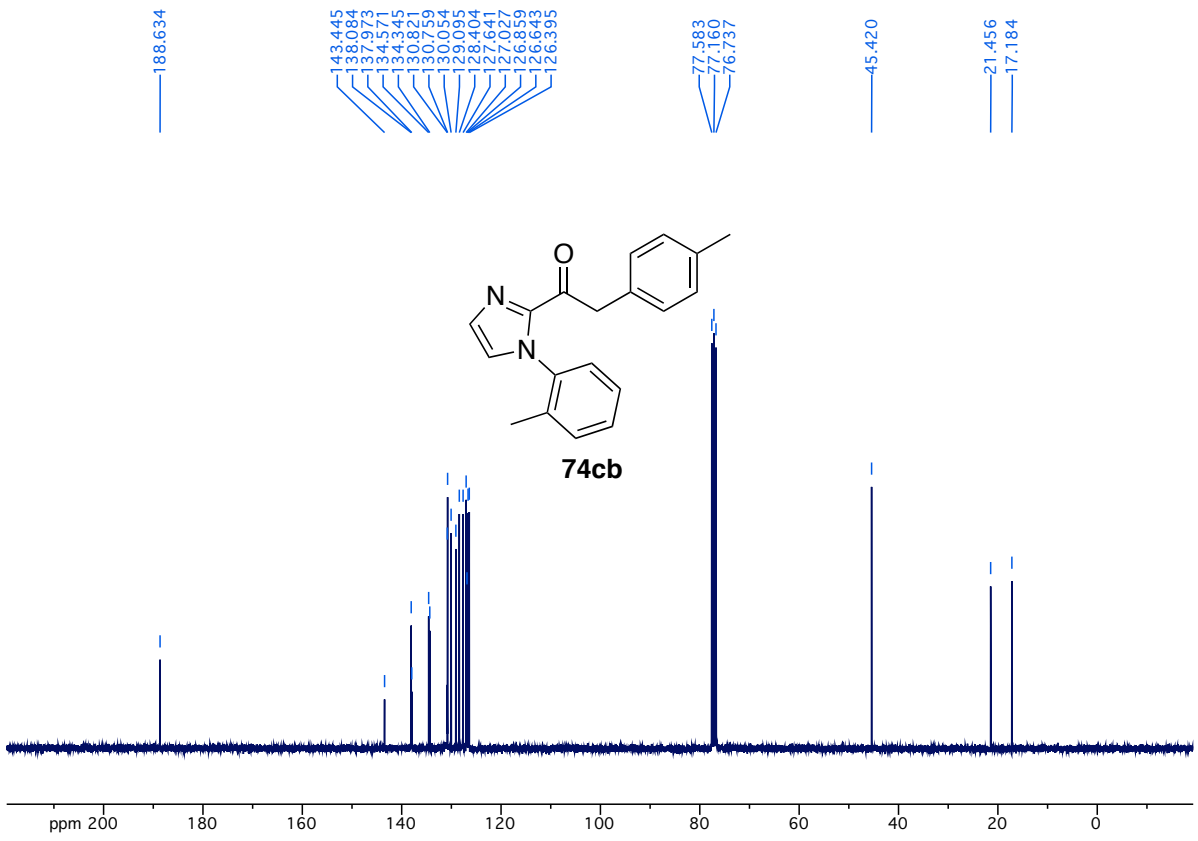

^{13}C-NMR spectrum of compound **74cb** (75.5 MHz, $CDCl_3$)

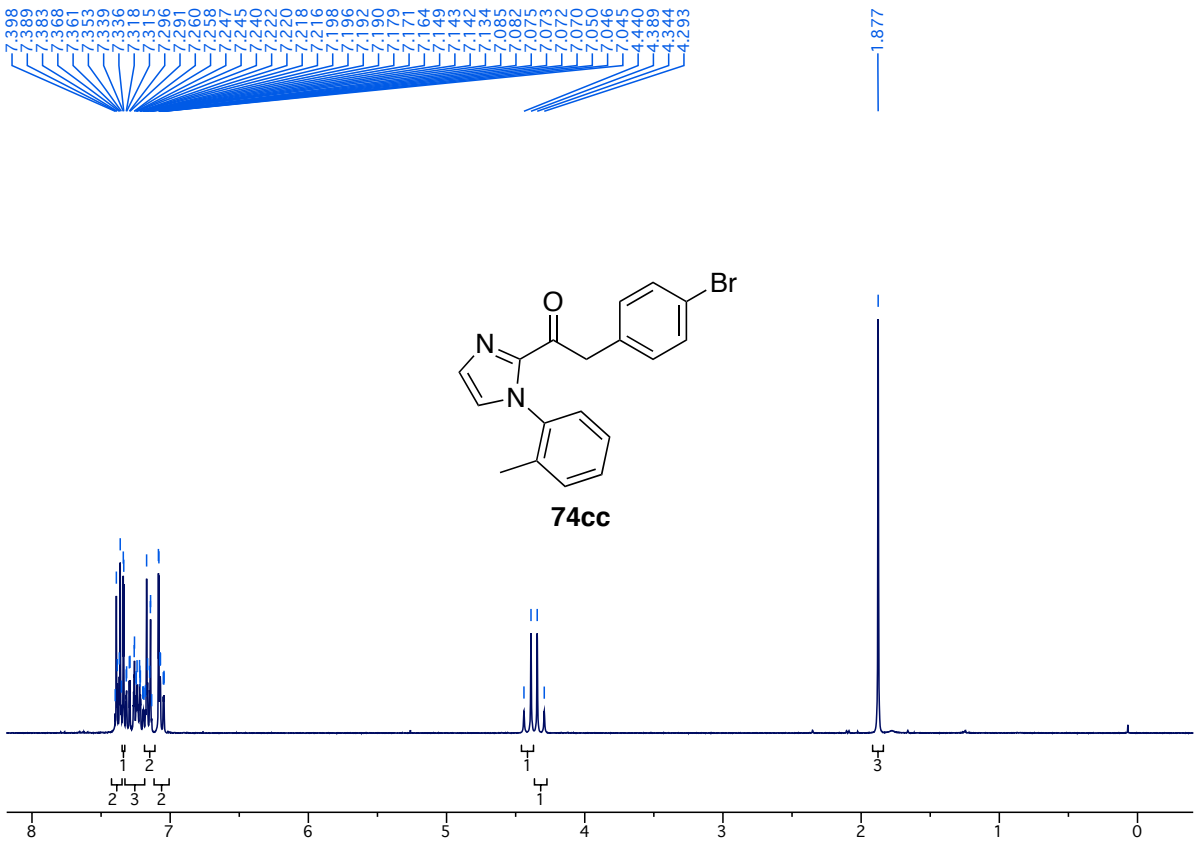

^{1}H-NMR spectrum of compound **74cc** (300 MHz, $CDCl_3$)

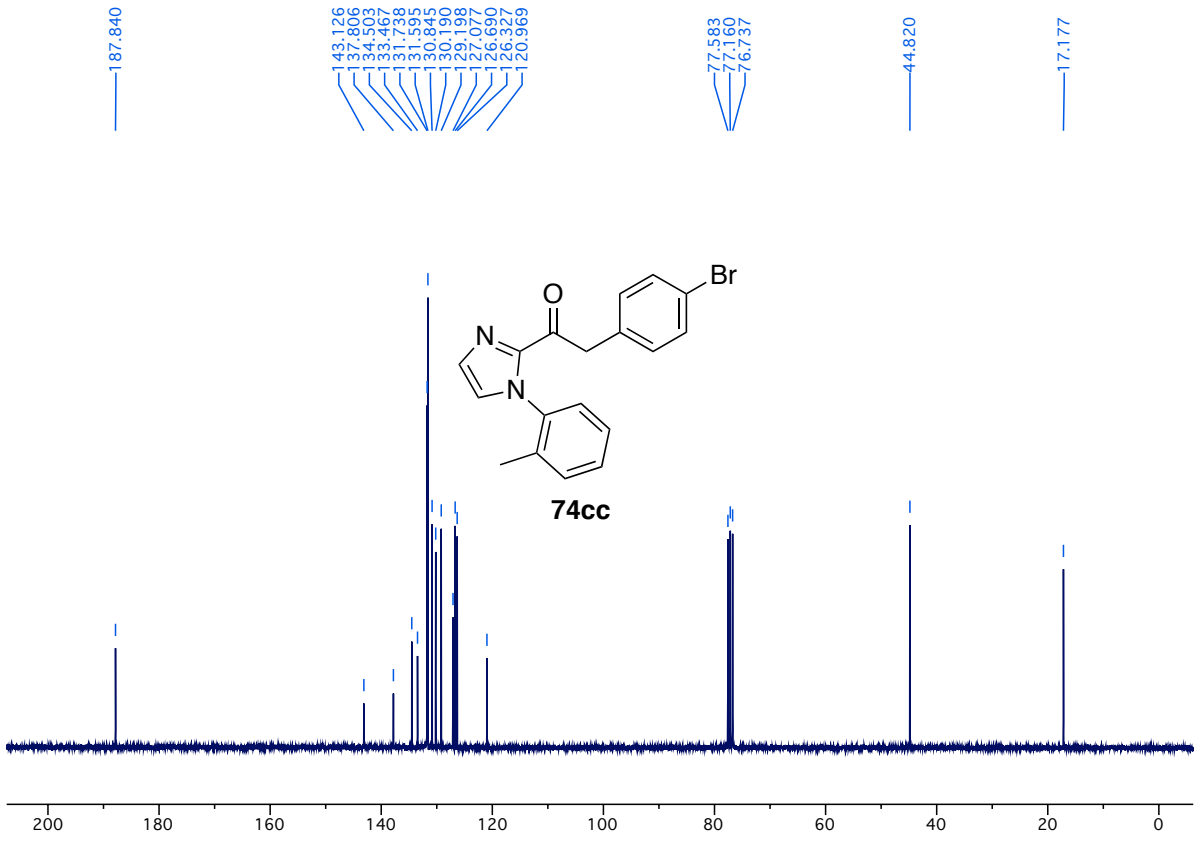

^{13}C-NMR spectrum of compound **74cc** (75.5 MHz, $CDCl_3$)

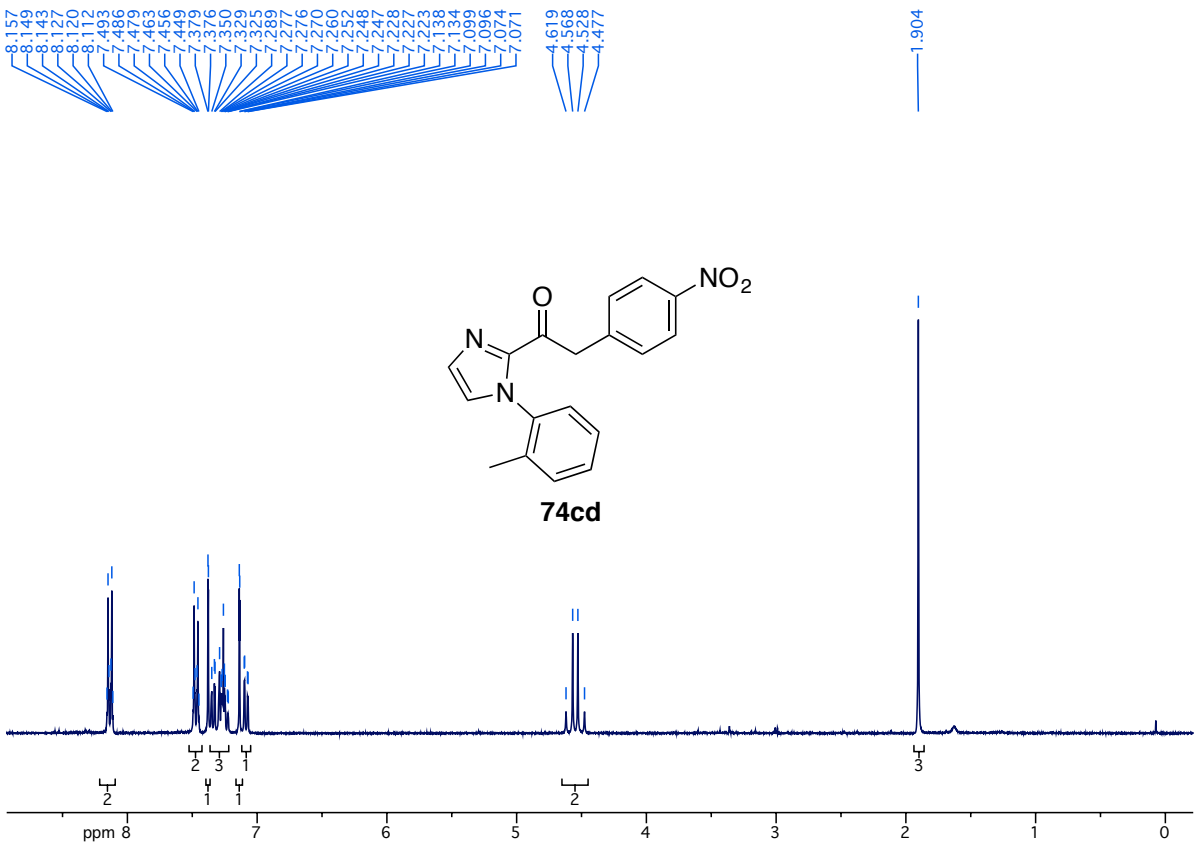

^{1}H-NMR spectrum of compound **74cd** (300 MHz, $CDCl_3$)

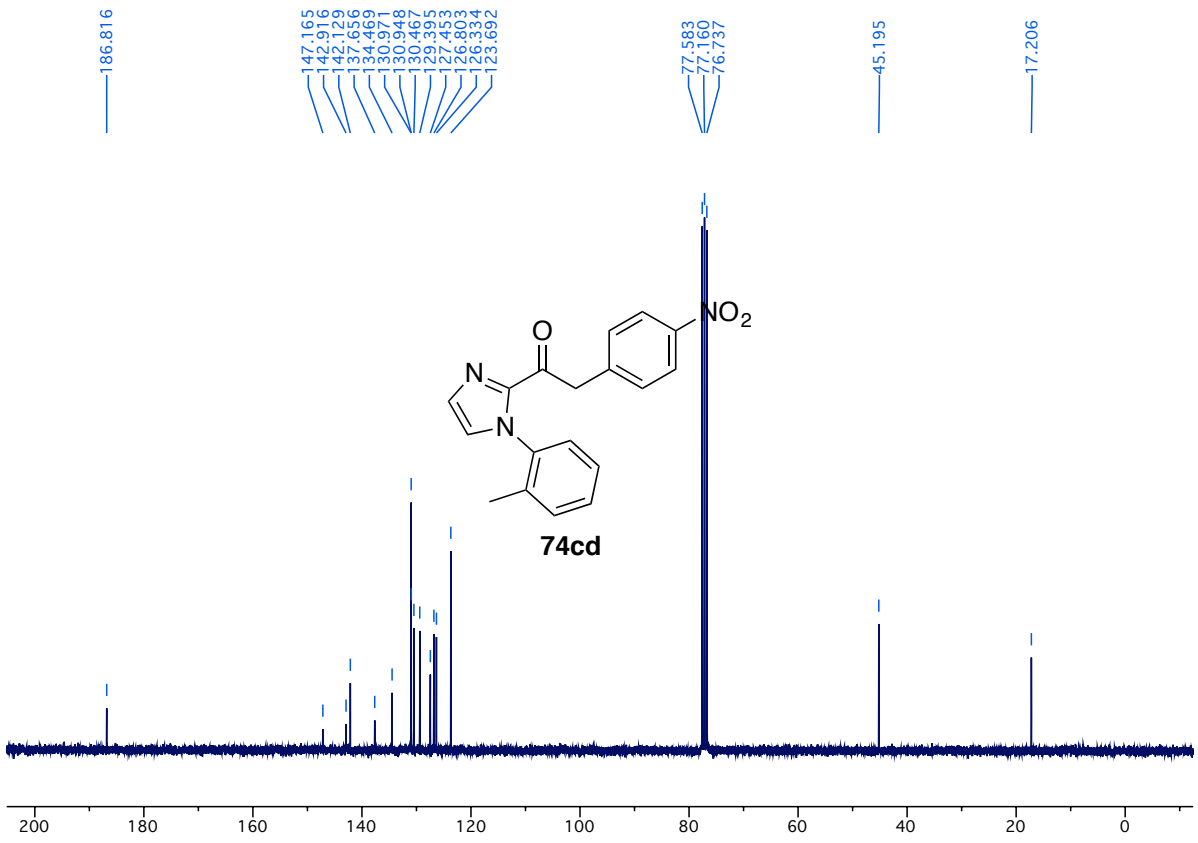

^{13}C-NMR spectrum of compound **74cd** (75.5 MHz, $CDCl_3$)

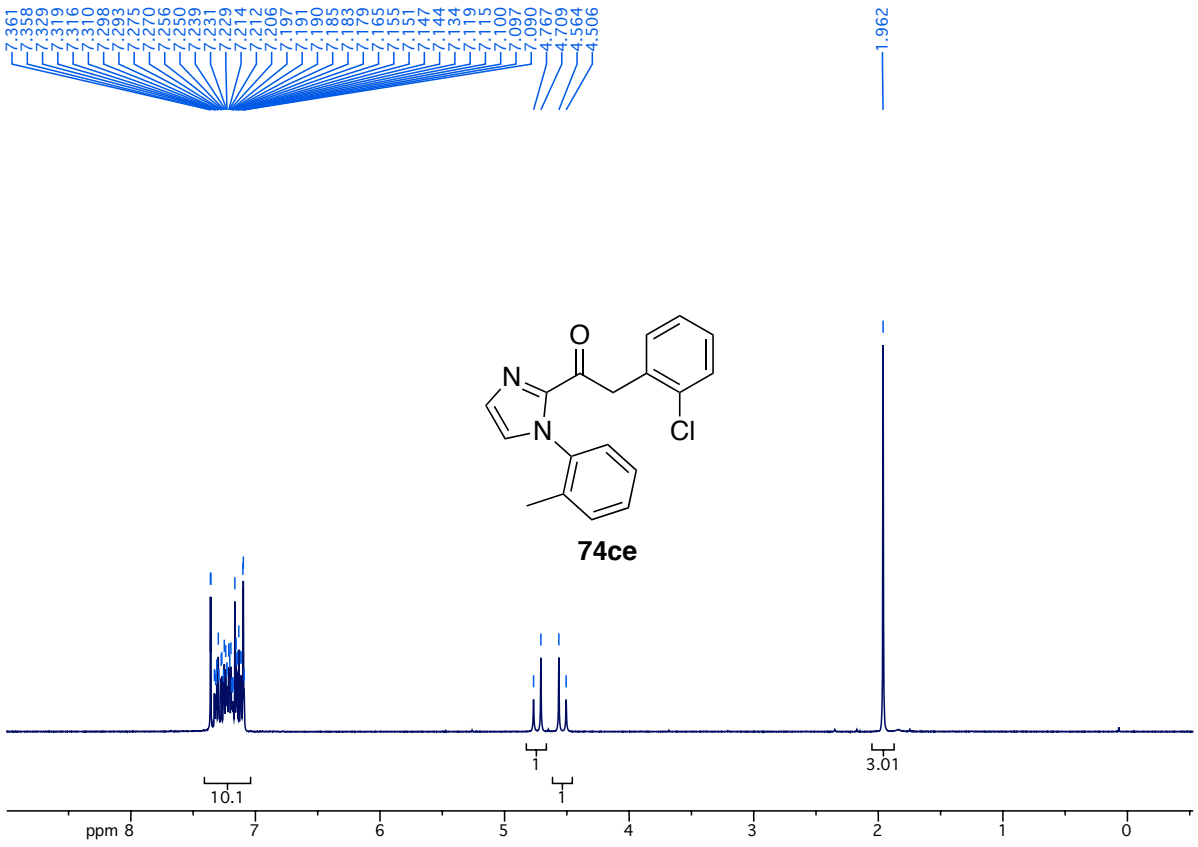

^{1}H-NMR spectrum of compound **74ce** (300 MHz, $CDCl_3$)

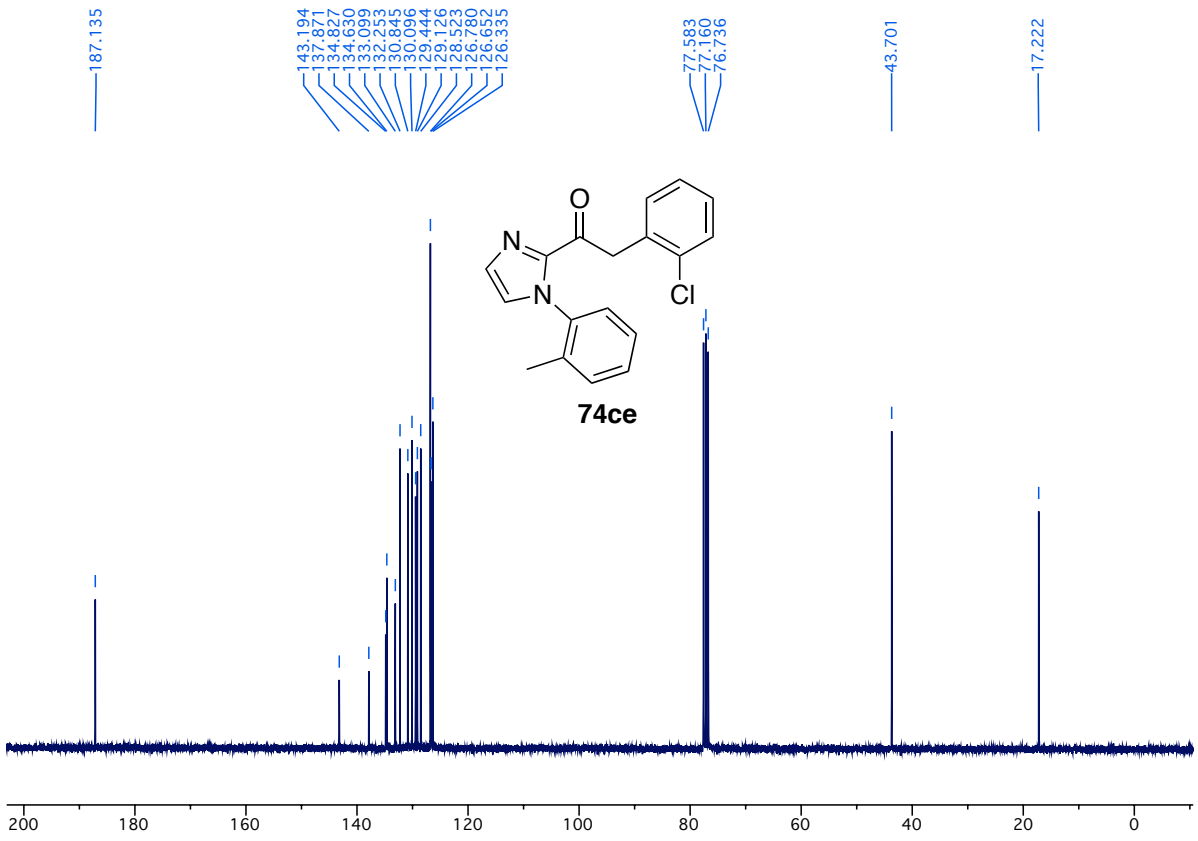

^{13}C-NMR spectrum of compound **74ce** (75.5 MHz, $CDCl_3$)

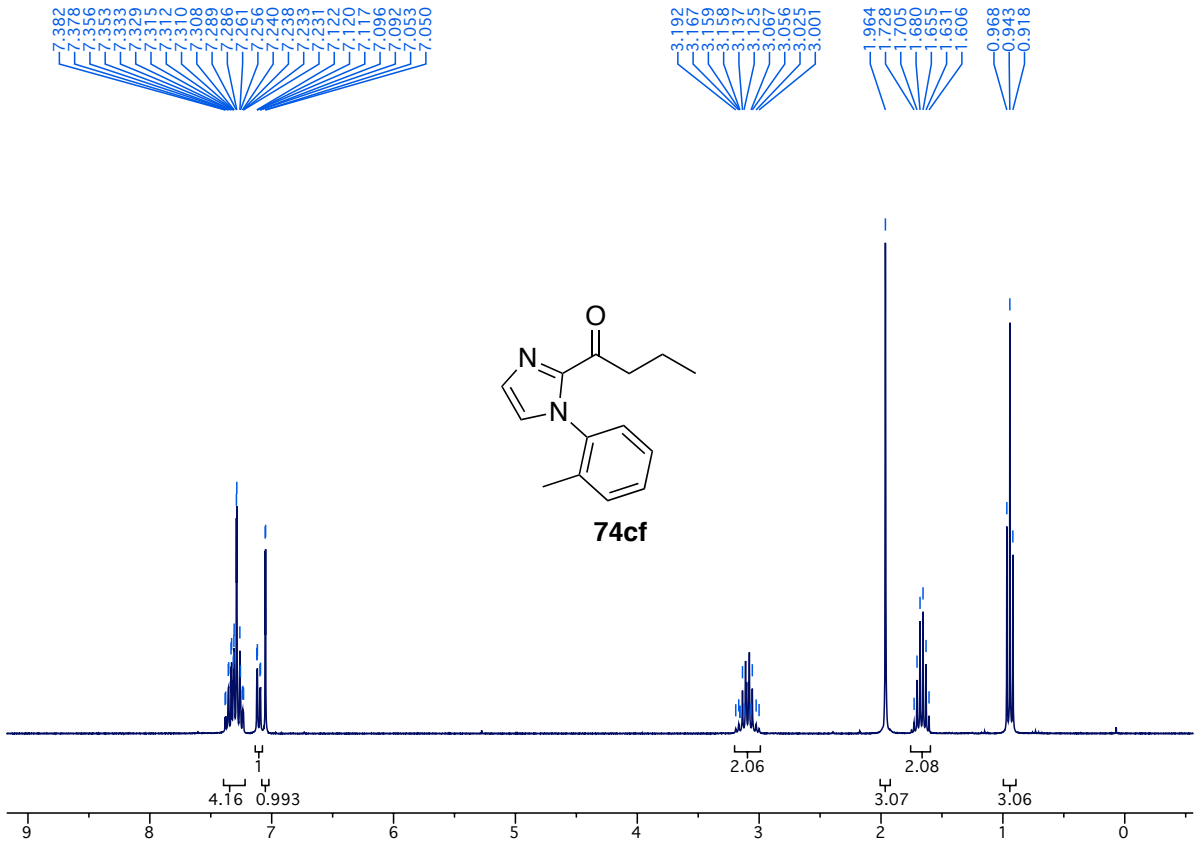

^{1}H-NMR spectrum of compound **74cf** (300 MHz, $CDCl_3$)

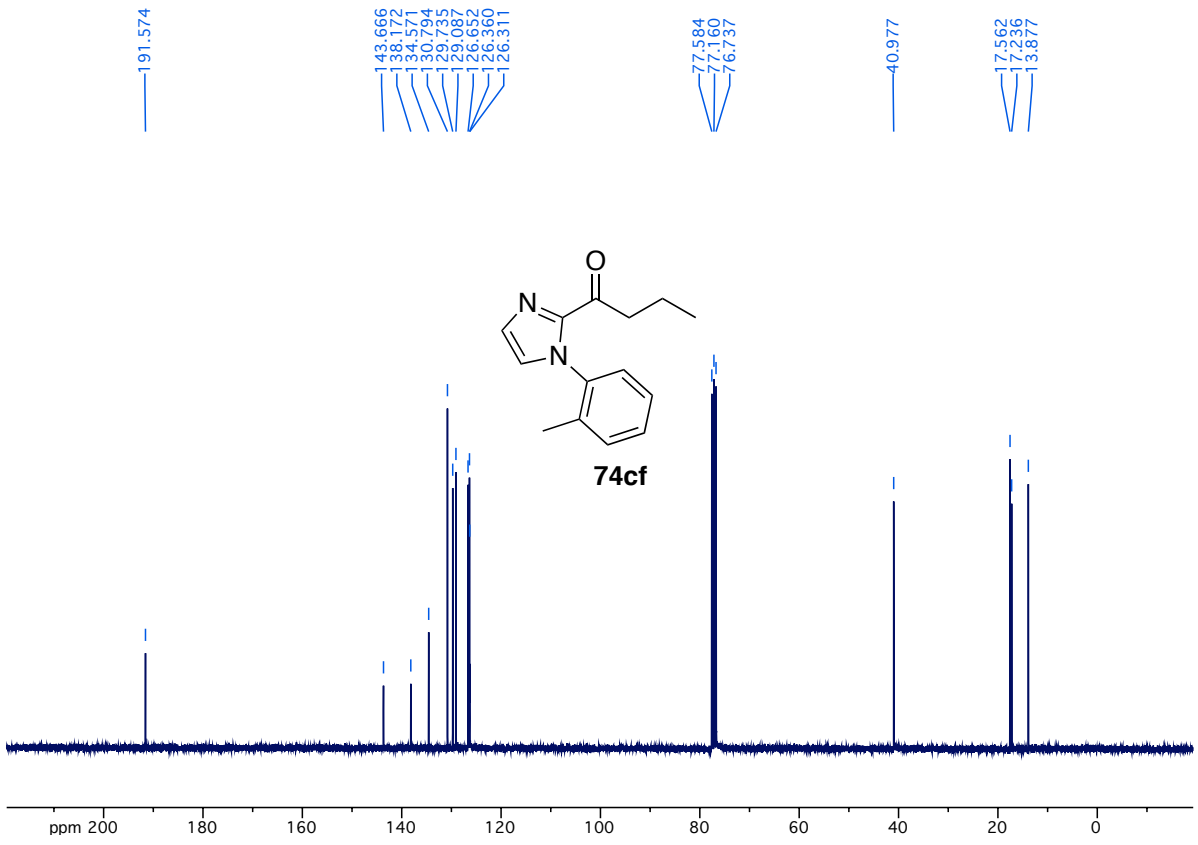

^{13}C-NMR spectrum of compound **74cf** (75.5 MHz, $CDCl_3$)

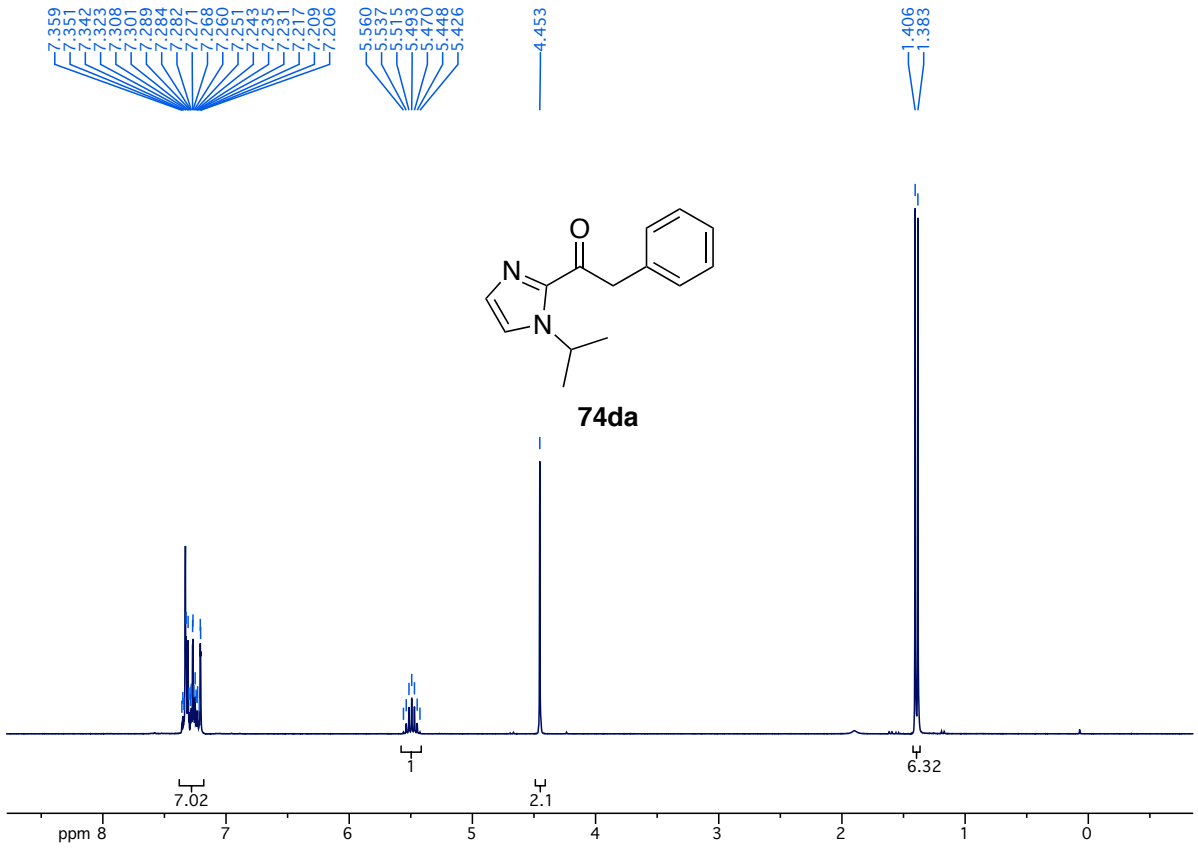

^{1}H-NMR spectrum of compound **74da** (300 MHz, $CDCl_3$)

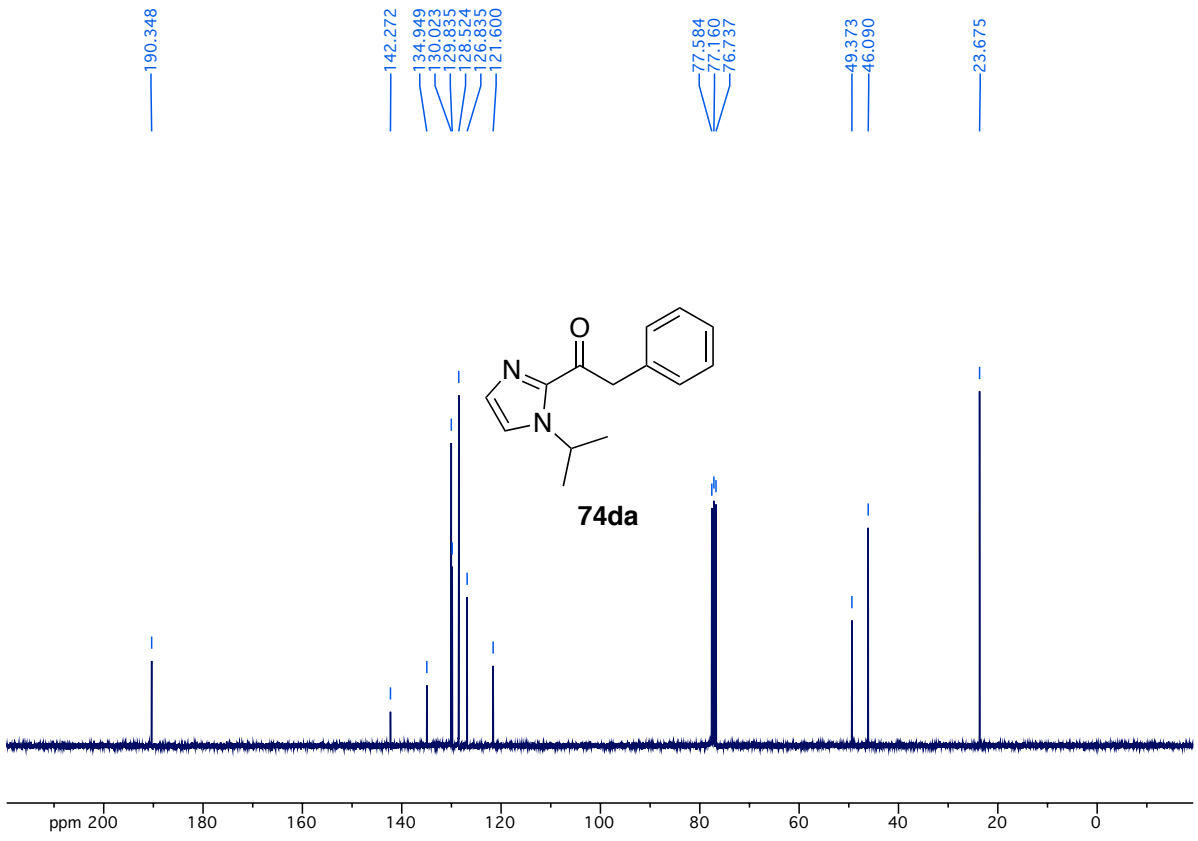

^{13}C-NMR spectrum of compound **74da** (75.5 MHz, $CDCl_3$)

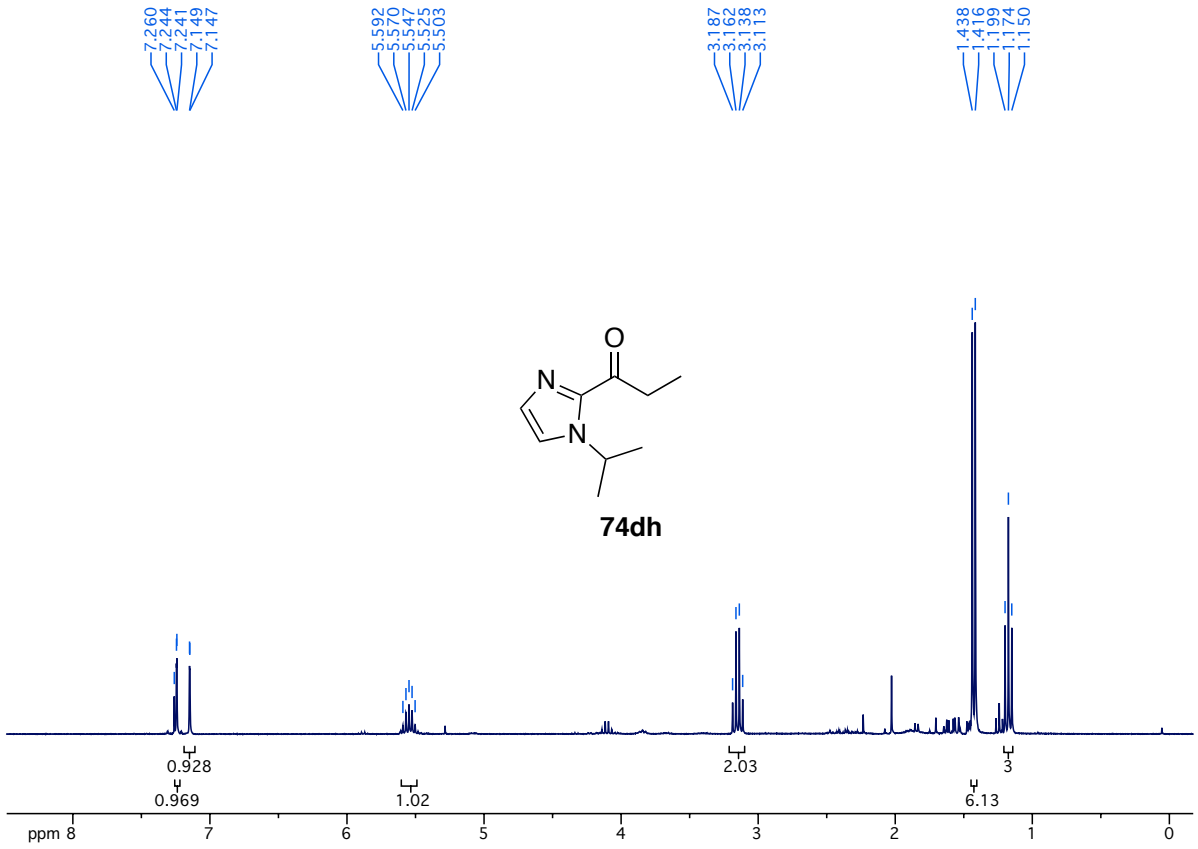

^{1}H-NMR spectrum of compound **74dh** (300 MHz, $CDCl_3$)

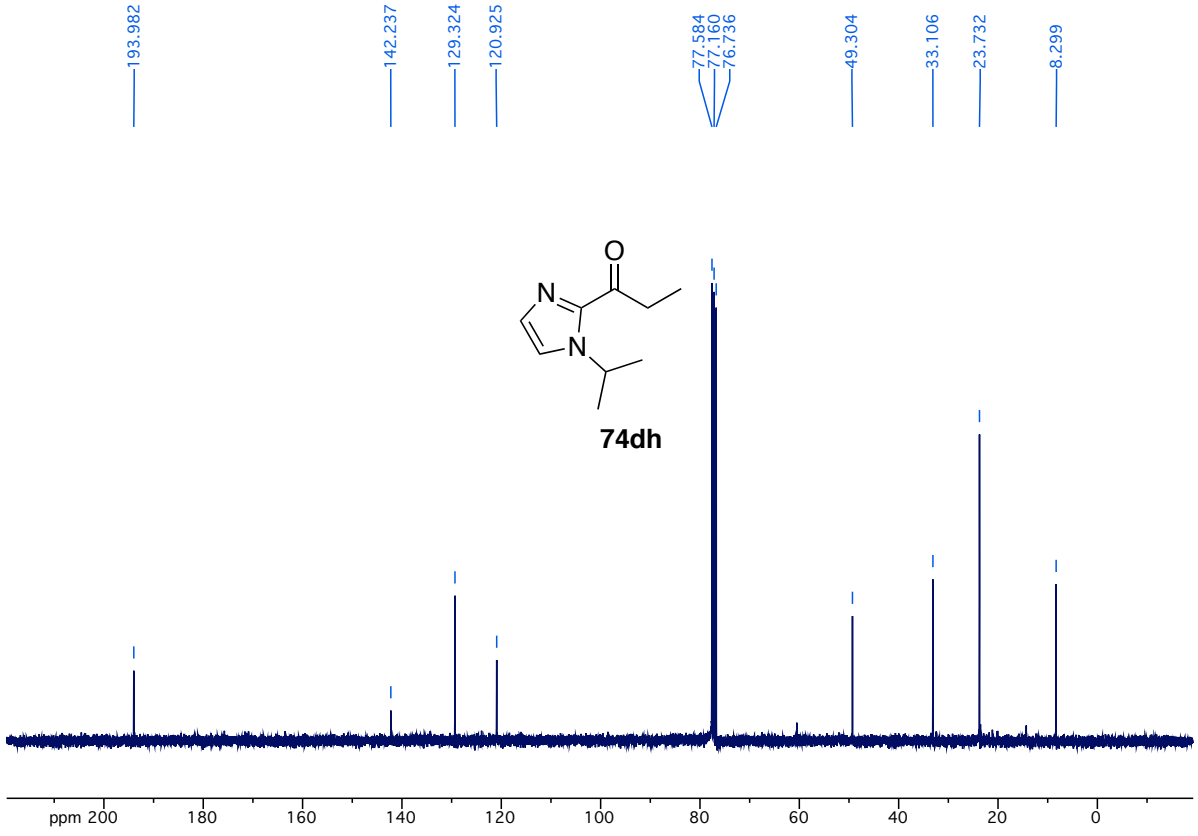

^{13}C-NMR spectrum of compound **74dh** (75.5 MHz, $CDCl_3$)

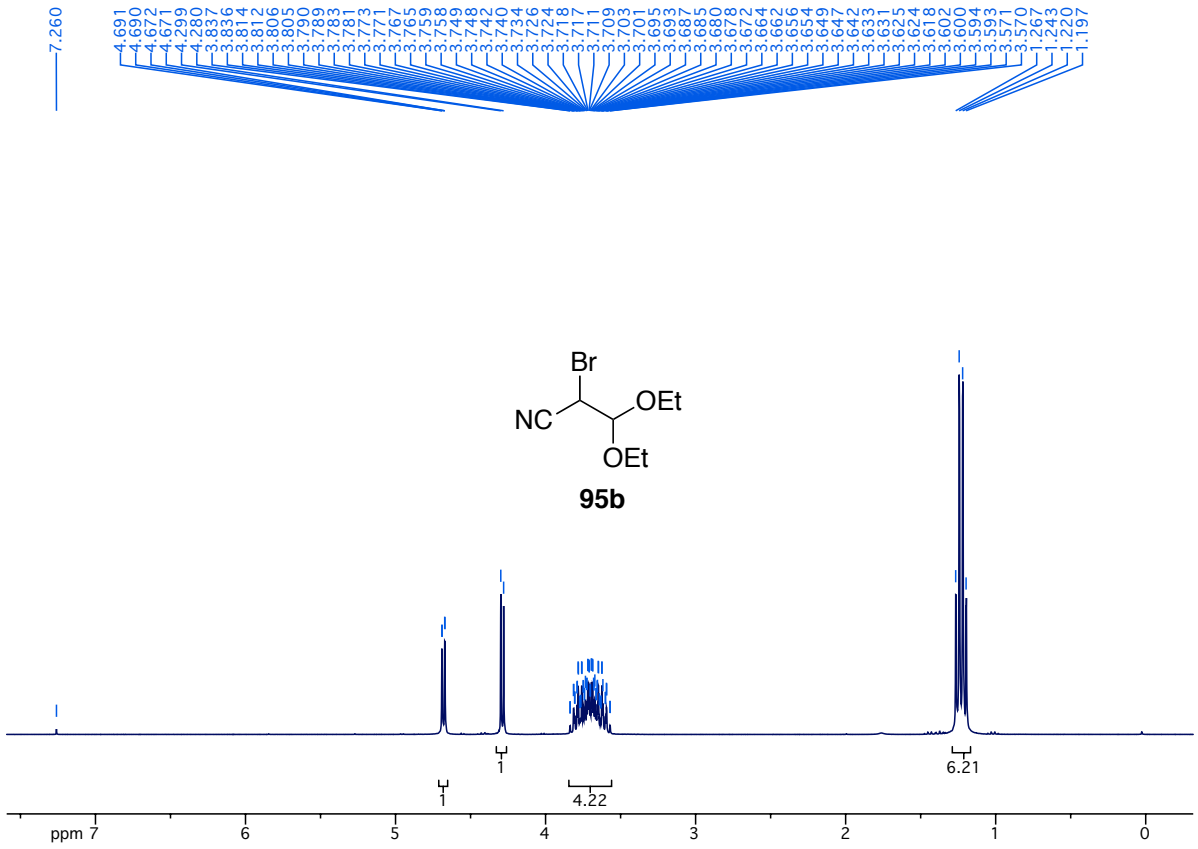

^{1}H-NMR spectrum of compound **95b** (300 MHz, $CDCl_3$)

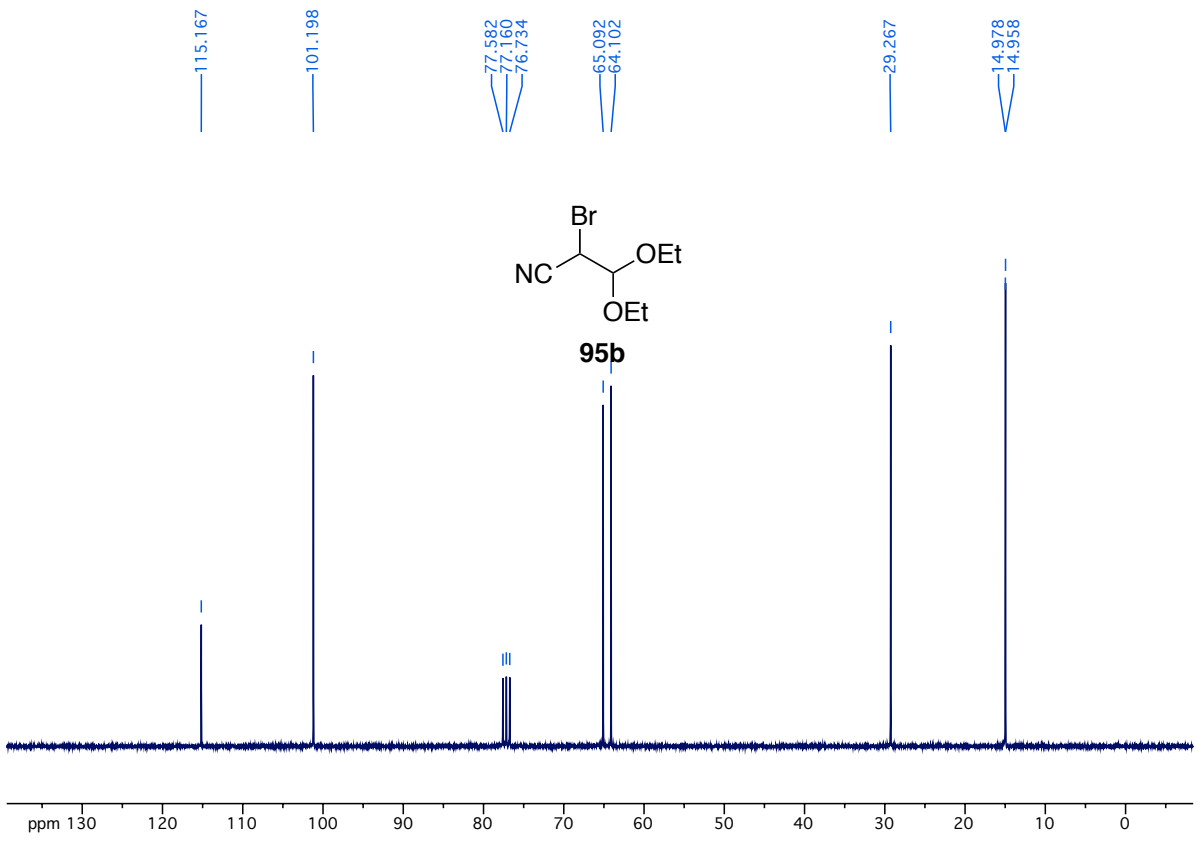

^{13}C-NMR spectrum of compound **95b** (75.5 MHz, $CDCl_3$)

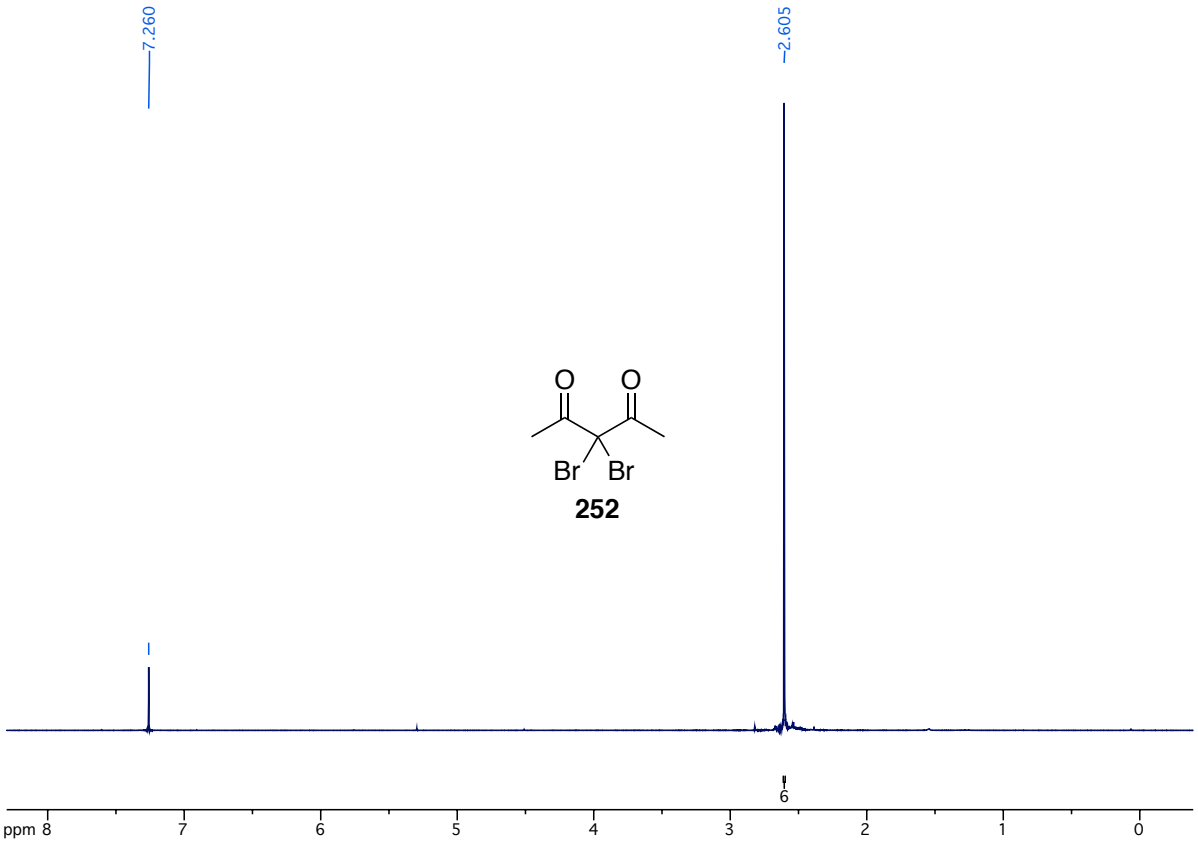

^{1}H-NMR spectrum of compound **252** (300 MHz, $CDCl_3$)

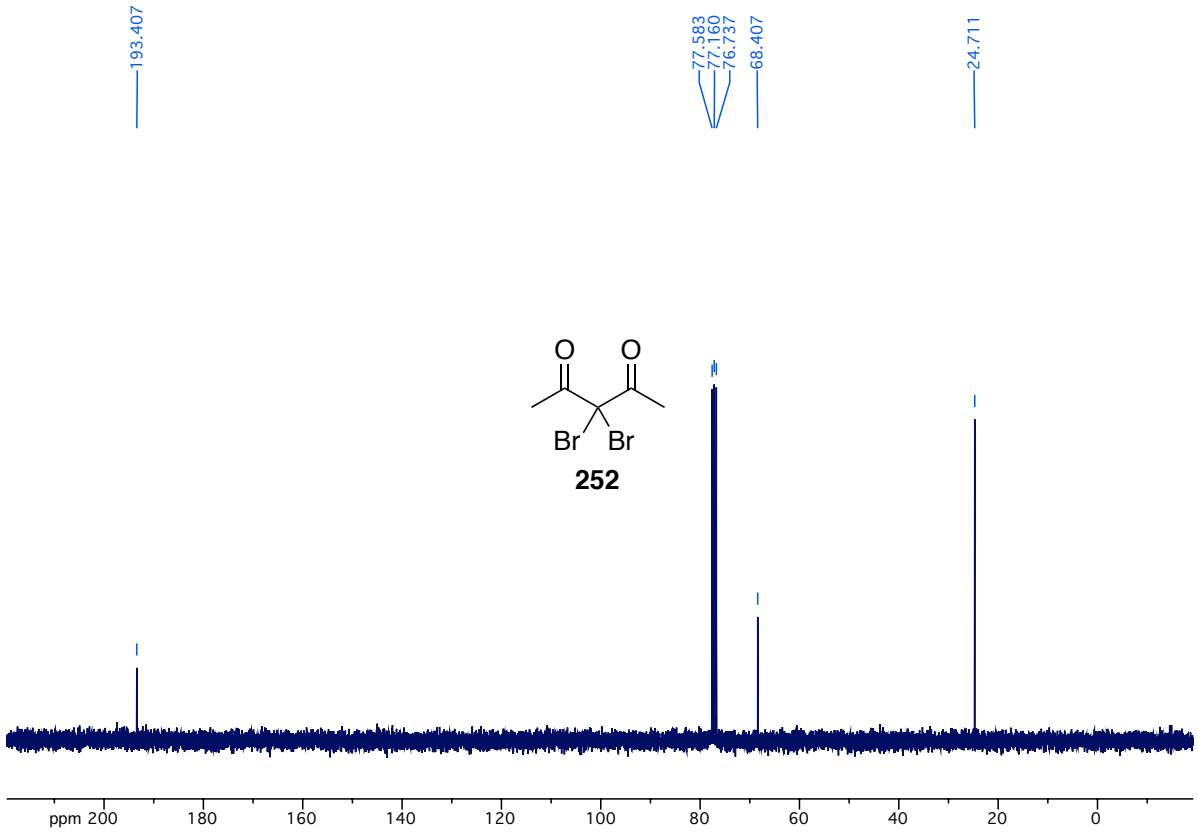

^{13}C-NMR spectrum of compound **252** (75.5 MHz, $CDCl_3$)

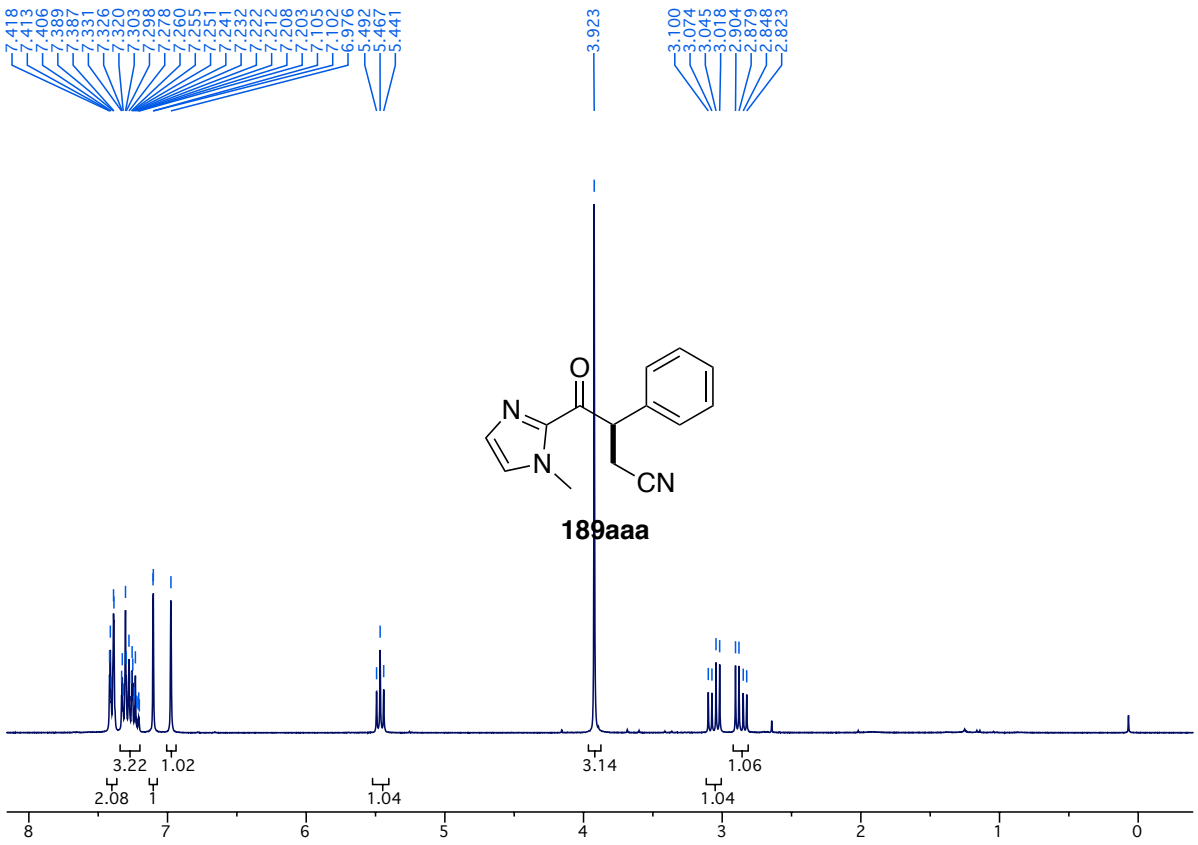

^{1}H-NMR spectrum of compound **189aaa** (300 MHz, $CDCl_3$)

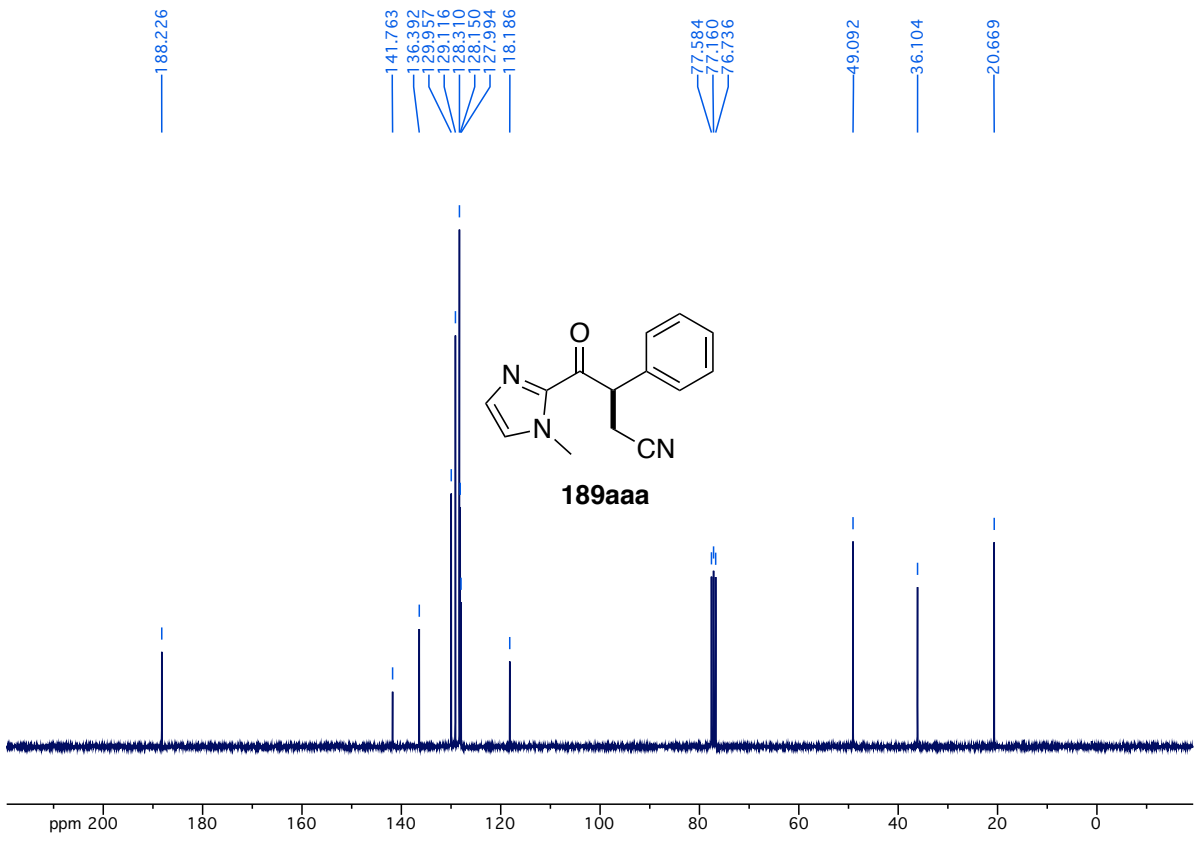

^{13}C-NMR spectrum of compound **189aaa** (75.5 MHz, $CDCl_3$)

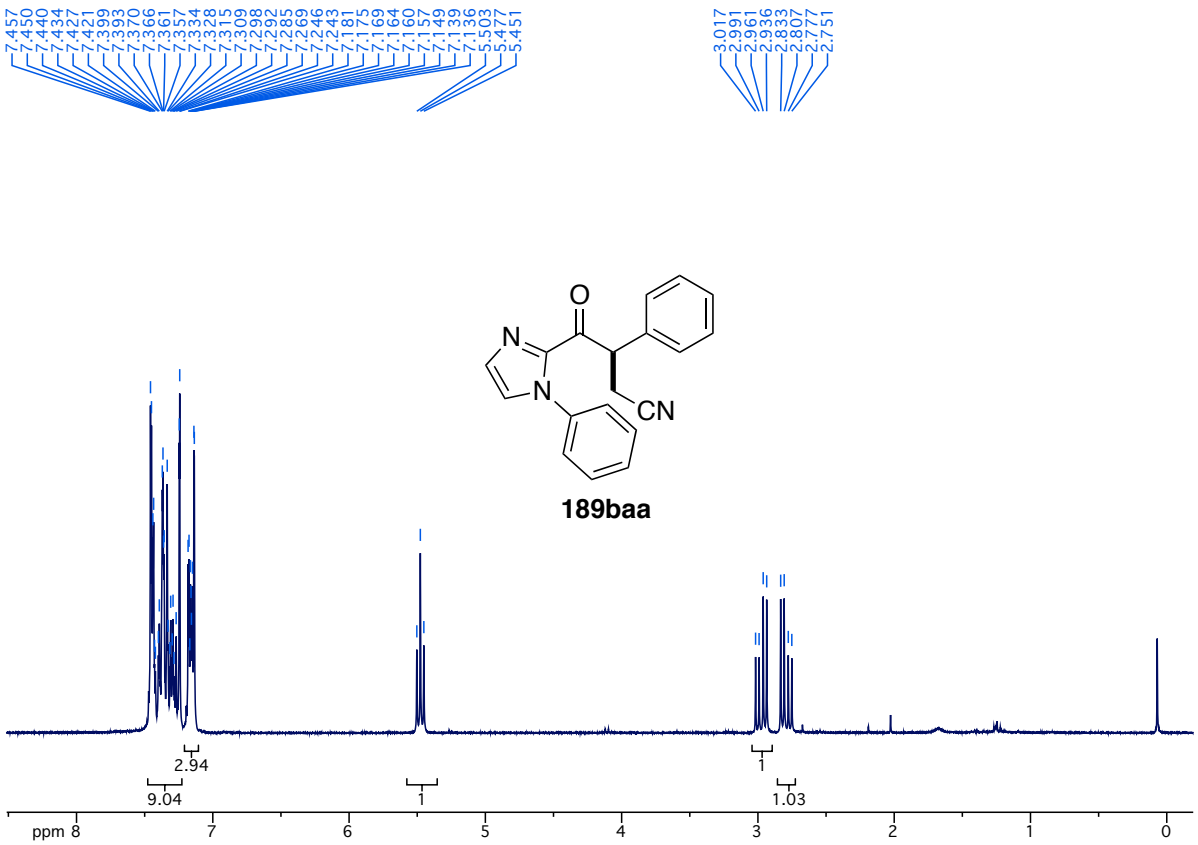

^{1}H-NMR spectrum of compound **189baa** (300 MHz, $CDCl_3$)

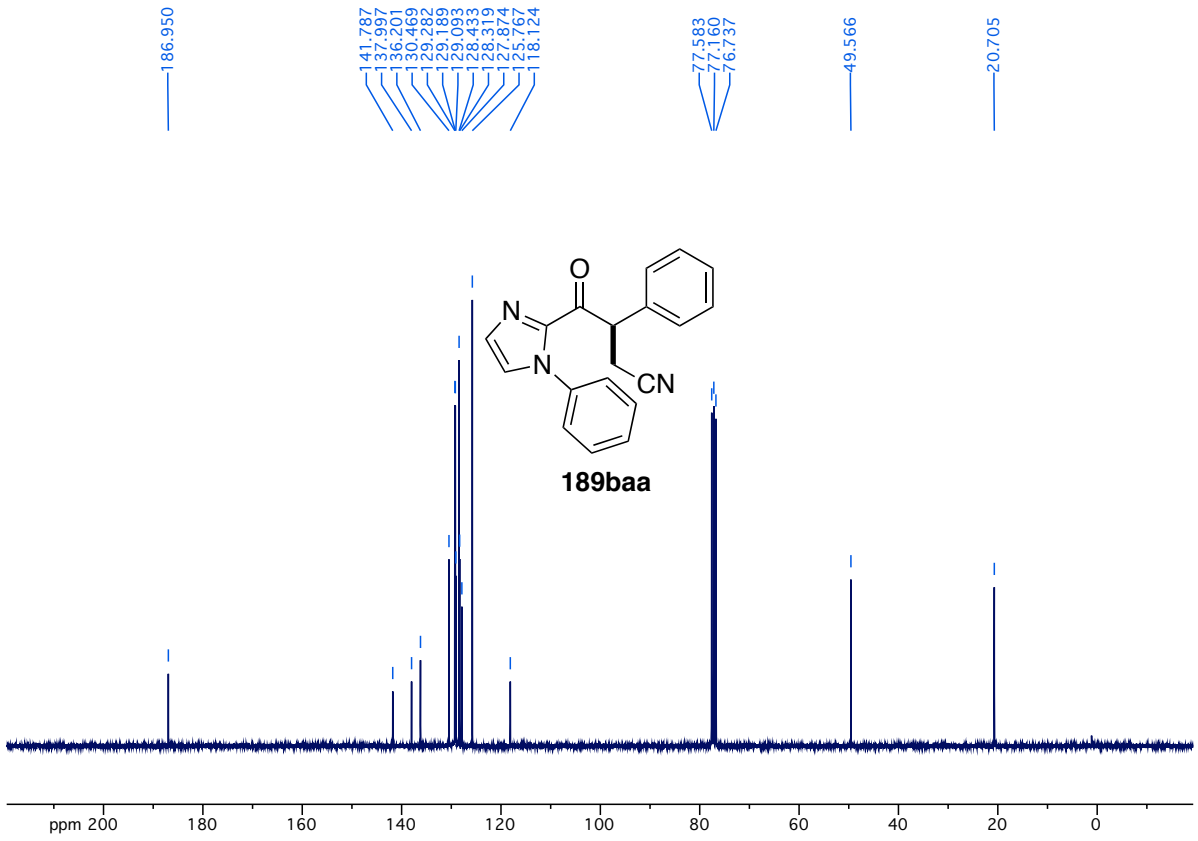

^{13}C-NMR spectrum of compound **189baa** (75.5 MHz, $CDCl_3$)

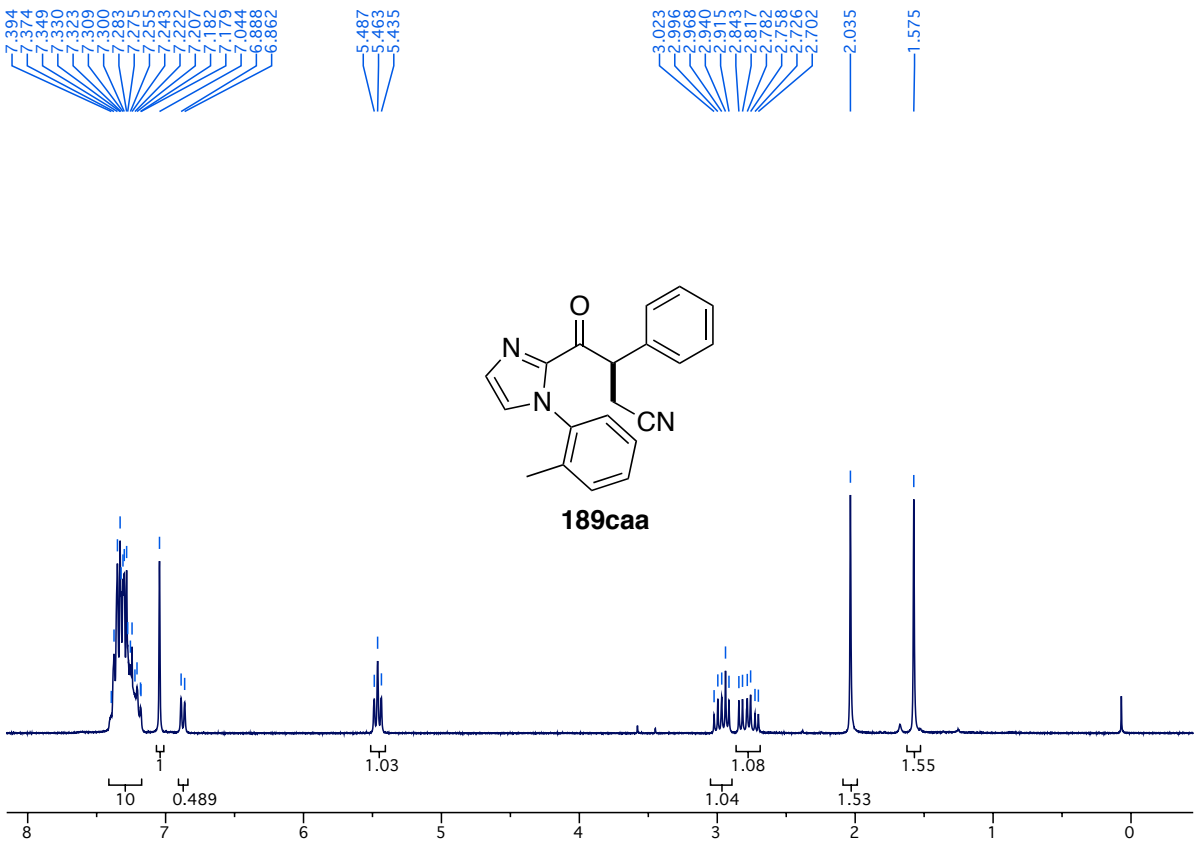

^{1}H-NMR spectrum of compound **189caa** (300 MHz, $CDCl_3$)

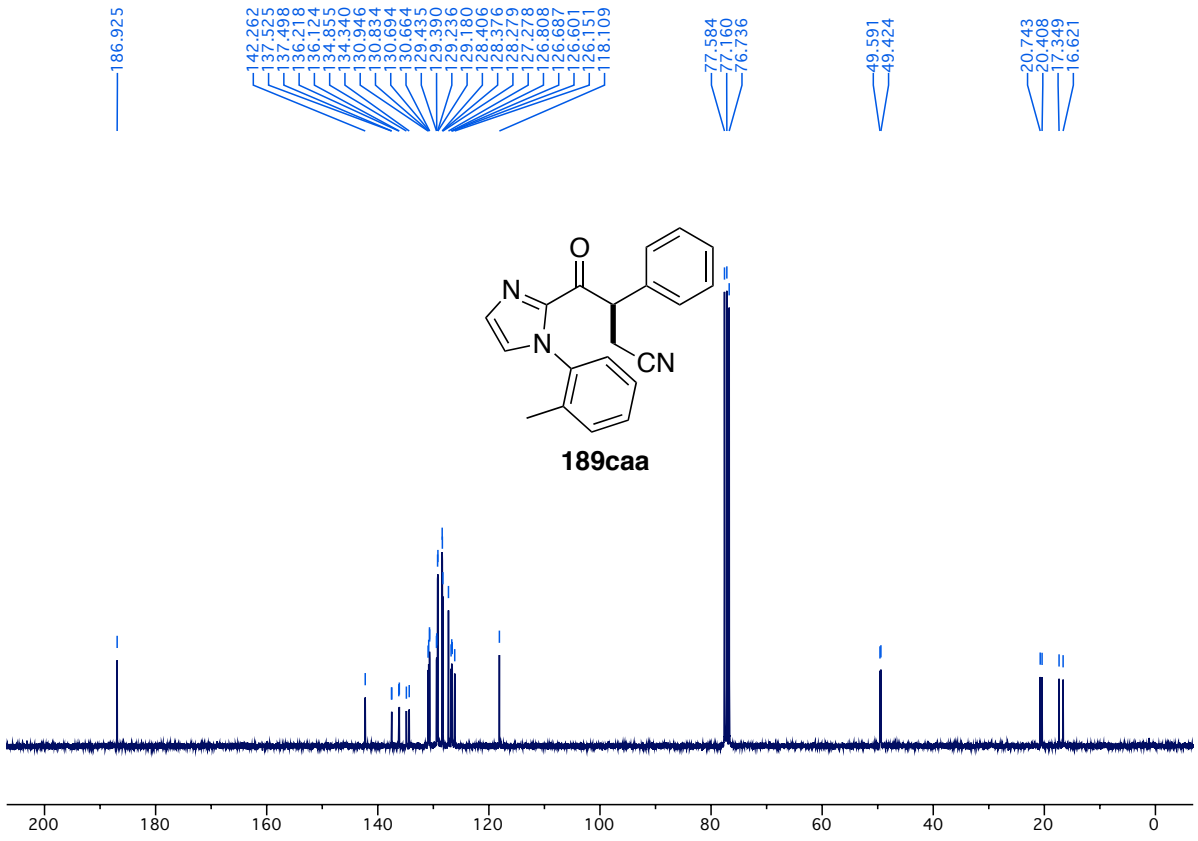

^{13}C-NMR spectrum of compound **189caa** (75.5 MHz, $CDCl_3$)

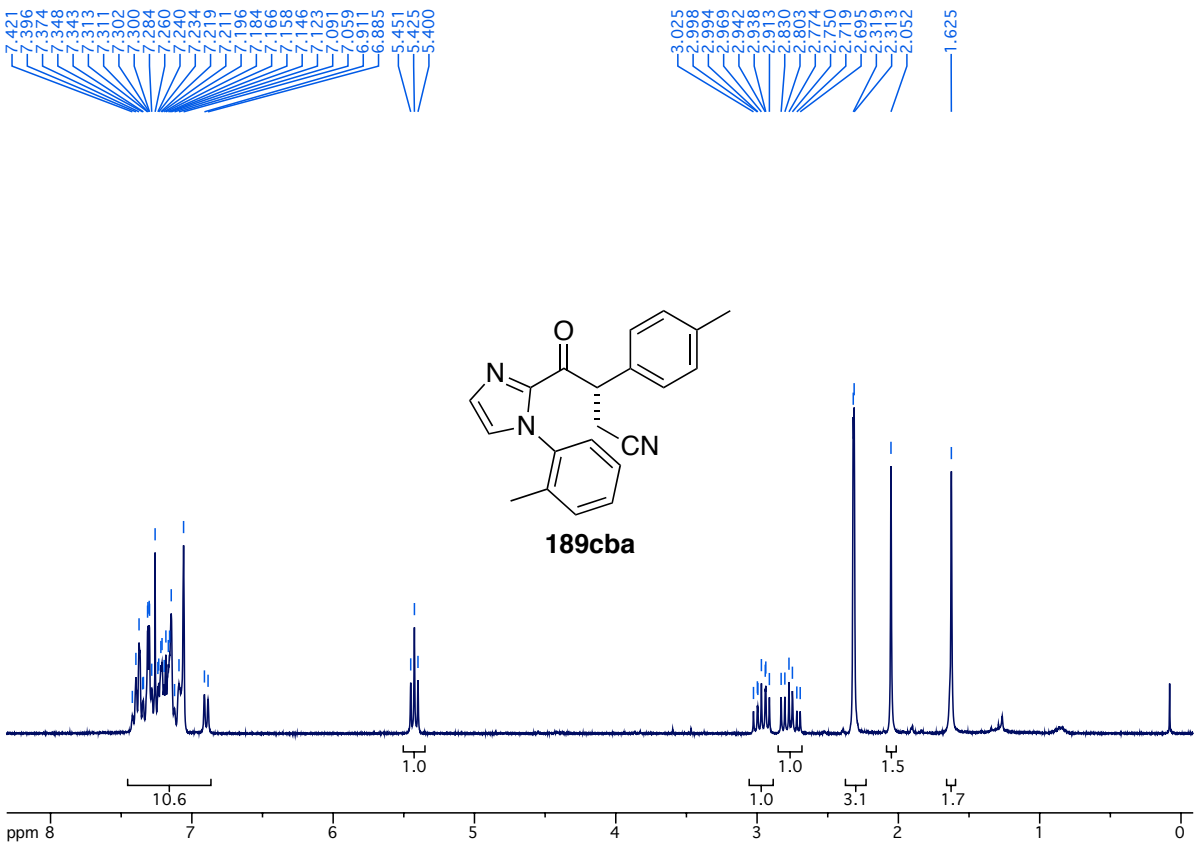

^{1}H-NMR spectrum of compound **189cba** (300 MHz, $CDCl_3$)

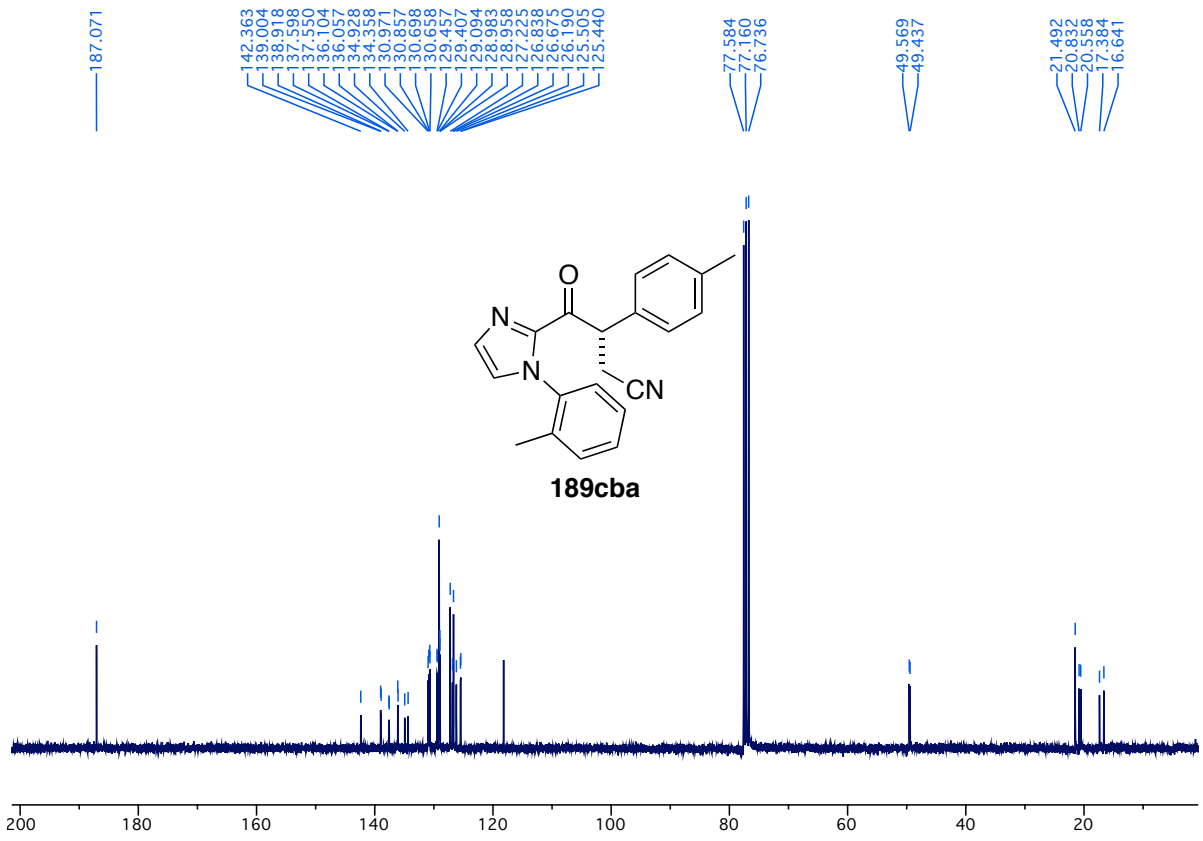

^{13}C-NMR spectrum of compound **189cba** (75.5 MHz, $CDCl_3$)

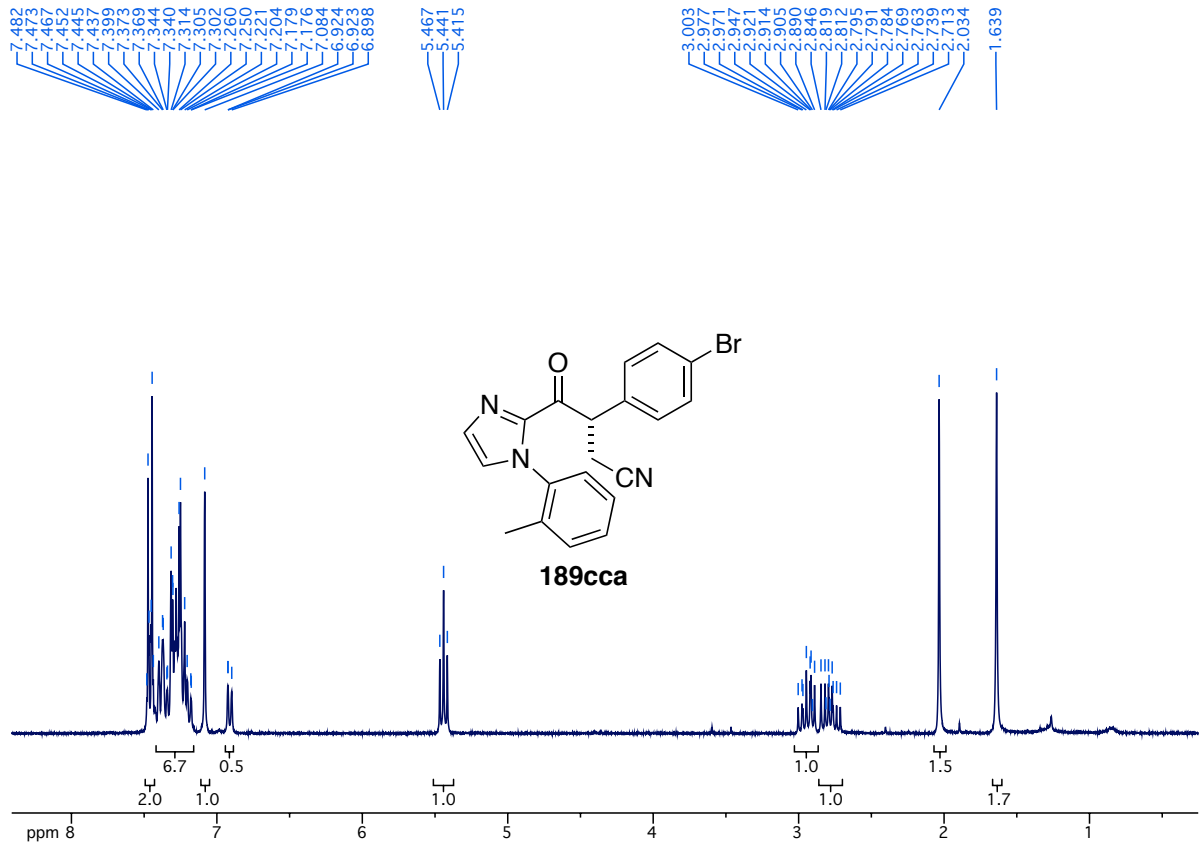

^{1}H-NMR spectrum of compound **189cca** (300 MHz, $CDCl_3$)

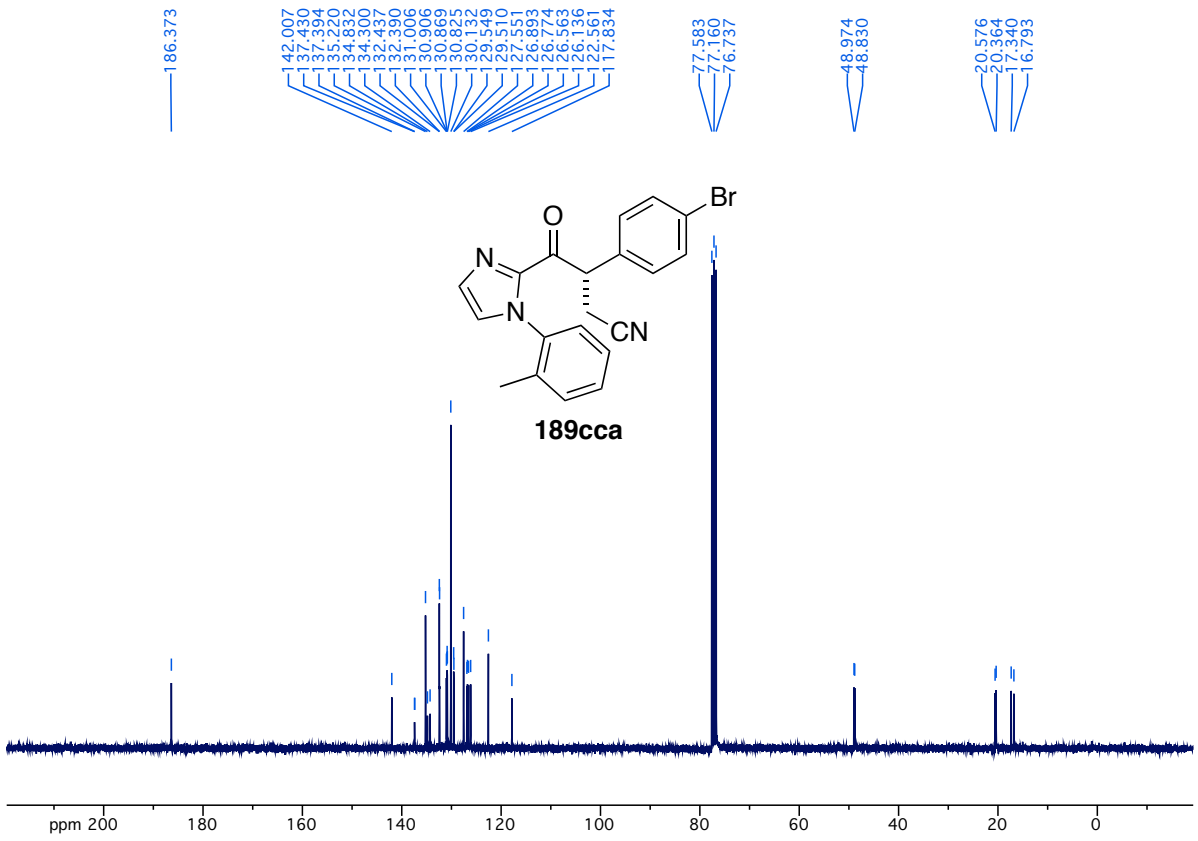

^{13}C-NMR spectrum of compound **189cca** (75.5 MHz, $CDCl_3$)

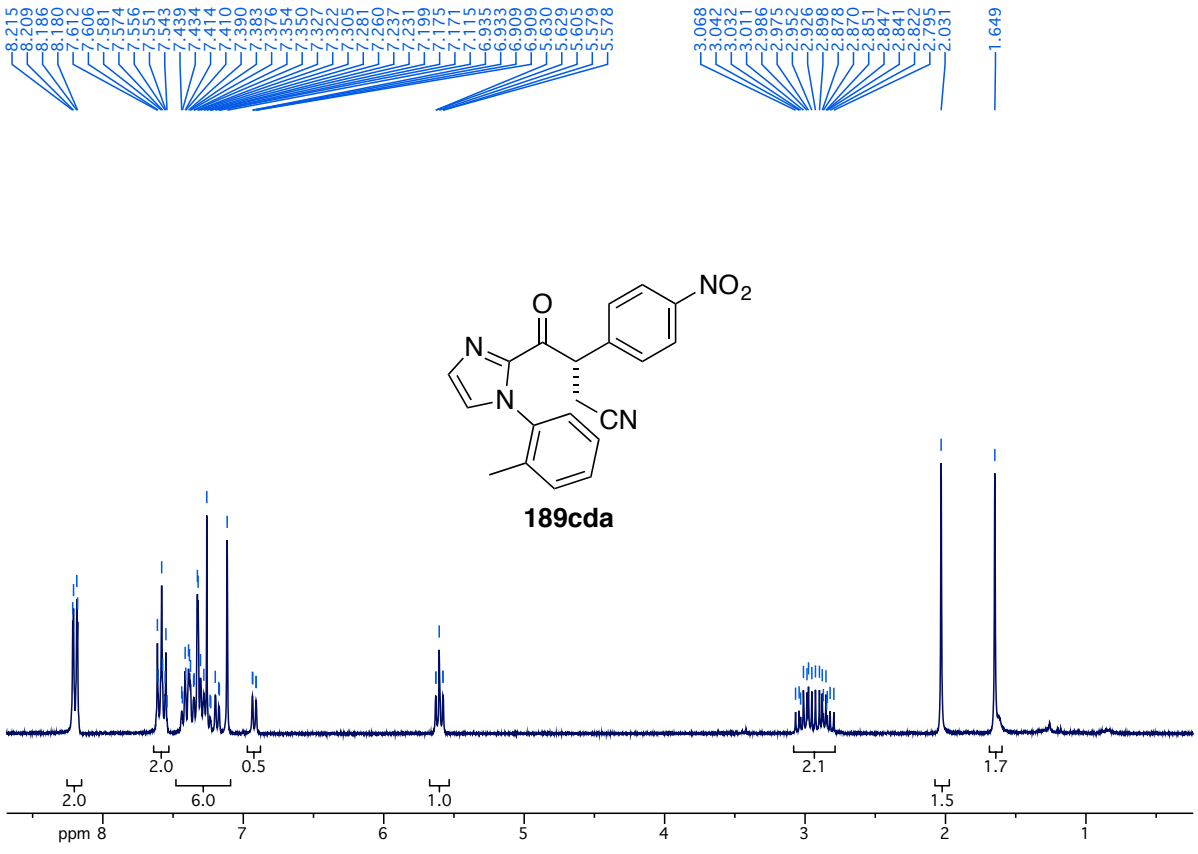

^{1}H-NMR spectrum of compound **189cda** (300 MHz, $CDCl_3$)

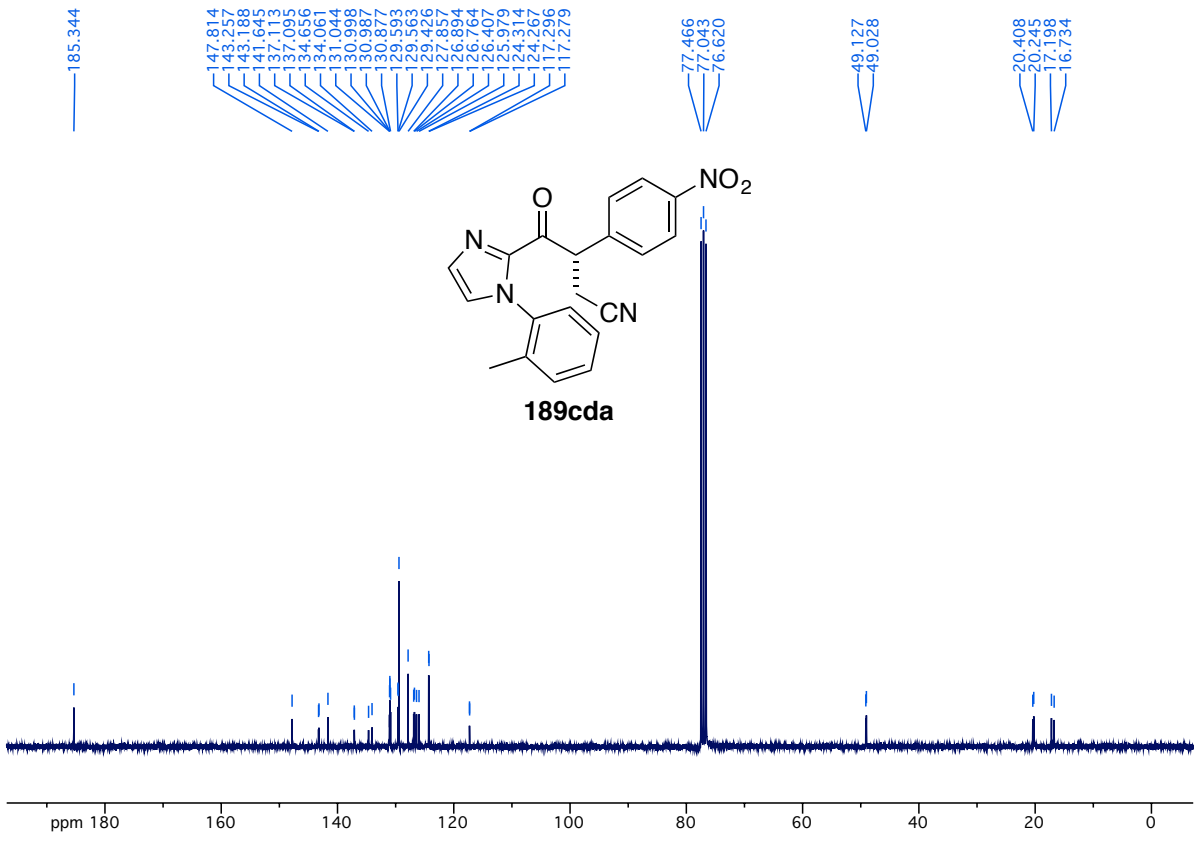

^{13}C-NMR spectrum of compound **189cda** (75.5 MHz, $CDCl_3$)

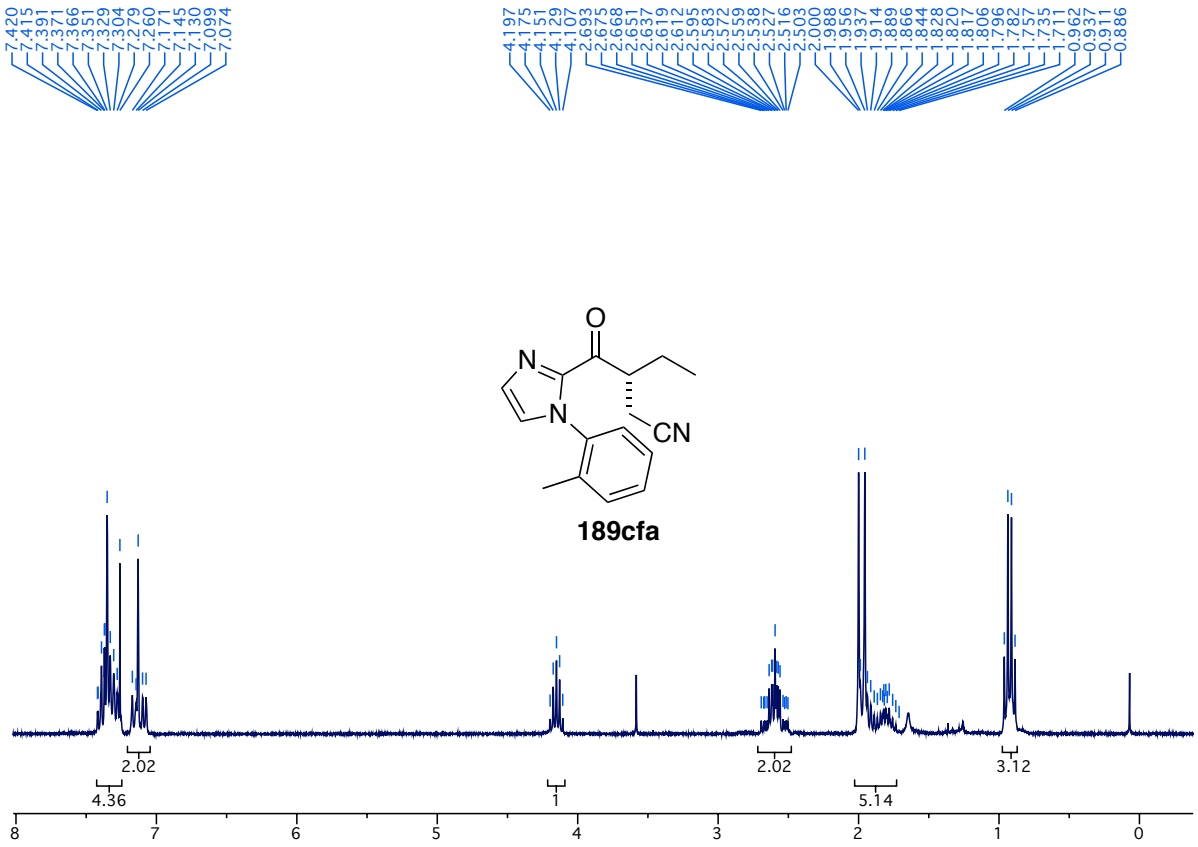

^{1}H-NMR spectrum of compound **189cfa** (300 MHz, $CDCl_3$)

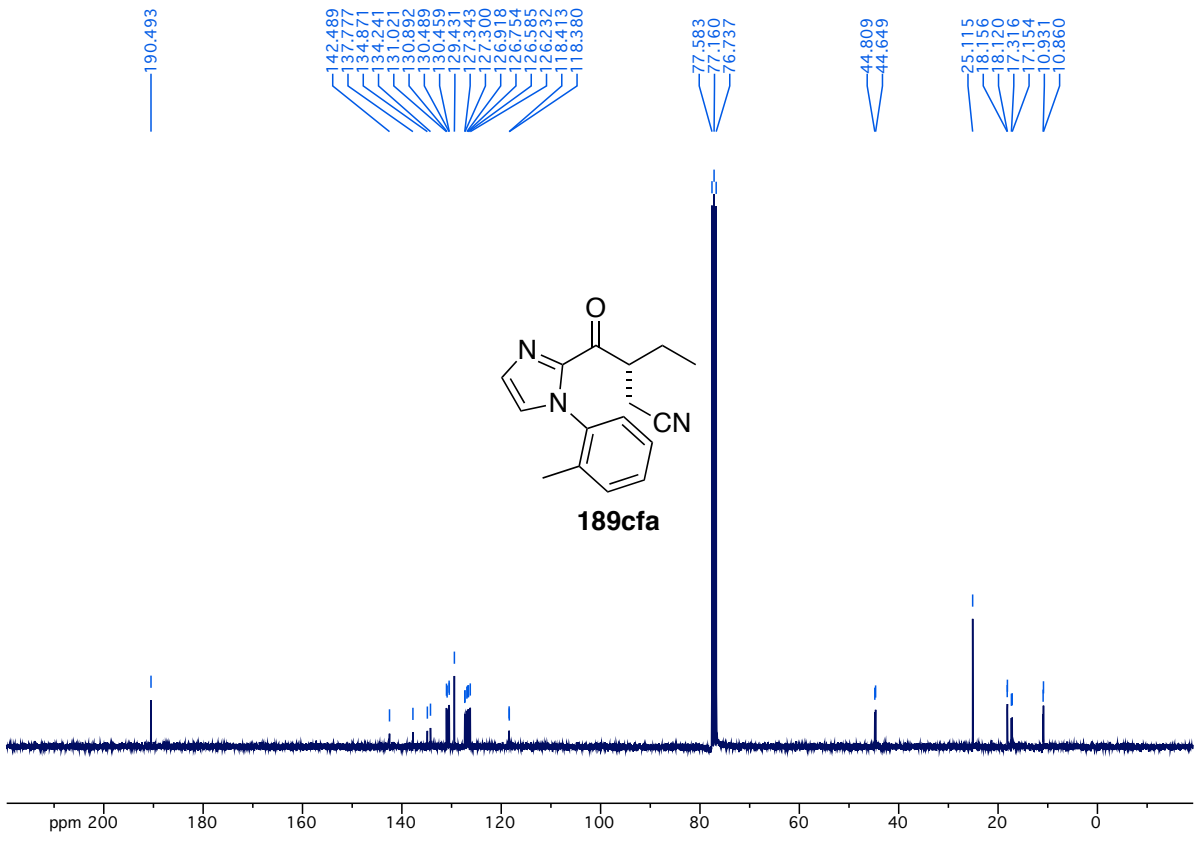

^{13}C-NMR spectrum of compound **189cfa** (75.5 MHz, $CDCl_3$)

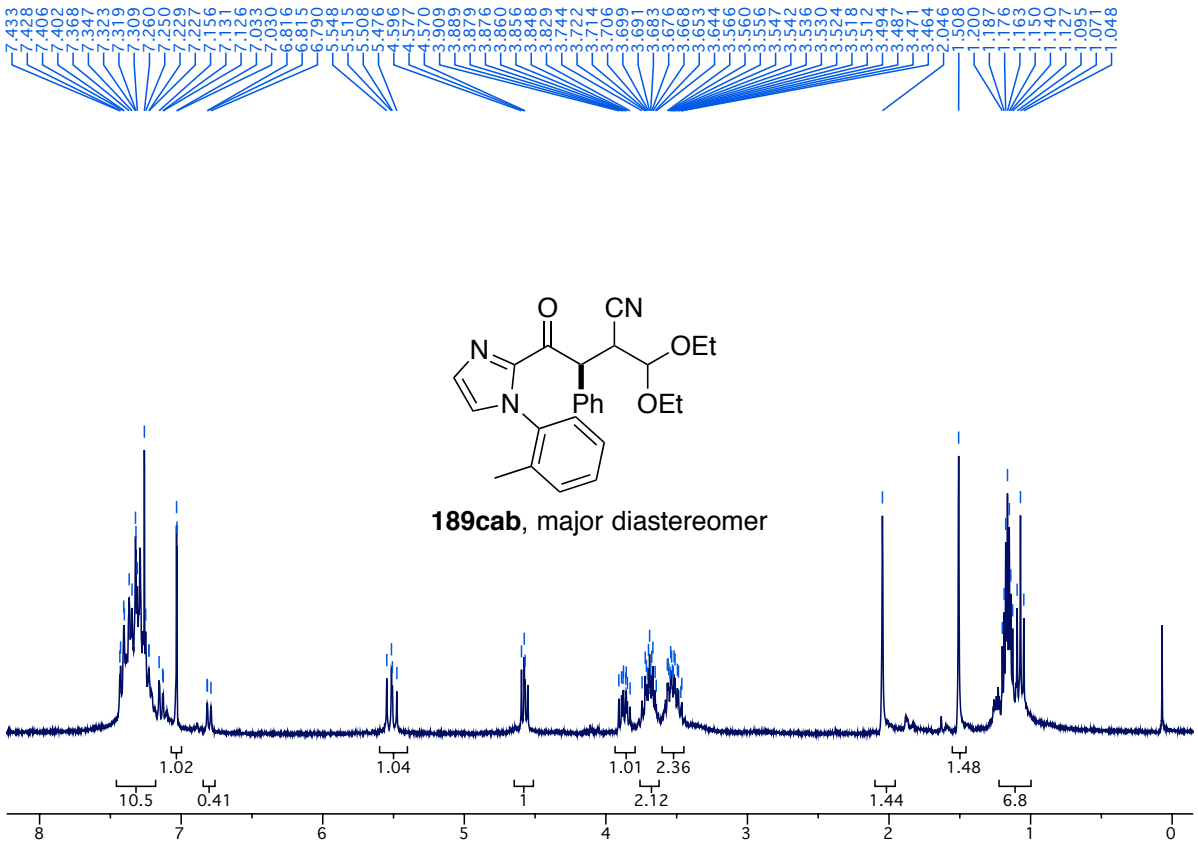

^{1}H-NMR spectrum of compound **189cab**: major diastereomer (300 MHz, $CDCl_3$)

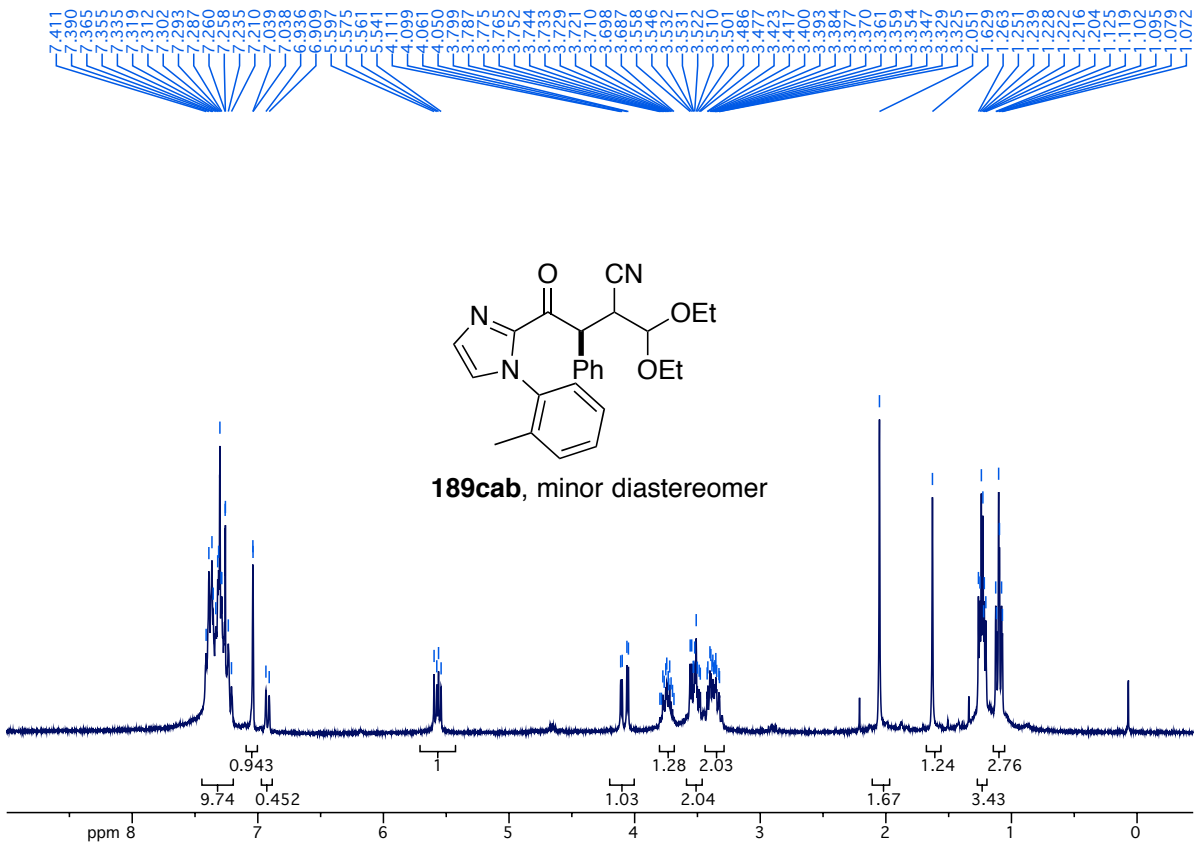

^{1}H-NMR spectrum of compound **189cab**: minor diastereomer (300 MHz, $CDCl_3$)

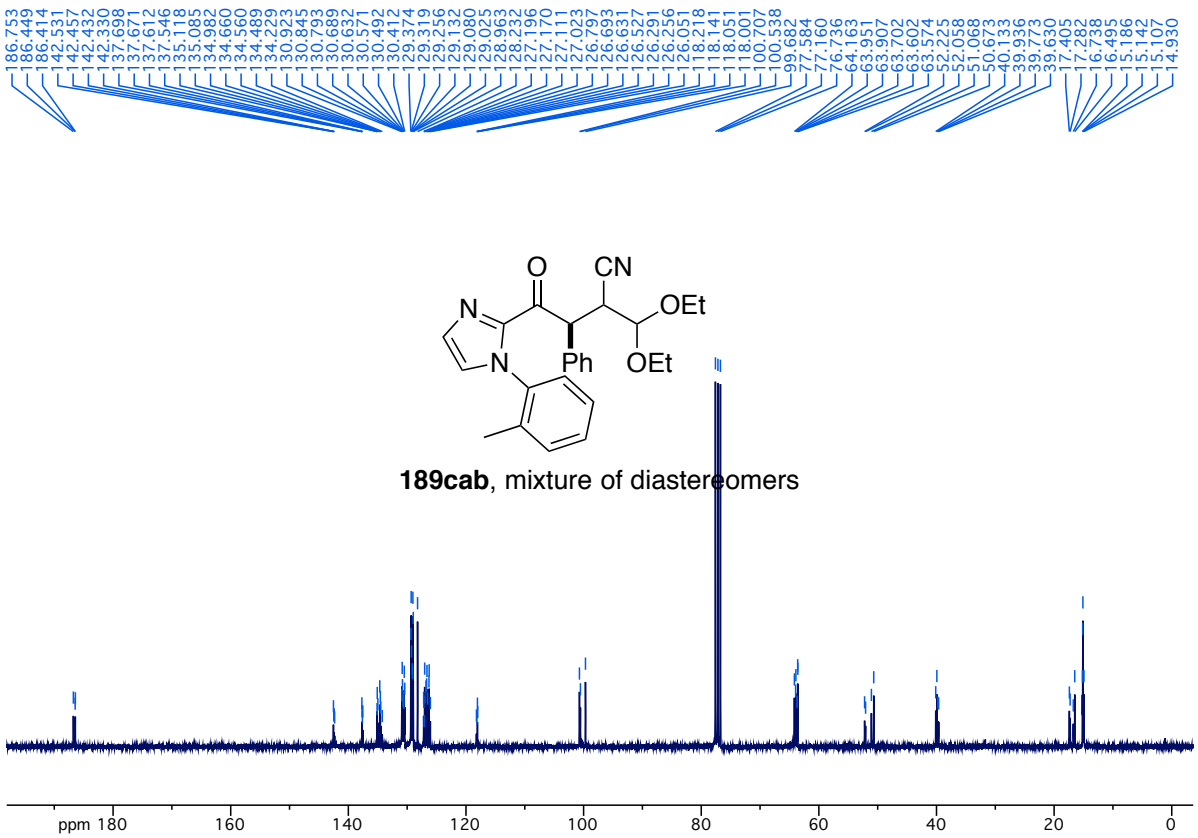

^{13}C-NMR spectrum of compound **189cab**: mixture of diastereomers (75.5 MHz, $CDCl_3$)

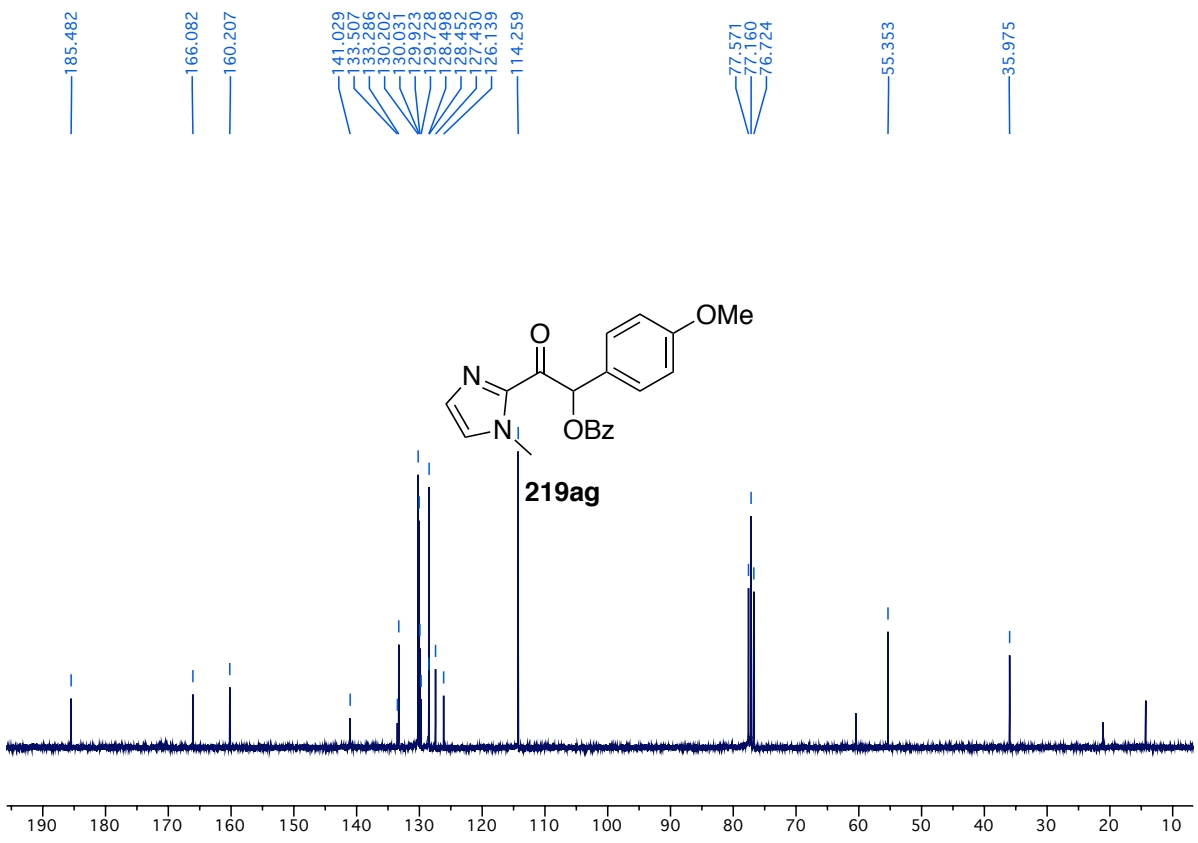

^{13}C-NMR spectrum of compound **219ag** (75.5 MHz, $CDCl_3$)

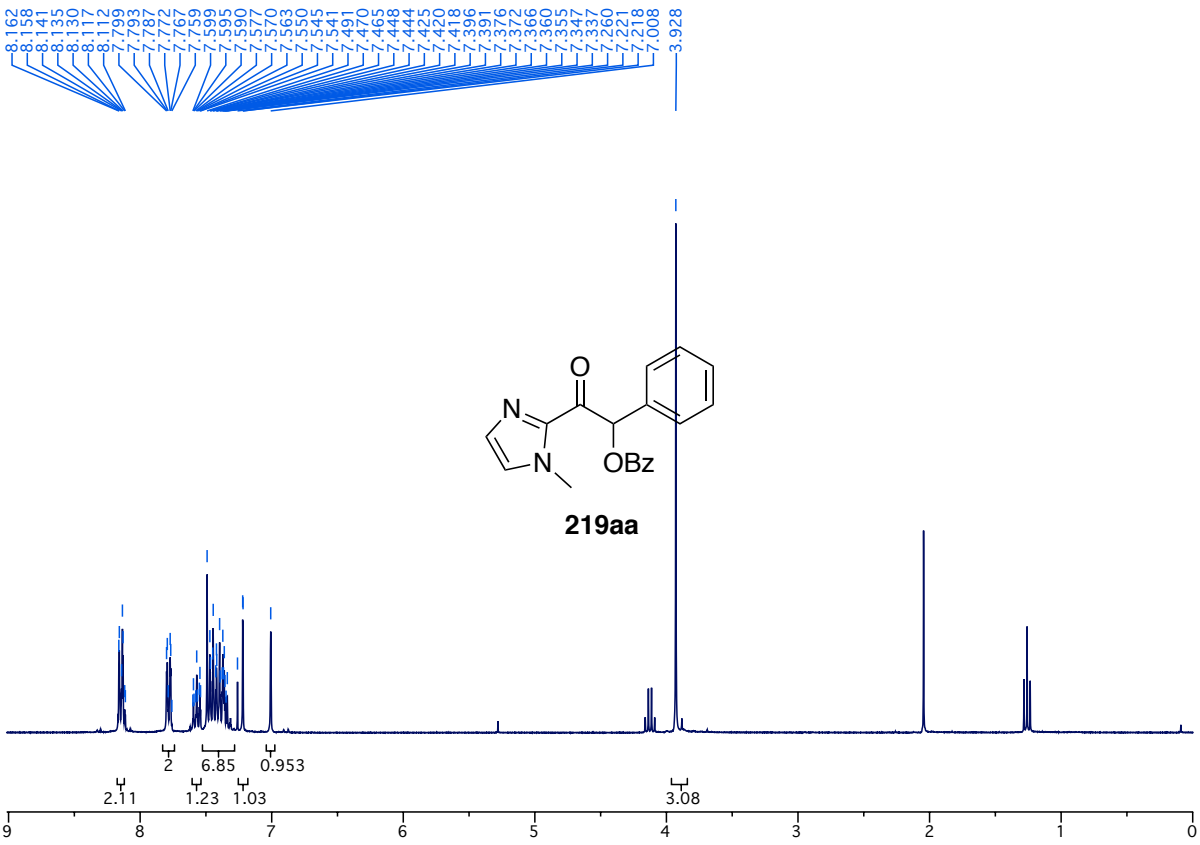

^{1}H-NMR spectrum of compound **219aa** (300 MHz, $CDCl_3$)

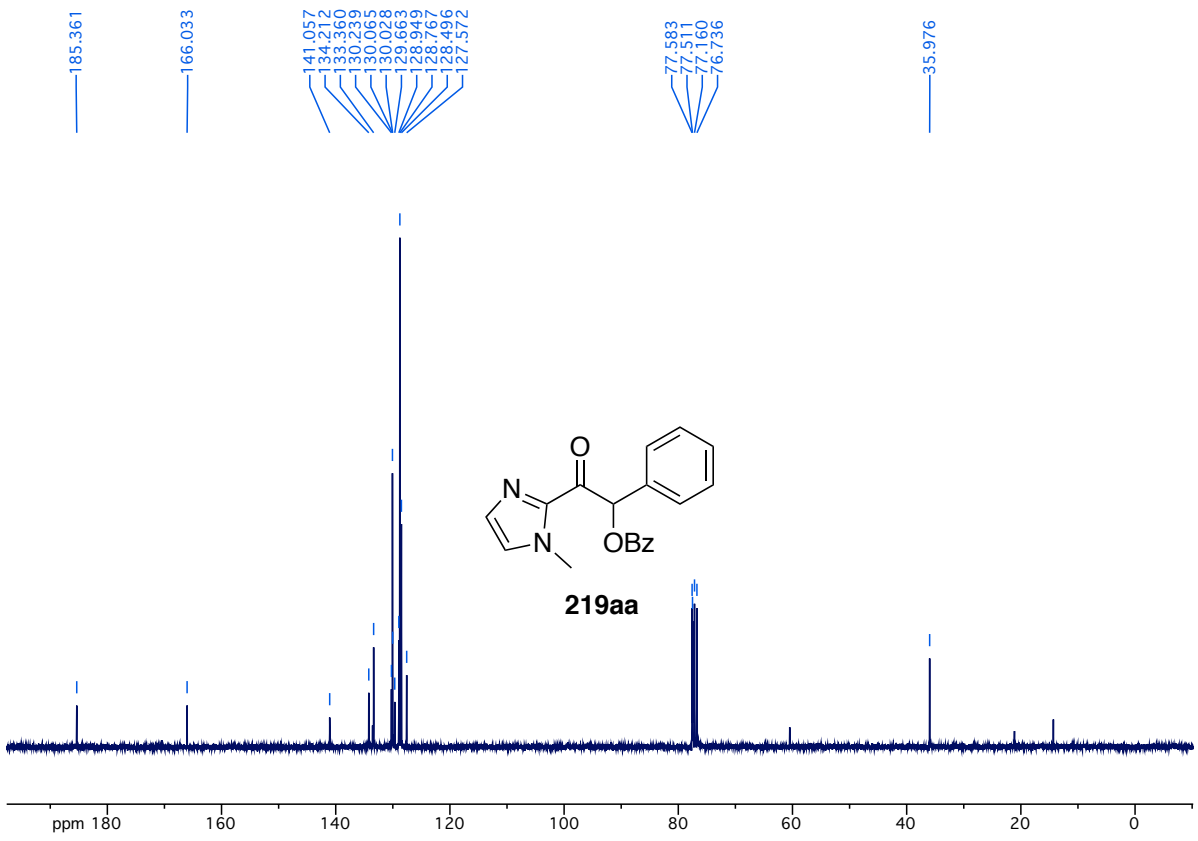

^{13}C-NMR spectrum of compound **219aa** (75.5 MHz, $CDCl_3$)

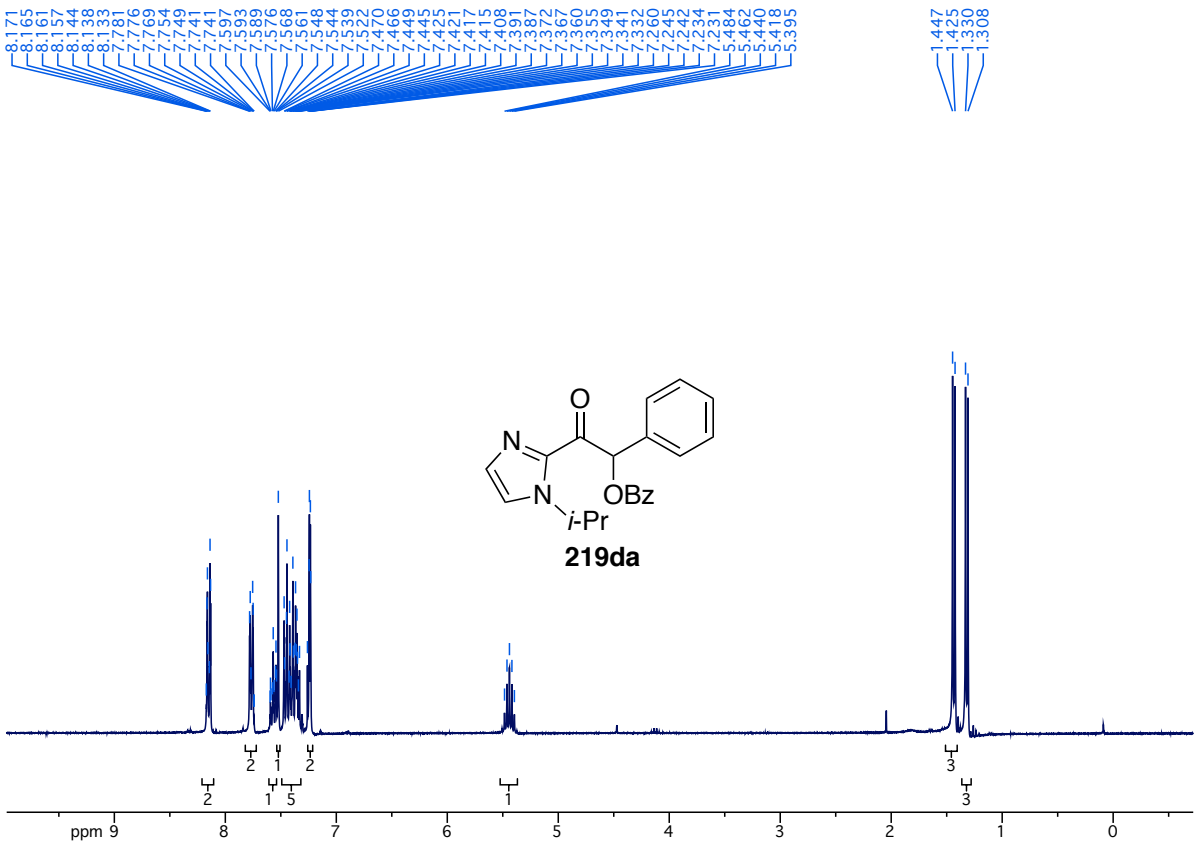

^{1}H-NMR spectrum of compound **219da** (300 MHz, $CDCl_3$)

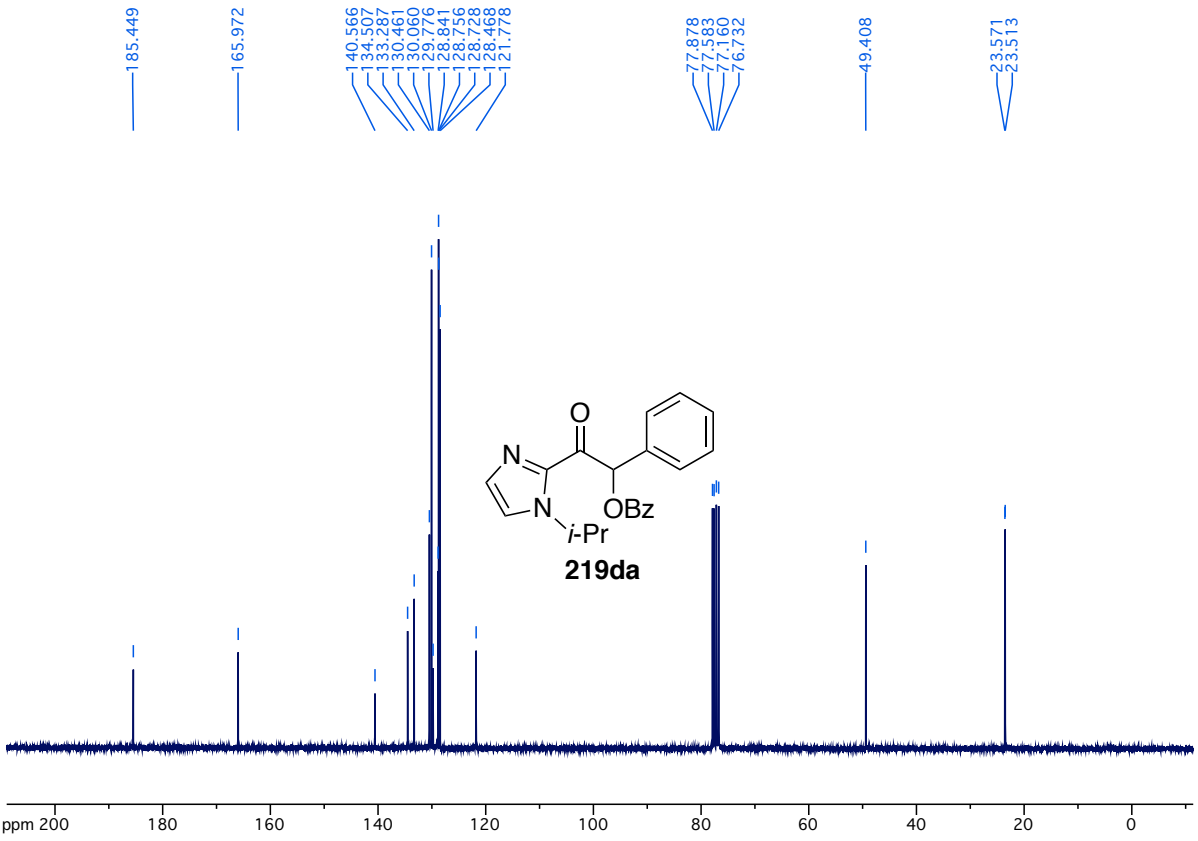

^{13}C-NMR spectrum of compound **219da** (75.5 MHz, $CDCl_3$)

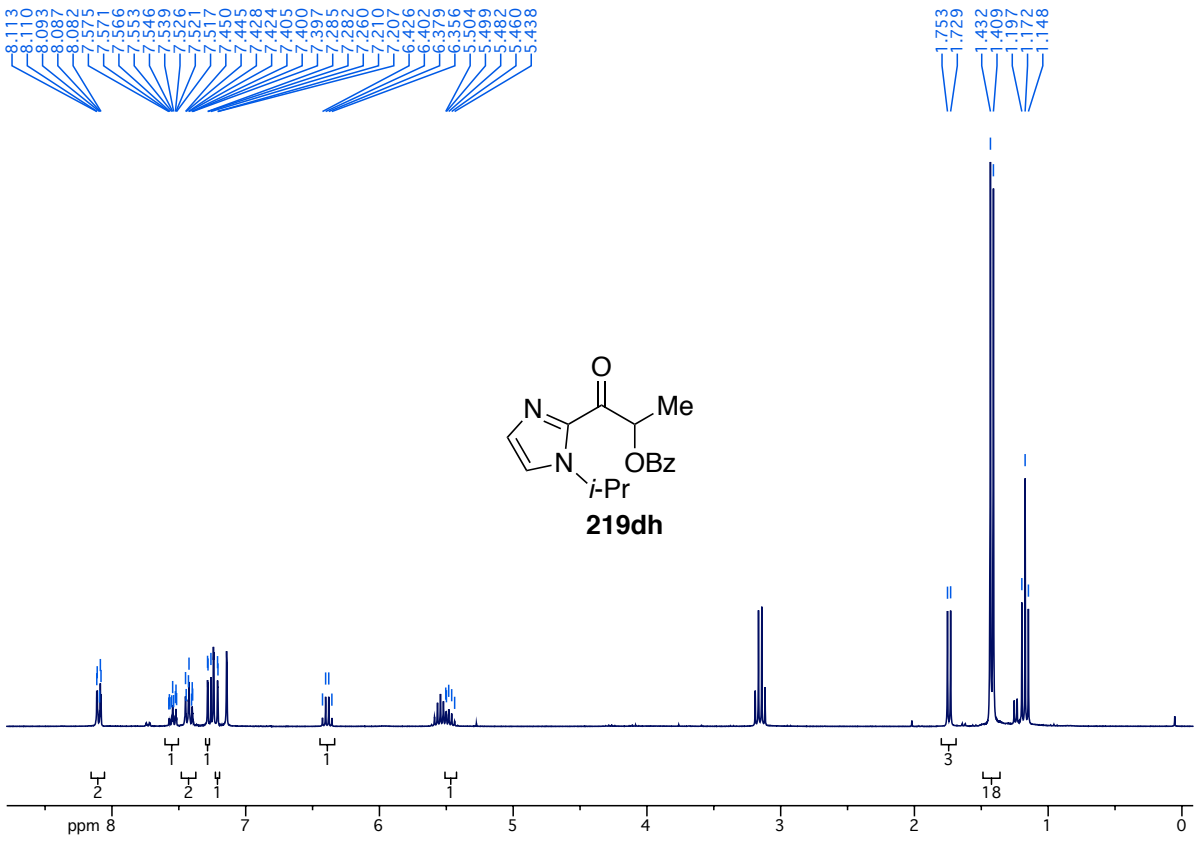

^{1}H-NMR spectrum of compound **219dh** (300 MHz, $CDCl_3$)

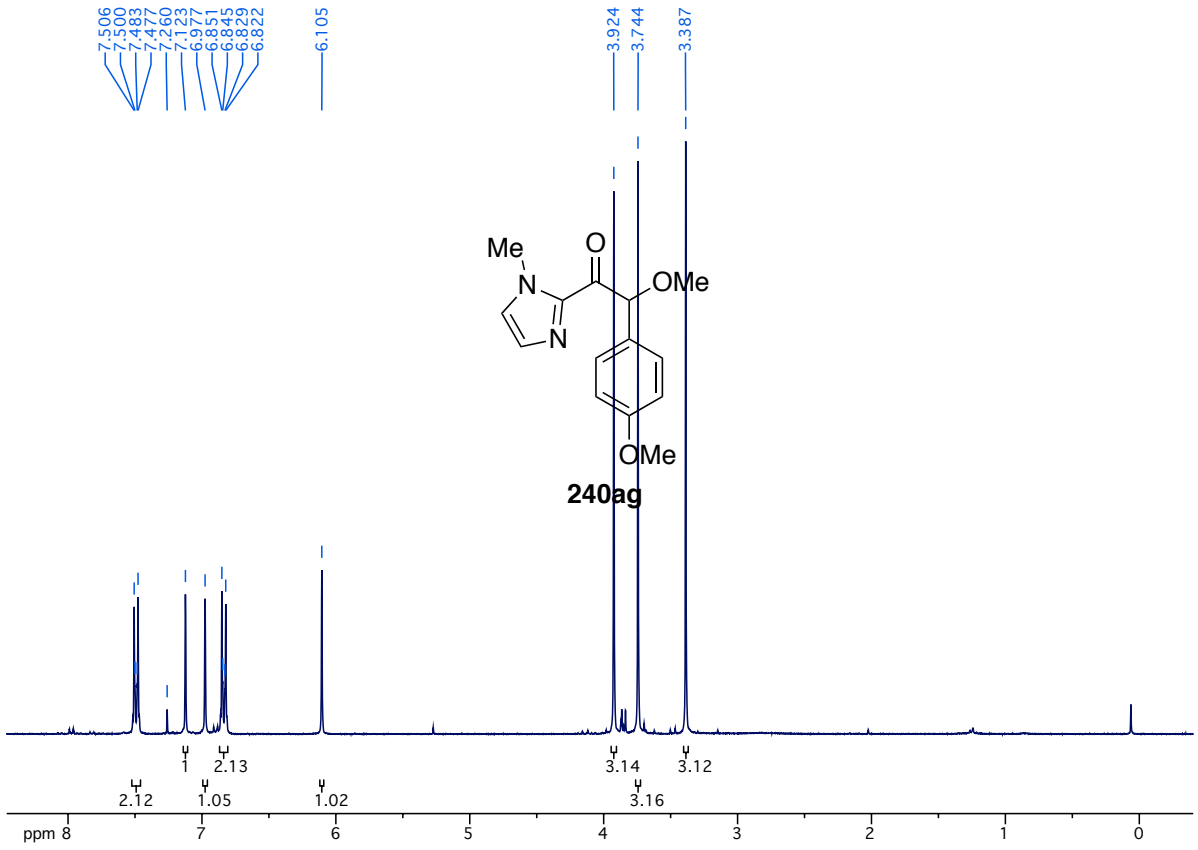

^{1}H-NMR spectrum of compound **240ag** (300 MHz, $CDCl_3$)

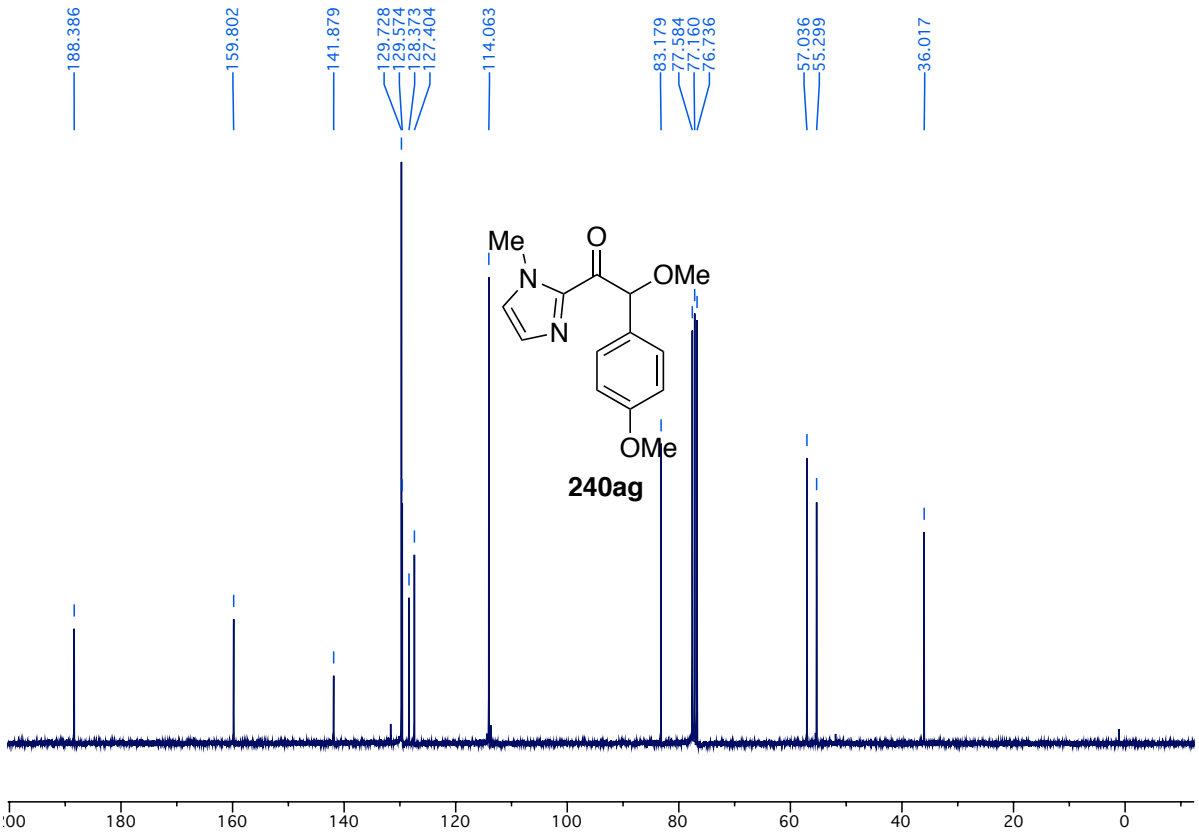

^{13}C-NMR spectrum of compound **240ag** (75.5 MHz, $CDCl_3$)

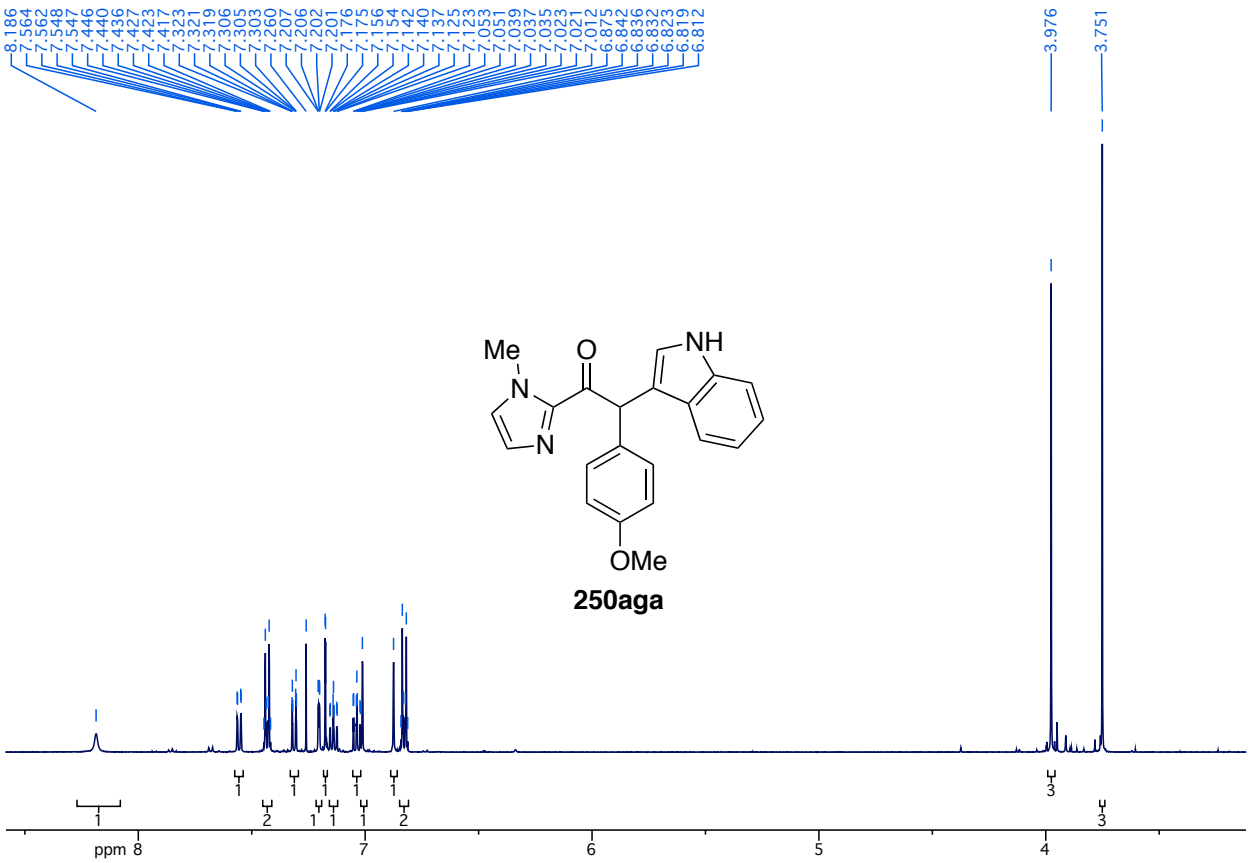

^{1}H-NMR spectrum of compound **250aga** (500 MHz, $CDCl_3$)

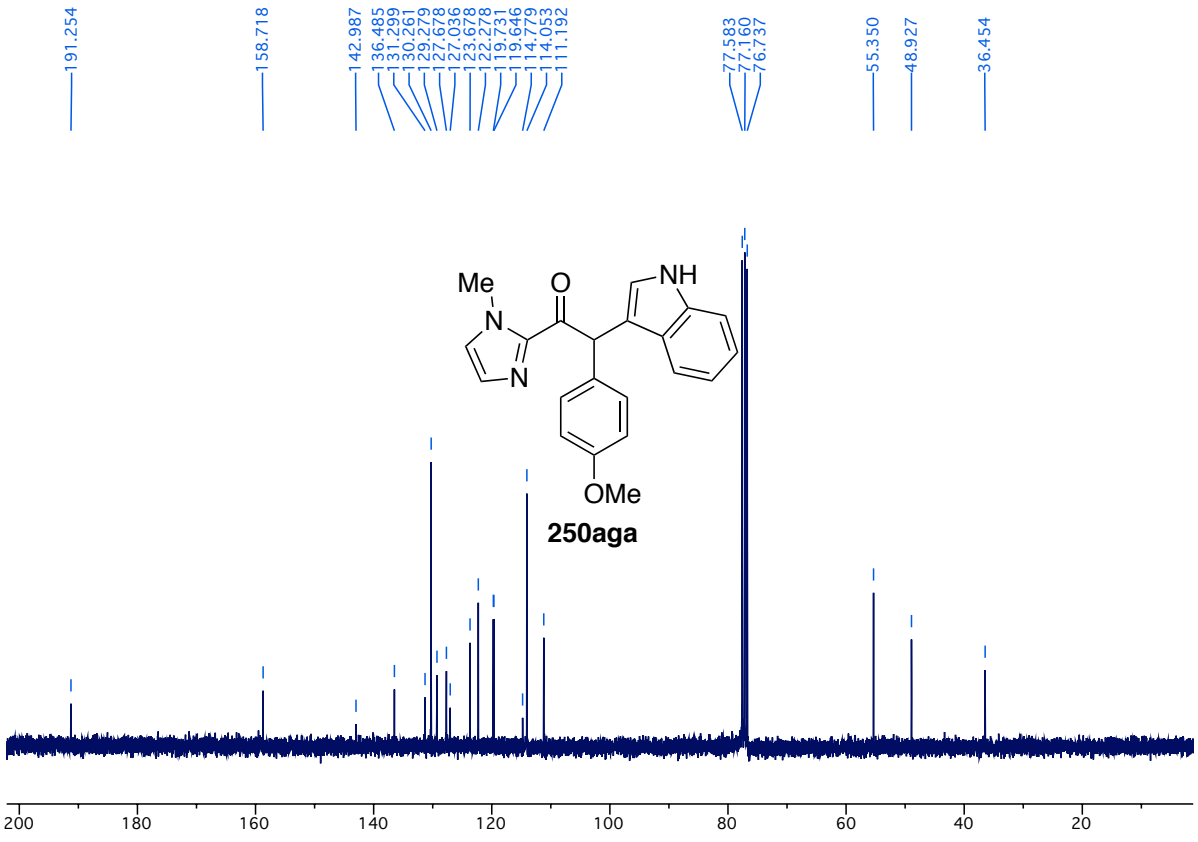

^{13}C-NMR spectrum of compound **250aga** (75.5 MHz, $CDCl_3$)

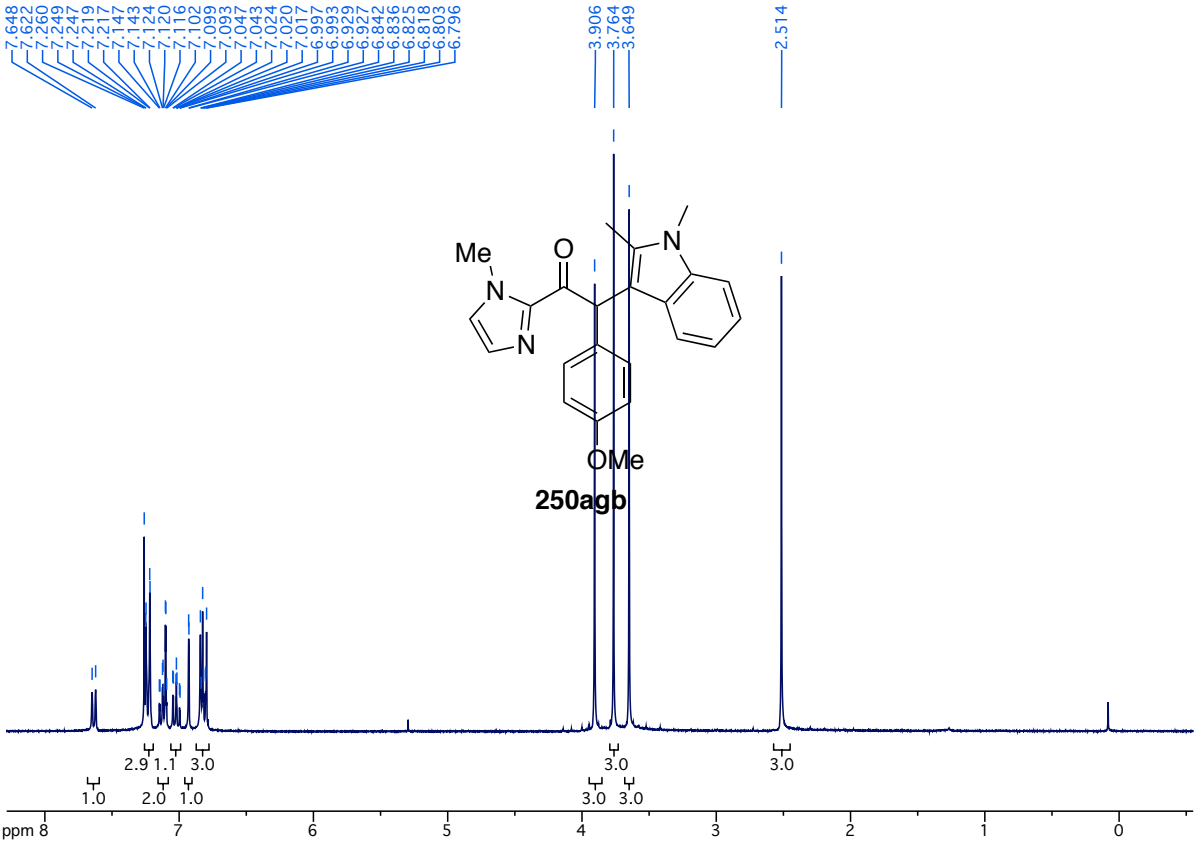

^{1}H-NMR spectrum of compound **250agb** (300 MHz, $CDCl_3$)

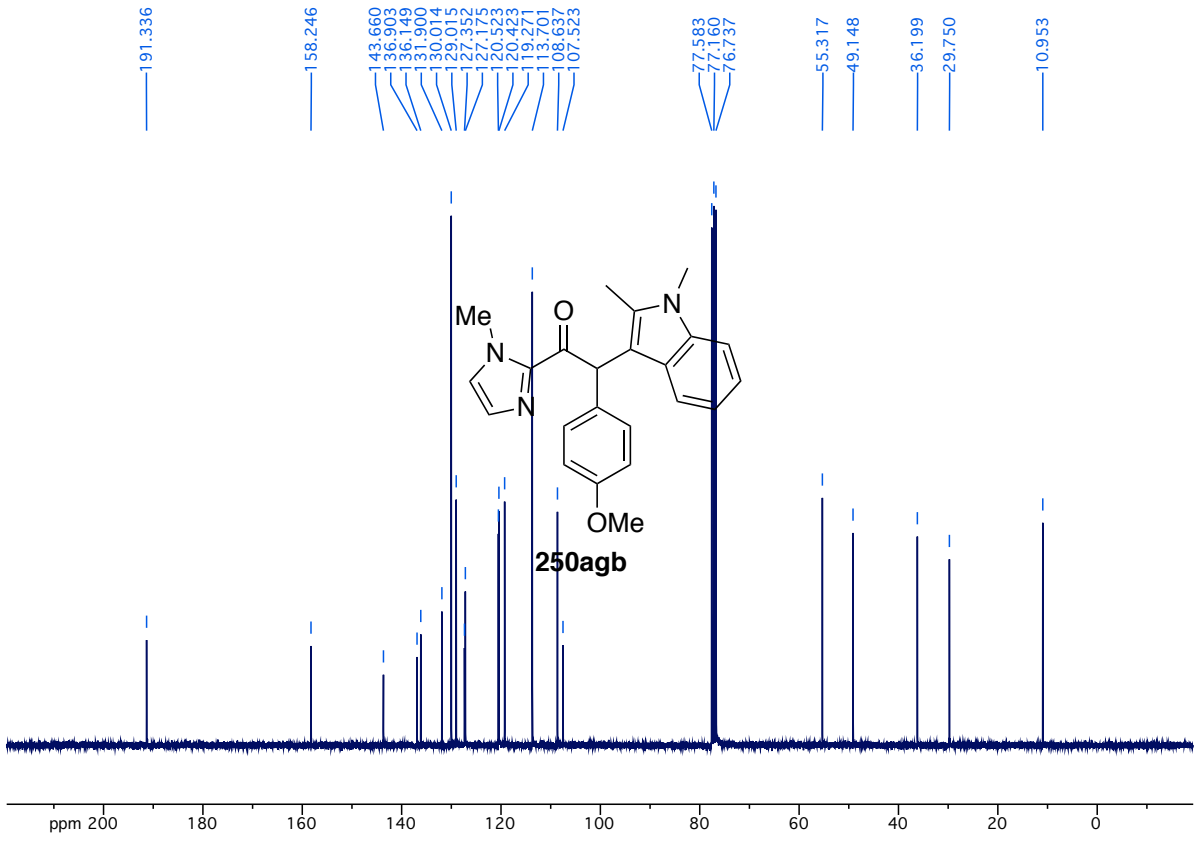

^{13}C-NMR spectrum of compound **250agb** (75.5 MHz, $CDCl_3$)

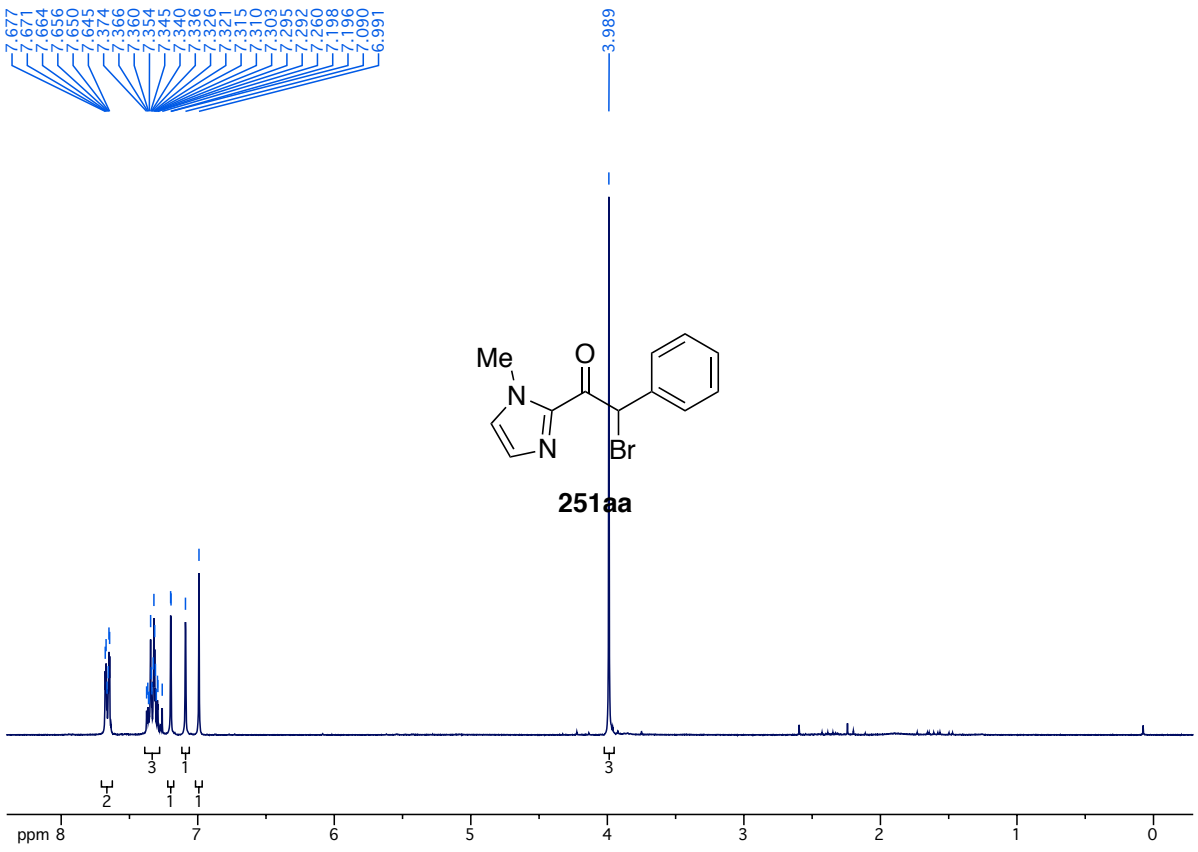

^{1}H-NMR spectrum of compound **251aa** (300 MHz, $CDCl_3$)

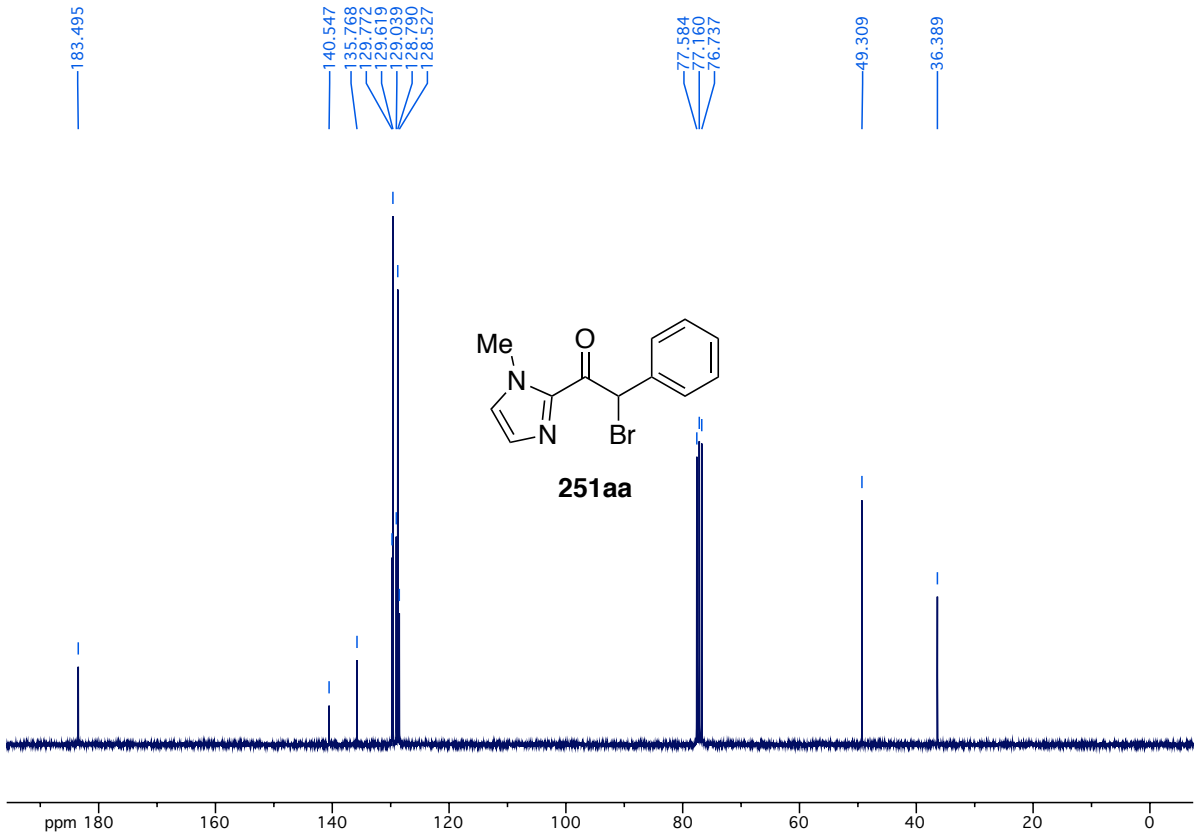

^{13}C-NMR spectrum of compound **251aa** (75.5 MHz, $CDCl_3$)

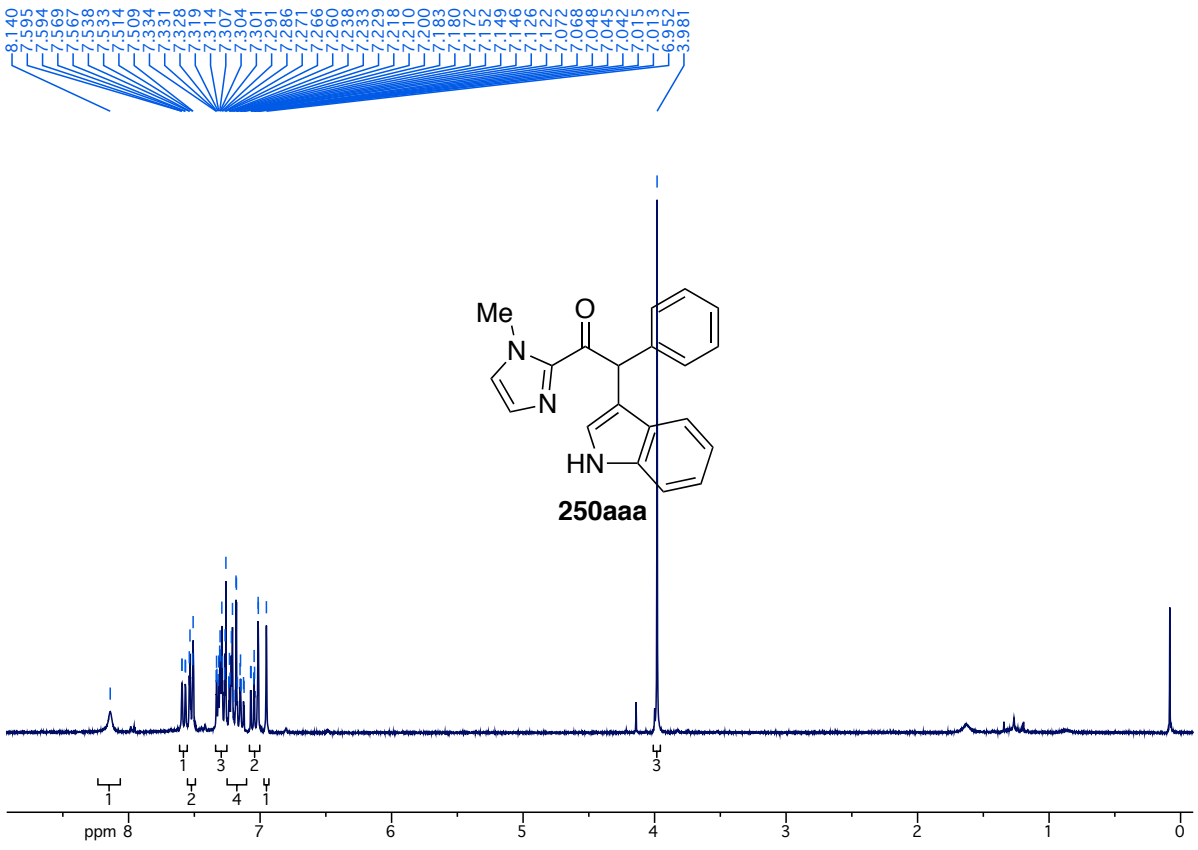

^{1}H-NMR spectrum of compound **250aaa** (300 MHz, $CDCl_3$)

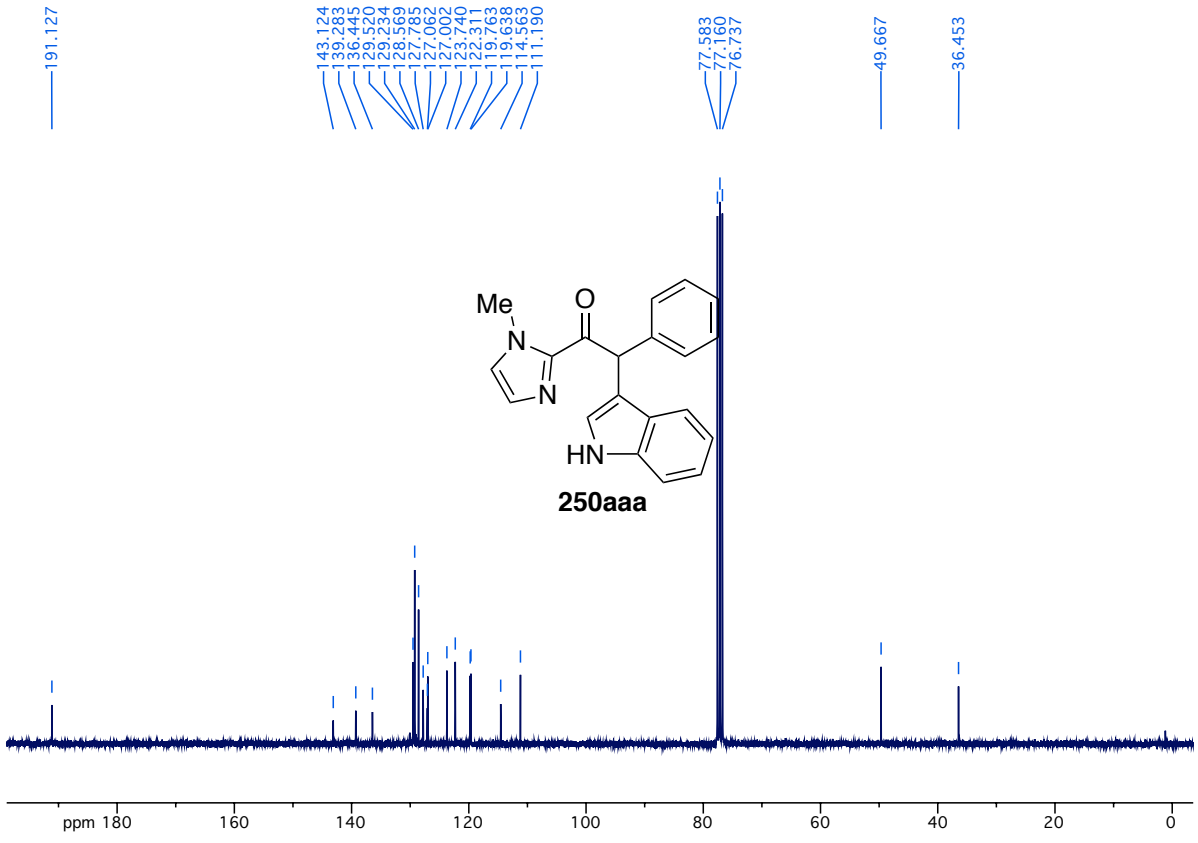

^{13}C-NMR spectrum of compound **250aaa** (75.5 MHz, $CDCl_3$)

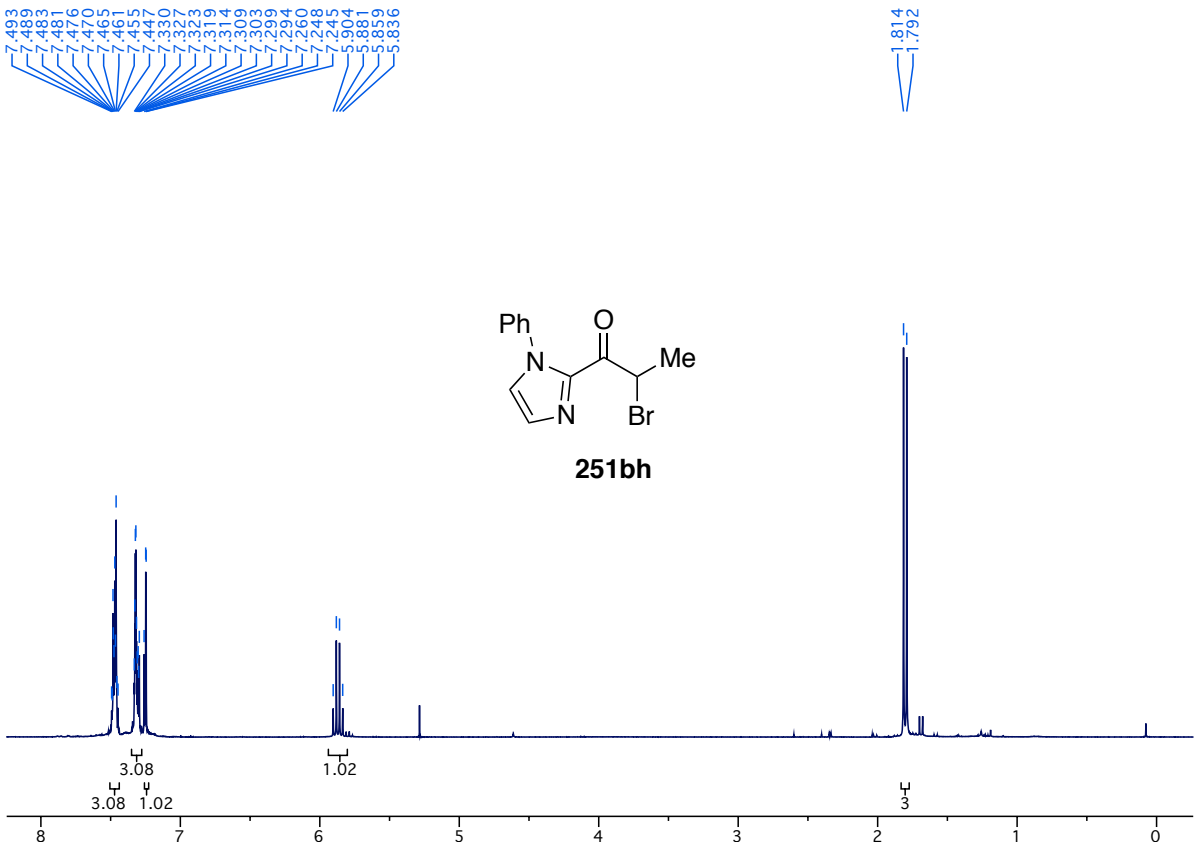

^{1}H-NMR spectrum of compound **251bh** (300 MHz, $CDCl_3$)

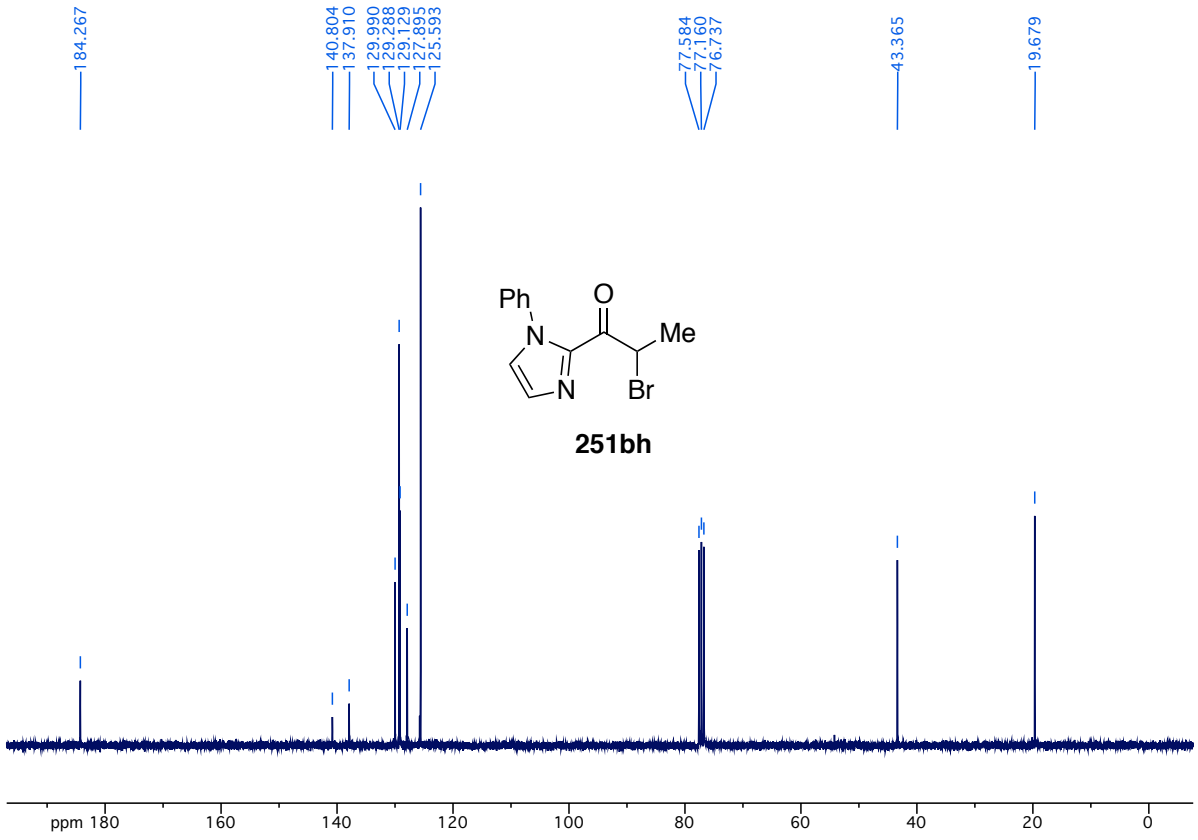

^{13}C-NMR spectrum of compound **251bh** (75.5 MHz, $CDCl_3$)

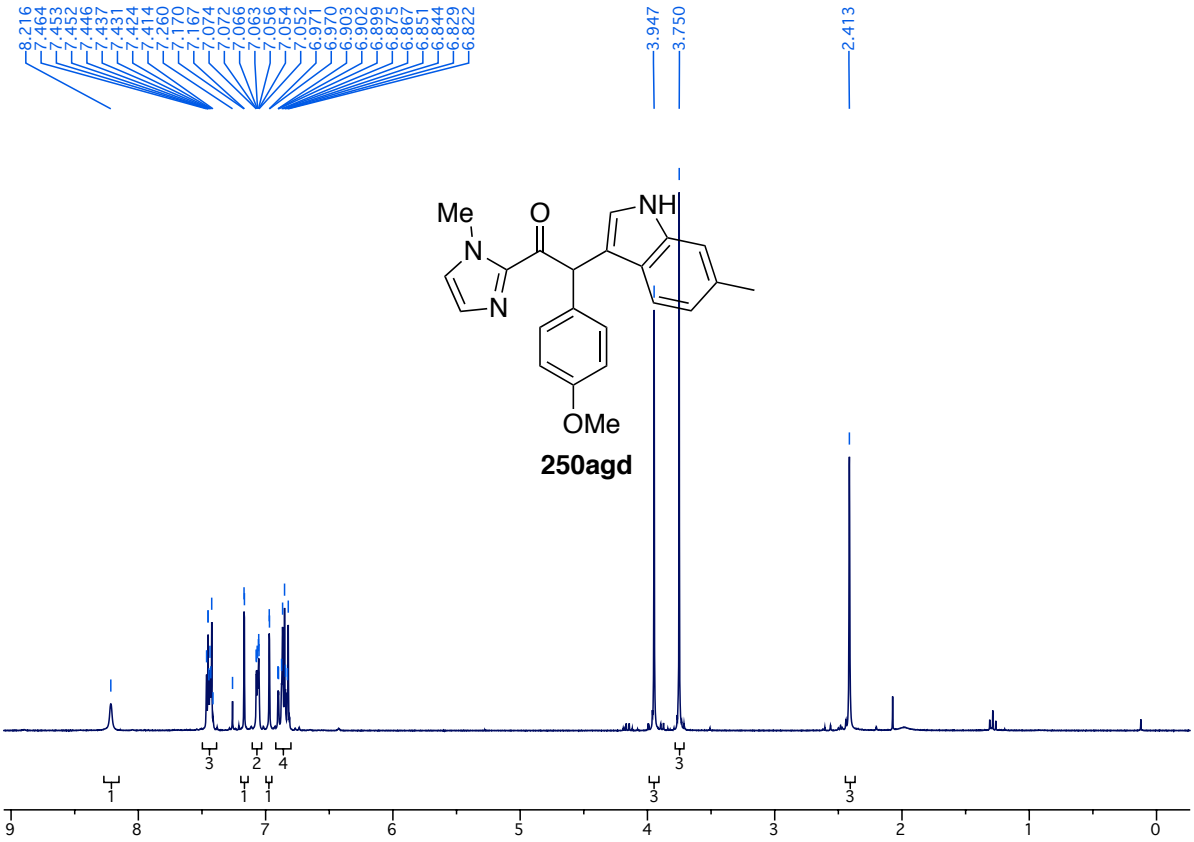

^{1}H-NMR spectrum of compound **250agd** (300 MHz, $CDCl_3$)

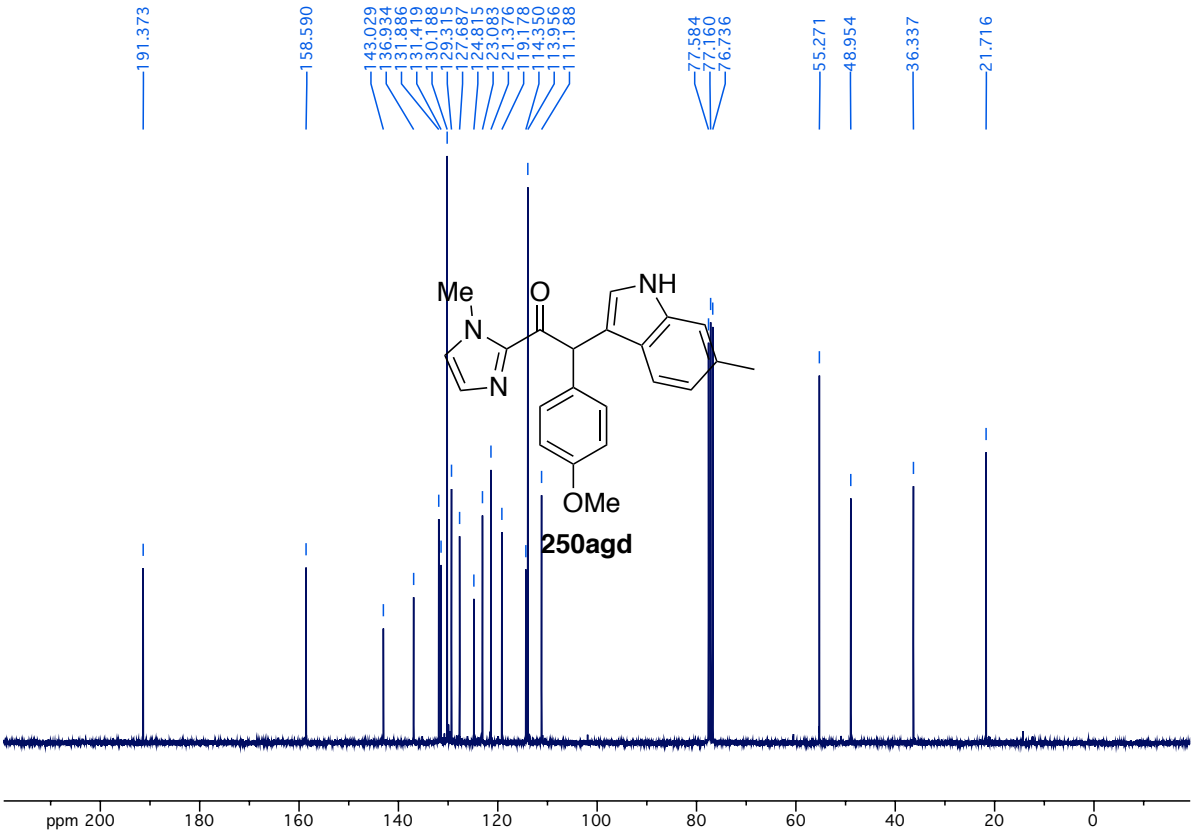

^{13}C-NMR spectrum of compound **250agd** (75.5 MHz, $CDCl_3$)

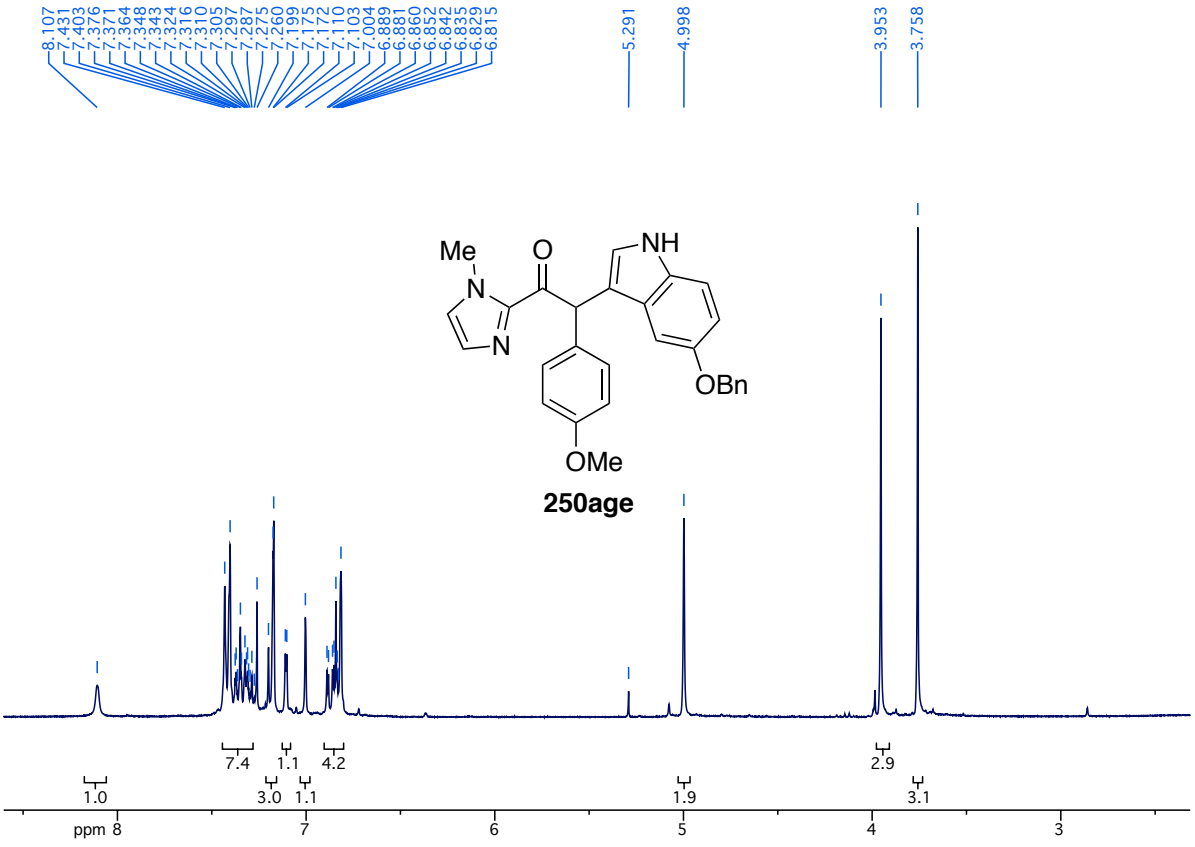

^{1}H-NMR spectrum of compound **250age** (300 MHz, $CDCl_3$)

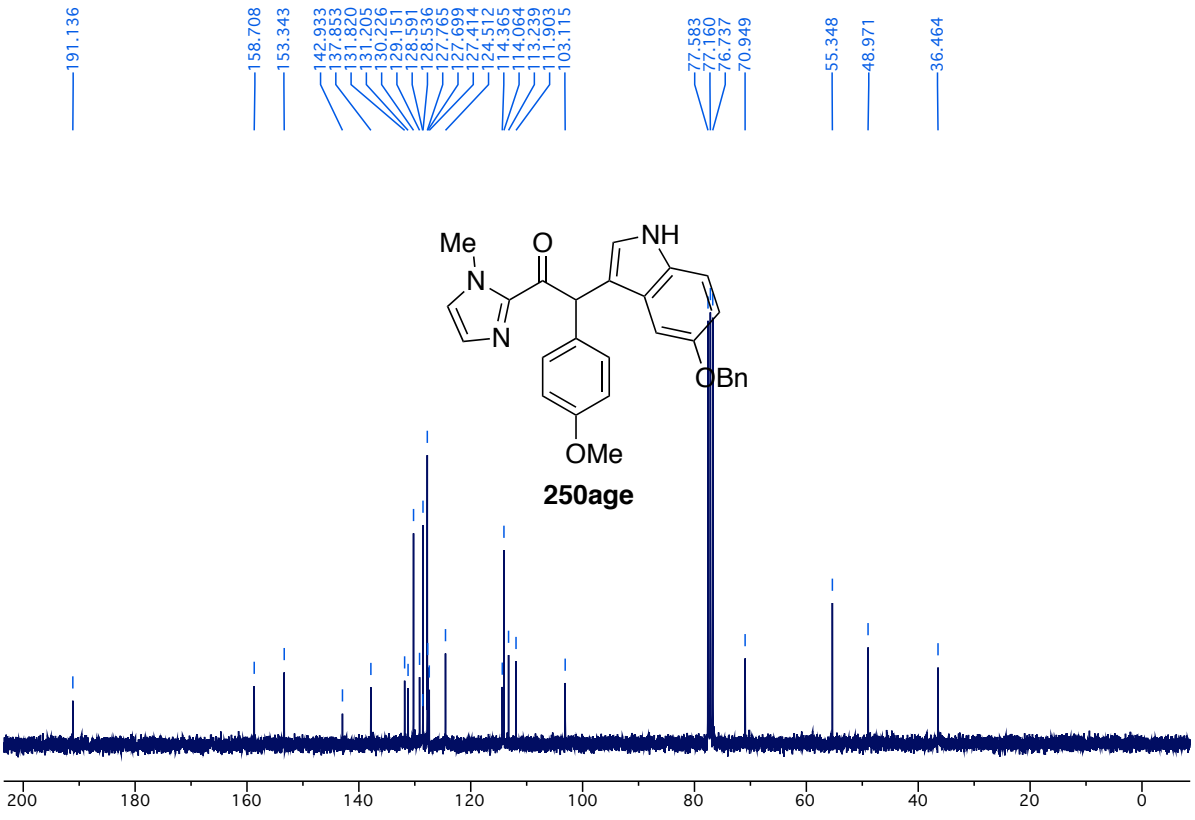

^{13}C-NMR spectrum of compound **250age** (75.5 MHz, $CDCl_3$)

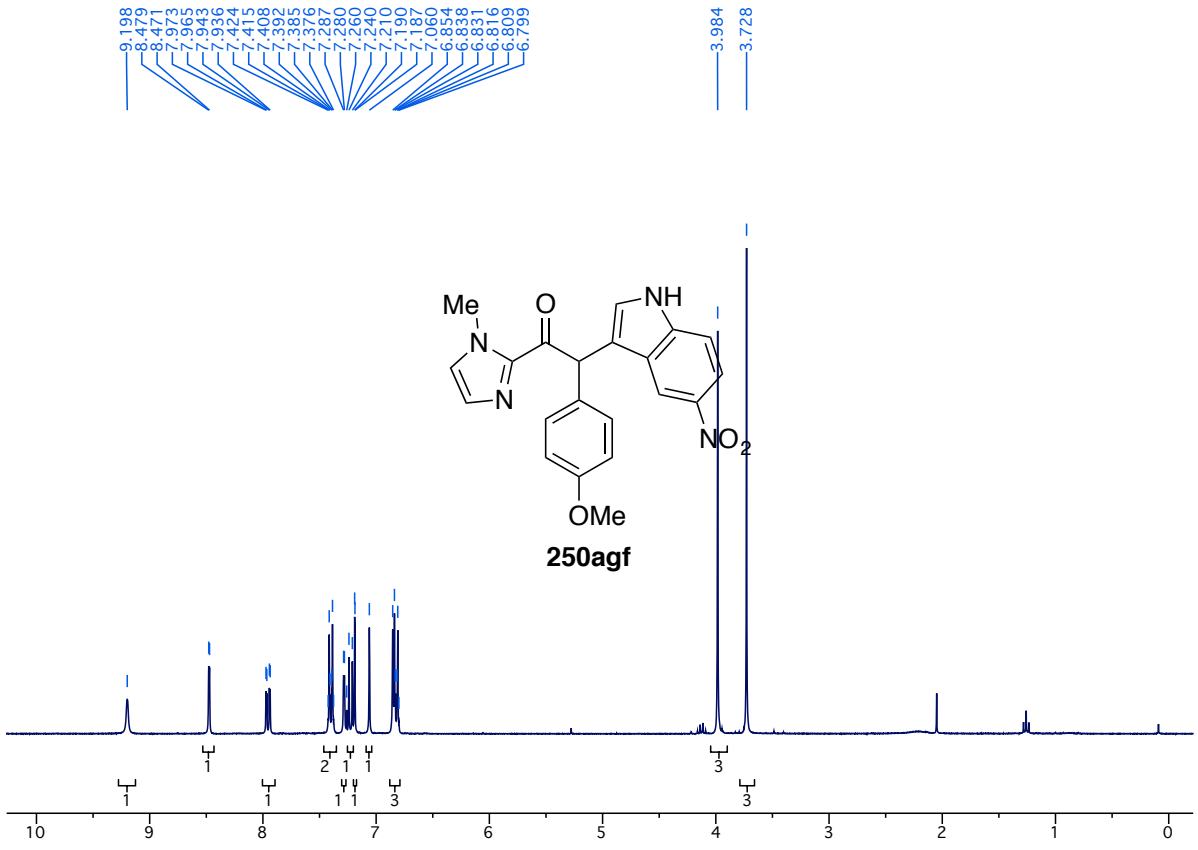

^{1}H-NMR spectrum of compound **250agf** (300 MHz, $CDCl_3$)

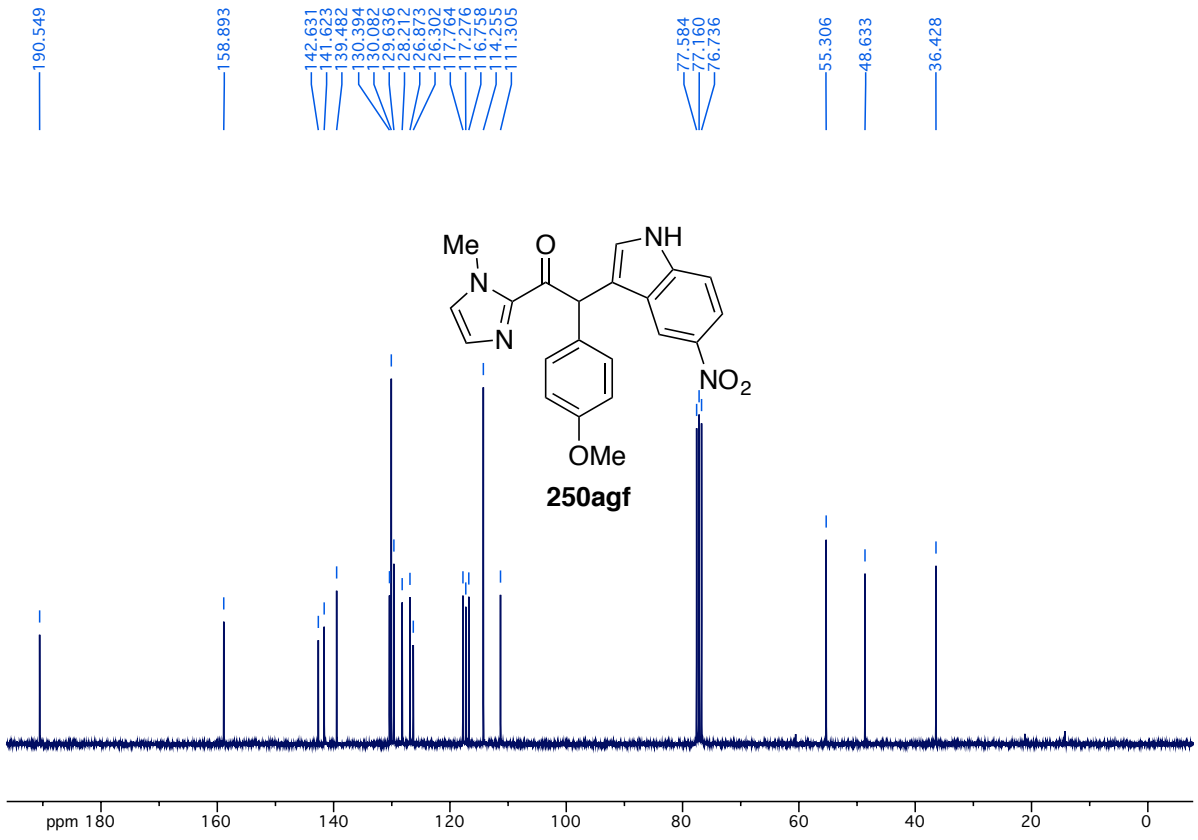

^{13}C-NMR spectrum of compound **250agf** (75.5 MHz, $CDCl_3$)

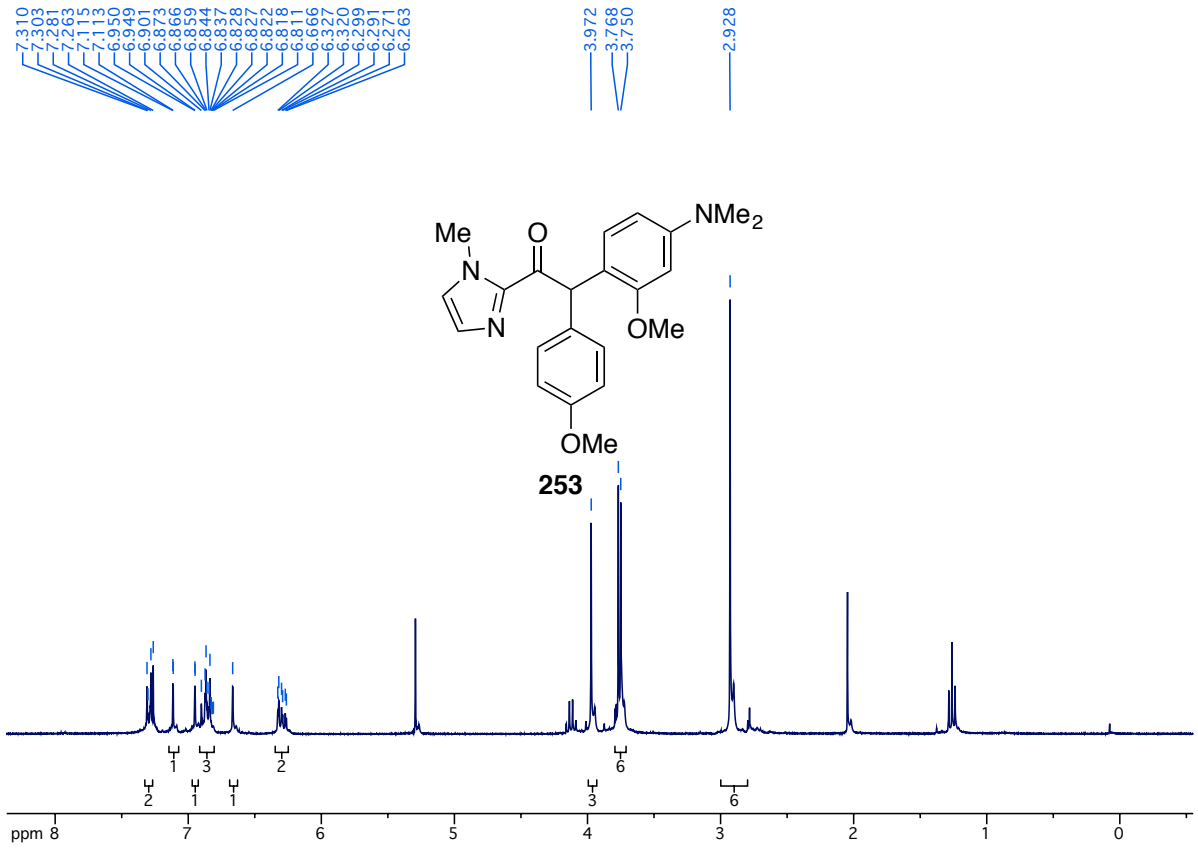

^{1}H-NMR spectrum of compound **253** (300 MHz, $CDCl_3$)

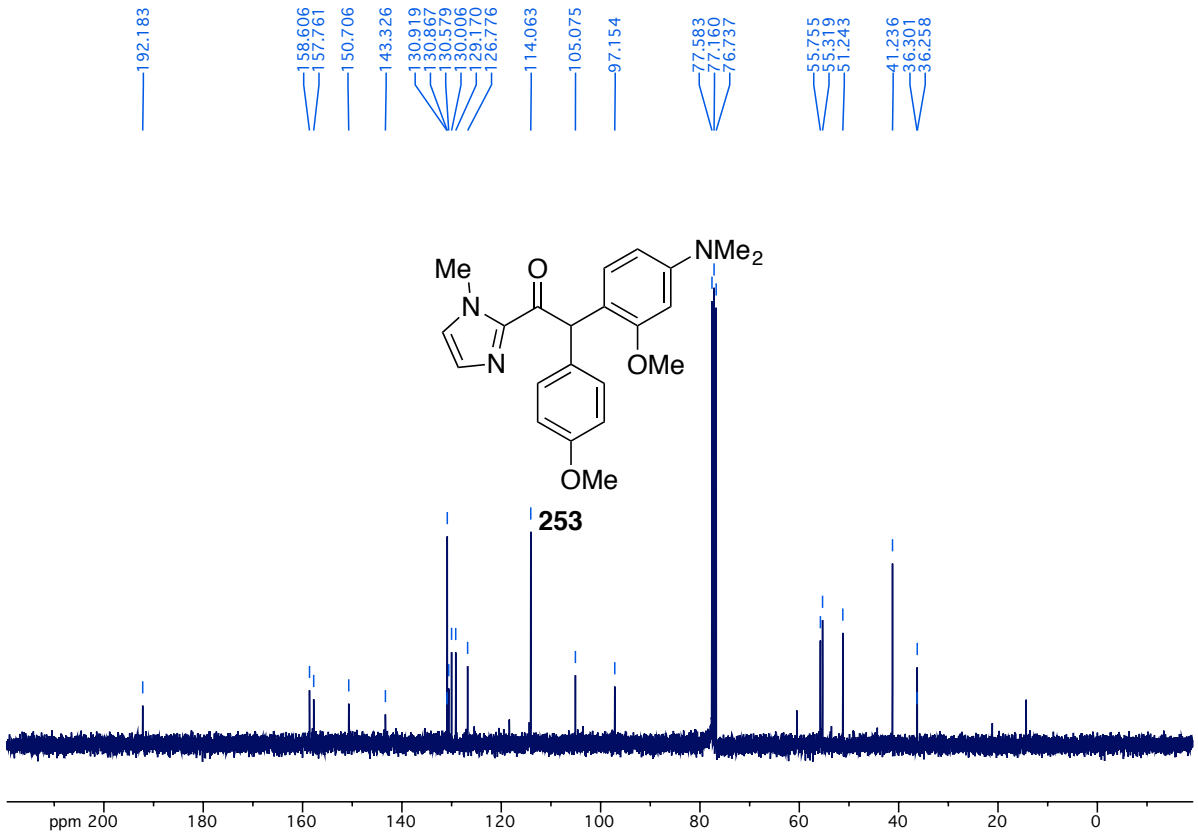

^{13}C-NMR spectrum of compound **253** (75.5 MHz, $CDCl_3$)

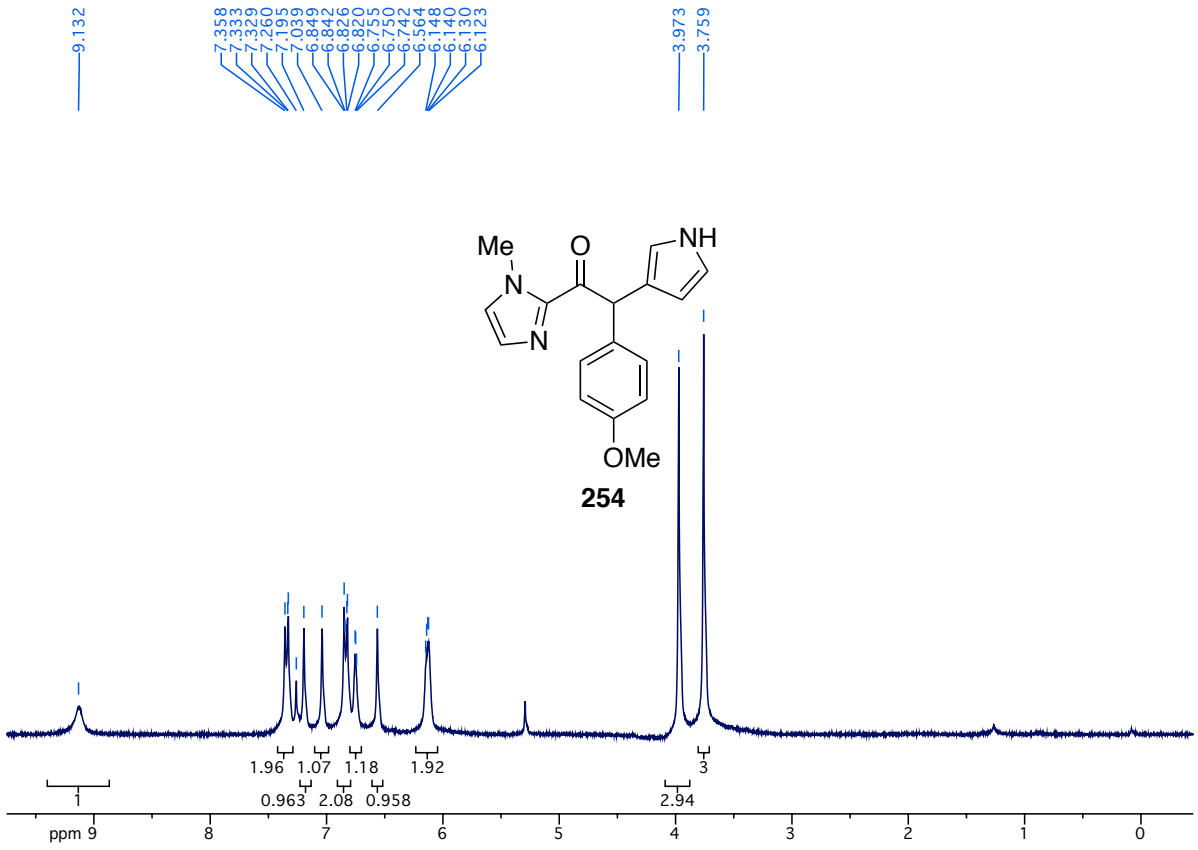

^{1}H-NMR spectrum of compound **254** (300 MHz, $CDCl_3$)

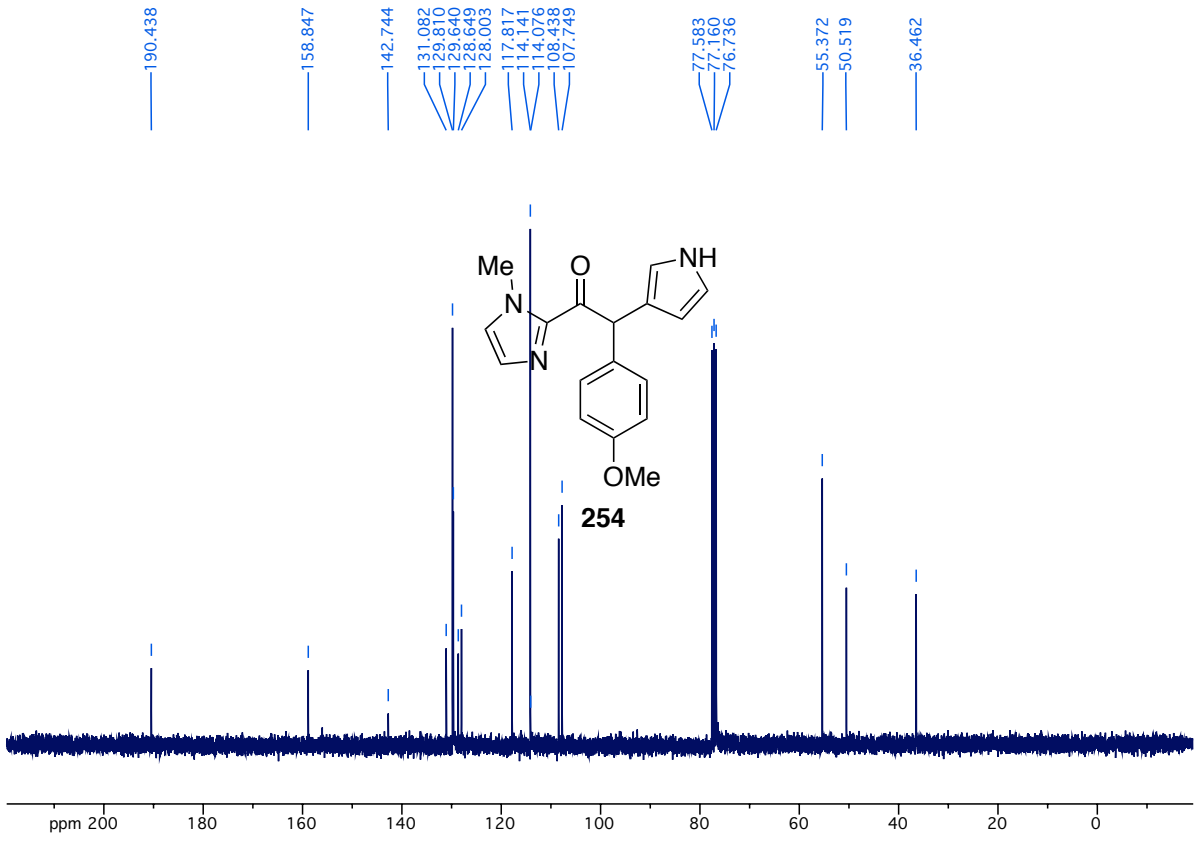

^{13}C-NMR spectrum of compound **254** (75.5 MHz, $CDCl_3$)

7.2. HPLC-Traces

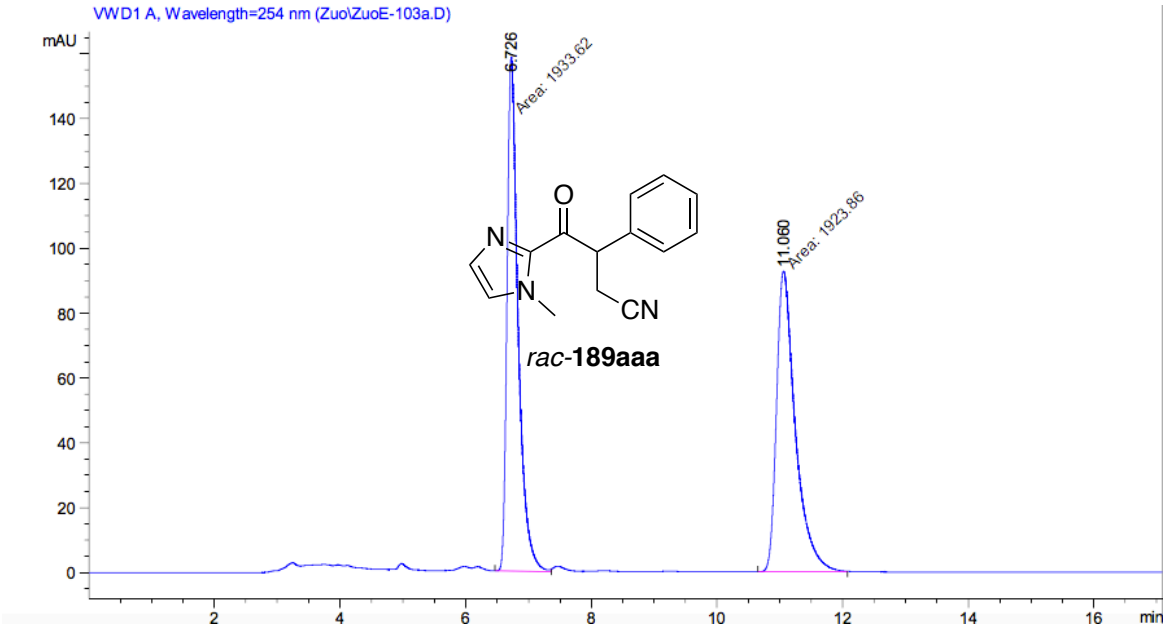

Peak #	Ret Time [min]	Type	Width [min]	Area [mAU*s]	Height [mAU]	Area %
1	6.726	MM	0.2034	1933.62366	158.43120	50.1266
2	11.060	MM	0.3458	1923.85645	92.72607	49.8734

HPLC chromatogram of compound *rac*-**189aaa**

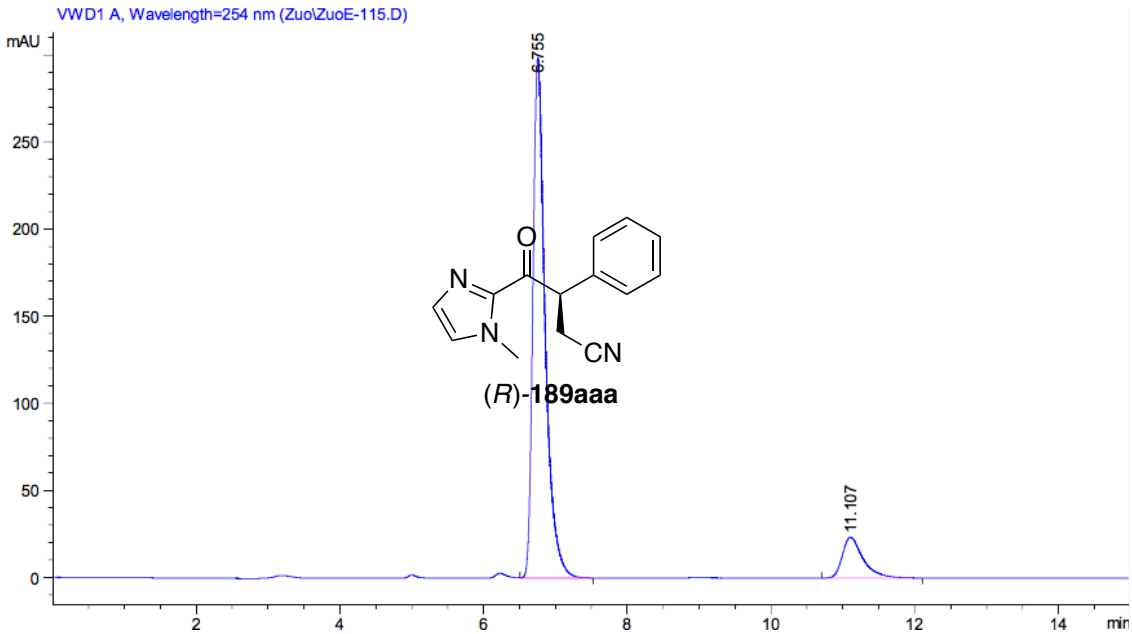

Peak #	Ret Time [min]	Type	Width [min]	Area [mAU*s]	Height [mAU]	Area %
1	6.755	VV R	0.1789	3540.64673	298.45129	88.2781
2	11.107	BB	0.2682	470.14124	23.47079	11.7219

HPLC chromatogram of compound (*R*)-**189aaa** with 77% *ee* (Table 4, entry 7, p.37)

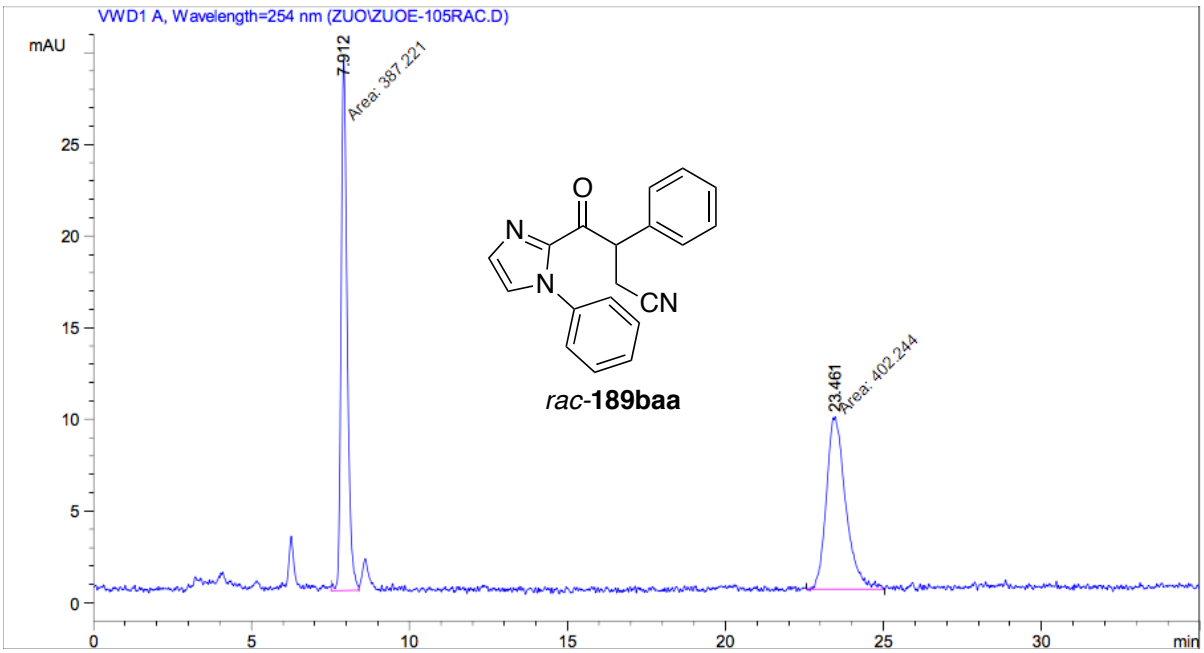

Peak #	RetTime [min]	Type	Width [min]	Area mAU *s	Height [mAU]	Area %
1	7.912	MF	0.2234	387.22104	28.89252	49.0486
2	23.461	MM	0.7115	402.24356	9.42225	50.9514

HPLC chromatogram of compound *rac*-**189baa**

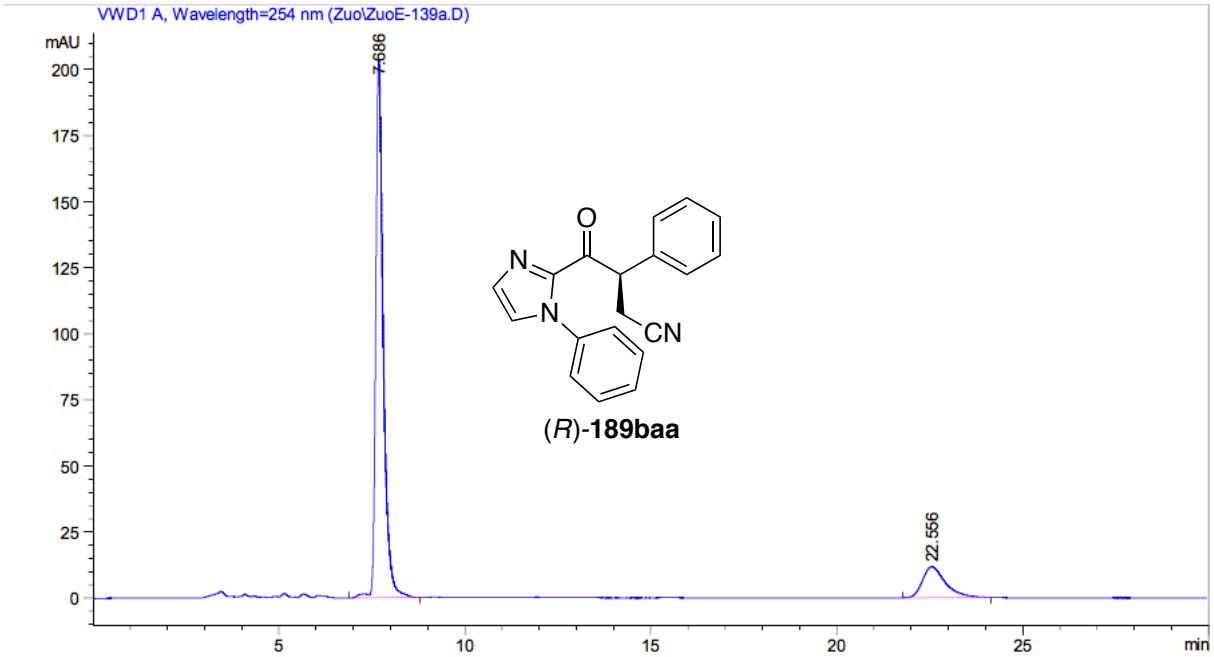

Peak #	Ret Time [min]	Type	Width [min]	Area [mAU*s]	Height [mAU]	Area %
1	7.686	VB R	0.2086	2854.84790	203.57301	84.9599
2	22.556	BB	0.5043	505.38196	11.76247	15.0401

HPLC chromatogram of (*R*)-**189baa** with 70% *ee* (Table 6, entry 3, p.40)

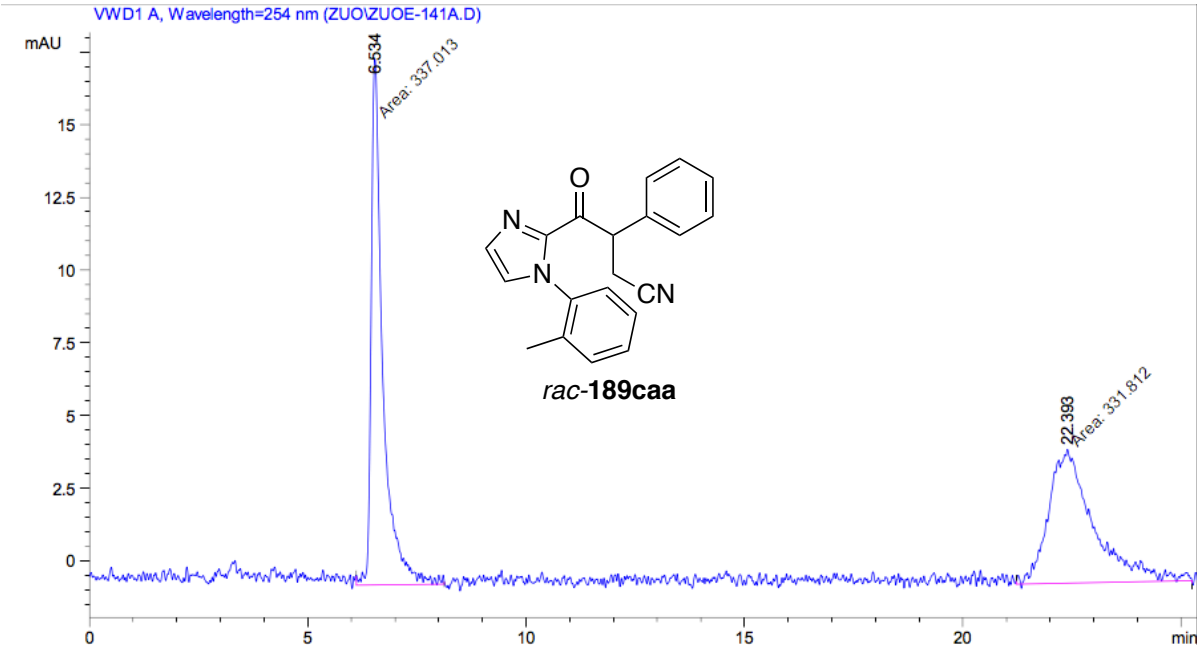

rac-**189caa**

Peak #	RetTime [min]	Type	Width [min]	Area mAU *s	Height [mAU]	Area %
1	6.534	MM	0.3102	337.01328	18.10982	50.3888
2	22.393	MM	1.2005	331.81244	4.60669	49.6112

HPLC chromatogram of compound *rac*-**189caa**

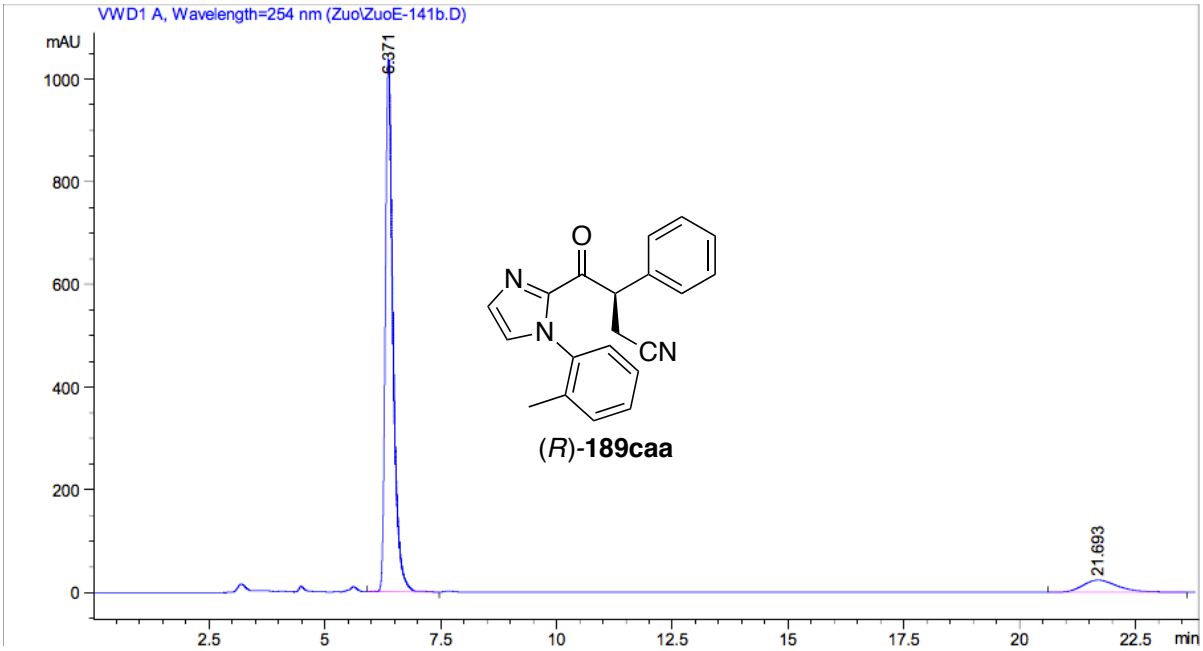

(*R*)-**189caa**

Peak #	Ret Time [min]	Type	Width [min]	Area [mAU*s]	Height [mAU]	Area %
1	6.371	VV R	0.1736	1.20336e4	1037.57532	90.3579
2	21.693	BB	0.6251	1284.09814	24.02547	9.6421

HPLC chromatogram of compound (*R*)-**189caa** with 80% *ee* (Table 6, entry 7, p.40)

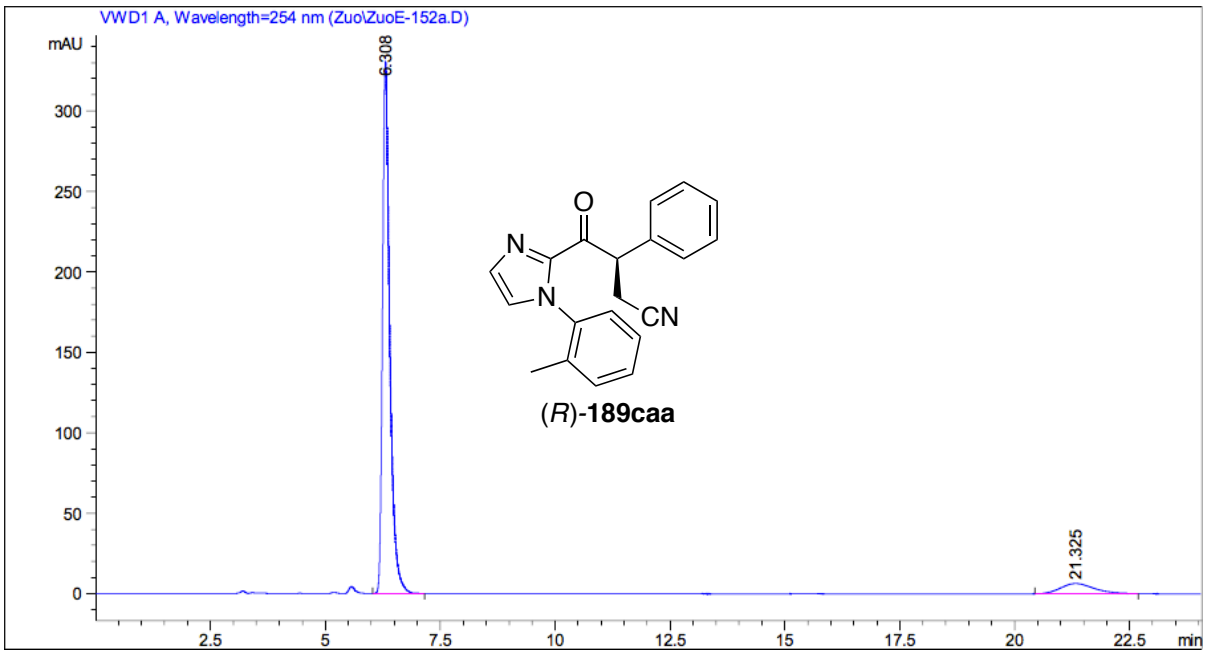

Peak #	Ret Time [min]	Type	Width [min]	Area [mAU*s]	Height [mAU]	Area %
1	6.308	BV R	0.1621	3628.15723	330.49603	91.8799
2	21.325	BB	0.5961	320.64664	6.31274	8.1201

HPLC chromatogram of compound (*R*)-**189caa** with 84% *ee* (Table 6, entry 8, p.40)

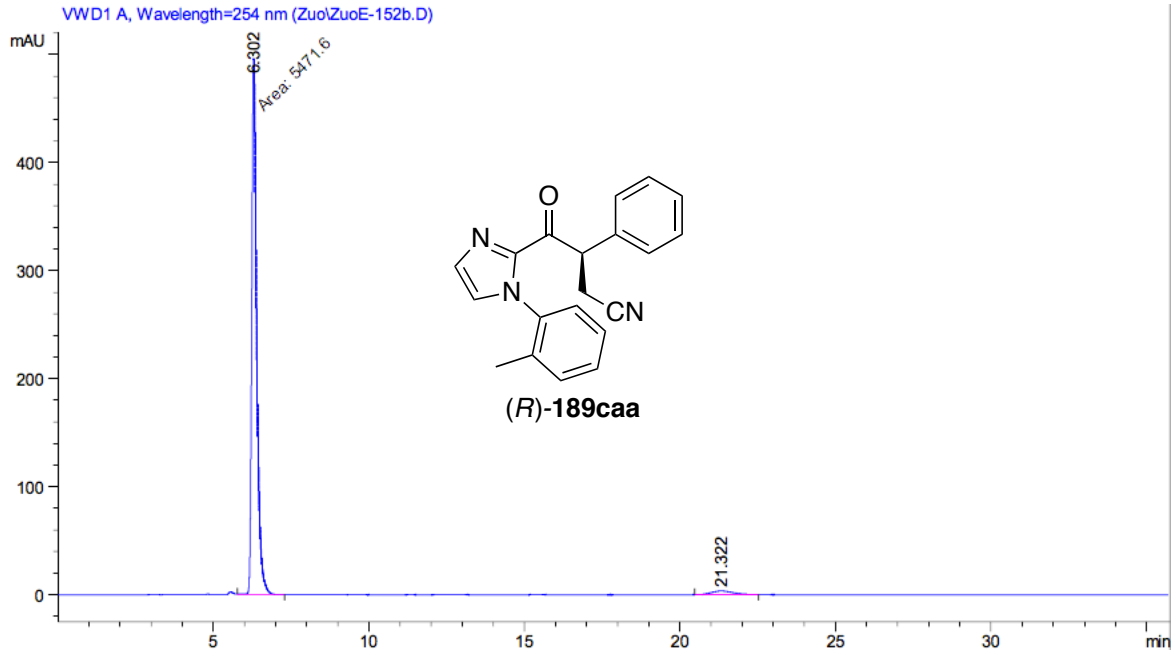

Peak #	Ret Time [min]	Type	Width [min]	Area [mAU*s]	Height [mAU]	Area %
1	6.302	MM	0.1839	5471.59912	496.00711	97.0159
2	21.322	BB	0.5849	168.29779	3.36577	2.9841

HPLC chromatogram of compound (*R*)-**189caa** with 94% *ee* (Table 6, entry 9, p.40)

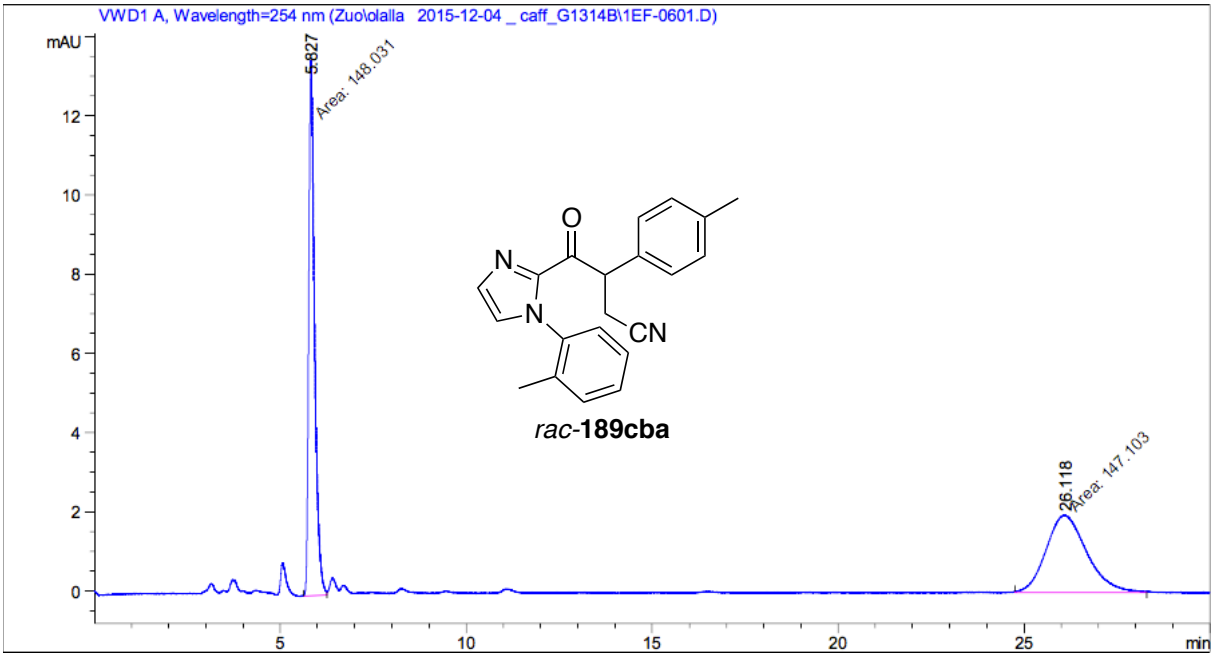

Peak #	Ret Time [min]	Type	Width [min]	Area [mAU*s]	Height [mAU]	Area %
1	5.827	MF	0.1825	148.03052	13.51754	50.1571
2	26.118	MM	1.2575	147.10342	1.94965	49.8429

HPLC chromatogram of compound *rac*-**189cba** (Table 7, entry 1, p.41)

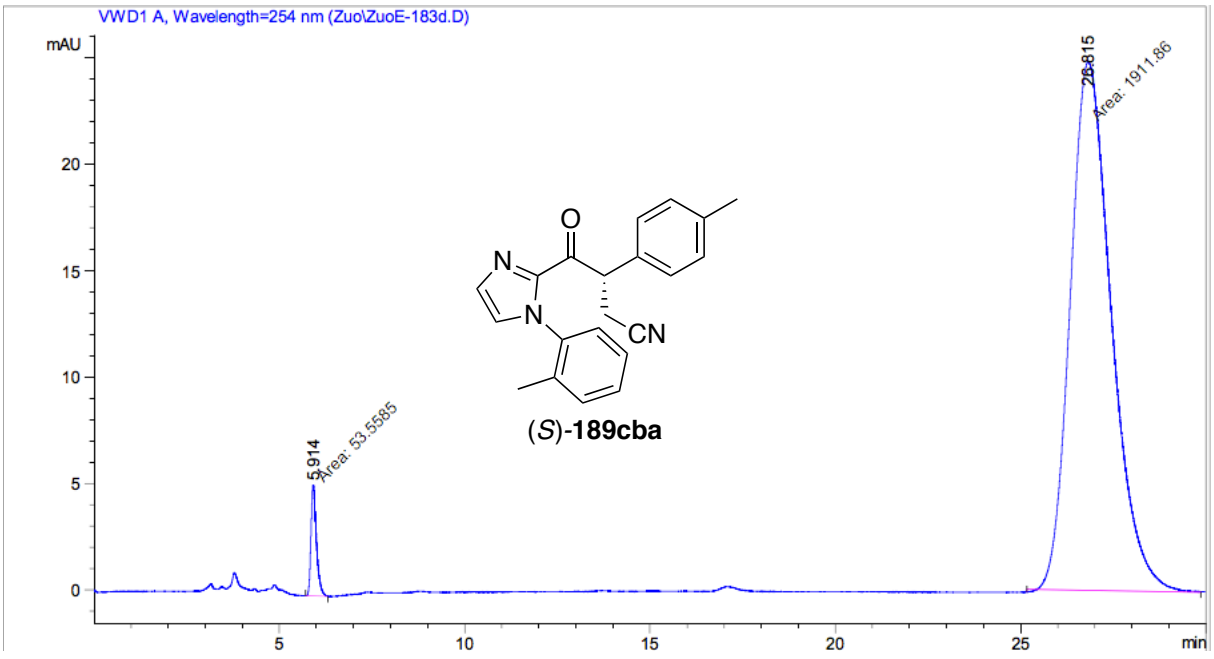

Peak #	Ret Time [min]	Type	Width [min]	Area [mAU*s]	Height [mAU]	Area %
1	5.914	MM	0.1706	53.55853	5.23369	2.7250
2	26.815	MM	1.2825	1911.86218	24.84499	97.2750

HPLC chromatogram of compound (*S*)-**189cba** with 95% *ee* (Table 7, entry 1, p.41)

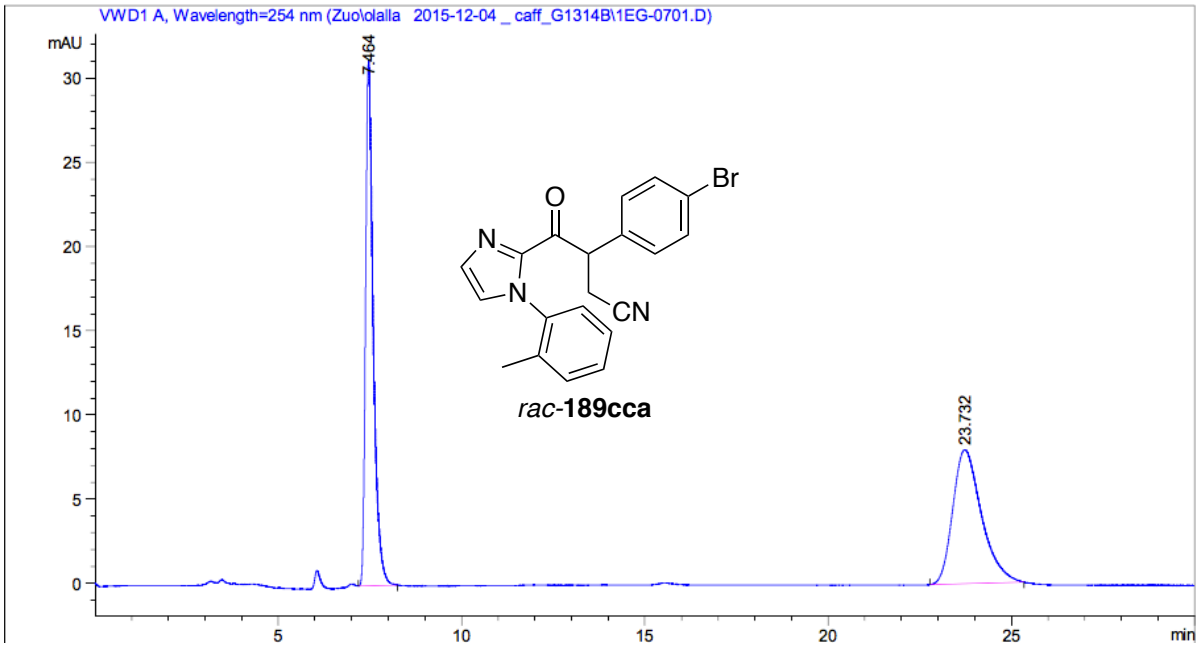

Peak #	Ret Time [min]	Type	Width [min]	Area [mAU*s]	Height [mAU]	Area %
1	7.464	BB	0.2105	453.50928	31.21653	51.0998
2	23.732	BB	0.6367	433.98874	7.97672	48.9002

HPLC chromatogram of compound *rac*-**189cca** (Table 7, entry 2, p.41)

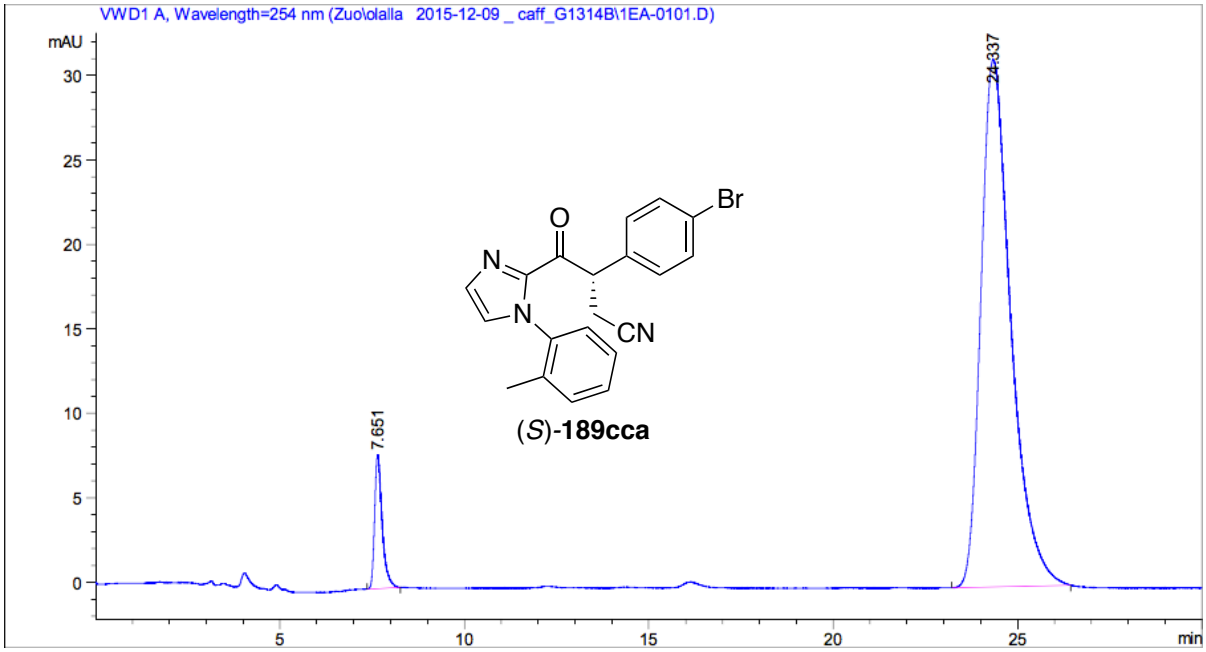

Peak #	Ret Time [min]	Type	Width [min]	Area [mAU*s]	Height [mAU]	Area %
1	7.651	BB	0.1744	112.91759	7.93921	6.0255
2	24.337	VB R	0.6590	1761.06482	31.22580	93.9745

HPLC chromatogram of compound (*S*)-**189cca** with 88% *ee* (Table 7, entry 2, p.41)

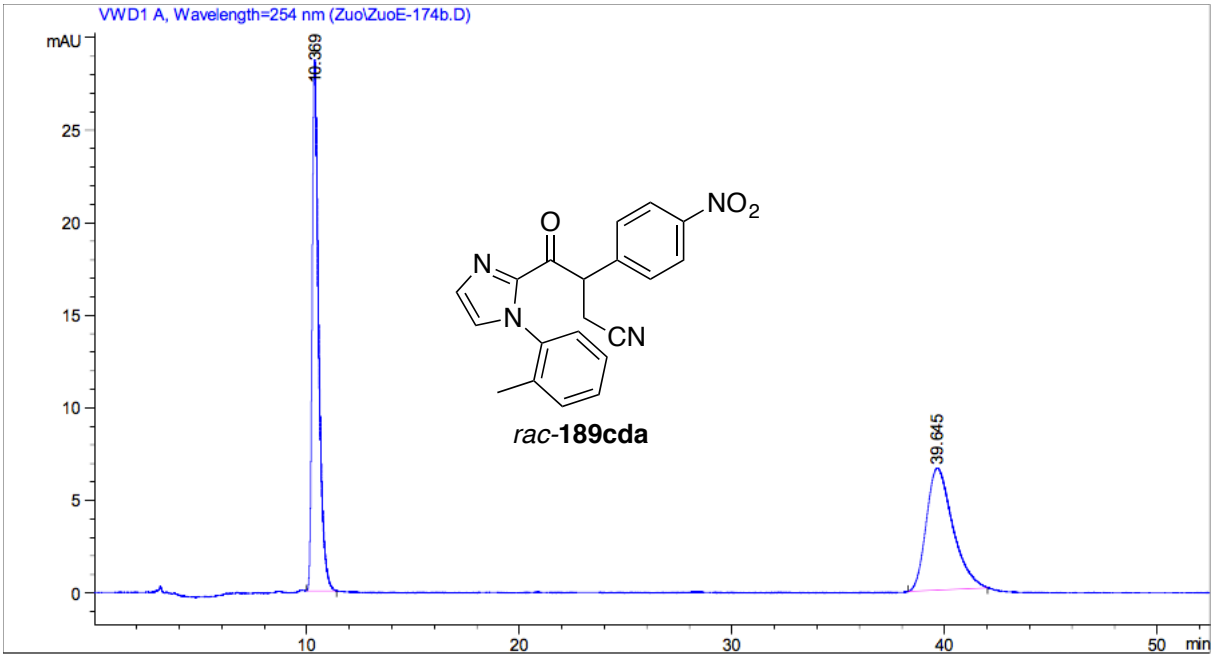

Peak #	Ret Time [min]	Type	Width [min]	Area [mAU*s]	Height [mAU]	Area %
1	10.369	BB	0.2785	614.06421	28.70809	51.8578
2	39.645	BB	1.0107	570.06659	6.59696	48.1422

HPLC chromatogram of compound *rac*-**189cda** (Table 7, entry 3, p.41)

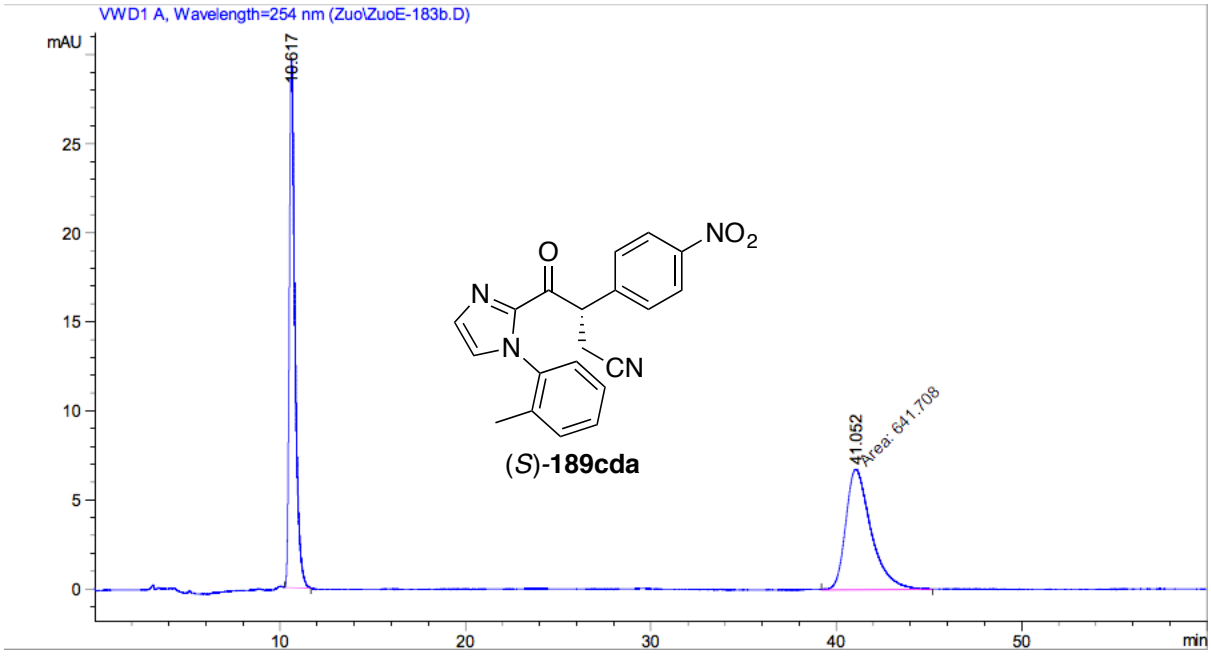

Peak #	Ret Time [min]	Type	Width [min]	Area [mAU*s]	Height [mAU]	Area %
1	10.617	BB	0.2802	629.67371	29.65191	49.5267
2	41.052	MM	1.5801	641.70752	6.76884	50.4733

HPLC chromatogram of compound (*S*)-**189cda** with 1% *ee* (Table 7, entry 3, p.41)

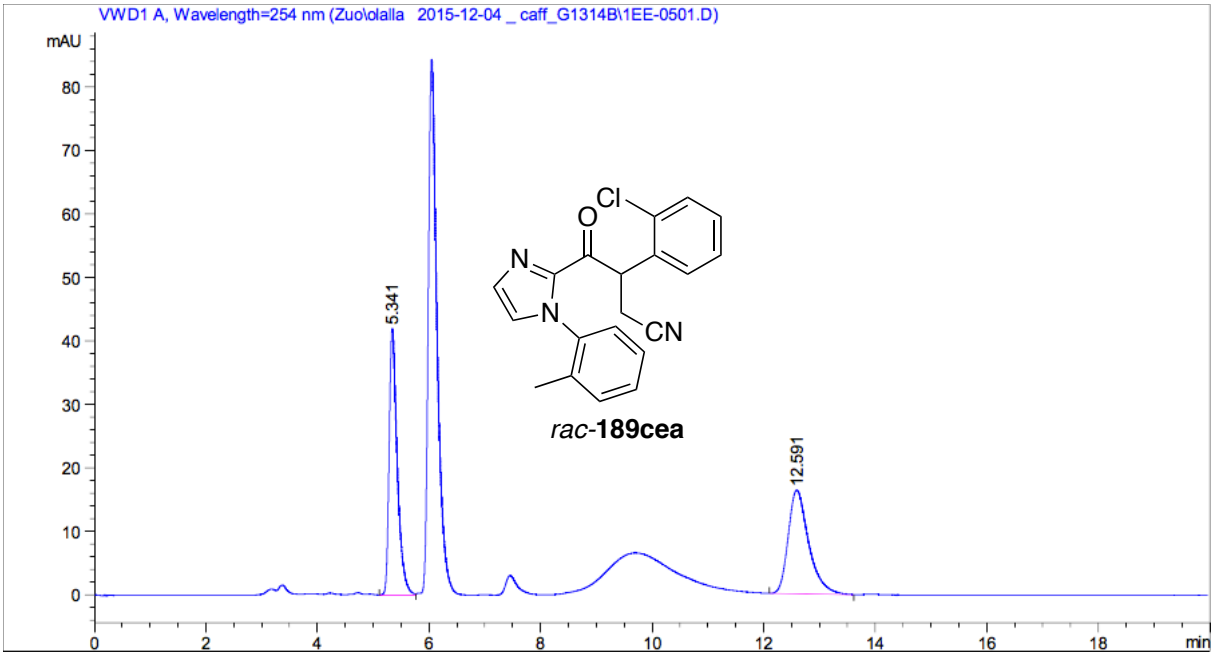

Peak #	Ret Time [min]	Type	Width [min]	Area [mAU*s]	Height [mAU]	Area %
1	5.341	BV	0.1493	423.74792	41.95168	50.4710
2	12.591	BB	0.2981	415.83963	16.35883	49.5290

HPLC chromatogram of compound *rac*-**189cea** (Table 7, entry 4, p.41)

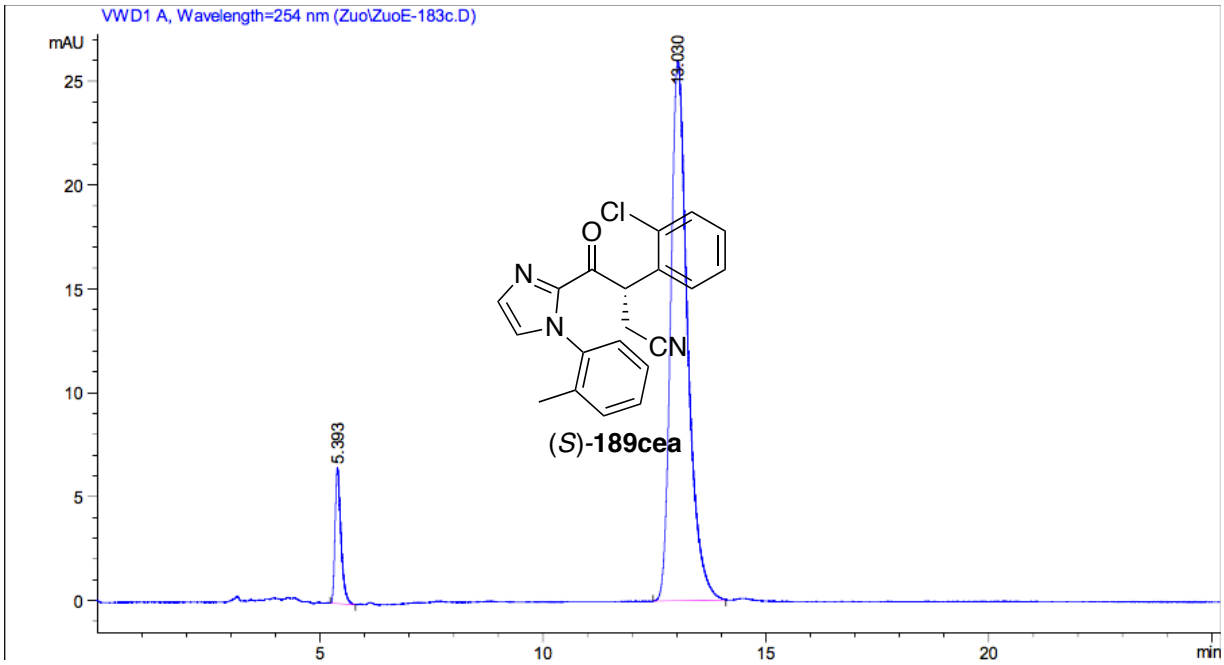

Peak #	Ret Time [min]	Type	Width [min]	Area [mAU*s]	Height [mAU]	Area %
1	5.393	BB	0.1282	60.14808	6.54664	8.0910
2	13.030	BB	0.3093	683.24994	25.98206	91.9090

HPLC chromatogram of compound (*S*)-**189cea** with 84% *ee* (Table 7, entry 4, p.41)

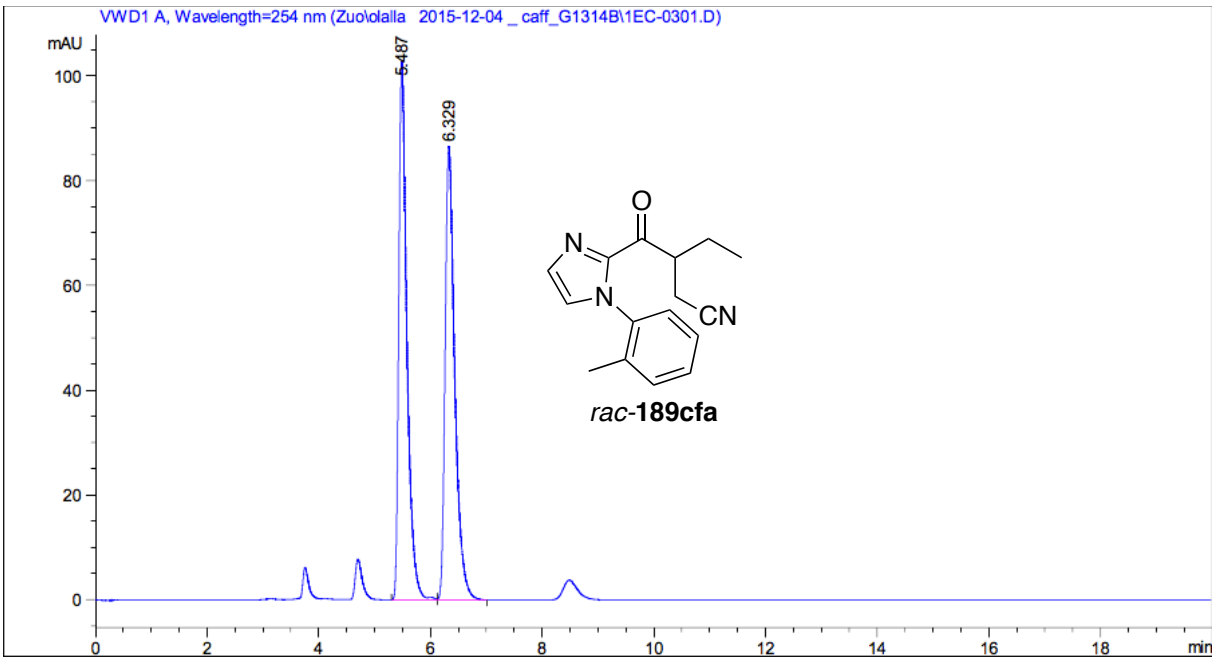

Peak #	Ret Time [min]	Type	Width [min]	Area [mAU*s]	Height [mAU]	Area %
1	5.487	BV R	0.1499	1043.25891	102.77842	50.1343
2	6.329	VB	0.1768	1037.66870	86.61980	49.8657

HPLC chromatogram of compound *rac*-**189cfa** (Table 7, entry 5, p.41)

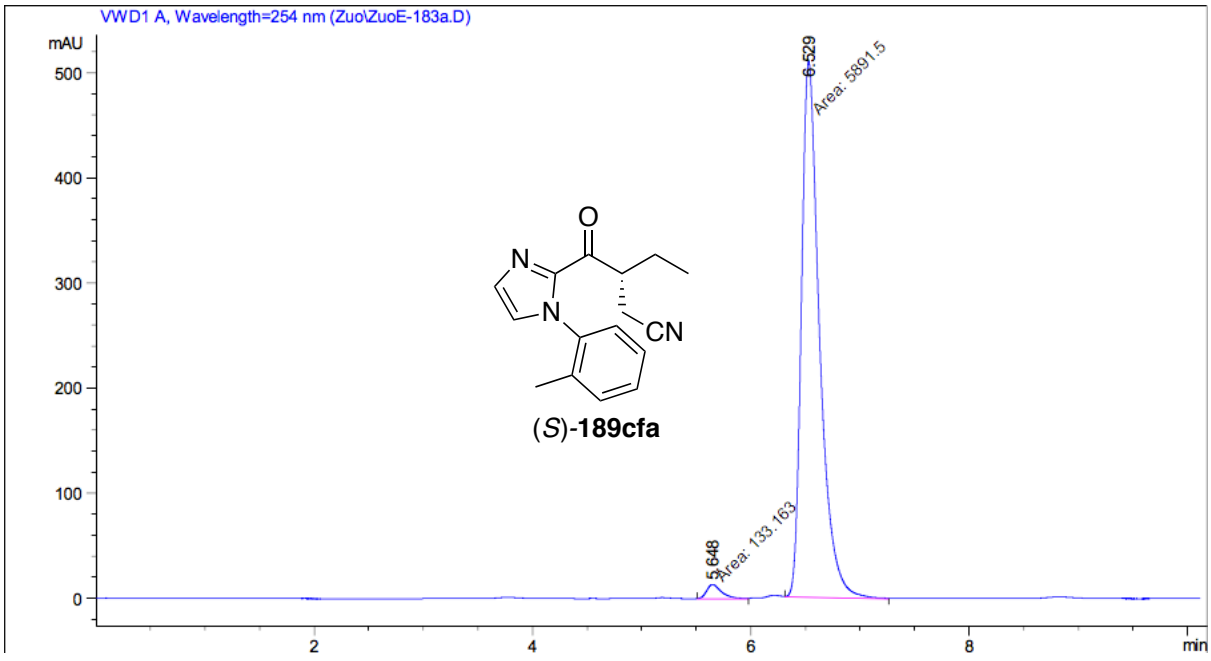

Peak #	Ret Time [min]	Type	Width [min]	Area [mAU*s]	Height [mAU]	Area %
1	5.648	MM	0.1615	133.16316	13.74349	2.2103
2	6.529	MM	0.1926	5891.50488	509.89795	97.7897

HPLC chromatogram of compound (*S*)-**189cfa** with 96% *ee* (Table 7, entry 5, p.41)

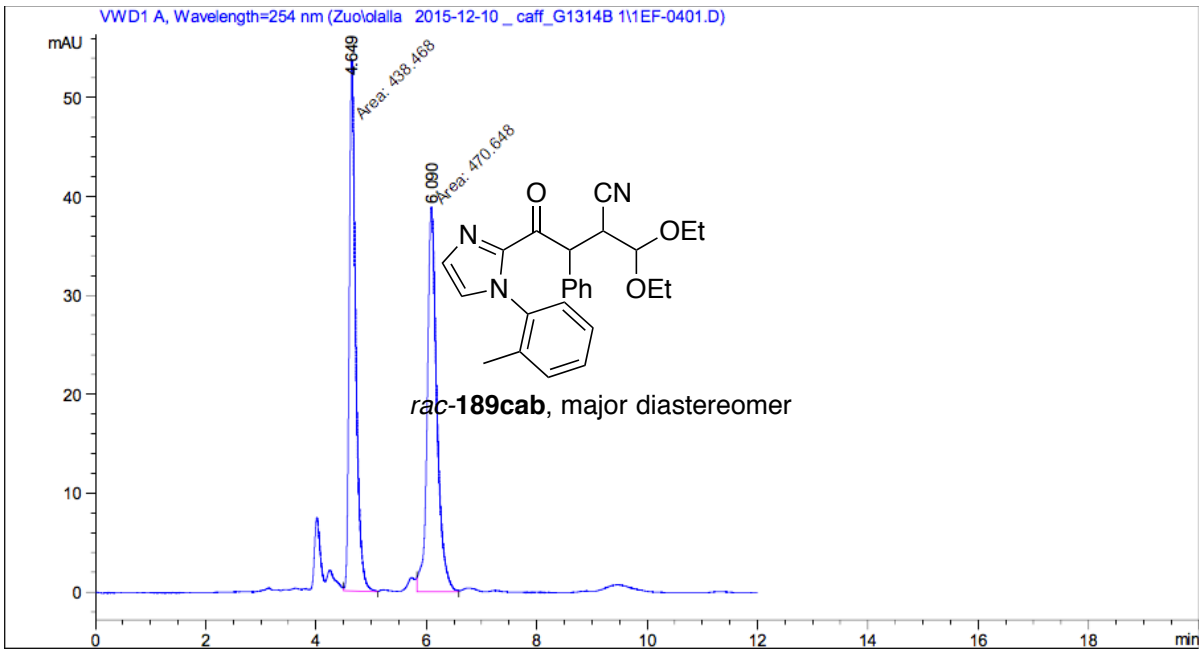

Peak #	Ret Time [min]	Type	Width [min]	Area [mAU*s]	Height [mAU]	Area %
1	4.649	FM	0.1363	438.46817	53.63160	48.2301
2	6.090	FM	0.2018	470.64844	38.87987	51.7699

HPLC chromatogram of compound *rac*-**189cab** major diastereomer (Scheme 49, p.41)

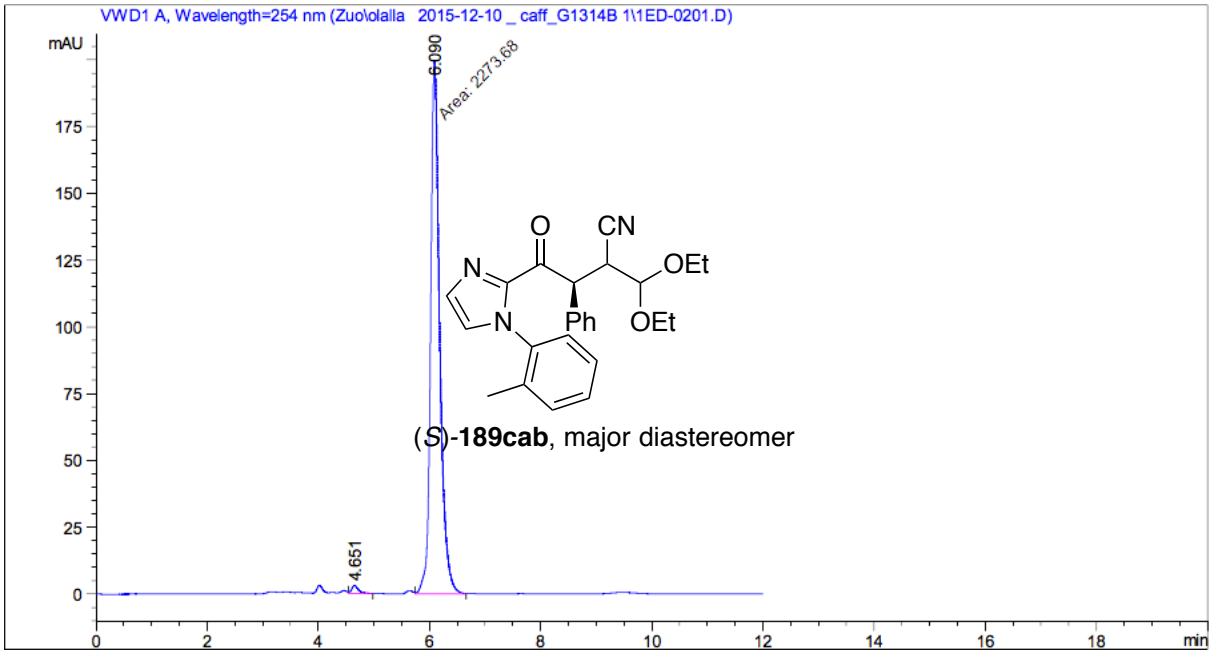

Peak #	Ret Time [min]	Type	Width [min]	Area [mAU*s]	Height [mAU]	Area %
1	4.651	VB	0.1108	25.39266	3.02847	1.1045
2	6.090	MF	0.1897	2273.68457	199.81311	98.8955

HPLC chromatogram of compound (*S*)-**189cab** major diastereomer with 98% *ee* (Scheme 50, p.42)

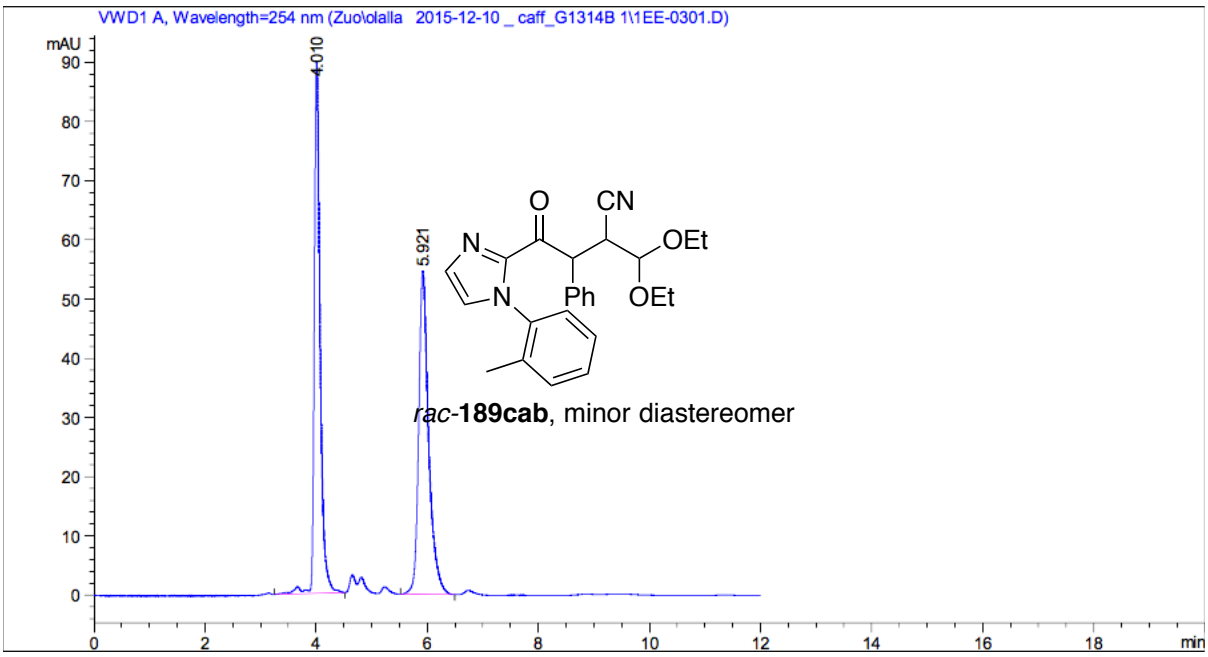

Peak #	Ret Time [min]	Type	Width [min]	Area [mAU*s]	Height [mAU]	Area %
1	4.010	VB R	0.1107	659.95923	89.79237	49.3090
2	5.921	BB	0.1834	678.45520	54.63861	50.6910

HPLC chromatogram of compound *rac*-**189cab** minor diastereomer (Scheme 49, p.41)

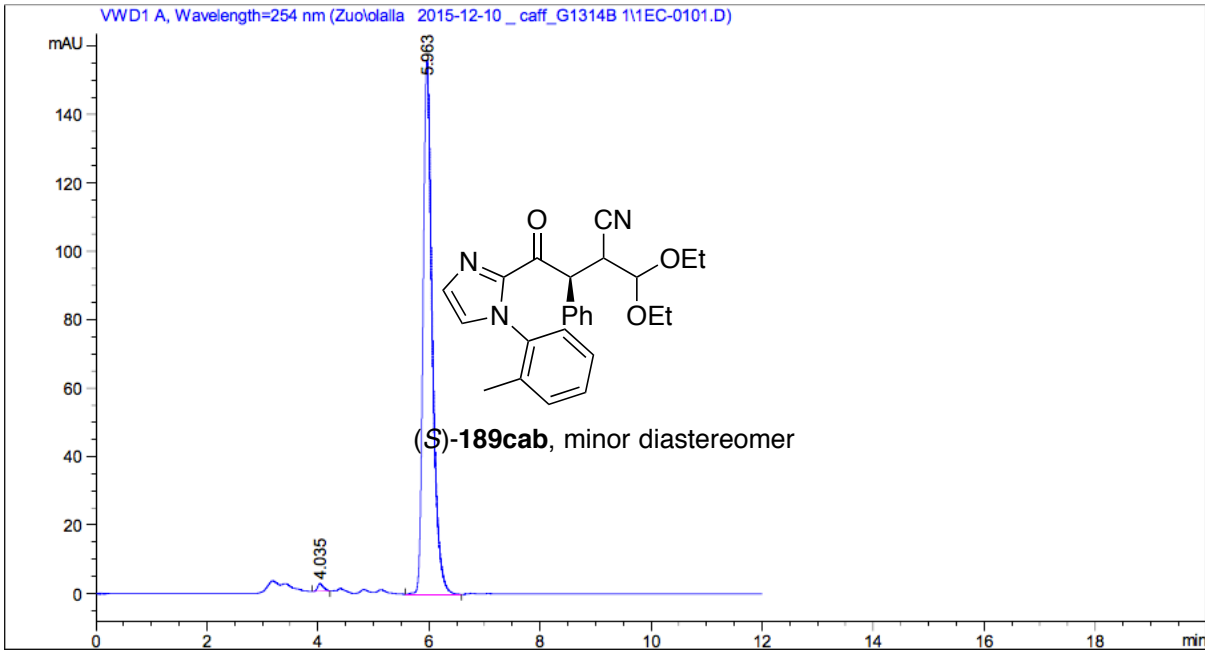

Peak #	Ret Time [min]	Type	Width [min]	Area [mAU*s]	Height [mAU]	Area %
1	4.035	BB	0.0926	16.25576	2.29677	0.9001
2	5.963	BB	0.1733	1789.77954	156.09813	99.0999

HPLC chromatogram of compound (*S*)-**189cab** minor diastereomer with 98% *ee* (Scheme 50, p.42)

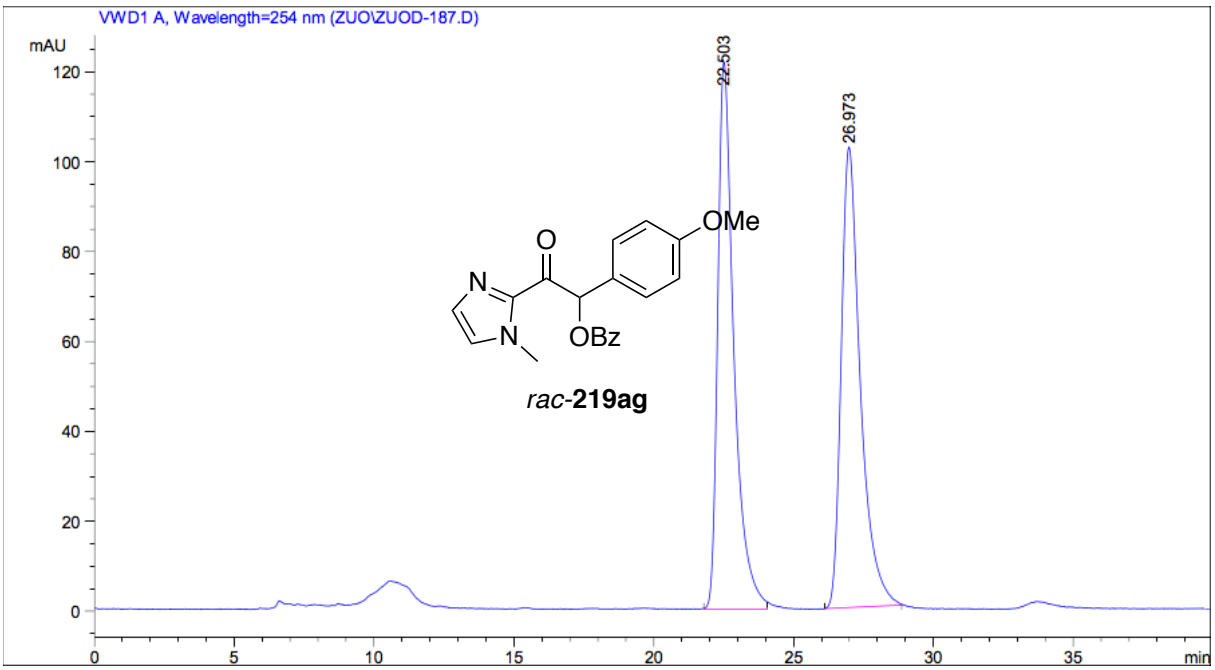

Peak #	RetTime [min]	Type	Width [min]	Area mAU *s	Height [mAU]	Area %
1	22.503	VV	0.5824	4872.58496	121.62259	49.9382
2	26.973	VB	0.7104	4884.64453	102.48278	50.0618

HPLC chromatogram of compound *rac*-**219ag**

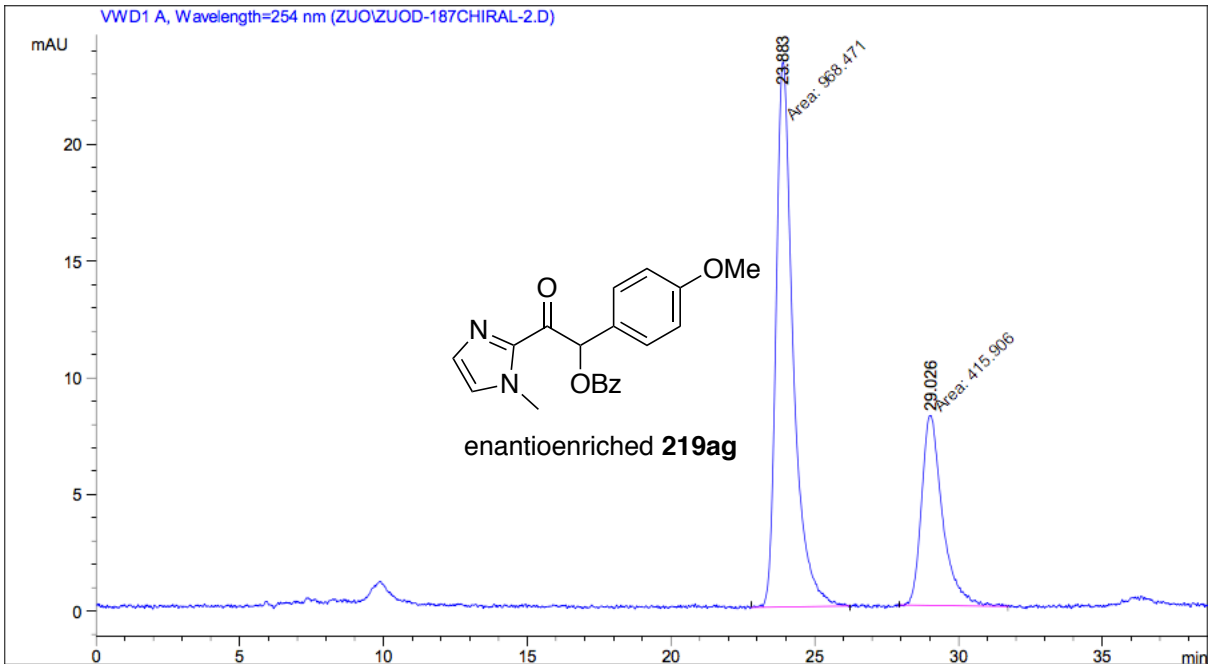

Peak #	RetTime [min]	Type	Width [min]	Area mAU *s	Height [mAU]	Area %
1	23.883	MM	0.6908	968.47058	23.36674	69.9572
2	29.026	MM	0.8504	415.90610	8.15101	30.0428

HPLC chromatogram of enantioenriched compound **219ag** with 40% *ee* (Scheme 62, p.50)

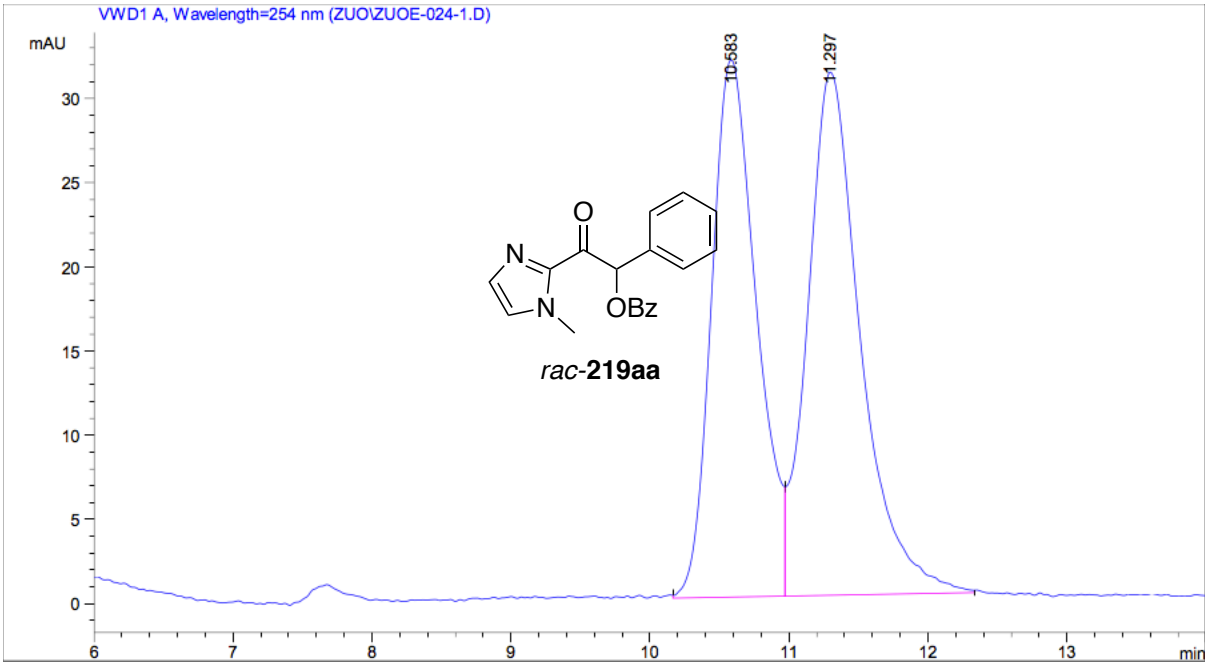

Peak #	RetTime [min]	Type	Width [min]	Area mAU *s	Height [mAU]	Area %
1	10.583	VV	0.3419	720.37048	31.92812	46.5366
2	11.297	VB	0.3935	827.59430	31.09032	53.4634

HPLC chromatogram of compound *rac*-**219aa**

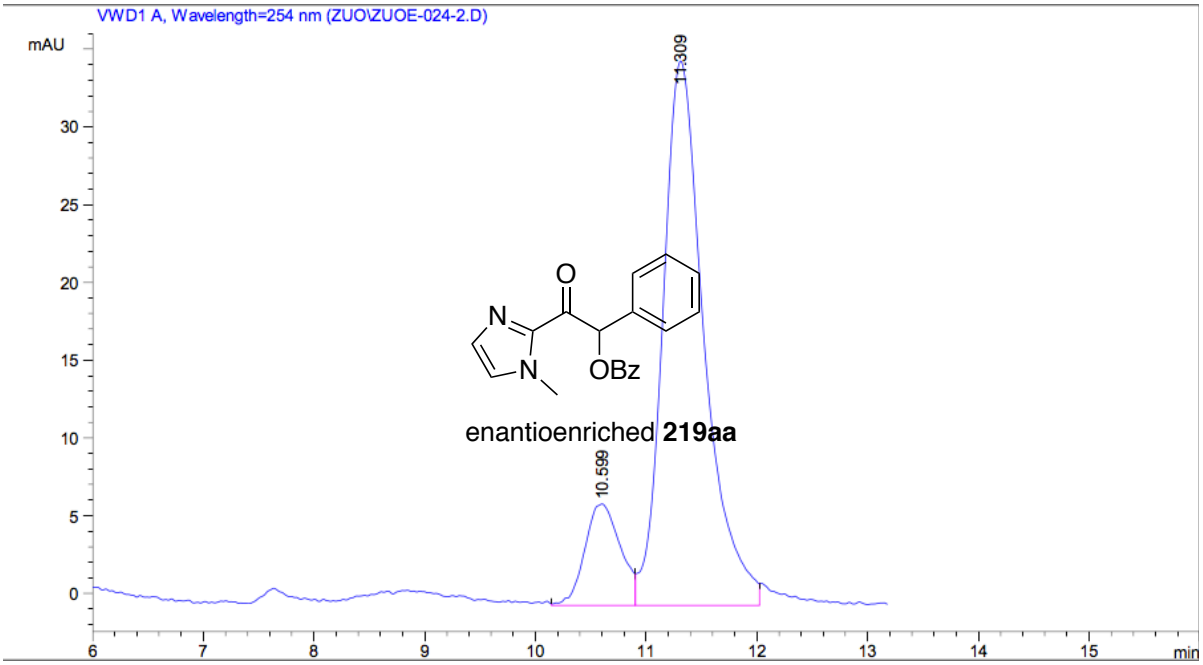

Peak #	RetTime [min]	Type	Width [min]	Area mAU *s	Height [mAU]	Area %
1	10.599	VV	0.2949	146.49054	6.53784	13.8693
2	11.309	VV	0.3860	909.72968	35.02222	86.1307

HPLC chromatogram of enantioenriched compound **219aa** with 72% *ee* (Scheme 63, p.53)

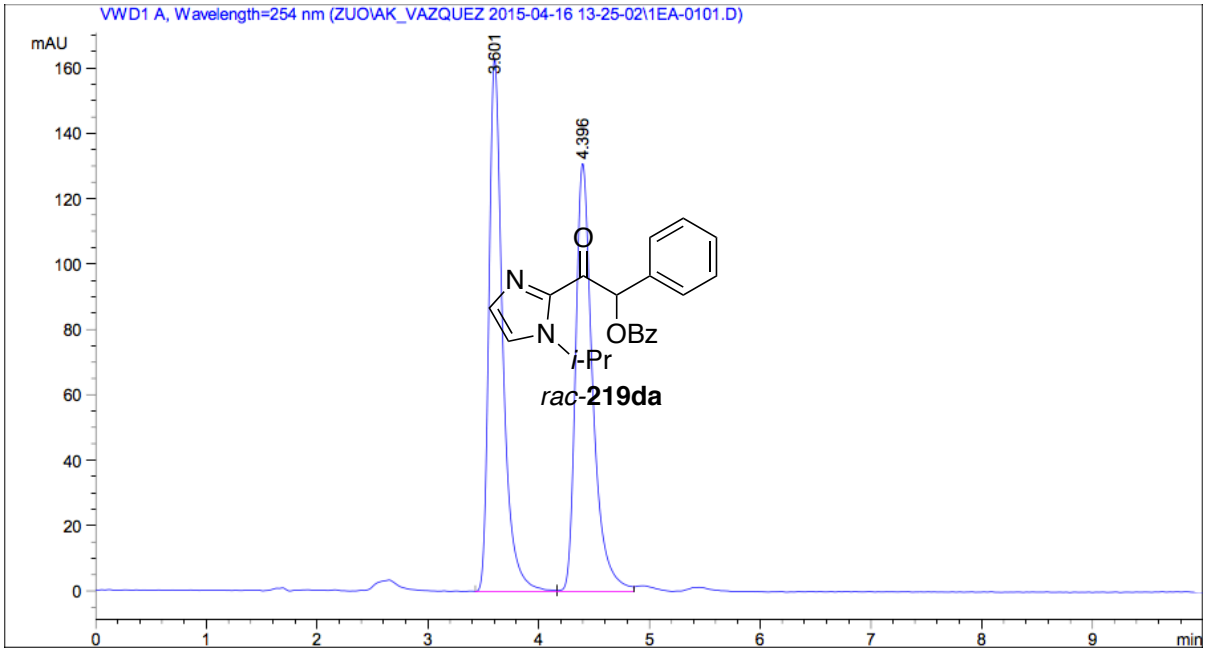

Peak #	RetTime [min]	Type	Width [min]	Area mAU *s	Height [mAU]	Area %
1	3.601	VV	0.1304	1412.85937	162.75661	50.1642
2	4.396	VV	0.1600	1403.60803	130.96902	49.8358

HPLC chromatogram of compound *rac*-**219da**

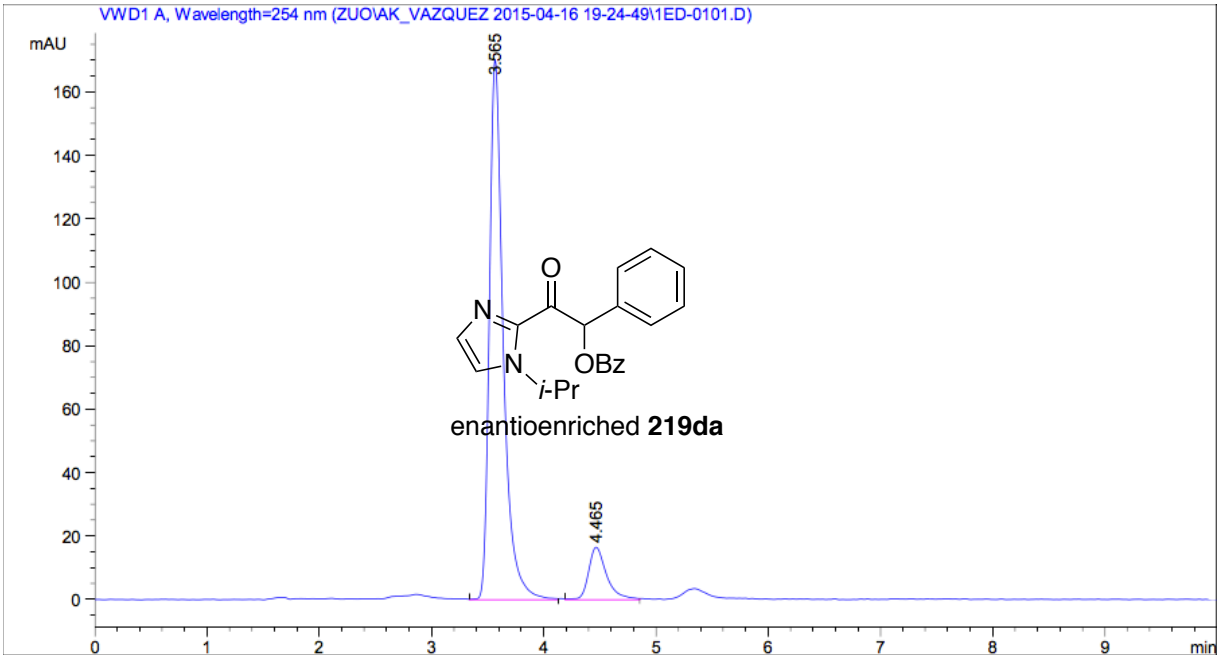

Peak #	RetTime [min]	Type	Width [min]	Area mAU *s	Height [mAU]	Area %
1	3.565	VV	0.1278	1463.87036	170.48497	88.7356
2	4.465	VV	0.1673	185.82898	16.56119	11.2644

HPLC chromatogram of enantioenriched compound **219da** with 79% *ee* (Scheme 63, p.53)

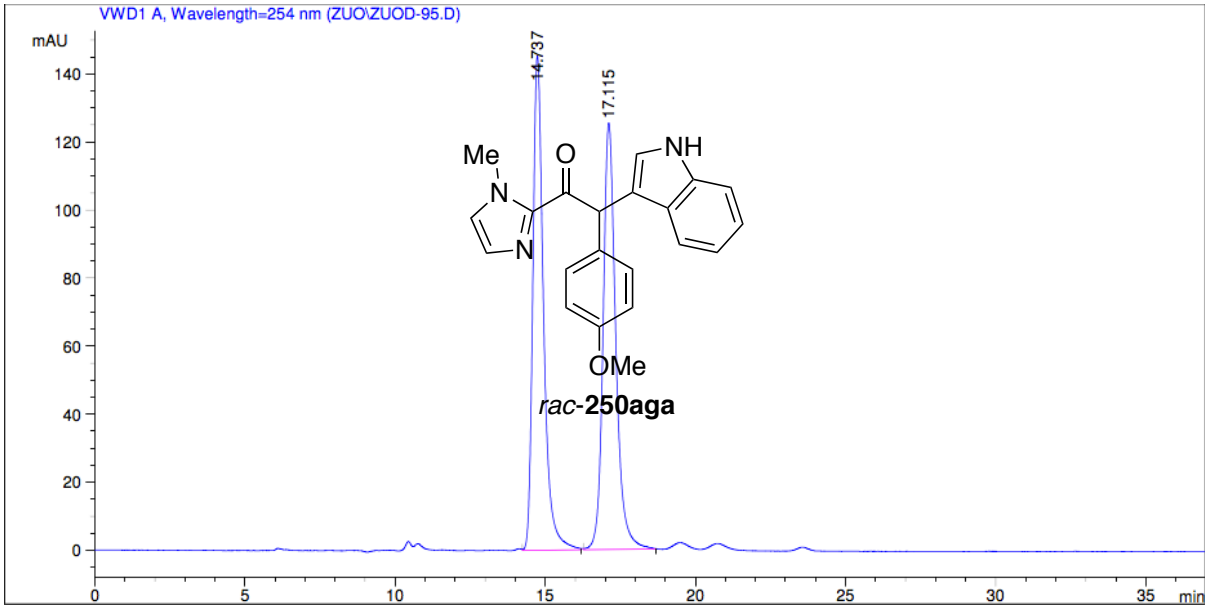

Peak #	RetTime [min]	Type	Width [min]	Area mAU *s	Height [mAU]	Area %
1	14.737	VB	0.3756	3610.80981	145.43683	49.5420
2	17.115	BB	0.4427	3677.56445	125.37881	50.4580

HPLC chromatogram of compound *rac*-**250aga**

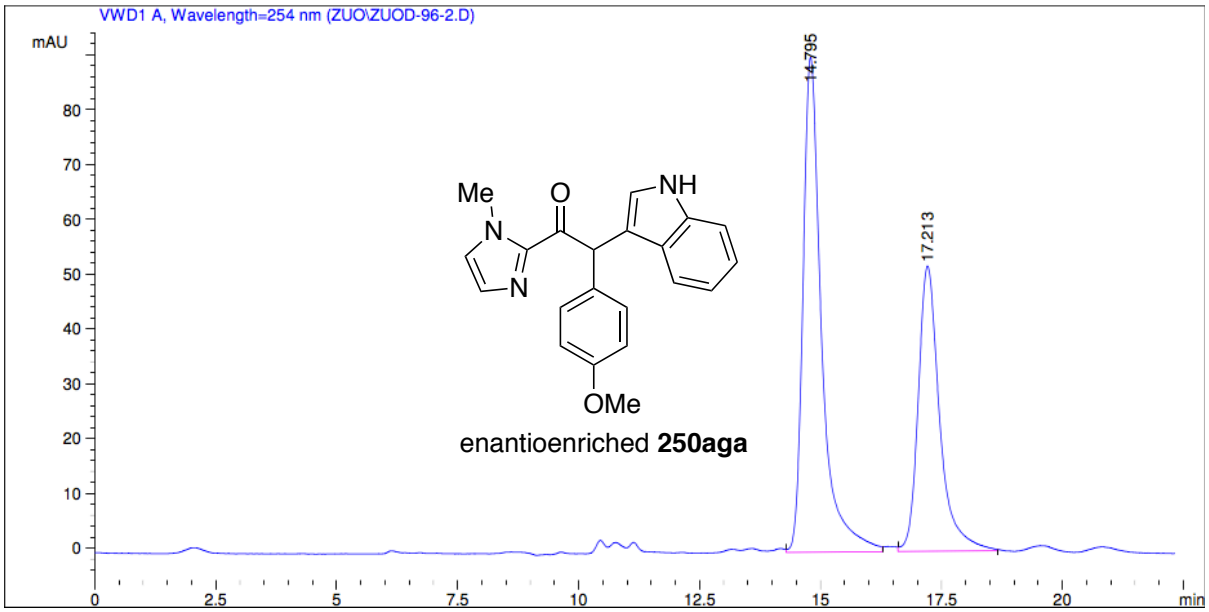

Peak #	RetTime [min]	Type	Width [min]	Area mAU *s	Height [mAU]	Area %
1	14.795	VB	0.3980	2413.69824	90.24113	60.0595
2	17.213	VB	0.4618	1605.14563	52.03101	39.9405

HPLC chromatogram of enantioenriched compound **250aga** with 20% *ee* (Scheme 76, p.61)

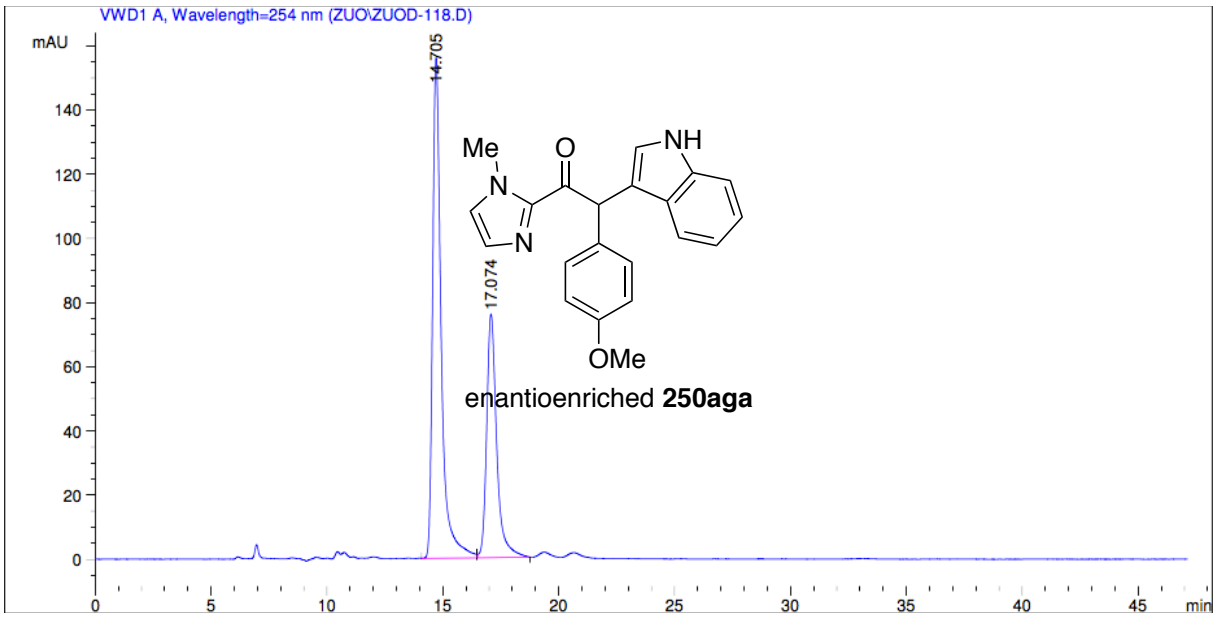

Peak #	RetTime [min]	Type	Width [min]	Area mAU *s	Height [mAU]	Area %
1	14.705	BV	0.3821	4018.03809	155.93918	63.8377
2	17.074	VB	0.4487	2276.11279	75.94535	36.1623

HPLC chromatogram of enantioenriched compound **250aga** with 28% *ee* (Scheme 76, p.61)

7.3. Crystallographic Data

(*S*)-3-(4-Bromophenyl)-4-oxo-4-(1-(*o*-tolyl)-1*H*-imidazol-2-yl)butanenitrile (189cca)

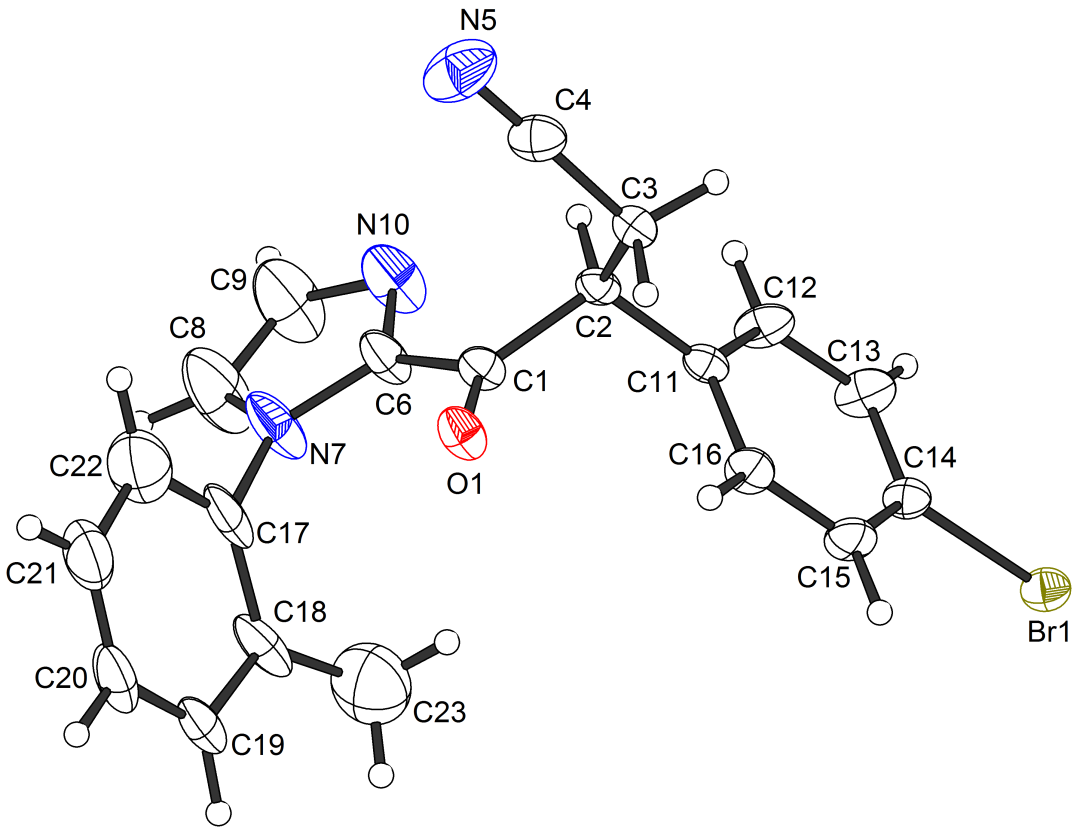

Crystal data and structure refinement

Crystal data

Identification code	ZuoE-183e	
Habitus, color	plate, colorless	
Crystal size	0.61 × 0.14 × 0.03 mm^3	
Crystal group	$P2_12_12_1$	
Unit cell dimensions	a = 9.7170(4) Å b = 12.4043(5) Å c = 15.5021(7) Å	α = 90°. β = 90°. γ = 90°.
Volume	1868.51(14) $Å^3$	
Z	4	
Cell determination	9896 peaks with Theta 2.5 to 27.4°.	
Empirical formula	$C_{20}H_{16}BrN_3O$	

Moiety formula	$C_{20}H_{16}BrN_3O$
Density (calculated)	1.402 Mg/m^3
Absorption coefficient	2.212 mm^{-1}
F(000)	800
Data collection	
Diffractometer type	Bruker D8 QUEST area Detektor
Wavelength	0.71073 Å
Temperature	115(2) K
Theta range for data collection	2.474 to 27.524º.
Index Ranges	-12<=h<=10, -16<=k<=16, -18<=l<=20
Data collection software	APEX3 (Bruker AXS Inc., 2015)
Cell refinement software	SAINT V8.35A (Bruker AXS Inc., 2015)
Data reduction software	SAINT V8.35A (Bruker AXS Inc., 2015)
Solution and refinement	
Reflections collected	41914
Independent reflections	4301 [R(int) = 0.0363]
Completeness to theta = 25.242º	100 %
Observed reflections	4085[I > 2(I)]
Reflections used for refinements	4301
Absorption correction	Semi-empirical from equivalents
Max. and min. transmission	0.94 and 0.65
Fleck parameter (absolute struct.)	-0.010(3)
Largest diff. peak and hole	0.854 and -0.429 $e.Å^{-3}$
Solution	Direct Methode
Refinement	Full-matrix least-squares on F^2
Treatment of hydrogen atoms	Calculated positions, constr. ref.
Programs used	XT V2014/1 (Bruker AXS Inc., 2014) SHELXL-2014/7 (Sheldrick, 2014) DIAMOND (Crystal Impact) ShelXle (Hübschle, Sheldrick, Dittrich, 2011)
Data / restrains / parameters	4301 / 798 / 330
Goodness-of-fit on F^2	1.108
R index (all data)	wR2 = 0.0753
R index conventional [I>2sigma(I)]	R1 = 0.0277

Atomic coordinates and equivalent isotropic displacement parameters (Å²)

U(eq) is defined as one third of the trace of the orthogonalized U^{ij} tensor

	x	y	z	U(eq)	Occupancy
Br1	0.59880(3)	0.78969(3)	0.48369(2)	0.02524(10)	1
C1	0.5178(3)	0.2527(3)	0.5839(2)	0.0228(7)	1
O1	0.3953(3)	0.2377(2)	0.57658(14)	0.0285(5)	1
C2	0.6074(3)	0.2921(2)	0.50991(18)	0.0204(5)	1
C3	0.5616(3)	0.2413(3)	0.4238(2)	0.0225(7)	1
C4	0.5849(4)	0.1241(3)	0.4245(2)	0.0308(8)	1
N5	0.6044(4)	0.0342(3)	0.4279(3)	0.0522(10)	1
C11	0.6022(3)	0.4139(2)	0.50498(18)	0.0198(6)	1
C12	0.7236(3)	0.4728(3)	0.5105(3)	0.0288(7)	1
C13	0.7230(3)	0.5845(3)	0.5042(3)	0.0308(9)	1
C14	0.5996(4)	0.6369(2)	0.4929(2)	0.0226(6)	1
C15	0.4765(3)	0.5810(3)	0.4877(3)	0.0278(7)	1
C16	0.4791(3)	0.4690(3)	0.4939(2)	0.0265(7)	1
C6	0.5881(9)	0.2230(8)	0.6642(5)	0.033(2)	0.65
N7	0.5240(6)	0.1885(8)	0.7379(4)	0.0488(18)	0.65
C8	0.6246(8)	0.1749(12)	0.7970(6)	0.071(3)	0.65
C9	0.7456(8)	0.1974(11)	0.7582(6)	0.066(3)	0.65
N10	0.7233(9)	0.2269(8)	0.6748(5)	0.047(2)	0.65
C17	0.3816(6)	0.1698(7)	0.7536(4)	0.0427(14)	0.65
C18	0.2920(7)	0.2542(6)	0.7811(4)	0.0392(14)	0.65
C19	0.1577(7)	0.2228(8)	0.8002(6)	0.0323(17)	0.65
C20	0.1141(7)	0.1148(6)	0.7896(4)	0.0435(15)	0.65
C21	0.2011(8)	0.0382(7)	0.7619(5)	0.0578(19)	0.65
C22	0.3372(12)	0.0579(10)	0.7421(8)	0.061(3)	0.65
C23	0.3344(18)	0.3665(12)	0.773(2)	0.078(2)	0.65
C6A	0.5899(17)	0.2600(11)	0.6673(10)	0.023(3)	0.35
N7A	0.5241(10)	0.2495(11)	0.7449(7)	0.037(2)	0.35
C8A	0.6254(13)	0.2473(14)	0.8058(8)	0.045(3)	0.35
C9A	0.7454(12)	0.2589(12)	0.7649(8)	0.033(3)	0.35
N10A	0.7241(15)	0.2702(9)	0.6787(9)	0.025(3)	0.35
C17A	0.3770(12)	0.2669(12)	0.7622(9)	0.054(3)	0.35
C18A	0.2963(14)	0.1805(12)	0.7779(10)	0.052(3)	0.35
C19A	0.1548(19)	0.1861(18)	0.7958(18)	0.054(4)	0.35
C20A	0.1069(16)	0.2956(13)	0.8018(9)	0.056(3)	0.35
C21A	0.1852(17)	0.3846(15)	0.7837(13)	0.073(4)	0.35
C22A	0.329(3)	0.384(2)	0.778(4)	0.078(2)	0.35

C23A	0.361(2)	0.0798(18)	0.7668(13)	0.056(5)	0.35

Bond lengths [Å] and angles [º]

Br1-C14	1.900(3)	C17-C18	1.427(10)
C1-O1	1.209(4)	C17-C22	1.465(15)
C1-C6	1.467(9)	C18-C19	1.393(8)
C1-C6A	1.473(16)	C18-C23	1.458(17)
C1-C2	1.521(4)	C19-C20	1.416(11)
C2-C11	1.514(4)	C19-H19	0.9500
C2-C3	1.542(4)	C20-C21	1.342(11)
C2-H2	1.0000	C20-H20	0.9500
C3-C4	1.472(5)	C21-C22	1.379(14)
C3-H3A	0.9900	C21-H21	0.9500
C3-H3B	0.9900	C22-H22	0.9500
C4-N5	1.132(5)	C23-H23A	0.9800
C11-C16	1.388(4)	C23-H23B	0.9800
C11-C12	1.390(4)	C23-H23C	0.9800
C12-C13	1.389(5)	C6A-N10A	1.322(15)
C12-H12	0.9500	C6A-N7A	1.369(15)
C13-C14	1.375(5)	N7A-C8A	1.364(14)
C13-H13	0.9500	N7A-C17A	1.471(14)
C14-C15	1.385(5)	C8A-C9A	1.335(15)
C15-C16	1.393(5)	C8A-H8A	0.9500
C15-H15	0.9500	C9A-N10A	1.360(14)
C16-H16	0.9500	C9A-H9A	0.9500
C6-N10	1.325(9)	C17A-C18A	1.350(17)
C6-N7	1.370(8)	C17A-C22A	1.55(2)
N7-C8	1.351(9)	C18A-C19A	1.404(18)
N7-C17	1.424(8)	C18A-C23A	1.41(2)
C8-C9	1.350(10)	C19A-C20A	1.44(2)
C8-H8	0.9500	C19A-H19A	0.9500
C9-N10	1.361(10)	C20A-C21A	1.370(18)

C9-H9	0.9500	C20A-H20A	0.9500
C21A-C22A	1.40(3)	C23A-H23D	0.9800
C21A-H21A	0.9500	C23A-H23E	0.9800
C22A-H22A	0.9500	C23A-H23F	0.9800
O1-C1-C6	119.9(4)	C15-C14-Br1	119.5(3)
O1-C1-C6A	124.0(7)	C14-C15-C16	118.7(3)
O1-C1-C2	122.8(3)	C14-C15-H15	120.6
C6-C1-C2	117.0(4)	C16-C15-H15	120.6
C6A-C1-C2	111.7(6)	C11-C16-C15	121.0(3)
C11-C2-C1	109.8(2)	C11-C16-H16	119.5
C11-C2-C3	110.7(2)	C15-C16-H16	119.5
C1-C2-C3	110.9(2)	N10-C6-N7	111.0(7)
C11-C2-H2	108.4	N10-C6-C1	123.9(7)
C1-C2-H2	108.4	N7-C6-C1	125.1(7)
C3-C2-H2	108.4	C8-N7-C6	106.0(6)
C4-C3-C2	110.6(3)	C8-N7-C17	124.6(6)
C4-C3-H3A	109.5	C6-N7-C17	129.4(6)
C2-C3-H3A	109.5	C9-C8-N7	107.6(7)
C4-C3-H3B	109.5	C9-C8-H8	126.2
C2-C3-H3B	109.5	N7-C8-H8	126.2
H3A-C3-H3B	108.1	C8-C9-N10	109.9(7)
N5-C4-C3	177.6(4)	C8-C9-H9	125.0
C16-C11-C12	118.7(3)	N10-C9-H9	125.0
C16-C11-C2	121.8(3)	C6-N10-C9	105.4(7)
C12-C11-C2	119.5(3)	N7-C17-C18	121.7(7)
C13-C12-C11	121.1(3)	N7-C17-C22	114.8(8)
C13-C12-H12	119.5	C18-C17-C22	123.5(7)
C11-C12-H12	119.5	C19-C18-C17	115.5(7)
C14-C13-C12	119.0(3)	C19-C18-C23	123.4(9)
C14-C13-H13	120.5	C17-C18-C23	120.2(9)
C12-C13-H13	120.5	C18-C19-C20	121.3(8)
C13-C14-C15	121.6(3)	C18-C19-H19	119.3
C13-C14-Br1	119.0(3)	C20-C19-H19	119.3

C21-C20-C19	121.3(7)	N10A-C9A-H9A	124.9
C21-C20-H20	119.4	C6A-N10A-C9A	105.8(12)
C19-C20-H20	119.4	C18A-C17A-N7A	118.8(13)
C20-C21-C22	123.3(9)	C18A-C17A-C22A	122.8(16)
C20-C21-H21	118.3	N7A-C17A-C22A	117.4(15)
C22-C21-H21	118.3	C17A-C18A-C19A	124.4(15)
C21-C22-C17	115.0(10)	C17A-C18A-C23A	114.9(15)
C21-C22-H22	122.5	C19A-C18A-C23A	120.4(16)
C17-C22-H22	122.5	C18A-C19A-C20A	112.1(17)
C18-C23-H23A	109.5	C18A-C19A-H19A	123.9
C18-C23-H23B	109.5	C20A-C19A-H19A	123.9
H23A-C23-H23B	109.5	C21A-C20A-C19A	124.6(15)
C18-C23-H23C	109.5	C21A-C20A-H20A	117.7
H23A-C23-H23C	109.5	C19A-C20A-H20A	117.7
H23B-C23-H23C	109.5	C20A-C21A-C22A	124.4(19)
N10A-C6A-N7A	110.6(13)	C20A-C21A-H21A	117.8
N10A-C6A-C1	126.3(12)	C22A-C21A-H21A	117.8
N7A-C6A-C1	122.9(12)	C21A-C22A-C17A	108(2)
C8A-N7A-C6A	105.9(11)	C21A-C22A-H22A	125.9
C8A-N7A-C17A	125.3(11)	C17A-C22A-H22A	125.9
C6A-N7A-C17A	126.9(12)	C18A-C23A-H23D	109.5
C9A-C8A-N7A	107.4(10)	C18A-C23A-H23E	109.5
C9A-C8A-H8A	126.3	H23D-C23A-H23E	109.5
N7A-C8A-H8A	126.3	C18A-C23A-H23F	109.5
C8A-C9A-N10A	110.2(11)	H23D-C23A-H23F	109.5
C8A-C9A-H9A	124.9	H23E-C23A-H23F	109.5

Symmetry transformations used to generate equivalent atoms

Anisotropic displacement parameters (Å²)

The anisotropic displacement factor exponent takes the form: $-2\pi^2[h^2 a^{*2} U^{11} + \ldots + 2 h k a^* b^* U^{12}]$

	U^{11}	U^{22}	U^{33}	U^{23}	U^{13}	U^{12}
Br1	0.02392(15)	0.02417(15)	0.02763(16)	-0.00387(14)	-0.00031(14)	0.00062(15)
C1	0.0165(15)	0.0316(16)	0.0204(15)	-0.0003(13)	-0.0018(12)	0.0002(12)
O1	0.0179(10)	0.0440(14)	0.0237(11)	0.0054(9)	-0.0019(10)	-0.0046(10)
C2	0.0137(11)	0.0272(14)	0.0203(13)	0.0002(14)	0.0009(12)	0.0028(14)
C3	0.0219(16)	0.0250(16)	0.0206(15)	-0.0014(12)	0.0025(12)	-0.0016(11)
C4	0.0240(17)	0.0314(19)	0.0370(19)	-0.0072(15)	0.0010(15)	-0.0011(15)
N5	0.046(2)	0.0302(18)	0.081(3)	-0.0099(17)	-0.004(2)	-0.0009(17)
C11	0.0153(12)	0.0267(14)	0.0175(15)	-0.0029(11)	0.0005(12)	-0.0008(12)
C12	0.0133(13)	0.0289(16)	0.044(2)	-0.0063(16)	-0.0053(14)	0.0018(12)
C13	0.0186(15)	0.0273(16)	0.047(2)	-0.0079(15)	-0.0046(14)	-0.0026(13)
C14	0.0232(14)	0.0214(13)	0.0232(16)	-0.0054(12)	0.0002(14)	-0.0002(14)
C15	0.0155(14)	0.0306(16)	0.0372(18)	0.0011(15)	0.0007(14)	0.0037(12)
C16	0.0142(15)	0.0288(16)	0.036(2)	0.0018(14)	0.0006(13)	-0.0029(11)
C6	0.020(2)	0.059(6)	0.020(3)	0.010(4)	0.0011(19)	0.001(4)
N7	0.024(2)	0.100(5)	0.022(3)	0.020(3)	0.0010(19)	0.001(3)
C8	0.043(4)	0.136(7)	0.034(3)	0.030(4)	-0.006(3)	0.000(4)
C9	0.035(3)	0.122(7)	0.042(4)	0.025(5)	-0.010(3)	-0.003(4)
N10	0.023(2)	0.086(6)	0.031(3)	0.012(4)	-0.006(2)	-0.003(4)
C17	0.025(3)	0.082(4)	0.021(3)	0.024(3)	0.005(2)	0.000(2)
C18	0.020(3)	0.076(4)	0.022(3)	0.007(3)	0.004(2)	-0.011(3)
C19	0.025(3)	0.055(4)	0.018(3)	0.008(3)	0.003(2)	-0.005(3)
C20	0.033(3)	0.059(3)	0.039(3)	0.022(3)	0.007(3)	-0.012(3)
C21	0.049(3)	0.066(4)	0.059(4)	0.030(3)	0.017(3)	0.001(3)
C22	0.043(4)	0.077(5)	0.061(6)	0.020(4)	0.001(4)	0.002(3)
C23	0.061(3)	0.086(4)	0.087(5)	0.008(5)	0.006(3)	-0.007(3)
C6A	0.023(4)	0.028(7)	0.018(4)	0.005(4)	-0.001(3)	0.003(4)
N7A	0.026(4)	0.063(6)	0.023(4)	0.003(4)	0.000(3)	-0.002(4)
C8A	0.032(5)	0.080(8)	0.022(4)	0.007(5)	-0.004(3)	0.002(5)
C9A	0.025(4)	0.050(6)	0.024(4)	0.006(4)	-0.005(3)	0.003(4)
N10A	0.019(4)	0.034(6)	0.022(4)	0.005(4)	-0.003(3)	0.001(4)
C17A	0.040(4)	0.086(5)	0.036(5)	0.001(5)	-0.001(4)	0.000(4)
C18A	0.042(5)	0.079(5)	0.033(6)	0.008(5)	0.003(5)	0.006(4)
C19A	0.046(6)	0.075(7)	0.041(8)	0.007(7)	0.011(5)	0.007(5)
C20A	0.049(5)	0.075(6)	0.043(6)	0.011(5)	0.004(5)	0.005(5)

C21A	0.059(5)	0.084(6)	0.075(8)	0.010(6)	0.005(6)	0.004(5)
C22A	0.061(3)	0.086(4)	0.087(5)	0.008(5)	0.006(3)	-0.007(3)
C23A	0.048(9)	0.082(7)	0.037(9)	-0.015(7)	-0.005(6)	0.012(6)

7.4. List of Synthesized Compounds

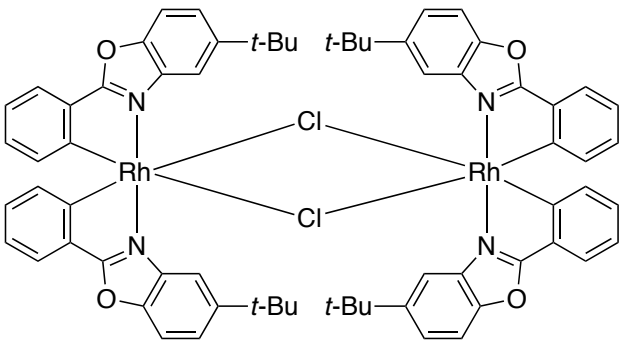

35

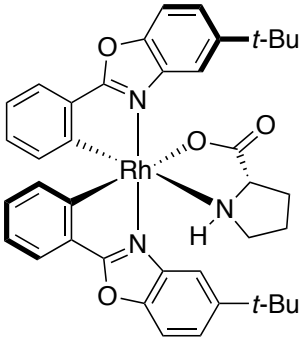

Λ-L-**37**

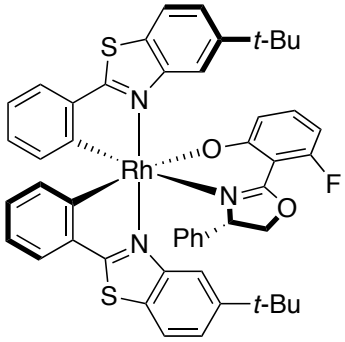

Λ-(*S*)-**39**

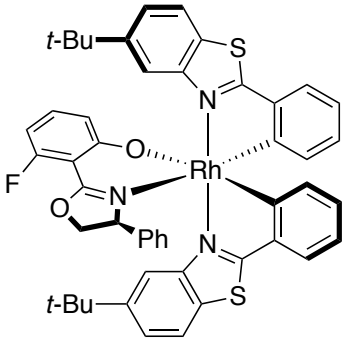

Δ-(*S*)-**39**

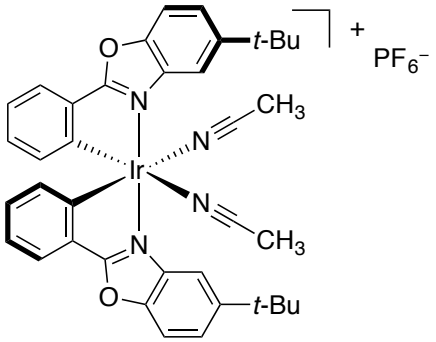

Λ-**60** (Λ-IrO)

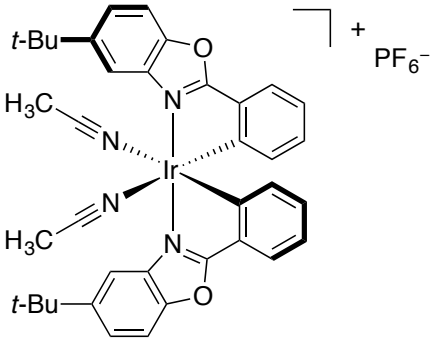

Δ-**60** (Δ-IrO)

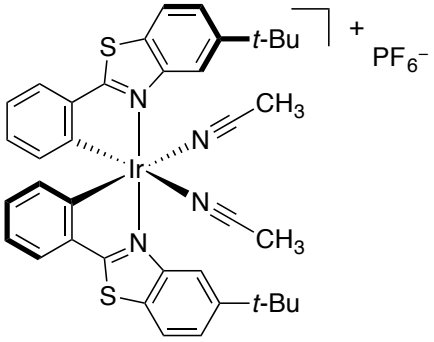

Λ-**64** (Λ-IrS)

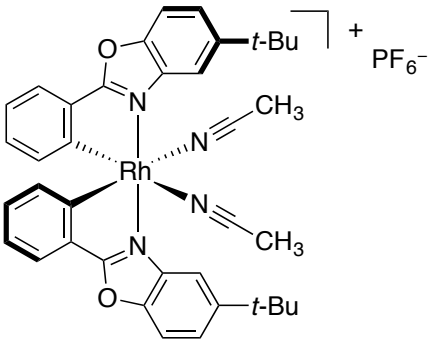

Λ-**70** (Λ-RhO)

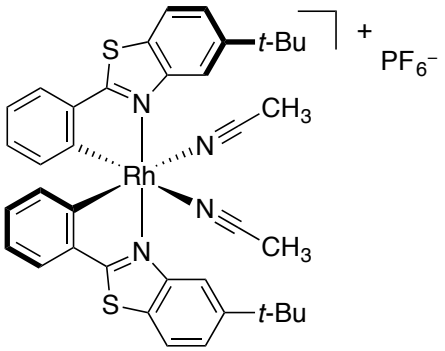

Λ-**71** (Λ-RhS)

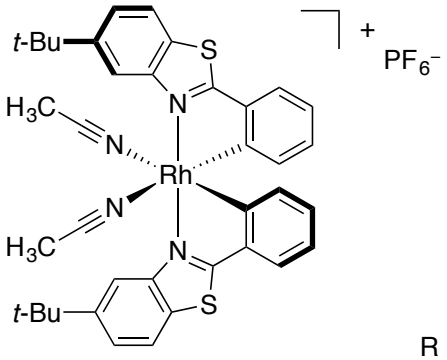

Δ-**71** (Δ-RhS)

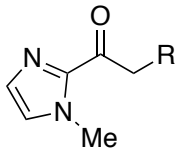

R = Ph: **74aa**
R = *p*-MeO-Ph: **74ag**

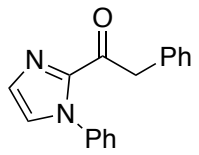

74ba

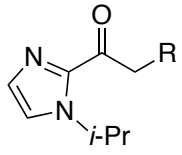

R = Ph: **74da**
R = Me: **74dh**

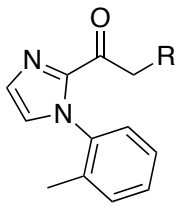

R = Ph: **74ca**
R = *p*-Me-Ph: **74cb**
R = *p*-Br-Ph: **74cc**
R = *p*-NO_2-Ph: **74cd**
R = *o*-Cl-Ph: **74ce**
R = Et: **74cf**

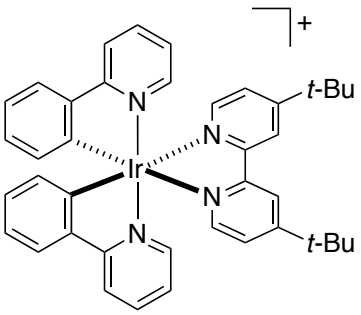

89·PF_6

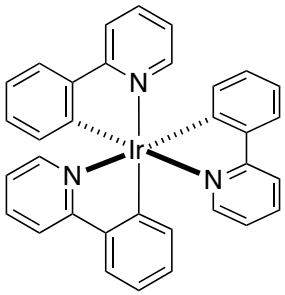

91

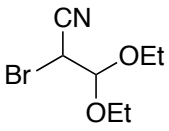

95b

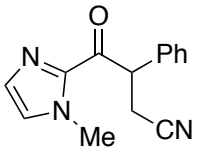

189aaa

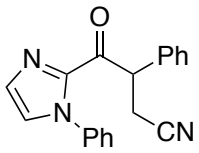

189baa

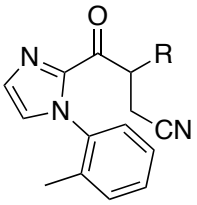

R = Ph: **189caa**
R = *p*-Me-Ph: **189cba**
R = *p*-Br-Ph: **189cca**
R = *p*-NO_2-Ph: **189cda**
R = *o*-Cl-Ph: **189cea**
R = Et: **189cfa**

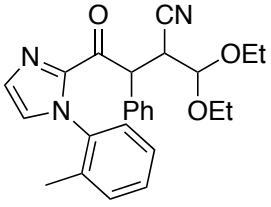

189cab

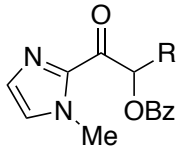

R = Ph: **219aa**
R = *p*-MeO-Ph: **219ag**

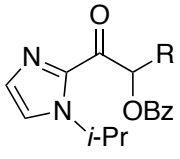

R = Ph: **219da**
R = Me: **219dh**

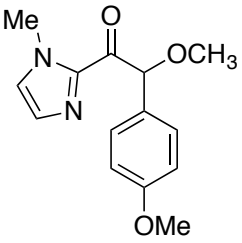

240ag

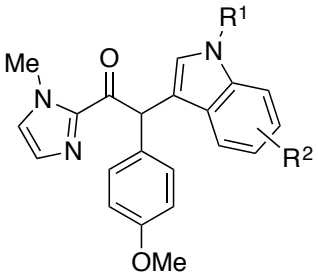

R^1 = H, R^2 = H: **250aga**
R^1 = Me, R^2 = 2-Me: **250agb**
R^1 = H, R^2 = 6-Me: **250agc**
R^1 = H, R^2 = 5-BnO: **250agd**
R^1 = Me, R^2 = 5-NO_2: **250age**

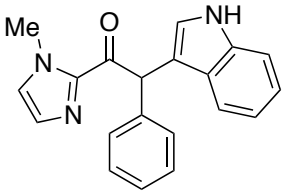

250aaa

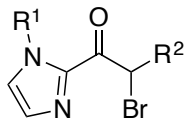

R^1 = Me, R^2 = Ph: **251aa**
R^1 = Ph, R^2 = Me: **251bh**

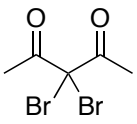

252

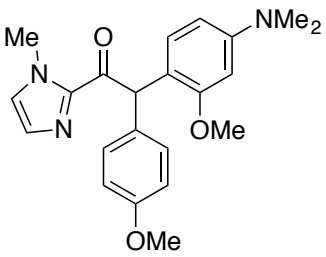

253

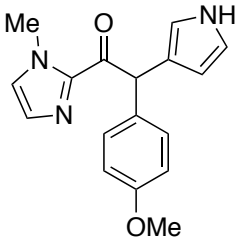

254

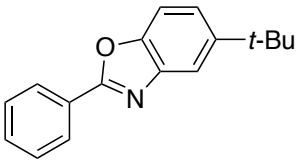

265

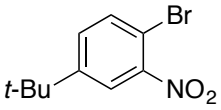

266

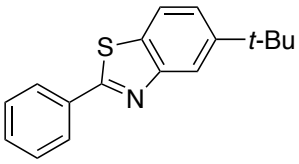

267

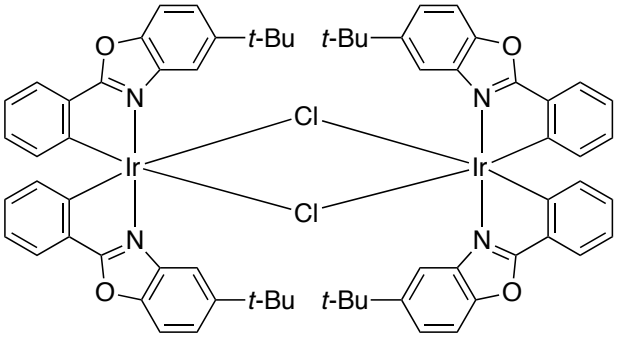

268

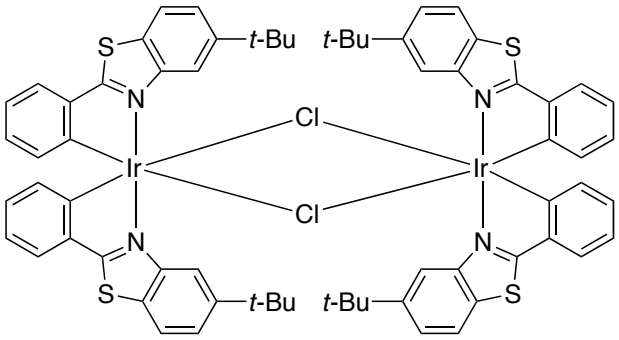

269

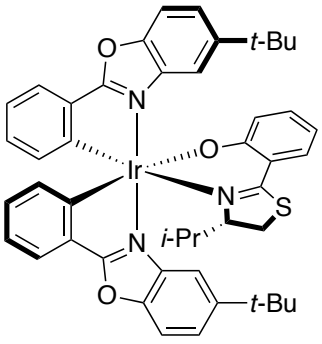

Λ-(*S*)-**270**

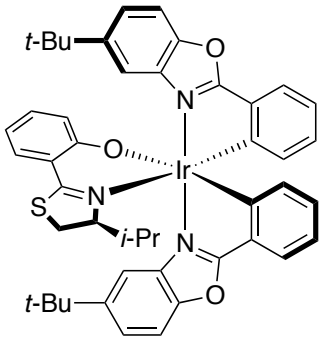

Δ-(*S*)-**270**

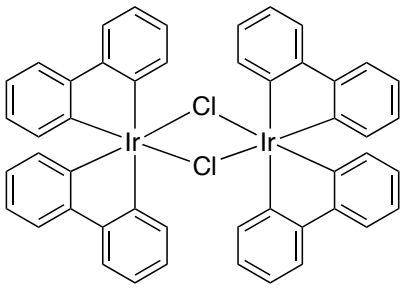

271

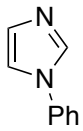

272b

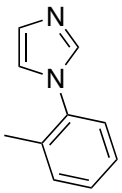

272c

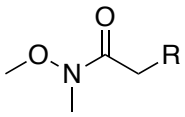

273

R = Ph: **273a**
R = *p*-CH_3-Ph: **273b**
R = *p*-Br-Ph: **273c**
R = *p*-NO_2-Ph: **273d**
R = *o*-Cl-Ph: **273e**
R = Et: **273f**
R = *p*-CH_3O-Ph: **273g**
R = CH_3: **273h**

7.5. Abbreviations and Symbols

Ac	acetyl
acac	acetylacetonato
AcO	acetate
Ar	aryl
aq.	aqueous
BArF	tetrakis[(3,5-trifluoromethyl)phenyl]borate
β-CD	β-cyclodextrin
BHT	2,6-di-*tert*-butyl-4-methylphenol
Bn	benzyl
Boc	*tert*-butyloxycarbonyl
BPO	benzoyl peroxide
bpy	2,2'-bipyridine
bpz	2,2'-pyrazine
Bu	butyl
BzO	benzoyl
cal	calorie
calcd.	calculated
CAN	ceric ammonium nitrate
cat.	catalyst
Cbz	carboxybenzyl
CFL	compact fluorescent lamp
conv.	conversion
COSY	correlation spectroscopy
D	dextrorotatory
d	day(s)
d	doublet
DMA	dimethylacetamide
DME	1,2-dimethoxyethane
DMF	*N*,*N*'-dimethylformamide
DMSO	dimethyl sulfoxide
DNA	deoxyribonucleic acid

dr	diastereomeric ratio
dtbbpy	4,4’-di-*tert*-butyl-2,2’-bipyridine
E	electrophile(s)
EDA	electron donor acceptor
EDCI	1-ethyl-3-(3-dimethylaminopropyl)carbodiimide
EDG	electron-donating group
ee	enantiomeric excess
en	ethylene-1,2-diamine
eq.	equivalent(s)
er	enantiomeric ratio
E_T	triplet energy
Et	ethyl
ESI	electrospray ionization
EWG	electron-withdrawing group
fac	*facial*
FG	functional group(s)
h	hour(s)
hex	hexyl
HMPA	hexamethylphosphoramide
HPLC	high performance liquid chromatography
HQ	hydroxyquinone
HRMS	high resolution mass spectrometry
i	*iso*
ISC	intersystem crossing
L	levorotatory
λ	wave length
LDA	lithium diisopropylamide
LED	light-emitting diode
m	*meta*
m	multiplet
M	molar(concentration)
Me	methyl
menbpy	4,4’-di(1*R*,2*S*,5*R*)-(−)-menthoxycarbonyl-2,2’-bipyridine

MLCT	metal-to-ligand charge transfer
MS	mass spectrometry
n	*normal*
n.d.	not determined
NHC	*N*-heterocyclic carbene
nm	nanometer
NMP	*N*-methyl-2-pyrrolidone
NMR	nuclear magnetic resonance spectroscopy
Nu-H/Nu	nucleophile(s)
o	*ortho*
ODN	2,4-dinitrophenylsulfonyloxy
OLED	organic light-emitting diode
p	*para*
Ph	phenyl
phen	1,10-phenanthroline
ppy	2-phenylpyridine
Pr	propyl
PS	photosensitizer
PyBOX	pyridine-2,6-bis(oxazoline)
rac	*racemic*
rt	room temperature
SCE	standard calomel electrode
SET	single electron transfer
SOMO	single occupied molecular orbital
T	temperature
t	*tertiary*
t	duration
TBHP	*tert*-butyl hydroperoxide
TBS	*tert*-butyldimethylsilyl
TEMPO	2,2,6,6-tetramethyl-1-piperidinyloxyl, free radical
TFA	trifluoroacetic acid
Tf	trifluoromethanesulfonyl
TfOH	trifluoromethanesulfonic acid

THF	tetrahydrofuran
TLC	thin layer chromatography
TMS	trimethylsilyl
TRISPHAT	tris[tetrachlorobenzene-1,2-bis(olato)] phosphate(V)
Ts	*para*-toluenesulfonyl
TsOH	*para*-toluenesulfonic acid
UV	ultraviolet

Statement

An den
Vorsitzenden des Prüfungsausschusses in Chemie
Fachbereich Chemie der Philipps-Universität Marburg
Hans-Meerwein-Strasße
D-35032 Marburg

Erklärung

gemäß §10, Abs. 1 der Promotionsordnung der Mathematisch-Naturwissenschaftlichen Fachbereiche und des Medizinischen Fachbereichs für seine mathematisch-naturwissenschaftlichen Fächer der Philipps-Universität Marburg vom 15.07.2009

Ich erkläre, dass eine Promotion noch an keiner anderen Hochschule als der Philipps-Universität Marburg, Fachbereich Chemie, versucht wurde und versichere, dass ich meine vorgelegte Dissertation

Chiral-at-Metal Iridium(III) and Rhodium(III) Lewis Acid Catalysts for the α-Functionalization of 2-Acyl Imidazoles

selbst und ohne fremde Hilfe verfasst, nicht andere als die in ihr angegebenen Quellen oder Hilfsmittel benutzt, alle vollständig oder sinngemäß übernommenen Zitate als solche gekennzeichnet sowie die Dissertation in der vorliegenden oder ähnlichen Form noch bei keiner anderen in- oder ausländischen Hochschule anlässlich einer Promotionsgesuches oder zu anderen Prüfungszwecken eingereicht habe.

Marburg, den Aug. 18, 2017

(Zuo, Wei)